

SECOND GENERATION ADVANCED REBURNING FOR HIGH EFFICIENCY NO_x CONTROL

DOE Contract No. DE-AC22-95PC95251

Final Report

Project Period: October, 1995 - June, 2001

Prepared by:

Vladimir M. Zamansky, Peter M. Maly, Vitali V. Lissianski,
Mark S. Sheldon, David Moyeda, and Roy Payne

Submitted by:

GE Energy and Environmental Research Corporation
18 Mason, Irvine, CA 92618

June 27, 2001



Disclaimer

This report was prepared as an account of work sponsored by an agency of the United States Government. Neither the United States nor any agency thereof, nor any of their employees, makes any warranty, express or implied, or assumes any legal liability or responsibility for the accuracy, completeness, or usefulness of any information, apparatus, product, or process disclosed, or represents that its use would not infringe privately owned rights. Reference herein to any specific commercial product, process, or service by trade name, trademark, manufacturer, or otherwise does not necessarily constitute or imply its endorsement, recommendation, or favoring by the United States Government or any agency thereof. The views and opinions of authors expressed herein do not necessarily state or reflect those of the United States Government or any agency thereof.

Abstract

This project develops a family of novel Second Generation Advanced Reburning (SGAR) NO_x control technologies, which can achieve 95% NO_x control in coal fired boilers at a significantly lower cost than Selective Catalytic Reduction (SCR). The conventional Advanced Reburning (AR) process integrates basic reburning and N-agent injection. The SGAR systems include six AR variants: (1) *AR-Lean* - injection of the N-agent and promoter along with overfire air; (2) *AR-Rich* - injection of N-agent and promoter into the reburning zone; (3) *Multiple Injection Advanced Reburning (MIAR)* - injection of N-agents and promoters both into the reburning zone and with overfire air; (4) *AR-Lean + Promoted SNCR* - injection of N-agents and promoters with overfire air and into the temperature zone at which Selective Non-Catalytic Reduction (SNCR) is effective; (5) *AR-Rich + Promoted SNCR* - injection of N-agents and promoters into the reburning zone and into the SNCR zone; and (6) *Promoted Reburning + Promoted SNCR* - basic or promoted reburning followed by basic or promoted SNCR process.

The project was conducted in two phases over a five-year period. The work included a combination of analytical and experimental studies to confirm the process mechanisms, identify optimum process configurations, and develop a design methodology for full-scale applications. Phase I was conducted from October, 1995 to September, 1997 and included both analytical studies and tests in bench and pilot-scale test rigs. Phase I moved AR technology to Maturity Level III - Major Subsystems. Phase II is conducted over a 45 month period (October, 1997 – June, 2001). Phase II included evaluation of alternative promoters, development of alternative reburning fuel and N-Agent jet mixing systems, and scale up. The goal of Phase II was to move the technology to Maturity Level IV- Subscale Integrated System.

Tests in combustion facility ranging in firing rate from 0.1×10^6 to 10×10^6 Btu/hr demonstrated the viability of the AR technology. The performance goals of the project to reduce NO_x by up to 95% with net emissions less than 0.06 lb/10⁶ Btu and to minimize other pollutants (N₂O and NH₃) to levels lower than reburning and SNCR have been met. Experimental data demonstrated that AR-Lean + SNCR and Reburning + SNCR are the most effective AR configurations, followed by AR-Lean and AR-Rich. Promoters can increase AR NO_x reduction efficiency. Promoters are the most effective at small amounts of the reburning fuel (6-10% of the total fuel heat input). Promoters provide the means to improve NO_x reduction and simultaneously decrease the amount of reburning fuel.

Tests also showed that alkali-containing compounds are effective promoters of the AR process. When co-injected with N-agent, they provide up to 25 % improvement in NO_x reduction.

A detailed reaction mechanism and simplified representation of mixing were used in modeling of AR processes. Modeling results demonstrated that the model correctly described a wide range of experimental data. Mixing and thermal parameters in the model can be adjusted depending on characteristics of the combustion facility. Application of the model to the optimization of AR-Lean has been demonstrated.

Economic analysis demonstrated a considerable economic advantage of AR technologies in comparison with existing commercial NO_x control techniques, such as basic reburning, SNCR, and SCR. Particularly for deep NO_x control, coal-based AR technologies are 50% less expensive than SCR for the same level of NO_x control. The market for AR technologies is estimated to be above \$110 million.

Table of Contents

<u>Section</u>	<u>Page</u>
Abstract	ii
Table of Contents	iii
List of Figures	vii
List of Tables	xiii
Nomenclature	xiv
Executive Summary	xvi
1.0 Introduction	1-1
2.0 Background	2-1
2.1 High Efficiency NO _x Control under Title 1 of the CAAA	2-1
2.2 Limitations of Available NO _x Control Technologies for Post-RACT Applications	2-2
2.3 Advanced Reburning	2-4
2.4 Second Generation Advanced Reburning (SGAR)	2-4
3.0 Phase I Results	3-1
3.1 Phase I Program Objectives	3-1
3.2 Summary of Phase I Results	3-2
3.3 Phase I Conclusions	3-4
4.0 Phase II Program Approach, Objectives and Tasks	4-1
4.1 Phase II Technical Approach	4-1
4.2 Phase II Objectives and Tasks	4-1
5.0 Task 2.1 Project Coordination and Reporting/Deliverables	5-1
6.0 Task 2.2 Studies of Prospective Additives	6-1
6.1 Bench-Scale Screening Tests	6-1
6.2 Pilot-Scale Test Results	6-5
6.2.1 Effect of Metals on NO _x Reduction	6-5
6.2.2 Effect of Ca on SO ₂ Emissions	6-8
6.2.3 Effect of Iron-Containing Compounds on NO _x Reduction	6-9
6.2.4 Effects of Fly Ash and Char on NO _x Reduction	6-12
6.3 Prospective Additives Search: Summary	6-14
7.0 Task 2.3 Development of Combined Chemistry/Mixing Model	7-1

7.1 Model Setup.....	7-2
7.1.1 Model Formulation.....	7-2
7.1.2 Estimation of Mixing Parameters	7-3
7.1.3 Mixing Mode.....	7-4
7.1.4 Mixture Stratification	7-6
7.2 Chemistry – Mixing Modeling of Gas Reburning	7-7
7.2.1 Comparison with Experimental Data Obtained in Bench- and Pilot-Scale Facilities	7-8
7.2.2 Comparison with Experimental Data of Kolb et al.....	7-11
7.2.3 Comparison with Experimental Data of Mereb and Wendt	7-12
7.3 Parametric Study of Basic Reburning	7-14
7.3.1 Effect of Fuel Stratification in the Reburning Zone	7-14
7.3.2 Effect of the Initial Temperature of the Reburning Fuel and Overfire Air	7-15
7.3.3 Reactions Responsible for NO _x Reduction	7-16
7.3.4 Gas Reburning Modeling: Summary	7-17
7.4 Chemistry-Mixing Modeling of Ammonia and Sodium Effects on Reburning.....	7-18
7.4.1 Combined Injection of N-Agent and Sodium Promoter.....	7-18
7.4.2 Injection of Promoters without N-Agent	7-22
7.4.3 Chemistry-Mixing Modeling of Ammonia and Sodium Effects: Summary.....	7-25
7.5 Optimization of AR via Modeling	7-26
7.5.1 AR-Lean Model Setup	7-26
7.5.2 Model Validation.....	7-27
7.5.3 Parametric Study of the AR-Lean Process.....	7-29
7.5.4 Mapping of the AR Process	7-34
7.5.5 AR Optimization: Summary	7-39
8.0 Task 2.4 Optimization of Process Synergism in 1×10 ⁶ Btu/hr Tests.....	8-1
8.1 Pilot-Scale Optimization Tests.....	8-1
8.1.1 Description of Greenidge AR System.....	8-1
8.1.2 Simulation of Greenidge Boiler	8-2
8.1.3 Baseline and Gas Reburning NO _x Data	8-3
8.1.4 Effect of Pulsing on Basic Reburning.....	8-5

8.1.5 AR-Lean Test Results	8-5
8.1.6 Comparison between Greenidge and Pilot-Scale AR-Lean Data.....	8-11
8.1.7 Reburning + SNCR	8-14
8.1.8 Comparison of Greenidge and Pilot-Scale Data: Summary	8-20
8.2 Coal Reburning Studies.....	8-22
8.2.1 Basic Coal Reburning Tests	8-22
8.2.2 Advanced Coal Reburning Tests	8-25
8.2.3 Advanced Coal Reburning: Summary	8-29
9.0 Task 2.5 10×10^6 Btu/hr Proof-of-Concept Tests.....	9-1
9.1 AR-Lean Tests.....	9-1
9.2 AR-Rich Tests	9-1
9.3 Reburning + SNCR Tests.....	9-2
9.4 MIAR Test Results	9-3
9.5 Ammonia Slip and N_2O Emissions Measurements	9-4
9.6 Proof-of-Concept Tests: Summary.....	9-5
10.0 Task 2.6 Design Methodology Validation	10-1
10.1 Full-Scale Implementation of AR	10-1
10.1.1 Activities at Martinez Refining Company Complex	10-1
10.1.2 AR-Lean Tests in Large Pilot-Scale	10-2
10.2 AR Economic and Market Update	10-12
10.2.1 NO_x Control Drivers	10-12
10.2.2 Economic Methodology and Case Studies	10-13
10.2.3 Technology Specific Inputs.....	10-14
10.2.4 Economic Results.....	10-16
10.2.5 Market Assessment	10-19
10.2.6 Economic and Market Analysis: Conclusions.....	10-19
10.3 Design Methodology and Application Conclusions	10-20
11.0 Experimental Facilities	11-1

11.1 Process Performance Characterization.....	11-1
11.2 Controlled Temperature Tower (CTT).....	11-2
11.3 Boiler Simulator Facility (BSF)	11-4
11.4 Tower Furnace (TF)	11-4
12.0 Conclusions.....	12-1
13.0 References.....	13-1
<i>Appendix A</i> Phase I Report	A-1
<i>Appendix B</i> Reaction Mechanism of C-H-O-N Species in Chemkin Format.....	B-1
<i>Appendix C</i> Thermodynamic Database for C-H-O-N Species in Chemkin Format.....	C-1
<i>Appendix D</i> Reaction Mechanism of Na Species in Chemkin Format	D-1
<i>Appendix E</i> Thermodynamic Database for Na Species in Chemkin Format.....	E-1
<i>Appendix F</i> Spray Evaporation Modeling Studies	F-1

List of Figures

<u>Figure</u>	<u>Page</u>
Figure 1-1. Schematic of different variants of AR	1-2
Figure 5-1. Phase II task structure	5-1
Figure 6-1. Alternative promoter AR-Rich screening test results.....	6-3
Figure 6-2. Performance of alternative promoter performance as a Function of injection temperature.....	6-4
Figure 6-3. Effect of FeSO ₄ on the reburning process	6-4
Figure 6-4. Promoter screening tests	6-5
Figure 6-5. Effect of metal-containing compounds injected with the main fuel on NO _x reduction	6-6
Figure 6-6. Na and K performance as a function of promoter concentration	6-6
Figure 6-7. NO _x reduction as function of Na concentration	6-7
Figure 6-8. Injection of 100 ppm Na and Ca into reburning zone at 1590 K	6-7
Figure 6-9. Effect of 100 ppm Na addition on CO emissions.....	6-8
Figure 6-10. Calcium promoter NO _x control performance during Utah coal firing.....	6-8
Figure 6-11. Calcium promoter SO ₂ capture during Utah coal firing.....	6-9
Figure 6-12. Test data on NO _x reduction in the presence of iron-containing compounds	6-11
Figure 6-13. Effect of fly ash co-injection with reburning fuel on NO _x reduction.....	6-13
Figure 6-14. Reburning performance of activated char as a function of char reburning heat input	6-13
Figure 7-1. Reactor diagram of model setup	7-2
Figure 7-2. A diagram of jet injection and model setup in the BSF reburning zone	7-4
Figure 7-3. Modeling setup in the BSF mixing zone	7-5
Figure 7-4. Comparison of BSF test results on reburning with modeling predictions	7-8
Figure 7-5. Performance of basic reburning in CTT.....	7-9
Figure 7-6. Performance of basic reburning in TF	7-9
Figure 7-7. Predicted effect of mixing time on NO _x reduction for typical BSF conditions	7-9
Figure 7-8. Modeling and experimental data on concentrations of N-containing species at the end of the BSF reburning zone.....	7-10
Figure 7-9. Comparison of experimental results on basic reburning with modeling predictions.....	7-11

Figure 7-10. Comparison of modeling predictions with experimental data of <i>Kolb et al.</i>	7-12
Figure 7-11. Effect of the reburning zone stoichiometry on efficiency of the reburning process.....	7-13
Figure 7-12. Comparison of modeling predictions with experimental data of <i>Mereb and Wendt</i>	7-14
Figure 7-13. Effect of fuel stratification in the mixing area of the reburning zone on modeling predictions for BSF conditions	7-15
Figure 7-14. Predicted effect of the initial temperature of the reburning fuel on NO reduction for BSF conditions	7-16
Figure 7-15. Predicted effect of the initial OFA temperature on NO reduction for BSF conditions	7-16
Figure 7-16. Performance of the reburning process for optimized and non optimized initial temperatures of the injected reburning fuel and overfire air	7-16
Figure 7-17. Concentrations of N-containing species in reburning and main reactions responsible for NO _x reduction in different zones	7-17
Figure 7-18. Comparison of modeling predictions with experimental data	7-19
Figure 7-19. Rate coefficient of the reaction $\text{NaOH} + \text{H} \rightarrow \text{Na} + \text{H}_2\text{O}$	7-21
Figure 7-20. Comparison of modeling predictions with experimental data on CO emissions.	7-21
Figure 7-21. CO emissions in the AR process as a function of flue gas temperature at the point of OFA injection.....	7-22
Figure 7-22. Comparison of modeling predictions with experimental data on the effect of Na ₂ CO ₃ injection in BSF at 18% reburning.....	7-24
Figure 7-23. Reactor diagram of AR-Lean model setup.....	7-27
Figure 7-24. Comparison of modeling predictions with experimental data on the effect of OFA/urea injection temperature on NO _x reduction in AR-Lean at 2% and 10% reburning.....	7-28
Figure 7-25. Comparison of modeling predictions with experimental data on basic reburning and AR-Lean reburning	7-28
Figure 7-26. Effect of CO on NO _x reduction by urea injection	7-29
Figure 7-27. Predicted effect of the reburning heat input on NO _x reduction at different OFA injection temperatures	7-31

Figure 7-28. Predicted effect of OFA/urea injection temperature in AR-Lean	7-31
Figure 7-29. Effect of droplet evaporation time on NO _x reduction	7-32
Figure 7-30. Predicted effects of droplet evaporation time on NO _x reduction at 10% and 5% reburning.....	7-33
Figure 7-31. Predicted effect of the amount of urea on NO _x reduction	7-34
Figure 7-32. Predicted effects of OFA and urea initial temperature on NO _x reduction	7-34
Figure 7-33. Performance of the AR-Lean process at NSR=1.5	7-36
Figure 7-34. Performance of the AR-Lean process at NSR=0.7	7-37
Figure 7-35. Performance of AR-Lean at NSR=0.7 as a function of the amount of the reburning fuel and droplet evaporation time of N-agent.....	7-38
Figure 7-36. Predicted performances of basic reburning, AR-Lean and Reburning+SNCR ...	7-39
Figure 8-1. Overview of the advanced gas reburning system installed on the Greenidge boiler.....	8-2
Figure 8-2. Comparison of Greenidge 1996 and 1997 gas reburning data.....	8-4
Figure 8-3. Comparison of gas reburning performance between Greenidge and BSF.....	8-4
Figure 8-4. Effect of fluctuations on reburning.....	8-5
Figure 8-5. AR-Lean performance vs. NSR at different CO concentrations	8-6
Figure 8-6. AR-Lean performance vs. NSR at different CO concentrations.....	8-7
Figure 8-7. AR-Lean performance vs. reburning zone CO concentration at 5% and 10% reburning.....	8-8
Figure 8-8. Incremental performance of N-agent alone in AR-Lean as a function of reburning zone CO concentration.....	8-8
Figure 8-9. AR-Lean performance versus additive injection temperature with and without main fuel pulsing at 10% reburning	8-9
Figure 8-10. AR-Lean performance versus additive injection temperature with main fuel pulsing at 5% reburning.....	8-9
Figure 8-11. AR-Lean performance versus NSR at initial NO concentrations of 300 and 600 ppm at 10% reburning	8-10
Figure 8-12. NO reduction in AR-Lean as a function of SR ₂ with and without pulsing.....	8-11
Figure 8-13. Comparison of the impacts of CO concentration on NO _x reduction in AR-Lean tests in Greenidge and BSF.....	8-12

Figure 8-14. Comparison of the impacts of injection temperature on NO _x reduction in Greenidge and BSF	8-13
Figure 8-15. NO _x reduction due to ammonia in AR-Lean in Greenidge and BSF	8-13
Figure 8-16. SNCR performance as a function of N-agent injection temperature with and without main fuel pulsing	8-14
Figure 8-17. Comparison of performance of different N-agents in the reburning + SNCR process without pulsing	8-15
Figure 8-18. Comparison of performance of different N-agents as a function of NSR at 1270 K and 1300 K (without pulsing)	8-15
Figure 8-19. Comparison of results obtained with the three N-agents during pulsing of the main fuel	8-16
Figure 8-20. NO reduction in reburning + SNCR as a function of pulsing frequency at 10% and 20% reburning	8-17
Figure 8-21. Comparison of results obtained at pulsing amplitudes of 5% and 10%.....	8-17
Figure 8-22. Promoted reburning + SNCR performance as a function of additive injection temperature at 10% reburning	8-18
Figure 8-23. Promoted reburning + SNCR performance as a function of sodium concentration at 10% reburning	8-18
Figure 8-24. Promoted reburning + SNCR performance as a function of reburning heat input	8-19
Figure 8-25. Ammonia slip results at different reburning + SNCR process conditions.....	8-20
Figure 8-26. Basic coal reburning performance as a function of reburning heat input with natural gas primary.....	8-24
Figure 8-27. Basic coal reburning performance as a function of reburning heat input with coal primary	8-24
Figure 8-28. AR-Lean performance at 10% reburning as a function of injection temperature for coals #1 and #3.....	8-25
Figure 8-29. Promoted AR-Lean performance at 10% reburning as a function of promoter concentration for coals #1 and #3	8-26
Figure 8-30. AR-Rich performance at 10% reburning as a function of injection temperature for coals #1 and #3.....	8-27

Figure 8-31. Promoted AR-Rich performance at 10% reburning as a function of promoter concentration for coals #1 and #3	8-27
Figure 8-32. Combined reburning and SNCR performance at 10% reburning as a function of injection temperature for coals #1 and #3	8-28
Figure 8-33. Combined reburning and SNCR performance as a function of reburning heat input for coals #1 and #3	8-28
Figure 8-34. Combined reburning and SNCR performance at 15% reburning as a function of promoter concentration for coals #1 and #3	8-29
Figure 8-35. Effect of Fe promoter concentration on reburning	8-30
Figure 9-1 AR-Lean performance vs. promoter concentration at 6% and 10 % reburning.....	9-2
Figure 9-2. AR-Rich performance vs. promoter concentration at 6% and 10 % reburning	9-2
Figure 9-3. Reburning+SNCR performance vs. promoter concentration at 10% and 20% reburning.....	9-3
Figure 9-4. MIAR: combined AR-Lean + AR-Rich performance vs. promoter concentration at 10% reburning	9-3
Figure 9-5. MIAR: combined AR-Lean + SNCR performance vs. promoter concentration at 6% and 10% reburning.....	9-4
Figure 9-6. Overall MIAR NO _x reduction under optimized conditions at 6% reburning	9-5
Figure 10-1. Atomization characteristics of test nozzle	10-3
Figure 10-2. Temperature profiles for the target boiler and the TF	10-4
Figure 10-3. Impact of atomization pressure for 5% urea solution on overall (a) and incremental (b) NO _x reduction by urea solution co-injected with OFA.....	10-5
Figure 10-4. Incremental NO _x reduction for co-injection of 5% urea solution with OFA ..	10-5
Figure 10-5. Incremental NO _x reduction for co-injection of different urea solution strengths with OFA	10-6
Figure 10-6. Comparison of overall NO _x reduction by urea solution for 3-port and 4-port configurations of OFA injection	10-7
Figure 10-7. Overall NO _x reduction at different urea injector positions. NSR = 1.0.....	10-7
Figure 10-8. Comparison of performance for urea and aqueous ammonia as a function of N-agent atomizing air pressure	10-8
Figure 10-9. Comparison of overall NO _x reduction at different OFA/urea injection temperatures	10-9

Figure 10-10. SNCR performance as a function of atomization pressure with and without reburning	10-9
Figure 10-11. Axial injector tests: impact of atomization pressure on overall NO _x reduction at different reburning heat inputs	10-10
Figure 10-12. Axial injector tests: comparison of urea and ammonium sulfate impacts on NO _x reduction.....	10-11
Figure 10-13. Comparison of cyclone-fired boiler NO _x control technology economics.....	10-16
Figure 10-14. Comparison of wall-fired boiler NO _x control technology economics	10-17
Figure 10-15. Impact of fuel differential on cyclone-fired boiler NO _x control economics.	10-18
Figure 10-16. Impact of fuel differential on wall-fired boiler NO _x control economics	10-18
Figure 11-1. Axial temperature profiles measured in CTT, BSF and TF	11-2
Figure 11-2. Controlled Temperature Tower (CTT).....	11-3
Figure 11-3. CTT temperature profiles.....	11-3
Figure 11-4. Boiler Simulator Facility (BSF).....	11-4
Figure 11-5. Schematic diagram of the Tower Furnace (TF)	11-5

List of Tables

<u>Table</u>	<u>Page</u>
Table 2-1. Performance of NO _x control technologies	2-3
Table 2-2. AR variants.....	2-5
Table 6-1. Compounds tested in CTT as advanced reburning promoters.....	6-2
Table 6-2. Mineral composition of fly ash generated by combustion of a Kentucky coal.....	6-12
Table 7-1. Characteristics of mixing in BSF and jet parameters	7-3
Table 7-2. Mixing parameters in CTT, BSF and TF.....	7-4
Table 7-3. Reburning parameters	7-7
Table 8-1. Test fuel analyses	8-23
Table 9-1. Results of ammonia slip tests.....	9-5
Table 10-1. Economic data.....	10-14
Table 10-2. NO _x control technologies and expected performance	10-15
Table 10-3. NO _x control technology economics	10-15
Table 10-4. Comparing the cost effectiveness for deep NO _x control	10-19

Nomenclature

AR	-	Advanced Reburning
AR-Lean	-	Advanced Reburning Lean
AR-Rich	-	Advanced Reburning Rich
BSF	-	Boiler Simulator Facility
Btu	-	British thermo units
CAAA	-	Clean Air Act Amendment
CFD	-	Computational Fluid Dynamics
CRF	-	Capital Recovery Factor
CTT	-	Controlled Temperature Tower
DOE	-	Department of Energy
EPRI	-	Electric Power Research Institute
ESP	-	Electrostatic Precipitator
FETC	-	Federal Energy Technology Center (U.S. Department of Energy)
GC	-	Gas Chromatography
GE-EER	-	General Electric Energy & Environmental Research Corp.
GRI	-	Gas Research Institute
JICFIS	-	Jets In Crossflow, Integral Solution code
LNB	-	Low NO _x Burners
MIAR	-	Multiple Injection Advanced Reburning
MS	-	Mass-Spectrometry
NAAQS	-	National Ambient Air Quality Standards
NEOTR	-	Northeast Ozone Transport Region
NESCAUM	-	Northeast States for Coordinated Air Use Management
NETL	-	National Energy Technology Laboratory (U.S. Department of Energy)
NSR	-	Nitrogen Stoichiometric Ratio
ODF	-	One Dimensional Flame code
OFA	-	Overfire Air
PFR	-	Plug Flow Reactor
RACT	-	Reasonably Available Control Technologies
SCR	-	Selective Catalytic Reduction
SGAR	-	Second Generation Advanced Reburning
SIP	-	Strategic Implementation Plan

g

SNCR	-	Selective Non-Catalytic Reduction
TAG	-	Technology Assessment Guide
TF	-	Tower Furnace
TFN	-	Total Fixed Nitrogen
WSR	-	Well-Stirred Reactor

Executive Summary

This project develops a family of novel Second Generation Advanced Reburning (SGAR) NO_x control technologies, which have the potential to achieve 95% NO_x control in coal fired boilers at a significantly lower cost than Selective Catalytic Reduction (SCR). AR systems integrate basic reburning and injection of an N-agent (a nitrogen-containing species, typically ammonia or urea, capable of converting NO to N₂). Specific features of the new AR systems in comparison with basic reburning include:

- Introduction of reburning fuel representing a small portion of the total fuel heat input, to provide slightly fuel-rich conditions in the reburning zone.
- N-agent injection at one or two locations, which may include the reburning zone, the point of overfire air injection, and/or downstream of overfire air injection.
- Injection of promoter additives which enhance the effectiveness of the N-agent.

The Advanced Reburning (AR) process is a GE-EER patented synergetic integration of basic reburning and N-agent injection. In this process, an N-agent is injected along with the overfire air (OFA) and the reburning system is adjusted to optimize the NO_x reduction due to the N-agent. By adjusting the reburning fuel injection rate to achieve near stoichiometric conditions (instead of the fuel rich conditions normally used for reburning), the CO level is controlled and the temperature window for selective NO_x reduction is broadened and deepened. The reburning fuel requirement is reduced from about 20% of total fuel heat input for basic reburning, to about 10% for AR, which has considerable economic benefits (the incremental cost of gas for gas reburning and the cost of the coal pulverization equipment for coal reburning). With AR, the NO_x control due to reburning fuel addition is somewhat reduced from basic reburning; however, this reduction is offset by the significant enhancement of the N-agent NO_x control.

This project develops AR systems which broaden technology applicability to a wide range of boiler designs. The AR systems incorporate several improvements over conventional AR, such as N-agent injection into the reburning zone, promoter additives which enhance the effectiveness of the N-agent, and injection of N-agents with or without promoters at two locations. Sodium salts, in particular sodium carbonate (Na₂CO₃), were identified as effective AR promoters. Salts of other alkali metals can also be used as promoters. This family of AR technologies is intended for post-RACT applications in ozone non-attainment areas where NO_x control in excess of 70%-80% is required. The AR systems are applicable to all types of coal fired boilers without massive hardware changes, without increasing air toxic and toxic waste problems, and at a cost for NO_x control on the order of half that of SCR. These systems will provide flexible installations and do not create secondary pollutants and can be integrated with SO₂ and air toxics control methods. They are also highly flexible, in that components can be added over time as NO_x emissions regulations become more stringent. Selection of a technology for a specific boiler can be made based on boiler access, thermal conditions, and NO_x control requirements.

In the AR processes, the N-agent can be injected with or without promoters at one or two of three chemically significant locations: into the reburning zone, along with OFA, or downstream of burnout in the temperature window for which Selective Non-Catalytic Reduction (SNCR) is effective, the SNCR zone. Accordingly, there are six AR variants:

- Promoted Advanced Reburning Lean (AR-Lean): Injection of the N-agent and promoter along with overfire air.
- Promoted Advanced Reburning Rich (AR-Rich): Injection of N-agent and promoter into the reburning zone.
- Multiple Injection Advanced Reburning (MIAR): Injection of N-agents and promoters both into the reburning zone and with overfire air.
- AR-Lean + Promoted SNCR: Injection of N-agents and promoters with overfire air and into the SNCR zone.
- AR-Rich + Promoted SNCR: Injection of N-agents and promoters into the reburning zone and into the SNCR zone.
- Reburning + Promoted SNCR: Basic or promoted reburning followed by basic or promoted SNCR process.

In each of these variants, the use of promoters is optional. When employed, promoters are typically co-injected with the N-agent.

The project was conducted in two phases over a five-year period. The work included a combination of analytical and experimental studies to confirm the process mechanisms, identify optimum process configurations, and develop a design methodology for full-scale applications. Phase I was conducted from October, 1995 to September, 1997 and included both analytical studies and tests in bench and pilot scale test rigs. Phase I moved AR technology to Maturity Level III - Major Subsystems. Phase II is conducted over a 45 month period (October, 1997 – June, 2001). Phase II is built on the Phase I results and includes evaluation of alternate promoters, development of alternative reburning fuel and N-Agent jet mixing systems, and scale-up. The goal of Phase II was to move the technology to Maturity Level IV- Subscale Integrated System.

The overall objective of Phase I was to demonstrate the effectiveness of the AR technologies at bench and pilot scale over a sufficiently broad range of conditions to provide all of the information needed for process optimization and scale up. Specific program objectives were as follows:

1. Develop an understanding of the mechanisms through which promoter additives improve N-agent effectiveness;
2. Develop a kinetic analytical model of the Promoted and Multiple Injection AR technologies;
3. Optimize the AR processes using the analytical model and the results of bench and pilot scale experiments under controlled mixing conditions; and
4. Upgrade GE-EER's AR design methodology to accommodate the technical advancements of AR.

Phase I project determined the ability of the AR technologies to meet the following technical performance goals:

- NO_x emissions from the 1×10⁶ Btu/hr coal fired Boiler Simulator Facility controlled to less than the requirements for post-RACT NO_x control in the NESCAUM area for the year 2003;
- Total estimated cost of controlling NO_x emissions, based on the 1×10⁶ Btu/hr coal fired tests, shown to be less than that currently projected for SCR NO_x control systems; and
- No significant reduction in boiler efficiency or significant adverse environmental impacts when compared to current reburning and SNCR technologies.

Phase I consisted of the following six tasks:

- Task 1.1 Project coordination and reporting/deliverables.
- Task 1.2 Kinetics of Na_2CO_3 reactions with flue gas components.
- Task 1.3 0.1×10^6 Btu/hr optimization studies.
- Task 1.4 1.0×10^6 Btu/hr process development tests.
- Task 1.5 Mechanism development and modeling.
- Task 1.6 Design methodology and application.

A flow system decomposition study in Task 1.2 revealed that the primary gas-phase decomposition products of Na_2CO_3 are Na atoms, NaOH and CO_2 . Extrapolating the results to higher temperatures showed that Na_2CO_3 decomposition at temperatures over 1400 K produced NaOH and CO_2 very quickly. NaOH then decomposed more slowly. These findings were incorporated into kinetic modeling in Task 1.5.

In Tasks 1.3 and 1.4 bench scale combustion tests in the 0.1×10^6 Btu/hr facility were conducted. These tests demonstrated NO_x reduction of 86%, 88%, and 91% for AR-Lean, AR-Rich, and MIAR, respectively. These levels of NO_x control were achieved with only 15 ppm Na_2CO_3 in flue gas. Pilot scale studies in the 1.0×10^6 Btu/hr combustion facility demonstrated the ability of the AR technologies to achieve NO_x reductions of 95+% during gas firing and 90+% during coal firing. Byproduct emissions were found to be lower than those generated by commercial reburning and SNCR technologies.

In Task 1.5 a detailed reaction mechanism was developed to model the AR chemical processes. Kinetic modeling provided insight into the controlling factors of the process and qualitatively described the observed reaction trends. Modeling predicted that the following factors mainly defined the efficiency of AR systems: equivalence ratio in the reburning zone, process streams injection temperatures (reburning fuel, N-agents, promoters, and OFA), concentrations of N-agents and promoters, delay times for injection of N-agents into the reburning and burnout zones, and characteristic mixing times of the injection streams with flue gas. The modeling predicted and explained the NO_x reduction enhancement of sodium promotion under both fuel-rich and fuel-lean conditions.

The AR design methodology was upgraded in Task 1.6 using experiments and analytical models to include the second generation improvements. This work took advantage of a full-scale demonstration of the original AR technology, already in progress under separate project funding, on a 105 MW tangentially fired boiler. The upgraded methodology was used to prepare process designs for three AR concepts on the 105 MW boiler, and to predict the impacts of the AR systems on boiler performance and NO_x emissions. Some elements of AR were tested in the boiler. These tests showed that the large scale stratification in the furnace gases affected the NO_x reduction and ammonia slip associated with N-agent injection.

An economic analysis was conducted to compare the cost effectiveness of AR and SCR using the EPRI Technology Assessment Guide methodology for two representative Title 1 CAAA applications: a cyclone fired boiler and a wall fired boiler equipped with low NO_x burners. The total cost of NO_x control (combining capital and operating cost components) for the AR systems was 48-69% less than for SCR depending on the specific application. The requirements for NO_x control under the CAAA were evaluated. The key drivers to implement AR are the current ozone non-attainment areas, the potential to expand those regions to the eastern half of the U.S., and the recent

tightening of the National Ambient Air Quality Standards for ozone and fine particulate which will require additional NO_x control nationwide. The market for AR technologies was estimated to be above \$1.5 billion.

Phase II filled the gap between the Phase I development and a long-term AR demonstration by doing the following:

- Identify alternative promoters based on the promotion mechanisms developed in Phase I.
- Identify and test coal mineral compounds responsible for the increased NO_x reduction in AR-Rich and MIAR with coal firing (about 10% higher than for gas firing).
- Optimize mixing (of reburning fuel, N-agents, and OFA into the furnace gas stream) via combined chemistry/mixing models.
- Optimize N-agent injection to maximize NO_x reduction with negligible ammonia slip.
- Evaluate the effect of N-agent/promoter mixing times representative of full scale.
- Optimize AR with new promoters and mixing regimes at 1×10⁶ Btu/hr scale.
- Scale up and confirm the design methodology via 10×10⁶ Btu/hr Proof-of-Concept tests as well as limited component tests conducted during the ongoing boiler AR tests.
- Update the economic and market analysis to confirm the advantages of AR.

Specific Phase II objectives were to:

1. Develop alternative NO_x control promoters for AR.
2. Develop a combined chemistry/mixing model of the process to optimize mixing regimes.
3. Confirm the design methodology via pilot scale experiments at 1.0×10⁶ and 10×10⁶ Btu/hr.

Phase II also determined the ability of the AR technologies to meet the following technical performance goals in the 10×10⁶ Btu/hr Proof-of-Concept coal firing tests:

1. Reduce NO_x by 95% with net emissions less than 0.06 lb NO_x/10⁶ Btu.
2. Minimize other pollutants (N₂O and NH₃) to levels lower than reburning and SNCR.
3. Minimize net parasitic power consumption to less than 0.5% of the power plant energy.
4. Minimize the total cost of NO_x control to less than half that of SCR.

Phase II included the following tasks:

- 2.1 Project coordination and reporting/deliverables.
- 2.2 Studies of other prospective promoters.
- 2.3 Development of a combined chemistry/mixing model.
- 2.4 Optimization of process synergism in 10×10⁶ Btu/hr tests.
- 2.5 10×10⁶ Btu/hr proof-of-concept tests.
- 2.6 Design methodology validation.

In Task 2.2 the effects of additives on AR-Rich and basic reburning were determined. Tests showed that co-injection of Li and K compounds resulted in 74-78% NO reduction, i.e. 17-21 percentage points improvement above the baseline reburning level. Although these effects are lower than those for sodium, they are significant. Thus, K and Li compounds can be used as AR promoters.

Compounds of Mg, Ca, Ba, and Zn provided relatively small promotional effect. When added to ammonia solution, they reduced NO by an additional 6-9 percentage points compared to unpromoted AR.

Tests also showed that metal-containing compounds could be effective reburning promoters without injection of N-agent. Fe-containing compounds were the most effective in reduction of NO_x emissions, followed by Na-, K-, and Ca-containing compounds. Co-injection of these compounds with the main fuel in the absence of reburning resulted in 16-30% NO_x reduction. Injection of metal compounds with the main fuel in the presence of reburning provided an additional 4-25% percentage points of NO_x reduction above the baseline reburning level. As the concentration of additive increased, so did the promotional effect. Co-injection of additives with reburning fuel and into the reburning zone had smaller effect than co-injection with the main fuel. Coal char and fly ash showed minimal effect on NO_x reduction. It is concluded that metals in coal char and fly ash were mainly present in the form of sulfides and silicate-alumosilicate matrixes that were more stable than carbonates and acetates at high temperatures. These compounds were not effective in reactions with combustion radicals and have a minimal effect on NO_x reduction.

Tests showed that not only did injection of Ca-containing compounds reduce NO_x emissions, but it also decreased SO₂ emissions: about 50% SO₂ reduction was achieved with the injection of 1,000 ppm of Ca(OH)₂ with main fuel.

The model of AR processes was updated in Task 2.3. Modeling results demonstrated that the model correctly described a wide range of experimental data obtained in five bench- and pilot-scale combustion facilities. This suggested that the model, as developed through Phase II, represented the main chemical and mixing features of the reburning process and could be used for process optimization. Mixing and thermal parameters in the model can be adjusted depending on the characteristics of the combustion facility. The following conclusions were drawn from modeling results:

- Stratification in the mixing zone improves reburning efficiency for small heat inputs of the reburning fuel and degrades reburning efficiency for large heat inputs. Based on modeling observations, it is suggested that design of the nozzle for the reburning fuel injection should be different depending on the amount of the injected reburning fuel. Injection of large amounts of the reburning fuel provides better NO_x reduction if mixing of reactants is fast. Injection of small amounts of the reburning fuel, on the other hand, should result in significant mixture stratification for better NO_x control (as long as complete mixing and burnout is ultimately achieved).
- Initial temperatures of the reburning fuel and OFA affect NO reduction and can be optimized for deeper NO control. Optimum temperatures depend on the mixture composition and on the injection location. By optimizing these parameters, NO_x reduction can be increased by several percentage points.
- Reactions of NH₃ in the burnout zone play an important role in NO reduction for large heat inputs of the reburning fuel.

The applicability of the model to the optimization of AR-Lean has been demonstrated. Modeling identified the following AR-Lean parameters as being most important: amounts of the reburning fuel and N-agent, temperature of flue gas at the point of OFA/N-agent injection, and evaporation time of the N-agent. Modeling predictions, supported by experiments, are that CO formed in the

reburning zone increases the efficiency of N-agent when the temperature of furnace gases at the point of OFA/N-agent injection is lower than 1200 K, and reduces its efficiency at higher injection temperatures. To reduce the negative effect of CO on NO_x reduction at OFA/N-agent injection temperatures typically utilized in utility boilers, the average droplet size of injected N-agent solution must be optimized to allow for CO oxidation in the burnout zone before a significant amount of N-agent evaporates.

In Task 2.4 BSF tests were conducted to determine the optimum process conditions at mixing and thermo characteristics of Greenidge 105 MW tangentially fired boiler. Tests focused on simulating the AR-Lean and reburning + SNCR performance as the most promising AR variants for deep NO_x control for the Greenidge unit. The results of the BSF simulation tests demonstrated that high CO concentrations typical for upper furnace of the Greenidge boiler have negative effects on AR-Lean performance at the NH₃/OFA injection location in the Greenidge boiler. For optimum AR-Lean performance, the CO concentration at the point of N-agent/OFA injection should be below 5000 ppm.

The Greenidge boiler is characterized by upper furnace fluctuations in gas concentrations, and contains zones that have simultaneously high levels of CO and O₂ due to incomplete mixing. To simulate boiler design, two cooling arrays were installed in the furnace of the BSF: one simulating the high temperature secondary superheater and one simulating the reheater. The pilot-scale test results demonstrated that pulsations of CO and O₂ concentrations did not affect the performance of basic reburning, but decreased NO_x reduction of SNCR by about 10% for tested experimental configuration. Performance in combined reburning + SNCR tests was almost independent on pulsing frequency and the reburning fuel flow rate, but decreased with pulsing amplitude. Results demonstrated that about 70-80% NO reduction could be achieved under Greenidge conditions using an optimized reburning + SNCR regime.

Another objective of Task 2.4 was to evaluate coal as a reburning fuel. The results of the experiments indicated that the four tested bituminous coals were capable of providing reasonably high NO_x control in basic reburning at the conditions available at the full-scale boilers. Over 90% NO_x reduction could be achieved in AR with utilization of coal as a reburning fuel. The most effective variant of AR was reburning + SNCR followed by AR-Lean and AR-Rich. Tests showed that injection of promoters could significantly improve the efficiency of AR.

Proof-of-concept tests in a 10×10⁶ Btu/hr combustion facility in Task 2.5 provided a final indication of the viability of the AR technology. The performance goals of Phase II to reduce NO_x by up to 95% with net emissions less than 0.06 lb/10⁶ Btu and to minimize other pollutants (N₂O and NH₃) to levels lower than reburning and SNCR have been met. The following conclusions were drawn from experimental data obtained in different combustion facilities ranging in firing rate from 0.1×10⁶ to 10×10⁶ Btu/hr:

- AR provides up to 95% NO_x reduction.
- AR-Lean + SNCR and Reburning + SNCR are the most effective AR configurations, followed by AR-Lean and AR-Rich.
- Promoters can increase the efficiency of NO_x reduction in AR. Promoters are most effective at a small amount of the reburning fuel (6-10% of total fuel heat input). This provides the means to improve NO_x reduction and simultaneously decrease the amount of reburning fuel required, relative to basic reburning.

In Task 2.6 economic and market analyses of AR technologies were updated. The main driver to implement AR is NO_x controls required in ozone non-attainment areas or areas which transport pollutants into ozone non-attainment areas. In the Northeastern portion of the country, this thirty-seven-state region consists of Pennsylvania and the States North and East of that state. This region can potentially be expanded to include Texas and all states North and East of this state. The NO_x control requirements developed by the EPA to date have been based on attaining the current National Ambient Air Quality Standards (NAAQS). However, the EPA has issued revised NAAQS for ozone and fine particulate that are substantially lower than the current standards. Since NO_x is a precursor of both pollutants, achieving the new NAAQS will require even greater reductions in NO_x emissions which provides additional driver for AR technologies.

The size of the market for AR technologies has been estimated to be above \$110 million by considering the existing and projected CAAA regulations, the power plants affected by the regulations, and industry projections for the mix of NO_x control technologies necessary for cost effective compliance with these regulations.

Economic analysis demonstrates a considerable economic advantage of AR technologies in comparison with existing commercial NO_x control techniques, such as basic reburning, SNCR, and SCR. Particularly for deep NO_x control, coal-based AR technologies are 50% less expansive than SCR for the same level of NO_x control.

All project objectives and technical performance goals have been met or exceeded, and it was demonstrated that AR technologies could achieve high efficiency and low cost NO_x control.

1.0 Introduction

This project develops a family of novel Second Generation Advanced Reburning (SGAR) NO_x control technologies, which have the potential to achieve 95% NO_x control in coal fired boilers at a significantly lower cost than Selective Catalytic Reduction (SCR). AR systems integrate basic reburning and injection of N-agents (nitrogen-containing compounds capable of reducing NO, typically ammonia or urea). The AR systems are intended for EPA SIP Call compliance that requires to reduce NO_x emissions from coal-fired facilities to the level of 0.15 lb/MMBtu in 22 states. Specific features of the new AR systems in comparison with basic reburning include:

- Introduction of reburning fuel representing a small portion of the total fuel heat input, to provide slightly fuel-rich conditions in the reburning zone.
- N-agent injection at one or two locations, which may include the reburning zone, the point of overfire air injection, and/or downstream of overfire air injection.
- Injection of promoter additives which enhance the effectiveness of the N-agent.

The project was conducted in two phases over a five year period. The work included a combination of analytical and experimental studies to confirm the process mechanisms, identify optimum process configurations, and develop a design methodology for full-scale applications. Phase I was conducted from October, 1995 to September, 1997 and included both analytical studies and tests in bench and pilot scale test rigs. Phase II is conducted over a 45 month period (October, 1997 –June, 2001). Phase II is based on the Phase I results and includes evaluation of alternate promoters, development of alternative reburning fuel and N-Agent jet mixing systems, and scale-up.

This report consists of 13 Sections and 6 Appendices. Sections 1 through 4 describe background of the AR technology, summary of Phase I results and Phase II objectives. A detailed description of Phase I results is presented in Appendix A. Sections 5 through 11 describe Phase II results. Sections 12 and 13 present conclusions and referenced literature. Appendices B through F include chemical mechanisms, thermodynamic property data used in kinetic modeling, and a description of Computational Fluid Dynamic (CFD) modeling used to correlate the droplet size of liquid N-agent with its evaporation time.

Extensive nomenclature is used in the description of different aspects of AR throughout this report. Figure 1-1 shows sketch of a boiler and summarizes the nomenclature for the various regions of the AR process. The region upstream of the reburning fuel injection is referred to as the primary zone or the main combustion zone. Combustion in the main combustion zone occurs in fuel lean environment so that the primary zone Stoichiometric Ratio (SR₁) is greater than 1.0. The initial NO concentration in this zone is referred to as NO_i. The region between the reburning fuel and overfire air (OFA) injection is referred to as the reburning zone and is maintained at stoichiometry SR₂ which is usually less than 1.0. In AR-Rich N-agent and promoter are injected into the reburning zone, typically with a delay after reburning fuel injection. OFA is injected to complete combustion, downstream at lower furnace gas temperatures (which drop rapidly due to the heat exchange surfaces used for steam generation). In AR-Lean, N-agent and promoter are injected along with OFA. The downstream region of OFA injection referred to as the burnout zone. Typically OFA serves as the carrier gas for injecting an N-agent and promoter in AR-Lean. This zone is always fuel lean, at a stoichiometric ratio (SR₃) greater than 1.0. An N-agent can also be injected (with or without promoter) downstream of the OFA injection location into the burnout zone at furnace gas

conditions (particularly temperature) characteristic of the Selective Non-Catalytic Reduction (SNCR) process. This variant is called reburning + SNCR.

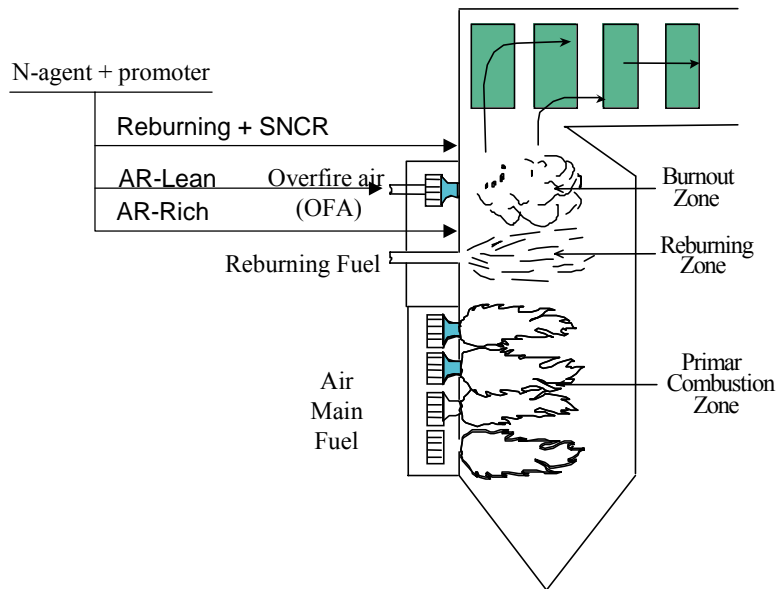


Figure 1-1. Schematic of different variants of AR.

2.0 Background

2.1 High Efficiency NO_x Control under Title 1 of the CAAA

Title 1 of the Clean Air Act Amendment (CAAA) of 1990 requires NO_x controls in ozone non-attainment areas. The initial Title 1 regulations required Reasonably Available Control Technologies (RACT). In most areas, the NO_x levels for RACT were based on Low NO_x Burners (LNB) and were in the range of 0.4 to 0.5 lb/10⁶ Btu. As a result, there has been little industry demand for higher efficiency and more expensive NO_x controls such as reburning, SNCR, and SCR.

Over the last ten years, U.S. Environmental Protection Agency (EPA) has developed most of the specific NO_x regulations authorized by the CAAA. The most stringent NO_x controls are required in ozone non-attainment areas or areas which transport pollutants into ozone non-attainment areas. In the Northeast, EPA has defined the Northeast Ozone Transport Region (NEOTR) consisting of Pennsylvania and the states North and East. In that zone, NO_x reductions of up to 75% are required by 2003 (SIP Call) with the potential for even deeper controls. The new control levels correspond to an average utility boiler NO_x emission rate of 0.15 lb/10⁶ Btu. EPA is now considering expanding the NEOTR to include Texas and all states North and East. In this 37 state region, it is projected that NO_x emissions may need to be reduced by as much as 85%.

As these specific regulations have developed, the trend has been towards cost effective emission controls. Rather than setting specific limits for each plant, in many areas the regulations have been established to provide the flexibility to over-control on some units and under-control on others, if that approach is cost effective. This can be of considerable advantage since the cost of NO_x control for some units (particularly smaller units) may be much higher than for others, on a basis of \$/ton of NO_x removed. This bubbling approach depends on the availability of NO_x control technologies which can achieve NO_x reductions greater than the nominal control levels (75-85%) at low cost.

Therefore, the goal established by DOE for this project, 95% NO_x control down to 0.06 lb/10⁶ Btu, is appropriate. NO_x control technologies which meet this goal will only be employed if their costs are competitive with conventional controls on a \$/ton basis. At present, the only commercial NO_x control technology capable of achieving such deep NO_x control is SCR. With SCR, NO_x is reduced to N₂ by reactions with N-agents on the surface of a catalyst. The SCR process effectively uses the N-agent. Injection at a Nitrogen Stoichiometric Ratio, NSR (NSR is defined as molar ratio of N atoms in N-agent to that in NO_x) of 1.0 typically achieves about 80% NO_x reduction (i.e., 80% N-agent utilization). SCR is fully commercialized in Europe and Japan and there are several U.S. installations. This is the reason for its extensive use as the basis of NO_x control requirements for post-RACT.

Since the post-RACT NO_x control requirements are largely based on SCR, achieving the required NO_x levels with SCR is relatively easy. However, SCR is far from an ideal utility solution. There are several important problems, and cost leads the list. SCR requires a catalyst in the flue gas exhaust stream. This catalyst, and the associated installation and boiler modifications, are expensive. As SCR technology has advanced over the last decade, the cost has decreased; however, at present, the initial cost of an 80% NO_x control SCR system for a coal fired boiler is still about a factor of four greater than that of LNB. Increasing the NO_x control to 95% approximately doubles the SCR system cost.

In addition, the SCR catalyst life is limited. Catalyst deactivation, through a number of mechanisms, typically limits catalyst life to about 4 years for coal fired applications. SCR catalysts are also toxic,

and therefore pose disposal problems. Since the catalyst is the major cost element in the SCR system, catalyst replacement and disposal contributes heavily to the total cost of NO_x control.

The AR technology developed in this project meets the following requirements:

1. NO_x control comparable with SCR;
2. Low capital cost compared to SCR;
3. Total cost of NO_x control (\$/ton of NO_x removal) low compared to SCR;
4. Compatible with all types of coal fired units (wall, tangential and cyclone fired);
5. Minimal plant modifications and no requirement to re-route and treat the entire flue gas stream;
6. No major components with limited life (such as the SCR catalyst);
7. No additional emissions of air toxics, criteria pollutants, or toxic solid or liquid waste materials;
8. Ability to integrate with technologies for controlling other pollutants, such as SO₂, air toxics and with projected CO₂ control strategies;
9. Minimal impact on boiler efficiency and operations; and
10. Flexibility to achieve the required level of control, with potential to readily implement add-on controls to reach more stringent control levels if required.

The main advantage of the AR technologies developed in this project is that they can provide the deep NO_x control of SCR at a considerable cost reduction.

2.2 Limitations of Available NO_x Control Technologies for Post-RACT Applications

The suitability of AR for post-RACT applications can best be appreciated by comparing it with the currently available NO_x control technologies. Table 2-1 shows the typical performance for a range of conventional NO_x controls applied to a pulverized coal fired boiler with baseline emissions of 1.0 lb/10⁶ Btu. Both the applicability of specific NO_x controls and their performance depend heavily on site specific factors. While the values in the table are generally representative of state of the art performance, each installation will be different.

Low NO_x burners and OFA provide only modest NO_x control. However, their capital costs are low and, since no reagents are required, their operating costs are near zero. This has made them the technologies of choice for the modest NO_x control required under Title 4 and the initial RACT under Title 1 of the CAAA. However, alone, they cannot approach the 0.15 lb/MMBtu NO_x control goal required by SIP Call.

For deeper NO_x control, reburning, SNCR or SCR can be added to low NO_x burners and OFA, or installed as stand alone systems.

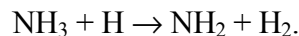
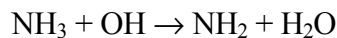
Reburning controls NO_x via fuel staging. The main portion of the fuel is fired through the conventional burners with a small portion of the fuel injected into the furnace above the burners. The result is a fuel rich "reburning zone" where NO_x is reduced by reactions with active radicals formed during interaction of the reburning fuel and oxygen from the main combustion zone.

Reburning, alone, can achieve only 50-70% NO_x control and, hence, may not be a candidate for most post-RACT applications.

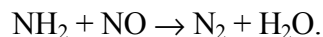
Table 2-1. Performance of NO_x control technologies.

Technology	Nominal Performance For Baseline NO _x 1.0 lb/10 ⁶ Btu	
	NO _x Reduction (%)	NO _x Emission (lb/10 ⁶ Btu)
Low NO _x Burners	30-50	0.5-0.7
Low NO _x Burners + Overfire Air	50-60	0.4-0.5
Reburning	50-70	0.3-0.5
Selective Non-Catalytic Reduction (SNCR)	40-70	0.3-0.6
Selective Catalytic Reduction (SCR)	> 80	< 0.2
Low NO _x Burners + AR systems	> 80	< 0.2

The reaction of N-agents with NO_x can proceed without a catalyst at high temperatures. This is the SNCR process. It is effective over a narrow "temperature window" typically centered about 1250 K where the N-agent forms NH₂ radicals which react with NO. The NH₂ radicals are formed from the N-agent via interaction with radicals. For example:



The NH₂ species can reduce NO to molecular nitrogen:



Under ideal laboratory conditions, deep NO_x control can be achieved. However, in practical, full scale installations, the non-uniformity of the temperature profile, difficulties of mixing the N-agent across the full boiler cross section, limited residence time for reactions, and any escape of unreacted ammonia ("ammonia slip"), combine to limit SNCR's effectiveness to about 40%. For typical SNCR conditions with a NSR of 1.5 and 40% NO_x control, the N-agent utilization is only 27%. Thus, while SNCR does not require a catalyst, and therefore has a low capital cost compared to SCR, it requires about four times as much N-agent resulting in higher operating costs.

2.3 Advanced Reburning

The AR process is a GE-EER patented (*Seeker et al., 1992*) synergetic integration of basic reburning and N-agent injection. In this process, an N-agent is injected along with the OFA and the reburning system is adjusted to optimize the NO_x reduction due to the N-agent. By adjusting the reburning fuel injection rate to achieve near-stoichiometric conditions (instead of the more fuel rich conditions normally used for reburning), the CO level is controlled and the temperature window for selective NO_x reduction is broadened to a greater temperature range, and deepened to greater maximum levels of NO_x control. The reburning fuel is reduced from about 20 to about 10% of the total heat input, which has considerable economic benefits (the incremental cost of natural gas for gas reburning, and the cost of additional coal pulverization equipment for coal reburning). With AR, the NO_x control due to the reburning process is somewhat reduced, however this reduction is offset by the significant enhancement of the N-agent NO_x control.

The AR process was developed by GE-EER as part of a DOE program (*Chen et al., 1991*) focusing on the optimization of basic reburning. Tests were conducted over a range of scales (up to 10×10⁶ Btu/hr) and achieved above 80% NO_x control. An AR design methodology was developed by extending GE-EER's reburning design methodology.

2.4 Second Generation Advanced Reburning (SGAR)

Improved versions of the AR process have been under development at GE-EER since 1993. They were first predicted by kinetic modeling and then confirmed by 300 kW combustion tests via GE-EER in-house R&D funds. The AR systems have the potential to achieve 95% NO_x control on all types of coal fired boilers without massive hardware changes, without increasing air toxic and toxic waste problems, and at a cost for NO_x control on the order of half that of SCR. The SGAR systems incorporate several improvements over conventional AR, such as:

- The alternative of N-agent injection into the reburning zone (as opposed to injection in the OFA zone);
- Optional use of promoter additives which enhance the effectiveness of the N-agent; and
- The option of injecting N-agents, with or without promoters, at multiple locations.

Sodium salts, in particular sodium carbonate (Na₂CO₃) were identified as effective AR promoters.

By integrating these improvements into AR, NO_x control can be increased to 90 - 95% for cyclone units and even higher for pulverized coal fired units (wall and tangentially fired) where AR can be further integrated with LNB and OFA. This family of AR technologies is intended for post-RACT applications in ozone non-attainment areas where NO_x control in excess of 80% is required.

Figure 1-1 presents a general schematic of the AR processes. The N-agent can be injected with or without promoters at selected locations (typically one or two), selected from the reburning zone, the point of OFA injection (typically co-injected), or downstream in the burnout (SNCR) zone. Accordingly, there are six AR variants, as shown in Table 2-2.

Table 2-2. AR variants (each N-agent can be injected with or without promoters).

AR Technology	Description
Advanced Reburning Lean - AR-Lean	Injection of the N-agent along with OFA
Advanced Reburning Rich - AR-Rich	Injection of N-agent and promoter into the reburning zone.
Multiple Injection AR - MIAR	Injection of N-agents and promoters both into the reburning zone and with OFA.
AR-Lean + SNCR	Injection of N-agents and promoters with OFA and into the SNCR zone.
AR-Rich + SNCR	Injection of N-agents and promoters into the reburning zone and into the SNCR zone.
Reburning + SNCR	Basic or promoted reburning followed by basic or promoted SNCR process

These AR technologies do not create secondary pollutants and can be integrated with SO₂ and air toxics control methods. They are also highly flexible, in that components can be added over time as NO_x emissions regulations become more stringent. Selection of a technology for a specific boiler can be made based on boiler access, thermal conditions, and NO_x control requirements.

30 Phase I Objectives and Results

The following sections describe Phase I objectives and present summary of Phase I results. Detailed description of Phase I results is presented in *Appendix A*.

31 Phase I Program Objectives

The overall objective of Phase I was to demonstrate the effectiveness of the AR technologies at bench and pilot scale over a sufficiently broad range of conditions to provide all of the information needed for process optimization and scale up. The Phase I program was conducted over a two-year period. Specific program objectives were as follows:

- Develop an understanding of the mechanisms through which promoter additives improve N-agent effectiveness;
- Develop a kinetic analytical model of the Promoted and Multiple Injection AR technologies;
- Optimize the AR processes using the analytical model and bench and pilot scale experiments under controlled mixing conditions; and
- Upgrade GE-EER's AR design methodology to include advances of SGAR.

Phase I project determined the ability of the AR technologies to meet the following technical performance goals:

- NO_x emissions from the 1×10⁶ Btu/hr coal fired Boiler Simulator Facility (BSF) controlled to less than the requirements for post-RACT NO_x control in the NESCAUM area for the year 2003 (0.15 lb/MMBtu);
- Total estimated cost of controlling NO_x emissions based on the 1×10⁶ Btu/hr coal fired tests less than that currently projected for SCR NO_x control systems; and
- No significant reduction in boiler efficiency or significant adverse environmental impacts when compared to current reburning and SNCR technologies.

Phase I consisted of the following six tasks:

Task 1.1 Project coordination and reporting/deliverables.

Task 1.2 Kinetics of Na₂CO₃ reactions with flue gas components.

Task 1.3 0.1×10⁶ Btu/hr optimization studies.

Task 1.4 1.0×10⁶ Btu/hr process development tests.

Task 1.5 Mechanism development and modeling.

Task 1.6 Design methodology and application.

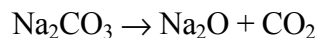
Task 1.1, *Project coordination and reporting/deliverables*, coordinated the efforts of the Key Personnel involved with the project so that the objectives of this project were met: on time, on

specification, and on budget. Phase I experimental work started from parametric screening tests at a bench scale facility (Task 1.3), followed by pilot scale developmental studies (Task 1.4). The Phase I program utilized two GE-EER test facilities providing nominal thermal capacities of 0.1×10^6 and 1×10^6 Btu/hr. The experimental work was paralleled by kinetic modeling (Task 1.5). A detailed reaction mechanism of the AR processes was developed based on available combustion chemistry data. Simultaneously, an experimental study (Task 1.2) was conducted at the University of Texas to define high-temperature chemistry of sodium carbonate under simulated flue gas conditions. The results were used for updating the kinetic model. The modeling used experimental data to define key process parameters, culminating in upgrading GE-EER's existing design methodology for conventional AR to include the second generation improvements (Task 1.6).

3 Summary of Phase I Results

Phase I included parametric screening tests which were conducted in a bench scale facility, followed by pilot scale developmental studies. Experimental work was paralleled by kinetic modeling which provided a scientific understanding of the process, including the activity of N-agent promoters. Simultaneously, an experimental study was conducted to define the high-temperature chemistry of sodium carbonate under simulated flue gas conditions. The modeling used experimental data to define key process parameters, culminating in a design methodology for the eventual scale-up and implementation of the technologies.

A kinetic study on thermal decomposition of Na_2CO_3 was conducted in Task 1.2 using a flow system with Gas Chromatography (GC) and Mass-Spectrometry (MS) analysis of products. It was found that significant decomposition of Na_2CO_3 occurred on a one second time scale at temperatures between 900 and 1300 K. The main decomposition products were identified as CO_2 , Na atoms, and Na_2O . The rate of Na_2CO_3 decomposition was measured as functions of temperature, residence time, and initial Na_2CO_3 concentration. The decomposition of Na_2CO_3 from 900 to 1190 K was described kinetically in terms of two irreversible and one reversible reactions:



In Task 1.3, 0.1×10^6 Btu/hr combustion tests were conducted with natural gas as main and reburning fuel. The promoted AR-Lean process achieved about 86% NO_x reduction at 10% reburning fuel heat input and only 15 ppm Na_2CO_3 in flue gas. The promoted AR-Rich process achieved 88% NO_x reduction at 10% reburning fuel and 15 ppm Na_2CO_3 . Thus, the presence of Na_2CO_3 promoted the effect of both "lean" and "rich" N-agent injection. Several sodium compounds (Na_2CO_3 , NaHCO_3 , and NaOH) were tested and achieved comparable promotion effectiveness. In AR-Rich, NO_x reduction was enhanced when the N-agent was injected into the reburning zone with a delay time after injection of the reburning fuel. The MIAR process achieved 90 - 91% NO_x reduction in these bench scale tests and was expected to improve at larger scales since the injectors adversely affected the temperature profile in these small scale tests.

Task 1.4 involved 1.0×10^6 Btu/hr tests in the BSF. Initial experiments were performed with natural gas firing. In AR-Lean, injection of urea or ammonia with OFA provided 45 - 82% NO_x reduction depending on the injection temperature. This was consistent with previous GE-EER research. Addition of 15 ppm of Na_2CO_3 promoter to the N-agent greatly improved NO_x reduction.

Performance was about equal for ammonia and urea with maximum of 89 - 94%. In AR-Rich, similar NO_x reduction was obtained for injection of ammonia and urea, 70 - 77%. However, addition of 15 - 25 ppm Na_2CO_3 significantly improved NO_x reduction, up to 94 - 95%. Two N-agent injections (MIAR) demonstrated 78 - 82% NO_x reduction without sodium and up to 98% NO_x reduction, with 15 ppm Na_2CO_3 . This was the maximum NO_x reduction achieved by AR systems.

Experiments were also conducted with coal firing. The results showed that the AR technologies could provide up to 95% NO_x control for a high-sulfur coal-fired combustor. The NO_x reduction due to N-agent injection was higher, but the effect of sodium promotion was lower in comparison with gas firing. Na_2CO_3 was found to promote performance only by 5 - 8 percentage points when added at 75 ppm. Maximum NO_x reductions achieved by the promoted AR technologies with coal firing were 90% for AR-Lean, 93% for AR-Rich, and 95% for MIAR. Three other AR modifications: AR-Lean + Promoted SNCR, AR-Rich + Promoted SNCR, and Reburning + Promoted SNCR, provided up to 95%, 92%, and 93% NO_x reduction, respectively.

A separate study was conducted to evaluate byproduct emissions from different AR variants in comparison with basic reburning and SNCR. The following emissions were characterized: NO_x , CO, CO_2 , O_2 , SO_2 , N_2O , total hydrocarbons, NH_3 , HCN, SO_3 , fly ash mass loading, size distribution, PM10, PM2.5, and carbon in ash. The results showed that in most configurations AR technologies have less byproduct emissions than basic reburning and SNCR processes under similar operating conditions.

In Task 1.5, a reaction mechanism, including 355 reactions of 65 chemical species, was developed to characterize the chemical processes of reburning and AR. The mechanism consists of C-H-O-N sub-mechanism (GRI-Mech-2.11, no variation of rate constants) and sub-mechanisms describing SNCR chemistry, and reactions of sodium, sulfur, and chlorine. Modeling was performed using three kinetic programs: Chemkin-2, Senkin (developed by Sandia National Laboratories) and GE-EER's One Dimensional Flame code (ODF). Modeling was capable of predicting major reaction trend, qualitatively describing AR processes, and, in some cases, was close to quantitative process description. Modeling explained why the delayed ammonia injection into the reburning zone is capable of reducing NO concentration and why certain additives, such as oxygen and active radicals, can promote the NO- NH_3 interaction in the reburning zone. Modeling also described the NO- NH_3 interaction in the burnout zone. A sensitivity analysis was conducted which revealed the most significant elementary reactions affecting formation and destruction of fuel-N compounds in the reburning zone under various conditions. Modeling with different mixing times demonstrated the importance of delayed mixing modes for efficient NO_x reduction. Modeling explained the effect of sodium promoters under both fuel-rich and fuel-lean conditions. Sodium reactions can affect NO_x control by decreasing or increasing the radical pool when it is needed. The radicals in turn can react with NH_3 to form NH_2 species which reduce NO to molecular nitrogen. The effect of promoters is most pronounced in systems with long characteristic mixing times, as is typical in full-scale industrial applications.

In Task 1.6, GE-EER's reburning design methodology was expanded to AR and an economic and market assessment was conducted. To demonstrate the applicability of the methodology, it was applied to a typical 100 MW coal-fired utility boiler with tangentially firing burners, resulting in development of conceptual designs for several AR systems, and predictions of their impacts on boiler NO_x emissions and operating performance. Thermal performance models were used to evaluate the impacts of implementing AR processes on the thermal performance of the boiler. For implementation of AR-Lean, AR-Rich, or MIAR processes, the reburning fuel would be injected

into the lower furnace and the overfire air would be injected into the upper furnace in a cavity between the first two tube banks of the convective pass. The overall boiler efficiency for operation with an AR system is similar to that for operation with a basic gas reburning system. The results of the analysis are specific to the boiler configuration evaluated and should not be generalized to other boiler designs. The results of injection system analysis indicate that good mixing of the process streams necessary to implement advanced reburning (AR-Lean, AR-Rich, and MIAR) on the case study boiler can be achieved. Natural gas can be injected from each wall in a pattern which achieves good distribution of the reburning fuel. Overfire air injection into a cavity in the convective pass, needed for implementation of each of the AR processes under consideration, can be achieved using high pressure wall jets. For the AR-Lean and MIAR processes, these ports can also be used to inject the reagent. Injection of reagent into the upper furnace, needed for the AR-Rich and MIAR processes, can be achieved using a lance-based system. Full scale NO_x reduction level is predicted to be above 90% and can be additionally increased with the use of promoters.

The original work scope for this task was based on applying the design methodology to a hypothetical case study; however, it was hoped that an initial AR demonstration could be developed in parallel with Phase I (outside the scope of this DOE project) to allow application to a real unit and evaluation of some of the AR elements. GE-EER was successful in developing an initial AR demonstration project. In 1995 GE-EER installed AR-Lean on a 105 MW tangentially fired boiler. Initial AR testing was conducted in 1996 and continued through 1998. This unit was used as the basis for extending the design methodology. AR-Lean tests on the boiler showed that stratification within the reburning zone could adversely affect the performance. Regions of inadequate CO in the reburning zone reduced the N-agent NO_x control and caused NH_3 slip.

While modifications were successful in reducing stratification, this experience showed the importance of mixing and scale up, two factors evaluated in Phase II. In addition to these AR-Lean tests, opportunity was taken to obtain preliminary larger scale data on several of the AR components including N-agent injection into the reburning zone, N-agent injection downstream of the reburning zone in an SNCR mode, and N-agent injection into the reburning zone and with the overfire air.

An economic analysis was conducted comparing AR technologies using gas and coal as reburning fuels with SCR for two representative Title 1 CAAA applications: a cyclone fired boiler and a wall fired boiler equipped with low NO_x burners. The analysis was based on the EPRI Technology Assessment Guide (TAG) methodology which evaluates the total annual levelized cost including capital and operating cost components (\$/ton). The unit cost of NO_x control (\$/ton) is also calculated. Depending on the specific application, AR offers total cost reductions of 48 to 69% over SCR. The market for AR technologies is estimated to be above \$1.5 billion.

3Phase I Conclusions

1. Bench scale combustion tests in the 0.1×10^6 Btu/hr facility demonstrated NO_x reduction of 86%, 88%, and 91% for AR-Lean, AR-Rich, and MIAR, respectively. These levels of NO_x control were achieved with only 15 ppm Na_2CO_3 in flue gas. Pilot scale studies in the 0.1×10^6 Btu/hr combustion facility demonstrated the ability of the AR technologies to achieve NO_x reductions of 95+% during gas firing and 90+% during coal firing. Byproduct emissions were found to be lower than those generated by commercial reburning and SNCR technologies.
2. A flow system decomposition study revealed that the primary gas-phase decomposition products of Na_2CO_3 were Na atoms, NaOH and CO_2 . Extrapolating the results to higher

temperatures showed that Na_2CO_3 decomposition at temperatures over 1400 K produced NaOH and CO_2 very quickly. NaOH then decomposes more slowly.

3. A detailed reaction mechanism was developed to model the AR chemical processes. Kinetic modeling provided insight into the controlling factors of the process and qualitatively described the observed reaction trends. The following factors mainly defined the efficiency of AR systems: equivalence ratio in the reburning zone, process streams injection temperatures (reburning fuel, N-agents, promoters, and OFA), concentrations of N-agents and promoters, delay times for injection of N-agents into the reburning and burnout zones, and characteristic mixing times of the injection streams with flue gas. The modeling predicted and explained the NO_x reduction enhancement of sodium promotion under both fuel-rich and fuel-lean conditions.
4. The AR design methodology was upgraded by using experiments and analytical models to include the second generation improvements. This work took advantage of a full-scale application of the original AR configuration in progress on a 105 MW tangentially fired boiler outside the scope of this project. The upgraded methodology was used to prepare process designs for three AR concepts on the 105 MW boiler and to predict the impacts of the AR systems on boiler performance and NO_x emissions. Some elements of AR were tested in the boiler. These tests showed that the large scale stratification in the furnace gases affected the NO_x reduction and ammonia slip associated with N-agent injection.
5. An economic analysis was conducted to compare the cost effectiveness of AR and SCR using the EPRI Technology Assessment Guide methodology for two representative Title 1 CAAA applications: a cyclone fired boiler and a wall fired boiler equipped with low NO_x burners. The total cost of NO_x control (combining capital and operating cost components) for the AR systems was 48-69% less than for SCR depending on the specific application. The requirements for NO_x control under the CAAA were evaluated. The key drivers are the current ozone non-attainment areas, the potential to expand those regions to the eastern half of the U.S. and the recent tightening of the National Ambient Air Quality Standards for ozone and fine particulate which will require additional NO_x control nationwide. The market for AR technologies was estimated to be above \$1.5 billion.
6. All Phase I objectives and technical performance goals have been met or exceeded, and it was demonstrated that AR technologies could achieve high efficiency and low cost NO_x control. However, additional work was needed in Phase II to move the technology to a demonstration stage. In particular, the following steps were necessary to optimize and scale up the AR technologies:
 - Identify alternative promoters based on the promotion mechanisms developed in Phase I.
 - Identify and test coal mineral compounds responsible for the increased NO_x reduction in AR-Rich and MIAR with coal firing (about 10% higher than for gas firing).
 - Optimize mixing (reburning fuel, N-agents, OFA) via combined chemistry/mixing models.
 - Optimize N-agent injection to maximize NO_x reduction with negligible ammonia slip.
 - Evaluate the effect of N-agent/promoter mixing times representative of full scale.
 - Optimize AR with new promoters and mixing regimes at 1×10^6 Btu/hr scale.

- Scale up and confirm the design methodology via 10×10^6 Btu/hr Proof-of-Concept tests and limited component tests during the ongoing boiler AR tests.
- Update the economic and market analysis to confirm the advantages of AR.

4 Phase II Program Approach, Objectives and Tasks

4.1 Phase II Technical Approach

This section presents an overview of GE-EER's technical approach to the development of the AR processes in Phase II. Phase I moved AR technology to Maturity Level III - Major Subsystems. Pilot scale tests have been conducted to evaluate all of the components including delayed injection of N-agents into the reburning zone and the use of sodium carbonate as a promoting additive for both fuel rich and lean N-agent injection. Limited component tests have been conducted in a boiler. Phase II moved the technology to Maturity Level IV- Subscale Integrated System. Maturity Level V (full-scale demonstration) and Level VI (commercial applications) will follow.

Phase II filled the gap between the Phase I development and a long-term AR demonstration by doing the following:

- Identifying alternative promoters based on the promotion mechanisms developed in Phase I.
- Optimizing mixing (reburning fuel, N-agents, OFA) via combined chemistry/mixing models.
- Optimizing N-agent injection to maximize NO_x reduction with minimum ammonia slip.
- Evaluating the effect of N-agent/promoter mixing times representative of full scale.
- Optimizing AR with new promoters and mixing regimes at 1×10^6 Btu/hr scale.
- Scaling up and confirming the design methodology via 10×10^6 Btu/hr Proof-of-Concept tests.
- Updating the economic and market analysis to confirm the advantages of AR.

Four types of experimental facilities were used in Phase II: (1) 0.1×10^6 Btu/hr Controlled Temperature Tower (CTT) to identify the prospective promoters, (2) 1×10^6 Btu/hr Boiler Simulator Facility (BSF) for combustion optimization tests, (3) 10×10^6 Btu/hr Tower Furnace (TF) for the Proof-of-Concept tests, and (4) the Greenidge boiler equipped with AR-Lean. (See description of GE EER facilities in Section 11). Phase II developed all information and know-how necessary prior to a full-scale AR demonstration.

4.2 Phase II Objectives and Tasks

Phase II work included a combination of experimental and modeling studies with the objective to demonstrate the effectiveness of the AR technologies in 10×10^6 Btu/hr Proof-of-Concept tests over a sufficiently broad range of conditions. Specific Phase II objectives were designed to overcome the remaining after Phase I technical barriers, broaden the range of applications and develop a data base for a subsequent full-scale demonstration. Specifically, Phase II objectives were to:

1. Develop alternative NO_x control promoters for AR.
2. Update a combined chemistry/mixing model of the process to optimize mixing regimes.
5. Confirm the design methodology via pilot scale experiments at 1.0 and 10×10^6 Btu/hr.

Phase II was build on the Phase I results and included the following tasks:

- 2.1 Project coordination and reporting/deliverables.
- 2.7 Studies of other prospective promoters.
- 2.8 Development of a combined chemistry/mixing model.
- 2.9 Optimization of process synergism in 10×10^6 Btu/hr tests.
- 2.10 10×10^6 Btu/hr proof-of-concept tests.
- 2.11 Design methodology validation.

The following sections describe Phase II results.

5.0 Task 2.1 Project Coordination and Reporting/Deliverables

Figure 5-1 shows the task structure and the major milestones of Phase II. Task 1.1, Project Coordination and Reporting/Deliverables, coordinated the efforts of the Key Personnel involved with the project so that the objectives of this project are met on time, on specification, and on budget. Phase II experimental work started from parametric screening tests of alternative promoters at a bench scale facility (Task 2.2), followed by pilot scale optimization studies (Task 2.4) and proof-of-concept tests (Task 2.5). The Phase II program utilized three test facilities providing nominal thermal capacities of 0.1, 1.0 and 10×10^6 Btu/hr. The experimental work was paralleled by kinetic modeling (Task 2.3) which provided a scientific understanding of the process, including the activity of N-agent promoters and effect of promoters on reburning and AR. The modeling used experimental data to define key process parameters, culminating in upgrading and validation of GE-EER's existing design methodology for AR (Task 2.6).

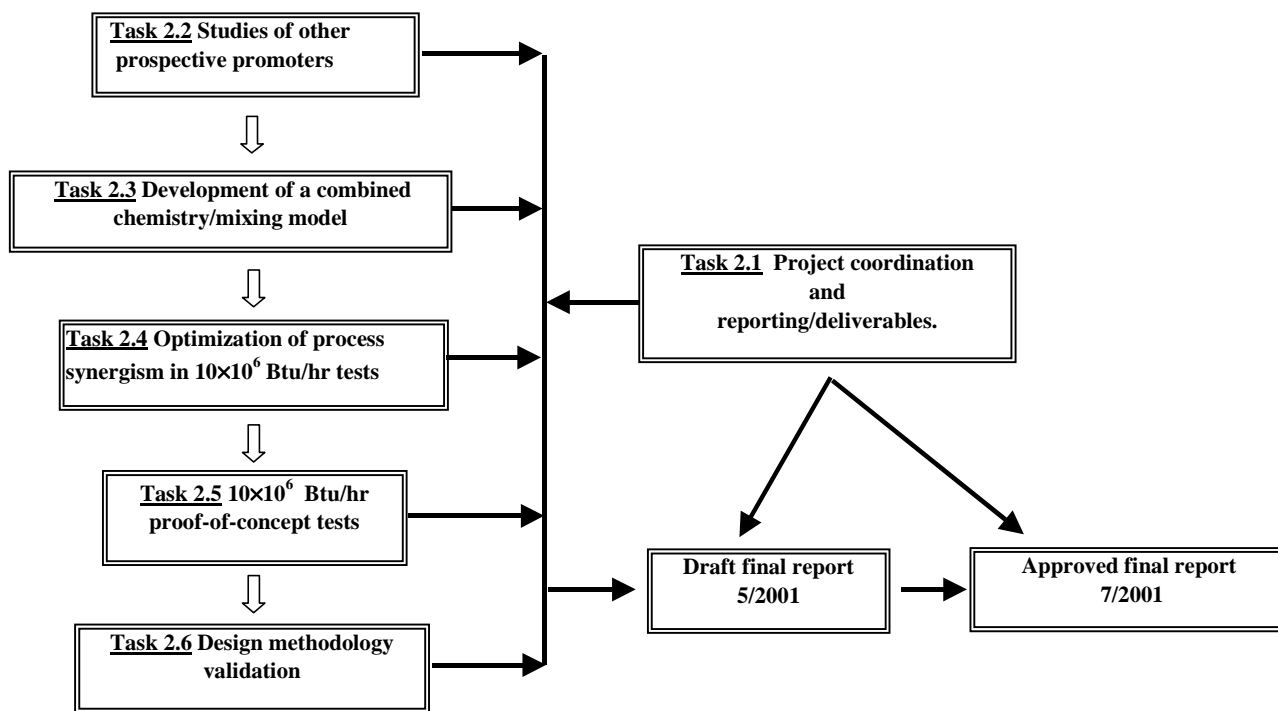


Figure 5-1. Phase II task structure and major milestones.

Significant efforts were undertaken to advertise AR technologies to make them visible to potential users. Project results were presented at the following conferences:

1. 26th International Symposium on Combustion, Naples, Italy, 1996.
2. The American Flame Research Committee International Symposium, Baltimore, MD, 1996.
3. 22nd International Technical Conference on Coal Utilization & Fuel Systems, Clearwater, FL, 1997.
4. 5th International Congress on Toxic Combustion Byproducts, Dayton, OH, 1997.
5. The American Society of Mechanical Engineers International Power Generation Conference, CO, 1997.

6. 4th International Conference on Technologies and Combustion for a Clean Environment, Lisbon, Portugal, 1997.
7. Conference on Advanced Coal-Based Power and Environmental Systems, Pittsburgh, PA, 1997.
8. 27th International Symposium on Combustion, Denver, CO, 1998.
9. International Gas Research Conference, San Diego, CA, 1998
10. 28th International Symposium on Combustion, Edinburgh, Scotland, 2000.

Project plans and results were also presented at FETC (now NETL) Contractor's Conferences in 1996, 1997 and 2000, during meetings at FETC (December 1995) and GRI (August 1995 and April 1997), as well as at Meetings of the Western States Section of the Combustion Institute in 1998 and 1999.

The following papers were published or submitted for publication:

1. Zamansky, V.M. and Lissianski, V.V. "Effect of Mixing on Natural Gas reburning", *Israel Journal of Chemistry* 39:63-71 (1999).
2. Han, D., Mungal, M.G., Zamansky, V.M. and Tyson, T.J. "Predicting of NO_x Control by Basic and Advanced Gas Reburning Using the Two-Stage Lagrangian Model", *Combust. Flame* 119:483-493 (1999).
3. Lissianski, V.V., Zamansky, V.M. and Sheldon, M.S. "Reburning Chemistry-Mixing Model", *Combust. Flame*, 2000 (accepted for publication).
4. Lissianski, V.V., Zamansky, V.M. and Maly, P.M. "Effect of Metal-Containing Additives on NO_x Reduction in Combustion and Reburning", *Combust. Flame*, 2000 (accepted for publication).
5. Zamansky, V.M., Maly, P.M., Lissianski, V.V. and Gardiner, W.C. "Utilization of Iron Additives for Advanced Control of NO_x Emissions from Stationary Combustion Sources", *Industrial & Engineering Chemistry Research*, 2001 (accepted for publication).

The following related patents were submitted and approved by the U.S. Patent and Trademark Office:

1. Zamansky, V.M., Maly, P.M. and Seeker, W.R. "Advanced Reburning Methods for High Efficiency NO_x Control", *U.S. Patent 5,756,059* (1998).
2. Zamansky, V.M.; Maly, P.M.; Cole, J.A.; Lissianski, V.V.; Seeker, W.R. Metal-Containing Additives for Efficient NO_x Control, *U.S. Patent 6,206,685* (2000).

The following patent has been submitted and is being considered by the U.S. Patent and Trademark Office:

Lissianski, V.V., Zamansky, V.M., Lyon, R.K. and Payne, R. "Method of Reducing NO_x via Selective Non-Catalytic Reduction".

6.0 Task 2.2 Studies of Other Prospective Additives

The goal of testing under Task 2.2 was to identify prospective promoters other than Na_2CO_3 . Phase I experiments (*Appendix A*) demonstrated that Na_2CO_3 is an effective promoter of AR. These tests also revealed that several other sodium salts have effects on AR which are similar to that of Na_2CO_3 . The mechanism of Na promotion was studied and explained in Phase I. Modeling predicted that Na-containing species increased the efficiency of NO_x reduction in the presence of N-agent by providing active species (e.g. H atoms and OH radicals). It was expected that other alkali compounds (lithium and potassium) would exhibit promotion effects based on the same principle. It was further anticipated that alkali earth metal compounds (Mg, Ca, and Ba) might have similar or stronger promotion effects.

The alternative promoter search included tests of a variety of relatively volatile metal salts that could potentially provide OH radicals in the reburning zone. A number of compounds that do not contain metals and nonvolatile metal-containing compounds were also screened to identify candidates which are effective in NO_x reduction. The following sections describe the results of screening tests conducted in the CTT (0.1×10^6 Btu/hr) and the BSF (1.0×10^6 Btu/hr).

6.1 CTT Screening Test

In CTT testing, natural gas was used as both the main and reburning fuel. Gaseous ammonia was added to the main fuel to provide a controlled primary NO concentration of 600 ppm. The reburning fuel, 10% by heat input, was injected at furnace gas temperatures of 1670 K, using bottled nitrogen as the transport medium. (Unless stated otherwise, temperature references in the context of injection locations refer to the local furnace gas temperature.) The OFA was injected at 1300 K, providing a reburning zone residence time of 0.50 s. Stoichiometric ratios in the main, reburning, and burnout zones were $\text{SR}_1=1.10$, $\text{SR}_2=0.99$, and $\text{SR}_3=1.15$, respectively. Additives were co-injected with aqueous ammonia into the reburning zone at 1460 K with $\text{NSR} = 1.5$. Promoters were dissolved in aqueous ammonia in a quantity corresponding to 30 ppm of metal concentration (or promoter concentration if metal is absent) in flue gas. These tests determined the efficiencies of various additives in promoting AR-Rich.

All tested compounds are presented in Table 6-1. Eight sodium salts were tested to determine the effect of anions in promoting NO_x reduction activity. Since preliminary tests of different sodium compounds, including carbonate and hydroxide forms, demonstrated identical NO_x reduction activity, only a limited set of potassium and lithium compounds (K_2CO_3 , KOH, and LiOH) was selected for testing. Additionally, one compound for each of five other metals (Mg, Ca, Ba, Zn, and Cu) was selected. Each of these compounds is soluble in water and was added to aqueous ammonia. Iron sulfate was also tested, but precipitated out of the basic ammonia solution, and therefore the concentration of iron in flue gas was difficult to control. Two non-metal compounds were selected for testing, methanol and dichloromethane. Methanol decomposes forming CH_3 and OH radicals under reburning conditions, and it was interesting to check how additional OH radicals affect NO concentration. Organic chlorides are known as radical inhibitors, and CH_2Cl_2 was added to see the effect of chlorinated compounds on the reburning process.

A summary of promoter screening results is presented in Figure 6-1. Sodium carbonates and sodium hydroxide provided the most significant promotion effect. Under the test conditions, the use of Na_2CO_3 , NaHCO_3 , their combination (trona), and NaOH provided about 89% NO reduction, or about a 32 percentage point increase above reburning + NH_3 injection. Some other sodium

compounds provided a smaller but significant promotional effect. Injection of NaNO_3 , NaAlO_2 , and NaCl resulted in 86%, 77%, and 74% NO reduction, respectively. The use of Na_2SiO_3 provided 60% NO reduction, only 4% increase compared with the case without promoters. Obviously, binding sodium with chlorine, aluminum, nitrate, and especially with silicate inhibits the effect of Na on NO reduction relative to the carbonate and hydroxide forms.

Table 6-1. Compounds tested in CTT as advanced reburning promoters.

Compound	Formula	Compound	Formula
<i>Sodium Compounds</i>		<i>Non-Sodium Metal Compounds</i>	
Sodium Carbonate	Na_2CO_3	Potassium Carbonate	K_2CO_3
Sodium Bicarbonate	NaHCO_3	Potassium Hydroxide	KOH
Trona	$\text{Na}_2\text{CO}_3 \cdot \text{NaHCO}_3$	Lithium Hydroxide	LiOH
Sodium Hydroxide	NaOH	Magnesium Acetate	$\text{Mg}(\text{CH}_3\text{COO})_2$
Sodium Chloride	NaCl	Calcium Acetate	$\text{Ca}(\text{CH}_3\text{COO})_2$
Sodium Nitrate	NaNO_3	Barium Hydroxide	$\text{Ba}(\text{OH})_2$
Sodium Silicate	Na_2SiO_3	Zinc Acetate	$\text{Zn}(\text{CH}_3\text{COO})_2$
Sodium Aluminate	NaAlO_2	Copper Acetate	$\text{Cu}(\text{CH}_3\text{COO})_2$
<i>Non-Metal Compounds</i>			
Dichloromethane	CH_2Cl_2	Methanol	CH_3OH

The difference in promotion efficiency of the different forms of sodium can be explained. In the case of NaNO_3 , thermal decomposition of the salt releases NO_x that naturally has an adverse impact on the net NO_x reduction efficiency. Sodium aluminate, chloride and silicate are very stable compounds which do not decompose to form significant concentrations of sodium atoms, which are necessary to promote NO reduction. Sodium chloride and sodium silicate are the typical forms of sodium in coal, and therefore sodium compounds in coal are not very effective AR promoters.

Co-injection of Li and K compounds with ammonia resulted in 74-78% NO reduction, i.e. 17-21 percentage points improvement. Although these effects are lower than those for sodium, they are significant. Thus, K and Li compounds can be used as AR promoters. Compounds of Mg, Ca, Ba, and Zn provided a relatively small promotional effect. When injected in solution with ammonia, they reduced NO by an additional 6-9 percentage points.

Injection of CH_2Cl_2 and $\text{Cu}(\text{CH}_3\text{COO})_2$ resulted in inhibition of the NO reaction with ammonia. The inhibition effect of dichloromethane was expected since Cl atoms reduce the concentration of OH radicals in the reaction media. The effect of $\text{Cu}(\text{CH}_3\text{COO})_2$ was surprising; it is difficult to explain because the rates of high temperature reactions of Cu compounds with radicals, NO and ammonia are not known.

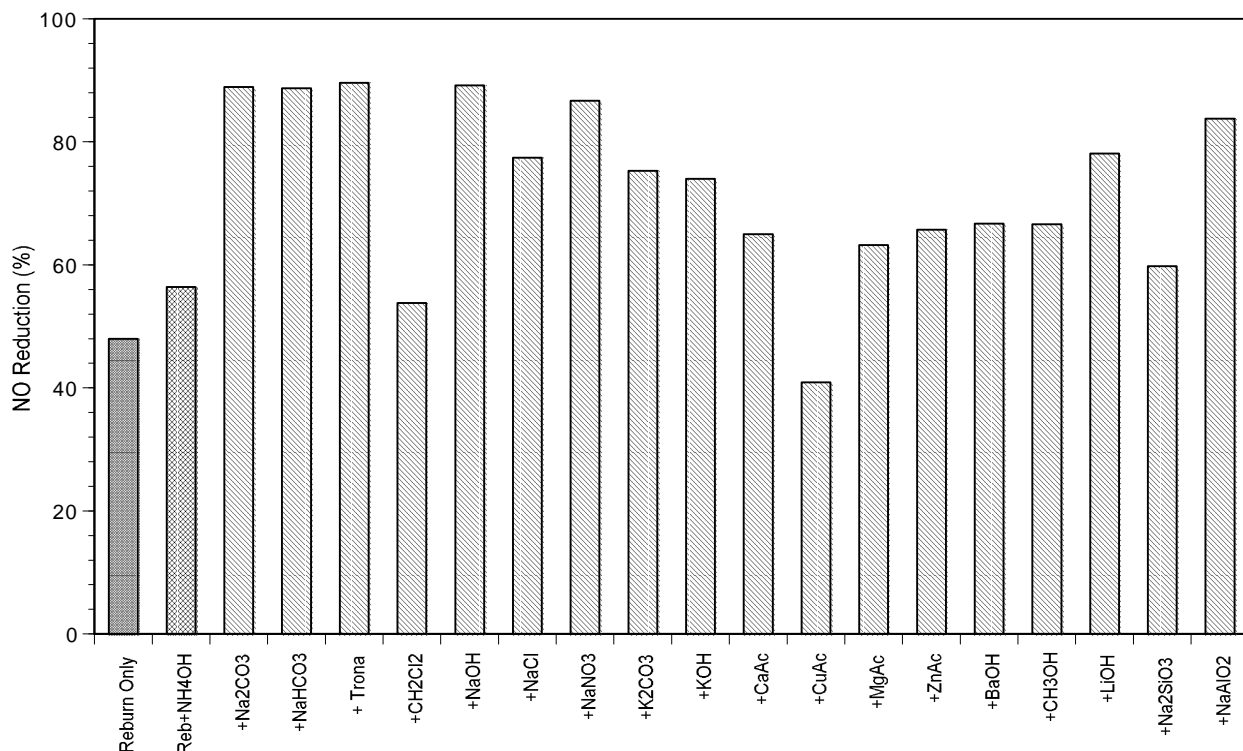


Figure 6-1. Alternative promoter AR-Rich screening test results. Additive (30 ppm) is co-injected with aqueous NH_3 at combustion gas temperatures of 1460 K.

Additional tests were then conducted to characterize the promotion effect of several compounds at different temperatures. Compounds with good and moderate promotion efficiency were selected for these tests. Additionally, one inhibiting compound was also tested. The furnace gas temperature at which promoters were injected was varied from 1170 K to 1590 K, for Na_2CO_3 , trona, K_2CO_3 , NaAlO_2 , and $\text{Cu}(\text{CH}_3\text{COO})_2$. At 1170 K the additives were injected with OFA (AR-Lean), while at higher temperatures they were injected under fuel-rich conditions (AR-Rich). The test results are summarized in Figure 6-2. As in the screening tests, the sodium additives resulted in significant promotion and potassium resulted in less significant promotion. The copper additive acted as inhibitor at higher temperatures and as a promoter at lower temperatures.

Tests at different injection temperatures were important in determining the effect of additives on CO emissions. As in the Phase I tests, injection of 30 ppm sodium resulted in high CO emissions (over 1000 ppm). Similar CO emissions were determined in tests with addition of potassium compounds. Injection of other promoters resulted in CO emissions lower than 70 ppm. This effect (higher CO emissions after injection of sodium under fuel rich conditions) was discussed and a hypothetical explanation of the Na effect on CO emissions was suggested in Phase I Final Report (*Appendix A*, pp. 7-8 to 7-9). High CO emissions show that in the presence of sodium and potassium the process of CO oxidation is inhibited. This inhibition effect is stronger under fuel rich conditions and especially pronounced in tests conducted in the CTT tests because of its very steep temperature profile at the point of ammonia/promoter injection.

Increasing the OFA temperature during the AR-Rich process, and conducting experiments in a larger facility with a lower temperature gradient (e.g. BSF) decreases CO emissions. As was demonstrated in Phase I (*Appendix A*), AR-Rich tests conducted in the BSF with two higher OFA

temperatures, 1380 and 1510 K, resulted in up to 90% NO reduction (in the presence of Na) and near baseline CO emissions.

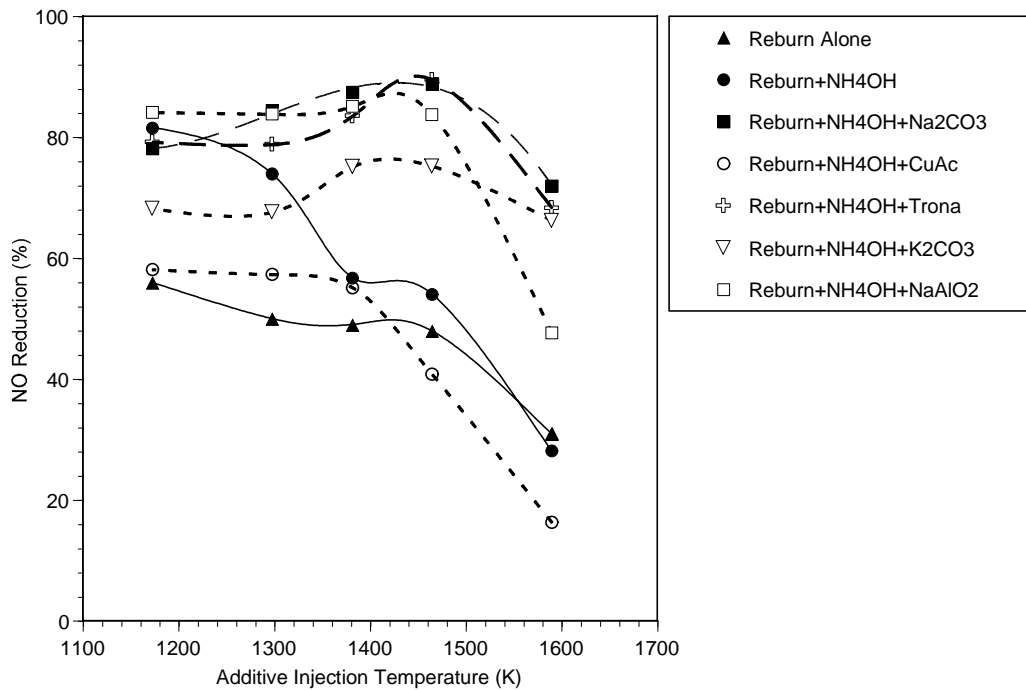


Figure 6-2. Performance of alternative promoters as a function of injection temperature.

Figure 6-3 shows the effect of FeSO_4 on the AR process. The promoter was co-injected with NH_3 in the reburning zone. The use of FeSO_4 provided 50% NO reduction, which is less than the effect of NH_3 alone. Thus, injection of FeSO_4 resulted in inhibition of the NO reaction with ammonia.

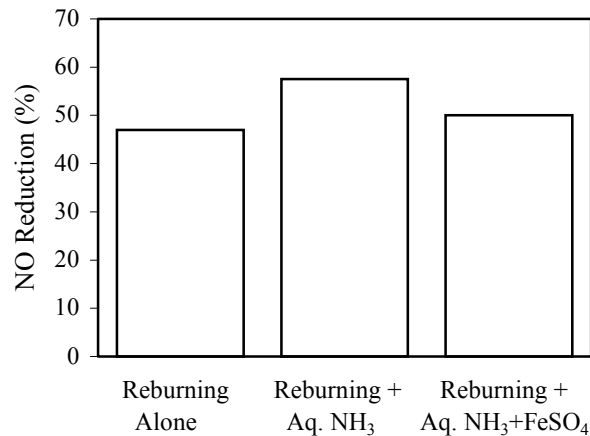


Figure 6-3. Effect of FeSO_4 on the reburning process.

6.2 BSF Test Results

Fly ash, char and several other additives were tested in the BSF as promoters of the reburning process. In these tests additives were injected without N-agent. The purpose of these tests was to determine if additives alone can improve the efficiency of the reburning process.

6.2.1 Effect of Metals on NO_x Reduction

Tests described in *Section 6.1* showed that some additives affect the AR process when co-injected with NH₃ in the reburning zone. It is worthwhile to determine if the same additives can affect the reburning process when injected alone. Figure 6-4 shows the effect of several additives on the reburning process. Injection of 30 ppm of sodium compounds without NH₃ provides up to 4% additional reduction in comparison with the unpromoted basic reburning process. This effect is much smaller than the effect of combined injection of NH₃ and Na compounds (*Section 6.1*). However, this effect can be more significant if the amount of additive is higher than 30 ppm. Additional tests were performed to provide more detailed information on the effect of metal-containing compounds on reburning.

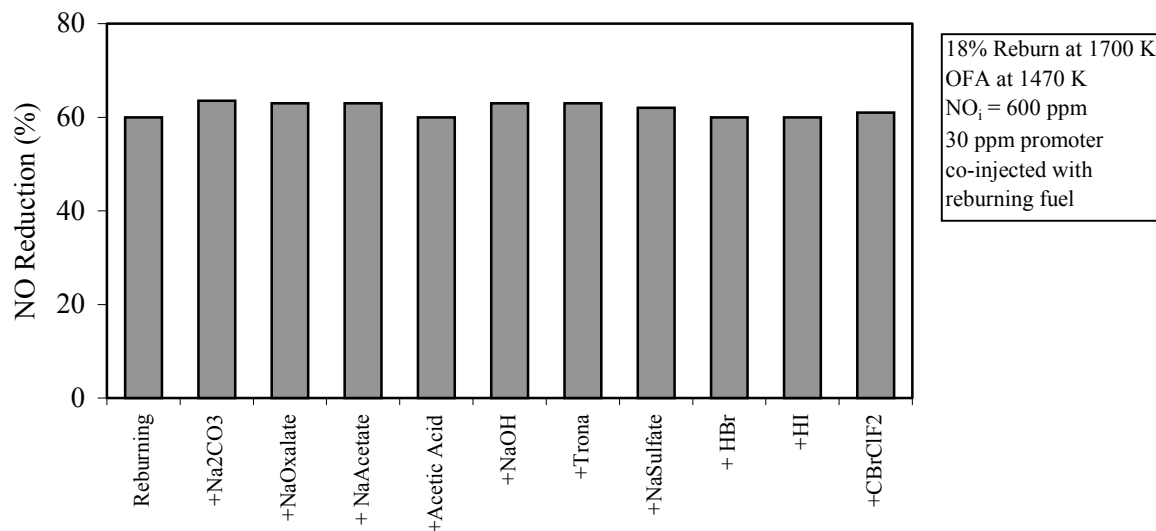


Figure 6-4. Promoter screening tests.

Sodium and potassium carbonates, and calcium acetate were selected for tests and were injected into BSF as aqueous solutions in one of the following configurations: with the main fuel, with the reburning fuel or into the reburning zone downstream of the reburning fuel injection. Solutions were injected by atomizing them with a twin-fluid nozzle. In all tests natural gas was used as main and reburning fuels. The amount of the reburning fuel was 18% of the total heat input. The reburning fuel was injected at a flue gas temperature of 1670 K and OFA was injected at 1300 K. Injection of additives into reburning zone downstream of the reburning fuel was performed at a flue gas temperature of 1590 K. The initial NO_x concentration was set to 600 ppm by adding ammonia to the combustion air.

Figure 6-5 shows the effect of these Na, K and Ca compounds, co-injected with the main fuel in the presence and in the absence of reburning. Injection of metal-containing compounds in the absence of reburning (“metal only” bars) resulted in 16%-21% NO_x reduction. Reburning itself provided 66% NO_x reduction. Injection of 100 ppm metal compounds (of total flue gas) with the main fuel in the presence of reburning provided an additional 4-7 percentage points of NO_x reduction. The amount of metal in flue gas is calculated assuming that all metal is in vapor phase. Results presented in Figure 6-5 illustrate that sodium- and potassium-containing additives are slightly more effective than calcium-containing compounds when added with the main fuel.

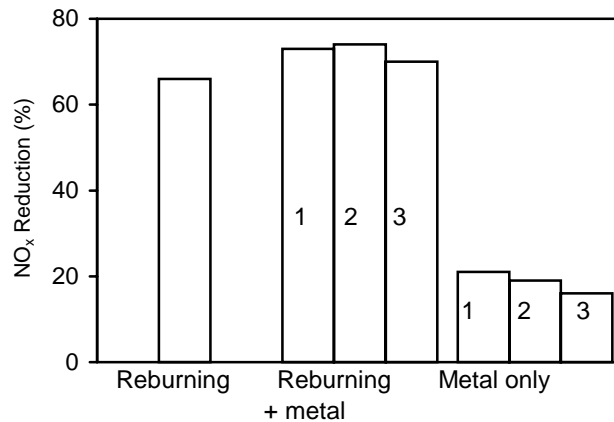


Figure 6-5. Effect of metal-containing compounds injected with the main fuel on NO_x reduction. Amount of metal is 100 ppm. 1 – Na, 2 – K, 3 – Ca.

Figure 6-6 shows the effect of promoter concentration on NO_x reduction. In the absence of reburning, the effect of the additive first increases as concentration of additive increases and then decreases. Up to approximately 28% NO_x reduction was achieved at 500 ppm of Na or K in the flue gas. The additives also improved the efficiency of reburning by 11 percentage points. The effect of additives on reburning also first increases and then slightly decreases (although not as significantly as in the absence of reburning). Both Na and K show similar effects on NO_x reduction.

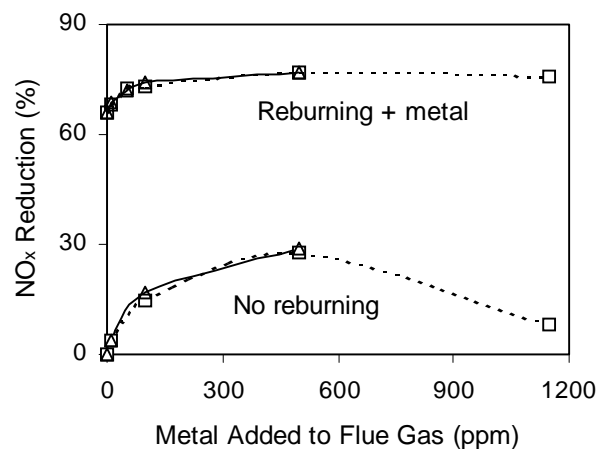


Figure 6-6. Na and K performance as a function of promoter concentration. Promoters are injected with the main fuel. Squares and dotted lines represent Na, triangles and solid lines represent K.

Figure 6-7 demonstrates that similar results were obtained by injecting sodium along with the reburning fuel at flue gas temperature of 1700 K. Injection of sodium carbonate improves NO_x control efficiency by up to 6 percentage points. This effect is slightly smaller than that observed for Na injection with the main fuel.

Figure 6-8 demonstrates the effects of Na and Ca injection into the reburning zone, but downstream of the reburning fuel. NO_x reduction in this case is less than that for the injection with main and reburning fuels. Injection of sodium carbonate reduces NO_x concentration by additional 4 percentage points, while calcium acetate reduces NO_x by 3 percentage points.

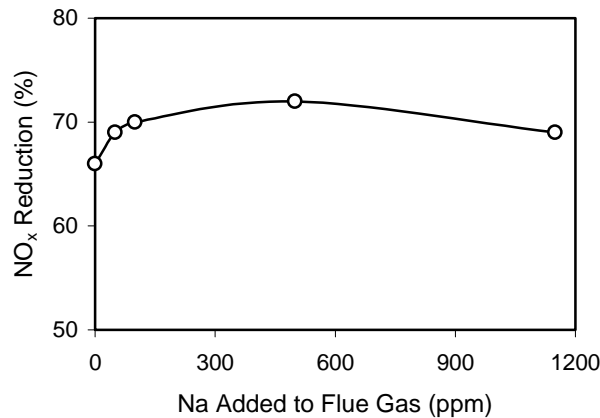


Figure 6-7. NO_x reduction as function of Na concentration. Na is co-injected with the reburning fuel.

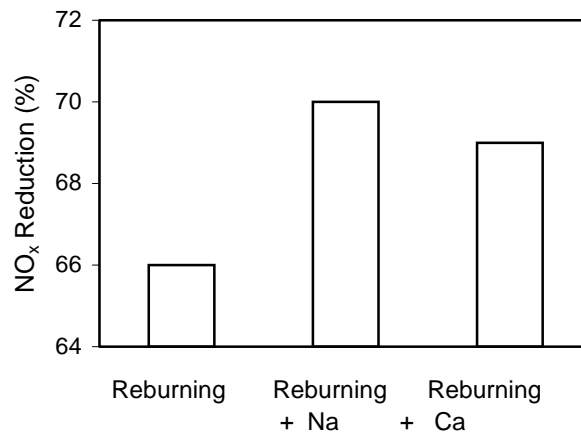


Figure 6-8. Injection of 100 ppm Na and Ca into reburning zone at 1590 K. Reburning fuel is injected at 1700 K.

Figure 6-9 shows the effect of sodium carbonate injection on CO emissions. The baseline corresponds to the level of CO in flue gas in the absence of reburning and additives. Reburning increases CO emissions by about 20%. The “Na only” bar corresponds to the injection of additive

with the main fuel in the absence of reburning. CO emissions appear to slightly increase during Na injection, most notably in the absence of reburning.

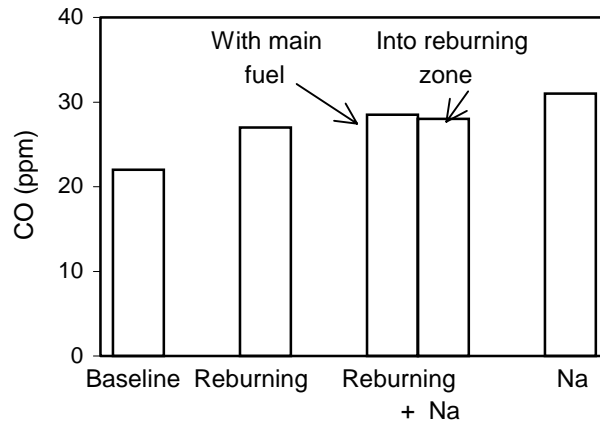


Figure 6-9. Effect of 100 ppm Na addition on CO emissions.

6.2.2 Effect of Ca on SO₂ Emissions

Tests showed that calcium-containing compounds were less effective than alkali metals in reduction of NO_x emissions. However, calcium has an advantage over alkali metals since it does not contribute to deposition on heat transfer surfaces and thus may be preferred in commercial applications. Another potential benefit of using calcium-containing compounds is reduced sulfur emissions from coal combustion due to the formation of CaS. To determine the efficiency of NO_x and SO₂ reduction during coal combustion, tests were conducted with Utah coal as the main fuel. The initial amount of SO₂ generated by coal combustion was 800 ppm. The reburning fuel was natural gas.

Figures 6-10 and 6-11 show effects of Ca(OH)₂ co-injection with main and reburning fuel on NO_x and SO₂ emissions. While the efficiency of NO_x reduction does not depend significantly on the method of additive injection, the efficiency of SO₂ reduction is much higher when the additive is injected with the main fuel (about 50%).

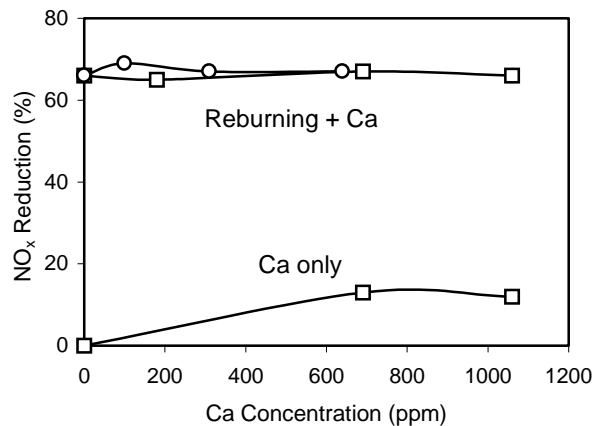


Figure 6-10. Calcium promoter NO_x control performance during Utah coal firing. Squares correspond to co-injection with main fuel, circles to co-injection with reburning fuel.

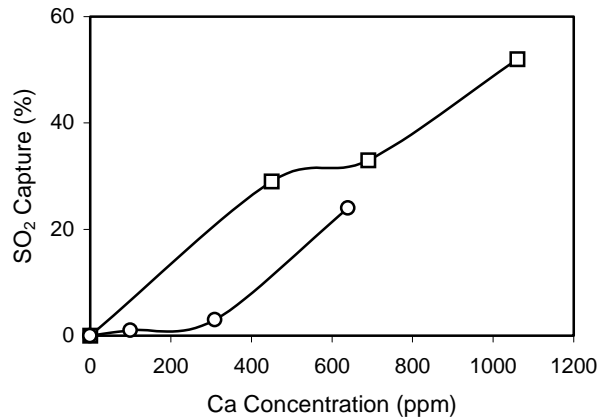


Figure 6-11. Calcium promoter SO₂ capture during Utah coal firing. Squares correspond to co-injection with main fuel, circles to co-injection with reburning fuel.

6.2.3 Effect of Iron-Containing Compounds on NO_x Reduction

While FeSO₄ additives showed an inhibiting effect on AR-Rich (Fig. 6-3), it was speculated that other Fe-containing compounds could be effective in promoting reburning. These speculations were based on experimental results (*Babushok et al, 1998*) demonstrating that under certain conditions Fe-containing compounds can have significant impact on the combustion process.

Experiments with injection of iron-containing additives were conducted in the BSF. For the natural gas firing tests, the initial NO_x concentration was set at 600 ppm by adding ammonia to the combustion air. With coal firing, no effort was made to control the initial NO_x concentration. Natural gas was used as the reburning fuel in all tests. The iron compounds were transported pneumatically as powders to the furnace and injected through a radial injector. Injection of the reburning fuel and OFA occurred at furnace gas temperatures of 1700 K and 1450 K, respectively. Iron compounds were added either with the main fuel, with the reburning fuel, or into the reburning zone at 1590 K.

The following additives were tested: metallic iron, iron oxides, iron waste, and Fe(CO)₅. Three test series were conducted. The first two, in which natural gas was fired as the main fuel, involved screening iron additives under constant baseline conditions and parametric evaluation of process variables. In the third series, coal was fired as the main fuel to provide conditions representative of industrial combustors. These studies involved screening the performance of four additives (metallic iron, two iron oxides and iron waste) selected to encompass a variety of attributes, including ferrous and ferric oxidation states and metallic iron itself, different particle sizes, and an industrial iron waste product tested as an example of a waste available at low or no cost. (The sample tested, a byproduct of the steel processing industry, consisted nominally of about 80% Fe₂O₃ and 20% impurities, primarily Ca(OH)₂.) Iron metal powder, 100% of which was smaller than 10 μm in diameter, was studied at a concentration corresponding to 1000 ppm mole fraction in the flue gas; Fe₂O₃ powder, 100% of which was smaller than 5 μm, over the range 0 to 1300 ppm; Fe₃O₄ (consisting of FeO and Fe₂O₃), 100% of which was smaller than 5 μm, at 1000 ppm; and iron oxide waste, 80% of which was smaller than 50 μm in diameter, at mole fractions ranging from 0 to 1000 ppm. The amount of metal in flue gas is expressed here as the number of Fe atoms per 10⁶

molecules present, calculated as if the entire flue gas content, aside from ash, were present as gas-phase molecules. The initial screening tests involved co-injecting each of the four additives together with the reburning fuel, at reburning heat inputs of 18% and 25%, in the amounts needed to provide 1000 ppm iron in the flue gas. Figure 6-12(a) summarizes the results. Reburning without additive provided 60-66% NO_x reduction; iron waste and Fe₂O₃ provided the greatest NO_x reductions, up to about 19 percentage points more than reburning alone. The maximum NO_x reductions observed were 77% and 85% for reburning heat inputs of 18% and 25%, respectively. Iron metal and Fe₃O₄ provided 3 to 9 percentage points of improvement.

After the screening tests, more detailed studies were performed to parametrically evaluate the process variables: injection mode (with the main fuel, with the reburning fuel, and into the reburning zone), additive concentration, and reburning heat input. The parametric tests focused on Fe₂O₃ and the iron waste product, which showed the greatest effects in the screening tests. Figure 6-12(b) shows the effect of iron waste compounds co-injected with the main fuel. In the absence of reburning, approximately 23% NO_x reduction was achieved by iron injection. Reburning without additives resulted in 60% NO_x reduction for 18% reburning and 66% NO_x reduction for 25% reburning. Additive injection improved the process efficiency by 8-10 percentage points.

Figure 6-12(c) shows the performance for Fe₂O₃ injection with the main fuel, with the reburning fuel, and into the reburning zone at 1590 K. The best performance was obtained for Fe₂O₃ co-injection with the reburning fuel, improving NO_x reduction by about 20 percentage points. Injection into the reburning zone was least effective.

Figure 6-12(d) shows the effect of iron oxide waste co-injected with the reburning fuel (for 25% reburning) as a function of additive concentration. In the absence of additive, conventional reburning again gave 66% NO_x reduction. NO_x reduction levels increased as the iron concentration increased from 0 to 600 ppm, after which further increase had little effect. About 86% NO_x reduction was achieved at 600-770 ppm additive in flue gas, that is, 21 percentage points greater than the baseline condition.

Reburning heat input was then varied from 10% to 25% with and without Fe₂O₃ additive. As shown in Figure 6-12(e), NO_x reduction appeared to increase with increasing reburning heat input. Fe₂O₃ additive increased NO_x reduction by 11 percentage points at 10% reburning and by 21 percentage points at 25% reburning. Figure 6-12(f) shows the effect of iron oxide co-injected with the reburning fuel during combustion of coal. A bituminous Utah coal containing 0.67% sulfur and 11.8% ash on a dry basis was used. The initial uncontrolled NO_x concentration it generated was 1200 ppm corrected to 0% O₂, dry basis. The iron additive caused NO_x reduction to increase by 6 to 9 percentage points. The maximum NO_x reduction efficiency with coal firing was 84%. Tests also showed that addition of an iron compound in both the main and the reburning zones could provide higher NO_x reduction than injection of the same amount of additive in one zone.

In some tests the iron oxide additive was co-injected with a small amount of the reburning fuel (about 6%). Since the total composition of the mixture was fuel lean, no OFA air was added. NO_x reduction increased from 32% to 38% as the additive amount increased from 0 to 1300 ppm.

To evaluate the effect of atomic iron, a few tests were conducted with injection of 450 ppm of iron pentacarbonyl together with the reburning fuel and downstream in the reburning zone. Iron pentacarbonyl quickly decomposes at reburning temperatures and produces Fe atoms and CO. An increase in NO_x reduction of 10-13 percentage points was obtained at 20% reburning heat input.

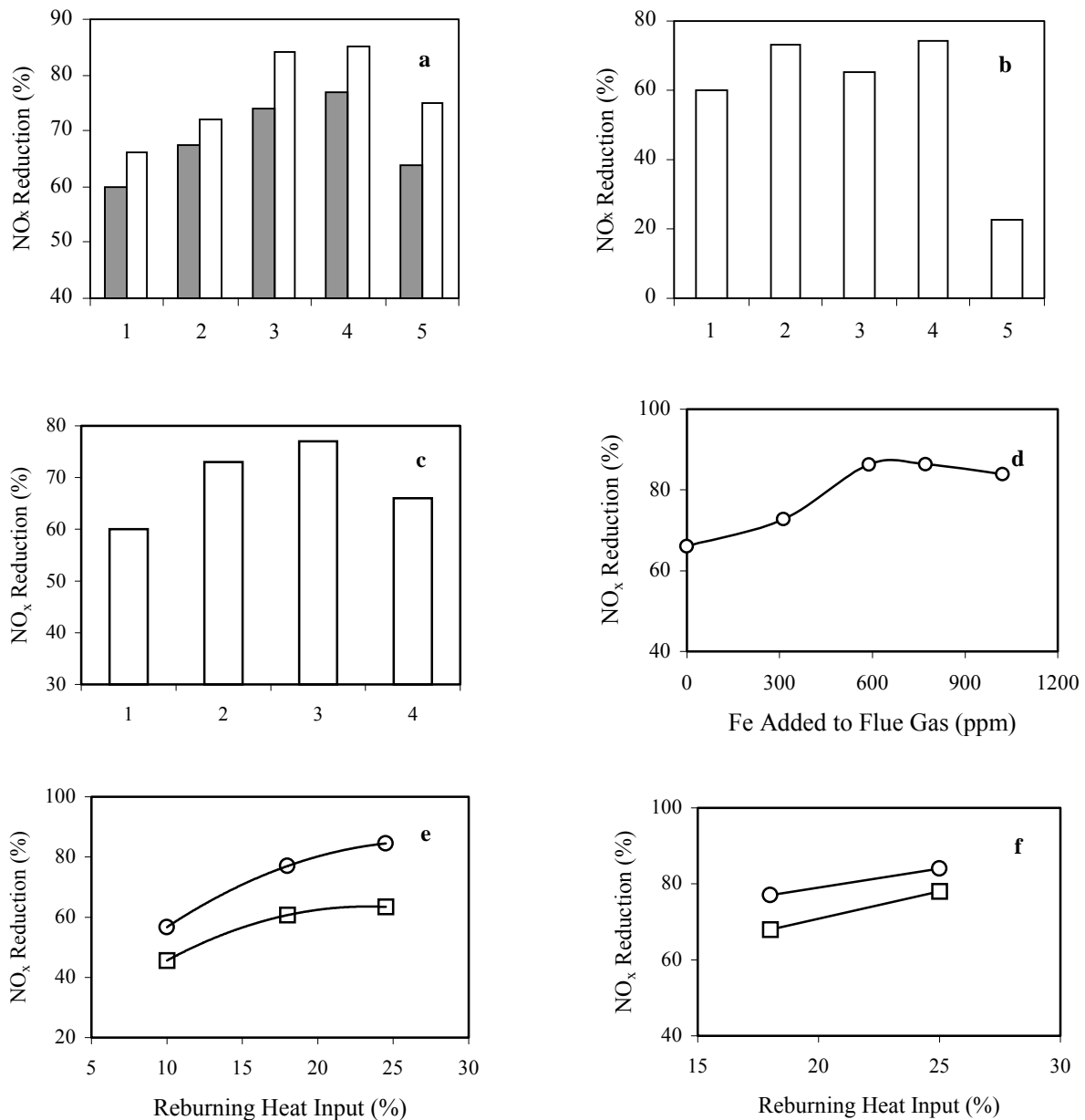


Figure 6-12. Test data on NO_x reduction in the presence of iron-containing compounds. (a) Co-injection of 1000 ppm of different additives with reburning fuel. Shaded bars represent 18% reburning, open bars represent 25% reburning. 1 - Reburning only; 2 - Fe metal; 3 - Fe waste; 4 - Fe₂O₃; 5 - Fe₃O₄. (b) Iron waste co-injection with the main fuel. 1 - 18% reburning alone; 2 - 18% reburning with 1000 ppm waste; 3 - 25% reburning alone; 4 - 25% reburning with 1000 ppm waste; 5 - 1000 ppm iron waste, no reburning. (c) Injection of 1000 ppm Fe₂O₃ at different locations for 18% reburning. 1 - Reburning alone; 2 - Co-injection with main fuel; 3 - Co-injection with reburning fuel; 4 - Injection into reburning zone. (d) Effect of iron waste co-injection with the reburning fuel at 25% reburning. (e) Effect of reburning heat input on Fe₂O₃ co-injection with reburning fuel. Circles 1000 ppm Fe₂O₃ added, squares without Fe₂O₃ addition. (f) Effect of iron waste co-injected with reburning fuel during coal combustion. Circles - 800 ppm waste added, squares - without waste addition. The initial level of NO_x was 1200 ppm.

6.2.4 Effects of Fly Ash and Char on NO_x Reduction

It is known that coals, chars and fly ash produced by coal combustion contain mineral compounds, including Na, K, Ca, Fe, and other metals that may become volatile at combustion temperatures and affect NO_x concentration. For example, the presence of CaO in char has been shown (*Guo and Hecker, 1996; Chen 1995; Illán-Gómez et al., 1995*) to increase reaction rate of NO with char. Catalytic decomposition of NO on various metallic oxides has been reported by *Winter, 1971*.

The amount of metals in fly ash varies and depends on the coal type. Table 6-2 shows the composition of fly ash used in current tests. It was generated from several coal sources, most notably Knott-Floyd Land which is a Kentucky coal. The iron content in fly ash is high (14.95%). It also has significant calcium oxide and potassium oxide content, 3.00% and 2.65% respectively. Figure 6-13 shows the effect of fly ash injected along with the reburning fuel. Fly ash was tested in two forms: calcinated at 1200 K, and calcinated/ground/hydrated. Both forms of fly ash showed minimal effect on NO_x reduction. However, grinding and hydrating slightly improve the efficiency of fly ash, probably by increasing surface area.

Table 6-2. Mineral composition of fly ash generated by combustion of a Kentucky coal.

Composition	Weight %
Silicon oxide	55.74
Aluminum oxide	18.68
Titanium dioxide	0.94
Iron oxide	14.95
Calcium oxide	3.00
Magnesium oxide	2.65
Potassium oxide	2.65
Sodium oxide	0.93
Sulfur trioxide	1.83
Phosphorus pentoxide	0.33
Barium oxide	0.16
Manganese oxide	0.01
Total	100.00

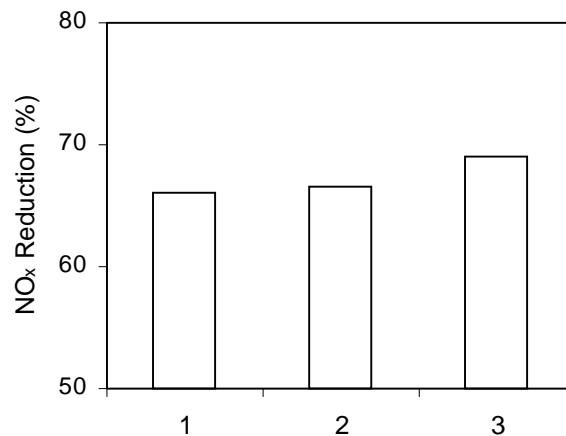


Figure 6-13. Effect of fly ash co-injection with reburning fuel on NO_x reduction. 1- Reburning, 2 – reburning + calcinated fly ash, 3 – reburning + calcinated/hydrated fly ash.

One can note that the metal additives are much more effective than the compounds of the same metals present in fly ash. The flow rate of fly ash injection in tests was such that concentrations of iron, calcium, potassium and sodium from fly ash in flue gas (if all metals were released in atomic form) would be approximately 400 ppm, 90 ppm, 120 ppm, and 60 ppm respectively. However, their effect on NO_x reduction is, as shown in Figure 6-13, only 1-4 percentage points. The small effect of fly ash can be explained by the difference in the chemical nature of metal compounds in the additives versus fly ash. Although traditional ash analyses present mineral composition in the form of metal oxides, the oxides are not the actual forms of metals in fly ash. The metals are mainly present in the form of sulfides and silicate-alumosilicate matrixes which are more stable than carbonates and acetates at high temperatures and, thus, are not effective in reactions with combustion radicals and have minimal effect on NO_x reduction.

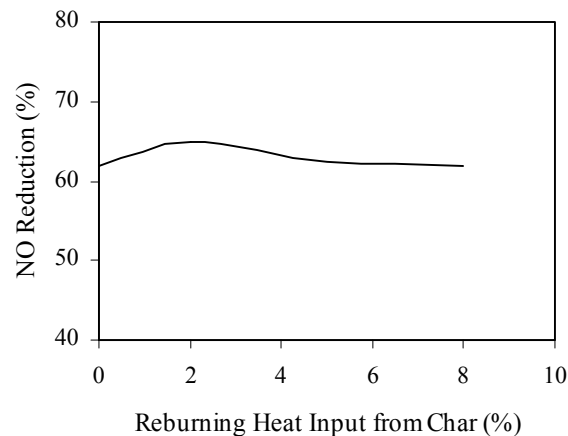


Figure 6-14. Reburning performance of activated char as a function of char reburning heat input.

Additional tests were conducted in which char comprised part of the reburning fuel. For these tests the char was activated by heating it to 600 K for one hour. The total reburning heat input was held

constant at 18% and the reburning heat input of the char was varied from 0 to 8%. Figure 6-14 shows that impact of char on reburning performance was minimal.

6.3 Prospective Additives Search: Summary

1. The effect of additives on AR-Rich and basic reburning were determined. Tests showed that co-injection of Li and K compounds resulted in 74-78% NO reduction, i.e. 17-21 percentage points improvement. Although these effects are lower than those for sodium, they are significant. Thus, K and Li compounds can be used as AR promoters. Compounds of Mg, Ca, Ba, and Zn provided relatively small promotional effect. When added to ammonia solution, they reduced NO by an additional 6-9 percentage points.
2. Tests also showed that metal-containing compounds could be effective promoters without injection of N-agents. Fe-containing compounds were the most effective in reduction of NO_x emissions followed by Na-, K-, and Ca-containing compounds. Co-injection of these compounds with the main fuel in the absence of reburning resulted in 16-30% NO_x reduction compared with basic reburning. Injection of metal compounds with the main fuel in the presence of reburning provided an additional 4-25% percentage points of NO_x reduction compared with basic reburning. As the concentration of additive increased, so did the promotional effect. Co-injection of additives with reburning fuel and into reburning zone had a smaller effect than co-injection with the main fuel. Coal char and fly ash showed a minimal effect on NO_x reduction. It was concluded that metals in coal char and fly ash were mainly present in the form of sulfides and silicate-alumosilicate matrixes that were relatively stable at high temperatures. These compounds are not effective in reactions with combustion radicals and have minimal effect on NO_x reduction.
3. Tests showed that injection of Ca-containing compounds can reduce NO_x emissions and simultaneously decrease SO₂ emissions: about 50% SO₂ reduction was achieved with injection of 1,000 ppm of Ca(OH)₂ with the main fuel.
4. Based on the observed effects of metal-containing compounds on NO_x formation and destruction under flame, reburning, and flue gas conditions, the following options for reducing NO_x emissions can be suggested:
 - Injection of metal-containing additives with the main fuel or into the main combustion zone, with or without reburning in operation. Up to approximately 30% NO_x reduction attributable to the presence of promoters can be obtained by this method.
 - Injection of metal-containing additives with the reburning fuel or into the reburning zone, with or without OFA injection (the latter only if the reburn zone stoichiometry is fuel lean). Up to about 20 percentage points of additional NO_x reduction, compared to conventional reburning, can be achieved by this method.
 - Injection of metal-containing additives with both the main fuel and the reburning fuel, or in the main combustion zone and the reburning zone, with or without OFA.
 - Metal-containing additives can be injected as solids or liquids (metal-organic compounds or as solutions of metal compounds in water or other solvents); they can also be components of the main fuel, the reburning fuel or products of their pyrolysis or gasification.

7.0 Task 2.3 Development of a Combined Chemistry Mixing Model

The objective of the combined chemistry-mixing modeling was to create a model for predicting the NO_x control performance via reburning and AR in a real boiler. Since the rates of chemical reactions responsible for NO_x reduction at typical reburning temperatures are faster than mixing processes, the latter has a rate-controlling effect on reburning performance. Thus, a realistic description of the mixing process is required to describe the main features of the reburning and AR processes.

Proper modeling of mixing requires a combination of kinetic and gas dynamic equations. Restrictions on computer time and storage requirements, however, allow one to use detailed chemistry modeling only with simplified fluid dynamics formulations, and conversely detailed three-dimensional modeling can be done only with simplified chemical reaction mechanisms. For a long time, modeling of the reburning process was subject to a choice between computational codes which focus on either multidimensional fluid mechanics with simplified chemical kinetics (for example, FLUENT, *Fluent*, 1998) or one dimensional flow codes with instantaneous or simplified mixing and with detailed chemical kinetics (e.g. SENKIN, *Lutz et al.*, 1987). There were successful attempts (*Luan et al.*, 1996; *Alzueta et al.*, 1998) to modify the SENKIN code, which assumes instantaneous mixing of reagents, to describe one dimensional mixing by combining several plug flow reactors. This approach is a good approximation of the fuel rich environment of the mixing zone. It fails, however, to take properly into account mixture stratification in the reburning zone which requires a more sophisticated representation of mixing. Since the kinetic mechanism of the reburning process is still not fully established, computational codes that simplify mixing processes and allow study of the detailed mechanism continue to be important modeling tools. The importance of the detailed chemistry became even more significant for AR applications, since the interaction of N-agents and promoters with C-H-O-N chemistry can not be understood without utilization of detailed chemical mechanisms.

The approach adopted in Phase II to model reburning and AR processes includes a combination of a detailed kinetic mechanism with a simplified representation of mixing. Such a model can be used not only for optimization of basic reburning, but can also be applied to AR to identify most important parameters affecting NO_x reduction.

The features that distinguish this model from other models is the utilization of distributed addition of reagents and the inverse mixing approach. The model utilizes plug flow reactors to describe processes that occur in the boiler: mixing of the reburning fuel with flue gas, NO_x reduction in the reburning zone, addition of OFA, and reactions in the burnout zone. The mixing is described using the Zweitering approach (*Zweitering*, 1959) (the secondary stream is distributed along the primary stream in a continuous fashion over certain period of time).

The model was first applied to the basic reburning process. After it was validated against experimental data, it was then applied to promoted reburning and AR. The following sections describe the modeling setup, the mixing approach which was adopted, validation of the model over a wide range of mixing conditions, and application of the model to the description of reburning and AR in several combustion facilities ranging from bench- to large pilot-scale.

Modeling was conducted with the kinetic mechanism described by *Glarborg et al.*, 1998. The mechanism included 447 reactions of 65 chemical species. Kinetic mechanism is presented in *Appendix B*. Thermodynamic data of C-H-O-N species are presented in *Appendix C*.

7.1 Model Setup

7.1.1 Model Formulation

The chemical kinetic code ODF, for “One Dimensional Flame” (Kau *et al.*, 1987) was employed in modeling. ODF treats a system as a series of one-dimensional reactors. Each reactor may be perfectly mixed (well-stirred reactor “WSR”) or unmixed (plug flow reactor “PFR”). Each ODF reactor may be assigned a variety of thermodynamic characteristics, including adiabatic, isothermal, or specified profiles of temperature or heat flux, and/or pressure. Process streams may be added over any interval of the plug flow reactor, with arbitrary mixing profiles along the reactor length. The flexibility in model setup allows many different chemical processes to be simulated in a variety of mixing regimes.

The reburning process was treated as series of five reactors (Figure 7-1). Each reactor described one of the physical and chemical processes occurring in a boiler: combustion of the main portion of fuel, addition of the reburning fuel (two parallel reactors as explained below), NO_x reduction as a result of the reaction with the reburning fuel, addition of overfire air, and completion of oxidation in the burnout zone.

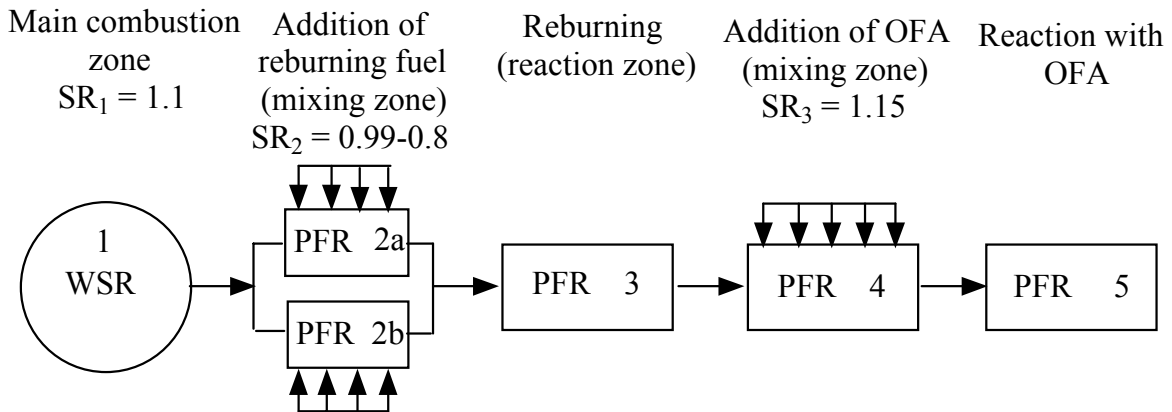
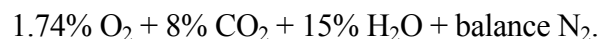


Figure 7-1. Reactor diagram of model setup.

The mixture entering the second reactor corresponds to products of natural gas combustion in air at $SR_1 = 1.1$ (first reactor). Assuming that the combustion process in the primary zone is complete, the mixture with $SR_1 = 1.1$ generates about 8% CO₂ and 15% H₂O. At the same time, 1.74% O₂ is left which is available for oxidation of the reburning fuel. Therefore, the premixed reactants entering the second reactor can be described as:



The reburning fuel is added to the main stream of reactants in the second reactor. Natural gas was used as a reburning fuel. The composition of natural gas was assumed to be the same as in experiments: 90.7% CH₄ + 7.5% C₂H₆ + 1.5% N₂ + 0.25% CO₂ + 0.05% O₂.

The third reactor described the continued process of NO removal in the reburning zone after the reburning fuel and flue gas are mixed. The fourth reactor described the process of OFA mixing with flue gas. The fifth reactor described oxidation of the products of incomplete combustion.

7.1.2 Estimation of Mixing Parameters

Mixing times and temperature profiles in mixing regions of CTT and BSF were calculated using a single jet in cross flow model (Cetegen *et al.*, 1986). A two-dimensional model was used because previous experience suggested relatively homogeneous distributions of temperature and mixture composition along cross sections of these combustors. Since the Tower Furnace (TF) is a much larger facility and is characterized by less uniform temperature and concentration fields across the furnace, mixing parameters in the TF were estimated using CFD modeling (Fluent, 1998).

A single jet model JICFIS (for “Jet in Crossflow, Integral Solution”) was used to estimate mixing time and mixture stratification in the reburning and OFA zones. JICFIS is a GE-EER model which numerically evaluates an integral solution to the trajectory and mixing of a single jet in cross flow. The mixing is determined by evaluating the entrainment rate of fluid from the crossflow into the jet. The model is based on a simplified two-dimensional representation of the fluid dynamic equations for the jet. These four equations (mass, two components of momentum, and energy) are integrated numerically, marching along the jet centerline, using the Runge-Kutta technique. Major inputs for the model for BSF are shown in Table 7-1 and include the velocity and density ratios of the crossflow to jet, their relative orientation in two dimensional rectangular coordinates, and the initial conditions (diameter, velocity, and temperature) of the jet. The model has been validated against experimental data and successfully employed in a number of jet injection studies.

Table 7-1. Characteristics of mixing in BSF and jet parameters.

Zone	Total flow rate lb/s, $\times 10^2$	Injector description	Injector characteristics
Primary zone	13.76		
Reburning zone	14.24	8 jets oriented 27° upstream	Injection rate 42.8 m/s Jet diameter 0.31 cm
After OFA	15.7	12 swirl jets oriented perpendicular to the stream	Injection rate 5.5 m/s Jet diameter 0.94 cm

Figure 7-2 shows trajectory of the jet in BSF as predicted by JICFIS model for the injection of the reburning fuel.

The JICFIS model was used up to the point where the amount of entrainment equals the main flux; after this, complete mixing is assumed (in Figure 7-2, this distance for the single jet corresponds to 0.25 m from the point of injection).

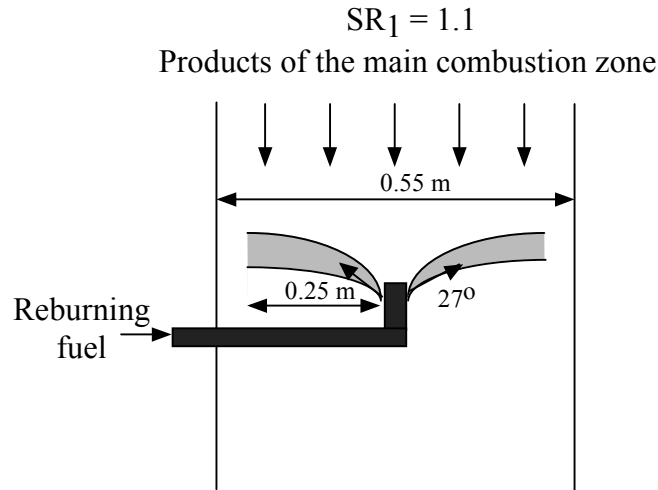


Figure 7-2. A diagram of jet injection and model setup in the BSF reburning zone.

A three-dimensional CFD model of the upper furnace and convective pass portion of the TF was set up in FLUENT to simulate mixing in the reburning and burnout zones. The temperature profile was calibrated to point measurements from the TF. Velocity profiles at the inlet reburning and overfire planes were obtained from physical flow modeling measurements. Once the temperature and convective pass pressure drop were calibrated in the model, reburning fuel and OFA were injected through appropriate ports. From these results, mixing times in the reburning and burnout zones were determined.

Table 7-2 presents calculated mixing parameters for CTT, BSF and TF. The effect of mixing time on modeling predictions is discussed in the following section.

Table 7-2. Mixing parameters in CTT, BSF and TF.

Combustion facility	Mixing time in the reburning zone (ms)	Mixing time in the burnout zone (ms)	Model used to estimate mixing parameters
CTT	100	100	Single jet in cross flow
BSF	120	120	Single jet in cross flow
TF	80	120	CFD modeling

7.1.3 Mixing Mode

Three different mixing modes were tested in calculations. The different models are judged based on best description of the rate at which injected streams are entrained into the main furnace gases and become available for reaction. The mixing modes are described here in the context of the reburning fuel injection stage, in which a jet of natural gas is injected into a crossstream consisting of the furnace flue gases from the primary zone.

In the first mode considered, natural gas was added to the stream of flue gas over the period of mixing time. The second mode was similar to the first one, except that the rate of natural gas addition linearly increased in time from zero to its final value (such that the total amount of natural gas added was the same as that for the same period of time at a constant entrainment rate). The third mode assumed that a mixture of NO, O₂, CO₂, H₂O and N₂ representing the flue gas was added to the stream of natural gas (so-called “inverse” mixing). The inverse mixing arrangement is opposite to apparent physical processes occurring in the combustor where reburning fuel is injected into the main stream, but from a chemical kinetic point of view it provides a description of the mixing process most closely resembling the real one: a high concentration of natural gas and low concentration of NO in the area of mixing. It was found that the mode of inverse mixing gave a better description of the experimental data than other models, and it was employed in calculations. This finding is in agreement with *Luan et al., 1996* and *Alzueta et al., 1998* studies which reported that the fuel-rich environment of the reburning mixing zone is better represented by addition of flue gases to the reburning fuel. The mixing process in the OFA zone was also described using the inverse mixing approach.

An example configuration describing the application of this approach to represent mixing in the reburning zone is shown in Fig. 7-3.

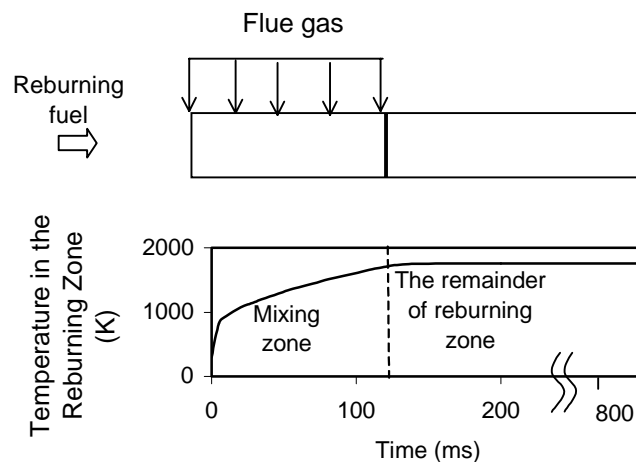


Figure 7-3. Modeling setup in the BSF mixing zone.

In the inverse mixing approach, the reburning fuel is the main stream in the one-dimensional reactor while flue gas exiting from the main combustion zone is added to it. As a result, the temperature history in the mixing region is described relative to the reburning stream rather than to the stream of flue gas. Thus, temperature in the mixing area at time $t = 0$ corresponds to the initial temperature of the reburning fuel. As mixing progresses, temperature increases until it reaches the temperature of flue gas. After reburning fuel and flue gas are completely mixed, there is no difference in their temperatures. This temperature profile neglected the thermal mass of the reburning jet in the final mixture, as well as non-monotonic aspects of the thermal profile due to local stoichiometry and reaction during mixing. These effects were judged to be minor in their overall impact on the reburning zone reactions.

Mixing time in the reburning zone depends on several factors including the reburning fuel injection configuration, velocities and temperatures of the reburning fuel and flue gas streams,

compositions of each stream, and related parameters. The temperature profile presented in Figure 7-3 represents the reburning fuel injection configuration used in BSF for flue gas at 1670 K and reburning fuel injected at 300 K. The mixing time determined using this profile and the corresponding flow parameters is about 120 ms. Based on this, the modeling setup used to represent the reburning zone of the BSF includes two plug-flow reactors. The first reactor (corresponding to Reactors 2a and 2b in Figure 7-1) has a residence time of 120 ms and treats the mixing of the reburning fuel and flue gas using the inverse mixing approach. The second reactor (Reactor 3 in Figure 7-1) has a residence time of 700 ms and describes the remainder of the reburning zone. The residence time in the second plug-flow reactor is determined by the difference in flue gas temperatures at which reburning fuel and OFA are injected, the temperature gradient in the BSF, and the mixing time in the first reactor.

OFA air injection and mixing is handled in the same manner as the reburning fuel. The times in Table 7-3 are approximate since the actual geometry does not precisely match the single jet treated by the JICFIS algorithm. However, the results are considered to reflect the magnitude of the mixing rate based on the general scale of the problem.

A similar approach was used in the model setup for the CTT and TF facilities.

7.1.4 Mixture Stratification

Injection of the reburning fuel results in mixture stratification, such that the composition in the mixing area is not uniform. The inverse mixing approach to describe the addition of reagents partially addresses the issue of mixture stratification in the mixing region: at the first moments of mixing, the reaction occurs in an extremely fuel-rich environment, which then progresses gradually to the final composition as determined by the relative amount of the injected reburning fuel. As this occurs, other portions of the furnace gas flow are incompletely covered by reburning fuel even though they are still within the reburning zone.

Since mixture stratification is an important factor that significantly affects NO reduction, additional efforts were undertaken to take it into account. Ideally, the mixing zone can be divided into infinite (or as many as possible) subzones each representing the local mixture composition. As a first approximation, the mixing zone was divided into two reactors (2a and 2b in Figure 7-1) that represented two extreme cases of mixture stratification: one reactor was assigned with a more fuel-rich mixture than average, another one with a less fuel-rich mixture. The fuel content of the two reactors corresponds to an average SR_2 reflecting total amount of added reburning fuel. For each reactor, 2a and 2b, the inverse mixing model was used to describe the addition of the reburning fuel. The distribution of reburning fuel between the two reactors was an adjustable parameter in modeling.

The results of JICFIS modeling for the BSF conditions were used to estimate the degree of mixture stratification in the mixing zone. Since the BSF arrangement is axisymmetrically symmetrical, the interaction of a single jet with the flue gas was described as a mixing zone divided into two reactors (2a and 2b in Figure 7-1), each with an equal mass flow of combustion gas. It was assumed that the injected fuel was distributed between reactors unevenly. The fuel distribution between the two reactors was described by a stratification coefficient K that can be determined as a ratio of the amount of reburning fuel in the first reactor to that in the second reactor. The case where $K = 1$ corresponds to reburning fuel distributed uniformly between two reactors.

The estimation of K is based on the following simple consideration. The radius at which complete mixing is achieved (within 0.25 m radial distance in a 0.55m diameter furnace, as shown in Fig. 7-2) corresponds to point at which the final mixture composition is attained, at a stoichiometric ratio of SR_2 . In the area of incomplete mixing, an unmixedness parameter can be defined which changes from 100% (100% unmixedness means that no oxygen is present in the jet mixture; this condition exists at the base of the jet) to 0% (mixture composition is determined by SR_2 ; exists in the jet at the point of complete mixing). Assuming that unmixedness within the jet is, on average, 50% (the concentration of fuel is 50% higher than that in the area of complete mixing), a geometrical consideration with distances shown in Figure 7-2 results in $K = 1.4$. It actually means that the mixture in the reactor 2a has 40% higher fuel concentration than that in the reactor 2b. This estimate is a simple approximation based on the non-uniform mixture composition along the jet. However, it provides a starting value of K for model development. K was then varied and compared with the experimental data. Final results reported here correspond to $K = 1.8$, for which the best agreement with experimental data was attained.

7.2 Chemistry -Mixing Modeling of Gas Reburning

This section describes the validation of the basic reburning model over wide range of process conditions. The data presented demonstrate that the model can be applied to describe basic reburning in different combustion facilities if their mixing and thermal characteristics can be characterized.

Experimental data under basic reburning conditions (no N-agent or promoter injection), used to evaluate modeling predictions, were obtained in three combustion facilities: the 0.1×10^6 Btu/hr CTT, the 1×10^6 Btu/hr BSF, and the 10×10^6 Btu/hr TF. These experimental facilities are described in *Section 11*. The data of *Kolb et al., 1988* and *Mereb and Wendt, 1990, 1991* were also used for model validation.

In all tests natural gas was used as both primary and reburning fuel. The flue gas temperature at the point of the reburning fuel and OFA injection, and the initial NO_x concentrations (NO_i) are presented in Table 7-3. Axial temperature profiles measured in the CTT, BSF and TF and subsequently utilized in modeling are presented in Section 11 (Figure 11-1).

Table 7-3. Reburning parameters.

Facility	Temperature at Reburning Fuel Injection (K)	Temperature at OFA Injection (K)	NO_i (ppm)
CTT	1630	1400	600
BSF	1670	1422	400-1000
TF	1800	1650	200

Combustion in the primary zone was characterized by operation at a stoichiometric ratio $SR_1 = 1.1$. The amount of the reburning fuel varied in the range from 5-25% of the total amount of fuel ($SR_2 = 0.83 - 1.05$). The mixture composition in the burnout zone (including previously added

fuel) corresponded to $SR_3 = 1.15$.

The following parameters were inputs for the model:

- Relative amount of the reburning fuel.
- Axial temperature gradient in the combustor.
- Temperatures of flue gas at the point where reburning fuel and OFA are injected.
- Initial temperatures of the reburning fuel and OFA.
- Initial NO_x concentration.
- Mixing times in the reburning and burnout zones.
- Temperature profiles in mixing regions.

7.2.1 Comparison with Experimental Data Obtained in CTT, BSF and TF

Influence of the Initial NO Concentration

The performance of the current model was verified against experimental data on NO reduction at different initial NO concentrations, $[NO]_i$. Figures 7-4 a-c show comparison of modeling predictions with experimental data from BSF for $[NO]_i = 416, 600, \text{ and } 970$ ppm, respectively. Figures 7-5 and 7-6 demonstrate comparison of modeling predictions with experimental data obtained in CTT and TF. For all initial amounts of NO the model at least qualitatively (and in most cases quantitatively) agrees with experiments within the data scatter. Modeling slightly underpredicts NO reduction efficiency at low reburning fuel heat inputs for all initial NO amounts. Modeling overpredicts NO reduction at the highest initial NO concentration for all but the lowest reburning fuel heat inputs.

Modeling predicted that the efficiency of NO reduction was higher as the amount of reburning fuel increase. However, at large heat inputs, the efficiency decreases so that there is an optimum amount of the reburning fuel which results in the greatest efficiency of NO reduction. As $[NO]_i$ increases, the optimum slightly shifts toward larger heat inputs.

The modeling results presented in Fig. 7-4 through 7-6 were obtained using values of mixing times from Table 7-2. Since two-dimensional models (for example, a single jet in planar cross flow) do not precisely match the experimental configurations employed for reburning fuel injection, a practical issue is determining how accurate the calculation of mixing time in the model should be to give reasonable agreement between modeling predictions and experimental data. Thus, it is important to determine the sensitivity of modeling predictions to the value of the mixing time. Figure 7-7 shows the effect of varying mixing time in the reburning zone on modeling predictions of NO_x Reduction, for typical BSF conditions. The experimental value of NO_x reduction for these conditions is also shown.

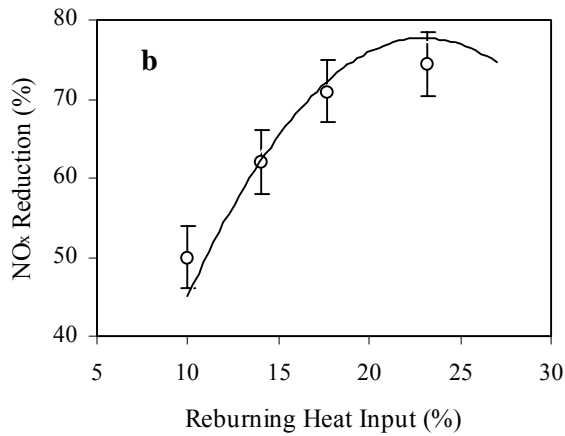
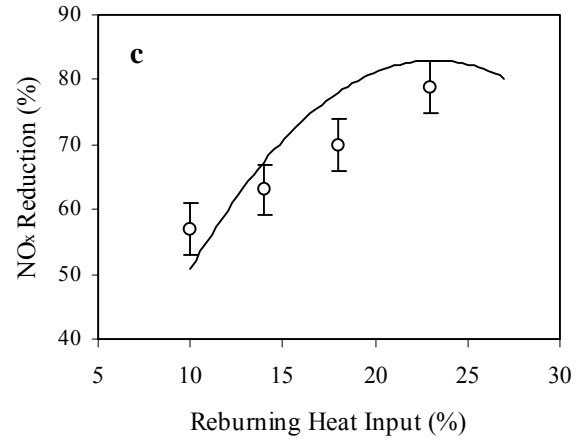
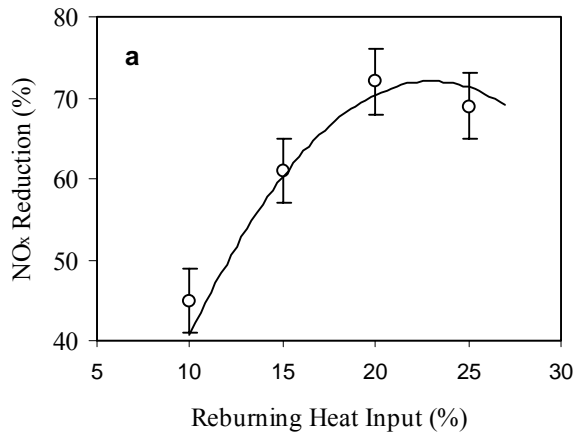


Figure 7-4. Comparison of BSF test results on reburning (symbols) with modeling predictions (lines). a: $[\text{NO}]_i=416$ ppm, b: $[\text{NO}]_i=600$ ppm, c: $[\text{NO}]_i=970$ ppm.

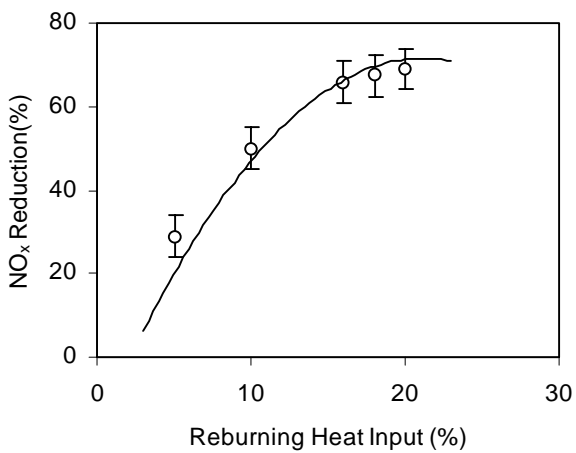


Figure 7-5. Performance of basic reburning in CTT. Lines represent calculations, symbols experimental data.

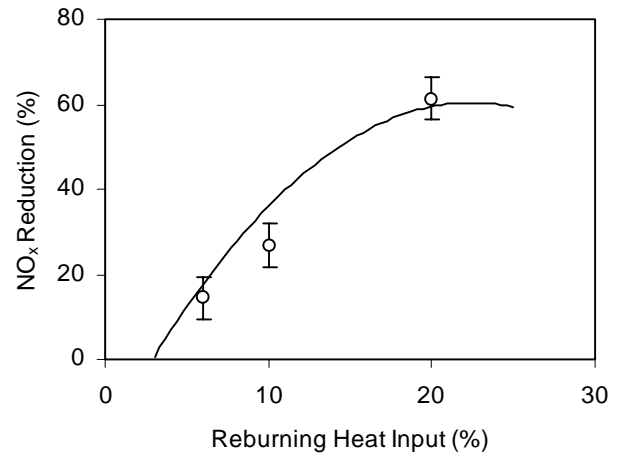


Figure 7-6. Performance of basic reburning in TF. Lines represent calculations, symbols experimental data.

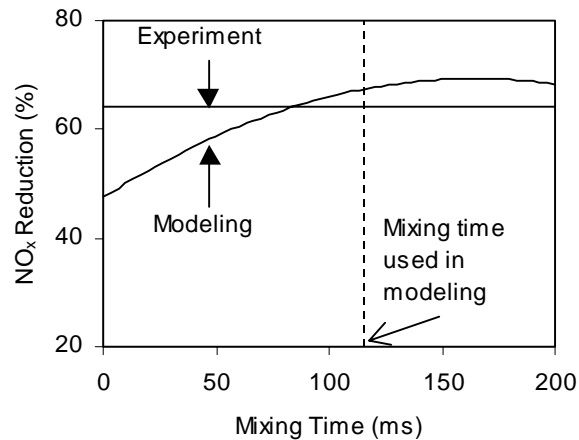


Figure 7-7. Predicted effect of mixing time on modeling predictions of NO_x reduction for typical BSF conditions. The amount of reburning fuel is 15% of total fuel. NO_i = 600 ppm.

Although Figure 7-7 demonstrates that mixing time has an impact on predicted NO_x reduction over the entire range evaluated, it also shows that it is the most significant at small mixing times (in the transition as finite-rate addition approaches the limit of instantaneous mixing). As mixing time increases, the effect of mixing time on NO_x reduction levels off. The characteristic mixing time and the sensitivity curve (Fig 7-7) change little over the range of operating conditions being considered here, so that any error due to the choice of mixing time has little effect on the *relative* changes predicted from one condition to another. This justifies the use of simple models for calculating mixing times. It should be remembered, however, that if the mixing region is characterized by significant radial and axial temperature non-uniformities, a more sophisticated approach is needed to describe mixing.

Concentrations of Intermediate Species in the Reburning Zone

Figures 7-8a,b compare modeling predictions and experimental data for the concentrations of NO, NH₃, HCN, and TFN (Total Fixed Nitrogen) at the end of the reburning zone (before OFA injection). NH₃ and HCN are formed in the reburning zone as a result of reactions between CH_i radicals and NO.

The concentration of NO at the end of the reburning zone depends on the relative heat input of the reburning fuel and decreases with as that parameter increases. For the range of relative heat inputs considered (except for lowest values), the concentrations of NH₃ and HCN at the end of the reburning zone are significant. The model qualitatively describes these trends. In agreement with the experiments, the model predicts that the TFN concentration at the end of the reburning zone is minimized in the neighborhood of 18% reburning fuel input.

The chemical mechanism (*Glarborg et al., 1998*) used in modeling is the current state of the art, but it is far from completion. The mechanism underpredicts NO and HCN concentrations in the reburning zone, especially at large relative heat inputs of the reburning fuel.

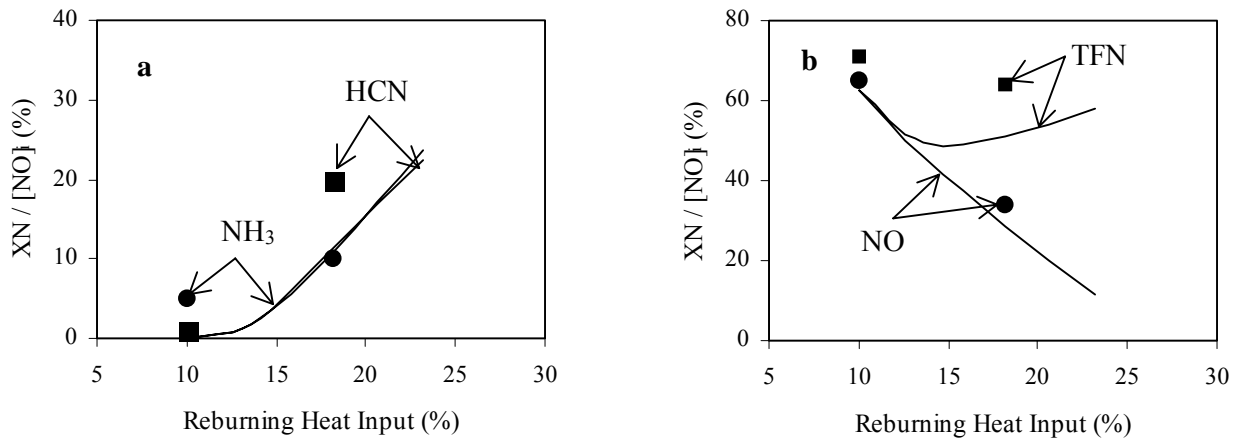


Figure 7-8. Modeling predictions (lines) and experimental data (symbols) for the concentrations of N-containing species at the end of the BSF reburning zone. $[\text{NO}]_i = 600$ ppm. a: NH_3 and HCN, b: NO and TFN. Residence time in the reburning zone is 0.93 s.

Influence of the OFA Injection Location

Due to the temperature gradient in a boiler, injection of OFA at different locations results in different flue gas temperatures at the point of injection. The position of the injector also determines the residence time in the reburning zone. For example, when OFA is injected at 1500 K, the reaction time available for NO reduction in the BSF reburning zone is 0.7 s. For OFA injection at 1300 K, the residence time (from reburning fuel injection at 1700 K) doubles.

Figure 7-9 shows influence of flue gas temperature at the point of OFA injection on NO removal. For 10% heat input from reburning fuel, modeling predicts slightly lower efficiencies of NO reduction than observed in experiments.

However, the model correctly represents the major process trends. Modeling predictions show that the flue gas temperature at the point of OFA injection has a weak effect on the efficiency of the reburning process. The relatively small dependence of NO reduction efficiency on the location of OFA injector at low heat inputs of the reburning fuel indicates that NO reduction in the reburning zone occurs in early reactions and is not affected by residence time in the reburning zone above some minimum value.

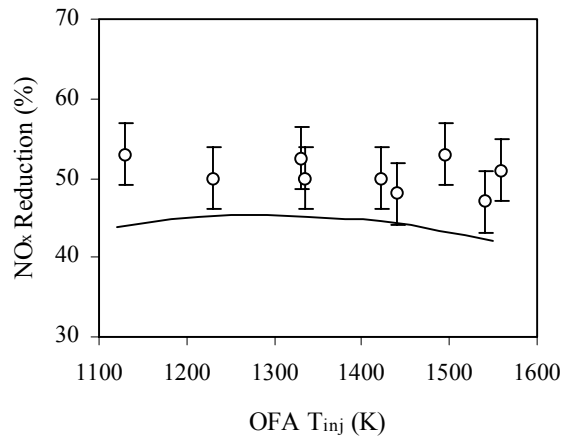


Figure 7-9. Comparison of experimental results for post-burnout NO_x Reduction under basic reburning (symbols) with modeling predictions (solid curve). 10% reburning fuel is added at 1700 K, [NO]_i = 600 ppm.

7.2.2 Comparison with Experimental Data of Kolb et al.

Modeling predictions were also compared with experimental data of *Kolb et al., 1988* who studied the effect of mixing on the reburning efficiency in a 1.2×10^6 Btu/hr combustor. The authors used methane doped with NH₃ as primary and reburning fuel. Variation in mixing time was achieved by changing jet momentum (adding nitrogen to the stream of the reburning fuel). In particular, experimental data are reported for two jet velocities which are referred by authors as the low and high momentum jets. Under tests conditions reported by *Kolb et al., 1988*, *Rota et al., 1997* calculated characteristic mixing times of the low and high momentum jets to be 50 and 10 ms. Calculations (*Rota et al., 1997*) using single jet in cross flow model also showed that the high velocity reburning fuel jet reached walls of the furnace before complete mixing with flue gas occurred. The 10 ms mixing time for this jet was taken as the time required for the jet to reach walls. Thus, “real” mixing time for the high velocity jet was probably longer than 10 ms. Since the actual configuration of the reburning fuel injection (twenty gas jets) does not precisely match the single jet, as specified by the single jet in cross flow model, these times are approximate and can be considered as order of magnitude estimations.

Figure 7-10 shows comparison of predicted by modeling and measured (*Kolb et al., 1988*) NO_x reduction at the end of the reburning zone for low and high momentum jets. Initial NO_x concentrations were 980 ppm for the high and 1,230 ppm for the low momentum jets. In modeling, mixing time was an adjustable parameter. For the low velocity jet, the best agreement with experimental data was achieved at 60 ms mixing time which is close to the estimate of 50 ms made by *Rota et al., 1997*. For high velocity jet, the best agreement was obtained at 40 ms mixing time which is longer than 10 ms *Rota et al., 1997* estimate. However, since actual mixing time of the high velocity jet is probably longer than 10 ms, this result can be considered to be in agreement with *Rota et al., 1997* estimate. Good agreement of modeling predictions with experimental data (Fig. 7-10) suggests that model correctly describes main features of the reburning process observed by *Kolb et al., 1988*.

Other observation regarding the effect of mixing on reburning can be derived from Fig. 7-10. Both experimental data and modeling predictions suggest that at low heat inputs of the reburning fuel (SR_2 in the range of 0.9-1.0) the process is more effective at longer mixing times (the low momentum jet), while at larger heat inputs ($SR_2 < 0.9$) better mixing (the high momentum jet) is more favorable. This finding suggests that injection of large amounts of the reburning fuel provides better NO_x reduction if mixing of reactants is fast, while injection of small amounts of the reburning fuel resulting in significant mixture stratification and longer mixing times gives better NO_x control.

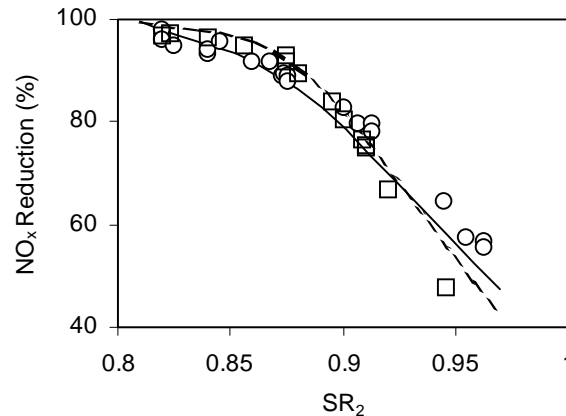


Figure 7-10. Comparison of modeling predictions (lines) with experimental data (symbols) of Kolb *et al.*, 1988. Squares and dashed line correspond to the high momentum jet, circles and solid line to the low momentum jet. Temperature in the reburning zone is 1600 K.

7.2.3 Comparison with Experimental Data of Merib and Wendt

Mereb and Wendt 1990 and Wendt and Mereb 1991 reported NO_x concentrations in the reburning zone of the laboratory combustor as function of SR_2 . Temperatures of flue gas at which reburning fuel was injected varied from 1380 to 1600 K. The reported mixing time was 0.18 s. The primary fuel was coal while reburning fuel was natural gas. Since the reburning fuel was deliberately injected significantly downstream from the primary coal flame to allow sufficient time for char burnout, the nature of the primary fuel probably had a little or no effect on the reactions in the reburning zone.

Figure 7-11 compares measured Wendt and Mereb, 1991 and predicted performances of the reburning process as a function of SR_2 . Modeling was done for 0.18 s mixing time. Modeling predictions agree well with experimental data at SR_2 in the range of 0.9-1.15 and slightly overpredicts the efficiency of the reburning process at $SR_2 < 0.9$. Maximum in the reburning efficiency at SR_2 about 0.9 is well predicted.

Figure 7-12 shows a comparison of predicted and measured (Mereb and Wendt, 1990) NO_x concentration profiles in the reburning zone for $SR_2 = 0.68$ and 0.80. While some deviations between experimental data and modeling predictions can be seen at the beginning and in the middle of the reburning zone, the predicted NO_x concentrations at the end of the reburning zone for both cases are in a good agreement with experimental values. This agreement is encouraging since

mixing time 0.18 s reported by *Mereb and Wendt, 1990* was used in modeling and none of the model parameters was adjusted to improve agreement with experimental data.

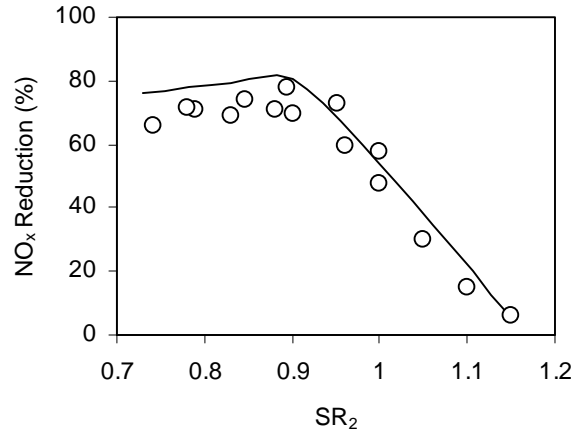


Figure 7-11. Effect of the reburning zone stoichiometry on efficiency of the reburning process. Symbols represent measurements *Wendt and Mereb, 1991*; line – model predictions. $SR_1 = 1.23$, $NO_i = 1,070$ ppm.

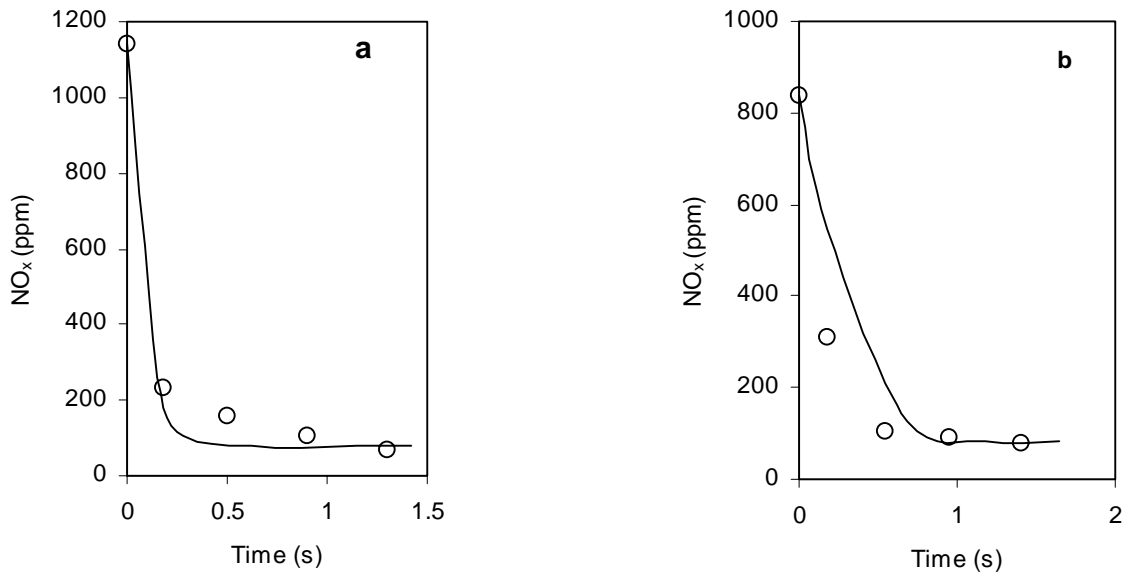


Figure 7-12. Comparison of modeling predictions with experimental data of *Mereb and Wendt, 1990*: (a) $SR_2 = 0.80$, $NO_i = 1,140$ ppm; (b) $SR_2 = 0.68$, $NO_i = 840$ ppm.

7.3 Parametric Study of Basic Reburning

There are several adjustable parameters in the model that affect the efficiency of NO_x reduction in basic reburning. They include fuel stratification in the reburning zone and temperatures of injected

reburning fuel and overfire air. Influence of these parameters on modeling predictions is discussed in the following Sections.

7.3 Effect of Fuel Stratification in the Reburning Zone

Fuel stratification after reburning fuel injection has a significant effect on modeling predictions. Figure 7-13 shows the effect of fuel stratification coefficient (K) on NO_x reduction. Value $K = 1$ corresponds to the case with no fuel stratification.

Modeling suggests that non-uniformity of fuel distribution within the reburning zone (increase in K) improves NO_x reduction for small heat inputs of the reburning fuel and degrades it for large heat inputs. This effect can be explained by the experimental observation (supported by modeling) that there is an optimum amount of the reburning fuel (usually about 20%) that results in maximum NO_x reduction (Figures 7-4 - 7-6). For small heat inputs of the reburning fuel, mixture stratification within mixing zone creates areas with a large amount of fuel that is still smaller than the optimum value. NO_x reduction in such areas significantly exceeds the level of NO reduction at the “average” fuel amount. Therefore, an increase in fuel stratification results in increasing NO_x reduction. For large heat inputs, due to the existence of the optimum in NO_x reduction, the efficiency of NO_x reduction in locally rich areas is lower than that for the “average” amount of fuel. Therefore, in this case, the total efficiency of reburning decreases with increased fuel stratification. Variation of the stratification coefficient achieved the best description of the experimental data at $K = 1.8$.

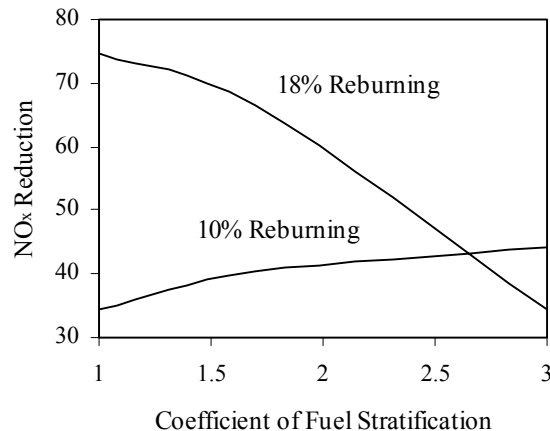


Figure 7-13. Effect of fuel stratification in the mixing area of the reburning zone on modeling predictions for BSF conditions. $[\text{NO}]_i = 416$ ppm.

7.3 Effect of the Initial Temperature of the Reburning Fuel and Overfire Air

Besides being injected at different locations (which correspond to different temperatures of flue gas at the moment of injection), reburning fuel and overfire air can be injected at different initial temperatures (temperatures of fuel and air streams at the moment of injection). Location of injection is usually determined by the geometry of the boiler and can not be easily changed, but the initial

temperature of the injected stream can be regulated, for example, by preheating prior to injection, by mixing with steam or hot flue gases, or by cooling the injector with water.

Figure 7-14 shows the effect of the initial temperature of the reburning fuel on NO_x reduction. Again, the effect is quite different for small and large heat inputs of the reburning fuel. Preliminary heating of the reburning fuel increases efficiency of the reburning process for large heat inputs of the reburning fuel and decreases it for small heat inputs. Influence of the jet temperature on the reburning performance can be explained by the fact that the initial temperature of the jet affects mixing time: an increase in the jet temperature provides in better jet mixing with the crossflow and as a result the mixing time in the reburning zone decreases.

Figure 7-15 shows the effect of the initial temperature of OFA on NO_x reduction at 10 and 23% heat input of the reburning fuel. OFA is injected into flue gas at temperatures 1422 K. At 23% reburning, as the initial temperature of OFA decreases, the efficiency of the reburning process increases. At 10% reburning, the initial temperature of OFA does not affect reburning efficiency.

These considerations suggest that initial temperatures of the injected reburning fuel and OFA are important parameters that affect the efficiency of the reburning process. NO_x reduction can be improved if values of these parameters are optimized.

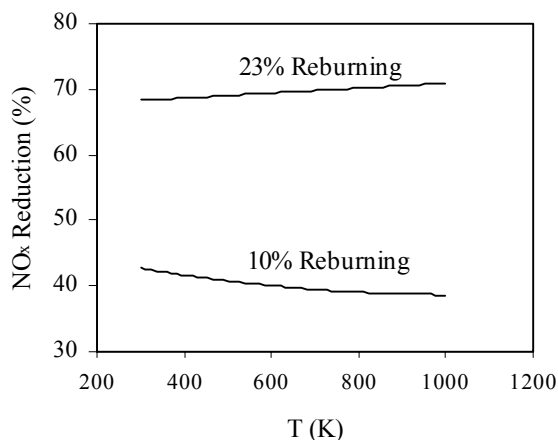


Figure 7-14. Predicted effect of the initial temperature of the reburning fuel on NO_x reduction for BSF conditions. $[\text{NO}]_i = 416$ ppm.

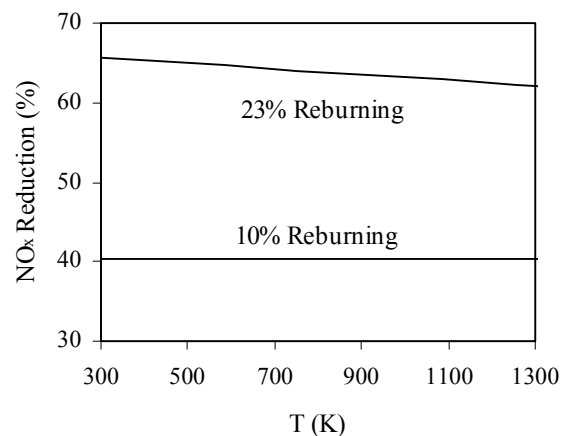


Figure 7-15. Predicted effect of the initial OFA temperature on NO_x reduction for BSF conditions. $[\text{NO}]_i = 416$ ppm.

Figure 7-16 shows comparison of the predicted efficiencies of the reburning process with optimized (dashed line) and non-optimized (solid line) initial temperatures of the reburning fuel and OFA with experimental data. Depending on heat input of the reburning fuel, optimization results in 2-10% increase in NO_x reduction.

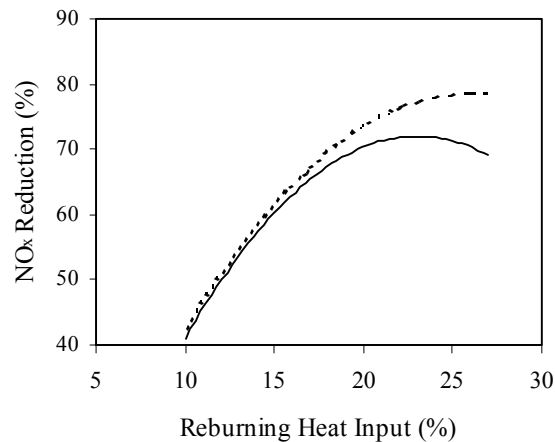


Figure 7-16. Performance of the reburning process for optimized (dashed line) and non optimized (solid line) initial temperatures of the injected reburning fuel and overfire air for BSF conditions. $[\text{NO}]_i = 416$ ppm.

7.3 Reactions Responsible for NO_x Reduction

Figures 7-17a,b show profiles of the main N-containing species in reburning and burnout zones and main reactions responsible for NO_x reduction for different heat inputs of the reburning fuel. The concentration profiles clearly show that major NO_x reduction occurs during addition of the reburning fuel within mixing zone and thus demonstrate that NO_x reduction is strongly affected by the mixing process.

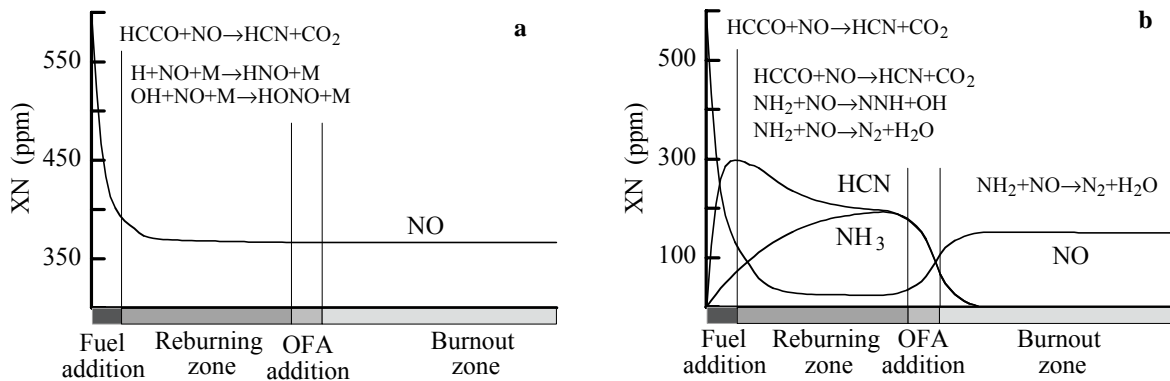


Figure 7-17. Concentrations of N-containing species in reburning and main reactions responsible for NO_x reduction in different zones. $[\text{NO}]_i = 600$ ppm. a - 10% reburning fuel, b - 27% reburning fuel.

For a small amount of the reburning fuel (Figure 7-17a), main changes in NO concentration occur during fuel fragmentation into CH_i radicals (mixing zone). As soon as fuel is consumed, NO reduction is practically ceased. Additional NO reduction occurs in reactions of NO with H and OH , but this is a minor contribution. Injection of OFA practically does not affect NO concentration.

Figure 7-17b demonstrates the importance of such species as HCN and NH₃ in the reburning process. Concentrations of these species at the end of the reburning zone (at least for large heat inputs of the reburning fuel) significantly exceed the concentration of NO. Major NO reduction occurs within mixing zone, similar to the case with small heat input of the reburning fuel. NH₂ radicals further reduce NO after mixing is completed. NH_i species play even more important role when OFA is injected. NH₂ radicals, formed as a result of NH₃ reaction with O₂, significantly reduce NO formed via HCN oxidation. Reactions of HCN and NH₃ in the burnout zone significantly affect final NO emissions, and if conditions in the burnout zone are optimized, can result in lower NO emissions.

7.3 Gas Reburning Modeling: Summary

Modeling results demonstrate that model of basic reburning correctly describes a wide range of experimental data obtained in five bench- and pilot-scale combustion facilities. This suggests that developed model represents the main chemical and mixing features of the reburning process and can be used for process optimization.

The following conclusions can be drawn from modeling results:

- The main features of reburning can be described using a detailed chemical mechanism with one-dimensional representation of mixing.
- Inverse addition of reactants in the mixing area gives much better approximation of fuel rich environment in the reburning zone compared to mixing of reburning fuel into the main stream.
- Stratification in the mixing zone improves reburning efficiency for small heat inputs of the reburning fuel and degrades reburning efficiency for large heat inputs. Based on modeling observations, it is suggested that design of the injector should be different depending on the amount of the injected reburning fuel. Injection of large amounts of the reburning fuel provides better NO_x reduction if mixing of reactants is fast. Injection of small amounts of the reburning fuel, on the other hand, should result in significant mixture stratification for better NO_x control (as long as complete mixing and burnout is ultimately achieved).
- Initial temperatures of the reburning fuel and OFA affect NO reduction and can be optimized for deeper NO control. Optimum temperatures depend on the mixture composition and on the injection location. By optimizing these parameters, NO_x reduction can be increased by several percentage points.
- Reactions of NH₃ in the burnout zone play important role in NO reduction for large heat inputs of the reburning fuel.

7.4 Chemistry-Mixing Modeling of Ammonia and Sodium Effects on Reburning

Model of basic reburning was applied to describe the effects of N-agent and promoter injection on NO_x reduction. The extension of the basic reburning model to describe the AR process required some modifications in the chemistry-mixing model described above. The kinetic mechanism (Glarborg *et al.*, 1999) which includes 447 reactions of 65 C-H-O-N chemical species was extended

to include reactions of Na-containing species (Zamansky *et al.*, 1999). Reactions of Na with components of flue gas have been studied (Zamansky *et al.*, 1999) in connection with reduction of NO emissions in the SNCR process. Reactions of Na-containing species and thermo data of Na-containing species are presented in *Appendices D* and *E*.

The following sections describe modeling of the effect of combined N-agent and Na injection, and injection of Na-containing species without N-agent on NO_x reduction and CO emissions.

7.4 Combined Injection of N-Agent and Sodium Promoter

Effect of N-Agent and Na Promoter on NO_x Reduction

The AR process was treated as series of six reactors: five reactors (Fig. 7-1) described reburning process and one reactor described addition of N-agent and promoter to flue gas. Mixing time of 130 ms was assumed for mixing of N-agent and promoter stream with flue gas. This time was estimated using a simple 2D-spray model to calculate evaporation time and a 2D jet in cross flow model to calculate the time required for the N-agent to fully entrain the furnace gas.

The initial concentration of NO in flue gas was 600 ppm, reburning fuel and OFA were injected at 1670 and 1300 K respectively. N-agent and Na-promoter were injected into the reburning zone at 1460 K.

Comparison of modeling predictions and experimental data obtained in CTT on AR process is shown in Fig. 7-18. The modeling result for reburning alone only slightly underpredicts the experimentally observed reburning efficiency. The difference, however, is within the scatter of experimental data ($\pm 10\%$). Injection of ammonia into the reburning zone results in an increase of NO_x reduction. Modeling overpredicts NO_x reduction observed experimentally in the presence of N-agent. Possible explanation of this effect is the uncertainty in the mixing model of N-agent injection. Due to a very steep temperature profile at the location of N-agent injection, small variations in the injector location, mixing time and local temperatures can significantly affect modeling predictions.

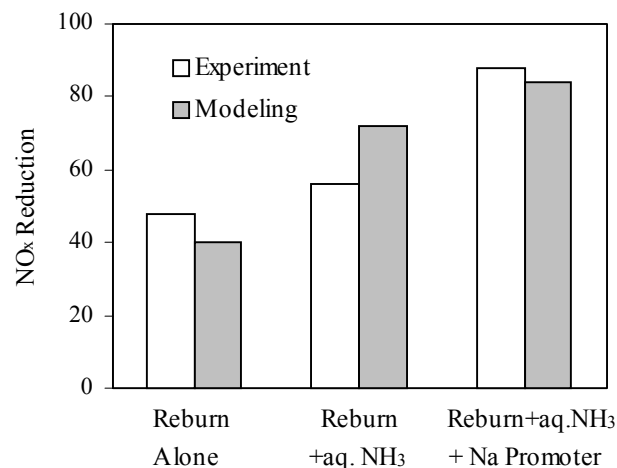


Figure 7-18. Comparison of modeling predictions with experimental data. NSR = 1.5, 30 ppm Na.

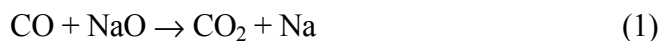
Sodium promoter (30 ppm of NaOH in flue gas) co-injected with N-agent further increases NO_x reduction. Modeling predicts that the efficiency of NO_x reduction increases about twice when N-agent and Na promoter are co-injected into reburning zone. Maximum NO_x reduction efficiency predicted by modeling is 85% for the selected conditions. Experiments show about 89% NO_x reduction.

Effect of N-Agent and Na Promoter on CO Emissions

Modeling showed that fuel oxidation in the reburning zone generated a significant amount of CO. For 10% reburning heat input, the concentration of CO at the end of the reburning zone was about 3800 ppm. The CO formed in the reburning zone is oxidized to CO₂ when OFA is injected to complete combustion. The temperature of OFA injection should be high enough to provide complete CO oxidation. Modeling predicted that concentration of CO in the flue gas decreased to 56 ppm after addition of OFA at 1300 K. This concentration was higher than that found in experiments (around 10 ppm) which can be attributed to the significant (-1240 K/s) temperature gradient in the experimental facility (CTT). Small uncertainties in the measured temperature profile can appreciably affect modeling predictions.

In agreement with experiments, modeling predicted that injection of NH₃ in the reburning zone resulted in a decrease of CO concentration in flue gas. Modeling showed that only a small fraction of the NH₃ reacted in the reburning zone. The remaining NH₃ reacts with oxygen in the OFA zone. This process generates active species (OH radicals, H atoms and others) which contribute to CO oxidation and account for the smaller CO concentration in flue gas.

However, modeling predictions were in contradiction with experiments when a Na promoter was co-injected with NH₃. Species flux calculations showed that a decrease in CO concentration predicted in modeling was a result of faster rate of CO oxidation in the presence of Na. To improve the model, routes for CO oxidation in the presence of Na-containing species were studied and identified to be the following:



The rate of CO oxidation in reaction (2) is much faster than that in reaction (1). Reaction (2) accounts for almost 100% of the total increase in CO oxidation in the presence of Na observed in modeling. Reactions (1) and (2) have not been studied experimentally. *Perry and Miller, 1996* estimated rate coefficients of these reactions to be $1.0 \times 10^{14} \text{ cm}^3 \text{ mol}^{-1} \text{ s}^{-1}$. Our modeling shows that to avoid a decrease in the CO concentration in flue gas in the presence of Na promoter, the rate coefficient of reaction (2) must be $\leq 1.0 \times 10^{10} \text{ cm}^3 \text{ mol}^{-1} \text{ s}^{-1}$.

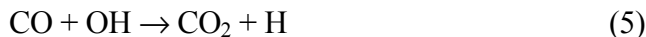
Adjustment of the rate coefficient for reaction (2) improved the agreement with experimental data. However, modeling still predicted much lower CO concentrations in flue gas than found in experiments. Sensitivity calculations showed that among reactions of Na-containing species the reaction



had the largest effect on the rate of CO oxidation. This reaction inhibited oxidation process by removing H atoms which otherwise react with O₂ via



Since CO oxidation mainly occurred in the reaction with OH radicals



which are mostly produced in reaction (4), the rate of reaction (3) actually controlled the rate of CO oxidation in the burnout zone when Na-containing species were present.

Review of the literature data showed that reaction (3) had not been studied extensively. Available information on the rate coefficient of reaction (3) at high temperatures is limited to flame measurements by *Jensen and Jones, 1982* (Figure 7-19). *Perry and Miller, 1996* gave an estimate of the rate coefficient of reaction (3) $5.0 \times 10^{13} \text{ cm}^3 \text{ mol}^{-1} \text{ s}^{-1}$ which is larger than experimentally reported by *Jensen and Jones, 1982* value. Our modeling shows that reasonable agreement with experimental data on CO emissions can be achieved if the rate coefficient of reaction (3) is equal to $1.0 \times 10^{14} \text{ cm}^3 \text{ mol}^{-1} \text{ s}^{-1}$.

Figure 7-20 shows comparison of modeling predictions with experimental data on CO emissions. An increase in NO_x reduction on this plot is achieved by injection of N-agent at NSR = 1.5 and Na promoter (0 – 200 ppm). Adjustment of the rate coefficients of reactions (2) and (3) resulted in significant improvement of the agreement between modeling predictions and experimental data. Although modeling results and experiments still do not agree quantitatively, modeling qualitatively describes the main features of the process.

Modeling predicts that CO emissions in the presence of NH₃ and Na additives depend on flue gas temperature at the point of OFA injection. Figure 7-21 shows that a decrease in this temperature results in an increase in CO emissions. Since OFA and the flue gas have different temperatures before mixing, the mixing area in the OFA zone is characterized by non-uniform temperature distribution and significant temperature fluctuations. This is the most likely reason why modeling predictions and experimental data do not agree quantitatively.

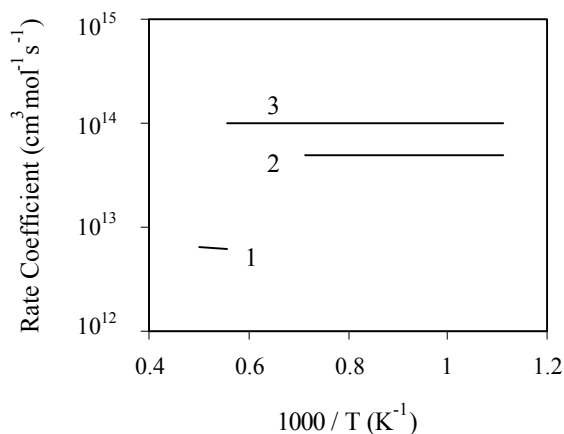


Figure 7-19. Rate coefficient of the reaction $\text{NaOH} + \text{H} \rightarrow \text{Na} + \text{H}_2\text{O}$. 1 – *Jensen and Jones, 1982* measurements, 2 – *Perry and Miller, 1996* estimate, 3 – this work.

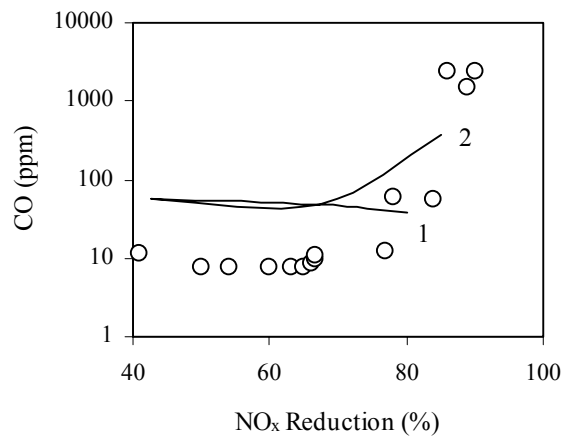


Figure 7-20. Comparison of modeling predictions (lines) with experimental data (symbols) on CO emissions at 10% reburning. OFA is injected at 1300 K. 1- modeling with default k_2 and k_3 , 2 – modeling with k_2 and k_3 adjusted.

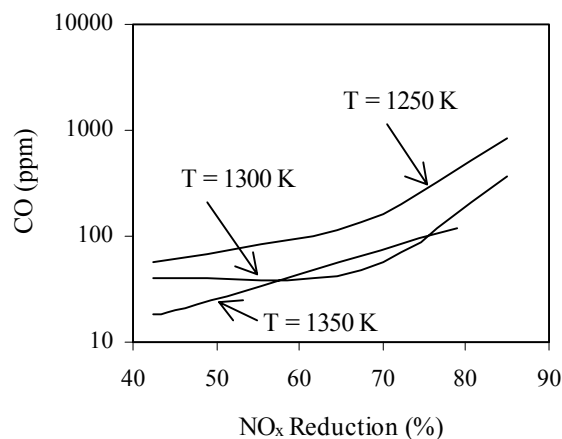


Figure 7-21. CO emissions in the AR process as a function of flue gas temperature at the point of OFA injection. Test conditions are the same as in Fig. 7-20.

To avoid high CO emissions, OFA has to be added at temperature higher than 1300 K. Figure 7-21 shows that an increase in OFA injection temperature results in a decrease in CO emissions in the AR process.

7.2 Injection of Promoters without N-Agent

Effect of Promoters on NO_x Emissions

Tests (Section 6.2.1) showed that injection of metal-containing compounds without N-agent into the main combustion or reburning zones resulted in NO_x reduction. The mechanism of this effect can be understood via kinetic modeling.

Since tests showed that Na had a significant effect on NO_x reduction in all tested configurations, and since the mechanism of Na₂CO₃ decomposition and reactions of Na-containing species are readily available (*Zamansky et al., 1999*), modeling work was conducted to describe to predict the effect of Na₂CO₃ injection on NO_x reduction. All three configurations used in tests (injection with main and reburning fuels, and into reburning zone) were considered in modeling.

The reduction of NO_x in the presence of Na-containing compounds can be explained by heterogeneous processes, reactions in the gas phase, or a combination of these two mechanisms. It was shown in Phase I that at temperatures higher than 1000 K Na₂CO₃ in the presence of water quickly decomposes to form NaOH(g) and CO₂. Thermodynamic calculations conducted with utilization of NASA equilibrium code (*McBride and Gordon, 1993*) also suggest that at temperatures relevant to the reburning process most Na is present in the gas-phase in the form of NaOH(g) (about 90% of the total Na) and in the atomic form Na(g). Thus, it is unlikely that any solid Na-containing species are present in a significant amount in flue gas at reburning conditions. Based on Phase I results and thermodynamic calculations, it was assumed in modeling that the homogeneous mechanism of NO_x reduction by Na-containing species was dominant.

Effect of Na on NO_x Reduction in the Main Combustion Zone

Experiments demonstrated that injection of Na with the main fuel in the absence of reburning reduced NO_x emissions by about 20%. Combustion in the main combustion zone is a complex process which is strongly affected by gas dynamic processes within combustion chamber. However, *chemistry* aspects of the effect of Na on NO_x formation and destruction in flame can be understood by isolating mixing effects from chemical kinetics. The main combustion zone in modeling was represented by a well-stirred reactor. The mixture entering the reactor corresponded to the methane–air mixture with SR = 1.15. It is known that the composition of products coming from well-stirred reactor depends on the reactor residence time. Thus, results of modeling are sensitive to the residence time. The residence time adopted in the model for the main combustion zone was 10 ms. Based on flame observations in the BSF main combustion zone, this time is believed to be representative of the residence time in the flame. While uncertainty in the value of the residence time in modeling affects the absolute value of the effect of Na on NO_x reduction, the chemical mechanism of the effect stays the same.

Modeling suggested that the effect of sodium additives on NO_x concentration in the main combustion zone could be explained as follows. Addition of sodium carbonate into the main combustion zone results in its fast decomposition and reaction with water to form sodium hydroxide, NaOH, CO₂ and sodium atoms. It is known (*Babushok et al., 1998*) that sodium-containing compounds are strong inhibitors of the combustion process. The suppression of flame occurs through the sequence of reactions in which active species are removed. Modeling (*Schofield and Steinberg, 1992*) suggested that the removal of radicals in flames could occur through the following chain reaction



The net action of sodium species in reactions (3), (6) and (7) is equivalent to the conversion of H atoms and OH radicals into H₂O.

Modeling predicted that concentrations of active species in the combustion zone decreased as a result of Na addition with the main fuel. For example, concentrations of oxygen and hydrogen atoms decrease in the presence of 100 ppm Na by 40% and 50% respectively. Since NO_x formation via thermal and fuel-NO mechanisms strongly depends on the local combustion environment, reduction in concentrations of major radicals results in decrease of NO_x concentration. Figure 7-22 shows a comparison between modeling predictions and experimental data for Na injection into the main combustion zone without reburning (“Na only” bars). Overpredicting the efficiency of NO_x reduction can be caused by several factors. The first factor is that well-stirred reactor does not give an exact representation of the main combustion zone. Particularly, a diffusion flame is formed in the main combustion zone, while in the model fuel and air are assumed premixed. Effect of turbulence on NO_x formation is not taken into account in the model either. Additionally, the residence time in the reactor can be different from 10 ms adopted in the model.

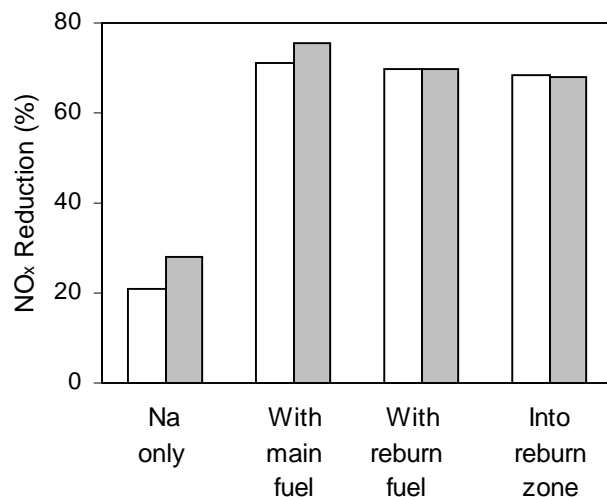


Figure 7-22. Comparison of modeling predictions with experimental data on the effect of Na₂CO₃ injection in BSF at 18% reburning. Open bars represent experimental data, shaded bars modeling.

Effect of Na on NO_x Reduction in the Reburning Zone

The effect of Na on NO_x reduction for the reburning configuration when additive is injected with the main fuel in the presence of reburning can be divided into two parts. First, Na reduces NO_x formation in the main combustion zone via the mechanism described in previous section. Second, Na reduces NO_x emissions in the reburning zone by affecting reburning chemistry.

Modeling suggested that sodium additives decreased NO_x concentration in the reburning zone by decreasing oxidation rate of the reburning fuel. The presence of sodium resulted in a decrease of radical concentrations in the reburning zone. It was observed in modeling that the reburning fuel was oxidized during the early part of the reaction with and without sodium addition. However, in the presence of sodium, the fuel was oxidized over a longer period of time. Fuel oxidation generated hydrocarbon-containing radicals which reduce NO to N₂. At the same time, the hydrocarbon

radicals reacted with other non-carbon atoms and radicals (H, OH, O etc.) and were transformed into other products. In the presence of sodium, the concentration of non-carbon radicals was smaller, reaction rates of hydrocarbon radicals with non-carbon radicals decreased that resulted in a higher rate of the reaction of hydrocarbon radicals with NO. Thus, modeling suggested that the effect of sodium addition could be explained by the removal of non-carbon radicals in the presence of sodium species via reactions (3), (6) and (7).

Additive co-injection with the reburning fuel was more effective than injection into reburning zone downstream of the reburning fuel because in the latter case by the time the additive evaporates and mixes with flue gas most reburning fuel had been oxidized and most NO_x reduction in the reburning zone had already occurred.

Figure 7-22 compares experimental data and modeling predictions on the effect of sodium injection both along with the reburning fuel and into reburning zone downstream of reburning fuel on NO_x reduction. Modeling results demonstrate good agreement with experimental data for both locations of additive injection. Both modeling and experimental data suggest that the additive is most effective when added with the main fuel, whereas the addition along with the reburning fuel is slightly less effective. Injection of Na with the main fuel is the most effective because in this case the additive reduces NO_x concentration both in the main and reburning zones.

Effect of Na on CO Emissions

Modeling also qualitatively explained experimental results on increasing CO emissions in the presence of Na additives. Fuel oxidation in the reburning zone generates a significant amount of CO. For 18% reburning heat input, the concentration of CO at the end of the reburning zone is about 2.2%. The CO formed in the reburning zone is oxidized to CO₂ when OFA is injected to complete combustion. The temperature of OFA injection should be high enough to provide complete CO oxidation. Since Na acts as an inhibitor of the combustion process, it decreases concentrations of active species in the burnout zone, including H atoms and OH radicals. Reaction (3) has the largest effect on the rate of CO oxidation among reactions of Na-containing species. This reaction inhibits the oxidation process by removing H atoms which otherwise would react with O₂ via



Since CO oxidation mainly occurs in the reaction with OH radicals



which are mainly formed in reaction (4), reaction (3) slows down the CO oxidation resulting in higher CO emissions. This mechanism is similar to that suggested in *Section 7.4.1* to explain the combined effect of N-agent and Na injection on CO emissions.

Quantitative description of experimental results on CO emissions is difficult within the framework of the adopted model since it does not take into account non-uniformity of temperature distribution in the BSF. Non-homogeneity of the temperature field in the burnout zone and incompleteness of mixing are the main reasons of CO emissions in tests even without additives. To avoid high CO concentrations in flue gas, OFA has to be added at temperatures higher than 1300 K.

7.4 Chemistry-Mixing Modeling of Ammonia and Sodium Effects: Summary

In summary, the developed kinetic model of AR correctly represents the major trends observed in experiments. It predicted that co-injection of N-agent with Na-containing promoter resulted in increase of NO_x reduction.

Modeling also demonstrates that small addition of Na-containing compounds increases the efficiency of NO_x control in combustion and reburning. While contribution of heterogeneous reactions to NO_x reduction in the presence of Na-containing additives can not be eliminated, the thermodynamic data suggest that most Na at the reburning conditions is present in the gas-phase. This makes the suggested homogeneous mechanism the most likely explanation of the effect of Na on NO_x reduction. The Na additives remove active combustion species (H and OH) via chain reaction and, thus, reduce the rate of NO formation in the main combustion zone. The increase in NO_x reduction in the reburning zone is due to slower oxidation of the reburning fuel in the presence of Na.

7.5 Optimization of AR via Modeling

Pilot scale experimental data on different AR systems demonstrate that these technologies can provide over 90% NO_x reduction while firing natural gas and coal. Each AR technology installation on a boiler will require practical expertise and intensive computer modeling to determine the most efficient process parameters such as the amount of the reburning fuel, the amount and location of N-agent injection, spray characteristics, etc. Since the efficiency of AR depends on many factors, the best performance can be achieved if the effects of these factors on the process performance are well determined and understood. The most efficient approach to the AR optimization is to explore the effects of different parameters on NO_x reduction via kinetic modeling, using the model for guidance to select the most effective test conditions, and then to optimize the technology in pilot- and full-scale combustion facilities. Thus, the kinetic model is an important tool in the development of AR technologies.

Modeling results reported in previous sections demonstrated that modeling based on a detailed chemical mechanism with a simplified representation of mixing can be used not only to explore the chemistry of the reburning and AR processes, but to identify ranges of process parameters that give the optimum process performance. The following sections describe further development of the AR model to describe the effect of N-agent injection on NO_x reduction. Modeling efforts concentrated on the description of the AR-Lean process since AR-Lean is seen as one of the most commercially attractive options because the N-agent is injected along with the OFA and thus does not require installation of additional ports.

7.5.1 AR-Lean Model Setup

The model of AR-Lean treats the reburning process as series of five plug-flow reactors (Figure 7-23). Each reactor describes one of the physical and chemical processes occurring in a boiler: addition of the reburning fuel, NO_x reduction as a result of the reaction with the reburning fuel, addition of OFA and N-agent, and NO_x reduction by N-agent and oxidation of partially oxidized products in the burnout zone. The first reactor describes mixing of the reburning fuel with flue gas. As was suggested earlier (*Section 7.1*), the mixing zone was divided into two reactors *R1a* and *R1b*. The reactor *R1a* was assigned with more fuel-rich mixture than average, the reactor *R1b* with a less

fuel-rich mixture. Averaging fuel contents distributed between the two reactors gave a mixture composition corresponding to the total amount of added reburning fuel. The model of inverse mixing was applied to both reactors *R1a* and *R1b*. The reburning fuel entering reactors *R1a* and *R1b* corresponds to natural gas. The mixture added to reactors *R1a* and *R1b* corresponds to products of natural gas combustion in air at a stoichiometric ratio (SR) = 1.1 in the main combustion zone. The flue gas was added to the reburning fuel at a constant rate over period of 120 ms. The second reactor *R2* described reactions in flue gas downstream from the mixing area up to the point where OFA and N-agent were injected. The reburning fuel and flue gas were uniformly mixed entering the second reactor. The third reactor *R3* described mixing of OFA and N-agent with flue gas using the model of inverse mixing. The mixture entering *R3* consisted of air and N-agent. It was assumed that N-agent and OFA were premixed prior to injection. The gas added to *R3* corresponds to products coming out of *R2*. The fourth reactor *R4* described reactions in the burnout zone.

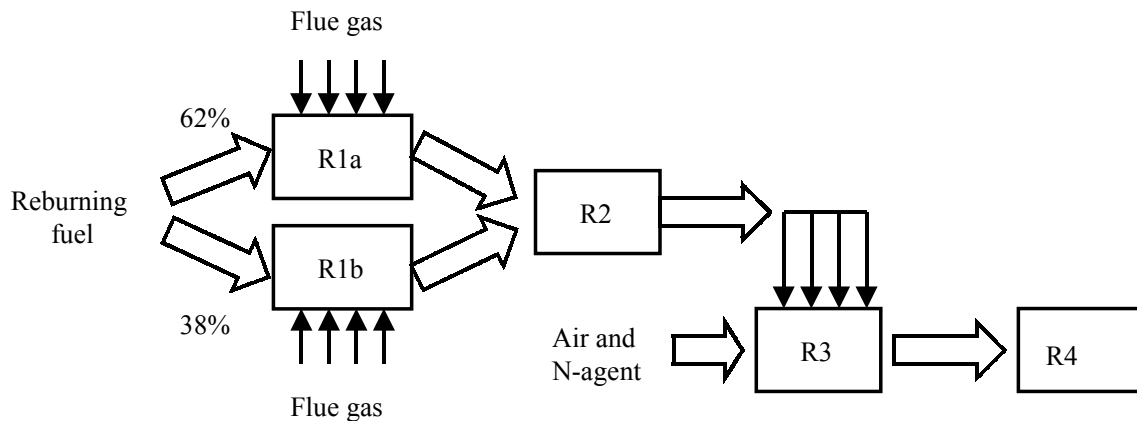


Figure 7-23. Reactor diagram of AR-Lean model setup.

7.5.2 Model Validation

Results presented in *Section 7.2* demonstrated that the model of basic reburning predicted the main trends of the reburning process. NO_x reduction efficiencies determined in experiments as functions of the initial NO_x amount, the amount of the reburning fuel and OFA injection temperature were well-described by the model. The AR-Lean model was validated based on experiments on co-injection of aqueous NH_3 and urea with OFA. The experimental data were obtained in the BSF.

The following parameters were varied in modeling:

- The amount of the reburning fuel (0-18% of the total fuel).
- Temperature at which OFA and N-agent are injected (1200-1500 K).
- Initial temperature of OFA and N-agent (300-600 K).
- Evaporation time of aqueous N-agent (urea).
- The amount of the N-agent.

Figures 7-24 and 7-25 show comparison of modeling predictions with experimental data at NSR = 1.5. Figure 7-24 shows that modeling describes main features of the AR-Lean process. At small reburning fuel heat inputs, the dependence of the process efficiency on the OFA/N-agent injection temperature is similar to that of SNCR. Modeling well predicts the maximum efficiency for 2%

reburning, and underpredicts and overpredicts efficiencies correspondingly at lower and higher than optimum temperatures. At 10% reburning, the optimum in the process performance occurs at 1100-1150 K (too low temperature for industrial applications).

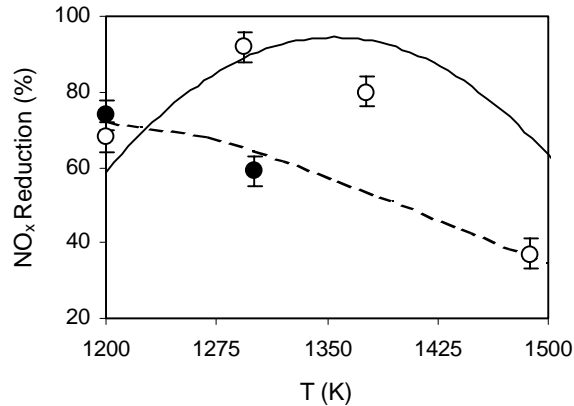


Figure 7-24. Comparison of modeling predictions (lines) with experimental data (symbols) on the effect of OFA/N-agent injection temperature on NO_x reduction in AR-Lean at 2% (open circles and solid line) and 10% reburning (filled circles and dashed line).

Figure 7-25 demonstrates good agreement between modeling predictions and experimental data for basic reburning and AR-Lean processes at an OFA injection temperature of 1300 K (this temperature was found in tests to give the highest AR-Lean efficiency). For less than 6% reburning fuel the efficiency of NO_x reduction is 90-94% and is insensitive to the amount of the reburning fuel. As the amount of the reburning fuel increases, the efficiency of the process decreases.

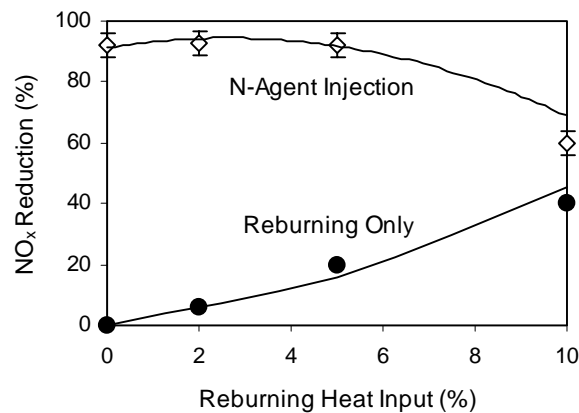


Figure 7-25. Comparison of modeling predictions (lines) with experimental data (symbols) on basic reburning (filled circles) and AR-Lean reburning (open circles).

Comparison of modeling predictions with experimental data for other conditions also demonstrated that the model of AR-Lean gave a realistic description of experimental data. This

confirmed that the mixing and kinetic submodels adequately described these processes and the model could be used to study the effects of different parameters on trends in AR-Lean performance.

7.5.3 Parametric Study of the AR-Lean Process

Since the efficiency of AR-Lean depends on many factors, the best performance can be achieved if the effects of these factors on the process performance are well determined and understood. The following sections describe results of a modeling study on the effect of the AR-Lean parameters on NO_x reduction.

Effect of CO on NO_x Reduction

Fuel fragments, such as CO and H_2 , formed in the reburning zone can significantly affect NO_x reduction by N-agent (Zamansky *et al.*, 1997; Alzueta *et al.*, 1997). However, previously it was difficult to determine this effect quantitatively since predictive model of AR-Lean has not been developed. The current model of AR-Lean has such quantitative predictive capabilities.

Figure 7-26 shows the predicted effect of CO on NO_x reduction by urea injection. In these calculations urea and air were injected into flue gas containing 600 ppm NO, 8% CO_2 , 16% H_2O , balance N_2 . The concentration of O_2 after injection was 1.7%. The amount of CO in flue gas was varied in modeling from 0 to 1%. The mark "10% reburning" on x -axis indicates the amount of CO coming from the reburning zone at 10% reburning fuel. At 1500 K OFA/N-agent injection temperature, CO inhibits NO_x reduction, while at 1200 K the presence of small amount of CO in flue gas promotes NO_x reduction.

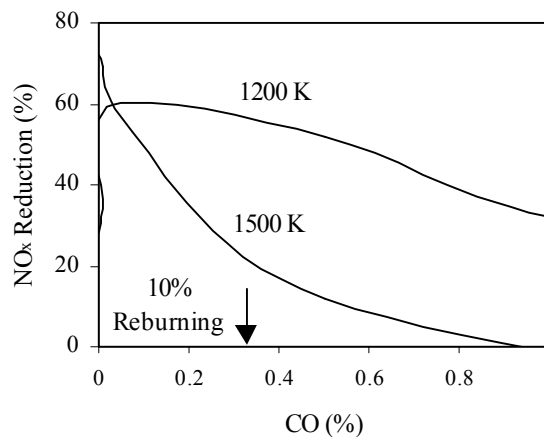
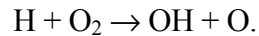
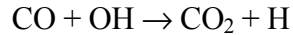


Figure 7-26. Effect of CO on NO_x reduction by urea injection. NSR = 1.5.

The relative effect of CO at 1200 K also depends on the amount of CO: small amounts of CO significantly promote NO_x reduction, while CO concentrations on the level of 0.05-1% decrease NO_x reduction. Thus, CO can increase or decrease the efficiency of the AR-Lean process depending

on the temperature at which OFA and N-agent are injected, and on CO concentration. At high temperatures, which are characterized by high concentrations of active species in flue gas, the CO oxidation reduces the efficiency of N-agent by competing for radicals with reactions of NO reduction. At low temperatures, the concentrations of active species in flue gas are much smaller, and the CO oxidation produces radicals via chain reaction



A similar observation was reported by *Leckner et al., 1991* for the effect of CO on Selective Non-Catalytic Reduction Process.

The following conclusion can be derived from modeling: for high efficiency NO_x control via AR-Lean, the CO concentration in flue gas entering the burnout zone has to be regulated.

Effect of Reburning Heat Input

Since the amount of CO present in flue gas at the point of OFA injection depends strongly on the amount of fuel injected in the reburning zone, the efficiency of the N-agent also depends on heat input of the reburning fuel. In basic reburning, efficiency of NO_x reduction increases as the amount of the reburning fuel increases. It also slightly increases as the temperature of flue gas at the point of OFA injection decreases. The situation is quite different when N-agent is co-injected with OFA (Figure 7-27). Modeling predicts that at an OFA/N-agent injection temperature of 1200 K, AR-Lean is more effective than basic reburning for reburning fuel heat inputs under 17%. The amount of CO entering the burnout zone for heat inputs less than 17% is relatively small. A small amount of CO enhances NO_x reduction at low temperatures. Since the concentration of CO coming from the reburning zone becomes higher as the amount of reburning fuel increases, the efficiency of AR-Lean becomes smaller than that of basic reburning at 18% reburning fuel. Modeling predicts that the concentration of CO in flue gas at 18% heat input of the reburning fuel is approximately 2.3%. At 1200 K, this amount of CO has an inhibiting effect on NO_x reduction.

At injection temperature of 1500 K AR-Lean is more effective than basic reburning for heat inputs less than 9%. As the amount of the reburning fuel increases in the range 0-5%, the combined effect of NO_x reduction in the reburning and burnout zones exceeds that of reburning only. However, as concentration of CO in flue gas entering the burnout zone increases at larger heat inputs, NO_x reduction decreases. This is because at high temperatures even small concentrations of CO inhibit NO_x reduction (Figure 7-26). High concentrations of H₂ in flue gas coming from the reburning zone also contribute to the degradation of AR-Lean performance at large reburning fuel heat inputs. Modeling suggests that the AR-Lean process is more effective than basic reburning at reburning fuel quantities smaller than those usually utilized in basic reburning (15-20%). Figure 7-28 supports these conclusions by demonstrating that AR-Lean at 5% reburning is predicted to be more effective than 10 and 18% reburning at practically all OFA injection temperatures. However, these modeling results are obtained under assumption that the evaporation time of N-agent is less than mixing time in burnout zone. The effect of N-agent evaporation time on NO_x reduction will be discussed in the following section.

Thus, the AR-Lean process can provide higher levels of NO_x reduction than basic reburning, and it also requires less reburning fuel. Modeling suggests that the efficiency of the AR-Lean process depends on the amount of the reburning fuel and OFA/N-agent injection temperature. The

amount of the reburning fuel determines the composition of flue gas entering the burnout zone. Among the species present in flue gas, CO has the strongest effect on the efficiency of N-agent. The larger the amount of the reburning fuel, the more CO is present in flue gas by the end of the reburning zone. Figure 7-27 implies that at high OFA/N-agent injection temperatures the presence of CO in flue gas decreases the efficiency of N-agent. At low OFA/N-agent injection temperatures, CO increases NO_x reduction by N-agent.

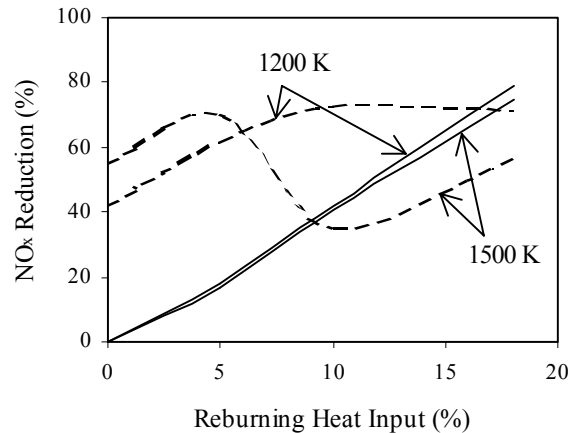


Figure 7-27. Predicted effect of the reburning heat input on NO_x reduction at different OFA injection temperatures. Solid lines correspond to basic reburning, dashed lines to AR-Lean. NSR = 1.5.

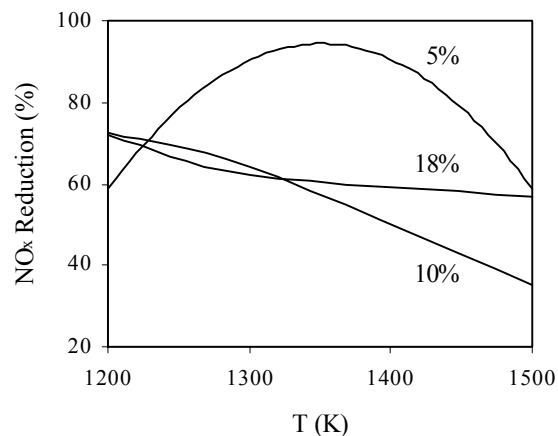


Figure 7-28. Predicted effect of OFA/urea injection temperature in AR-Lean.

Effect of N-Agent Evaporation Time

To reduce influence of CO on NO_x reduction at large reburning fuel heat inputs, the N-agent can be injected with a delay (as it is done in Reburning + SNCR), or injection can be arranged in such a way that the release of N-agent into the gas phase occurs over longer period of time. The later can be done, for example, by injecting large droplets of aqueous solution containing N-agent. Because

of the longer time required for large droplets to evaporate and mix with flue gas, N-agent will be delivered to the flue gas with some delay. Both approaches result in N-agent entering flue gas after air and flue gas are already mixed and thus allow for most of the CO to be oxidized before N-agent reacts with NO_x .

Estimates of droplet evaporation time for the conditions of the BSF tests show (*Attachment F*) that this time is smaller than the OFA mixing time. Droplet evaporation time can be increased by increasing droplet size, or by varying spray angle.

Figure 7-29 shows the effect of droplet evaporation time on NO_x reduction by urea at an OFA/N-agent injection temperature of 1500 K. As the evaporation time increases, the efficiency of the AR-Lean process also increases. At longer evaporation times the dependence becomes less prominent since at 1500 K most of the CO is oxidized within first 200 ms.

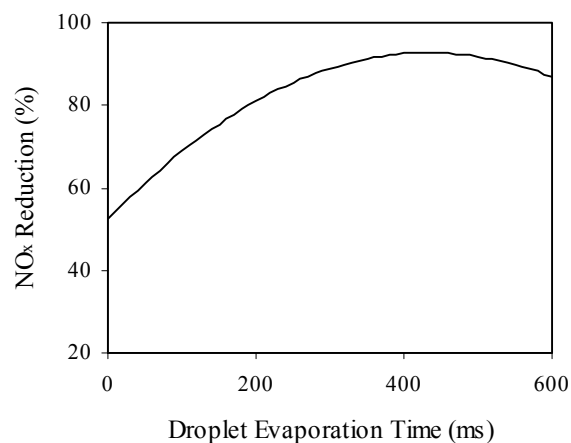


Figure 7-29. Effect of droplet evaporation time on NO_x reduction. 10% reburning, $[\text{NO}]_i = 600$ ppm, OFA/urea are injected at 1500 K. NSR = 1.5.

Figure 7-30 compares predicted effects of N-agent evaporation time on NO_x reduction at 5% and 10% reburning. At evaporation times smaller than mixing time in OFA zone, the maximum in NO_x reduction at 10% reburning occurs in the temperature range 1150-1200 K and at 1300 K at 5% reburning. As evaporation time increases, the maximum shifts toward higher temperatures. The maximum NO_x reduction slightly decreases at longer evaporation times. Figure 7-30 demonstrates that by regulating evaporation time of N-agent, it is possible to achieve high levels of NO_x reduction at larger amounts of the reburning fuel at temperatures that can be utilized in large-scale combustion facilities. This approach can result in higher levels of NO_x reduction since larger amounts of the reburning fuel provide higher levels of NO_x reduction before injection of N-agent.

Thus, the modeling results suggest that utilization of droplets of larger size increases the efficiency of AR-Lean process at large heat inputs of the reburning fuel and practically does not affect efficiency of the process at small heat inputs.

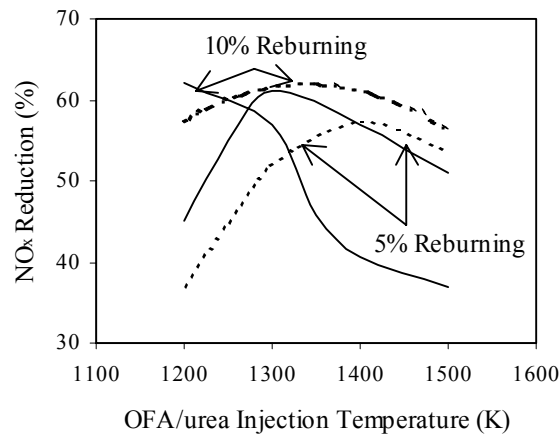


Figure 7-30. Predicted effects of urea droplet evaporation time on NO_x reduction at 10% and 5% reburning. Solid lines correspond to evaporation time smaller than mixing time of OFA, dashed lines correspond to 380 ms evaporation time. $\text{NSR} = 0.7$.

Effect of the Amount of N-Agent

Figure 7-31 shows the predicted effect of the amount of urea on NO_x reduction under conditions found in experiments and modeling to give the highest level of NO_x reduction (OFA/N-agent injection temperature = 1300 K, 5% reburning). It is assumed that evaporation time of the N-agent is smaller than the OFA mixing time in the burnout zone. Modeling shows that efficiency of NO_x reduction increases as the amount of N-agent increases in the range $\text{NSR} = 0 - 1.5$. The dependence of NO_x reduction on the amount of N-agent at $\text{NSR} > 1.5$ is not strong.

Modeling thus demonstrates that the amount of N-agent co-injected with OFA is an important parameter that can affect the efficiency of NO_x reduction.

Effect of the Initial OFA/N-Agent Injection Temperature

Figure 7-32 demonstrates the effect of the initial OFA/urea injection temperature on NO_x reduction. The initial OFA/urea injection temperature is defined here as temperature of the OFA/urea mixture prior to injection into flue gas. Preheating OFA results in decrease of NO_x reduction efficiency. This effect does not depend on the temperature of flue gas at the point of OFA injection. The main reason for the negative impact of elevated initial temperatures of OFA on NO_x reduction is that the increase in OFA initial temperature results in decreased mixing time of OFA and flue gas according to jet in crossflow model. As mixing time in the burnout zone decreases, the efficiency of the process also decreases. For example, modeling shows that as the initial temperature of OFA increases from 300 K to 600 K, the mixing time decreases from 120 ms to 80 ms and NO_x reduction at 10% reburning decreases on average by 10 percentage points.

This conclusion is similar to observations made for basic reburning: the efficiency of the basic reburning process for small heat inputs of the reburning fuel does not depend significantly on the initial temperature of OFA and slightly decreases with increase in OFA initial temperature for large heat inputs of the reburning fuel.

Modeling thus suggests that the initial temperature of OFA/N-agent is not an important parameter in AR-Lean.

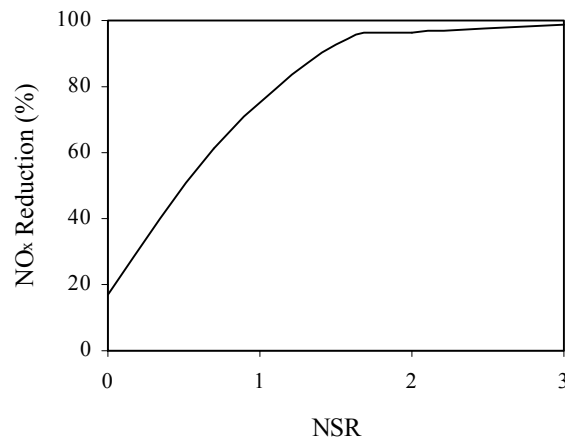


Figure 7-31. Predicted effect of the amount of urea on NO_x reduction. 5% reburning, OFA/urea injection temperature 1300 K.

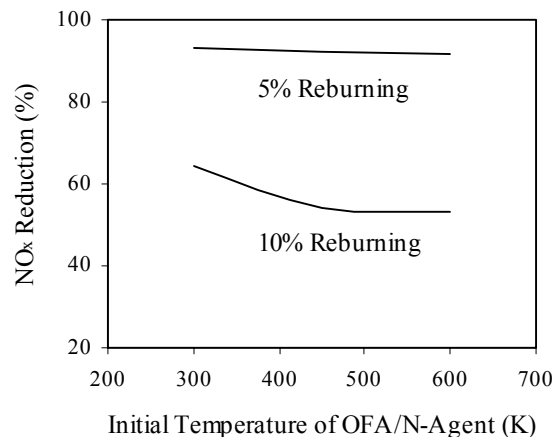


Figure 7-32. Predicted effects of OFA and urea initial temperature on NO_x reduction. OFA and urea are injected at flue gas temperature 1300 K. NSR = 1.5.

7.5. Mapping of the AR Process

As it was demonstrated earlier in this Section, the AR model correctly describes the main features of the process observed in experiments. This allows use of the model to optimize AR to obtain the best possible performance. Because of the model limitations (mostly due to simplified representation of mixing), this approach can hardly be used to determine exact values of parameters (for example, the amount of the reburning fuel and N-agent, temperature of flue gas at the point of N-agent injection, etc.) that result in the best performance. However, the model can determine ranges of these parameters that are required for the best performance. The guidance of the model then can be used for experimental optimization of the AR technology.

The developed model of the AR process incorporates some features that are specific for the BSF. For example, mixing time in the reburning and OFA zones were estimated using characteristics of nozzles utilized in the BSF. Modeling also took into account temperature profile measured in the BSF. Other combustion facilities have different thermal and mixing characteristics, and this may result in different optimum conditions for AR. However, differences in the process characteristics can be taken into account by adjusting appropriate parameters in the model to optimize AR for a specific facility.

The following sub-sections describe how the proposed approach can be used to “map” the AR process. “Mapping” is defined here as creation of diagrams that show efficiency of NO_x reduction as a function of two parameters while other parameters are kept constant. Such diagrams can be used to identify effective ranges of process parameters. They also can be used to estimate the maximum level of NO_x reduction that can be achieved at optimum conditions in a particular facility.

This mapping approach was used to determine the effects of several process parameters on performance of AR-Lean. The following parameters were considered:

- The amount of the reburning fuel.
- Temperature of flue gas at the point of OFA/N-agent injection.
- Evaporation time of the N-agent.
- The amount of N-agent.
- Initial temperature of OFA/N-agent.

Modeling predicted that selection of these parameters in the optimum range resulted in the efficiency of the AR-Lean process in BSF as high as 90+%. It also showed that some of the parameters could be excluded from consideration since their variations have small or negative impact on NO_x reduction. For example, it was shown that preheating of OFA and N-agent results in degradation of the AR-Lean performance (Figure 7-32). Thus, minimum available initial temperature of OFA gives the best process performance. Modeling also identified optimum range for the amount of N-agent (Figure 7-31). Assuming that the amount of N-agent is in this range (for example, NSR = 1.5), the remaining parameters of interest are amount of the reburning fuel, temperature of flue gas at the point of OFA/N-agent injection and evaporation time of N-agent.

Experimental data on AR-Lean that were used for the model development were obtained at constant N-agent spray characteristics. Thus, evaporation time of N-agent was not a test variable. To enable comparison of model predictions with experimental data, the mapping of AR-Lean at NSR = 1.5 was limited to two parameters only: the amount of the reburning fuel and temperature of flue gas at the point of OFA/N-agent injection. It was assumed in modeling that evaporation of N-agent was fast and occurred within time scale of the mixing process in OFA zone. This assumption was made based on estimation of droplet evaporation times for typical BSF conditions. The effect of N-agent evaporation time on NO_x reduction will be considered in a latter section.

Fast Evaporation of N-Agent

At NSR=1.5 a series of modeling runs were conducted to determine the effects of the amount of reburning fuel and the temperature of flue gas at the point of OFA/N-agent injection on AR-Lean NO_x reduction (Figure 7-33). The amount of reburning fuel varied from 0 to 10% of the total heat input. For each amount of reburning fuel, the OFA/N-agent injection temperature varied from 1200 K to 1650 K. The experimental data are shown in Fig. 7-33 as symbols. Comparison of modeling predictions with experimental data shows agreement for a wide range of conditions. The first region with high NO_x reductions identified by modeling corresponds to the amount of the reburning fuel in the range 0-6%, and OFA/N-agent injection temperatures about 1280-1350 K. Modeling suggests (and is confirmed by experiments) that the efficiency of NO_x reduction in this region is about 90-95%.

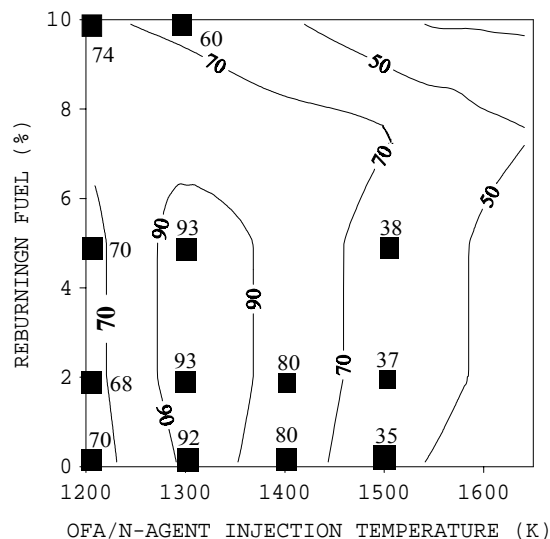


Figure 7-33. Performance of the AR-Lean process at NSR=1.5. Lines represent calculations, symbols experimental data. Numbers indicate levels of NO_x reduction. Evaporation time of the N-agent is less than OFA mixing time.

As the amount of reburning fuel increases over 6%, the amount of CO coming from the reburning zone becomes significant. Since the optimum temperature range for reaction of N-agent and NO in the presence of CO shifts toward lower temperatures, an increase in AR-Lean performance occurs at higher than 6% reburning fuel for OFA/N-agent injection temperatures less than 1300 K (the second region of high NO_x reduction). At 10% reburning, the optimum OFA/N-agent injection temperatures are lower than 1200 K.

Modeling predicts (and experiments confirm) that due to effective mixing, the efficiency of the SNCR process in BSF at 1300 K and NSR=1.5 is very high (over 90% NO_x reduction at reburning fuel equals zero in Figures 7-25 and 7-33). Therefore, increasing the amount of reburning fuel up to 6% does not significantly improve NO_x reduction. However, in full-scale installations, non-uniformity of the temperature profile, difficulties in mixing the N-agent across the full boiler cross section, and limited residence time for reactions limit effectiveness of SNCR to 30-50%. Some amount of N-agent passes through the system and appears as ammonia slip. Under such mixing conditions, the efficiency of the AR-Lean process may depend more strongly

on the amount of reburning fuel. One way to simulate poor mixing of N-agent with flue gas is to reduce the amount of N-agent to the level that provides 40-50% NO_x reduction, reflecting the N-agent available to react. Thus, it is of practical interest to study AR-Lean at NSR less than 1.5.

Figure 7-34 shows performance of the AR-Lean process at NSR=0.7. The maximum NO_x reduction in the SNCR process (no reburning fuel), predicted by modeling, is 54%. Modeling results show that at 1300 K (close to optimum temperature for OFA/N-agent injection) the efficiency of AR-Lean process first increases as the amount of the reburning fuel increases, and then decreases. The maximum NO_x reduction predicted by modeling is 62%, which is achieved at 5% reburning and is about 8 percentage points higher than the efficiency of SNCR under similar conditions.

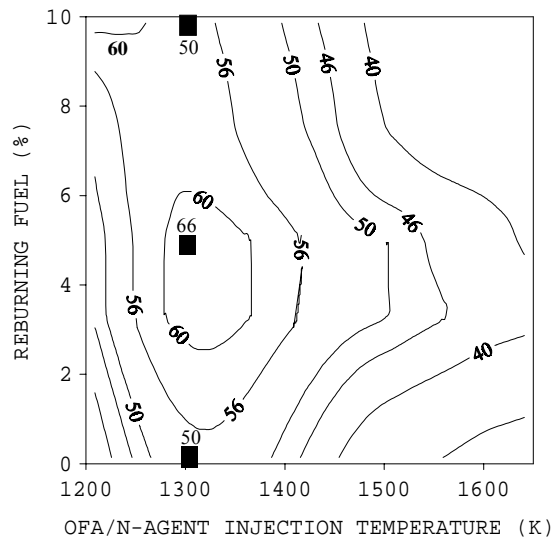


Figure 7-34. Performance of the AR-Lean process at NSR=0.7. Lines represent calculations, symbols experimental data. Numbers indicate levels of NO_x reduction. Evaporation time of the N-agent is less than OFA mixing time.

Based on modeling predictions, a series of tests were conducted in the BSF to determine the effect of the amount of reburning fuel on NO_x reduction in AR-Lean. Test results are shown in Figure 7-34 as symbols. Tests confirmed that maximum NO_x reduction at NSR=0.7 and 1300 K is achieved around 5% reburning fuel. Maximum reduction observed in tests was 66% - slightly higher than that predicted by modeling.

Thus when droplet evaporation time is smaller than mixing time of OFA in the burnout zone (N-agent is injected as a gas or as small droplets), the AR-Lean process is most efficient at about 5% reburning fuel and OFA/N-agent injection temperatures in the range of 1280-1350 K.

The second region of high NO_x reduction identified by modeling for NSR=0.7 is located at 10% reburning fuel and an OFA/N-agent injection temperature of about 1200 K. Since in full-scale boilers OFA is usually injected at temperatures higher than 1200 K to achieve full burnout, this result can be considered as being mostly of theoretical interest. The occurrence of high NO_x reduction at relatively large reburning heat inputs and low OFA/N-agent injection temperatures is due to the fact that CO formed in the reburning zone interacts with NO_x/N-agent chemistry in the OFA zone. As a result, the optimum conditions for NO_x reduction are shifted toward lower temperatures.

Slow Evaporation of N-Agent

To reduce the influence of CO on NO_x reduction at large reburning fuel heat inputs, the injection of N-agent can be arranged in such a way that the release of N-agent into the gas phase occurs over a longer period of time. This can be done, for example, by injecting larger droplets of aqueous solution containing N-agent. This approach results in N-agent entering flue gas after the OFA and flue gas are already mixed and thus allows for most of the CO to be oxidized before N-agent reacts with NO_x.

Figure 7-35 shows the predicted performance of AR-Lean as functions of the amount of reburning fuel and evaporation time of N-agent at NSR=0.7. Temperature of flue gas at the point of OFA/N-agent injection is optimized with respect to NO_x reduction. Optimum temperatures increase from 1300 K at instantaneous evaporation of N-agent to 1500 K at droplet evaporation times close to 800 ms. Modeling predicts that injection of larger droplets of N-agent and utilization of larger amounts of the reburning fuel result in higher levels of NO_x reduction. Figure 7-35 demonstrates that combining 18% reburning with N-agent injection results in about 80% NO_x reduction when droplets with an evaporation time of 100 ms or higher are used, while 5% reburning provides no more than 60% NO_x reduction at any droplet evaporation time. Figure F-3b (*Appendix F*) demonstrates that droplets larger than about 170 μm provide evaporation times longer than 100 ms at BSF conditions.

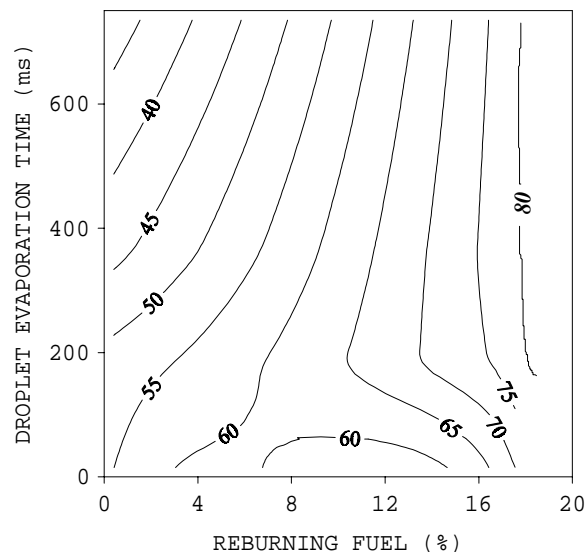


Figure 7-35. Performance of AR-Lean at NSR=0.7 as a function of the amount of the reburning fuel and droplet evaporation time of N-agent. Numbers indicate levels of NO_x reduction. Temperature of flue gas at the point of OFA/N-agent injection is optimized.

Injection of larger droplets of N-agent along with OFA is the equivalent of combining reburning with SNCR. Thus, performances of AR-Lean and Reburning+SNCR at optimum conditions should be similar. Note, however, that AR-Lean is much more attractive than Reburning+SNCR from a practical standpoint since no additional N-agent ports are required and OFA serves as the N-agent carrier (no flue gas recirculation required). Figure 7-36 compares predicted performances of basic reburning, AR-Lean and Reburning+SNCR at conditions (temperatures of flue gas at the point of N-agent injection and droplet evaporation times) that result in the highest optimized level of NO_x reduction. Figure 7-36 also shows AR-Lean performance for injection of

small droplets of N-agent (non-optimized AR-Lean). AR-Lean and Reburning+SNCR result in a significant increase in NO_x reduction in comparison with basic reburning. Figure 7-36 shows that by adjusting the N-agent injection temperature and droplet evaporation time, the efficiency of AR-Lean can be as high as the efficiency of Reburning+SNCR. Figure 7-36 also demonstrates the importance of optimizing droplet evaporation time in AR-Lean to achieve higher NO_x reduction at larger heat inputs of the reburning fuel.

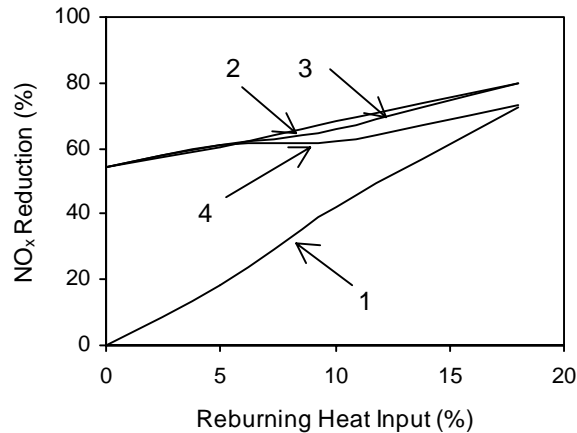


Figure 7-36. Predicted performances of basic reburning, AR-Lean and Reburning+SNCR. 1 – basic reburning, 2 – Reburning+SNCR, 3 – AR-Lean optimized, 4 – AR-Lean non-optimized. NSR=0.7.

7.5.5 AR-Lean Optimization: Summary

The model developed in this work describes major trends of AR and can be used for process optimization. Mixing and thermal parameters in the model can be adjusted depending on characteristics of the combustion facility. To demonstrate the optimization procedure, optimization of AR-Lean was conducted. The following AR-Lean parameters were identified as being most important: amounts of the reburning fuel and N-agent, temperature of flue gas at the point of OFA/N-agent injection, and evaporation time of the N-agent. Modeling predicts (and supported by experiments) that CO formed in the reburning zone increases the efficiency of N-agent at temperatures of OFA/N-agent injection lower than 1200 K and reduces its efficiency at higher injection temperatures. To reduce the negative effect of CO on NO_x reduction at temperatures of OFA/N-agent injection utilized in utility boilers, the average droplet size of injected N-agent solution has to be optimized to allow for CO oxidation in the burnout zone before significant amount of N-agent evaporates.

8.0 Task 2.4 Optimization of Process Synergism in 1 $\times 10^6$ Btu/hr Tests

The objective of this task was twofold: firstly, using pilot-scale tests to determine the optimum process conditions at mixing and thermo characteristics of a full-scale boiler and secondly, to evaluate coal as a reburning fuel. Task 2.4 included detailed pilot scale natural gas and coal firing tests at the BSF designed to evaluate the prospective promoters and mixing schemes, culminating in the final definition of optimum process conditions. The following sections describe results of these tests.

8.1 BSF Optimization Tests

This section discusses the BSF tests design to give better understanding of different AR components in a potential target boiler for the demonstration of AR technologies. Pilot scale tests were performed with the objective of simulating furnace conditions at the Greenidge boiler and defining the processes controlling AR performance. Tests focused on simulating the boiler AR-Lean and reburning + SNCR performance as the most promising AR variants for deep NO_x control for the Greenidge unit. The BSF heat extraction system was configured to simulate the temperature profile of the full-scale unit. The process parameters were varied to optimize NO_x reduction and to minimize byproduct emissions.

The unit is Greenidge Unit 4, which is owned and operated by New York State Electric and Gas (NYSEG). All of NYSEG's units are located within NEOTR and as a result are subject to Title 1 NO_x control requirements. NYSEG's compliance plan involved a system-wide daily cap on NO_x emissions. After considering a number of alternatives, NYSEG decided to utilize reburning and AR-Lean for NO_x control at Greenidge. GE-EER installed the gas reburning system as part of a commercial project with guaranteed performance. The upgrade to AR-Lean was conducted as a cooperatively funded demonstration project with the support of NYSEG and a number of co-funding organizations including the Electric Power Research Institute, Empire State Electric Energy Research Corporation, Gas Research Institute, Gaz de France, New York State Energy Research & Development Authority, and Orange & Rockland Utilities.

The following sections describe Greenidge AR system, experimental methods, and performance test results in BSF on AR-Lean and reburning + SNCR.

8.1.1 Description of Greenidge AR System

The Greenidge boiler is a tangentially fired boiler rated at 105 MWe with four burner packs located at the furnace corners. Each corner has four burners, totaling 16 burners. Figure 8-1 shows an overview of the advanced gas reburning system installed on the Greenidge boiler. The reburning fuel system consists of 16 gas injectors, with four injectors located at each corner a short distance above the burner pack. The furnace OFA system, which is used during gas reburning tests only, consists of four OFA ports, with one port located at each corner. The convective pass OFA system, which is used for advanced gas reburning, consists of a total of 10 ports; with five ports located on each sidewall at the convective pass cavity between the superheater and the reheater platens. Ammonia is injected along with OFA through the convective pass OFA ports. During 1996 parametric tests, ammonia was sprayed into two sidewall ducts upstream of the OFA openings via two individual spray nozzles located in the ducts. This spray system was tested during 1996

parametric tests and indicated maldistribution of ammonia among the East and the West OFA ports. In 1997, the spray system was modified using an individual spray nozzle in each port to provide flexibility in controlling splits among the ports and between each side of the boiler.

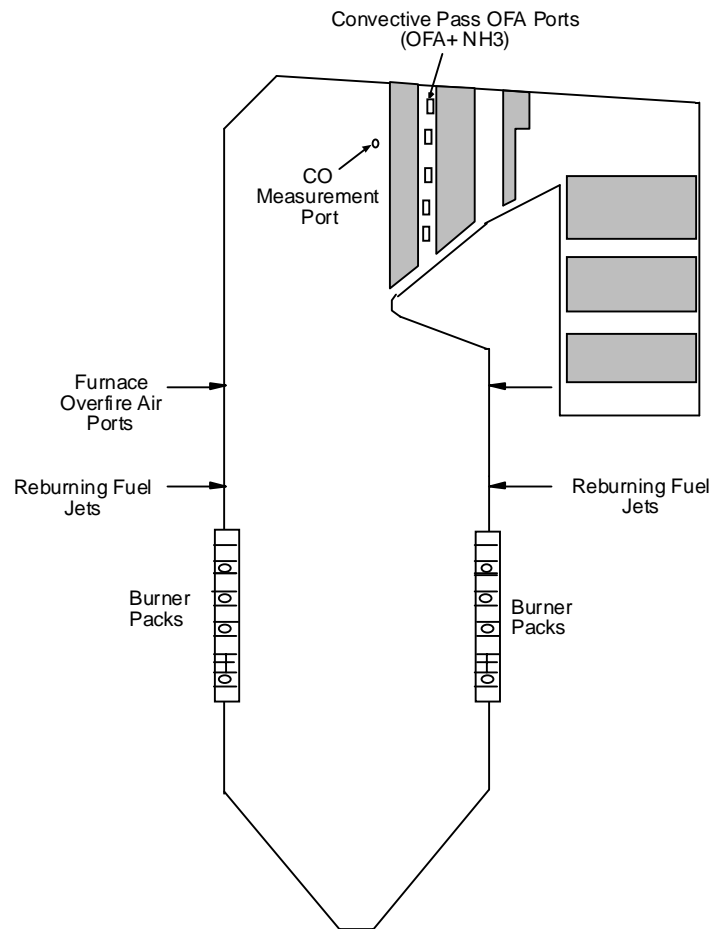


Figure 8-1. Overview of the advanced gas reburning system installed on the Greenidge boiler.

8.1.2 Simulation of Greenidge Boiler

The Greenidge boiler is characterized by upper furnace fluctuations in gas concentrations, and contains zones that have simultaneously high levels of CO and O₂ due to incomplete mixing. To evaluate and optimize AR process performance for Greenidge it was necessary to simulate these fluctuations along with boiler design features. To simulate boiler design, two cooling arrays were installed in the furnace of the BSF: one simulating the high temperature secondary superheater, which lowers gas temperature from 1450 K to 1340 K, and one simulating the reheater, which lowers gas temperature from 1280 K to 1170 K. Reburning fuel was injected upstream of the first cooling array. N-agent and OFA were injected between the two cooling banks. CEM sampling was performed at three locations: just upstream of the first cooling array, just downstream of the second cooling array, and in the convective pass.

To simulate the fluctuations in furnace gas composition that occur at Greenidge, a system was installed at the BSF to pulse the main natural gas. The fuel delivery system consisted of two lines. One carried the nominal main burner gas at a constant flow rate. The other carried 5% of the total

main fuel flow rate, and was pulsed from full-open to full-closed. The valve was open and closed for equal time periods. The system was designed to nominally provide square wave pulsations, although the compressibility of the gas affected this to some degree. An electronic timer and solenoid-actuated diaphragm valve were used for the pulsing. It was found that by varying the period of the pulsing it was possible to control the degree of unmixedness, thus providing control over furnace gas O₂ and CO concentrations. It was also found that CO emissions decreased across the three CEM ports due to progressive gas mixing. Actual time-averaged SR₂ values were determined by measuring all air flow rates and exhaust O₂ in the convective pass after burnout of most CO and performing a mass balance.

For the Greenidge simulation tests natural gas was used as both the main and reburning fuels. The reburning injector was elbow-shaped, and was installed along the centerline of the furnace, aligned in the direction of gas flow. Overfire air was injected through an elbow-shaped injector to burn out combustibles generated in the reburning zone. Gaseous ammonia was used as the N-agent. The N-agent was co-injected with the overfire air.

8.1.3 Baseline and Gas Reburning NO_x Data

Since the performance of ammonia is calculated based on the initial NO_x levels after reburning, the gas reburning data were determined for reference purposes. Figure 8-2 shows a plot comparing the gas reburning data obtained during 1996 and 1997 parametric tests at Greenidge. As can be seen, the 1997 baseline NO_x level was slightly less than the 1996 level. After the first round of AR tests in 1996, GE-EER recommended to conduct burner modifications to try improving CO/O₂ distribution in the furnace. In 1997, some riffle box modifications were performed as well as tests to determine the degree of burner air/fuel distribution. These activities resulted in slight decreases in baseline NO_x emissions and moderate increases in LOI as compared to pre-reburning system installation levels. At typical boiler stoichiometry of 25% excess air, the 1996 baseline NO_x emissions was 0.56 lb/10⁶ Btu (485 ppm @ 0% O₂) and the 1997 baseline NO_x level was 0.52 lb/10⁶ Btu (450 ppm @ 0% O₂). GE-EER also recommended replacing the gas injectors with supersonic injectors to try improving CO/O₂ distribution in the upper furnace. This resulted in better NO_x reductions, as shown in the plot.

Figure 8-3 shows a comparison of NO_x reduction efficiency due to reburning alone for the Greenidge and BSF systems. It can be seen that reburning efficiency was high for both systems, with the BSF showing a slight better NO_x reduction. At SR₂ of 0.99, which was the typical SR₂ level during the AR-Lean tests, reburning resulted in approximately 39% NO_x reduction in the BSF and about 35 to 40% reduction in the Greenidge boiler.

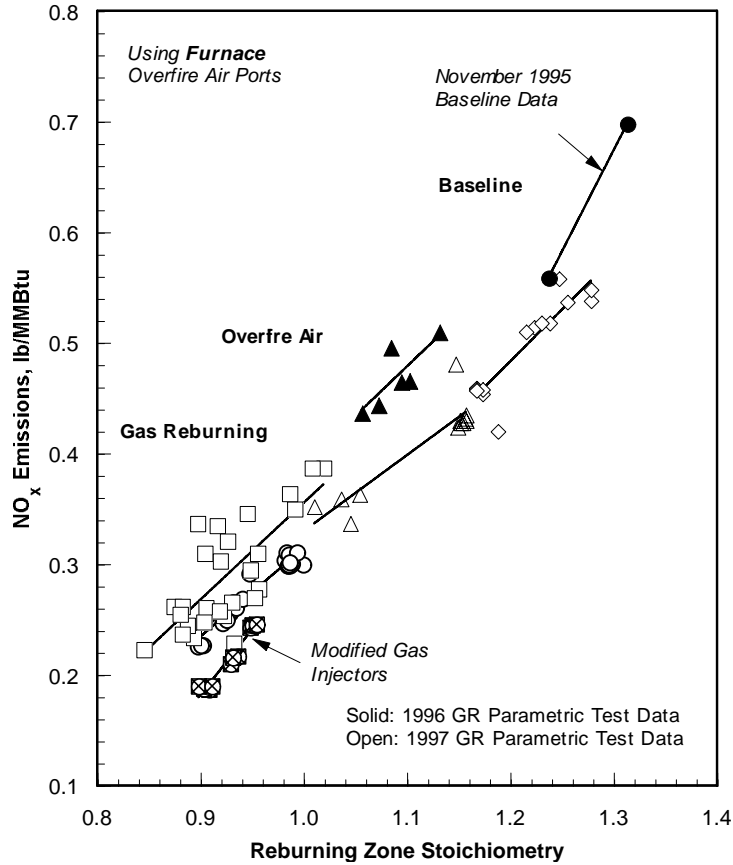


Figure 8-2. Comparison of Greenidge 1996 and 1997 gas reburning data.

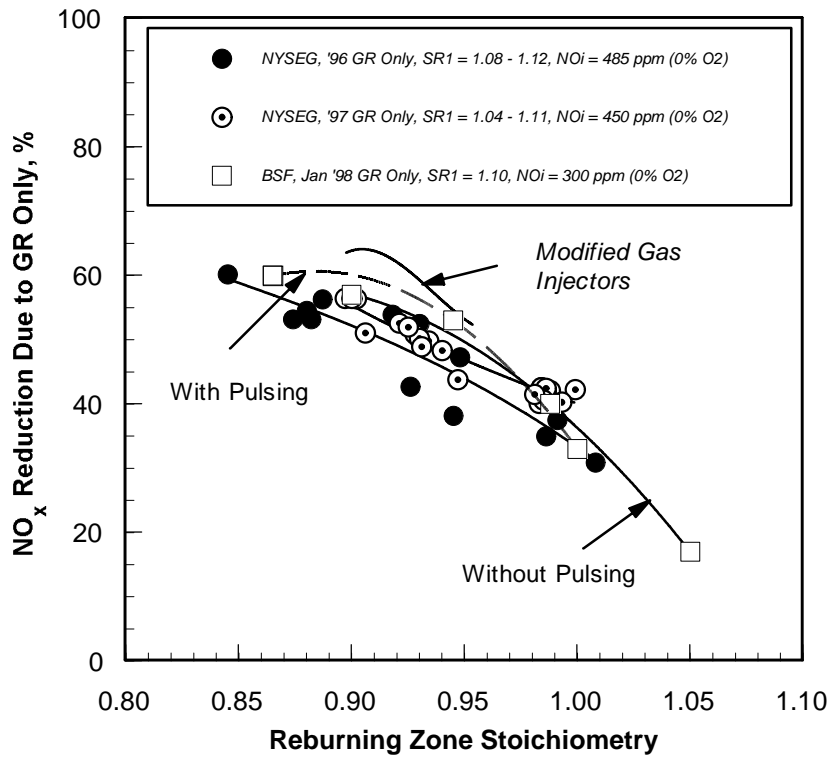


Figure 8-3. Comparison of gas reburning performance between Greenidge and BSF.

8.1.4 Effect of Pulsing on Basic Reburning

A series of tests was conducted in BSF to determine the effect of fluctuations on reburning. Data presented in Figure 8-4 compare NO reduction for basic reburning at different time-averaged SR_2 and pulsing frequencies. The results suggest that there is no visible effect of pulsing on basic reburning. Fuel fluctuations form regions with increased and decreased SR_2 , but the time-averaged SR_2 value is the main parameter defining NO emissions. Observed performance, 17-60% NO reduction, is somewhat low for reburning systems, primarily due to short residence time (0.4 sec) and low initial NO concentration (300 ppm).

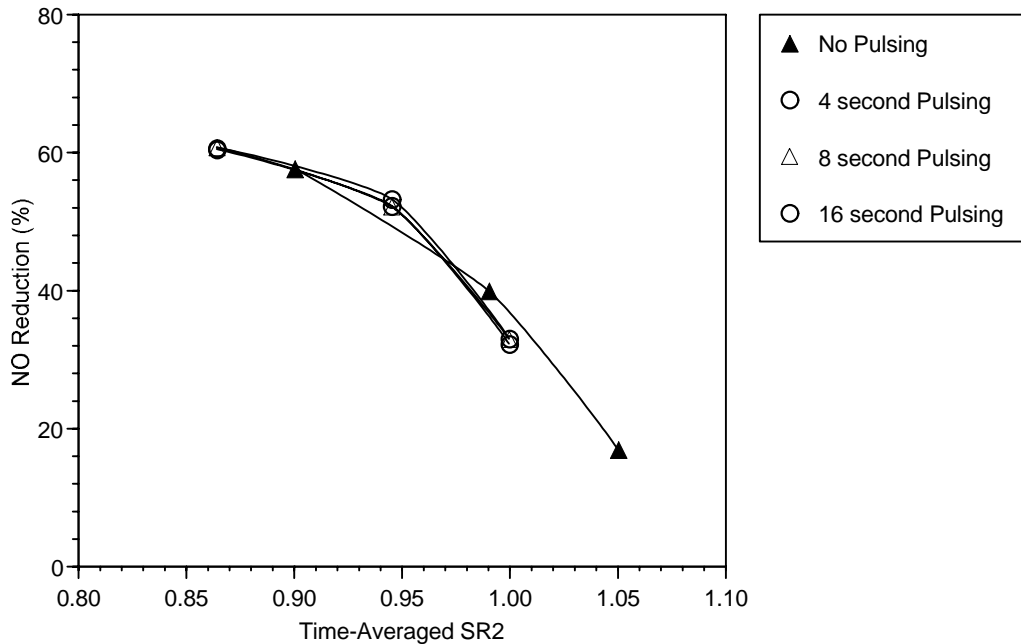


Figure 8-4. Effect of fluctuations on reburning.

8.1.5 AR-Lean Test Results

A series of tests was conducted at the BSF to parametrically evaluate the effect of N-agent co-injection with OFA (AR-Lean) on NO_x reduction. The objective of the tests was to define the processes controlling NO_x reduction in light of the gas fluctuations and incomplete mixing at the Greenidge boiler. Test variables included the NSR of the additive, furnace gas CO concentration (varied using the pulsation system), N-agent injection temperature, and initial NO concentration (NO_i). In addition, several tests were conducted with SNCR alone.

Impact of NSR and CO Concentration on AR-Lean

AR tests were conducted during operation of the pulsing system in which NSR was varied from 0 to 2.0. Reburning heat inputs of 10% and 5% were tested, corresponding to reburning zone stoichiometry (SR_2) values of 0.99 and 1.05, respectively. To achieve different CO concentrations, the natural gas pulsing system was operated at four cycle frequencies, ranging from 0 (i.e. no pulsing) to 16 seconds. Although reburning zone CO concentration did not vary directly with

pulsing frequency, the pulsing system did provide a means of obtaining high CO levels such as those found at the Greenidge boiler. Specifically, reburning zone CO concentrations were measured to be 2,000 ppm with no pulsing, 13,000 ppm with 4 second pulsing, 15,000 ppm with 8 second pulsing, and 14,000 ppm with 16 second pulsing.

Figure 8-5 shows AR performance at 10% reburning as a function of NSR at different CO concentrations. With no pulsing, NO reduction increased from 38% at NSR = 0 to 69% at NSR = 1.5. However, during pulsing NO reduction decreased from 52% at NSR = 0 to 30-38% at NSR = 2.0. This suggests that high CO concentrations are bad for AR performance. The fact that a net decrease in NO reduction was seen with increasing NSR indicates that some of the N-agent was actually being oxidized to form NO. It can also be noted that performance of reburning alone (i.e. at NSR = 0) improved from 38% to 52% during pulsing. This is attributed to the fact that SR_2 decreased slightly due to the pulsing system.

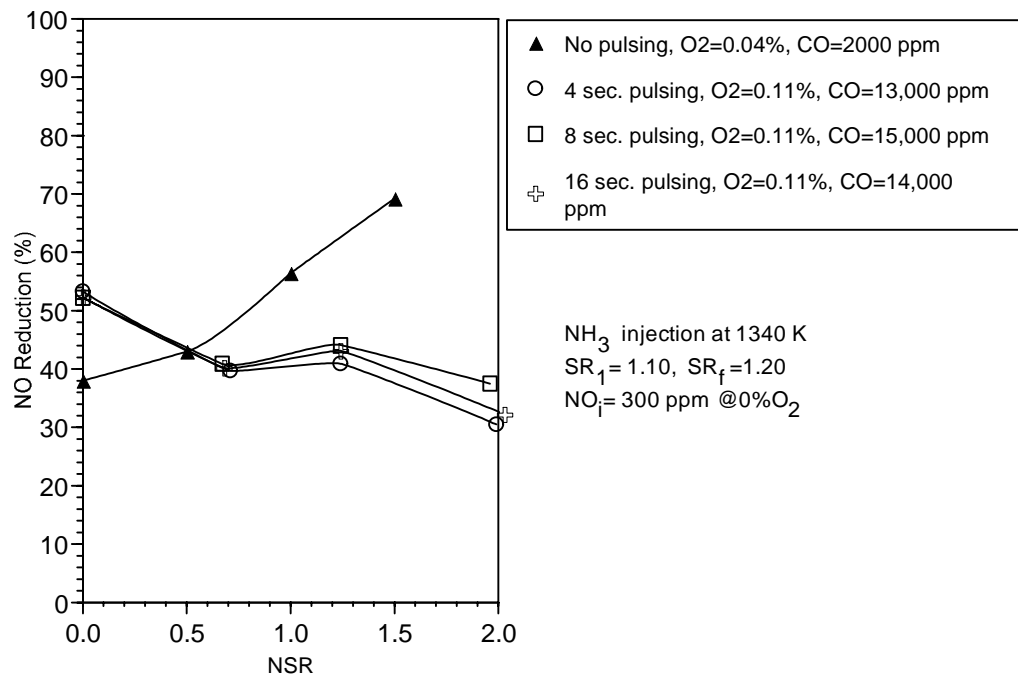


Figure 8-5. AR-Lean performance vs. NSR at different CO concentrations, 10% reburning.

Figure 8-6 shows AR-Lean results at 5% reburning for different pulsing frequencies. Reburning zone CO concentrations ranged from 200 ppm with no pulsing to 8,000 ppm with 8 second pulsing. With no pulsing, NO reduction increased from 17% at NSR = 0 to 71% at NSR = 1.5. During pulsing NO reduction increased with increasing NSR, but by a lesser degree than with no pulsing. Again performance of reburning alone improved during pulsing.

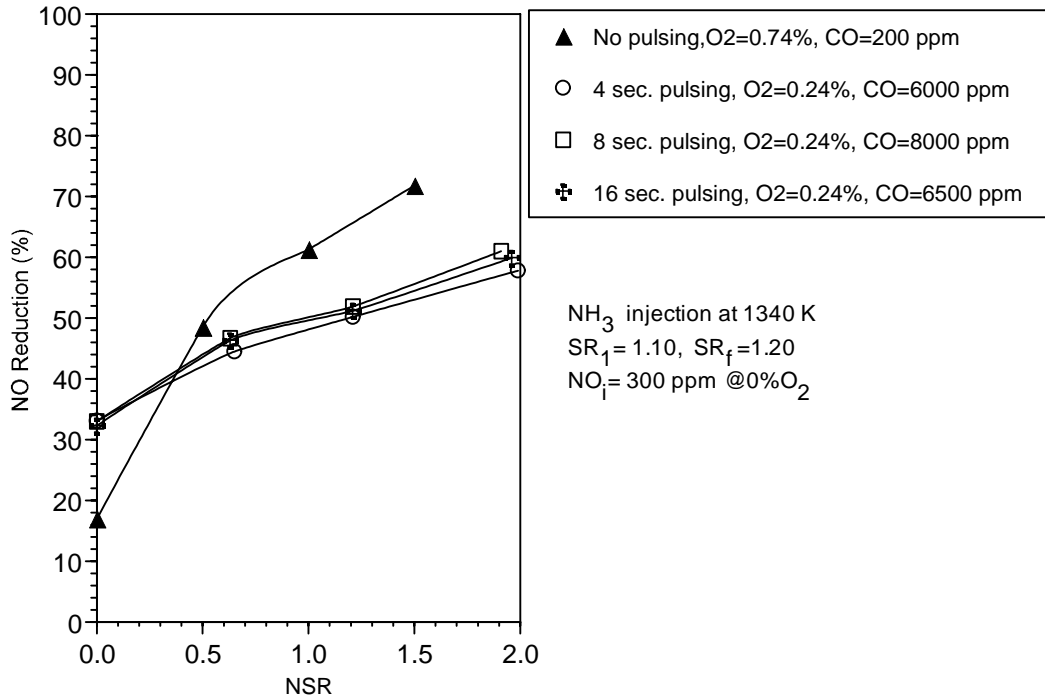


Figure 8-6. AR-Lean performance vs. NSR at different CO concentrations, 5% reburning.

Figure 8-7 shows NO reduction as a function of reburning zone CO concentration. For the purpose of this plot no differentiation has been made between the different reburning heat inputs. At all NSR values, AR-Lean performance appears to decrease with increasing CO. Figure 8-8 shows the incremental performance of the N-agent alone for these same AR tests, as calculated by the difference between overall NO reduction and reburning-only NO reduction. Again performance decreases with increasing CO. NO reduction falls off more rapidly at 10% reburning than at 4.6% reburning. At 10% reburning, negative NO reductions (i.e. NO increases) were observed during all high-CO pulsing conditions.

Impact of Additive Injection Temperature on AR-Lean

AR-Lean tests were then conducted in which the OFA/NH₃ injection temperature was varied from 1200 K to 1500 K. Figure 8-9 compares AR-Lean performance with and without pulsing at 10% reburning ($SR_2 = 0.99$). For all cases NO reduction increased with decreasing injection temperature. At NSR values of 1.0 and 1.5, NO reduction was significantly worse during pulsing.

Figure 8-10 shows AR-Lean results obtained at 5% reburning ($SR_2 = 1.05$). These tests were conducted only with 8 second fuel pulsing to allow direct comparison to the pulsing tests at 10% reburning. NO reduction generally increased with decreasing injection temperature, reaching a maximum at about 1280 K. AR performance during pulsing was significantly better at 5% reburning than at 10% reburning. For example, at an OFA/NH₃ injection temperature of 1280 K, NO reduction was 78% at 5% reburning, as compared to 55% at 10% reburning.

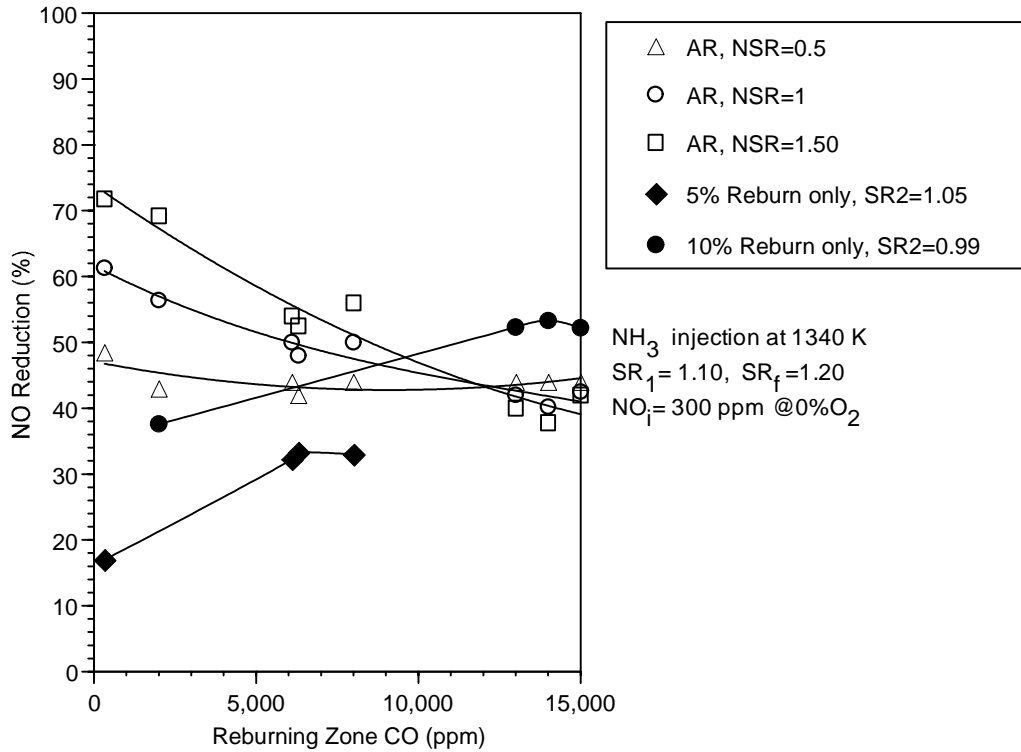


Figure 8-7. AR-Lean performance vs. reburning zone CO concentration at 5% and 10% reburning.

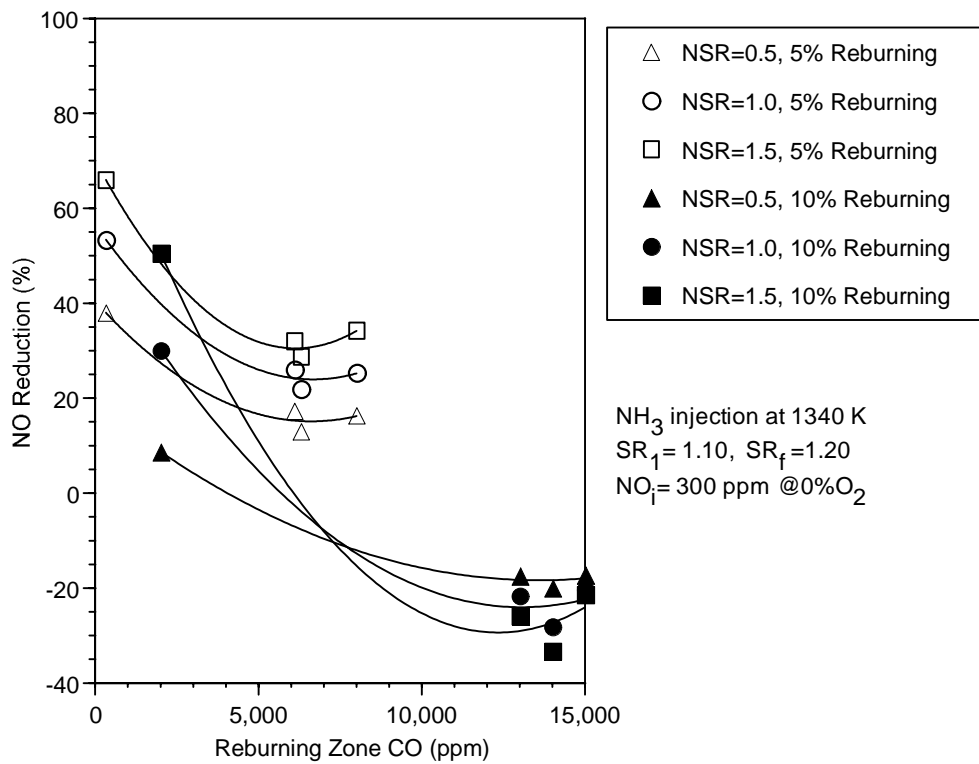


Figure 8-8. Incremental performance of N-agent alone in AR-Lean as a function of reburning zone CO concentration.

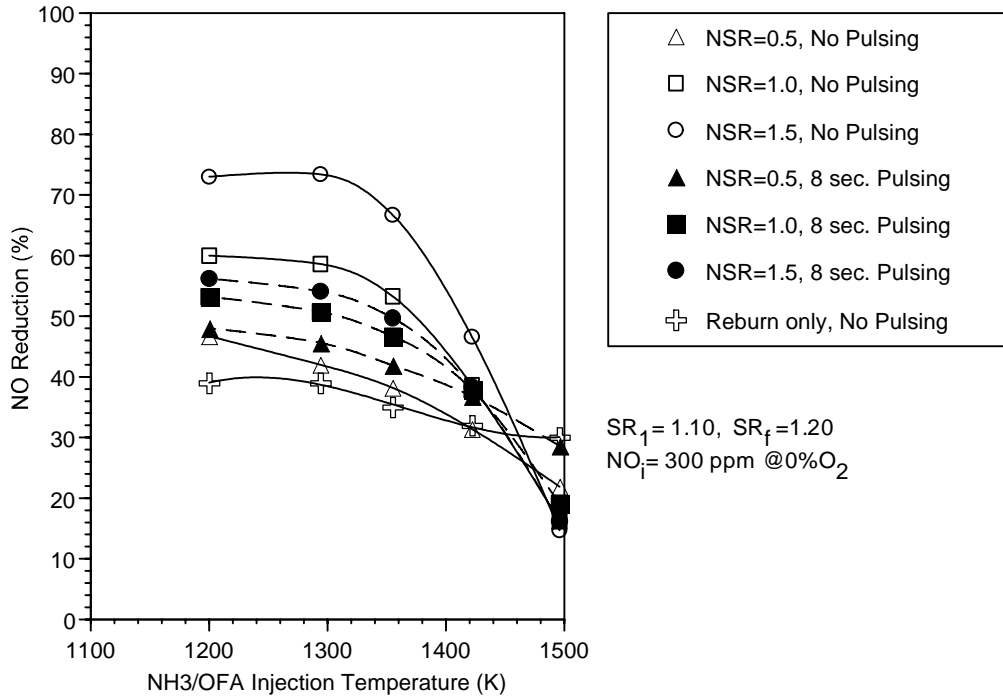


Figure 8-9. AR-Lean performance versus additive injection temperature with and without main fuel pulsing at 10% reburning.

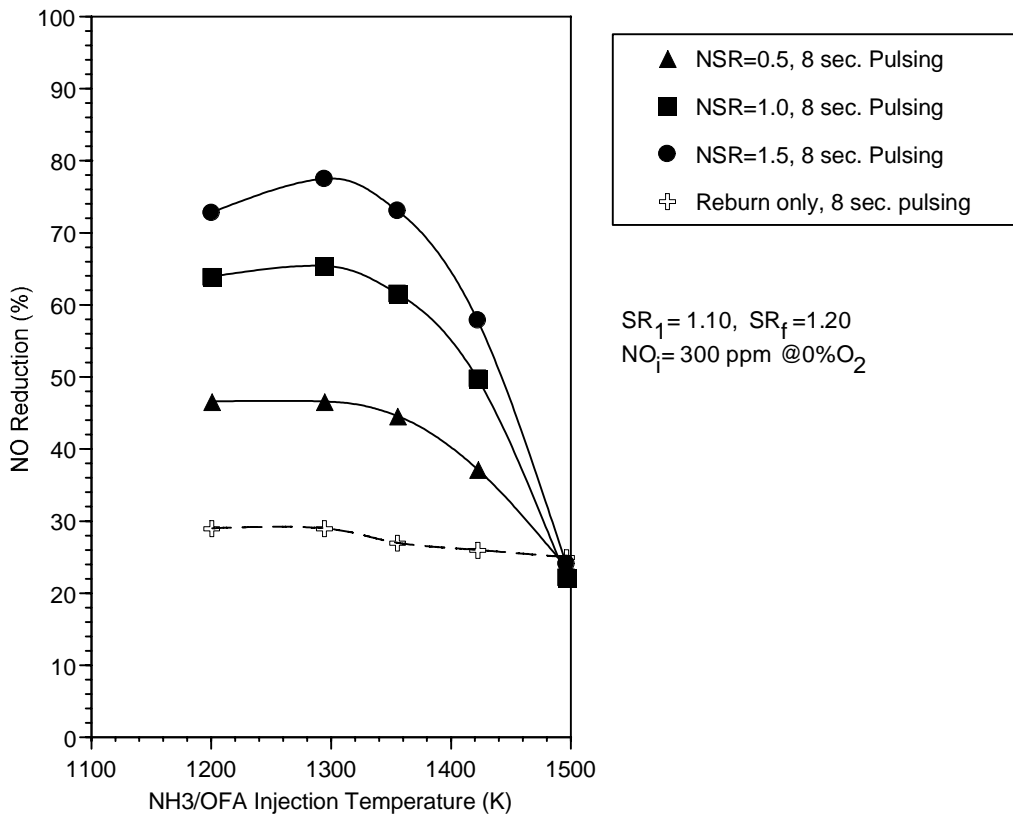


Figure 8-10. AR-Lean performance versus additive injection temperature with main fuel pulsing at 5% reburning.

Impact of NO_i on AR-Lean

Most of the BSF tests were conducted at an initial NO_i concentration of 300 ppm to simulate the Greenidge boiler conditions. To determine the functional dependence of AR on NO_i , several tests were also conducted at $\text{NO}_i = 600$ ppm. The tests were performed at 10% reburning with no pulsing of the main natural gas. Figure 8-11 shows the impact of NSR upon AR-Lean performance at NO_i concentrations of 300 and 600 ppm. NO reductions were 5 to 10 percentage points better at the higher NO_i concentration. Performance was also significantly better at an injection temperature of 1350 K than at 1420 K.

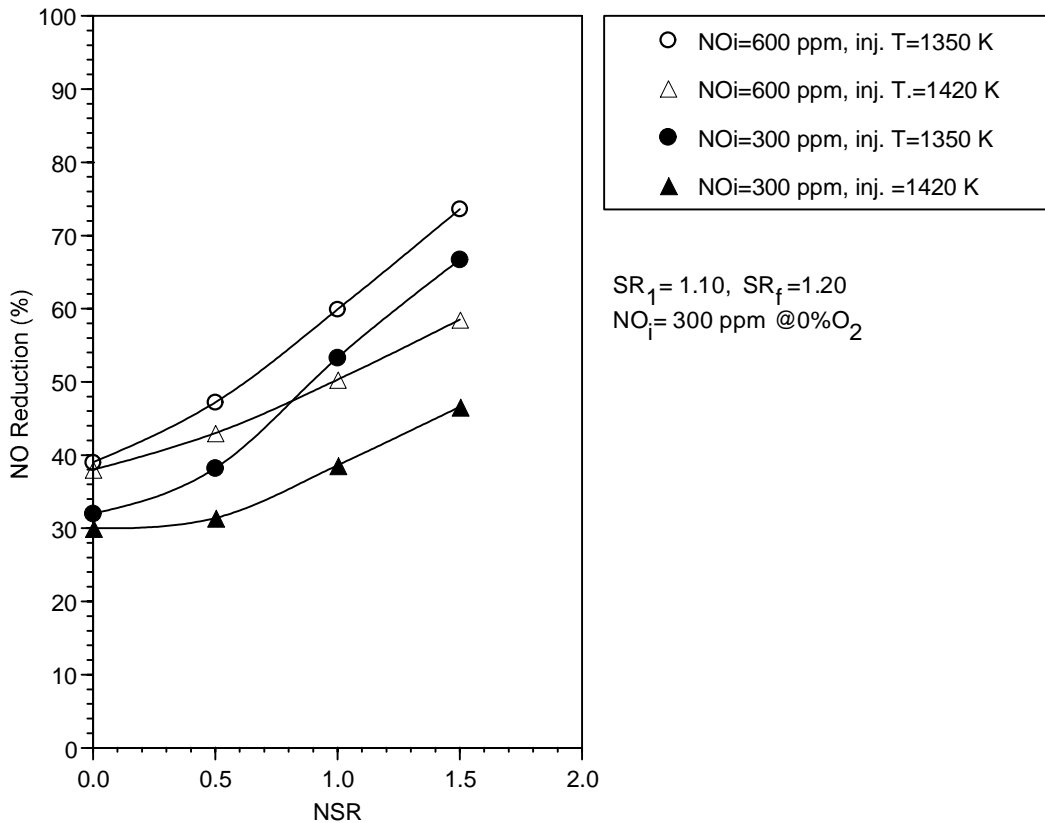


Figure 8-11. AR-Lean performance versus NSR at initial NO concentrations of 300 and 600 ppm at 10% reburning.

Impact of the Amount of the Reburning Fuel on AR-Lean

Figure 8-12 shows NO reduction at SR_2 values of 1.10 (no reburning), 1.05 (5% reburning), and 0.99 (10% reburning). For each condition NSR was 1.0. Both with and without pulsing NO reduction increased with increasing SR_2 . Thus in general the test results would appear to indicate that furnace gas fluctuations and high CO concentrations decrease performance of the AR-Lean process.

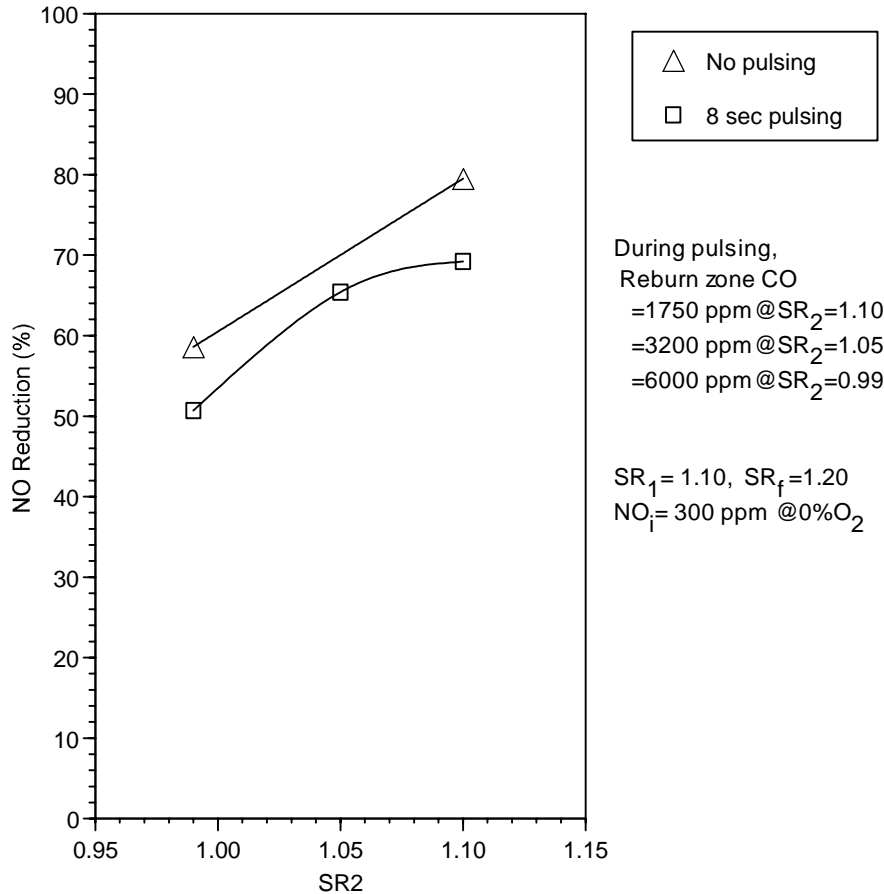


Figure 8-12. NO reduction in AR-Lean as a function of SR₂ with and without pulsing.

8.1.6 Comparison between Greenidge and BSF AR-Lean Data

This section presents a comparison of AR-Lean data of the Greenidge and BSF systems. Figure 8-13 shows a plot comparing the impacts of CO concentration on NO_x reduction for the Greenidge and BSF systems. (Please note that the 1996 Greenidge data, which had high NH₃ slip (0 - 100 ppm), were obtained before modifications to the ammonia injection system. The 1997 data, which had much better NH₃ slip (0 - 25 ppm), were obtained after the ammonia system modifications). This plot shows the key difference between the Greenidge and BSF systems. In the BSF furnace, high CO concentrations showed a detrimental impact on NO_x reduction, which is consistent with the results, obtained during the Phase I studies. As CO concentration in the furnace increased, NO_x reduction performance decreased. Quantitatively, as CO concentration increased to about 15,000 ppm, NO_x reduction percentage decreased to 20% below the gas reburning initial NO_x level. In the Greenidge furnace, CO concentrations varied significantly, both temporal and spatial. In addition, the control for a specific level of CO concentration had been extremely difficult. Although the reburning zone in both systems was set at 0.99, there was no guarantee that they would have had similar levels of CO concentration at the ammonia injection location. One of the key differences might have been due to fluctuating characteristics associated with a full-scale system caused by the unmixedness of the flow from the burners and reburning fuel injectors. Another difference might have been due to the air leakage of the furnace OFA ports in the Greenidge system. The furnace OFA ports might have burned some CO as CO entered the superheater platens. Therefore, CO

concentrations at the ammonia injection location might actually have been lower than the concentration levels measured in front of the superheater platens. Another piece of data to show the impacts of the furnace OFA ports was the test A, during which the furnace OFA ports were shut down. Test A resulted in negative NO_x reduction (-27% at NSR = 1.0), similar to the BSF results. Because the opacity was very unstable during this test, in-furnace data were not recorded. However, readings during the test set-up indicated CO concentration levels of approximately 20,000 ppm.

Figure 8-14 shows the impacts of injection temperature on NO_x reduction performance of ammonia for both systems. The figure shows three plots for NSR at 0.5, 1.0 and 1.5. Temperatures in the BSF were measured at the NH₃/OFA injection elevation. Injection temperatures for Greenidge were determined by subtracting 125 K (based upon heat transfer modeling results) from the measured temperatures in front of the superheater platens. The BSF data indicated that injecting ammonia at high temperatures, i.e., greater than 1367 K, had negative impacts on AR-Lean performance, as indicated by decreases in NO_x reduction efficiency as temperature increased. The full-scale data appear to be in the range with the pilot-scale data, with and without pulsing. The comparison seems to suggest that the injection location for the Greenidge AR system is reasonable because the injection temperatures reside at the region before performance starts to drop off. The rapid quench rate of the Greenidge reheater section may have been responsible for the relatively high ammonia slip that was obtained in the field.

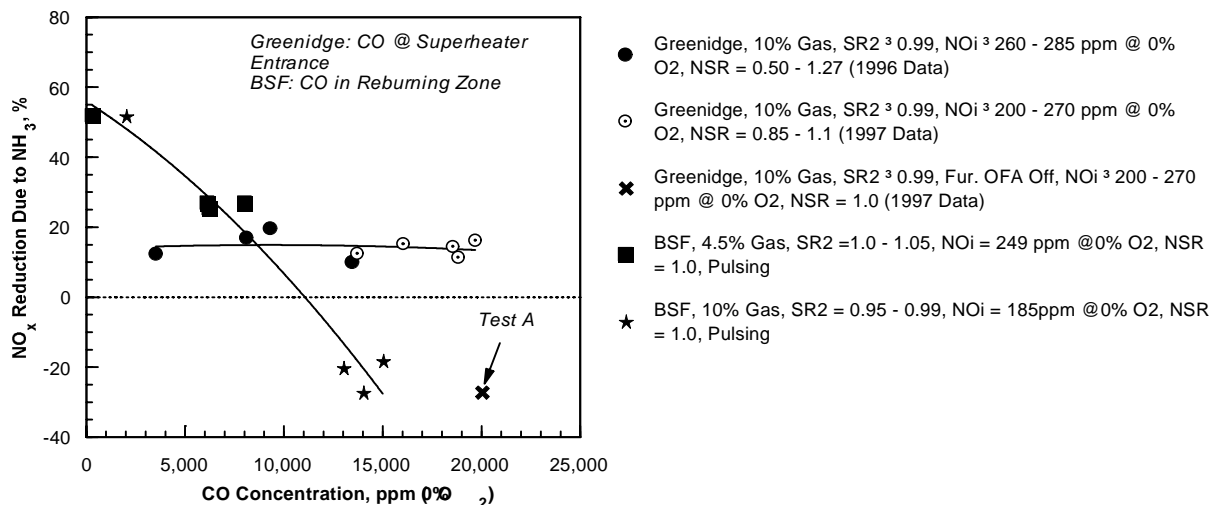


Figure 8-13. Comparison of the impacts of CO concentration on NO_x reduction in AR-Lean tests in Greenidge and BSF. The furnace OFA ports were shut down during test A.

Figure 8-15 shows a plot of NO_x reduction due to ammonia only as a function of NSR. For the BSF, the data were collected with ammonia injected with OFA at 1355 K and two levels of CO concentration: 2,000 and 6,000 ppm. The plot shows that the full-scale system was substantially less effective than the pilot-scale system. As previously discussed about the effect of CO concentration, the data seems to suggest that (keeping the effect of flow field stratification in mind) the average CO concentrations at the convective pass cavity of Greenidge must have been higher than 6,000 ppm, possibly in the order of 10,000 ppm. The measured CO concentrations in front of the superheater platens were 14,000 to 20,000 ppm.

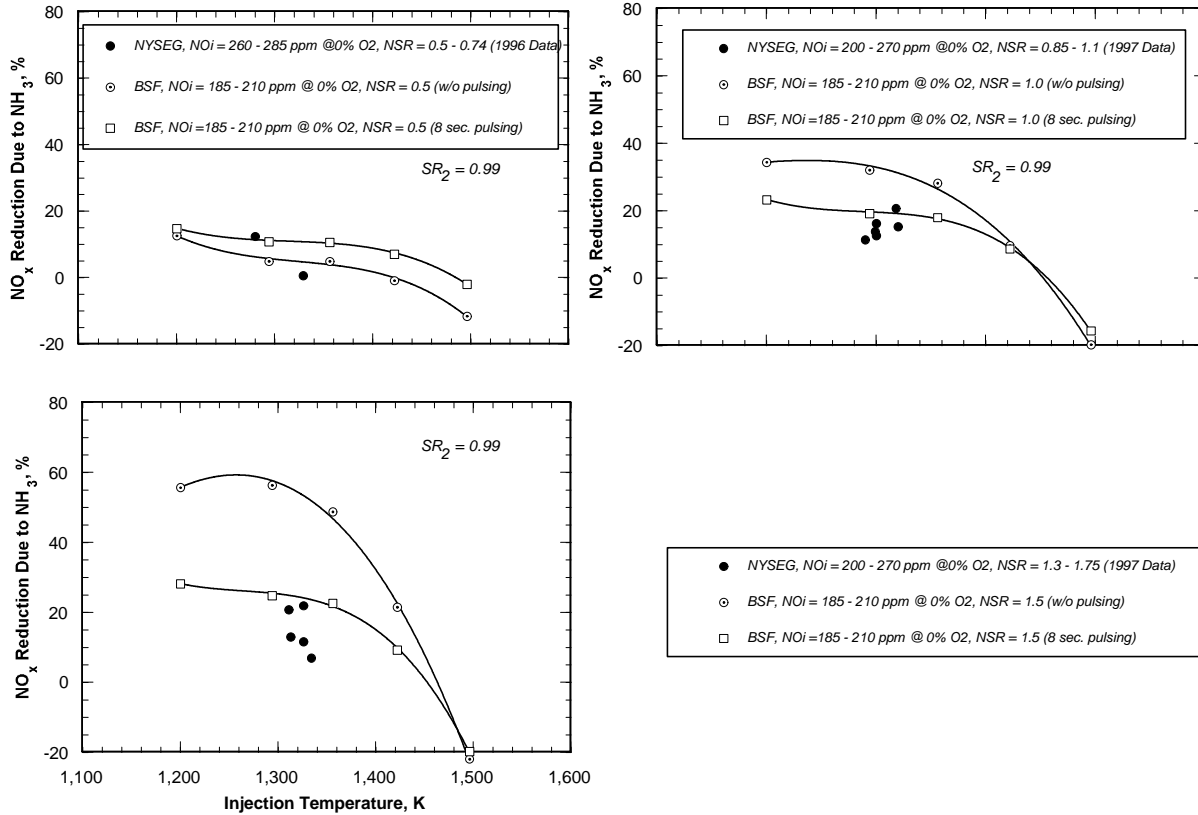


Figure 8-14. Comparison of the impacts of injection temperature on NO_x reduction in Greenidge and BSF.

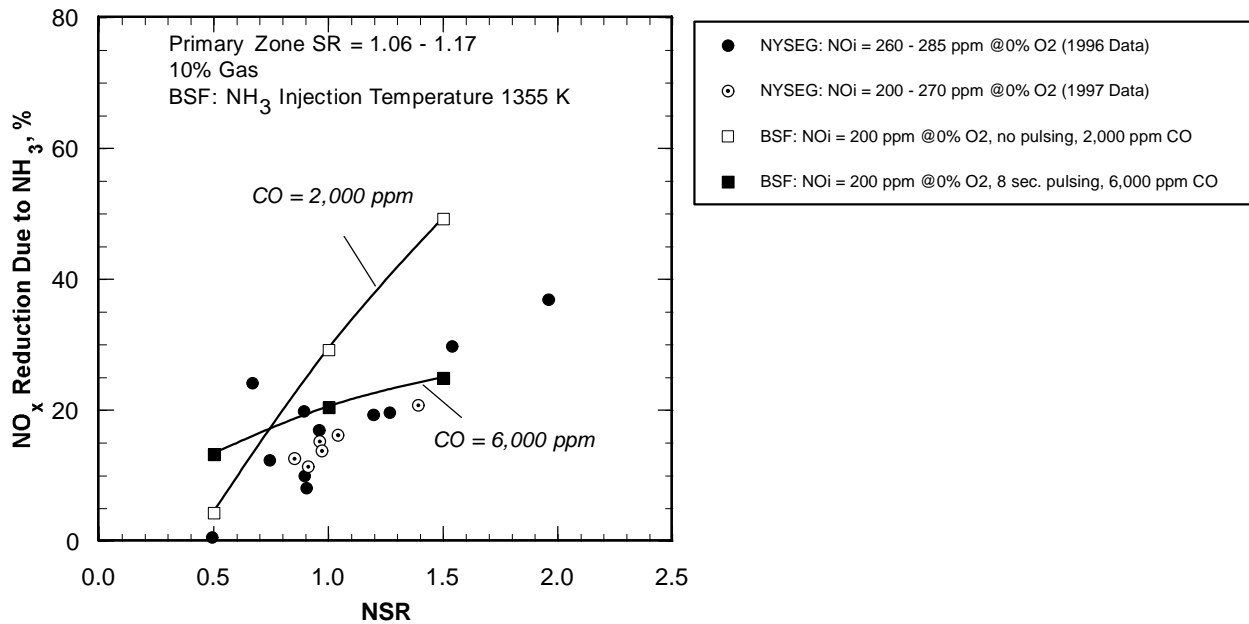


Figure 8-15. NO_x reduction due to ammonia in AR-Lean in Greenidge and BSF.

8.1.7 Reburning + SNCR

Effect of Pulsing on SNCR

BSF tests were conducted with SNCR alone, to determine how gas fluctuations and high CO concentrations affect N-agent performance in the absence of reburning. Tests were conducted at NSR values ranging from 0.5 to 1.5 at different ammonia injection temperatures. Figure 8-16 shows SNCR performance with and without pulsing. NO reduction increased with increasing NSR and was, at the optimum point, about 10 percentage points better with no pulsing. At NSR = 1.5, a maximum of 88% NO reduction was obtained at 1280 K without pulsing and 78% with pulsing.

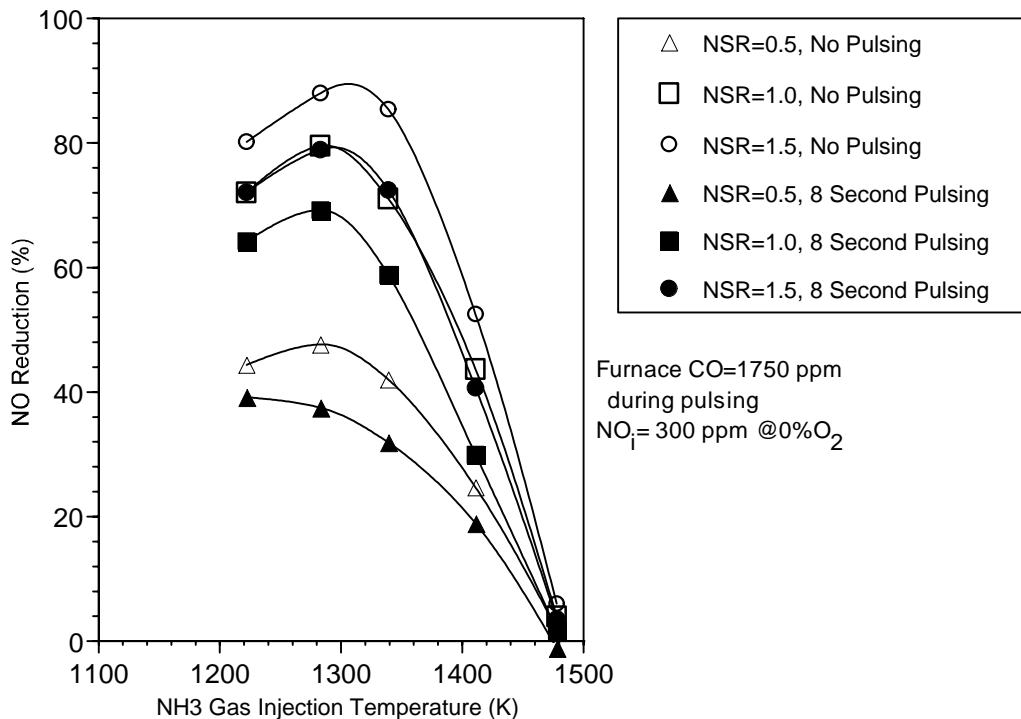


Figure 8-16. SNCR performance as a function of N-agent injection temperature with and without main fuel pulsing.

Initial Characterization of Combined Reburning + SNCR Performance

The initial BSF tests were designed to provide combined reburning and SNCR performance data for injection temperatures and residence times simulating those available at Greengidge. Aqueous NH_3 and gaseous NH_3 were tested along with urea as N-agents. Figure 8-17 compares performance of different N-agents in the reburning + SNCR process without pulsing. It appears that gaseous NH_3 has a lower optimum injection temperature than urea or aqueous NH_3 . Figure 8-18 compares performance of the different N-agents as a function of NSR at two different injection temperatures (also without pulsing). At the lower temperature (1270 - 1300 K), best performance was obtained with gaseous NH_3 . At the higher temperature (1340 K), best performance was obtained with urea.

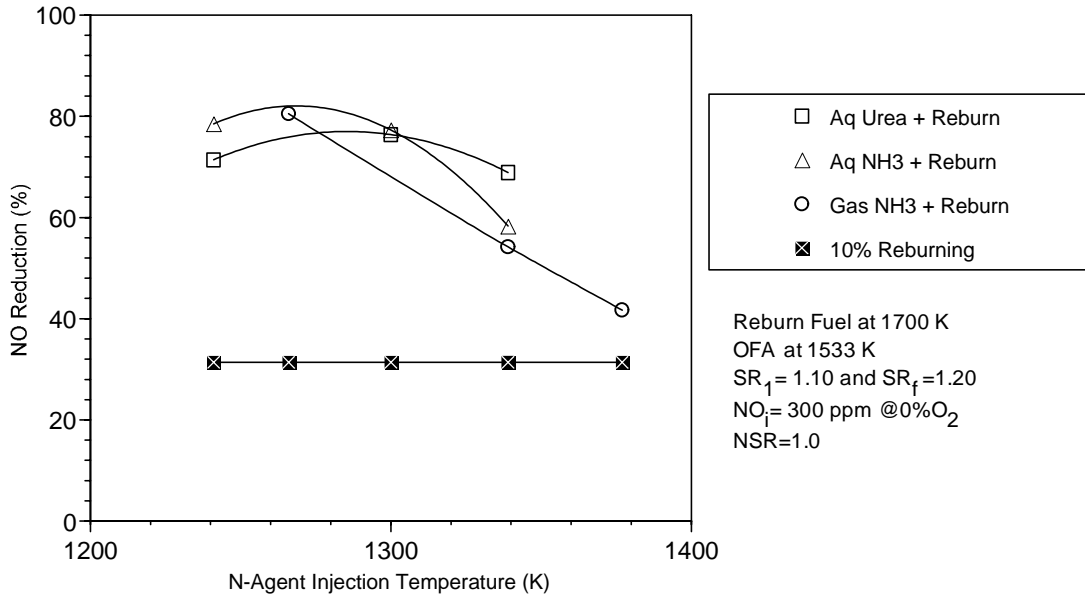


Figure 8-17. Comparison of performance of different N-agents in the reburning + SNCR process without pulsing.

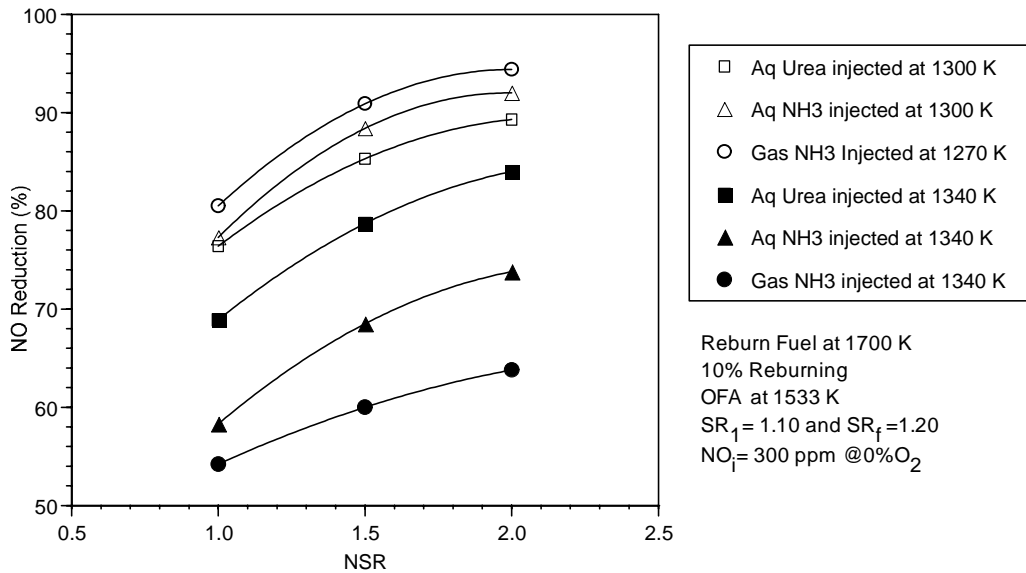


Figure 8-18. Comparison of performance of different N-agents as a function of NSR at 1270 K and 1300 K (without pulsing).

Figure 8-19 compares results obtained with the three N-agents during pulsing of the main fuel. High NO reductions, in the range of 73 - 87%, were obtained in these tests. Results appear to be best with gaseous NH₃, although this is largely a function of the injection temperature selected (see Figure 8-17). The impacts of pulsing frequency upon performance were minimal, again suggesting that injecting the N-agent downstream of the OFA might minimize the detrimental impacts of furnace fluctuations.

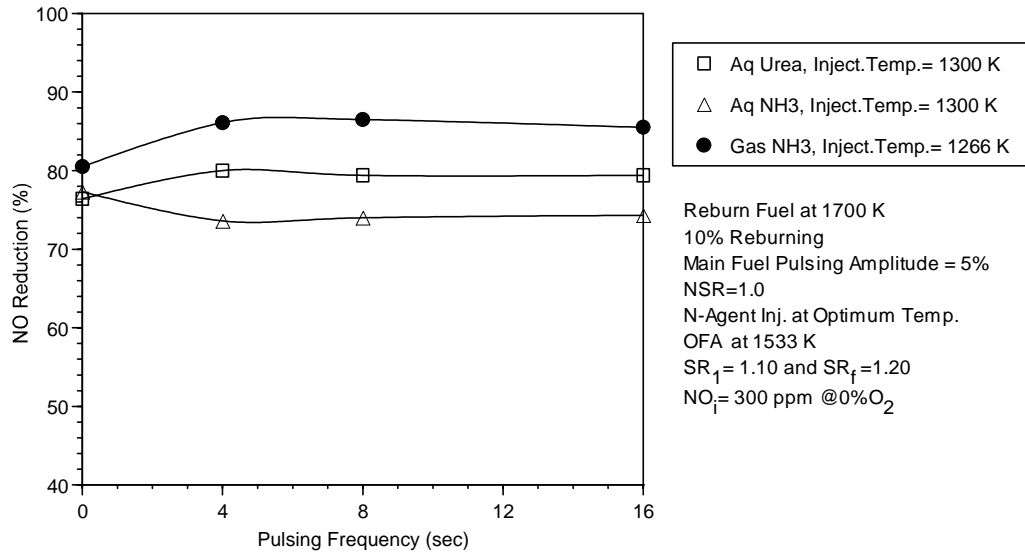


Figure 8-19. Comparison of results obtained with the three N-agents during pulsing of the main fuel.

Effects of Fuel Pulsing Parameters on Performance

BSF tests were performed to characterize the concentration of CO in the reburning and SNCR zones and to examine the effects of reburning fuel flow rate and pulsing amplitude. CEM sampling was performed at three locations: in the reburning zone, in the N-agent injection zone (downstream of the OFA) and in the convective pass. The frequency and amplitude of the pulsing were each varied at 10% and 20% reburning. Measurements of CO concentrations as a function of pulsing frequency demonstrated that CO levels were high in the reburning zone (8,000-40,000 ppm depending on reburning heat input), but were lower than 50 ppm in the N-agent injection zone and convective pass.

Figure 8-20 shows reburning + SNCR results as a function of pulsing frequency at 10% and 20% reburning. Varying pulsing frequency did not significantly impact NO reduction. It can be also observed that results are similar at 10% and 20% reburning. It is noted that the urea injection location was the same for 10% and 20% reburning, but injection temperature varied slightly due to impacts of reburning heat input on temperature profile. Figure 8-21 compares results obtained at different pulsing amplitudes. Performance was worse at 10% pulsing than at 5% pulsing.

Effect of Sodium on Reburning + SNCR Performance

BSF tests were conducted in which the effects of sodium on reburning + SNCR performance were characterized under furnace conditions simulating a full-scale boiler. Reburning fuel was injected at 1700 K, just below the flame. Overfire air was injected at various locations depending on target injection temperature. N-agent was injected downstream of the OFA, also at varying locations. When sodium promoter was used, it was co-injected with the N-agent. To quantify emissions as a function of axial position in the furnace, continuous emissions monitor sampling was performed at three locations: just below the reburning fuel injector, between the secondary superheater and reheater cooling arrays, and at the furnace exhaust.

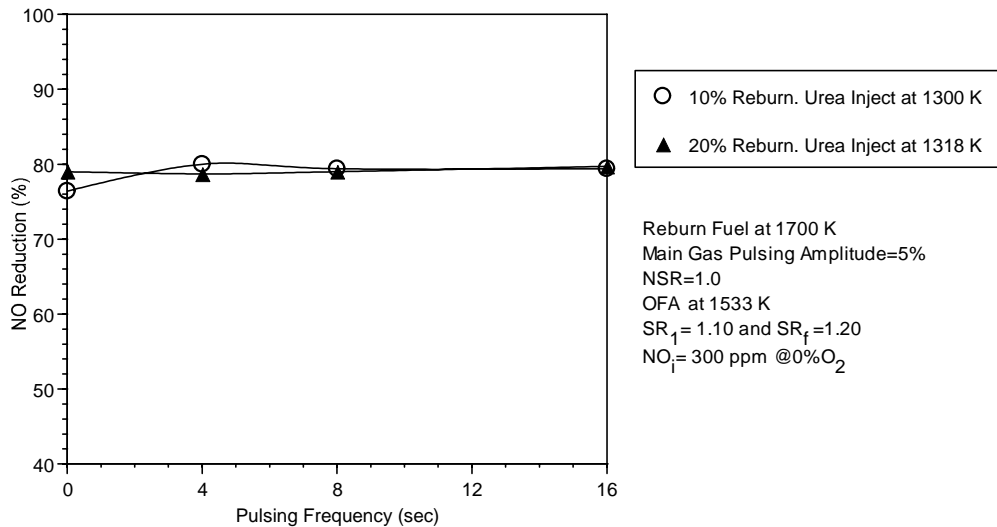


Figure 8-20. NO reduction in reburning + SNCR as a function of pulsing frequency at 10% and 20% reburning.

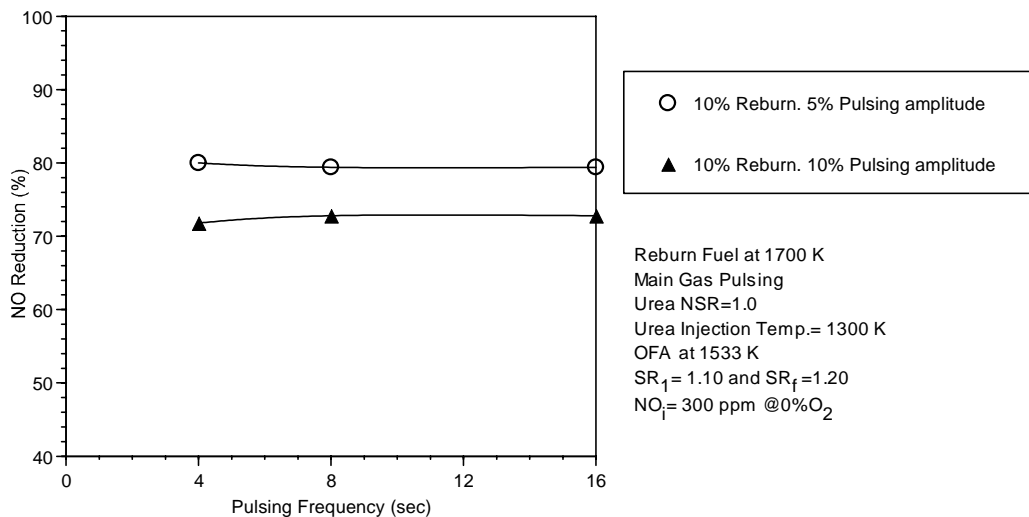


Figure 8-21. Comparison of results obtained at pulsing amplitudes of 5% and 10%.

For the reburning + SNCR sodium injection studies, test variables included additive injection temperature, sodium concentration, and reburning heat input. In the first test series, additive injection temperature was varied from 1240 K to 1340 K. Reburning heat input was set at 10% and OFA was injected at 1530 K. The additives consisted of either urea alone or urea plus Na_2CO_3 , at 30 ppm Na in the flue gas. NSR was 1.0. Figure 8-22 shows NO reduction as a function of additive injection temperature. Reburning alone gave about 32% NO reduction. Sodium had a significant promotional effect at 1240 K and 1300 K, but not at 1340 K. Maximum NO reduction achieved was 84%, obtained with urea plus sodium at an injection temperature of 1300 K.

Figure 8-23 shows NO reduction as a function of Na concentration at 10% reburning. The injection temperature was 1300 K, and NSR ranged from 1.0 to 2.0. NO reduction increased by 6 to 8 percentage points as Na was increased from zero to 10 ppm, and then increased minimally as Na

was further increased to 60 ppm. Maximum NO reductions were 97% at NSR=2.0 and 94% at NSR=1.5.

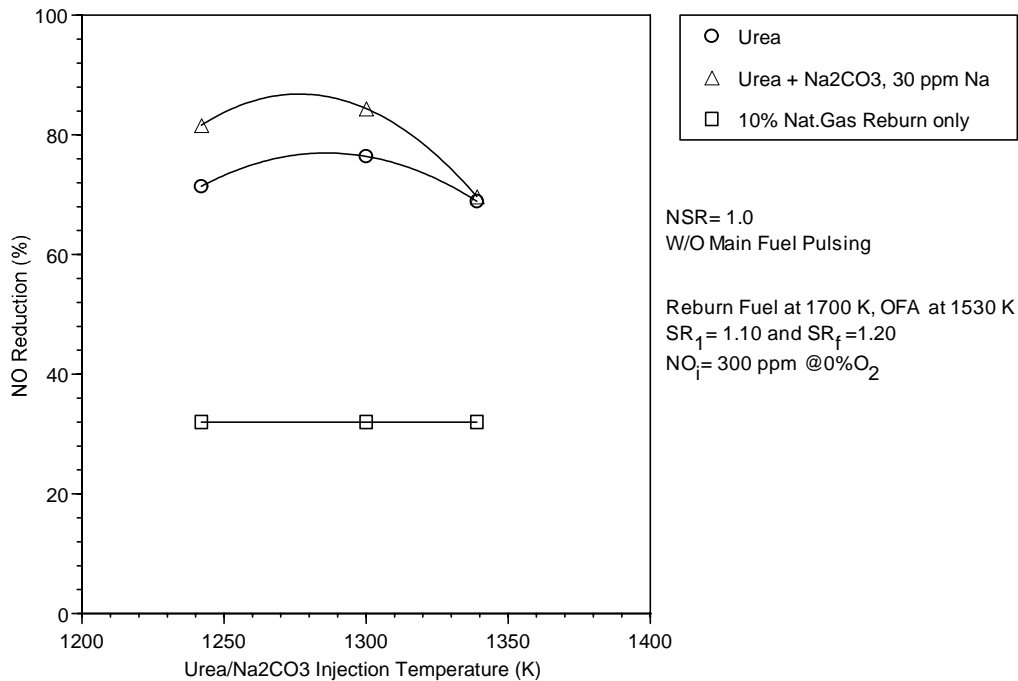


Figure 8-22. Promoted reburning + SNCR performance as a function of additive injection temperature at 10% reburning.

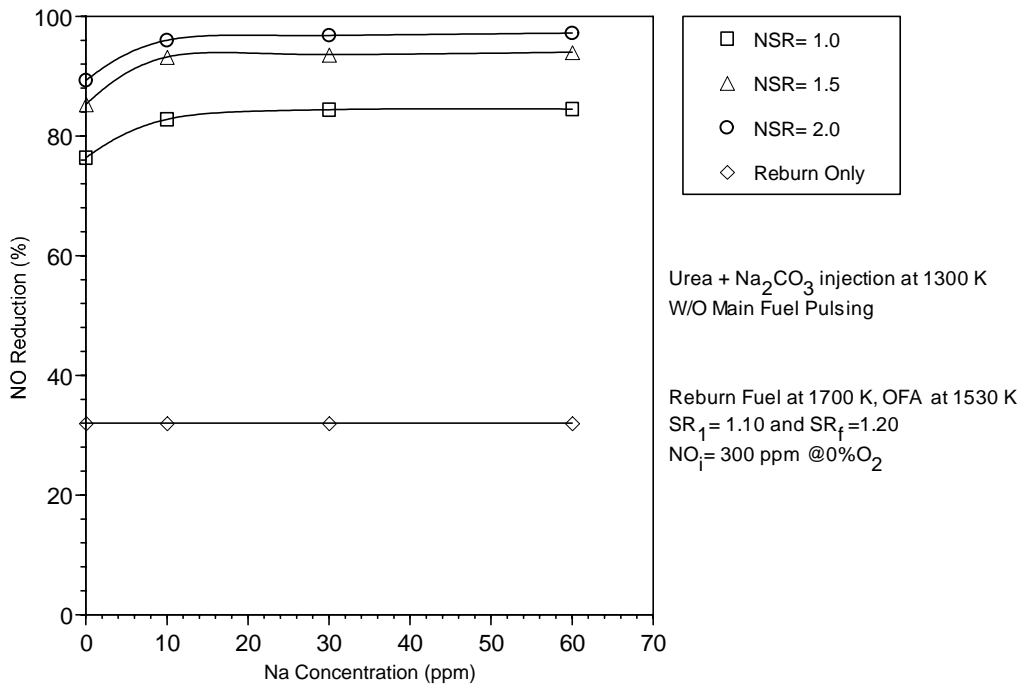


Figure 8-23. Promoted reburning + SNCR performance as a function of sodium concentration at 10% reburning.

Figure 8-24 shows the impact of sodium addition for different reburning heat inputs. The incremental performance benefit provided by urea is greatest at 10% and 15% reburning. The promotional effect of sodium is also largest at the lower reburning heat inputs.

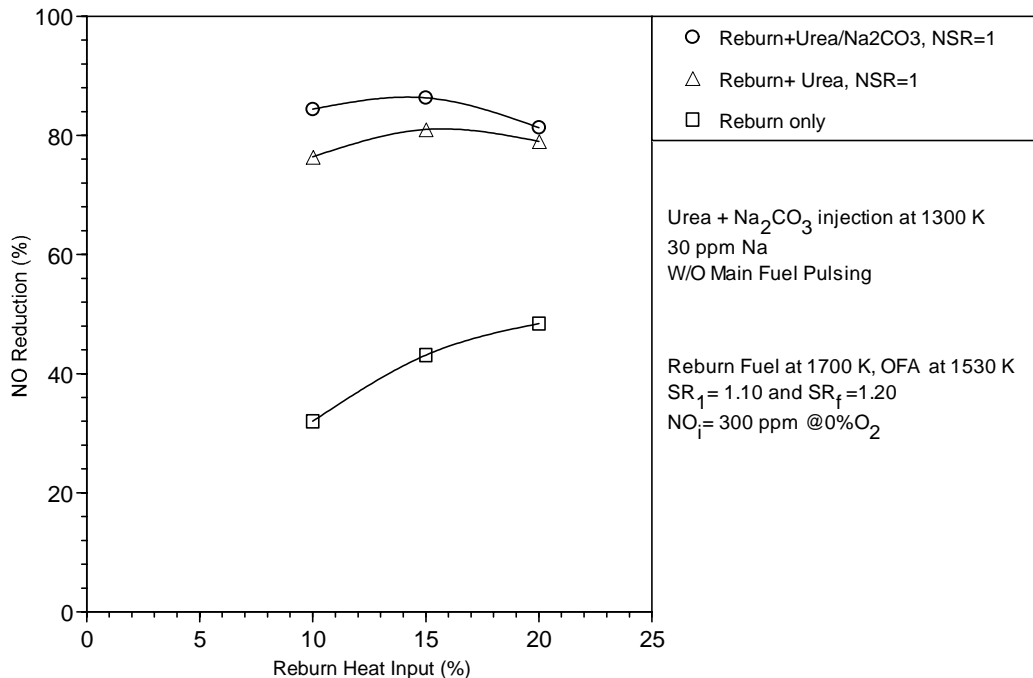


Figure 8-24. Promoted reburning + SNCR performance as a function of reburning heat input.

CO and Ammonia Emissions During Reburning + SNCR

A series of BSF tests was conducted with the objective to define process conditions providing high NO reduction with low byproduct emissions. Sampling was performed for CO by continuous monitoring and for NH₃ by manual methods at various reburning + SNCR test conditions. CO emissions were measured in the reburning zone, in the convective pass, and in the furnace exhaust. During implementation of main fuel pulsing, reburning zone CO concentrations were found to be as high as 38,000 ppm. However, exhaust CO levels remained below 100 ppm for all conditions.

For the ammonia slip tests, reburning heat input was 10%. N-agents tested included aqueous urea and gaseous NH₃. NSR was 1.0 for all tests. Injection temperatures ranged from 1270 K to 1340 K. Tests were conducted both with and without the natural gas pulsing system. Sodium concentrations of zero and 30 ppm were tested.

Figure 8-25 shows ammonia slip results, along with process conditions and corresponding NO reductions. NH₃ emissions were generally higher during pulsing, likely because mixing between the air and furnace gases was poorer during pulsing. Sodium evidently reduced ammonia slip. With urea injection at 1300 K with no sodium, ammonia slip results were 11.4 ppm with pulsing off and 16.9 ppm with pulsing on. At the same conditions with 30 ppm sodium added, ammonia slip results were 2.8 ppm with pulsing off and 2.7 ppm with pulsing on. NO reductions for these conditions were greater than 80%, and were also slightly better with sodium addition.

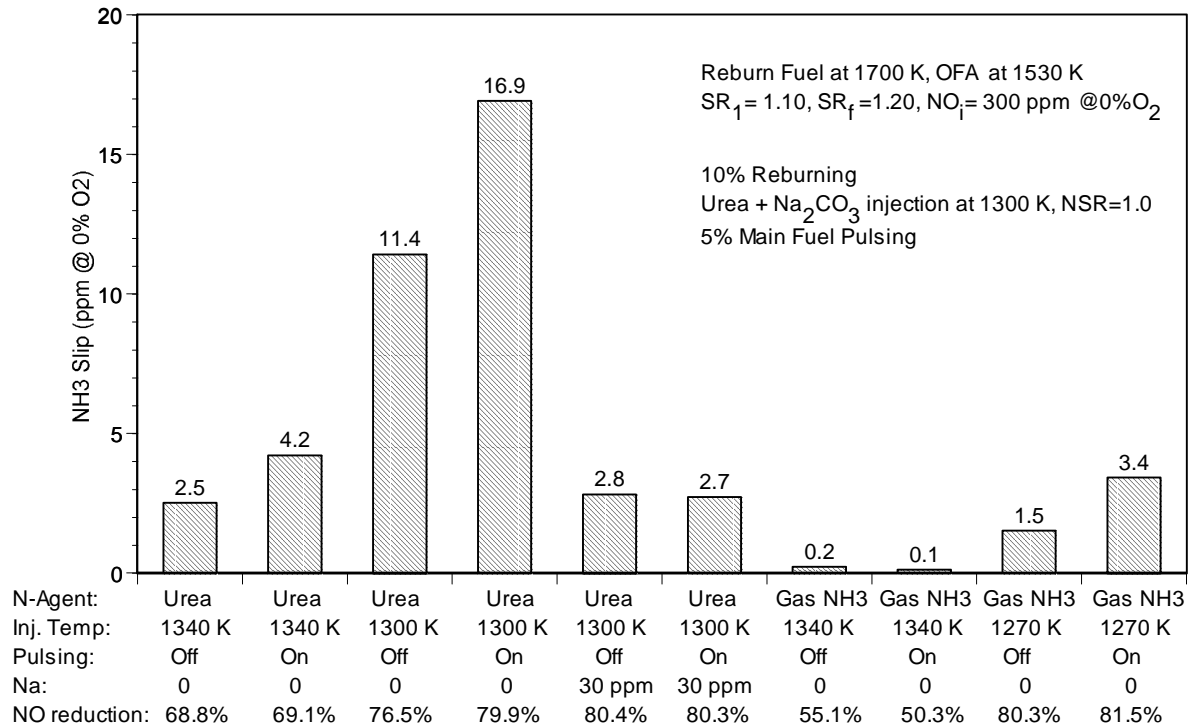


Figure 8-25. Ammonia slip results at different reburning + SNCR process conditions.

With gaseous NH_3 , ammonia slip measurements were made at injection temperatures of 1270 and 1340 K. At 1340 K, ammonia slip was extremely low (well below 1 ppm). However, only moderate NO control was achieved (i.e. 50%-55%). Decreasing the gaseous NH_3 injection temperature to 1270 K increased NO reduction to over 80%, while maintaining NH_3 slip below 4 ppm, both with and without pulsing. Therefore, process conditions at the BSF have been identified that can provide over 80% NO reduction while maintaining ammonia slip below 4 ppm.

8.1.8 Comparison of Greenidge and BSF Data: Summary

Pilot-scale BSF tests were conducted under different process conditions to simulate and predict the performance of AR-Lean and reburning + SNCR in the Greenidge 105 MW tangentially fired boiler. The boiler is characterized by upper furnace fluctuations in CO and O_2 concentrations due to incomplete mixing. A pulsing system was installed in the main fuel delivery line to simulate the fluctuations in furnace gas composition that occur at Greenidge. Pilot-scale test results are discussed separately for two experimental configurations: AR-Lean and reburning + SNCR.

AR-Lean

The NO_x reduction performance at Greenidge is similar to that of the BSF pulsing tests for basic reburning, but less than the BSF counterpart for AR-Lean. This discrepancy is most likely due to the difficulty in controlling the amount of CO concentration in the ammonia injection elevation at full scale. The rapid quench rate at the Greenidge reheater section is probably responsible for the relatively high ammonia slip.

The results of the BSF simulation tests demonstrated that high CO concentrations have negative effects on AR-Lean performance at the NH₃/OFA injection location in the Greenidge boiler. For optimum AR-Lean performance, the CO concentration at the point of N-agent/OFA injection should be below 5000 ppm, preferably 1,000-2,000 ppm, with a low (less than 0.5%) concentration of oxygen. Experimental observations at Greenidge demonstrate that the upper furnace zone is affected by stratification and there are regions with much higher and much lower CO and O₂ concentrations. In both cases, the performance of AR-Lean is lower than under optimum conditions. The results show that high CO concentrations in the N-agent/OFA injection zone of AR-Lean may result in negative NO reductions, i.e. NO increases. This effect can be explained by formation of higher concentrations of active species (OH radicals and O atoms) due to the chain branching reaction of CO oxidation. Under these conditions, the NH₂ radicals formed from the N-agent have higher tendency for oxidation to NO than for NO reduction.

The performance of AR-Lean is better at lower flow rate of the reburning fuel. For instance, 78% NO reduction was achieved at 5% reburning and ammonia/OFA injection at 1280 K compared to only 55% NO reduction at 10% reburning (Figs. 8-13 and 8-14). This can be attributed to the negative effect of higher CO levels formed in the gas mixture due to increased fuel concentration.

The comparison of OFA/N-agent injection temperatures suggests that the Greenidge OFA/NH₃ ports, located at a temperature of about 1300 K, approximately correspond to optimum injection temperature for urea and slightly higher than the optimum injection temperature for gaseous ammonia.

Reburning + SNCR

Test results demonstrated that fuel pulsing, and consequently pulsations of CO and O₂ concentrations, do not affect the performance of basic reburning, but decrease NO_x reduction of SNCR by about 10% for tested experimental configuration.

Performance in combined reburning + SNCR tests was almost independent on pulsing frequency and the reburning fuel flow rate, but decreased with pulsing amplitude. NO reduction in the range of 73-87% was achieved at a pulsing amplitude of 5% for 10% reburning and NSR=1.0 (Fig. 8-19). Higher N-agent levels (NSR = 1.5 and 2) increased NO reduction to 85-94% (Fig. 8-18). Results demonstrate that about 70-80% NO reduction can be achieved under Greenidge conditions using an optimized reburning + SNCR regime. Higher NO_x reduction with lower NH₃ slip can be achieved in the presence of Na₂CO₃ additive. Combination of reburning and SNCR has the following synergistic advantages over using reburning or SNCR alone:

- The combined method can provide higher level of NO reduction at full scale than individual technologies.
- SNCR performance is higher at low fuel pulsations and relatively low concentration of CO in the gas mixture. Injection of OFA upstream of the N-agent injection provides additional mixing in the upper furnace zone, reduces the concentrations of CO, and prepares conditions for a more effective SNCR process. Thus, deterioration of SNCR performance in the presence of CO might be minimized by injecting the N-agent after the OFA.
- Combined reburning + SNCR process requires relatively low input of the reburning fuel. As shown in Fig. 8-20, injection of 10% and 20% reburning fuel resulted in almost identical high level of NO reduction, about 80%.

- High NO reduction level can be achieved with relatively low input of the N-agent compared to SNCR alone. For example, if the initial NO concentration is 300 ppm, SNCR alone requires 300 ppm ammonia or urea to provide NSR=1. In the combined process, reburning reduces NO by about 50-60%, and 120-150 ppm of N-agent is necessary for providing NSR=1. Reduced consumption of N-agent reduces ammonia slip and N₂O emissions.
- Reburning and SNCR promoters can be used to increase the total efficiency of the technology.

8.2 Coal Reburning Studies

Basic reburning and advanced reburning tests were performed in which coal was used as the reburning fuel. These tests were performed in conjunction with South Carolina Electric and Gas (SCE&G) that is considering installing basic coal reburning on multiple boilers with potential to subsequently utilize advanced coal reburning. Coal can be effectively used as a reburning fuel given the right fuel properties and process conditions. In some boiler applications the use of coal as a reburning fuel is limited by the fact that furnace temperatures and residence times are insufficient to fully combust the reburning coal, leading to high carbon-in-ash levels. However, the boilers of interest are equipped with carbon recovery units and thus can tolerate relatively high carbon-in-ash levels. Therefore, these boilers are ideal targets for application of coal reburning and advanced coal reburning.

Two test series were conducted, including basic reburning and promoted advanced reburning. All test work was conducted at BSF. The following sections describe results of coal reburning studies.

8.2.1 Basic Coal Reburning Tests

Studies conducted by GE-EER have shown that a number of fuels can be used effectively in the reburning process. However, due to the heterogeneous nature of coal, it is difficult to predict how a specific coal will perform as a reburning fuel based upon easily characterized fuel properties. Therefore, combustion tests were performed to evaluate the reburning performance of four coals of specific interest to SCE&G. The primary objective of the basic reburning tests was to characterize the impacts of reburning process parameters on NO_x reduction at conditions typical of the full-scale boilers.

For the initial experiments, the main burner was fired with natural gas. Ammonia was premixed with the combustion air to provide a controlled initial NO_x level. Four bituminous coals were tested as reburning fuels. Fuel characteristics are shown in Table 8-1. Each fuel was pulverized in a CE-Raymond deep bowl mill such that 70% passed through a 200 mesh sieve.

The reburning fuel was injected into the furnace through an injector designed to provide rapid dispersion of the fuel into the flue gas. The transport medium for the fuel was nitrogen (to simulate recycled flue gas). The range of parameters investigated in the study represented the range of conditions available at the full-scale units. The main burner was fired at an excess air level of 10%. The reburning fuel was injected at a temperature of 1700 K at rates between 10% and 20% of the total furnace heat input. For the tests with natural gas primary the OFA was injected at 1400 K, corresponding to a reburning zone residence time of 800 ms. The initial NO_x level was set at 400 ppm on a dry, corrected to 3% O₂ basis.

Table 8-1. Test fuel analyses.

Parameter	Units	Coal #1	Coal #2	Coal #3	Coal #4
Proximate					
Moisture	%	4.32	5.35	8.22	5.62
Ash	%	7.16	8.49	14.72	8.26
Volatiles	%	34.30	33.12	31.41	31.82
Fixed Carbon	%	54.22	53.04	45.65	54.3
Total	%	100.00	100.00	100.00	100.00
Calorific Value	Btu/lb	13288	13217	11283	13124
Ultimate					
Carbon	% dry	78.63	78.77	69.50	77.03
Hydrogen	% dry	4.91	4.89	4.46	4.71
Nitrogen	% dry	1.62	1.50	1.39	1.41
Sulfur	% dry	0.82	0.91	1.11	0.82
Ash	% dry	7.48	8.97	16.04	8.75
Oxygen	% dry	6.54	4.96	7.50	7.28
Total	% dry	100.00	100.00	100.00	100.00

Figure 8-26 compares reburning performance of the four coals. The best performance was obtained with the coal #1, followed in order by coal #4, coal #3, and coal #2. It is believed that these trends are related to the composition and volatility of each reburning fuel. More volatile fuels tend to release the bound-nitrogen species and fuel fragments quicker. This allows the reburning chemistry more time to occur, and enables nitrogen-bound species to be processed in an environment where they can be reduced to molecular nitrogen.

Another factor that can affect reburning performance is the nitrogen content of the coal; higher nitrogen concentrations result in poorer reburning performance. However, in this case the nitrogen contents of the four test fuels vary by only 0.2%, so this factor has minimal impact on reburning performance.

The second series of tests was performed with coal as the primary fuel. For each of the four coals the same coal was used as both the main and reburning fuel. OFA was injected at 1500 K, corresponding to a reburning zone residence time of 400 ms. Figure 8-27 compares reburning performance of the four test fuels. For these conditions, coal #3 performed best, followed by coal #2, coal #1, and coal #4. NO_x reductions for these tests were lower than those obtained during the previous tests with natural gas primary. This is mainly attributed to the fact that reburning zone residence time during the coal primary tests (400 ms) was lower than during the natural gas tests (800 ms).

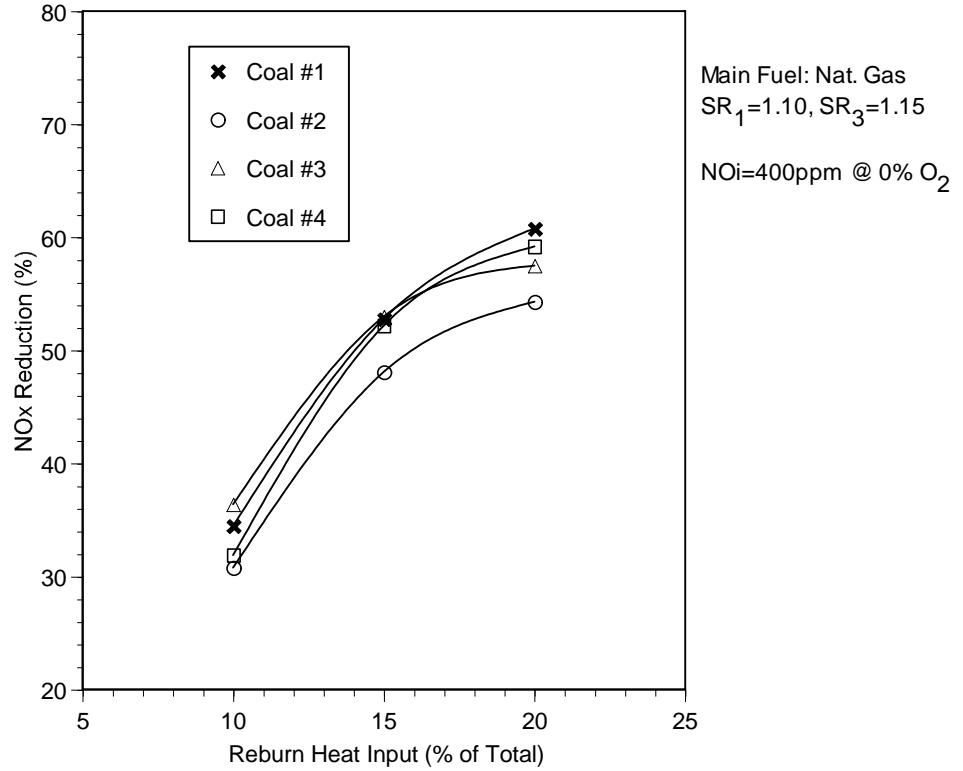


Figure 8-26. Basic coal reburning performance as a function of reburning heat input with natural gas primary.

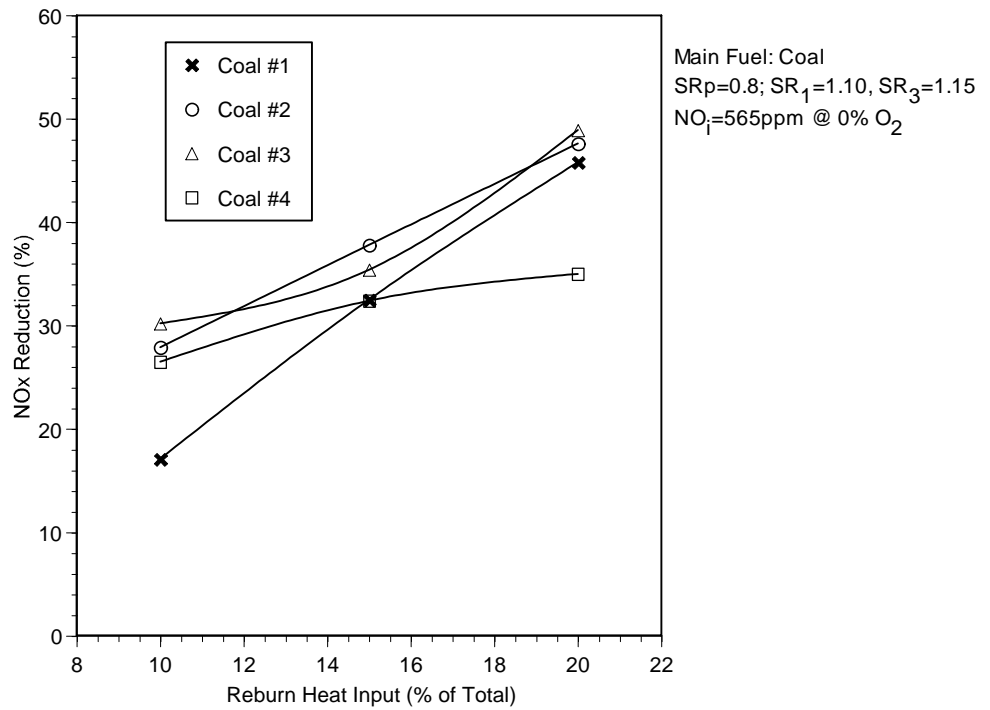


Figure 8-27. Basic coal reburning performance as a function of reburning heat input with coal primary.

8.2.2 Advanced Coal Reburning Tests

Two coals selected for these tests based on results of basic reburning studies were coal #1 and coal #3. Three test series were performed including AR-Lean, AR-Rich, and reburning + SNCR. For these tests natural gas was used as the primary fuel. Initial NO_x concentration was 400 ppm. In all tests $\text{SR}_1 = 1.1$ and $\text{SR}_3 = 1.15$ while SR_2 was a variable. Urea was injected at $\text{NSR} = 1.5$.

AR-Lean with Coal Reburning

Figure 8-28 shows AR-Lean performance as a function of injection temperature for coals #1 and #3. Reburning heat input was 10%. With each coal performance increased with decreasing injection temperature. Maximum NO_x reductions were 57% for coal #3 and 62% for coal #1, both obtained at an injection temperature of 1310 K. These results represent an incremental improvement of 17-20 percentage points over basic reburning.

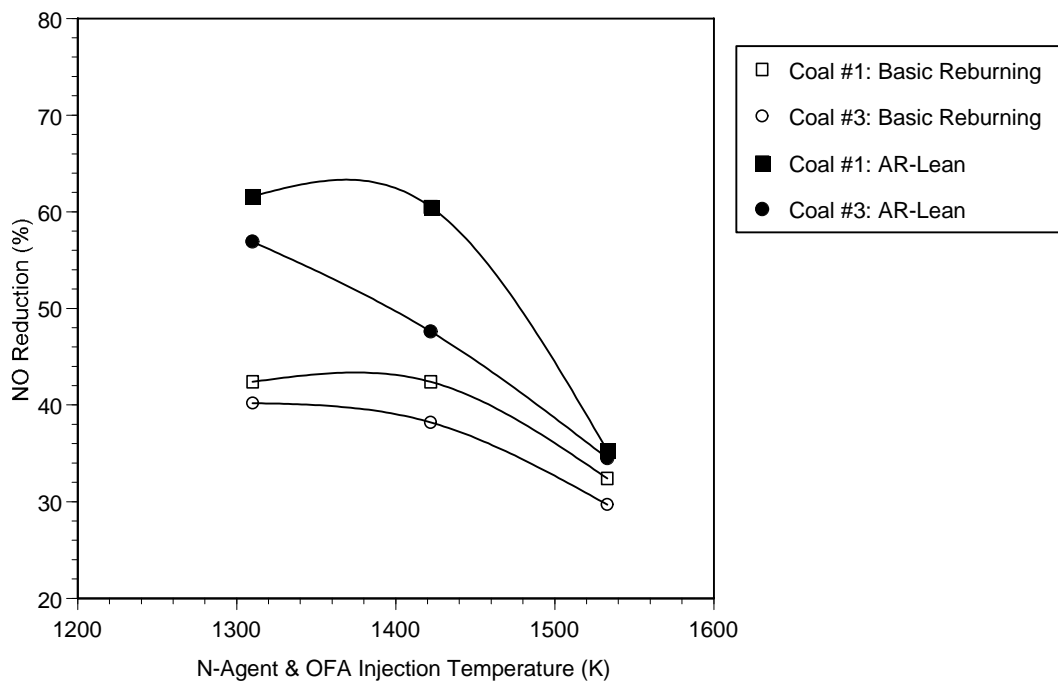


Figure 8-28. AR-Lean performance at 10% reburning as a function of injection temperature for coals #1 and #3.

Figures 8-29 shows promoted AR-Lean performance as a function of flue gas sodium concentration for coals #1 and #3. OFA was injected at 1310 K. With each coal sodium dramatically increased NO_x reduction. With coal #1, NO_x reduction increased from 62% with no sodium to 90% with 150 ppm sodium. With coal #3 under similar conditions NO_x reduction increased from 57 to 82%.

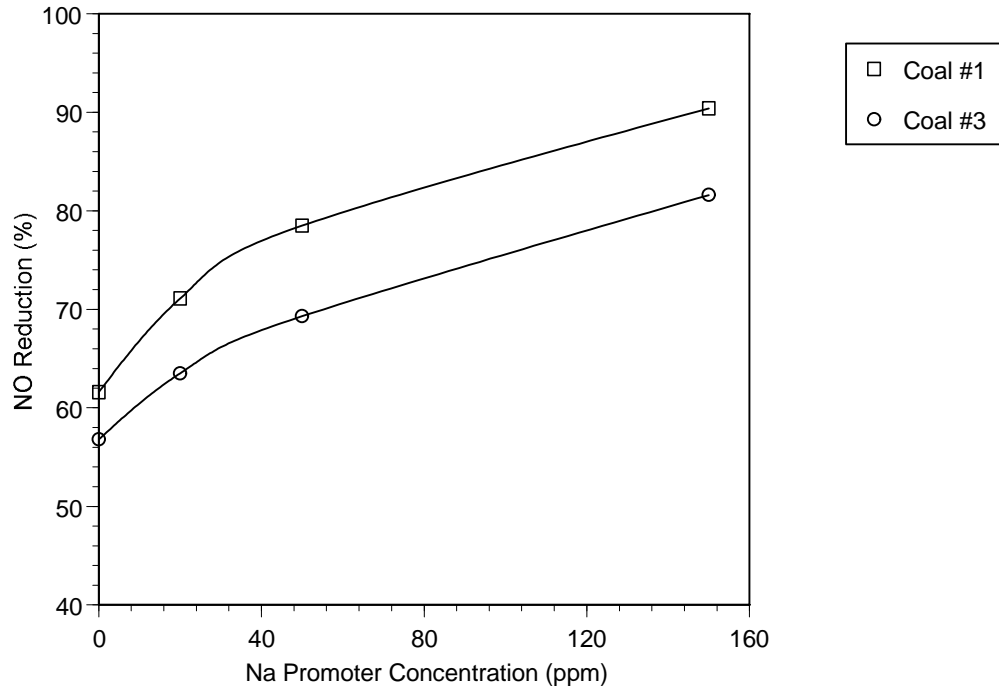


Figure 8-29. Promoted AR-Lean performance at 10% reburning as a function of promoter concentration for coals #1 and #3. Na_2CO_3 is co-injected with urea.

AR-Rich with Coal Reburning

Figure 8-30 shows AR-Rich performance as a function of injection temperature for coals #1 and #3. Urea was injected at 1310-1530 K and OFA was injected at 1300 K. Maximum NO_x reduction for coal #1 and coal #3 was 58% and 61%, obtained at injection temperature of 1400 K. Figure 8-31 shows promoted AR-Rich performance as a function of flue gas sodium concentration. Adding 150 ppm sodium caused NO_x reduction to increase from 57% with no promoter to 65% with 150 ppm Na for coal #3 and from 53% to 72% for coal #1, which is a lower increase than that observed during AR-Lean tests.

Coal Reburning + SNCR

Reburning + SNCR tests were conducted as a function of N-agent injection temperature, reburning heat input, and sodium promoter concentration. Figure 8-32 shows results as a function of N-agent injection temperature for coals #1 and #3. With each coal NO_x reduction increased with decreasing injection temperature. Maximum NO_x reduction for both coals was about 90%, achieved at an injection temperature of 1230 K.

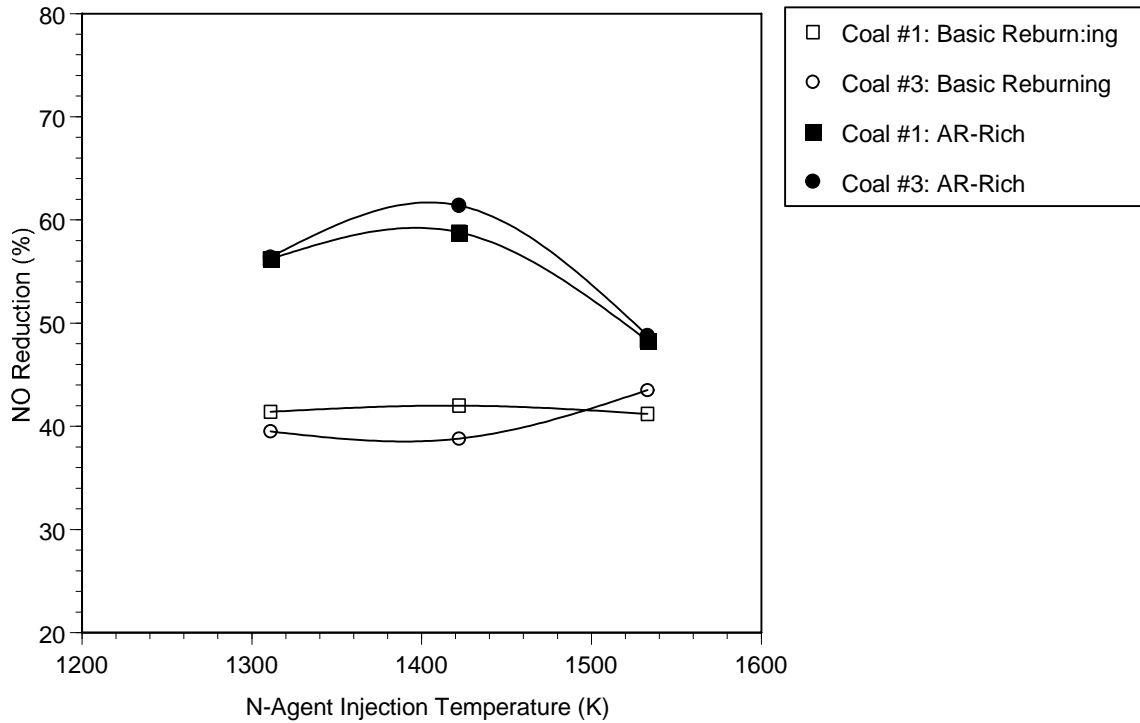


Figure 8-30. AR-Rich performance at 10% reburning as a function of injection temperature for coals #1 and #3.

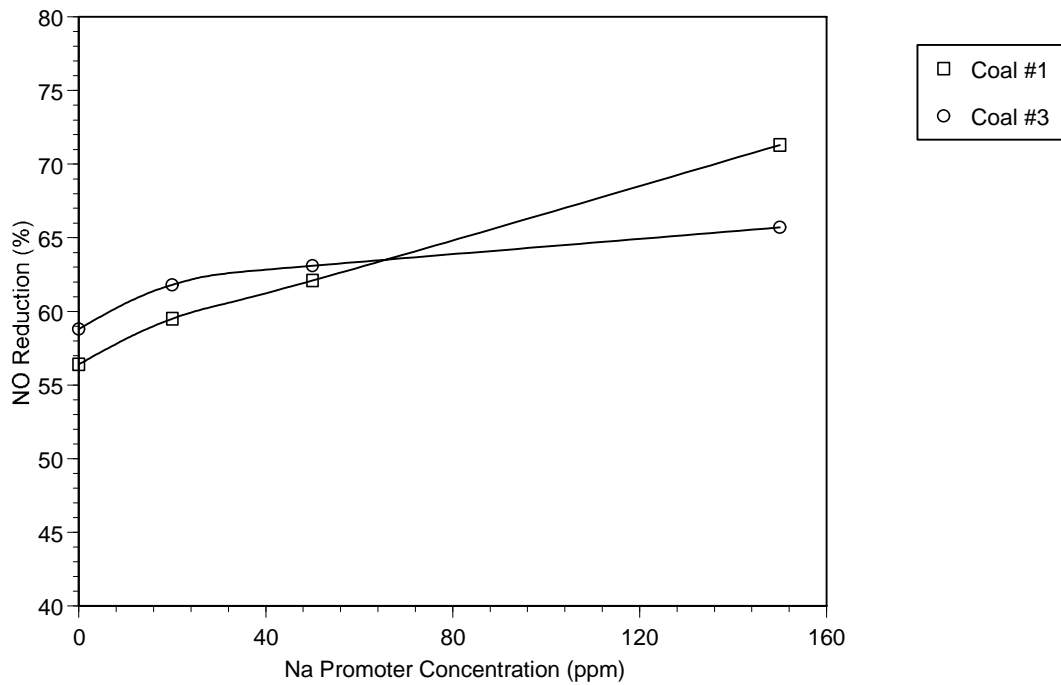


Figure 8-31. Promoted AR-Rich performance at 10% reburning as a function of promoter concentration for coals #1 and #3. Na_2CO_3 is co-injected with urea.

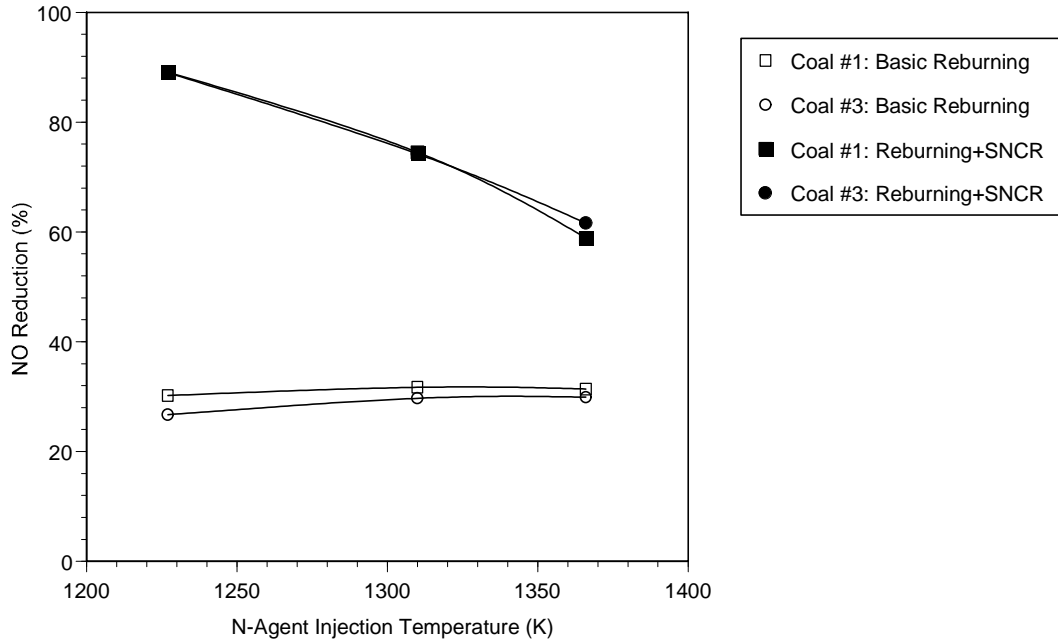


Figure 8-32. Combined reburning and SNCR performance at 10% reburning as a function of injection temperature for coals #1 and #3.

Figure 8-33 shows reburning + SNCR results as a function of reburning heat input. OFA was injected at 1530 K, urea at 1200 K. With each coal, overall NO_x reduction showed minimal dependence on reburning heat input. Better performance was achieved with the coal #1 than the coal #3.

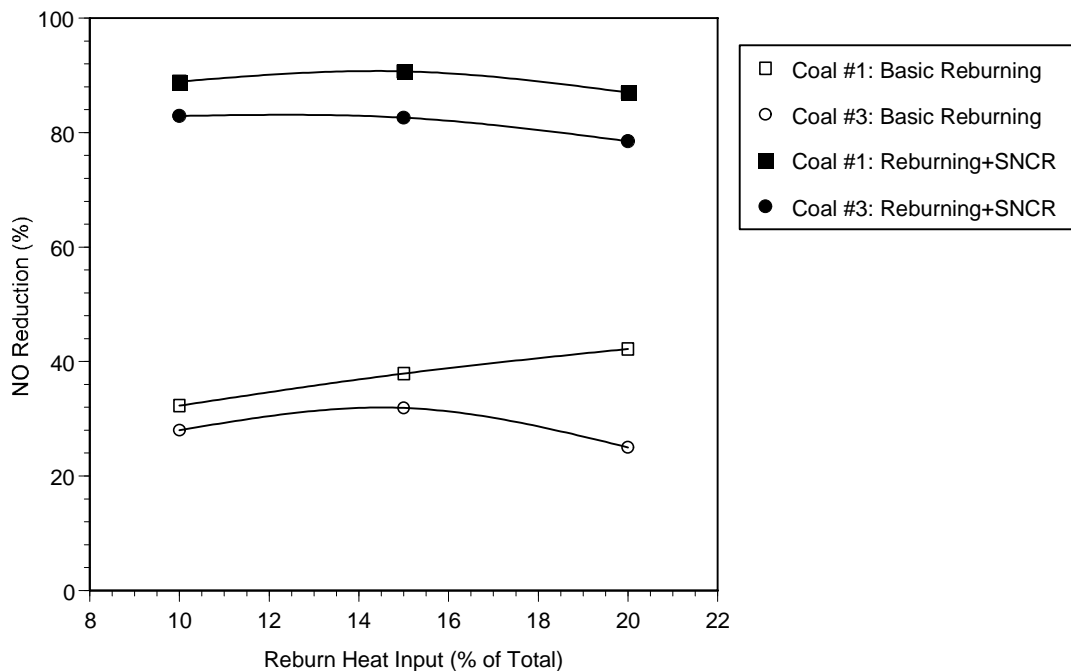


Figure 8-33. Combined reburning and SNCR performance as a function of reburning heat input for coals #1 and #3.

Figure 8-34 shows reburning + SNCR results as a function of sodium promoter concentration. The sodium was co-injected with the N-agent at 1230 K. In each case the sodium had minimal effect on performance, likely because the injection temperature was too low.

The final series of tests involved promoted reburning with no N-agent. The promoter consisted of an iron oxide waste material that was co-injected with the reburning coal. Fe concentration in the flue gas was varied from 0 to 1,000 ppm. Figure 8-35 shows NO_x reduction as a function of Fe promoter concentration for coal #1. Co-injection of 1,000 ppm iron oxide waste with the reburning fuel increased NO_x reduction by 10% in comparison with reburning only.

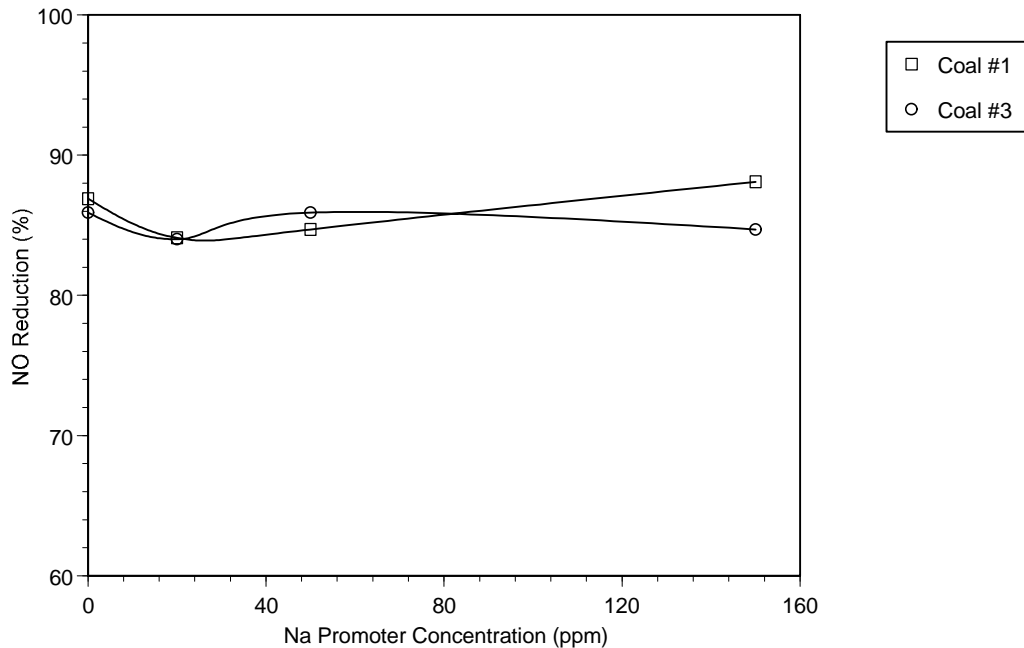


Figure 8-34. Combined reburning and SNCR performance at 15% reburning as a function of promoter concentration for coals #1 and #3.

8.2.3 Advanced Coal Reburning: Summary

1. The results of the experiments indicate that the four tested bituminous coals are capable of providing reasonably high NO_x control at the conditions available at the full-scale boilers. At the BSF, at 20% reburning each of the four coals provided over 50% NO_x reduction in basic reburning. Defining the level of control at full-scale will depend on the extent to which effective mixing of the reburning fuel can be achieved, and the extent to which the furnace flow field characteristics impact the reburning zone residence time.
2. Over 90% NO_x reduction can be achieved with utilization of coal as a reburning fuel in AR. The most effective AR variant is reburning + SNCR followed by AR-Lean and AR-Rich. The same order of AR efficiencies was found for firing natural gas as a reburning fuel. Tests showed that injection of promoters could significantly improve efficiency of AR.

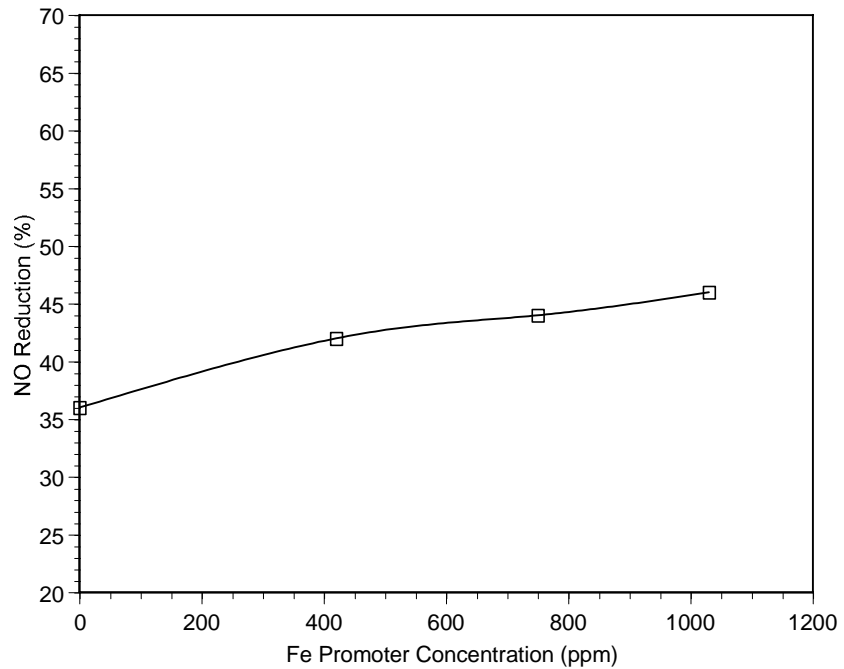


Figure 8-35. Effect of Fe promoter concentration on coal #1 reburning. Amount of the reburning fuel is 15%.

9.0 Task 2.5 10×10^6 Btu/hr Proof of Concept Tests

The objective of Task 2.5 tests was to provide a final indication of the viability of the AR technologies before proceeding to a full-scale demonstration. The tests were conducted in TF at nominally 10×10^6 Btu/hr. The performance goals in the proof-of-concept tests were to: (1) reduce NO_x by up to 95% with net emissions less than $0.06 \text{ lb NO}_x/10^6 \text{ Btu}$ and (2) minimize other pollutants (N_2O and NH_3) to levels lower than reburning and SNCR. Several variants of AR were studied, including AR-Lean, AR-Rich, reburning + SNCR, and MIAR. All variants were evaluated both with and without promoters.

A high-sulfur, bituminous Illinois coal was used as the main fuel for all tests. An air-staging system was applied to the primary burner to simulate a commercial LNB, thus providing initial NO_x concentrations similar to those obtained in full-scale boilers. Natural gas was used as the reburning fuel. Reburning fuel transport media was nitrogen, which simulated an inert media such as steam. Reburning fuel was injected at 1800 K, while OFA injection temperature varied from 1285 to 1380 K. The N-agent and promoter consisted of urea and sodium carbonate, respectively. Basic test conditions were those found to be optimum in previous sub-scale experiments. Initial uncontrolled amount of NO_x resulting from coal combustion was 820 ppm. An air-staging resulted in reduction of NO_x to 340 ppm. Stoichiometric ratios in the main combustion and burnout zones were 1.1 and 1.15, respectively. The NSR varied from 1.3 to 1.6.

The following sections summarize results of AR tests in TF.

9.1 AR-Lean Tests

AR-Lean tests were conducted in which urea and promoter were injected along with the OFA at 1300 K. Flow rate of sodium carbonate was varied such that the concentration of sodium in the flue gas varied from 0 to 150 ppm. Figure 9-1 shows results obtained at 6% and 10% reburning heat input. Basic reburning provided 27% and 40% NO_x reduction. These values increased to 65% and 66% for unpromoted AR-Lean. Addition of sodium carbonate caused performance to increase significantly for 6% reburning and minimally for 10% reburning. Thus the promoter was significantly more effective at 6% reburning than at 10% reburning.

9.2 AR-Rich Tests

AR-Rich tests were conducted in which urea and promoter were injected into the fuel-rich reburning zone at 1450 K and OFA was injected at 1320 K. The concentration of sodium in the flue gas was varied from 0 to 150 ppm. Reburning heat inputs of 6% and 10% were tested (Figure 9-2). NO_x reduction in unpromoted AR-Rich was 58% and 64% for 6% and 10% reburning, respectively. Addition of sodium carbonate had minimal effect. Thus AR-Rich performance was worse than that of AR-Lean, and the promoter had a lesser impact upon performance.

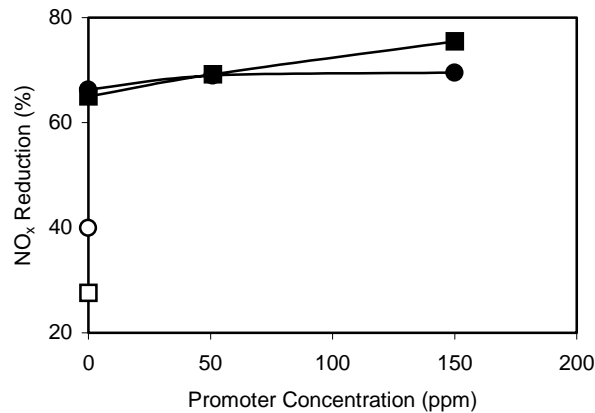


Figure 9-1 AR-Lean performance vs. promoter concentration at 6% (squares) and 10 % (circles) reburning. Open symbols represent basic reburning, filled symbols represent AR-Lean.
NSR = 1.5

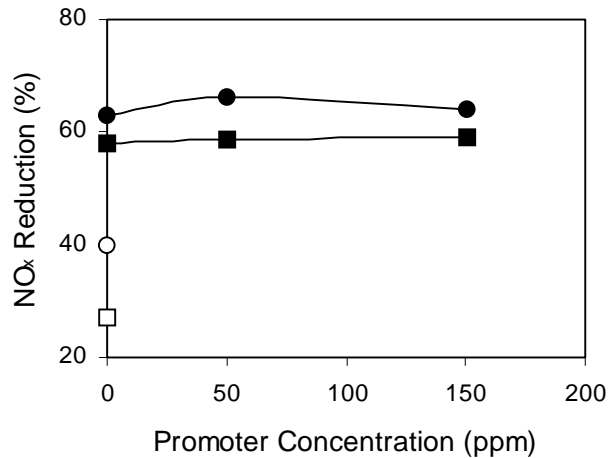


Figure 9-2. AR-Rich performance vs. promoter concentration at 6% (squares) and 10 % (circles) reburning. Open symbols represent basic reburning, filled symbols represent AR-Rich.
NSR = 1.5.

9.3 Reburning + SNCR Tests

Reburning + SNCR tests were conducted at 10% and 20% reburning, OFA was injected at 1560 K. Two urea injection temperatures were tested, including 1285 K and 1380 K. Results of tests are presented in Figure 9-3. The maximum achievable performance was better with urea injection at 1285 K than at 1380 K. Similar overall performance levels were obtained at 10% and 20% reburning, although it is noted that at 10% reburning more urea is required and at 20% reburning more natural gas is required. The promoter again had minimal impact on performance.

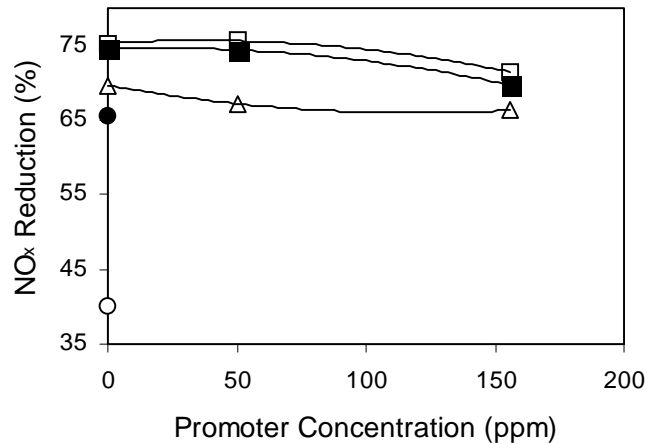


Figure 9-3. Reburning + SNCR performance vs. promoter concentration at 10% and 20% reburning. Open symbols represent 10% reburning, filled symbols represent 20% reburning. Circles represent basic reburning. Urea is injected at 1285 K (squares) at NSR = 1.4 and at 1380 K (triangles) at NSR = 1.6 .

9.4 MIAR Test Results

Several MIAR variants were tested to optimize overall process performance. The first MIAR tests involved AR-Rich + AR-Lean. The first N-agent was injected at 1480 K, the second N-agent and promoter were injected with the OFA at 1370 K. Reburning heat input was 10%. As shown in Figure 9-4, basic reburning provided 40% NO_x control, AR-Rich NO_x reduction was 58%. MIAR NO_x reduction was 78%. The sodium promoter had minimal impact on performance.

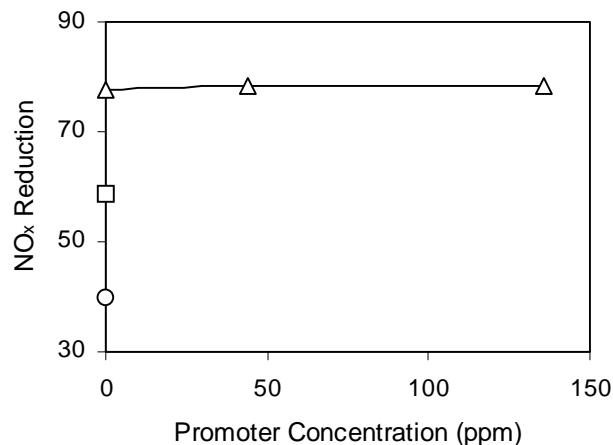


Figure 9-4. MIAR: combined AR-Lean + AR-Rich performance vs. promoter concentration at 10% reburning. Circle represents basic reburning, square represents AR-Rich, triangles represent AR-Rich + AR-Lean. NSR₁ = 1.6, the second urea is injected at 1370 K at NSR₂ = 1.4.

MIAR tests were then conducted involving AR-Lean + SNCR. The first N-agent was injected along with the OFA at 1350 K, the second N-agent was injected at 1280 K. Two reburning heat inputs were tested: 6% and 10%. At 10% reburning, sodium promoter was injected along with the second N-agent. At 6% reburning, the sodium promoter was injected along with the first N-agent. As shown in Figure 9-5, basic reburning provided 27% and 40% NO_x control for 6% and 10% reburning, respectively. AR-Lean NO_x reductions were 64% for both inputs of the reburning fuel. MIAR NO_x reductions were 84% and were also independent of the amount of the reburning fuel. With sodium promoter, NO_x reductions increased to 91% at 6% reburning. The sodium promoter had minimal impact on performance at 10% reburning.

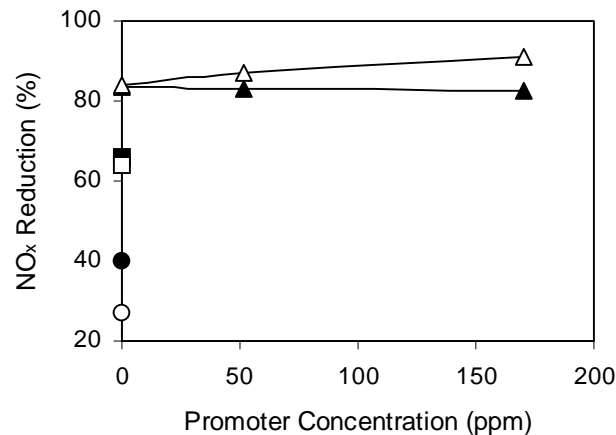


Figure 9-5. MIAR: combined AR-Lean + SNCR performance vs. promoter concentration at 6% (open symbols) and 10% reburning (filled symbols). Circles represent basic reburning, squares represent AR-Lean, triangles represent AR-Lean + SNCR. $NSR_1 = NSR_2 = 1.5$.

9.5 Ammonia Slip and N₂O Emissions Measurements

Table 9-1 shows results of ammonia slip measurements. Two conditions were tested: MIAR and AR-lean. For MIAR, the first urea was injected at 1450 K and 1390 K, the second urea was injected at 2000 K and 1920 K. For the MIAR tests, ammonia slip increased with decreasing temperature of the coldest N-agent. For AR-lean ammonia was below the detection limit of about 1 ppm.

Tests also demonstrated that there were no hydrocarbon emissions in any of conducted tests. The N₂O emissions were 0 ppm for the basic reburning, 6 ppm for the basic SNCR and 11 ppm for the MIAR tests.

9.6 Proof of Concept Tests: Summary

For the optimized MIAR condition, Figure 9-6 shows overall NO_x reductions for each process component, including the burner air staging system, which simulates a low-NO_x burner. Staging provided 57% NO_x control. Basic reburning increased this to 70%. Adding SNCR increased overall NO_x reduction to 85%. Adding AR-Lean increased performance to 94%. Overall NO_x reduction for the complete MIAR process, including sodium promoter, was 96%. The complete process caused NO_x emissions to decrease from a baseline concentration of 820 ppm to 32 ppm.

Proof-of-concept tests in 10×10^6 Btu/hr combustion facility provided a final indication of the viability of the AR technology. The performance goal of Phase II to reduce NO_x by up to 95% with net emissions less than $0.06 \text{ lb}/10^6 \text{ Btu}$ has been met.

Table 9-1. Results of ammonia slip tests.

Technology	AR-Lean	MIAR	MIAR
Reburn heat input (%)	6	6	6
OFA temperature (K)	1380	1450	1390
1 st N-agent temperature (K)	1380	1450	1390
1 st N-agent NSR	1.60	1.35	1.48
2 nd N-agent temperature (K)		1370	1320
2 nd N-agent NSR		1.35	1.44
Promoter temperature (K)	1380	1450	1390
Promoter concentration (ppm)	265	268	246
Overall NO_x control (%)	67	91	91
Exhaust NO_x (ppm @ 0% O_2)	140	45	32
Exhaust NH_3 (ppm @ 0% O_2)	<1	6.1	36.2

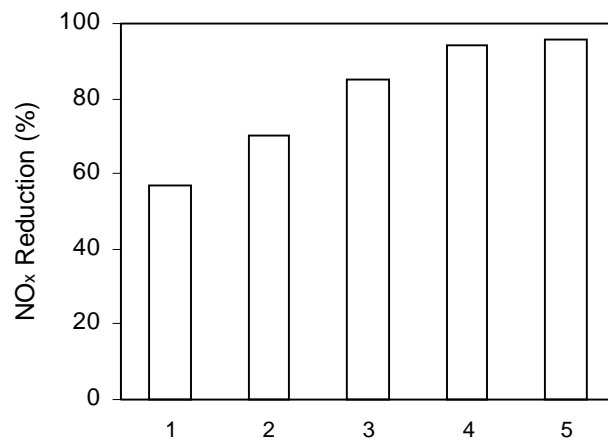


Figure 9-6. Overall MIAR NO_x reduction under optimized conditions at 6% reburning. OFA is injected at 1340 K. Urea is injected with OFA (NSR = 1.3) and in burnout zone (NSR = 1.3, 1270 K). 1 – LNB, 2 – basic reburning, 3 – Reburning + SNCR, 4 – AR-Lean + SNCR, 5 – AR-Lean + SNCR (250 ppm promoter).

10.0 Task 2.6 Design Methodology Validation

Goals of this task were to (1) provide a conduit for translation of the analytical and experimental AR configurations into practical full-scale designs and (2) update AR economics and market potential for U.S. utility boilers.

Section 10.1 discusses activities that were undertaken for full-scale implementation of SGRA. These activities included Tower Furnace tests to determine efficiency of AR-Lean at higher than optimum temperatures and implementation of AR at the Martinez Refining Company complex in Martinez, CA. Section 11.2 presents update of AR economic and market analyses.

10.1 Full-Scale Implementation of AR

10.1.1 Activities at Martinez Refining Company Complex

GE-EER has undertaken in 1998-1999 a multi-phase program to identify and select a technology for reducing NO_x emissions from the CO boilers at the Martinez Refining Company complex in Martinez, CA (MRC). The MRC CO boiler was characterized as a unit with a high level of complex chemical kinetics and minimal slow stream mixing. The front wall fired unit burned a refinery fuel gas, an off gas fed from the exhaust of a catalytic cracking unit, and a low BTU content flexigas. These three fuel streams with varying characteristics (heating value, flow, density, temperature) were burned simultaneously in the refractory lined horizontal firebox. The CO off gas mass flow was so great compared to the other fuels that mixing between the CO off gas and those other fuel and air streams was relatively slow. This slow mixing behavior was one of the parameters that were believed to limit NO_x reduction performance on the MRC CO boilers.

As a result of the initial phase of this project, CO boiler #3 was retrofitted with an AR NO_x control system consisting of air staging, gas injection, and SNCR. The technologies were selected to work in conjunction to reach the project goals of reducing NO_x emissions by 67.5% while maintaining ammonia slip and carbon monoxide below regulatory levels.

Earlier design validation field trials simulating air staging and SNCR showed that NH₃ slip resulting from air staging was being oxidized by the OFA jets, thus compromising some of the benefits of air staging. One of the options that was considered during final stage of the project to reduce this negative impact was *injection of natural gas* in the vertical section of the CO duct. Chemical kinetic modeling predicted that the gas injection process might limit NH₃ slip at the stack to less than 50 ppm. The process works by injecting natural gas to create a slightly fuel rich reburning zone.

Tests were performed to investigate potential benefit of the gas injection on ammonia slip. The test results, however, showed that gas injection into the CO gas resulted in a slight increase in NO_x emissions. Effectively, little difference was observed between the tests with air staging alone and air staging with gas injection. It is believed that poor mixing between the CO gas and the refinery gas flame was the primary cause of this negative result.

An alternative approach to reduce NO_x emissions was considered. This approach includes an improvement of the air/SNCR concept by stoichiometric adjustments and *Na promotion*. Kinetic modeling predicted that this approach could result in significant performance improvement, up to 70% NO_x reduction. However, additional, more detailed modeling analysis suggested that the furnace temperature was too highly stratified to obtain the full benefit of Na injection.

While gas injection and Na promotion were not implemented in boiler #3 and project objectives were met by using other available options (improving air staging and SNCR system), this work provided additional insight into the AR methodology and demonstrated potential applications and benefits of different aspects of AR technologies.

10.1.2 TF AR-Lean Tests

Tests conducted in the CTT, BSF and TF demonstrated that efficiency of NO_x reduction in AR could be up to 95%. This high efficiency of NO_x reduction can be achieved if process parameters including temperature of OFA injection are optimized. However, in many boilers that are equipped with OFA injection system the injection occurs at higher than optimum temperatures. Utilization of already existing ports for OFA injection would decrease cost of AR installation. However, efficiency of NO_x reduction in this case is expected to be lower than that at optimum conditions.

The objective of current tests was to determine efficiency of co-injection of N-agent with OFA (AR-Lean) in large pilot-scale combustor at temperatures that are higher than optimum. Specifically, it was of interest to demonstrate the effect of large N-agent droplets, the approach that was identified as promising in the modeling studies (Section 7.5). Tests were conducted in the TF. Temperature profile in TF was modified to match conditions in an industrial boiler that is currently being considered for demonstration of the AR-Lean technology.

The test approach was to parametrically vary key process parameters in order to characterize sensitivity and optimize performance. Test variables included:

- Urea atomization pressure
- Urea nitrogen stoichiometric ratio
- Urea solution strength
- OFA/Urea port configuration
- Nitrogen agent type
- OFA/Urea injection temperature
- Injector position

Each of these variables was evaluated as reburning heat input was varied from 10% to 20%. For comparison, a series of basic SNCR tests was also performed.

The following subsections describe nozzle development studies, test facility configuration and the impacts of each test variable upon performance.

Atomization Notes

Prior to the test work, a series of nozzle development studies was performed. The objective was to develop nozzles capable of providing controllable droplet mean diameters in the range of 200 to 1000 μm. The nozzles were of the twin-fluid type, with pressurized gas used to provide energy to atomize the liquid. A total of 5 nozzle designs were developed, labeled A-1 through A-5. The design had different orifice diameters for the liquid and gas streams. Design A-4 was selected for the pilot scale tests.

A total of five nozzles of the A-4 design were built and characterized as a function of atomization gas pressure using a Malvern particle sizer. Figure 10-1 shows droplet mean diameter as a function of atomization gas pressure. As pressure was increased from 10 to 40 psig, mean diameter decreased from approximately 1000 to 100 μm . Results were similar for all nozzles. At gas pressures of 5 psig and lower the atomizers began to fail, with the liquid spray sputtering and becoming off-center.

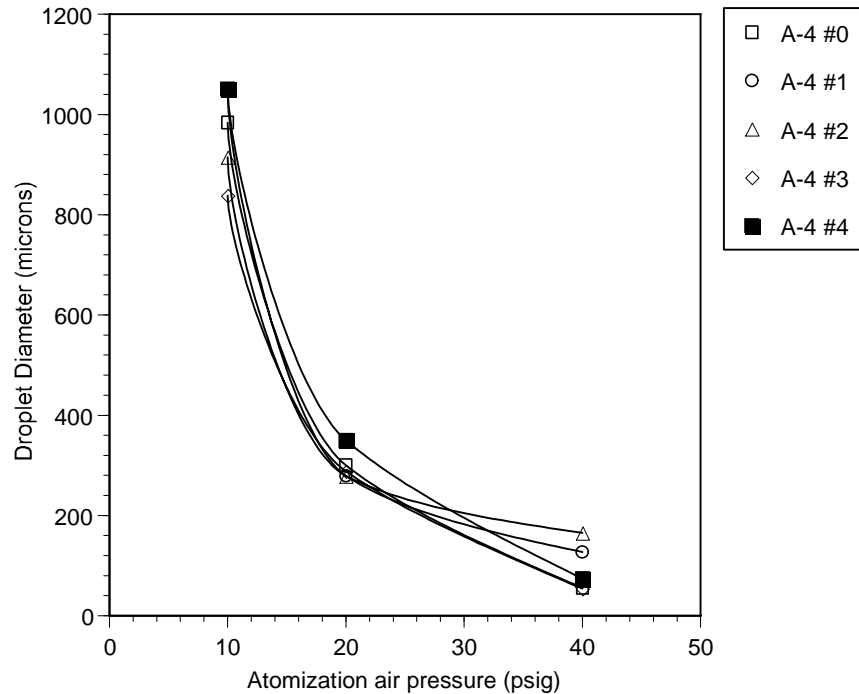


Figure 10-1. Atomization characteristics of test nozzle.

A series of qualitative flow visualization tests was also performed in which the nozzle was oriented horizontally, simulating the configuration used in the pilot scale tests. Atomization pressure was varied from 0 to 60 psig. The liquid spray was observed to extend horizontally outward by a maximum of about 2 feet. Since the TF is 4 feet across, it was believed that the liquid spray would not impinge upon the far wall unless it was carried there by the overfire air.

Test Facility Configuration

The tests were conducted in the TF. Natural gas was used as main and reburning fuels. For the current tests the furnace was configured to nominally simulate the thermal conditions of the target boiler. Figure 10-2 compares the TF temperature to that of the target boiler. The thermal quench rate through the furnace agreed fairly well for the two units.

Urea was injected along with OFA at 1650 K. For comparison, tests were also conducted at OFA injection temperature of 1520 K to demonstrate the effect of temperature on N-agent performance. The injectors were designed with a central urea atomizer surrounded by an annular OFA port. Two configurations were used for the OFA/urea injectors, one with four ports and the other with three ports. These configurations were designed to provide different mixing and entrainment characteristics. A brief series of tests was also conducted using axial injectors. This involved

inserting two L-shaped injectors into the furnace such that urea was injected axially, co-current to the furnace gas flow. The axial injectors were oriented to provide maximum flow field coverage. Initial NO_x concentration was 240 ppm.

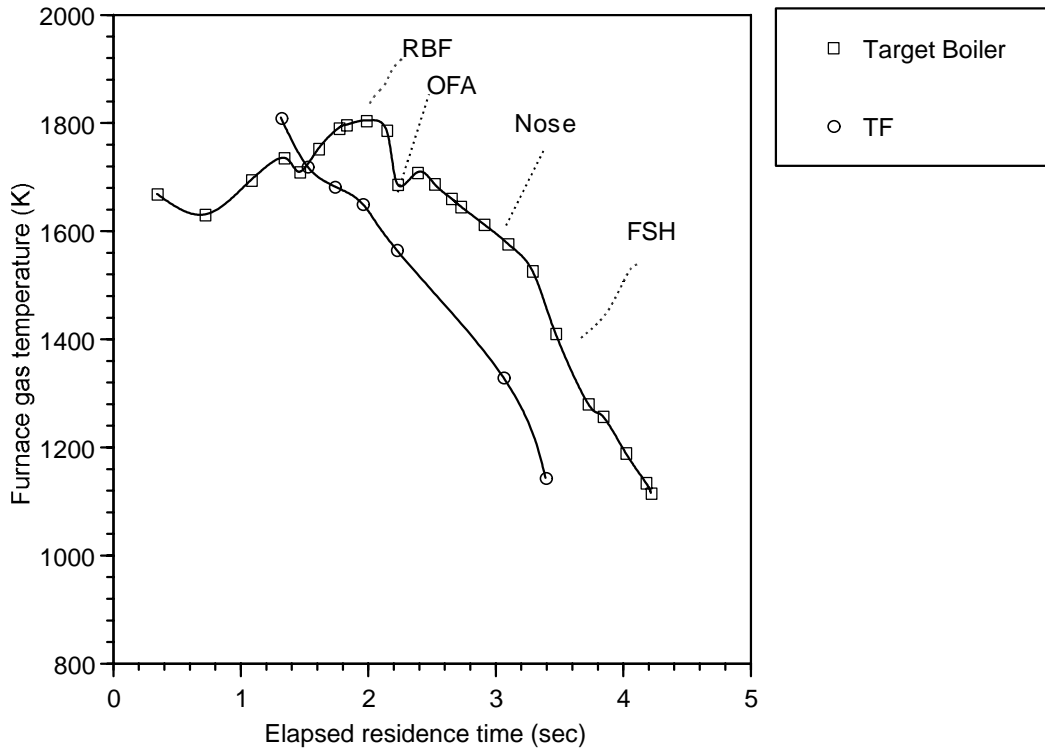


Figure 10-2. Temperature profiles for the target boiler and the TF.

Effect of Atomization Pressure

Atomization pressure was varied from 5 to 20 psig. As shown in Fig. 10-3a, overall NO_x reduction improved with decreasing pressure, particularly at 10% reburning. However, the highest incremental NO_x reduction achieved by urea (Fig. 10-3b) for any condition was 9%. The incremental reduction here is defined as NO_x reduction by N-agent only.

Effect of Urea Nitrogen Stoichiometric Ratio

Urea NSR was varied from 1.0 to 1.5. As shown in Figure 10-4, performance was slightly better at the higher NSR. However, the incremental NO_x reduction provided by urea remained below 15% in all cases.

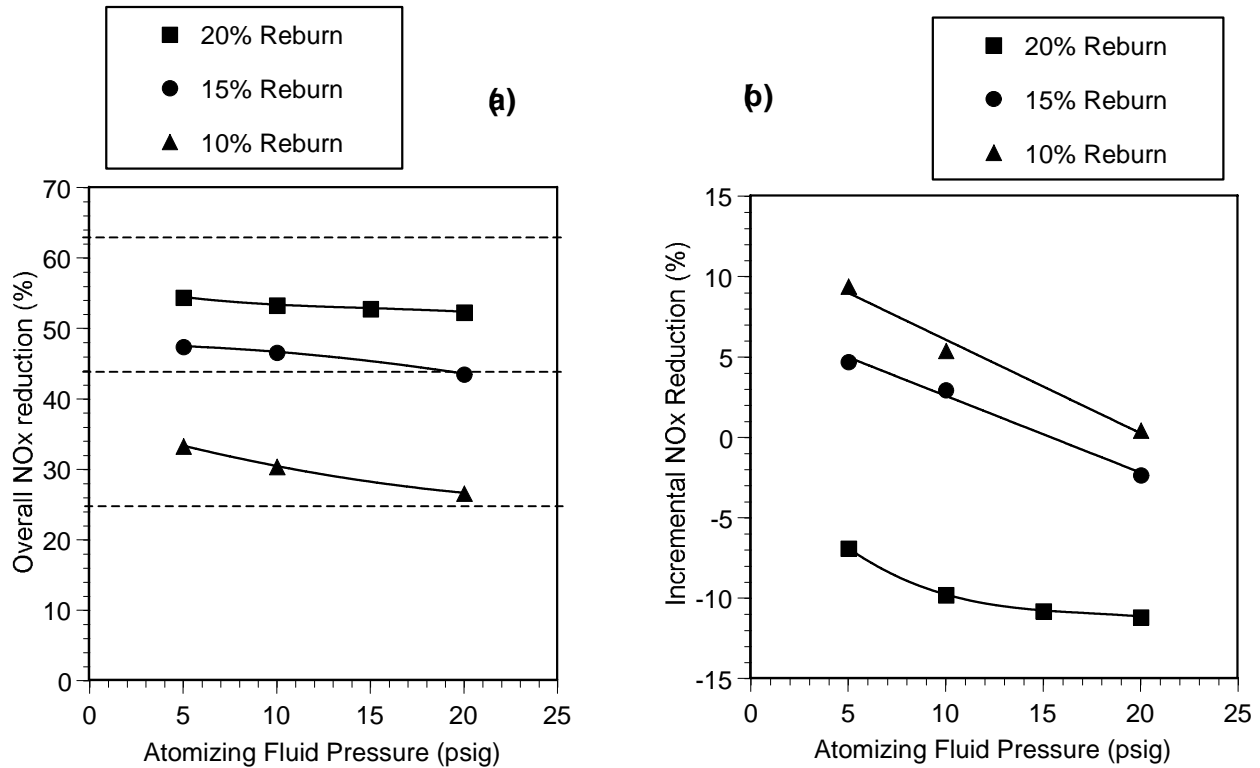


Figure 10-3. Impact of atomization pressure for 5% urea solution on overall (a) and incremental (b) NO_x reduction by urea solution co-injected with OFA. Dashed lines represent NO_x reduction without urea. NSR = 1.0.

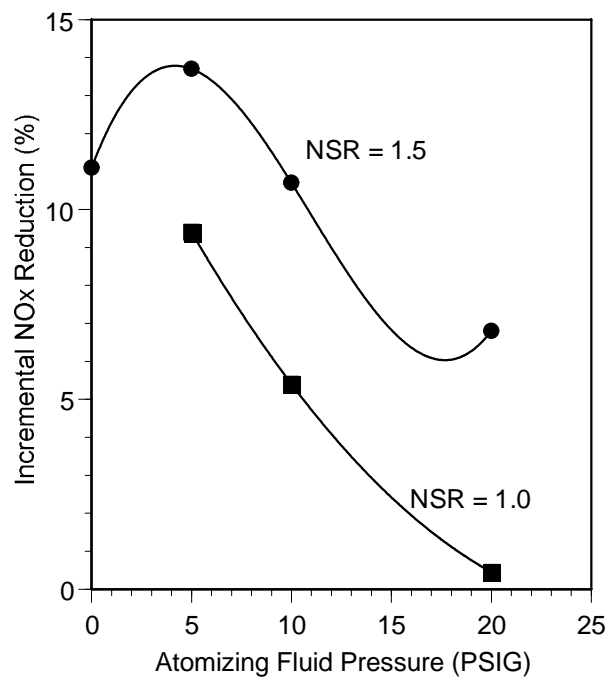


Figure 10-4. Incremental NO_x reduction for co-injection of 5% urea solution with OFA at 10% reburning.

Effect of Urea Solution Strength

The Malvern tests revealed that the atomization nozzles tended to produce larger droplets at higher liquid flow rates. Therefore, as a means of further evaluating impacts of droplet size upon performance, tests were conducted in which the urea solution strength was varied, with a corresponding change in liquid flow rate. Figure 10-5 shows incremental performance of the urea at solution strengths of 2.5%, 5%, and 10%. Performance was best with the most dilute solution, corresponding to the highest liquid flow rate. This implies that better performance was achieved with larger droplets.

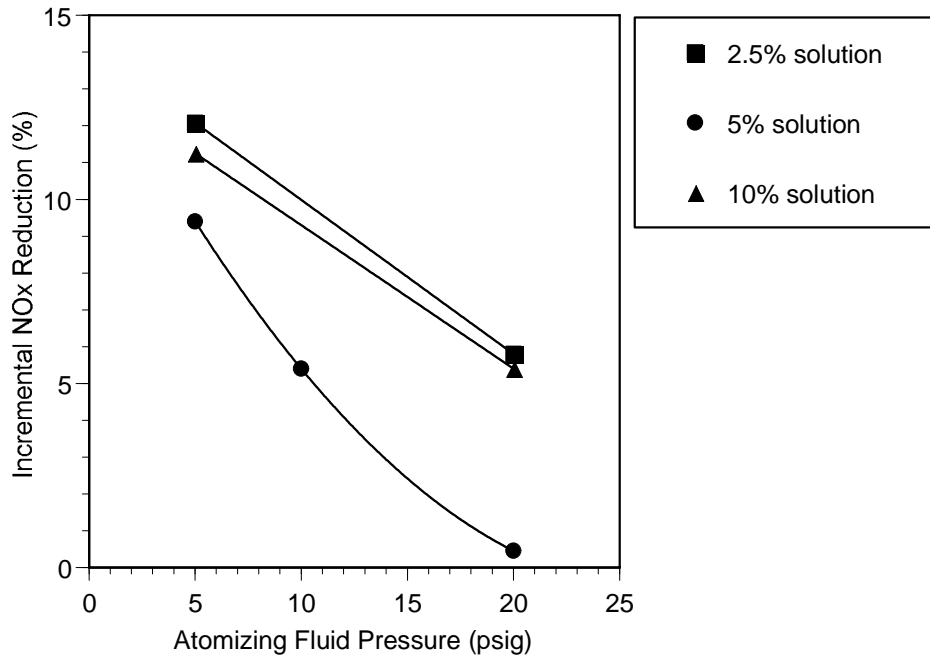


Figure 10-5. Incremental NO_x reduction for co-injection of different urea solution strengths with OFA. 10% reburning.

Effect of OFA Port Configuration

To evaluate mixing and thermal effects, two OFA configurations were tested, including one with four ports and one with three ports. Figure 10-6 shows overall NO_x reduction for each configuration at 10% and 20% reburning. At 10% reburning, similar results were obtained for the two configurations. At 20% reburning, performance was slightly better with the three-port configuration.

Effect of Injector Position

The baseline position for the urea injectors was flush with the inner wall of the furnace. A test series was also conducted in which the injectors were recessed back into the OFA port by 5 inches. The objective was to provide time for the velocity of the liquid stream to approach that of the OFA stream, potentially allowing the OFA to better shield the droplets. However, as shown in Figure 10-7, similar results were obtained for each injector position.

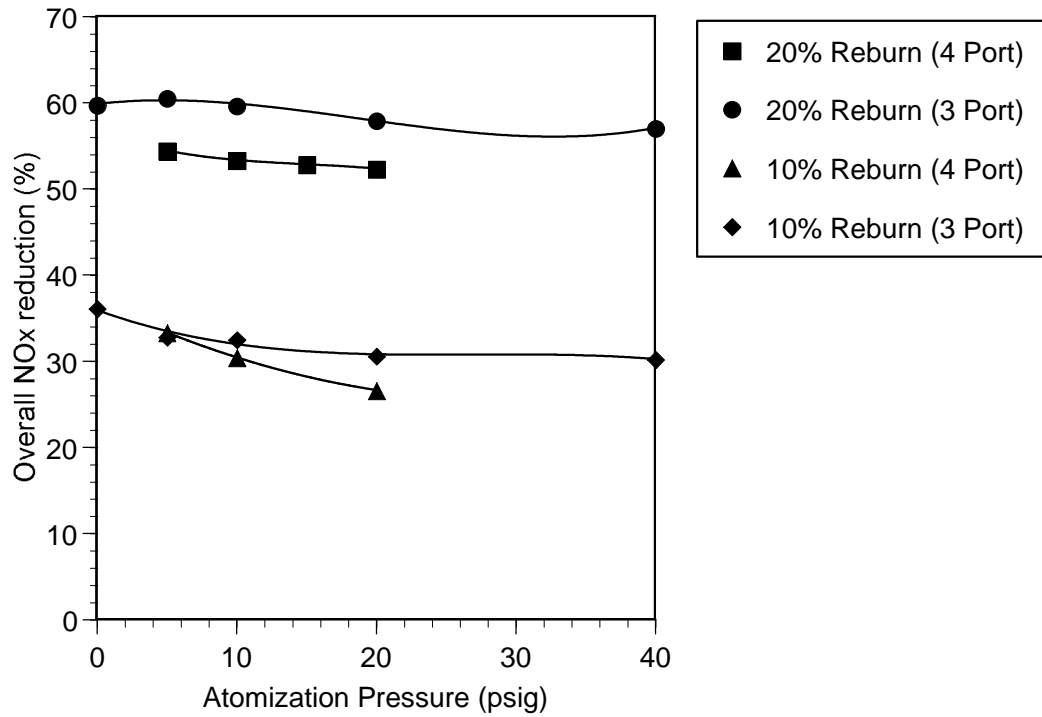


Figure 10-6. Comparison of overall NO_x reduction by urea solution for 3-port and 4-port configurations of OFA injection. NSR = 1.0.

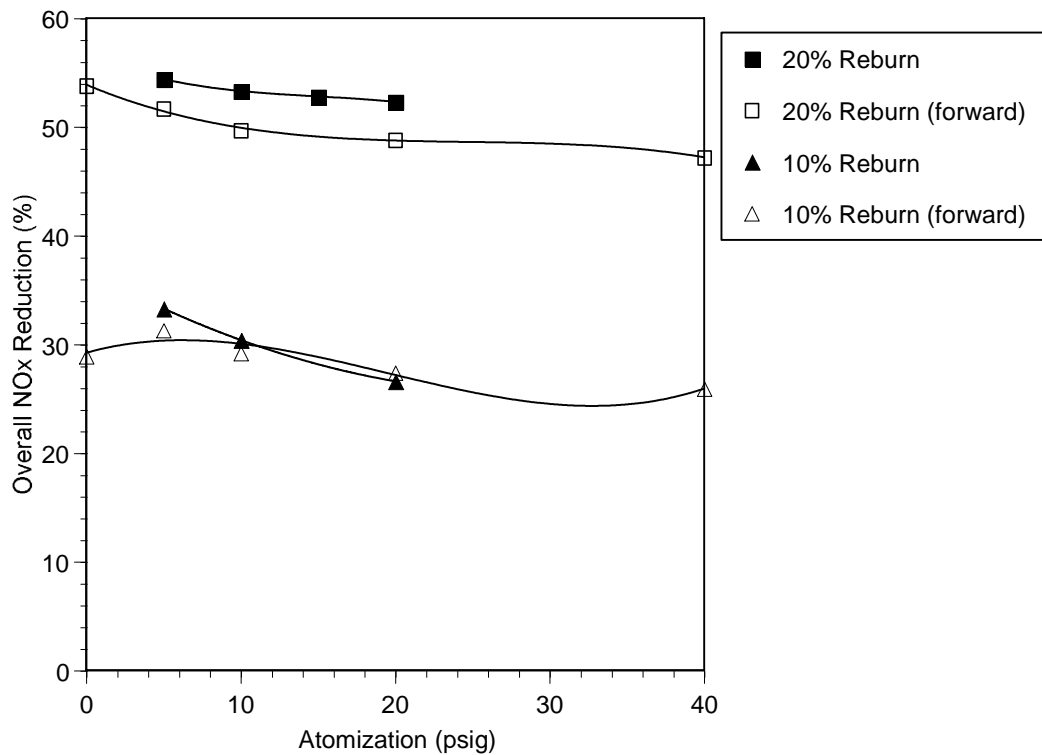


Figure 10-7. Overall NO_x reduction at different urea injector positions. NSR = 1.0.

Effect of N-Agent Type

Urea requires an extra step to decompose relative to ammonia. Thus it was believed that urea would perform better under the subject test conditions that require a delay time. To validate this reasoning, a series of tests was conducted in which aqueous ammonia was used as the N-agent. OFA and N-agent were injected at 1650 K. Figure 10-8 shows performance of urea and aqueous ammonia as a function of atomization pressure. While at 10% reburning performance was similar for the two additives, at 20% reburning urea performed significantly better than aqueous ammonia.

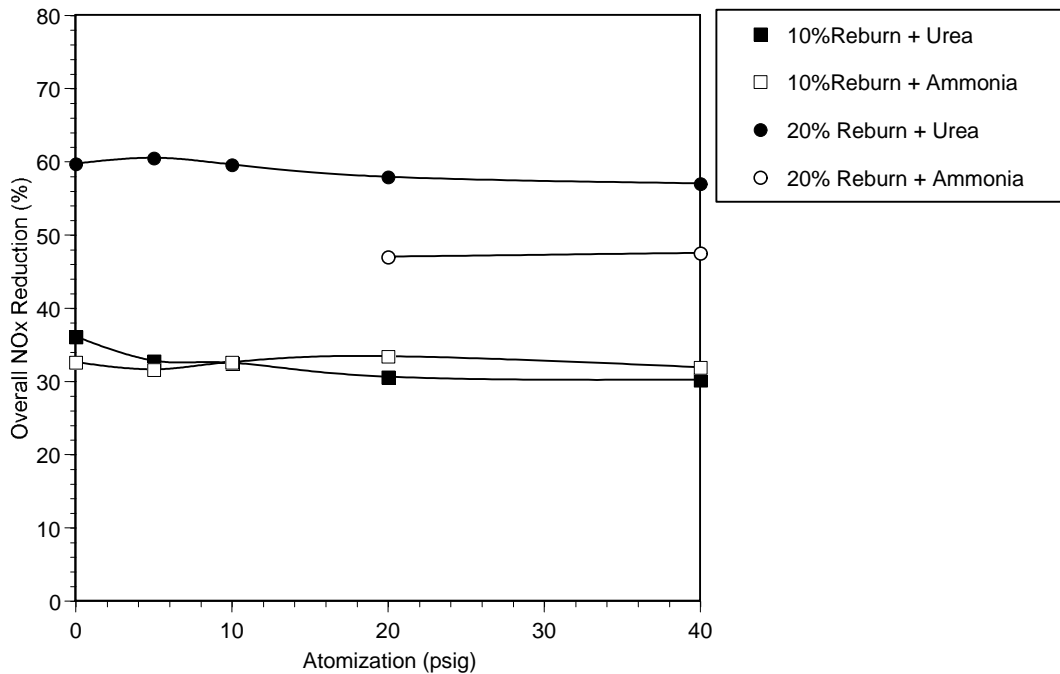


Figure 10-8. Comparison of performance for urea and aqueous ammonia as a function of N-agent atomizing air pressure. NSR = 1.0.

Effect of OFA Injection Temperature

To determine the impacts of injection temperature, a series of tests was performed in which the OFA and urea were moved downstream in the furnace by 24". This corresponded to a furnace gas temperature of about 1520 K, as compared to 1650 K in previous tests. Figure 10-9 compares performance at 10% and 20% reburning. In each case overall NO_x reduction was about 10 percentage points higher at the lower temperature.

SNCR Test Results

Reburning generates CO concentrations that can impact performance of the N-agent. To characterize these effects, a series of tests was performed involving basic SNCR without reburning. In all cases OFA was injected to maintain the same furnace mixing patterns. Figure 10-10 shows urea performance as a function of atomization pressure with and without reburning. Significantly higher NO_x reduction was obtained without reburning, indicating that under these conditions CO had a negative impact on performance.

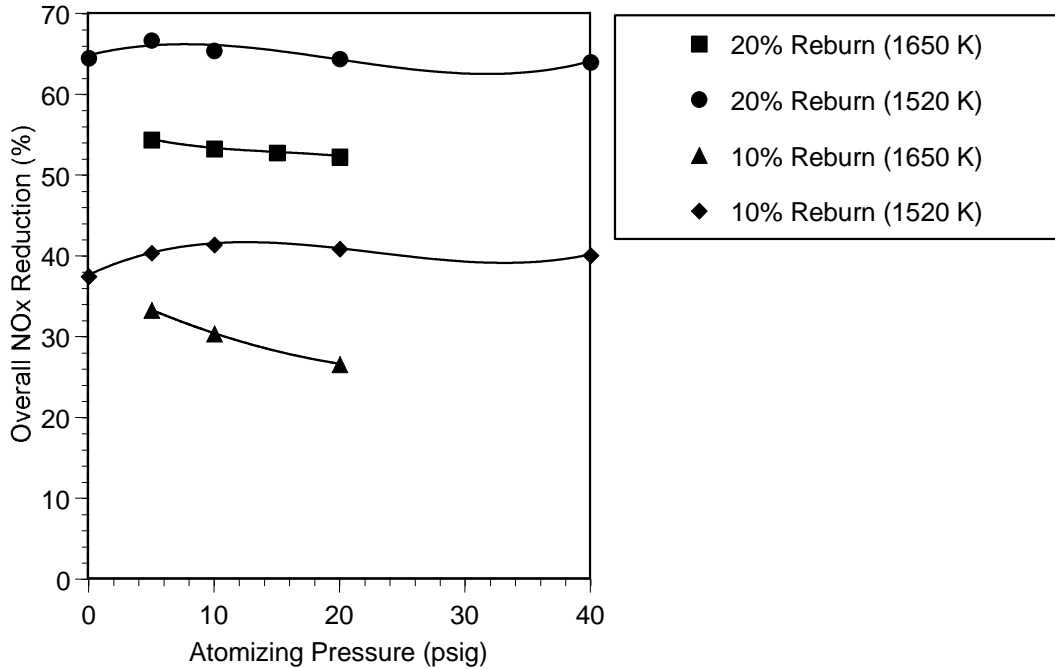


Figure 10-9. Comparison of overall NO_x reduction at different OFA/urea injection temperatures. NSR =1.0.

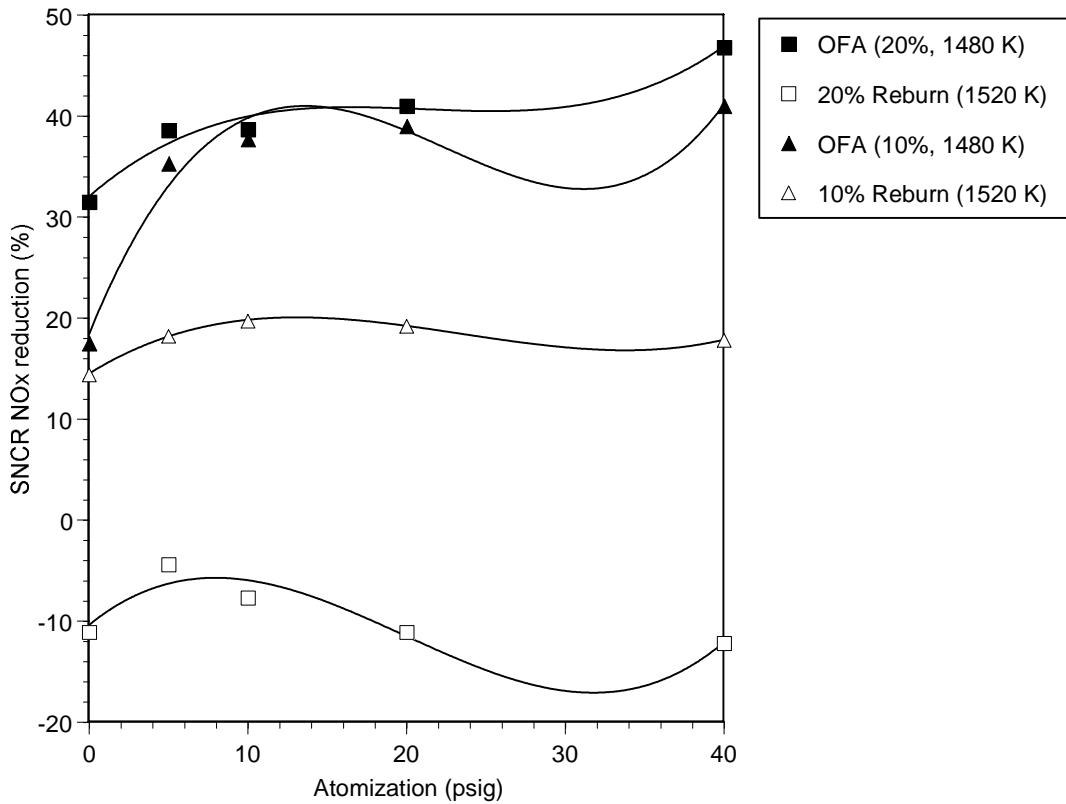


Figure 10-10. SNCR performance as a function of atomization pressure with and without reburning. NSR = 1.0.

Axial Injector Tests

Near the end of the test program a series of tests was conducted using axial injectors. This involved inserting two L-shaped injectors into the furnace such that urea was injected axially, co-current to the furnace gas flow. The axial injectors were oriented to provide maximum flow field coverage. The axial injector tests were intended to minimize potential ballistic and wall-impingement effects. For these tests both the OFA and urea injectors were located at 1650 K. Reburning heat inputs of 6%, 10%, and 20% were tested with urea injection. One series of tests was also conducted using ammonium sulfate as the N-agent, at 10% reburning. The objective of these tests was to determine whether the ammonium sulfate would have different evaporation characteristics, and thus different NO_x control performance, than urea.

Figure 10-11 shows NO_x reduction as a function of atomization pressure for the axial injector tests. Incremental SNCR performance was better at lower reburning heat inputs, pointing to possible CO effects. Urea performance improved with decreasing atomization pressure. At an atomization pressure of zero, overall NO_x reductions were 47% at 10% reburning and 37% at 6% reburning. Incremental urea NO_x reductions at these conditions were 25% at 10% reburning and 26% at 6% reburning. This performance is significantly better than that achieved with the wall injectors. For comparison, under similar conditions at 10% reburning the incremental NO_x control achieved by urea with the wall injection system was 8%.

Both urea and ammonium sulfate were tested with the axial injectors at 10% reburning. Figure 10-12 shows performance as a function of atomization pressure. At low pressures, performance was similar for the two additives. At higher pressures, urea performed significantly better, possibly indicating that it was less prone to vaporizing prior to complete evaporation of the water droplet.

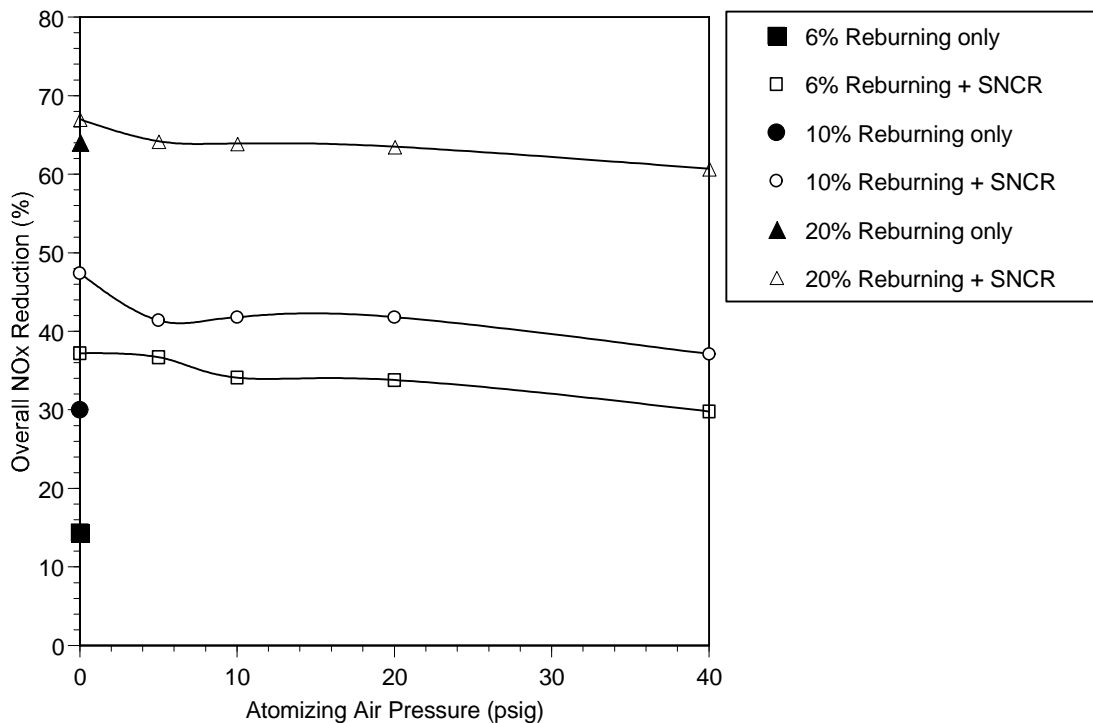


Figure 10-11. Axial injector tests: impact of atomization pressure on overall NO_x reduction at different reburning heat inputs. NSR = 1.0.

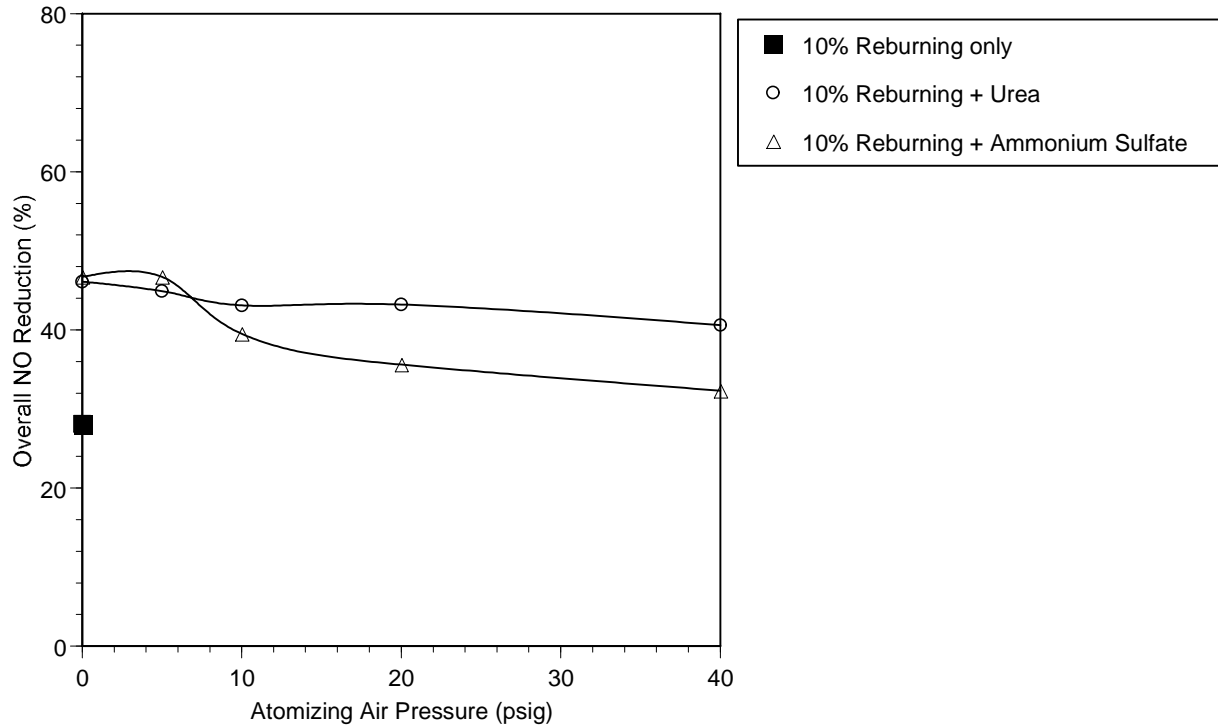


Figure 10-12. Axial injector tests: comparison of urea and ammonium sulfate impacts on NO_x reduction. NSR = 1.0.

TF AR-Lean Tests: Summary

Tests in 10×10^6 Btu/hr TF demonstrated that efficiency of NO_x reduction in AR-Lean at OFA/N-agent injection temperature of 1520 K is about 60% and is significantly smaller than 96% achieved in the same combustor under optimized conditions. The incremental NO_x reduction provided by N-agent only at this temperature did not exceed 15%. However, model of AR (Section 7.5) predicted that up to 40% incremental NO_x reduction could be achieved at urea injection temperature of 1520 K if droplet size of urea solution is optimized. Model predicted that optimized droplet size for the TF conditions was 300 μm .

A three-dimensional CFD model of the TF was simulated in FLUENT (*FLUENT, 1998*) to gain an understanding of the physical phenomena that could have resulted in smaller than predicted by modeling NO_x reduction efficiency. The FLUENT model predicted that droplets larger than 200 μm do not easily make the turn into the superheater and sweep against the TF wall. Many of the larger droplets that escape upper wall impingement were unable to make the turn at the "nose" into the convective pass. Results also showed that certain injection locations were better than others in allowing the droplets to reach the convective pass. Optimized locations could be found for the injectors to minimize the momentum from the OFA flow from sweeping the droplets into the walls. However, even in locations that were considered optimized, some droplet sizes were still impinging against the sidewalls. The CFD modeling predicted that higher than observed in the TF tests efficiencies of NO_x reduction could be achieved in a larger scale combustion facility since wall impingement could be avoided for longer droplet penetration distances.

Thus, the importance of optimization of process conditions for achieving high efficiency of NO_x reduction in AR was demonstrated. Tests also indicated that moderate NO_x control can be achieved

in boilers with existing systems for OFA injection even if temperatures of the OFA injection are too high for the gaseous N-agent to be effective. Since additional port for N-agent is not required in AR-Lean, injection of an aqueous solution of N-agent presents an opportunity to provide moderate NO_x control at low cost in boilers already equipped with OFA ports.

10.2 AR Economic and Market Update

This section discusses the economics of NO_x control via AR and the potential market for the AR technologies in the U.S. for compliance under the 1990 CAAA. The following section, Section 10.2.1, discusses the market drivers and the nominal NO_x control requirements to meet existing and projected regulations (see also Section 2.1). Section 10.2.2 outlines an economic methodology for comparing the cost effectiveness of conventional and AR technologies and defines case studies for a typical cyclone-fired boiler and a typical wall-fired boiler. The methodology was used to compare the costs of conventional NO_x controls (SNCR, SCR and OFA) with the costs of reburning-based technologies including basic reburning and the full range of AR technologies evaluated in this project. Section 10.2.3 discusses the cost and performance of each NO_x control technology and Section 10.2.4 presents the results. The results show a considerable economic advantage for the AR technologies particularly for deep NO_x control with cost savings in the range of 50%. The resulting market for these AR technologies is discussed in Section 10.2.5.

10.2.1 NO_x Control Drivers

The Clean Air Act Amendments of 1990 (CAAA) established the framework for NO_x emission regulations to mitigate ozone non-attainment areas and acid rain. Over the last decade, the U.S. EPA has developed most of the specific NO_x regulations authorized by the CAAA. The most stringent NO_x controls are required in ozone non-attainment areas or areas which transport pollutants into ozone non-attainment areas. In the Northeastern portion of the country, the EPA has defined the NEOTR which consists of Pennsylvania and the States North and East of that state. In the NEOTR, NO_x reductions of up to 75% are required by the year 2003 with the potential for even deeper controls depending on the results of dispersion modeling over the next few years. The EPA is considering the potential to expand the NEOTR to include Texas and all states north and East of this state. In this thirty-seven-state region, it is projected that NO_x emissions may need to be reduced by as much as 85%.

As these regulations have developed, the trend has been towards permitting industry to comply by implementation of cost-effective emission controls. Rather than setting specific limits for each plant, the regulations in many areas provide the flexibility to over-control on some units and under-control on others if that approach is cost effective. This “cap and trade” approach can be of considerable advantage since the cost of NO_x control for some units (particularly smaller units) may be much higher than for others, on a \$/ton basis. This bubbling approach depends on the availability of NO_x control technologies that can achieve NO_x reductions greater than the nominal control levels (75-85%) with low costs.

The NO_x control requirements developed by the EPA to date have been based on attaining the current NAAQS. However, the EPA has issued revised NAAQS for ozone and fine particulate that are substantially lower than the current standards. Since NO_x is a precursor of both pollutants, achieving the new NAAQS will require even greater reductions in NO_x emissions.

The goal that was established by DOE for this project was to achieve 95% NO_x control or emissions rates of 0.06 lb/10⁶ Btu. This goal assumes that future regulations will continue to require substantial reductions in NO_x emissions. NO_x control technologies that can meet this goal will be employed if their costs are competitive with conventional controls on a \$/ton basis. At present, the only commercial NO_x control technology capable of achieving such deep NO_x control is SCR. The advantage of the AR technologies being developed on this project is that they can provide the deep NO_x control of SCR at a considerable cost reduction.

10.2.2 Economic Methodology and Case Studies

To evaluate the cost effectiveness of the AR technologies, an economic analysis was conducted using the EPRI Technology Assessment Guide (TAG) methodology, which is widely used in the utility industry to evaluate advanced emission control technologies. The TAG methodology calculates the total levelized annual costs including capital and operating cost components. The resulting levelized annual cost and emissions reduction can be expressed in terms of \$/ton of NO_x controlled. In the TAG methodology, the total installed cost (capital cost) of the control technology is estimated and distributed over the operating life in a series of uniform annual costs by applying a Capital Recovery Factor (CRF). The CRF depends on the operating life, time value of money, depreciation, etc. In this analysis, a CRF of 0.131 was utilized. This is equivalent to simple amortization at an annual interest rate of 10% over a 15 year operating life. The annual operating costs for the technology are calculated for the first year and then levelized over the life of the technology by applying an annual levelization factor. In this analysis, a constant dollar approach was utilized so that the levelization factor was 1.0.

AR technologies can be applied to all types of combustion systems including the three most common utility boiler firing systems (wall, tangential and cyclone fired). Two applications were selected for the economic evaluation: a cyclone-fired boiler and a dry-bottom wall-fired unit equipped with low-NO_x burners.

Reburning applications on cyclones are particularly attractive for several reasons:

1. The baseline NO_x levels are high. Since NO_x is a reactant in the reburning reactions, high baseline NO_x increases the rate of NO_x reduction. Thus, the cost of NO_x control for units with high baseline NO_x is low for reburning-based technologies.
2. Furnace temperatures are high. High furnace temperatures improve reburning NO_x control since the reduction reactions are kinetically controlled.
3. Low-NO_x burners cannot be used with cyclones. This makes reburning based controls SNCR, and SCR the only alternatives.

In contrast to the cyclone application, dry-bottom wall-fired units can be equipped with low-NO_x burners and OFA. In fact, Title 4 of the CAAA mandates that “Low-NO_x Burner Technology” be applied to all dry-bottom wall-fired units by the year 2000 with a NO_x emissions limit of 0.46 lb/10⁶ Btu.

The assumptions utilized in the analysis and those specific to the two applications (cyclone and wall-fired) are summarized in Table 10-1.

Table 10-1. Economic data.

Parameter	Units	Value	
Unit Specifications			
Unit Capacity	MW	200	
Capacity Factor	%	65	
Heat Rate	Btu/KWH	10,000	
Fuels data			
Coal Sulfur	lb/10 ⁶ Btu	1.2	
Coal Heating Value	Btu/lb	12,000	
Coal Cost	\$/10 ⁶ Btu	1.5	
Gas Cost	\$/10 ⁶ Btu	2.5 – 4.5	
Coal Ash Content	%	10	
Unit costs			
Value of SO ₂ Reduction	\$/ton	125	
Ash Disposal Cost	\$/ton	10	
Economic Factors			
Capital Recovery Factor		0.131	
Escalation		Constant dollar	
Boiler Data			
Firing Configuration		Cyclone	Wall-Fired
Baseline NO _x controls		None	Low-NO _x Burners
Baseline NO _x	\$/10 ⁶ Btu	1.2	0.46

10.2.3 Technology Specific Inputs

The NO_x control technologies selected for evaluation are presented in Table 10-2 along with the assumed control performance. The reburning-based technologies were evaluated using both gas and coal as reburning fuels. The key technology specific assumptions are presented in Table 10-3 and are discussed further below.

The performance of SNCR is highly site specific. A typical performance in full-scale applications with modest ammonia slip is in the range of 25-35% NO_x reduction with injection of a reagent (such as urea or ammonia) at a nitrogen stoichiometric ratio (NSR) of 1.5. For this analysis, the lower performance level was used for the wall-fired boiler and the higher performance level was used for the cyclone-fired boiler. The capital cost was based on discussions with SNCR vendors. The SNCR reagent was assumed to be Fuel Tech's NO_xOut A, a commercially available aqueous urea solution.

Costs and performance for SCR were initially obtained from an EPA report (*Phase II NO_x Control, 1996*) which presented DOE estimates for a high-sulfur coal-fired unit of 200 MW capacity with initial NO_x of 1.0 lb/10⁶ Btu and 80% NO_x reduction. Current information indicates that the cost for SCR technology is somewhat lower than that presented in the EPA report (~35% lower). Therefore,

the EPA cost data were scaled to the conditions of the model plants and reduced to account for lower cost SCR systems.

Table 10-2. NO_x control technologies and expected performance.

Technology	NO _x Reduction (%)		NO _x Emissions (lb/MMBtu)	
	Cyclone	Wall	Cyclone	Wall
Conventional NO _x Controls				
Overfire Air		25		0.35
Selective Non-Catalytic Reduction (SNCR)	35	25	0.78	0.35
Selective Catalytic Reduction (SCR)	80	80	0.24	0.09
Selective Catalytic Reduction (SCR)	90	90	0.12	0.05
Reburning NO _x Controls				
Basic Reburning	60	50	0.48	0.23
Advanced Reburning—Rich (AR-Rich)	80	80	0.24	0.09
Advanced Reburning—Lean (AR-Lean)	80	80	0.24	0.09
Promoted Advanced Reburning—Lean (PAR-Lean)	90	90	0.12	0.05
Promoted Advanced Reburning—Rich (PAR-Rich)	90	90	0.12	0.05
Multiple Injection Advanced Reburning (MIAR)	95	95	0.06	0.02

Table 10-3. NO_x control technology economics.

Parameter	Units	OFA	SNCR	Basic Reburn	AR R/L	PAR R/L	MIAR	SCR 80%	SCR 95%
Capital Cost									
Conventional	\$/kw	10	5					52	71
Gas Reburning	\$/kw			15	20	20	25		
Coal Reburning	\$/kw			25	30	30	35		
Reburning Fuel Firing									
Gas Reburning	%			18	12	12	12		
Coal Reburning	%			25	20	20	20		
Catalyst Life	Years							4	4
SO ₂ Control (via gas)	%	0	0	18	12	12	12	0	0

Reburning costs and performance were based on EER's extensive database and the experimentally determined effectiveness of the AR technologies developed in this project. For the coal reburning systems, costs were included for addition of pulverizers to produce the fine-grind (micronized) coal necessary to minimize carbon loss. Pulverizers are required for the cyclone-fired boiler, but are not necessarily required for the wall-fired boiler. For wall-fired boilers, the capital cost for a coal reburning system can be significantly reduced by using one of the existing mills for the reburning

system. There is no incremental fuel cost for the coal reburning system (except for an efficiency penalty due to potential for increased carbon loss) since the normal plant coal is used for reburning. For gas reburning systems, no pulverizers are required, but the gas cost is greater than coal. A price differential ranging between 1.00 to 3.00 $\$/10^6$ Btu was assumed. Although the cost of natural gas has significantly increased in recent years, it is expected that significant price differentials cannot be sustained in the future. It is assumed that coal and gas reburning technologies can achieve comparable NO_x reduction.

10.2.4 Economic Results

Figures 10-13 and 10-14 show the results of the economic comparison as plots of the total annual cost of NO_x reduction versus percentage NO_x reduction. Lines of constant unit cost of NO_x control ($\$/\text{ton}$ of NO_x reduced) are also shown on the plots. As discussed above, the unit cost of NO_x control is the appropriate figure of merit since utilities will apply controls to a number of units, bubbling to achieve the lowest total cost.

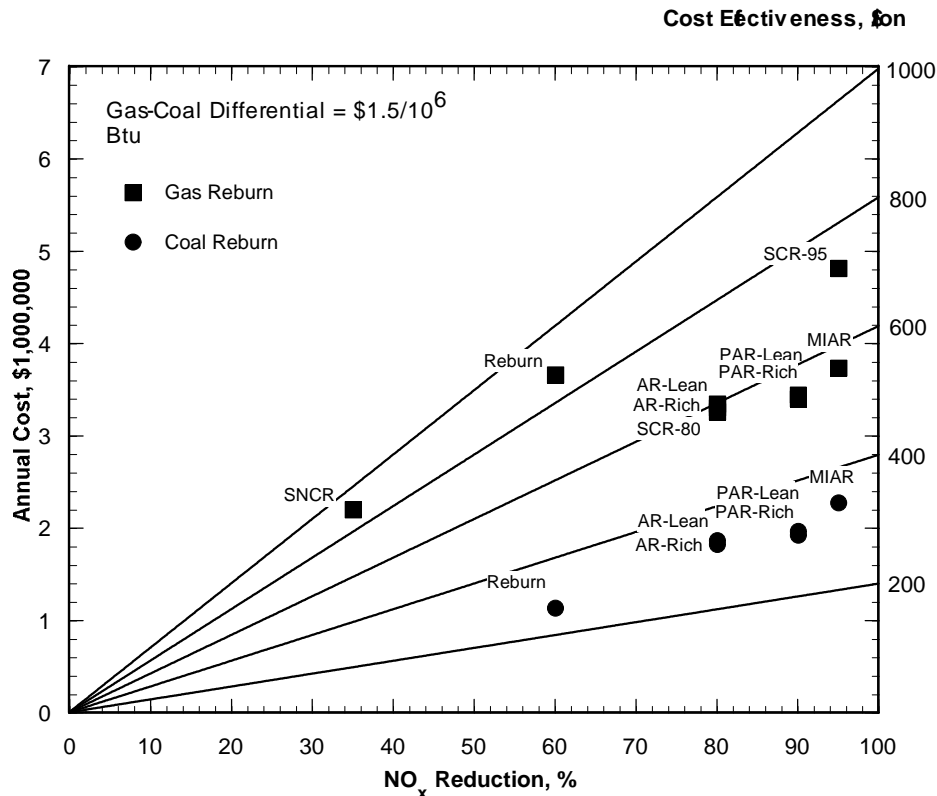


Figure 10-13. Comparison of cyclone-fired boiler NO_x control technology economics.

Figure 10-13 shows the results for the cyclone-fired boiler. The technologies with the highest unit cost of NO_x control are SNCR, gas reburning, and high-performance SCR with costs in the range of 700-1,000 $\$/\text{ton}$. The reburning-based technologies are considerably lower in cost. The unit cost of NO_x control for gas-based reburning technologies is comparable to low-performance SCR. Coal-based reburning technologies are the most cost effective since they have the lowest unit cost of NO_x control.

Figure 10-14 shows the results for the wall-fired boiler. Since the baseline NO_x is lower than for the cyclone application (0.46 versus 1.2 lb/10⁶ Btu), the unit cost of NO_x control is higher. As with the cyclone-fired boiler results, the reburning technologies have a considerable cost advantage. OFA has been included for this application. While the total annual cost of OFA is low, the low NO_x reduction (25%) results in a relatively high unit cost of NO_x control.

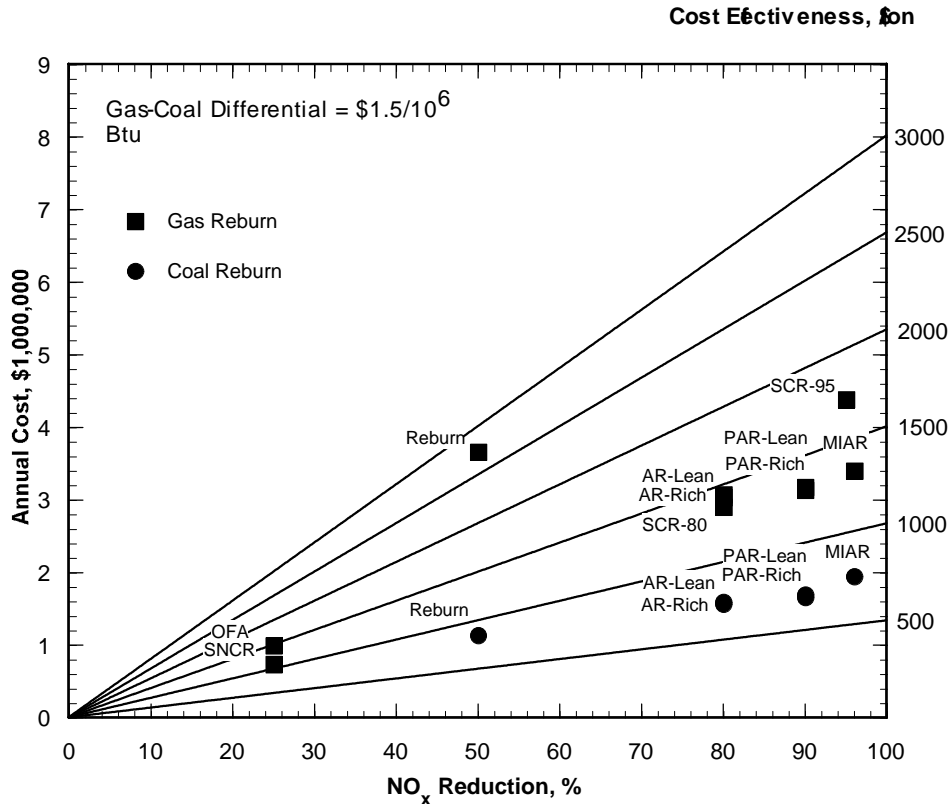


Figure 10-14. Comparison of wall-fired boiler NO_x control technology economics.

The cost effectiveness of gas-based reburning technologies depends upon the price differential between coal and natural gas. The impacts that this parameter has on the cost effectiveness of gas-reburning technologies are shown in Figures 10-15 and 10-16. In these plots, the cost effectiveness of reburning and MIAR technologies is compared to that for SNCR and SCR. For the cyclone-fired boiler application, basic gas reburning is more cost effective than SCR for fuel price differentials less than approximately \$1.2 while MIAR is more cost effective for differentials less approximately \$2.2. Based on the assumptions used for this study, the costs for coal as the reburning fuel are lower than for gas. However, it should be noted that site specific considerations might favor gas in some situations. Factors favoring gas include a low gas-coal cost differential, problems related to carbon loss which are more significant with coal as the reburning fuel, and space limitations which make pulverizer installation expensive, difficult or impossible.

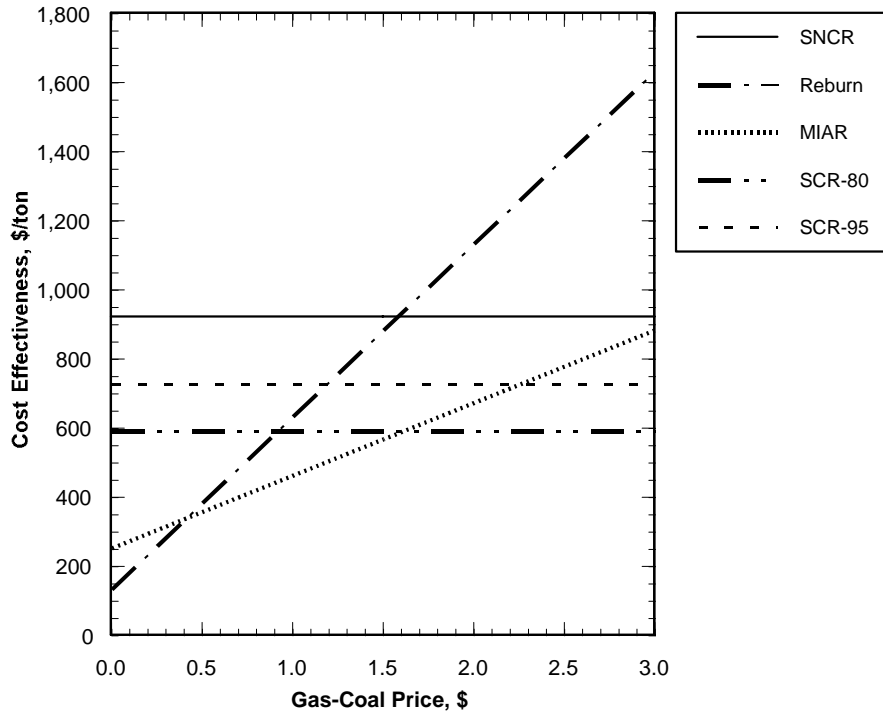


Figure 10-15. Impact of fuel differential on cyclone-fired boiler NO_x control economics.

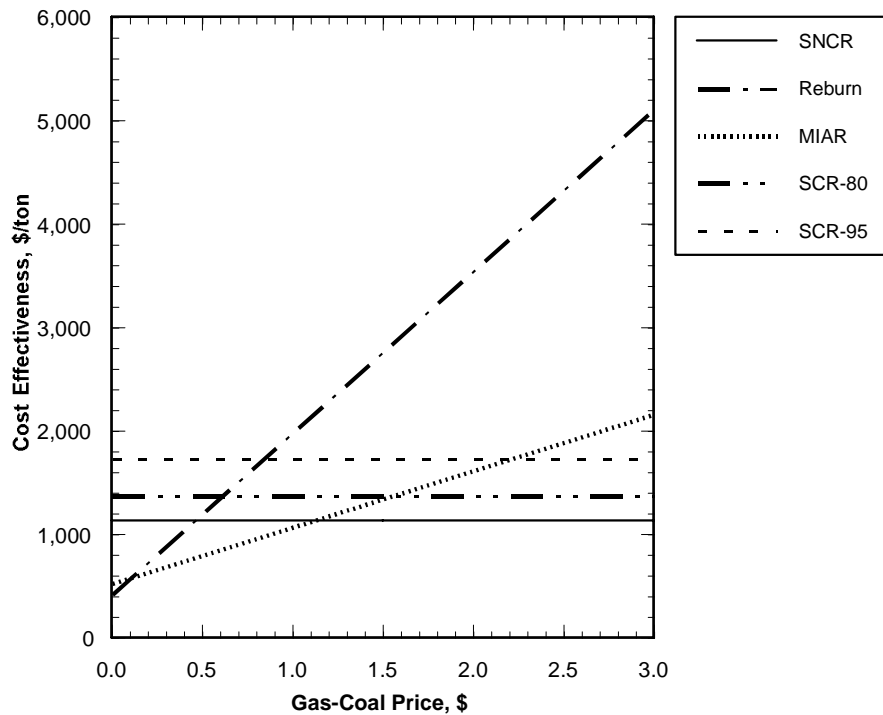


Figure 10-16. Impact of fuel differential on wall-fired boiler NO_x control economics.

These results show the significant economic advantage of the technologies developed on this project for the projected NO_x control market characterized by deep NO_x control and the potential for

bubbling. For example, in the cyclone application, the total annual cost of SNCR is comparable to MIAR using coal, but MIAR provides more than twice the NO_x reduction.

Table 10-4 compares the economics of technologies capable of achieving deep NO_x control (between 80 to 95% reduction). This comparison shows that coal reburning based AR technologies have are 44% to 56% more cost effective than SCR. As discussed above, the cost effectiveness of gas reburning based AR technologies depends upon the price of natural gas.

Table 10-4. Comparing the cost effectiveness for deep NO_x control.

NO _x Control AR Technology	Cyclone, Baseline NO _x 1.2 lb/10 ⁶ Btu				Wall, Baseline NO _x 0.46 lb/10 ⁶ Btu			
	80%		95%		80%		95%	
	AR-Rich		MIAR		AR-Rich		MIAR	
	106 \$/yr	\$/ton NO _x	106 \$/yr	\$/ton NO _x	106 \$/yr	\$/ton NO _x	106 \$/yr	\$/ton NO _x
Costs								
SCR	3.27	592	4.82	728	2.91	1,374	4.39	1,729
AR (gas reburning)	3.31	600	3.74	569	3.04	1,438	3.41	1,346
AR (coal reburning)	1.83	332	2.28	347	1.57	740	1.95	767
Cost Reduction								
AR (gas reburning)	-1		22		-5		22	
AR (coal reburning)	44		53		46		56	

10.2.5 Market Assessment

The size of the market for AR technologies has been estimated and presented in Phase I Report by considering the existing and projected CAAA regulations, the power plants affected by the regulations, and industry projections for the mix of NO_x control technologies necessary for cost effective compliance with these regulations. In 2000, H&W Management Science Consultants (*H&W Management Science Consultants, 2000*) analyzed the U.S. air pollution control market through 2003. The total NO_x control markets in 2001, 2002 and 2003 were projected to be \$1,570 million, \$1,480 million, and \$1,380 million, respectively. The reburning/SNCR share of this market was estimated to be \$82 million, \$101 million, and \$134 million, respectively, of which share of AR was 35%. Thus, total market share of AR technologies by 2003 was projected to be \$110 million. It is expected that the size of the AR market will increase as result of utilities SIP Call compliance in 2004. Since the EPA is considering the expansion of the NEOTR to include Texas and all states north and East of this state, it will further increase the market share of AR technologies.

10.2.6 Economic and Market Analysis: Conclusions

Economic analysis demonstrates a considerable economic advantage of AR technologies in comparison with existing commercial NO_x control techniques, such as basic reburning, SNCR, and SCR. Particularly for deep NO_x control, coal-based AR technologies are 50% less expansive than SCR for the same level of NO_x control. The market for AR technologies is estimated to be above \$110 million.

10.3 Design Methodology and Application Conclusions

A design methodology, which consists of various computational and analytical models, was generalized for use with AR technologies. This methodology was then applied to develop conceptual designs for application of three AR concepts—AR-Lean, AR-Rich, and MIAR to a typical 100 MW tangentially fired utility boiler, and to predict the impacts of the AR systems on boiler performance and NO_x emissions.

The design methodology uses various experimental and analytical tools to develop the injector specifications and operating characteristics of the AR system with the objective of meeting specific process requirements for optimum emissions control performance while maintaining boiler operation and performance at normal levels.

Thermal performance models were used to evaluate the impacts of implementing AR processes on the thermal performance of a nominally 100 MW tangentially fired boiler. For implementation of AR-Lean, AR-Rich, or MIAR processes on this boiler, the reburning fuel would be injected into the lower furnace and the overfire air would be injected into the upper furnace in a cavity between the first two tube banks of the convective pass. The model results indicate that this configuration is expected to increase carbon loss and reduce main and reheat steam temperatures in comparison to baseline or gas reburning operation. Changes in the operating settings of the AR process can be used to mitigate some of the increase in carbon loss. However, the overall boiler efficiency for operation with an AR system is similar to that for operation with a basic gas reburning system. Changes in the operating settings of the AR process or in the boiler operating settings can be used to mitigate the impacts of AR on main and reheat steam temperatures. It should be noted that the results of this analysis are specific to the boiler configuration evaluated and should not be generalized to other boiler designs. The results of injection system analysis indicate that good mixing of the process streams necessary to implement advanced reburning (AR-Lean, AR-Rich, and MIAR) on the case study boiler can be achieved. Natural gas can be injected from each wall in a pattern that achieves good distribution of the reburning fuel. Overfire air injection into a cavity in the convective pass, which is needed for implementation of each of the AR processes under consideration, can be achieved using high-pressure wall jets. For the AR-Lean and MIAR processes, these ports can also be used to inject the reagent. Injection of reagent into the upper furnace, needed for the AR-Rich and MIAR processes, can be achieved using a lance-based system. The overall boiler efficiency for operation with AR systems is similar to that for operation with a basic gas reburning system. Full scale NO_x reduction level is predicted to be about 80% and can be additionally increased with the use of promoters.

The original work scope was based on applying the design methodology to a hypothetical case study; however, it was hoped that an initial AR demonstration could be developed outside the scope of this DOE project to allow application to a real unit and evaluation of some of the AR elements. EER was successful in developing an AR demonstration project. In 1995, EER installed AR-Lean on the Greenidge 105 MW tangentially fired boiler. AR testing was conducted in 1996-98. This unit was used as the basis for extending the design methodology. AR-Lean tests on the boiler showed that stratification within the reburning zone could adversely affect the performance. Regions of inadequate CO in the reburning zone reduced the N-agent NO_x control and caused NH₃ slip. While modifications were successful in reducing stratification, this experience showed the importance of mixing and scale up. In addition to these AR-Lean tests, opportunity was taken to obtain preliminary larger scale data on several of the AR components, including N-agent injection into the

reburning zone, N-agent injection downstream of the reburning zone in an SNCR mode, and N-agent injection into the reburning zone and with the overfire air.

11.0 Experimental Facilities

Most of experimental work in Phase II was conducted at the GE-EER test site in Irvine, California. Three combustion facilities were used in experiments, including the 0.1×10^6 Btu/hr Controlled Temperature Tower (CTT), the 1.0×10^6 Btu/hr Boiler Simulator Facility (BSF), and the 10×10^6 Btu/hr Tower Furnace (TF). Utilization of combustion facilities ranging in firing rate by two orders of magnitude allowed to study AR processes at different mixing and thermo conditions and to determine effect of scaling on the AR performance. The following sections describe process performance characterization and combustion facilities.

11.1 Process Performance Characterization

Process performance was characterized by continuous emissions monitors (CEMs), which provided an online analysis of flue gas composition. Identical CEMs systems were used at each of the three test facilities. Each system consisted of a water cooled sample probe, sample conditioning system (to remove water and particulate), and gas analyzers. Species analyzed, detection principles, and detection limits were as follows:

- O₂: paramagnetism, 0.1%
- NO_x: chemiluminescence, 1 ppm
- CO: nondispersive infrared, 1 ppm
- CO₂: nondispersive infrared, 0.1%
- SO₂: nondispersive ultraviolet, 1 ppm
- N₂O: nondispersive infrared, 1 ppm
- NH₃: SCAQMD Method 207 (sampling, Nessler reagent, colorimetry), 1 ppm
- HCN: sampling, ion-specific electrode, 1 ppm

High purity dry nitrogen was used to zero the analyzers. Certified span gases were used to calibrate and check linearity of the analyzers. A chart recorder was used to obtain a hard copy of analyzer outputs. A personal computer based data acquisition system (LabTech Notebook) was used for storage and analysis of test data. Furnace gas temperatures were periodically measured using a calibrated suction pyrometer.

Process equipment included gas reburning and additive delivery systems. Reburning natural gas and burnout air flow rates were measured using calibrated rotameters at each facility. Bottled nitrogen were premixed with the natural gas to ensure good penetration and entrainment with furnace gases. The natural gas and OFA injectors consisted of water cooled elbow probes aligned along the centerline of each facility. N-Agents and promoters were dissolved to form aqueous solutions. Solution flow rates were monitored by measuring mass loss (via a load cell) as a function of time.

Figure 11-1 shows axial temperature profiles for all three combustion facilities. Temperature gradients were adjusted to simulate environment in large-scale boilers.

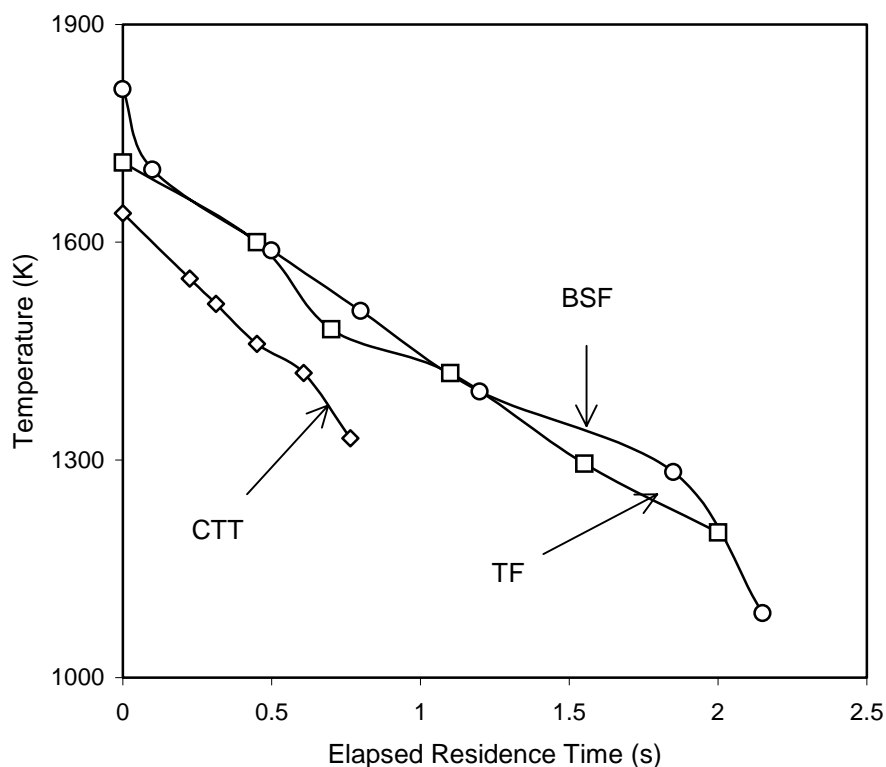


Figure 11-1. Axial temperature profiles measured in CTT, BSF and TF. Elapsed time corresponds to the time after injection of the reburning fuel.

11.2 Controlled Temperature Tower (CTT)

The Controlled Temperature Tower (CTT) is a downfired tunnel furnace with a nominal firing capacity of 0.1×10^6 Btu/hr. A schematic of the CTT is presented as Figure 11-2. The facility has an inside diameter of 8 inches and a furnace length of 96 inches. Furnace walls consist of layers of high temperature castable refractory. The furnace is equipped with numerous axial ports to allow introduction of additive injectors and sample probes. The furnace entry consists of an 18 inch long conical quarl that diverges from 2 inches to 8 inches. The quarl stabilizes the flame in the center of the furnace. The CTT is equipped with a variable swirl diffusion burner that is capable of firing coal, oil, or natural gas. Burner swirl number can be varied to control flame characteristics and initial NO_x concentrations. The CTT is designed to provide precise control of furnace thermal characteristics. Backfired heating channels run along the outside of the refractory in the upper and lower furnace. Rate of furnace heat extraction can be varied by varying the heat input to these backfired channels. Additional control over furnace temperatures can be obtained by inserting circulating water cooling coils along the furnace axis. Because of its relatively small scale, bottled gases can be used to control furnace gas composition. Specifically, a metered amount of NH_3 can be added to the flame, oxidizing to provide control over initial NO_x . The CTT's versatility and ability to provide precise control of test conditions make it an ideal facility for conducting parametric screening studies.

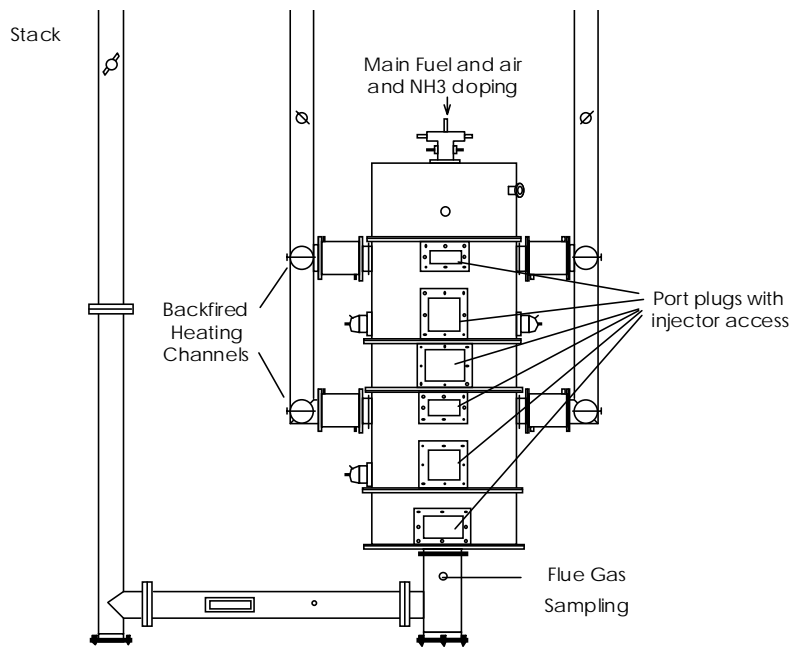


Figure 11-2. Controlled Temperature Tower (CTT).

Because of its small scale, temperature profile in CTT is affected by the injection of the reburning fuel and additives. Figure 11-3 shows effects of 10% reburning and water injection (to simulate injection of N-agent) on axial temperature profile in CTT.

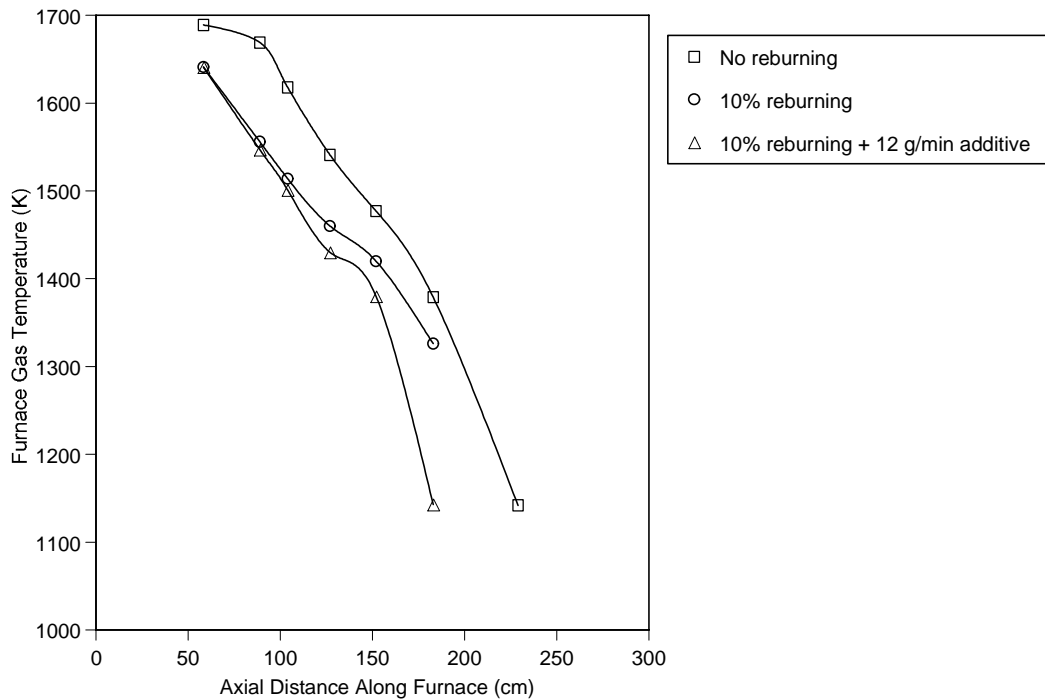


Figure 11-3. CTT temperature profiles.

11.3 Boiler Simulator Facility

The Boiler Simulator Facility (BSF) is a down-fired combustion research facility with a nominal firing rate of 1.0×10^6 Btu/hr. It is designed to simulate the thermal characteristics of a utility boiler. As shown in Figure 11-4, the BSF consists of a burner, vertical radiant furnace, and horizontal convective pass. The facility's variable swirl diffusion burner is equipped to fire coal, oil, or natural gas. The furnace is constructed of eight modular refractory lined spool sections with access ports. The furnace has an inside diameter of 22 inches and a height of 18 feet. The radiant is equipped with adjustable heat removal panels. Configuration of these panels is usually adjusted such that the BSF matches the residence time-temperature profile and furnace exit gas temperature of a specific full scale boiler. The convective pass is equipped with air-cooled tube bundles designed to simulate the superheater and economizer sections of a coal fired boiler. The facility has a baghouse at the end of the convective pass to control fly ash emissions. Because it accurately simulates the thermal environment of a full scale boiler, the BSF is ideally suited to process optimization studies leading to utility boiler application.

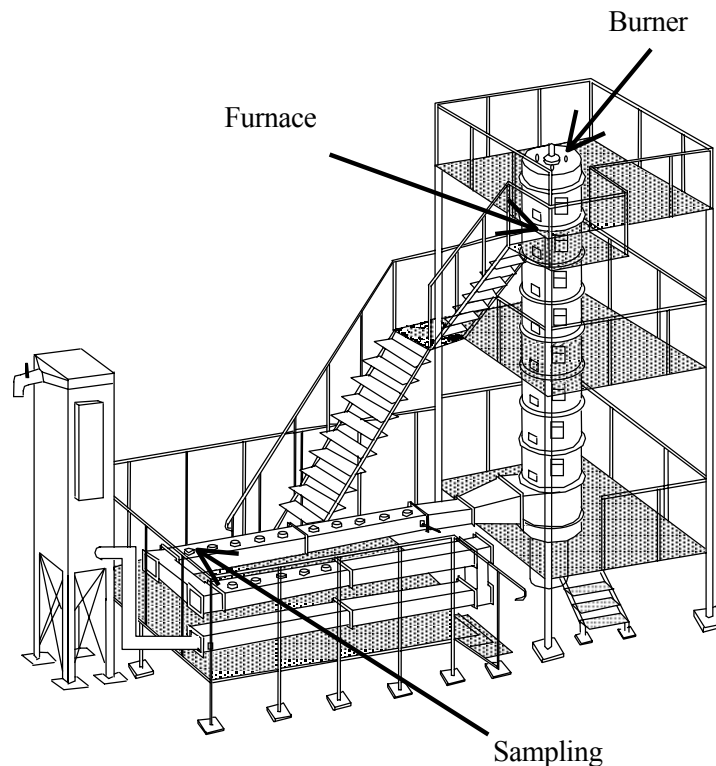


Figure 11-4. Boiler Simulator Facility (BSF).

11.4 Tower Furnace

The Tower Furnace (TF) is a downfired pilot plant combustor with a nominal firing rate of 10×10^6 Btu/hr. The facility is designed to provide a large-scale simulation of the flame properties, temperatures, gas compositions, and characteristic mixing times of a coal-fired boiler. As shown in Fig. 11-5, the TF consists of a burner section, radiant furnace, convective pass, and set of air

pollution control devices. The burner section can be configured with a single burner or an array of four burners to simulate different types of flames. The facility is equipped with a video camera at the bottom of the furnace, allowing direct monitoring of flame characteristics. The furnace is a refractory lined, water-cooled steel shell. It is square, having dimensions of four feet across and 30 feet in height. It has numerous axial ports, allowing access for injectors and sample probes. The furnace has a turbulent flow field, allowing the impacts of furnace gas mixing and additive entrainment upon process performance to be evaluated. The transition between the furnace and convective pass is a nose section, having geometry and gas flow field characteristics similar to those of a coal fired boiler. Facility air pollution control equipment, which includes a cyclone, baghouse, ESP, and wet scrubber, can be used in varying configurations depending upon test requirements. Because the TF provides an accurate simulation of the temperatures, gas compositions, and flow field characteristics of a coal fired boiler, it provides a means of directly applying results to full-scale systems.

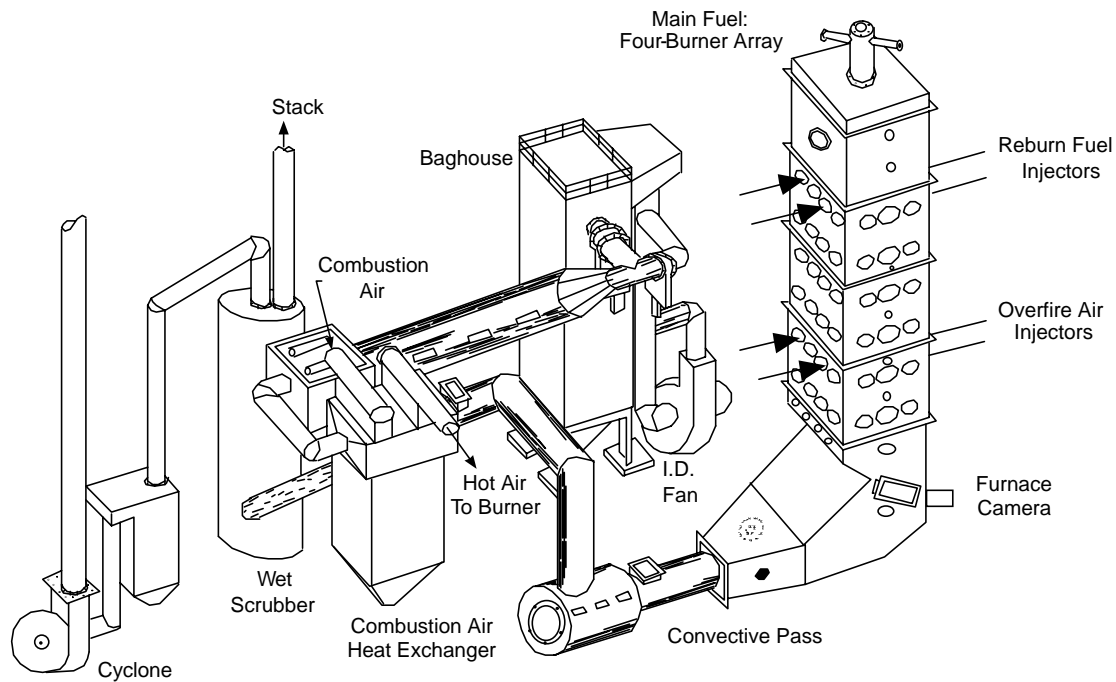


Figure 11-5. Schematic diagram of the Tower Furnace (TF).

12.0 Conclusions

This project develops a family of novel Second Generation Advanced Reburning NO_x control technologies, which have been demonstrated to achieve up to 95% NO_x control in coal fired boilers. AR systems integrate basic reburning and injection of an N-agent which can be injected with or without promoters at one or two boiler locations. The work included a combination of analytical and experimental studies to confirm the process mechanisms, identify optimum process configurations, and develop a design methodology for full-scale applications. The overall objective of the project was to demonstrate the effectiveness of the AR technologies at bench and pilot scale over a sufficiently broad range of conditions, optimize AR with natural gas and coal firing, and develop modeling tools required for scaling and optimization of AR at full scale. The information from Phase I and Phase II provides all the information needed for a process design evaluation of AR for a full-scale installation. All project objectives and technical performance goals have been met or exceeded, and it was demonstrated that AR technologies could achieve high efficiency and low cost NO_x control. The following conclusions can be drawn from results of the work:

1. Tests in combustion facilities ranging in firing rate from 0.1×10^6 to 10×10^6 Btu/hr demonstrated that AR provided up to 95% NO_x reduction. Among different AR variants AR-Lean + SNCR and Reburning + SNCR were found to be the most effective configurations, followed by AR-Lean and AR-Rich. Under optimized conditions these technologies reduce NO_x by up to 95% with net emissions less than 0.06 lb/10⁶ Btu and minimize other pollutants (N₂O and NH₃) to about the same levels achieved by reburning and SNCR.
2. Four different coals were evaluated as reburning fuel for basic reburning and AR. The results of the experiments indicated that the four tested bituminous coals were capable of providing reasonably high NO_x control in basic reburning at the full-scale boiler conditions evaluated. Over 90% NO_x reduction could be achieved in AR using coal as a reburning fuel. The most effective variant of AR with coal firing was reburning + SNCR followed by AR-Lean and AR-Rich. Tests showed that injection of promoters could significantly improve the NO_x reduction efficiency of coal serving as the reburning fuel in AR.
3. Tests showed that promoters could increase the efficiency of NO_x reduction in several AR variants. Promoters are most effective with small relative quantities of reburning fuel (6-10% of total fuel heat input). The use of promoters provides the means to improve NO_x reduction and simultaneously decrease the amount of reburning fuel required, relative to basic reburning.
4. Different metal-containing compounds were evaluated as AR promoters. Tests showed that co-injection of Na, Li and K compounds with N-agent resulted in 17-25 percentage points improvement compared to the NO_x reduction level provided by N-agent injection alone. Compounds of Mg, Ca, Ba, and Zn provided a relatively small promotional effect. When injected with the N-agent, they reduced NO by an additional 6-9 percentage points compared to unpromoted AR.
5. Tests demonstrated that metal-containing compounds could be effective reburning promoters without injection of N-agent. Fe-containing compounds were the most effective in reduction of NO_x emissions, followed by Na-, K-, and Ca-containing compounds. Co-injection of these compounds with the main fuel in the absence of reburning resulted in 16-

30% NO_x reduction. Co-injection of metal compounds with the main fuel in the presence of reburning provided an additional 4-25% percentage points of NO_x reduction above the baseline reburning level. Co-injection of these additives with reburning fuel and into the reburning zone had smaller effect than co-injection with the main fuel.

6. The kinetics of Na₂CO₃, one of the most effective AR promoters, was studied in a flow reactor. The study revealed that the primary gas-phase decomposition products of Na₂CO₃ are Na atoms, NaOH and CO₂. Extrapolating the results to higher temperatures showed that Na₂CO₃ decomposition at temperatures over 1400 K produced NaOH and CO₂ very quickly. The NaOH product then decomposed more slowly. These findings were used in the development of the kinetic mechanism of AR promotion.
7. The model of AR processes was developed. This model combined a detailed reaction mechanism with a simplified description of the mixing process. Modeling results demonstrated that the model correctly described a wide range of experimental data obtained in five bench- and pilot-scale combustion facilities. Mixing and thermal parameters in the model can be adjusted depending on the characteristics of the combustion facility. Kinetic modeling provided insight into the controlling factors of the process and predicted that the efficiency of AR systems are primarily determined by the following factors: equivalence ratio in the reburning zone, injection temperatures of process streams (reburning fuel, N-agents, promoters, and OFA), concentrations of N-agents and promoters, delay times for injection of N-agents into the reburning and burnout zones, and characteristic mixing times of the injection streams with flue gas.
8. The applicability of the model to the optimization of AR-Lean has been demonstrated. Modeling identified the following AR-Lean parameters as being most important: amounts of the reburning fuel and N-agent, temperature of flue gas at the point of OFA/N-agent injection, and evaporation time of the N-agent. Modeling predictions, supported by experiments, show that CO formed in the reburning zone increases the efficiency of N-agent when the temperature of furnace gases at the point of OFA/N-agent injection is lower than 1200 K, and reduces its efficiency at higher injection temperatures. To reduce the negative effect of CO on NO_x reduction at higher OFA/N-agent injection temperatures encountered in typical utility boiler installations, the average droplet size in the spray of injected N-agent solution must be optimized to allow for CO oxidation in the burnout zone before a significant amount of N-agent evaporates.
9. Pilot-scale tests were conducted to determine the optimum AR conditions at mixing and thermal characteristics of the Greenidge 105 MW tangentially fired boiler. Tests focused on simulating this boiler's AR-Lean and reburning + SNCR performance, considered to be the most promising for deep NO_x control for the unit. The results of the pilot-scale simulation tests demonstrated that high CO concentrations typical for upper furnace of the Greenidge boiler had negative effects on AR-Lean performance at the OFA/NH₃ injection location in the Greenidge boiler. The results predicted that about 70-80% NO_x reduction could be achieved under Greenidge conditions using an optimized reburning + SNCR regime.
10. The AR design methodology was created using experiments and analytical models to characterize the process elements of AR. This work took advantage of a full-scale demonstration of the original AR configuration on a 105 MW tangentially fired boiler, conducted outside the scope of this project. The AR methodology was used to prepare

process designs for implementation of three of the AR concepts on the 105 MW boiler, and to predict the impacts of each AR system on boiler performance and NO_x emissions.

11. Economic analysis demonstrates a considerable economic advantage of AR technologies in comparison with existing commercial NO_x control techniques, such as basic reburning, SNCR, and SCR. Particularly for deep NO_x control, coal-based AR technologies are 50% less expensive than SCR for the same level of NO_x control. The market for AR technologies is estimated to be above \$110 million.

13 References

- Alzueta, M.U., Bilbao, R., Millera, A., Glarborg, P., Østberg, M., and Dam-Johansen, K., *Energy & Fuels* 12:329 (1998).
- Alzueta, M.U., Røjel, H., Kristensen, P. G., Glarborg, P., and Dam-Johansen, K., *Energy and Fuels* 11:716-723 (1997).
- Babushok, V., Tsang, W., Linteris, G.T., and Reinelt, D., *Combust. Flame* 115:551 (1998).
- Cetegen, B. M., Johnson, T. R.; Payne, R., Moyeda, D. K., and Sheldon, M. S. Effective Mixing Processes for SO_x, Sorbent, and Coal Combustion Products, *U.S. Environmental Protection Agency Report No. EPA/600/7-87/013*, 1986.
- Chen, W.-Y., Extent of Heterogeneous Mechanisms During Reburning of Nitrogen Oxide, *Presented at the Annual Meeting of American Institute of Chemical Engineers*, Paper #78k, 1995.
- Chen, S.L., Lyon, R.K. and Seeker, W.R., *Environ. Progress*, V. 10, P. 182, August, 1991.
- FLUENT, *Fluent 5 User's Guide*, Fluent, Inc., Lebanon, NH, 1998.
- Glarborg, P., Alzueta, M.U., Dam-Johansen, K., and Miller, J.A., *Combust. Flame* 115:1 (1998).
- Illán-Gómez, M.J., Linares-Solano, A., Radovic, L.R., and Salinas-Martínez de Lecea, C., *Energy Fuels* 9, 97 (1995).
- Guo, F., Hecker, W.C., *Proc. Combust. Inst.* 26:2251 (1996).
- Hewson, T.A., and Stamberg, J.B. Evaluation of Proposed 37 State Seasonal NO_x Control Program. Compliance Costs and Issues, *Report by Energy Ventures Analysis, Inc.*, Arlington, VA, 1995.
- H&W Management Science Consultants, *Air Pollution Control Equipment Market Forecasts*, Issue No. 19, September 2000.
- Jensen, D.E., and Jones, G.A., *J. Chem. Soc. Faraday Trans. 1*, 78:2843 (1982).
- Kau, C. J., Heap, M. P., Seeker, W. R., and Tyson, T. J., Fundamental Combustion Research Applied to Pollution Formation. *U.S. Environmental Protection Agency Report No. EPA-6000/7-87-027, Volume IV: Engineering Analysis*, 1987.
- Kolb, T., Jansohn, P., and Leuckel, W., *Proc. Combust. Inst.* 22:1193 (1988).
- Leckner, B., Karlsson, M., Kilpinen, P., and Hupa, M., *Ind. Eng. Chem. Res.* 30:2396-2404 (1991).
- Luan, T., Liu, H., Gibbs, B.M., and Hampartsoumian, E., *The 9th International Symposium on Transport Phenomena in Thermal-Fluids Engineering*, p. 268, 1996.
- Lutz, A.E., Kee, R.J., and Miller, J.A., *SENKIN: A Fortran Program for Predicting Gas Phase Chemical Kinetics with Sensitivity Analysis*, Sandia National Laboratories, Report SAND87-8248, 1987.
- McBride, B. and Gordon, S. Chemical Equilibrium with Thermal Transport Properties, Lewis Research Center, Cleveland, Ohio, 1993.

- Mereb, J.B. and Wendt, J.O.L., *Proc. Combust. Inst.* 23:1271 (1990).
- Perry, R.A., and Miller, J.A., *Int. J. Chem. Kinetics*, 28:217 (1996).
- Phase II NO_x Controls for the MARAMA and NESCAUM Regions, EPA-453/R-96-002, 1996.
- Rota, R., Bonini, F., Servida, A., Morbidelli, M., and Carra, S., *Combust. Sci. and Tech.* 123:83 (1997).
- Schofield, K. and Steinberg, M., *J. Phys. Chem.* 96:715 (1992).
- Seeker, W.R., Chen, S.L., and Kramlich, J.C., U.S. *Patent 5,139,755*, August 18, 1992.
- Wendt, J.O.L and Mereb, J.B., Nitrogen Oxide Abatement by Distributed Fuel Addition, *FETC Quarterly Report No. 13*, Contract DE-AC22-87PC79850, 1991.
- Winter, E.R.S., *J. of Catalysis* 22:158 (1971).
- Zamansky, V.M., Lissianski, V.V., Maly, P.M., Ho, L., Rusli, D., and Gardiner, W.C., Jr. *Combust. Flame*, 117:821 (1999).
- Zamansky, V.M., Ho, L., Maly, P.M. and Seeker, W.R. (1996) *American Flame Research Committee (AFRC) International Symposium*, Baltimore, MD, (1996).
- Zamansky, V.M., Ho, L., Maly, P.M., and Seeker, W.R., *The Fourth International Conference on Technologies and Combustion for a Clean Environment*, Lisbon, Portugal, 1997.
- Zwietering, T.N., *Chem. Eng. Scie.* 11:1 (1959).

Appendix A Phase I Report

Appendix A includes description of Phase I work which started in October, 1995 and was finished in September, 1997. Phase I Final Report was submitted to U.S. DOE in July, 1997.

***SECOND GENERATION ADVANCED REBURNING
FOR HIGH EFFICIENCY NO_x CONTROL***

Phase I Final Report

Project Period: October 1, 1995 - September 30, 1997

Prepared by:

Vladimir M. Zamansky, Peter M. Maly, Loc Ho, Mark S. Sheldon, David Moyeda,
Blair A. Folsom, W. Randall Seeker, William C. Gardiner, Jr. and Vitaly V. Lissianski

July 31, 1997

DOE Contract No. DE-AC22-95PC95251

Phase I

Submitted by:

Energy and Environmental Research Corporation
18 Mason, Irvine, CA 92618

Disclaimer

This report was prepared as an account of work sponsored by an agency of the United States Government. Neither the United States nor any agency thereof, nor any of their employees, makes any warranty, express or implied, or assumes any legal liability or responsibility for the accuracy, completeness, or usefulness of any information, apparatus, product, or process disclosed, or represents that its use would not infringe privately owned rights. Reference herein to any specific commercial product, process, or service by trade name, trademark, manufacturer, or otherwise does not necessarily constitute or imply its endorsement, recommendation, or favoring by the United States Government or any agency thereof. The views and opinions of authors expressed herein do not necessarily state or reflect those of the United States Government or any agency thereof.

ABSTRACT

This project develops novel Advanced Reburning (AR) concepts for high efficiency and low cost NO_x control from coal fired utility boilers. AR technologies are based on combination of basic reburning and N-agent/promoter injections. Phase I demonstrated that AR technologies are able to provide effective NO_x control for coal fired combustors. Three technologies were originally envisioned for development: AR-Lean, AR-Rich, and Multiple Injection AR (MIAR). Along with these, three additional technologies were identified during the project: reburning plus promoted SNCR, AR-Lean plus promoted SNCR, and AR-Rich plus promoted SNCR. The promoters are sodium salts, in particular sodium carbonate. These AR technologies have different optimum reburn heat input levels and furnace temperature requirements. For full scale application, an optimum technology can be selected on a boiler-specific basis depending on furnace temperature profile and regions of injector access.

The experimental program included combustion tests in 20 and 200 kW facilities. Pilot scale studies in the 200 kW combustor demonstrated the ability of the AR technologies to achieve NO_x reductions of 95+% during gas firing and 90+% during coal firing. Byproduct emissions were found to be lower than those generated by commercial reburning and SNCR technologies.

A detailed reaction mechanism was developed to model the AR chemical processes. The mechanism (355 reactions of 65 species) includes the following submechanisms: GRI-Mech-2.11, SNCR chemistry, sodium chemistry with Na_2CO_3 decomposition reactions, SO_2/SO_3 reactions, and interaction of HCl with flue gas components. Modeling provided insight into the controlling factors of the process and qualitatively described the observed reaction trends. Modeling predicted and explained the effect of sodium promotion under both fuel-rich and fuel-lean conditions. The sensitivity analysis revealed the most significant elementary reactions affecting formation and destruction of NO and other N-containing compounds in the reburning and burnout zones.

The AR design methodology was updated by using experiments and analytical models to include the second generation improvements. This methodology was then used for application of the novel AR concepts to a 100 MW tangentially fired utility boiler, and to predict the impacts of the AR systems on boiler performance and NO_x emissions. A parallel AR-Lean demonstration (outside the scope of this project) provided an opportunity to test several novel AR components in the field.

Economic analysis demonstrates a considerable economic advantage of AR technologies in comparison with existing commercial NO_x control techniques, such as basic reburning, SNCR, and SCR. Particularly for deep NO_x control, AR results in 2-3 times lower costs (in \$/ton of NO_x removed) than SCR for the same level of NO_x control. The market for AR technologies is estimated to be above \$1.5 billion.

TABLE OF CONTENTS

<u>Section</u>	<u>Page</u>
1.0 EXECUTIVE SUMMARY	1-1
2.0 INTRODUCTION	2-1
3.0 BACKGROUND	3-1
3.1 High Efficiency NO _x Control under Title 1 of the CAAA	3-1
3.2 Limitations of Available NO _x Control Technologies for Post-RACT Applications	3-3
3.3 Advanced Reburning	3-5
3.4 Second Generation Advanced Reburning (SGAR)	3-5
4.0 PHASE I PROGRAM OBJECTIVES	4-1
5.0 KINETICS OF Na ₂ CO ₃ REACTIONS WITH FLUE GAS	5-1
5.1 Literature Review	5-1
5.2 Thermodynamics of Sodium in Combustion Flue Gas	5-3
5.2.1 The Solid to Gas-Phase Transition	5-3
5.2.2 Available Thermodynamic Data on Sodium in the Gas-Phase	5-8
5.3 Experimental Methods	5-15
5.3.1 Flow System	5-15
5.3.2 Mass Spectrometric Analysis	5-17
5.4 Rate of Sodium Carbonate Decomposition	5-17
5.4.1 Sodium Carbonate Decomposition in Nitrogen	5-17
5.4.2 Reactions of Sodium Carbonate with Components of Flue Gas ..	5-25
5.5 Mass Spectrometry of Decomposition Products	5-26
5.6 Kinetics of Na ₂ CO ₃ Reactions: Conclusions	5-32
6.0 BENCH SCALE PROCESS OPTIMIZATION STUDIES	6-1
6.1 Controlled Temperature Tower	6-1
6.2 Reburning Alone	6-4
6.3 Promoted AR-Lean	6-6
6.4 Promoted AR-Rich	6-7
6.5 Multiple Injection AR (MIAR)	6-12
6.6 Bench Scale Combustion Tests: Conclusions	6-13
7.0 PILOT SCALE DEVELOPMENT TESTS	7-1
7.1 Preparation of Pilot Scale Combustion Facility	7-1
7.1.1 Boiler Simulator Facility	7-1

7.1.2	Reburning and Additive Injection Systems	7-3
7.1.3	Sampling and Analysis Methods	7-4
7.2	Pilot Scale Combustion Tests with Natural Gas Firing	7-4
7.2.1	Promoted AR-Lean	7-4
7.2.2	Promoted AR-Rich	7-7
7.2.3	Hybrid AR-Lean/SNCR	7-12
7.2.4	MIAR	7-14
7.3	Pilot Scale Combustion Tests with Coal Firing	7-16
7.3.1	Promoted AR-Lean	7-17
7.3.2	Promoted AR-Rich	7-18
7.3.3	Hybrid AR-Lean/SNCR	7-23
7.3.4	Hybrid AR-Rich/SNCR	7-26
7.3.5	MIAR	7-27
7.3.6	Byproduct Sampling Tests	7-31
7.4	Pilot Scale Combustion Tests: Conclusions	7-38
8.0	MECHANISM DEVELOPMENT AND KINETIC MODELING	8-1
8.1	Mechanism Development	8-1
8.1.1	GRI-Mech	8-2
8.1.2	SNCR Reations	8-2
8.1.3	Reactions of Sodium	8-5
8.1.4	Reactions of Sulfur and Chlorine	8-7
8.1.5	Mechanism Development: Summary	8-9
8.2	Modeling with Instantaneous Mixing Times	8-9
8.2.1	Modeling of the Basic Reburning Process	8-13
8.2.2	Injection of Ammonia into the Reburning Zone (AR-Rich)	8-32
8.2.3	Promotion of the NO-NH ₃ Interaction in the Reburning Zone	8-42
8.2.4	Effect of Different Factors on the NO-NH ₃ Interaction in the Reburning Zone	8-48
8.2.5	Injection of Ammonia into the Burnout Zone (AR-Lean)	8-50
8.2.6	Modeling with Instantaneous Mixing Times: Summary	8-51
8.3	Evaluation of Mixing Effects	8-52
8.3.1	Approach	8-52
8.3.2	Effect of Mixing Times on Basic Reburning	8-54
8.3.3	Effect of Mixing Times on AR-Rich	8-55
8.3.4	Effect of Mixing Times on AR-Lean	8-58
8.3.5	Mixing Studies: Summary	8-60
8.4	Effect of Sodium	8-61
8.4.1	Effect of Sodium Promotion in AR-Rich	8-62
8.4.2	Effect of Sodium Promotion in AR-Lean	8-76
8.5	Summary of Modeling Studies	8-84

9.0	DESIGN METHODOLOGY AND APPLICATION	9-1
9.1	AR Design Methodology	9-1
9.1.1	General Approach	9-1
9.1.2	Case Study Boiler Characteristics	9-3
9.1.3	Heat Transfer Analysis	9-4
9.1.4	Injection System Studies	9-14
9.1.5	Full Scale Performance Prediction	9-18
9.2	AR Application	9-19
9.3	Economic and Market Analysis	9-24
9.3.1	NO _x Control Drivers	9-25
9.3.2	Methodology and Cases Evaluated	9-26
9.3.3	Technology Specific Inputs	9-27
9.3.4	Economic Results	9-29
9.3.5	Market Assessment	9-31
9.4	Design Methodology and Application: Conclusions	9-33
10.0	CONCLUSIONS	10-1
11.0	ACKNOWLEDGEMENTS	11-1
12.0	REFERENCES	12-1
Appendix 1.	Reaction Mechanism in Chemkin/Senkin Interpreter Format	A-1
Appendix 2.	Thermodynamic database for Reaction Mechanism in Chemkin Format .	A-12
Appendix 3.	Thermodynamic database for sodium compounds	A-17

LIST OF FIGURES

<u>Figure</u>	<u>Page</u>
2.1 SGAR schematic - definitions	2-2
4.1. Phase I task structure and major milestones	4-2
5.2.1 Dependence of $\Delta_r G^\circ$ (EER thermochemistry) for $\text{Na}_2\text{CO}_3 \leftrightarrow \text{Na}_2\text{O} + \text{CO}_2$ and $\text{Na}_2\text{CO}_3 + \text{H}_2\text{O} \leftrightarrow 2\text{NaOH} + \text{CO}_2$ on temperature	5-5
5.2.2 Dependence of Na_2CO_3 to CO_2 conversion according to equation (5.13)	5-6
5.2.3 Comparison between experimental and calculated equilibrium conversions of Na_2CO_3 to CO_2	5-8
5.2.4 Equilibrium distribution of sodium-containing species at 1 atm pressure in 80% N_2 , 20% H_2O and 300 ppm Na_2CO_3	5-13
5.2.5 Equilibrium distribution of sodium-containing species at 1 atm pressure in a flue-gas-like mixture with 300 ppm of added Na_2CO_3	5-13
5.3.1 Flow system diagram	5-16
5.4.1 Comparison of experimental and calculated Na_2CO_3 conversion profiles	5-20
5.4.2 Temperature dependence of the decadic logarithm of time required for decomposition of 30% of the initial amount of Na_2CO_3	5-21
5.4.3 Sensitivity spectrum for decomposition of Na_2CO_3	5-23
5.4.4 Rate coefficient inferred for $\text{Na}_2\text{CO}_3 \rightarrow \text{Na}_2\text{O} + \text{CO}_2$ (5.16)	5-23
5.4.5 Rate coefficient inferred for $\text{Na}_2\text{O} + \text{CO}_2 \rightarrow \text{Na}_2\text{CO}_3$ (5.17)	5-24
5.5.1 Time histories of ion currents at $m/z = 44$ and 106 and total ion current	5-27
5.5.2 Mass spectrum at 62 s on the x-axis of Figure 5.5.1	5-27
5.5.3 Mass spectrum at the time $m/z = 23$ reaches its maximum	5-28
5.5.4 Mass spectrum at the time $m/z = 23$ reaches its maximum in thermal ionization mode	5-28
5.5.5 Time histories of ions with $m/z = 23$ (Na^+), 44 (CO_2^+), 53 ($\text{Na}_2\text{CO}_3^{++}$), 106 (Na_2CO_3^+), 129 (Na_3CO_3^+), and total ion current	5-29
5.5.6 Time histories of Ag^+ (109) and total ion current for experiments with Ag wire .	5-30
5.5.7 Mass spectrum at 1235 K	5-31
5.5.8 Time histories of ions with $m/z = 23$ (Na^+) and 109 (Ag^+), and total ion current through the detector for thermal ionization mode	5-31
5.5.9 Mass spectrum corresponding to the moment of burnout of Ag wire for thermal ionization mode	5-32
6.1 Controlled Temperature Tower (CTT)	6-2
6.2 CTT temperature profiles	6-3
6.3 NO reduction vs. reburn heat input for CTT gas reburn: No additives or promoters	6-5
6.4 NO reduction vs. reburn zone residence time for gas reburn: No additives or promoters	6-6
6.5 AR-Lean performance	6-7

6.6	AR-Rich performance	6-8
6.7	Alternative promoter screening test results	6-9
6.8	NO control vs. Na promoter concentration	6-10
6.9	NO reduction vs. NO _i for rich side injection of NH ₄ OH + Na ₂ CO ₃	6-11
6.10	NO reduction vs. NSR for rich side injection of NH ₄ OH + Na ₂ CO ₃	6-12
6.11	MIAR: NO reduction vs. additive injection temperature for reburn with both rich and lean side additives	6-13
7.1	Boiler Simulator Facility (BSF)	7-2
7.2	BSF temperature profile during 10% reburning	7-3
7.3	AR-Lean with aqueous urea/sodium injection	7-5
7.4	AR-Lean with aqueous ammonia/sodium injection	7-6
7.5	AR-Rich with urea/sodium injection	7-7
7.6	AR-Rich with ammonia/sodium injection	7-8
7.7	AR-Rich with urea/sodium injection	7-10
7.8	AR-Rich with urea/sodium injection	7-11
7.9	Effect of sodium on NO reduction in AR-Rich	7-12
7.10	NO reduction during natural gas firing by combined AR-Lean/SNCR with urea injection at two locations	7-13
7.11	Effect of rich side additive injection temperature upon MIAR performance during natural gas firing at SR ₂ = 0.99	7-15
7.12	Effect of rich side additive injection temperature upon MIAR performance during natural gas firing at SR ₂ = 0.90	7-16
7.13	NO reduction by AR-Lean during coal firing	7-17
7.14	AR-Lean tests: Effect of N-agent/OFA injection temperature upon performance	7-18
7.15	Effect of urea injection temperature and concentration of sodium on NO reduction in AR-Rich with coal firing	7-19
7.16	Effect of urea injection temperature and concentration of sodium on NO reduction in AR-Rich with coal firing	7-20
7.17	AR-Rich tests: Effect of N-agent injection temperature upon performance	7-21
7.18	AR-Rich tests: Effect of OFA injection temperature upon performance	7-22
7.19	AR-Rich tests: Effect of sodium promoter concentration upon performance	7-23
7.20	NO reduction during coal firing by combined AR-Lean/SNCR with urea injection at two locations	7-24
7.21	AR-Rich + SNCR tests: Effect of second additive injection temperature upon performance	7-26
7.22	MIAR tests: Effect of first additive injection temperature upon performance at 18% reburning	7-27
7.23	MIAR tests: Effect of first additive injection temperature upon performance at 9% reburning	7-28
7.24	MIAR tests: Effect of second additive injection temperature upon performance at 18% reburning	7-29

7.25	MIAR tests: Effect of second additive injection temperature upon performance at 9% reburning	7-30
7.26	CO and N ₂ O emissions for AR technologies	7-33
7.27	NH ₃ and HCN emissions for AR technologies	7-34
7.28	SO ₃ emissions for AR technologies	7-35
7.29	Fly ash size distribution	7-36
7.30	Fly ash total loading, PM 10 and PM 2.5	7-37
7.31	Carbon in ash results	7-38
8.1.1	Comparison of experimental data and modeling with mechanisms A and B for the Thermal DeNO _x process	8-4
8.1.2	Effect of sulfur and chlorine on equilibrium concentrations of sodium species in flue gas	8-10
8.2.1	Kinetic curves of the main species in the reburning zone at SR ₂ = 0.99 and injection temperature T ₁ = 1700 K	8-14
8.2.2	Kinetic curves of the main species in the reburning zone at SR ₂ = 0.95 and injection temperature T ₁ = 1700 K	8-14
8.2.3	Kinetic curves of the main species in the reburning zone at SR ₂ = 0.90 and injection temperature T ₁ = 1700 K	8-15
8.2.4	Kinetic curves in the reburning zone at SR ₂ = 0.99, T ₁ = 1700 K and t = 5ms ..	8-16
8.2.5	Kinetic curves in the reburning zone at SR ₂ = 0.90, T ₁ = 1700 K and t = 5ms ..	8-18
8.2.6	Modeling and experimental data on concentrations of NO, NH ₃ , HCN, and TFN in the reburning zone (t = 0.5 s) at T ₁ = 1700 K for different concentrations of reburning fuel, SR ₂	8-20
8.2.7	Modeling data on concentrations of NO, NH ₃ , HCN, and TFN in the reburning zone (t = 0.5 s) at T ₁ = 1500 - 1700 K for different concentrations of reburning fuel, SR ₂	8-21
8.2.8	NO contribution factors at SR ₂ = 0.99 in the fast NO decrease region	8-23
8.2.9	NO contribution factors at SR ₂ = 0.99 in the slow NO decrease region	8-24
8.2.10	NO sensitivity coefficients at SR ₂ = 0.99 in the fast NO decrease region	8-26
8.2.11	NO sensitivity coefficients at SR ₂ = 0.99 in the slow NO decrease region	8-27
8.2.12	NO contribution factors at SR ₂ = 0.90 in the fast NO decrease region	8-29
8.2.13	NO contribution factors at SR ₂ = 0.90 in the slow NO decrease region	8-30
8.2.14	NO sensitivity coefficients at SR ₂ = 0.90 in the slow NO decrease region	8-31
8.2.15	Effect of ammonia co-injection with the reburning fuel and 0.1 s delayed NH ₃ injection on fuel-N species in the reburning zone	8-34
8.2.16	Effect of the delay time of NH ₃ injection into the reburning zone at SR ₂ = 0.99 ..	8-35
8.2.17	Effect of the NH ₃ concentration injected into the reburning zone at SR ₂ = 0.99 and 0.1 s delay time	8-35
8.2.18	Kinetic curves of species in the reburning zone at SR ₂ = 0.99 for injection of 800 ppm ammonia along with the reburning fuel at 1700 K	8-37
8.2.19	NO contribution factors for conditions of Figure 8.2.18	8-38

8.2.20	Kinetic curves of species in the reburning zone at $SR_2 = 0.99$ for injection of 800 ppm ammonia with a 0.1 s delay after the reburning fuel injected at 1700 K	8-39
8.2.21	NO contribution factors for conditions of Figure 8.2.20	8-40
8.2.22	NO sensitivity coefficients for conditions of Figure 8.2.20	8-41
8.2.23	Effect of NH_3 injection temperature and NH_3 concentration in mixture I on NO/TFN reduction	8-44
8.2.24	Effect of radicals co-injection with 500 ppm NH_3 into mixture I, $T_2 = 1600$ K	8-45
8.2.25	Comparison of the promotion effect of different compounds	8-46
8.2.26	Modeling of the promotion effect at different preexponential factors A	8-47
8.2.27	Effect of O_2 co-injection with 500 ppm NH_3 into mixture I at different injection temperatures	8-49
8.2.28	Effect of FA co-injection with NH_3 on the final NO concentration	8-51
8.3.1	Kinetic curves of important species in the reburning zone at $SR_2 = 0.99$ and with mixing of the reburning fuel over an interval of 30 ms	8-55
8.3.2	Kinetic curves of important species in the reburning zone at $SR_2 = 0.99$ and with mixing of the reburning fuel over an interval of 300 ms	8-56
8.3.3	Kinetic curves of important species in the reburning zone at $SR_2 = 0.99$ and with mixing of the reburning fuel over an interval of 30 ms	8-57
8.3.4	Kinetic curves of important species in the reburning zone at $SR_2 = 0.99$ and with mixing of the reburning fuel over an interval of 300 ms	8-58
8.3.5	AR-Rich NO emissions, for $SR_2 = 0.99$ and NH_3 added at $NSR = 1$	8-59
8.3.6	AR-Lean NO emissions, for $SR_2 = 0.99$ and NH_3 added at the same time as overfire air, at $NSR = 1$	8-60
8.3.7	AR-Lean NO emissions, for $SR_2 = 0.99$ and NH_3 added 0.1 s after burnout air at $NSR = 1$	8-61
8.4.1	AR-Rich kinetic curves with instantaneous mixing, from the point of reburn fuel injection with NH_3 ($NSR = 1$) injected after 0.1 s	8-63
8.4.2	AR-Rich kinetic curves with 30 ms mixing, from the point of reburn fuel injection with NH_3 ($NSR = 1$) injected after 0.1 s	8-64
8.4.3	AR-Rich kinetic curves with 300 ms mixing, from the point of reburn fuel injection with NH_3 ($NSR = 1$) injected after 0.1 s	8-65
8.4.4	NO and total fuel nitrogen before burnout for AR-Rich vs. mixing time, $NSR = 1.0$	8-67
8.4.5	NO and total fuel nitrogen before burnout for AR-Rich vs. mixing time, 800 ppm NH_3 added	8-67
8.4.6	NO concentration prior to start of overfire air injection at 1300 K, as a function of N-agent/promoter injection delay time	8-69
8.4.7	TFN concentration prior to start of overfire air injection at 1300 K, as a function of N-agent/promoter injection delay time	8-69
8.4.8	Final NO concentration at 600 K, as a function of N-agent/promoter injection	

delay time	8-70
8.4.9 Kinetic curves after NH ₃ (NSR = 1) injection in AR-Rich 500 ms after reburn fuel, with and without 50 ppm	8-72
8.4.10 Effect of promoter on NO exit concentrations for AR-Lean	8-77
8.4.11 AR-Lean kinetic curves with 30 ms mixing from the point of NH ₃ injection, which is 0.1 s after OFA injection at 1280 K	8-79
8.4.12 AR-Lean kinetic curves with 30 ms mixing from the point of NH ₃ injection, which is 0.1 s after OFA injection at 1380 K	8-81
9.1.1 Generalized design methodology for AR technologies	9-2
9.1.2 Schematic of case study boiler	9-3
9.1.3 Furnace heat transfer model set up	9-6
9.1.4 Comparison of predicted and measured furnace gas temperatures	9-7
9.1.5 Predicted bulk mean temperatures in upper furnace of case study boiler	9-8
9.1.6 Implementation of AR technologies on case study boiler	9-9
9.1.7 Projected impacts of AR processes on furnace exit gas temperature	9-11
9.1.8 Projected impacts of AR processes on carbon in ash	9-11
9.1.9 Projected impacts of AR processes on ASME heat loss efficiency	9-12
9.1.10 Projected impacts of AR processes on steam temperatures	9-13
9.1.11 Baseline flow field characteristics	9-15
9.1.12 Dispersion pattern for preferred reburning fuel injector configuration	9-16
9.1.13 Dispersion pattern for preferred overfire air port configuration	9-17
9.2.1 Isometric view of Greenridge Unit 4 showing gas reburning and AR-Lean components external to the boiler	9-20
9.2.2 Gas reburning and AR-Lean NO _x data, Greenridge Unit 4	9-22
9.3.1 Cyclone fired boiler NO _x economics	9-30
9.3.2 Wall fired boiler NO _x economics	9-30

LIST OF TABLES

<u>Table</u>	<u>Page</u>
3.1 Performance of NO _x control technologies	3-3
5.2.1 JANAF standard enthalpies of formation at 298 and 1500 K	5-9
5.2.2 JANAF standard enthalpies of formation at 298 and 1500 K	5-10
5.2.3 Thermochemistry for breaking Na—X bonds at 1500 K	5-10
7.1 Comparison of NO reduction for hybrid AR-Lean/SNCR with gas and coal firing	7-25
7.2 Byproduct sampling conditions and results	7-32
8.2.1 Comparison of NO reaction rates with C-radicals at SR ₂ = 0.99, T ₁ = 1700 K and t = 2ms	8-17
8.4.1 Results of AR-Rich at different delay times	8-71
8.4.2 Results of AR-Lean at different injection temperatures, with and without sodium	8-78
9.3.1 Economic data	9-27
9.3.2 Evaluated NO _x control technologies	9-28
9.3.3 NO _x control technology data	9-28
9.3.4 Comparing cost effectiveness for deep NO _x control	9-31
9.3.5 Estimated market for AR technologies	9-32
9.3.6 Total estimated AR market	9-33

1.0 EXECUTIVE SUMMARY

In this project EER is developing second generation enhancements to Advanced Reburning (AR). AR is an NO_x control technology which integrates reburning with injection of a nitrogen reducing agent (N-agent), two well known commercial NO_x control technologies. Reburning involves injection of a hydrocarbon fuel above the burners to produce a fuel rich zone where NO_x is reduced to elemental nitrogen. Overfire air is added to burn out combustibles. Reburning can typically achieve about 60% NO_x reduction in full scale applications. N-agent injection involves the injection of an N-agent such as ammonia or urea into high temperature gases in the convective pass of a boiler where it reduces NO_x to elemental nitrogen. The commercial version of this system is termed Selective Non-Catalytic Reduction (SNCR) and typically achieves 20-40% NO_x reduction in full scale applications.

EER's original configuration of AR (now termed AR-Lean) was developed prior to this project and is currently being demonstrated at full scale. AR-Lean is expected to achieve NO_x reduction in the range of 75-85% in compatible boiler designs. This project is developing second generation AR (SGAR) systems which increase the NO_x reduction to over 95% and broaden applicability to a wide range of boiler designs. This family of SGAR technologies includes various combinations of the following elements:

- Injection of a reburning fuel to produce slightly fuel-rich conditions in the reburn zone where a portion of the NO_x reduction occurs.
- Injection of overfire at a lower temperature range than conventional reburning, typically (1250-1420°K).
- N-agent injection at one or multiple locations: in the reburning zone, with overfire air, and downstream of the overfire air injection to provide the remainder of the NO_x reduction.
- Addition of water soluble promoter additives which enhance the effectiveness of the N-agent NO_x reduction.

By selecting various combinations of these elements, the SGAR systems can be tailored to site specific boiler characteristics to achieve NO_x control ranging from about 60% for reburning alone to as high as 95% for the most complex SGAR system. These SGAR systems can meet the most stringent NO_x control requirements of Title 1 of the Clean Air Act Amendment at considerably less cost than Selective Catalytic Reduction, the only commercial NO_x control technology which can achieve comparable NO_x reduction. In addition, SGAR avoids the massive duct modifications and catalyst replacement/disposal problems of SCR.

At the beginning of the project, EER proposed the development of three SGAR systems differing in the way in which the N-agent injection is integrated with reburning:

- Promoted Advanced Reburning - Lean (AR-Lean) -- This is the original AR configuration but with a promoter added to the N-agent. The N-agent and promoter are injected with

the overfire air.

- Advanced Reburning - Rich (AR-Rich) -- Here, the N-agent is injected into the reburning zone with or without a promoter. This provides increased flexibility in locating the overfire air ports to match the boiler convective pass configuration.
- Multiple Injection Advanced Reburning (MIAR) -- This involves two stages of N- agent injection with promoters: in the reburning zone and with the overfire air. NO_x reduction as high as 95% is achieved by three stages: reburning, rich injection of the N-agent and lean injection o the N-agent.

During the project, the family of SGAR systems was expanded with three additional configurations:

- AR-Lean + SNCR -- This is the integration of the AR-Lean with conventional SNCR where the N-agent is injected downstream of the overfire air with a promoter.
- AR-Rich + SNCR -- This is the integration of AR-Rich with conventional SNCR where the N-agent is injected downstream of the overfire air with a promoter.
- Reburning + Promoted SNCR -- This is basic reburning followed by the promoted SNCR process.

This family of six SGAR configurations allows the NO_x control system to be tailored to site specific requirements. Also, components can be added in building block fashion to increase NO_x reduction as the NO_x regulations become more stringent over time.

This project is being conducted in two phases: Phase I -- Development of a Design Methodology, and Phase II -- Process Optimization and Scale-up.

Phase I consists of the following six tasks:

Task 1.1	Project Coordination and Reporting/Deliverables
Task 1.2	Kinetics of Na ₂ CO ₃ Reactions with Flue Gas Components
Task 1.3	0.1 x 10 ⁶ Btu/hr Optimization Studies
Task 1.4	1.0 x 10 ⁶ Btu/hr Process Development Tests
Task 1.5	Mechanism Development and Modeling
Task 1.6	Design Methodology and Application

This report presents the results of Phase I which was conducted over a period of two years. The objectives of Phase I were as follows:

1. Develop an understanding of the mechanisms through which promoter additives improve N-agent effectiveness.
2. Develop a kinetic analytical model of the Promoted and Multiple Injection AR technologies.
3. Optimize the SGAR processes using the analytical model and bench and pilot scale experiments under controlled mixing conditions.
4. Upgrade EER's AR design methodology to include the second generation advances.

The following Phase I technical performance goals were established in the Project Management Plan:

- NO_x emissions from the 1.0 x 10⁶ Btu coal fired Boiler Simulator Facility should be controlled to less than the requirements for post-RACT NO_x control in the Northeast Ozone Transport Region for the year 2003.
- The total estimated cost of controlling NO_x emissions based on the 1.0 x 10⁶ Btu/yr coal fired tests should be less than that currently projected for SCR NO_x control systems.
- SGAR should not cause a significant reduction in boiler efficiency or significant adverse environmental impacts compared to basic reburning and SNCR technologies.

All Phase I objectives and technical performance goals have been met or exceeded, and it was demonstrated that AR technologies can achieve high efficiency and low cost NO_x control.

Initial parametric screening tests were conducted in a bench scale facility, followed by pilot scale developmental studies. Experimental work was paralleled by kinetic modeling which provided a scientific understanding of the process, including the activity of N-agent promoters. Simultaneously, an experimental study was conducted to define the high-temperature chemistry of sodium carbonate under simulated flue gas conditions. The results were used for updating the kinetic model. The modeling used experimental data to define key process parameters, culminating in a design methodology for the eventual scale-up and implementation of the technologies.

A kinetic study on thermal decomposition of Na₂CO₃ was conducted in Task 1.2 using a flow system with Gas Chromatography (GC) and Mass-Spectrometry (MS) analysis of products. It was found that significant decomposition of Na₂CO₃ occurs on a one second time scale at temperatures between 900 and 1300 K. The main decomposition products were identified as CO₂, Na atoms, and Na₂O. The rate of Na₂CO₃ decomposition was measured as functions of temperature, residence time, and initial Na₂CO₃ concentration. The decomposition of Na₂CO₃

from 900 to 1190 K was described kinetically in terms of two irreversible and one reversible reactions: $\text{Na}_2\text{CO}_3 \rightarrow \text{Na}_2\text{O} + \text{CO}_2$; $\text{Na}_2\text{O} + \text{CO}_2 \rightarrow \text{Na}_2\text{CO}_3$; and $\text{Na}_2\text{O} + \text{H}_2\text{O} \rightleftharpoons 2\text{NaOH}$.

In Task 1.3, 0.1×10^6 Btu/hr combustion tests were conducted with natural gas as main and reburning fuel. The promoted AR-Lean process achieved about 86% NO_x reduction at 10% reburning fuel heat input and only 15 ppm Na_2CO_3 in flue gas. The promoted AR-Rich process achieved 88% NO_x reduction at 10% reburning fuel and 15 ppm Na_2CO_3 . Thus, the presence of Na_2CO_3 promotes the effect of both "lean" and "rich" N-agent injection. Several sodium compounds (Na_2CO_3 , NaHCO_3 , and NaOH) were tested and achieved comparable promotion effectiveness. In AR-Rich, NO_x reduction was enhanced when the N-agent was injected into the reburning zone with a delay time after injection of the reburning fuel. The MIAR process achieved 90-91% NO_x reduction in these bench scale tests and was expected to improve at larger scales since the injectors adversely affected the temperature profile in these small scale tests.

Task 1.4 involved 1.0×10^6 Btu/hr tests in a Boiler Simulator Facility (BSF). Initial experiments were performed with natural gas firing. In AR-Lean, injection of urea or ammonia with OFA provided 45-82% NO reduction depending on the injection temperature. This was consistent with previous EER research. Addition of 15 ppm of Na_2CO_3 promoter to the N-agent greatly improved NO_x reduction. Performance was about equal for ammonia and urea with maximum of 89-94%. In AR-Rich, similar NO_x reduction was obtained for injection of ammonia and urea, 70-77%. However, addition of 15-25 ppm Na_2CO_3 significantly improved NO_x reduction, up to 94-95%. Two N-agent injections (MIAR) demonstrated 78-82% NO_x reduction without sodium and up to 98% NO_x reduction, with 15 ppm Na_2CO_3 . This was the maximum NO_x reduction achieved by AR systems.

Experiments were also conducted with coal firing. The results showed that the AR technologies can provide up to 95% NO_x control for a high-sulfur coal-fired combustor. The NO_x reduction due to N-agent injection was higher, but the effect of sodium promotion was lower in comparison with gas firing. Na_2CO_3 was found to promote performance only by 5-8 percentage points when added at 75 ppm. Maximum NO_x reductions achieved by the promoted AR technologies with coal firing were 90% for AR-Lean, 93% for AR-Rich, and 95% for MIAR. Three other AR modifications: AR-Lean+Promoted SNCR, AR-Rich+Promoted SNCR, and Reburning+Promoted SNCR, provided up to 95, 92, and 93% NO_x reduction, respectively.

A separate study was then conducted to evaluate byproducts emissions from different AR variants in comparison with basic reburning and SNCR. The following emissions were characterized: NO_x , CO, CO_2 , O_2 , SO_2 , N_2O , total hydrocarbons, NH_3 , HCN, SO_3 , fly ash mass loading, size distribution, PM10, PM2.5, and carbon in ash. The results showed that in most configurations AR technologies have less byproduct emissions than basic reburning and SNCR processes under similar operating conditions.

In Task 1.5, a reaction mechanism, including 355 reactions of 65 chemical species, was developed to characterize the chemical processes of reburning and AR. The mechanism consists of C-H-O-N submechanism (GRI-Mech-2.11, no variation of rate constants) and submechanisms describing SNCR chemistry, and reactions of sodium, sulfur, and chlorine. Modeling was performed using three kinetic programs: Chemkin-2, Senkin (developed by Sandia National Laboratories) and EER's One Dimensional Flame code (ODF). Modeling was capable of predicting major reaction trend, qualitatively describing AR processes, and, in some cases, was close to quantitative process description. Modeling explained why the delayed ammonia injection into the reburning zone is capable of reducing NO concentration and why certain additives, such as oxygen and active radicals, can promote the NO-NH₃ interaction in the reburning zone. Modeling also described the NO-NH₃ interaction in the burnout zone. A sensitivity analysis was conducted which revealed the most significant elementary reactions affecting formation and destruction of fuel-N compounds in the reburning zone under various conditions. Modeling with different mixing times demonstrated the importance of delayed mixing modes for efficient NO_x reduction. Modeling explained the effect of sodium promoters under both fuel-rich and fuel-lean conditions. Sodium reactions can affect NO_x control by decreasing or increasing the radical pool when it is needed. The radicals in turn can react with NH₃ to form NH₂ species which reduce NO to molecular nitrogen. The effect of promoters is most pronounced in systems with long characteristic mixing times, as is typical in full-scale industrial applications.

In Task 1.6, EER's reburning design methodology was expanded to SGAR and an economic and market assessment was conducted. To demonstrate the applicability of the methodology, it was applied to a typical 100 MW coal-fired utility boiler with tangentially firing burners, resulting in development of conceptual designs for several second generation AR systems, and predictions of their impacts on boiler NO_x emissions and operating performance. Thermal performance models were used to evaluate the impacts of implementing AR processes on the thermal performance of the boiler. For implementation of AR-Lean, AR-Rich, or MIAR processes, the reburning fuel would be injected into the lower furnace and the overfire air would be injected into the upper furnace in a cavity between the first two tube banks of the convective pass. The overall boiler efficiency for operation with an AR system is similar to that for operation with a basic gas reburning system. The results of the analysis are specific to the boiler configuration evaluated and should not be generalized to other boiler designs. The results of injection system analysis indicate that good mixing of the process streams necessary to implement advanced reburning (AR-Lean, AR-Rich, and MIAR) on the case study boiler can be achieved. Natural gas can be injected from each wall in a pattern which achieves good distribution of the reburning fuel. Overfire air injection into a cavity in the convective pass, needed for implementation of each of the AR processes under consideration, can be achieved using high pressure wall jets. For the AR-Lean and MIAR processes, these ports can also be used to inject the reagent. Injection of reagent into the upper furnace, needed for the AR-Rich and MIAR processes, can be achieved using a lance-based system. Full scale NO_x reduction level is predicted to be above 90% and can be additionally increased with the use of promoters.

The original work scope for this task was based on applying the design methodology to a hypothetical case study; however, it was hoped that an initial AR demonstration could be developed in parallel with Phase I (outside the scope of this DOE project) to allow application to a real unit and evaluation of some of the SGAR elements. EER was successful in developing an initial AR demonstration project. In 1995 EER installed AR-Lean on a 105 MW tangentially fired boiler. Initial AR testing was conducted in 1996 and will continue through 1998. This unit was used as the basis for extending the design methodology. AR-Lean tests on the boiler showed that stratification within the reburn zone could adversely affect the performance. Regions of inadequate CO in the reburning zone reduced the N-agent NO_x control and caused NH₃ slip. While modifications were successful in reducing stratification, this experience shows the importance of mixing and scale up, two factors to be evaluated in Phase II. In addition to these AR-Lean tests, opportunity was taken to obtain preliminary larger scale data on several of the SGAR components including N-agent injection into the reburning zone, N-agent injection downstream of the reburning zone in an SNCR mode, and N-agent injection into the reburning zone and with the overfire air.

An economic analysis was conducted comparing SGAR technologies using gas and coal as reburning fuels with SCR for two representative Title 1 CAAA applications: a cyclone fired boiler and a wall fired boiler equipped with low NO_x burners. The analysis was based on the EPRI Technology Assessment Guide (TAG) methodology which evaluates the total annual levelized cost including capital and operating cost components (\$/ton). The unit cost of NO_x control (\$/ton) is also calculated. Depending on the specific application, SGAR offers total cost reductions of 48 to 69% over SCR. The market for AR technologies is estimated to be above \$1.5 billion.

Additional work is needed in Phase II to move the technology to a demonstration stage. In particular, the following steps are necessary to optimize and scale up the SGAR technologies:

- Identify alternative promoters based on the promotion mechanisms developed in Phase I.
- Identify and test coal mineral compounds responsible for the increased NO_x reduction in AR-Rich and MIAR with coal firing (about 10% higher than for gas firing).
- Optimize mixing (reburn fuel, N-agents, OFA) via combined chemistry/mixing models.
- Optimize N-agent injection to maximize NO_x reduction with negligible ammonia slip.
- Evaluate the effect of N-agent/promoter mixing times representative of full scale.
- Optimize SGAR with new promoters and mixing regimes at 1 x 10⁶ Btu/hr scale.
- Scale up and confirm the design methodology via 10 x 10⁶ Btu/hr Proof-of- Concept tests and limited component tests during the ongoing boiler AR tests.
- Update the economic and market analysis to confirm the advantages of SGAR.

2.0 INTRODUCTION

This project develops a family of novel Advanced Reburning (AR) NO_x control technologies, which have the potential to achieve 95% NO_x control in coal fired boilers at a significantly lower cost than Selective Catalytic Reduction (SCR). AR systems integrate basic reburning and N-agent injection (typically ammonia or urea). Specific features of the new AR systems in comparison with basic reburning include:

- Low heat input of reburn fuel to provide slightly fuel-rich conditions in the reburning zone.
- N-agent injection at one or two locations, including in the reburning zone, along with overfire air, and/or downstream of the overfire air injection.
- Low temperature of overfire air injection (1250-1400 K).
- Injection of promoter additives which enhance the effectiveness of the N-agent.

Phase I consists of six tasks:

Task 1.1	Project Coordination and Reporting/Deliverables
Task 1.2	Kinetics of Na ₂ CO ₃ Reactions with Flue Gas Components
Task 1.3	0.1 x 10 ⁶ Btu/hr Optimization Studies
Task 1.4	1.0 x 10 ⁶ Btu/hr Process Development Tests
Task 1.5	Mechanism Development and Modeling
Task 1.6	Design Methodology and Application

The project is currently in schedule, about 94% of the planned activities are completed, and all project objectives and technical performance goals have been met or exceeded. The project work under Tasks 1.2 and 1.6 is underway, however, these results will not change the main conclusions.

Figure 2.1 summarizes the nomenclature for the various regions of the Second Generation Advanced Reburning (SGAR) process. The region upstream of the reburning fuel injection is referred to as the “primary zone” or the main combustion zone. The primary zone Stoichiometric Ratio (SR_1) was maintained at $SR_1=1.1$ for all tests and the initial NO concentration in this zone is referred to by a subscript “i”. The region between the reburning fuel and overfire air (OFA) injection is referred to as the “reburning zone” or reburn zone and is maintained at stoichiometry SR_2 . The reburning fuel is injected at a temperature of T_1 . An N-agent (A_1) can be introduced into the reburn zone at T_2 with a Nitrogen Stoichiometric molar Ratio $NSR_1=A_1/NO$. The NO concentration for NSR calculations is the local amount at the point of N-agent injection. All N-agents can be injected with or without promoters. The rich side N-agent and promoter (Pr_1) are injected with a t_1 delay time after reburn fuel injection. Overfire air is injected at T_3 . OFA can serve as a carrier gas for injecting an N-agent (A_2) and promoter Pr_2 . A_2 is injected with $NSR_2=A_2/NO$. The downstream region of OFA injection is referred to as the “burnout zone”. Stoichiometric ratio in this zone is SR_3 . An N-agent (A_3) can also be injected (with or without promoter Pr_3) downstream of the OFA injection location (t_2 delay time, $NSR_3=A_3/NO$) into the burnout zone under conditions of the Selective Non-Catalytic Reduction process (SNCR).

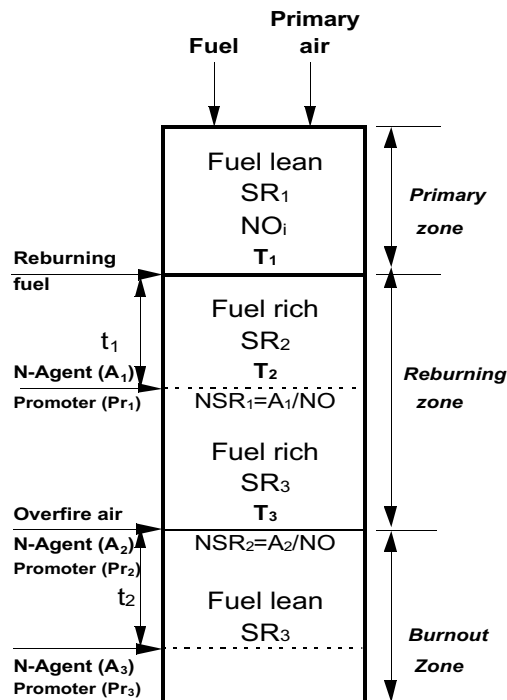


Figure 2.1 SGAR schematic - definitions.

3.0 BACKGROUND

3.1 High Efficiency NO_x Control under Title 1 of the CAAA

Title 1 of the Clean Air Act Amendment (CAAA) of 1990 requires NO_x controls in ozone non-attainment areas. The initial Title 1 regulations, implemented over the last few years, required Reasonably Available Control Technologies (RACT). In most areas, the NO_x levels for RACT are based on Low NO_x Burners (LNB) and are in the range of 0.4 to 0.5 lb/10⁶ Btu. As a result, there has been little industry demand for higher efficiency and more expensive NO_x controls such as reburning, SNCR, and SCR. However, the current RACT requirements are not the end of NO_x regulations. Much more stringent NO_x control will be required to bring many of the ozone non-attainment areas into compliance, particularly in the Northeast. The post-RACT requirements are based, to a large extent, on SCR, the commercial technology with the highest NO_x control efficiency.

With SCR, NO_x is reduced to N₂ by reactions with N-agents on the surface of a catalyst. The SCR process effectively uses the N-agent. Injection at a NSR of 1.0 typically achieves about 80% NO_x reduction (i.e., 80% N-agent utilization). SCR is fully commercial in Europe and Japan and there are a few US installations. This is the reason for its extensive use as the basis of NO_x control requirements for post-RACT.

Since the post-RACT NO_x control requirements are largely based on SCR, achieving the required NO_x levels with SCR is relatively easy. However, SCR is far from an ideal utility solution. There are several important problems, and cost leads the list. SCR requires a catalyst in the flue gas exhaust stream. This large catalyst, and its related installation and boiler modifications, are expensive. As SCR technology has advanced over the last decade, the cost has decreased; however, at present, the initial cost of an 80% NO_x control SCR system for a coal fired boiler is

still about a factor of four greater than that of LNB. Increasing the NO_x control to 95% approximately doubles the SCR system cost.

In addition, the SCR catalyst life is limited. Catalyst deactivation, through a number of mechanisms, typically limits catalyst life to about 4 years for coal fired applications. SCR catalysts are also toxic and, therefore, pose disposal problems. Since the catalyst is the major cost element in the SCR system, catalyst replacement and disposal contributes heavily to the total cost of NO_x control.

Thus, there is a need for a high efficiency, low cost NO_x control which utilities could apply to meet post-RACT NO_x control requirements without the problems of SCR discussed above. Ideally, such a technology would meet the following requirements:

1. NO_x control comparable or greater than SCR;
2. Low capital cost compared to SCR;
3. Total cost of NO_x control (\$/ton) low compared to SCR and ideally comparable to LNB;
4. Compatible with all types of coal fired units (wall, tangential and cyclone fired);
5. Minimal plant modifications and no requirement to re-route and treat the entire flue gas stream;
6. No major components with limited life (such as the SCR catalyst);
7. No additional emissions of air toxics, criteria pollutants, or toxic solid or liquid waste materials;
8. Ability to integrate with technologies for controlling other pollutants, such as SO₂, air toxics and with projected CO₂ control strategies;
9. Minimal impact on boiler efficiency and operations; and
10. Flexibility to achieve the required level of control with potential to readily implement add-on controls to reach more stringent control levels if required.

3.2 Limitations of Available NO_x Control Technologies for Post-RACT Applications

The suitability of AR for post-RACT applications can best be appreciated by comparing it with the currently available NO_x control technologies. Table 3.1 shows the typical performance for a range of conventional NO_x controls applied to a pulverized coal fired boiler with baseline emissions of 1.0 lb/10⁶ Btu. Both the applicability of specific NO_x controls and their performance depend heavily on site specific factors. While the values in the table are generally representative of state of the art performance, each installation will be different.

Table 3.1. Performance of NO_x control technologies.

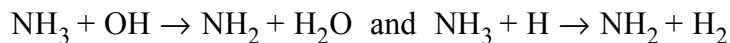
Technology	Nominal Performance For Baseline NO _x 1.0 lb/10 ⁶ Btu	
	NO _x Reduction (%)	NO _x Emission (lb/10 ⁶ Btu)
Low NO _x Burners	30-50	0.5-0.7
Low NO _x Burners + Overfire Air	50-60	0.4-0.5
Reburning	50-70	0.3-0.5
Selective Non-Catalytic Reduction (SNCR)	40-70	0.3-0.6
Selective Catalytic Reduction (SCR)	80	0.2
AR systems (projected)	80-95	0.05-0.2

Low NO_x burners and overfire air (OFA) provide only modest NO_x control. However, their capital costs are low and, since no reagents are required, their operating costs are near zero. This has made them the technologies of choice for the modest NO_x control required under Title 4 and the initial RACT under Title 1 of the CAAA. However, alone, they cannot approach the NO_x control required for post-RACT or the 90-95% NO_x control goal of the near future.

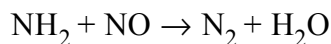
For deeper NO_x control, reburning, SNCR or SCR can be added to low NO_x burners and OFA, or

installed as stand alone systems. Reburning controls NO_x via fuel staging. The main portion of the fuel is fired through the conventional burners with a small portion of the fuel injected into the furnace above the burners. The result is a fuel rich "reburning zone" where NO_x is reduced by reactions with active radicals formed during interaction of the reburn fuel and oxygen from the main combustion zone. Reburning, alone, can achieve only 50-70% NO_x control and, hence, may not be a candidate for most post-RACT applications.

The reaction of N-agents with NO_x can proceed without a catalyst at high temperatures. This is the SNCR process. It is effective over a narrow "temperature window" centered about 1250 K where the N-agent forms NH_2 radicals which react with NO. The NH_2 radicals are formed from the N-agent via interaction with radicals, e.g.



The NH_2 species can reduce NO to molecular nitrogen



Under ideal laboratory conditions, deep NO_x control can be achieved; however, in practical, full scale installations, the non-uniformity of the temperature profile, difficulties of mixing the N-agent across the full boiler cross section, limited residence time for reactions, and ammonia slip, limit SNCR's effectiveness to about 40%. For typical SNCR conditions with a NSR of 1.5 and 40% NO_x control, the N-agent utilization is only 27%. Thus, while SNCR does not require a catalyst, and, therefore, has a low capital cost compared to SCR, it requires about four times as much N-agent resulting in higher operating costs.

In summary, the NO_x control technologies listed above all have limitations which may prevent

them from successfully achieving cost effective post-RACT compliance.

3.3 Advanced Reburning

The conventional AR process is an EER patented (Seeker et al., 1992) synergetic integration of basic reburning and N-agent injection. In this process, an N-agent is injected along with the OFA and the reburning system is adjusted to optimize the NO_x reduction due to the N-agent. By adjusting the reburning fuel injection rate to achieve near stoichiometric conditions (instead of the fuel rich conditions normally used for reburning), the CO level is controlled and the temperature window for selective NO_x reduction is broadened and deepened. The reburning fuel is reduced from about 20 to about 10% which has considerable economic benefits (the incremental cost of gas for gas reburning and the cost of the coal pulverization equipment for coal reburning). With AR, the NO_x control due to reburning is somewhat reduced, however, this reduction is offset by the significant enhancement of the N-agent NO_x control.

The AR process was developed by EER as part of a DOE program (Chen et al., 1989) focusing on the optimization of basic reburning. Tests were conducted over a range of scales (up to 10 x 10⁶ Btu/hr) and achieved above 80% NO_x control. An AR design methodology was developed by extending EER's reburning design methodology. Conventional AR is now being demonstrated at the NYSEG 105 MW Greenidge Station.

3.4 Second Generation Advanced Reburning (SGAR)

Improved versions of the conventional AR process are under development at EER since 1993. They were first predicted by kinetic modeling and then confirmed by 300 kW combustion tests via EER in-house R&D funds. The SGAR systems have the potential to achieve 95% NO_x control on all types of coal fired boilers without massive hardware changes, without increasing air toxic and toxic waste problems, and at a cost for NO_x control on the order of half that of SCR.

These systems will provide flexible installations that allow NO_x levels to be lowered as new elements of the technology become available. The SGAR systems incorporate several improvements over conventional AR, such as:

- N-agent injection into the reburning zone;
- Promoter additives which enhance the effectiveness of the N-agent; and
- Injection of N-agents with or without promoters at two locations.

Sodium salts, in particular sodium carbonate (Na₂CO₃) were identified as effective AR promoters. By integrating these improvements with conventional AR, NO_x control can be increased to 90-95% for cyclone units and even higher for pulverized coal fired units (wall and tangentially fired) where AR can be further integrated with low NO_x burners and overfire air. This family of AR technologies is intended for post-RACT applications in ozone non-attainment areas where NO_x control in excess of 80% is required.

Three SGAR systems were originally proposed to DOE under the 1994 PRDA solicitation. They include:

- Promoted Advanced Reburning - Lean (AR-Lean) - conventional AR (N-agent injected with the OFA) which can be used with a promoter added to the agent.
- Advanced Reburning - Rich (AR-Rich) - N-agent injection with or without a promoter into the reburning zone.
- Multiple Injection Advanced Reburning (MIAR) - N-agents with promoters injected in two locations: within the reburning zone and with the OFA.

4.0 PHASE I PROGRAM OBJECTIVES

The overall objective of Phase I was to demonstrate the effectiveness of the SGAR technologies at bench and pilot scale over a sufficiently broad range of conditions to provide all of the information needed for process optimization and scale up. The Phase I program is conducted over a two year period. Specific program objectives were as follows:

1. Develop an understanding of the mechanisms through which promoter additives improve N-agent effectiveness;
2. Develop a kinetic analytical model of the Promoted and Multiple Injection AR technologies;
3. Optimize the SGAR processes using the analytical model and bench and pilot scale experiments under controlled mixing conditions; and
4. Upgrade EER's AR design methodology to include the second generation advances.

Phase I project determines the ability of the SGAR technologies to meet the following technical performance goals:

- NO_x emissions from the 1×10^6 Btu/hr coal fired Boiler Simulator Facility controlled to less than the requirements for post-RACT NO_x control in the NESCAUM area for the year 2003;
- Total estimated cost of controlling NO_x emissions based on the 1×10^6 Btu/hr coal fired tests less than that currently projected for SCR NO_x control systems; and
- No significant reduction in boiler efficiency or significant adverse environmental impacts when compared to current reburning and SNCR technologies.

Figure 4.1 shows the task structure and the major milestones for the program. Task 1.1, Project Coordination and Reporting/Deliverables, coordinates the efforts of the Key Personnel involved with the project so that the objectives of this project are met: on time, on specification, and on budget. Phase I experimental work started from parametric screening tests at a bench scale facility (Task 1.3), followed by pilot scale developmental studies (Task 1.4). The Phase I program utilized two EER test facilities providing nominal thermal capacities of 0.1 and 1×10^6 Btu/hr. The experimental work was paralleled by kinetic modeling (Task 1.5) which provided a scientific understanding of the process, including the activity of N-agent promoters. A detailed reaction mechanism of the SGAR processes was developed based on available combustion chemistry data. Simultaneously, an experimental study (Task 1.2) was conducted at the University of Texas to

define high-temperature chemistry of sodium carbonate under simulated flue gas conditions. The results were used for updating the kinetic model. The modeling used experimental data to define key process parameters, culminating in upgrading EER's existing design methodology for conventional AR to include the second generation improvements (Task 1.6).

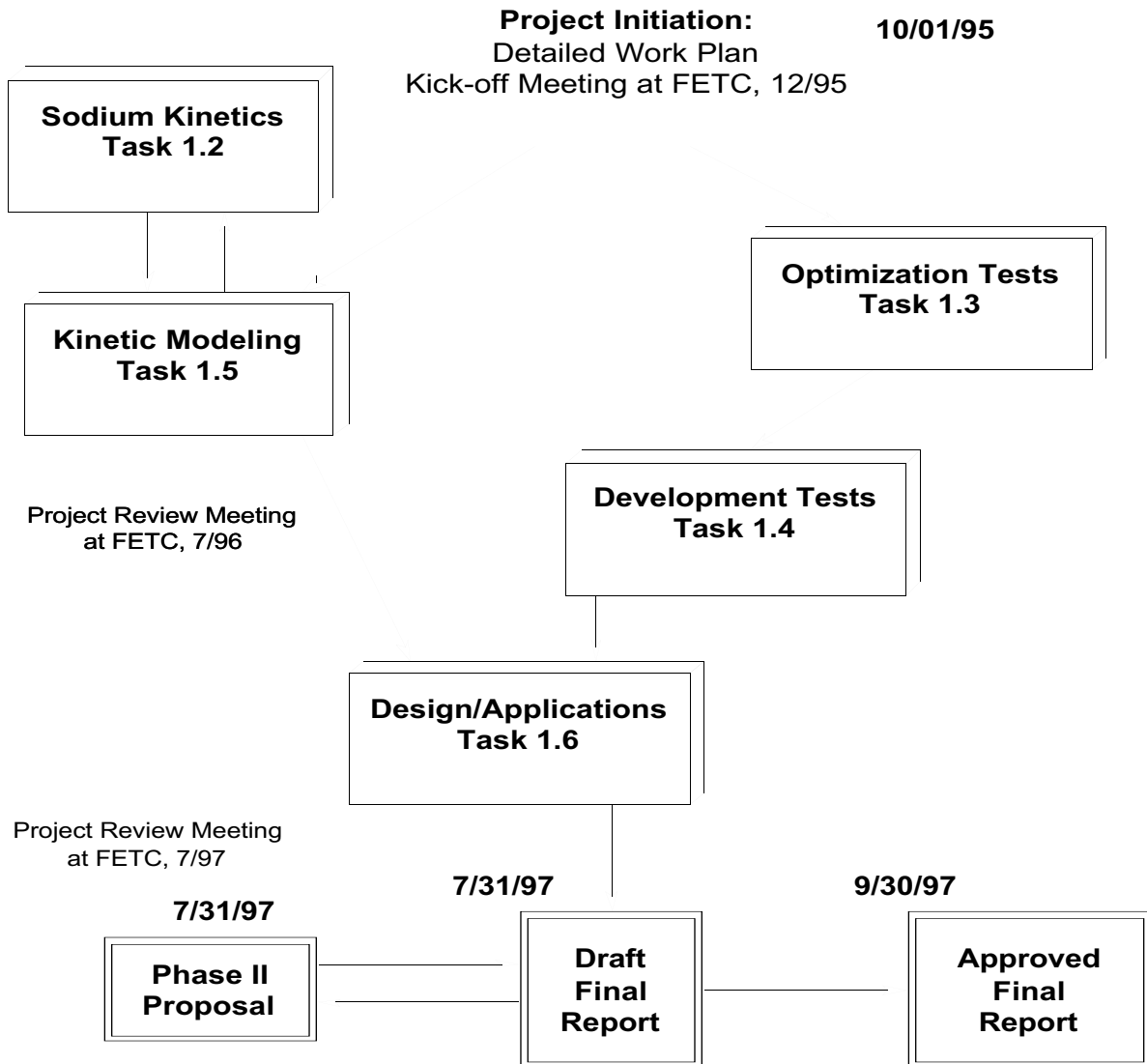
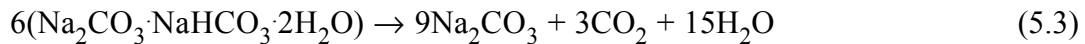
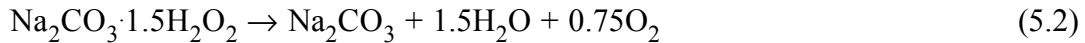


Figure 4.1. Phase I task structure and major milestones.

5.0 KINETICS OF Na₂CO₃ REACTIONS WITH FLUE GAS

5.1 Literature Review

Although salts of alkali metals have long been used as flame inhibitors (Mitani and Nioka, 1984; Jensen and Jones, 1982), the chemical mechanism of their decomposition at high temperatures is not well known. On the other hand, decomposition of sodium bicarbonate NaHCO₃, (Wu and Shih, 1993; Heda et al., 1995) sodium carbonate perhydrate Na₂CO₃·1.5H₂O₂ (Galwey and Hood, 1979) and double salts which occur in the Na₂CO₃·NaHCO₃·H₂O system (Ball et al., 1992) at low temperatures has been studied intensively, primarily because thermal decomposition of these salts can produce a highly porous Na₂CO₃ product which can be used for SO₂ removal from waste gases. It was found that decomposition of these salts starts at around 350 K; by 500 K they are practically completely converted into Na₂CO₃ and H₂O



Decomposition of Na₂CO₃ thus determines rate of decomposition of other salts of Na and carbonic acid at still higher temperatures, and very little is known about the decomposition mechanism of Na₂CO₃. It was found that the time scale for flame inhibition by Na₂CO₃ is about 10 ms at 1200 K and 0.5 ms at 1800 K, which is thought to correspond to the decomposition time of Na₂CO₃. (Mitani and Nioka, 1984) The inhibiting effect of salts on flame was attributed (Jensen and Jones, 1982) to catalytic removal of H atoms and OH radicals in the chain





While Na atoms in flames have been studied for years, (Carabetta and Kaskan, 1968; Hynes et al., 1984; Srinivasachar et al., 1990; Schofield and Steinberg, 1992) their reaction mechanisms are not well understood, and the rate coefficients of some important reactions are not known. Apparently Na, NaO, NaO₂, and NaOH are coupled to one another in flames by fast reactions which rapidly interconvert one species to another as conditions vary. (Hynes et al., 1984; Schofield and Steinberg, 1992) Analysis of Na influences on H₂-O₂-N₂ flames led to the conclusion that the Na chemistry is largely controlled by



At temperatures above 2300 K the main channel for Na disappearance is reaction (5.6). As temperature decreases, however, the importance of NaO₂ increases and the predominant depletion of sodium is via reaction (5.7). Kaskan (1971) concluded that reaction (5.7) is the dominant Na oxidation process in lean H₂-O₂-N₂ flames at temperatures from 1400 to 1700 K. Other observations also support NaO₂ as an important intermediate species at temperatures below 1900 K. (McEwan and Phillips, 1966) However, contradictory values of the rate coefficient for the reaction (5.7) have been reported. (Kaskan, 1971; McEwan and Phillips, 1966; Husain and Plane, 1982)

Ho et al. (1993) and Chen et al. (1993) considered the feasibility of using sodium (a representative alkali metal) salts to control N₂O emissions from combustion sources. Perry and Miller (1996) investigated this process by dynamic modeling and concluded that the key reaction

is



where sodium atoms are produced by the reverse of reaction (5.6). This explanation, however, is not the only possible one. The same effect of N_2O removal could be explained by the reaction



since sodium hydroxide additive enhances production of active species like OH (reaction (5.5)) already present in exhaust gases.

The literature review thus shows that practically no information is available about the rate of Na_2CO_3 decomposition at high temperatures. The active species formed during decomposition are not well defined either, and as a result the mechanism of Na_2CO_3 influences on high temperature chemistry is essentially unknown.

5.2 Thermodynamics of Sodium in Combustion Flue Gas

5.2.1 The Solid to Gas-Phase Transition

Sodium carbonate melts at 1120 K and is relatively stable at still more elevated temperatures—according to a textbook of inorganic chemistry (Bailar et al. 1973) it does not decompose until 1220 K. Thermodynamic calculations based on the EER thermochemical data base show that $\Delta_r G^\circ$ for the reaction



changes sign from positive to negative in the temperature range 2400–2500 K (Figure 5.2.1), making reaction (5.12) “spontaneous” only at temperatures above 2400 K. Since the most common way to supply Na_2CO_3 is as an aqueous solution, one also has to consider the spontaneity of



Figure 5.2.1 shows that reaction (5.13) becomes spontaneous (in the sense that P_{CO_2} is greater than $P_{\text{H}_2\text{O}}$) at temperatures above 2000 K. Thermodynamic calculations thus show that reactions (5.12) and (5.13) for all species in their standard states are not spontaneous at temperatures normally achieved in the flow system, i.e., less than 1400 K. This statement does not mean, however, that at low Na_2CO_3 concentrations significant conversion of Na_2CO_3 to products can not be achieved. The equilibrium partial pressure of CO_2 in reaction (5.12) over the surface of liquid or solid Na_2CO_3 calculated using values of $\Delta_r G^\circ$ from Figure 5.2.1 is equal to 0.01 Torr at 1400 K. The statement “reaction (5.12) is not spontaneous at 1400 K” means that Na_2CO_3 decomposes at that temperature only until the partial pressure of CO_2 reaches 0.01 Torr. Thus if the amount of Na_2CO_3 is very small, all of it might decompose and the partial pressure of CO_2 still be less than 0.01 Torr. Figure 5.2.2 illustrates this idea by showing how Na_2CO_3 to CO_2 conversion (based on equation (5.13)) at chemical and phase equilibrium at a total pressure of 1 atmosphere depends on temperature at initial Na_2CO_3 concentrations of 100, 300 and 500 ppm, typical concentrations used in our flow system experiments and proposed for pollution control in flue gas. The assumed amount of H_2O in the mixture is 20%, the rest is N_2 . Conversion in Figure 5.2.2 is defined as the concentration ratio $[\text{CO}_2]/[\text{Na}_2\text{CO}_3]_0$, where $[\text{Na}_2\text{CO}_3]_0$ is the initial concentration of sodium carbonate. The calculations were performed using the EER thermochemistry data base and the NASA program CET89 (Feitelberg, 1994), which calculates chemical equilibrium compositions taking into account both gaseous and condensed-phase reactants and products. It is clear from Figure 5.2.2 that significant decomposition of Na_2CO_3

occurs in the temperature range from 1000 to 1500 K even though reaction (5.12) is not spontaneous at these temperatures in the ordinary thermochemical sense. The dependence of conversion on the initial amount of Na_2CO_3 is evident—as the initial concentration decreases, fractional conversion of Na_2CO_3 to CO_2 is more complete.

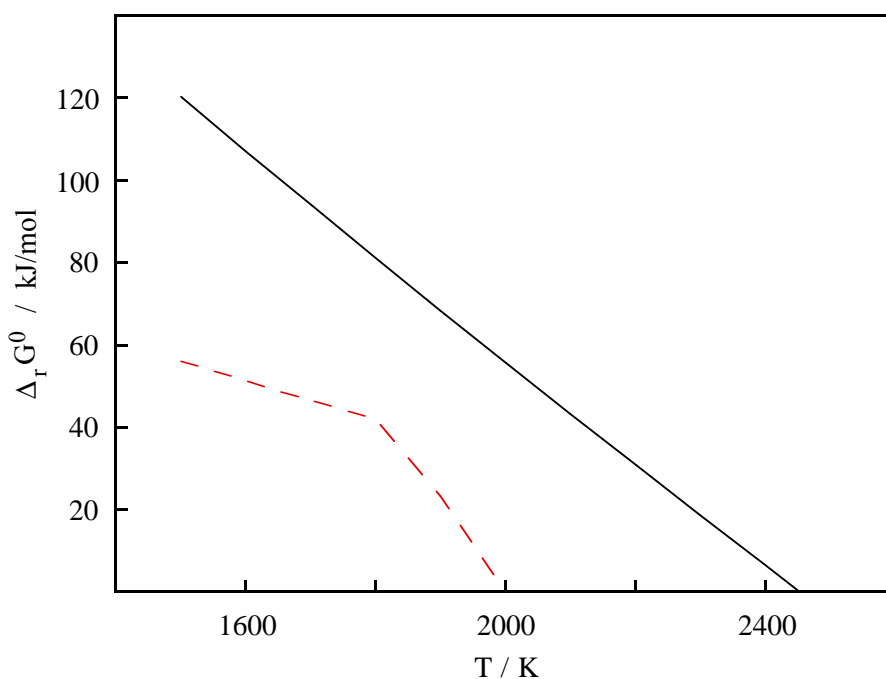


Figure 5.2.1. Dependence of $\Delta_r G^\circ$ (EER thermochemistry) for $\text{Na}_2\text{CO}_3 \leftrightarrow \text{Na}_2\text{O} + \text{CO}_2$ (solid) and $\text{Na}_2\text{CO}_3 + \text{H}_2\text{O} \leftrightarrow 2\text{NaOH} + \text{CO}_2$ (dashed) on temperature. The break in the dashed line corresponds to the melting temperature of NaOH.

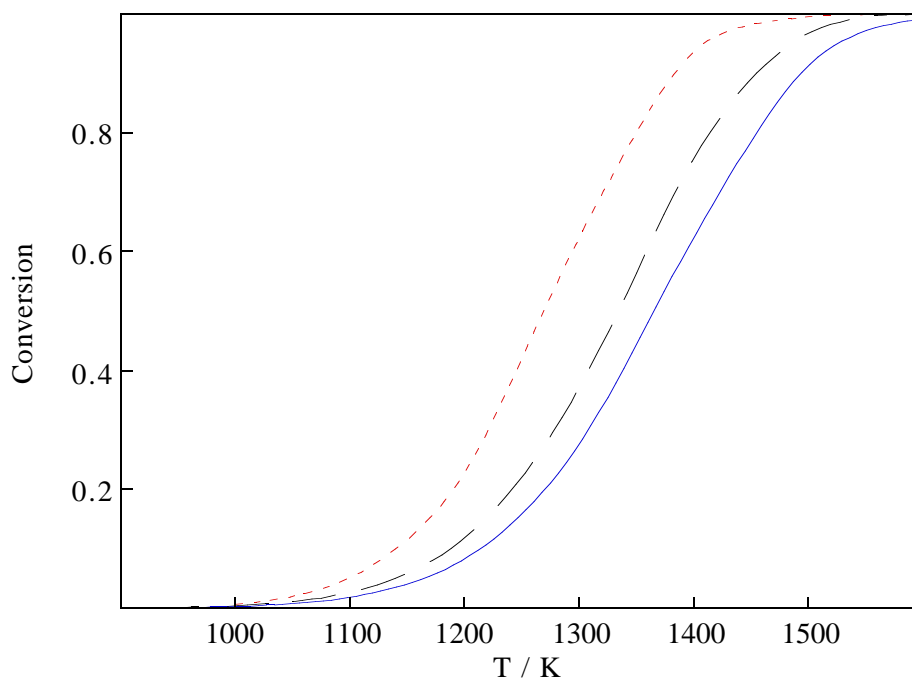
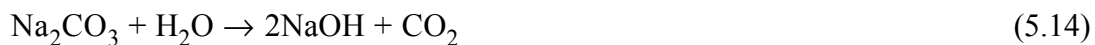


Figure 5.2.2. Dependence of Na_2CO_3 to CO_2 conversion according to equation (5.13). Solid line corresponds to an initial Na_2CO_3 concentration of 500 ppm in the gas phase, the dashed line to 300 ppm, and the dotted line to 100 ppm.

These simple one-reaction calculations for conditions typical of the experiments thus confirm that significant fractional decomposition of Na_2CO_3 in the presence of water is thermochemically favored beginning at temperatures slightly above 1000 K.

Our flow system experiments, however, show significant Na_2CO_3 decomposition also at temperatures below 1000 K. Figure 5.2.3 shows a comparison between calculated equilibrium conversions and those derived from experimental profiles at long residence times. It indicates that at the conditions of our experiments the Na_2CO_3 decomposition reaction is not equilibrated as predicted by the thermochemistry used. Because we felt that the thermochemical model was uncertain, particularly for its gas-phase Na_2CO_3 component, and could not explain the experimental decomposition profile, and because reaction (5.13) oversimplifies a complex process that involves many chemical reactions, we composed a dynamic model to fit the data. For the

conditions of our experiments Na_2CO_3 decomposition can be described as consisting of two opposed irreversible steps



occurring in the directions indicated. An alternative model of Na_2CO_3 decomposition is



that can also proceed in irreversible steps



which in presence of water can be followed by NaOH formation



making the ultimate effect of model (5.12) identical to model (5.13).

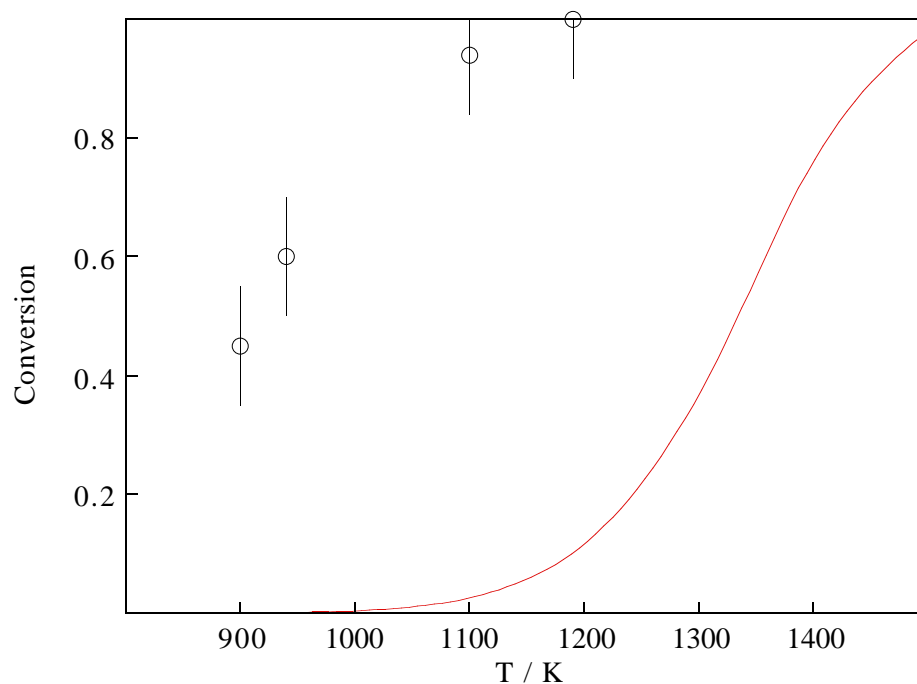


Figure. 5.2.3. Comparison between experimental and calculated (Feitelberg, 1994) equilibrium conversions of Na_2CO_3 to CO_2 . The initial concentration of Na_2CO_3 was 300 ppm.

5.2.2 Available Thermodynamic Data on Sodium in the Gas-Phase

The documented gas-phase thermochemistry of sodium compounds is sparse. The 1985 JANAF table provides for non-halogen neutral compounds the information shown in Table 5.2.1. The tabulated enthalpy of formation values for 1500 K can be combined with the 1500 K values for the radicals H, O, OH and CN and the stable molecules HCN, H_2 , H_2O and H_2SO_4 to derive the bond strengths of the sodium bonds in these molecules and the enthalpy changes of reaction for the key atom exchange reactions that establish the equilibrium composition of high temperature systems containing sodium. The JANAF values for these species at 1500 K are summarized in Table 5.2.2.

Table 5.2.1. JANAF standard enthalpies of formation at 298 and 1500 K.

Species	$\Delta_f H_{298}$ (kJ)	$\Delta_f H_{1500}$ (kJ)	Error @ 298 K	Source
Na	107.3	0	± 0.7	Vapor pressure data at 298 K; reference state above 1170.5 K.
Na ₂	142.07	-75.2	± 1.2	Spectroscopic bond dissociation energy value.
NaO	83.68	-23.7	± 41.8	Estimated bond dissociation energy from $k_e r_e D^\circ = \text{constant}$ and spectroscopic D° for LiO.
Na ₂ SO ₄	-1033.6	-1294.5	± 25.1	Thermo of solid and average of various vapor measurements.
NaH	124.26	15.6	± 19.2	Spectroscopic measurement of D° .
NaOH	-197.76	-303.7	± 12.6	Complex but secure thermochemical cycles
(NaOH) ₂	-607.5	-822.5	± 25.1	Mass-spectrometric study of vapor-phase dissociation equilibria
NaCN	94.27	-12.8	± 2.1	Vapor pressure and composition measurements, thermo of crystal
(NaCN) ₂	-8.8	-213.2	± 13	1200 K vapor composition.

Table 5.2.2. JANAF standard enthalpies of formation at 298 and 1500 K.

Species	$\Delta_f H_{1500}$ (kJ)	Species	$\Delta_f H_{1500}$ (kJ)
H	224.8	H ₂	0
O	254.2	H ₂ O	-250.3
OH	124.8	H ₂ SO ₄	-788.8
CN	259.7	HCN	132.1

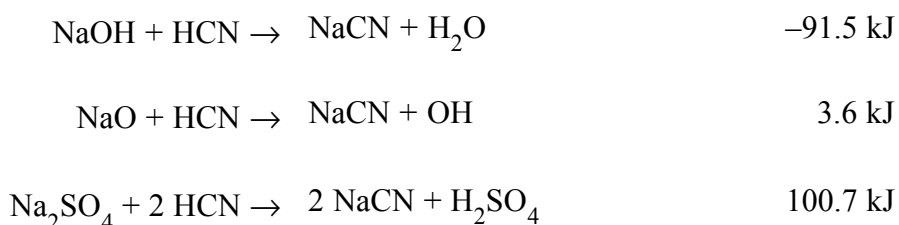
The dissociation reactions breaking off the Na atom can then be compared with one another and with the corresponding reactions for breaking off a hydrogen atom at 1500 K as shown in Table 5.2.3.

Table 5.2.3. Thermochemistry for breaking Na–X bonds at 1500 K.

Reaction	$\Delta_r H_{1500}$ (kJ)	$\Delta_r H_{1500}$ (kJ) for Na = H	Difference between H and Na
Na ₂ → Na + Na	75.2		
NaH → Na + H	208.2	449.6	241.4
NaCN → Na + CN	272.5	352.4	79.9
NaO → Na + O	277.9	354.2	75.3
NaOH → Na + OH	428.5	599.9	171.4
NaOH → NaO + H	504.8	599.9	95.1

The sense of the results is not surprising: The strength of the Na–X bond increases with increasing electronegativity difference between Na and X, and Na bonds to other atoms and radicals less strongly than does H. The numerical comparisons shown in the fourth column are disappointing, however, in that there is neither consistency nor an understandable trend in the comparison to be seen in the compounds for which there is data to analyze this way.

Another way to compare sodium bonding with hydrogen bonding is through an isodesmic reaction series, in which sodium trades partners with hydrogen in a reaction that conserves the number and type of chemical bonds. The following linearly independent reactions illustrate the results of this alternative analysis style for HCN as the trading partner.



In all three cases an Na atom (2 of them in the third reaction) trades bonding to an O for bonding to CN. The trade is exothermic if the O is a hydroxyl O atom, essentially thermoneutral for a lone O atom, and endothermic for a sulfate O atom.

Two conclusions emerge from the foregoing overview of gas-phase sodium thermochemistry.

The first is an assessment of the available high temperature thermochemical data base: It is too small, and has too-large error bounds, to permit reliable estimation of the energetics of other sodium-containing species by an analog of the group additivity methods that have proved to be successful in correlating the thermochemistry of gas-phase molecules (Cohen, 1996) and radicals (Lay et al., 1995). Neither the bond dissociation energies nor the isodesmic reaction series that can be constructed from the available information suffice for extrapolation purposes.

The second is that while sodium bonding is characteristically weaker than bonding of its Group I fellow hydrogen in all gas phase species, this bonding is not so weak that only the most stable sodium species need be considered for modeling purposes. As example, formation of the O–H bond in NaOH provides 505 kJ/mol, implying that NaO is readily able to abstract H atoms from most of the H-containing species present in flue gas. It is thus necessary to estimate thermochemical and kinetic parameters for many more sodium-containing species than the

JANAF set if one is to hope for adequate dynamic modeling of sodium chemistry under flue gas conditions.

Mention should be made of two other gas phase sodium species that have been discussed. The first is the sodium analog of water, Na_2O , for which thermochemical data have been generated based on the experiments of Hildenbrand and Murad (1970). As shown below, the binding of the second Na atom is sufficiently weak that very small amounts of it are formed at low total sodium concentrations. The second species is the superoxide NaO_2 , which has been invoked to explain Na concentration measurements in flames, Knudsen cells and flow reactors. The thermochemical inferences show disappointingly large scatter, i.e., dissociation energy values in kJ/mol of <115, >145, 163 ± 21 , <184, <195, >202, 234 ± 13 , 230 ± 5 , and 243 ± 21 . (Marshall et al., 1990 and references cited therein.) Theoretical values of 150, 151, 156, 185, 196 and 199 kJ/mol have been reported for various levels of theory (Partridge et al., 1992 and references cited therein). The experimental and theoretical values are consistently large enough to demonstrate that NaO_2 has to be considered as an intermediate in high-temperature sodium chemistry, but its thermochemistry is clearly as much or more a problem as that of NaO.

Taking the available thermochemical data all together permits one to generate more complete overviews of the species expected to be present at chemical equilibrium than is seen in the foregoing more narrowly targeted discussion. Leaving out the uncertain NaO_2 and solving the equilibrium at 1 atm pressure over the temperature range of interest here provides the overviews shown below. Figure 5.2.4 shows an equilibrium composition chart for the conditions of our laboratory experiments, in which the only source of CO_2 was the small addition of Na_2CO_3 , and Figure 5.2.5 shows the corresponding distribution for conditions that can be encountered at flue gas compositions, when there is an exogenous source of CO_2 corresponding to an equivalence ratio of 1 for a fuel containing equimolar amounts of C and H.

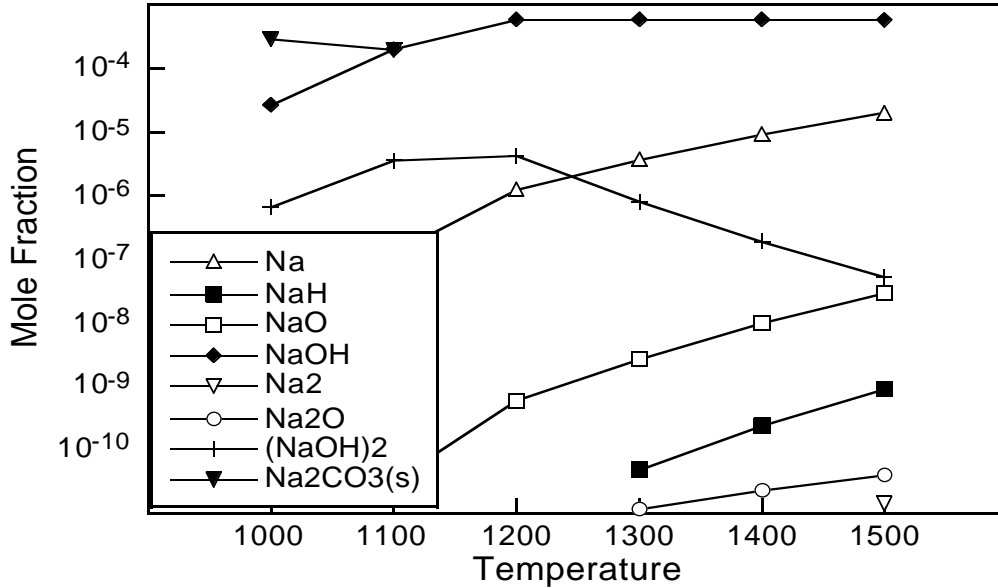


Figure 5.2.4. Equilibrium distribution of sodium-containing species at 1 atm pressure in 80% N₂, 20% H₂O and 300 ppm Na₂CO₃. The only condensed phase stable for these conditions is solid Na₂CO₃ below 1100 K.

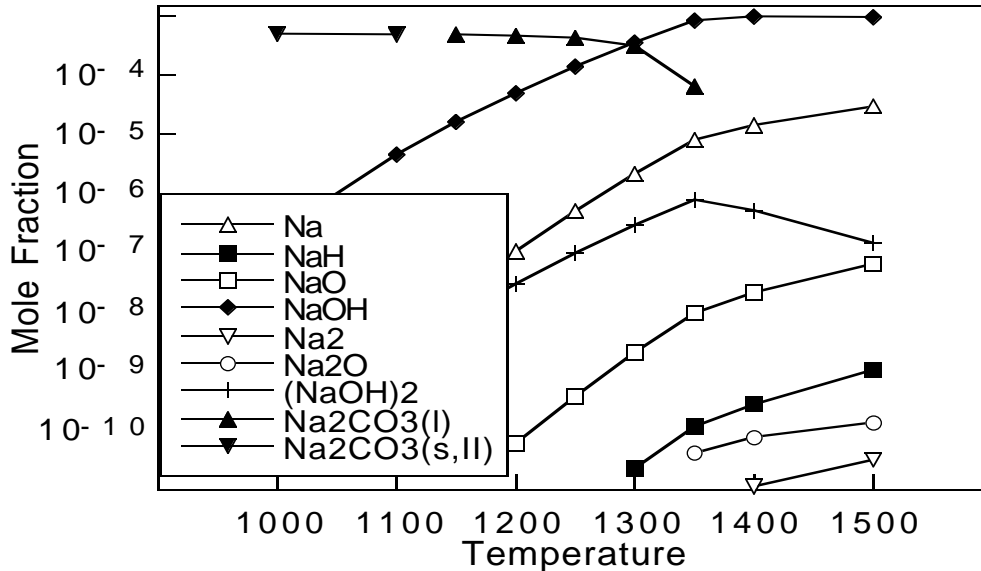


Figure 5.2.5. Equilibrium distribution of sodium-containing species at 1 atm pressure in a flue-gas-like mixture with 300 ppm of added Na₂CO₃. The assumed fuel had C:H and equivalence ratios of 1. The high concentration of CO₂ forces the condensed phase to be solid or liquid sodium carbonate rather than the intrinsically more stable hydroxide. Aside from this difference the composition is quite similar to that of the CO₂-free case, especially at higher temperatures.

Based upon the JANAF species and NaO_2 , one can start to model flue gas conditions to examine the basic flow of sodium chemistry. Such models have been composed for example by Plane (1991) and Schofield and Steinberg (1992). In these mechanisms additional species are advanced, with provision of estimated, if any, thermochemical data. The additional species include NaO_3 , NaHCO_3 , and NaCO_3 in the Plane (1991) model, designed to describe sodium chemistry in the mesosphere, and NaS , NaSH , NaS_2 , NaOS and NaSO_2 in the Schofield and Steinberg (1992) model, designed to describe sodium-sulfur interactions in flames; the latter authors describe structural and thermochemical estimation procedures in detail. Calculations using the Chemkin program and these reactions are in progress.

It is clear that the JANAF species and NaO_2 do not suffice to give a complete picture of the interactions of sodium species with the advanced reburning process. The strength of sodium bonds to other prominent radicals (as we have calculated, but not reported here) at the 6-31G(d)++/MP2 level with isodesmic series) is sufficient to enable many such species to interact with not only the common flame radicals but also with the ones that are specific to the AR chemistry, such as the NH_i species. Translating our molecular electronic structure results for these species into temperature-dependent thermodynamics for these species is in progress. We assume that the results of simulations that include these species will support the basic conclusion of our Phase I research—that the sodium enhancement effect arises from general increased radical availability—but until the main candidate sodium species relevant to the advanced reburning environment are tested in simulations, as Plane and coworkers did for the atmospheric case and Schofield and coworkers did for the sulfur-interactions, this conclusion must remain tentative.

5.3 Experimental Methods

Most of our experiments on Na_2CO_3 decomposition were done in a flow system over the

temperature range from 900 to 1300 K. These experiments provided information about the rate of Na_2CO_3 decomposition and reactions of Na_2CO_3 with components of flue gas. In place of our early intention to identify gas-phase species by shock tube experiments, we decided to substitute mass spectrometric ones in order to get a broader range of information about the product distribution resulting from high temperature Na_2CO_3 decomposition.

The following sections give descriptions of the experimental apparatus used in our work.

5.3.1 Flow System

The flow system used for our experiments is shown in Figure 5.3.1. Our efforts began with the construction of the flow and gas handling systems for our gas chromatograph (GC). The gas handling system was made with a combination of glass and metal components so as to enable both high and low pressure operation. A new reactor for the flow system was constructed that took advantage of an ultrasonic atomizing nozzle system supplied by EER, which provided a reliable way to spray aqueous Na_2CO_3 solution with salt concentrations up to 15% by weight. The reactor was initially horizontal and later rearranged in a vertical orientation to suppress deposition of Na_2CO_3 on the walls. The second design also included preheating the carrier gas to temperatures in the range 300–400 °C and use of a ceramic adapter between the nozzle system and the reactor. The adapter allowed mixing hot carrier gas with the spray from the nozzle without overheating the nozzle itself. (The specified working temperature range of the nozzle is up to 200 °C). The original GC columns were replaced with new ones packed with molecular sieve and HAYESEP Q to enable measurements of CO_2 and surrogate components of flue gas. The sensitivity of the GC to CO_2 was enhanced by use of high-sensitivity thermal conductivity filaments and by prolonged pretreatment of the columns at 200 °C. These modifications resulted in a sensitivity level of 50 ppm of CO_2 and permitted us to work with the flow system at Na_2CO_3 levels close to those used by EER in their field experiments.

Preliminary experiments showed that temperature measurements taken inside of the reactor were significantly different from measurements taken in the furnace area that originally were used for temperature determinations. To enable correct temperature measurements, the construction of the flow reactor was changed to enable a thermocouple to be inserted directly into the gas flow. Measurements showed that by adjusting the current through each of three segments of the furnace a uniform temperature distribution inside of the reactor can be created with temperature variations within ± 10 degrees.

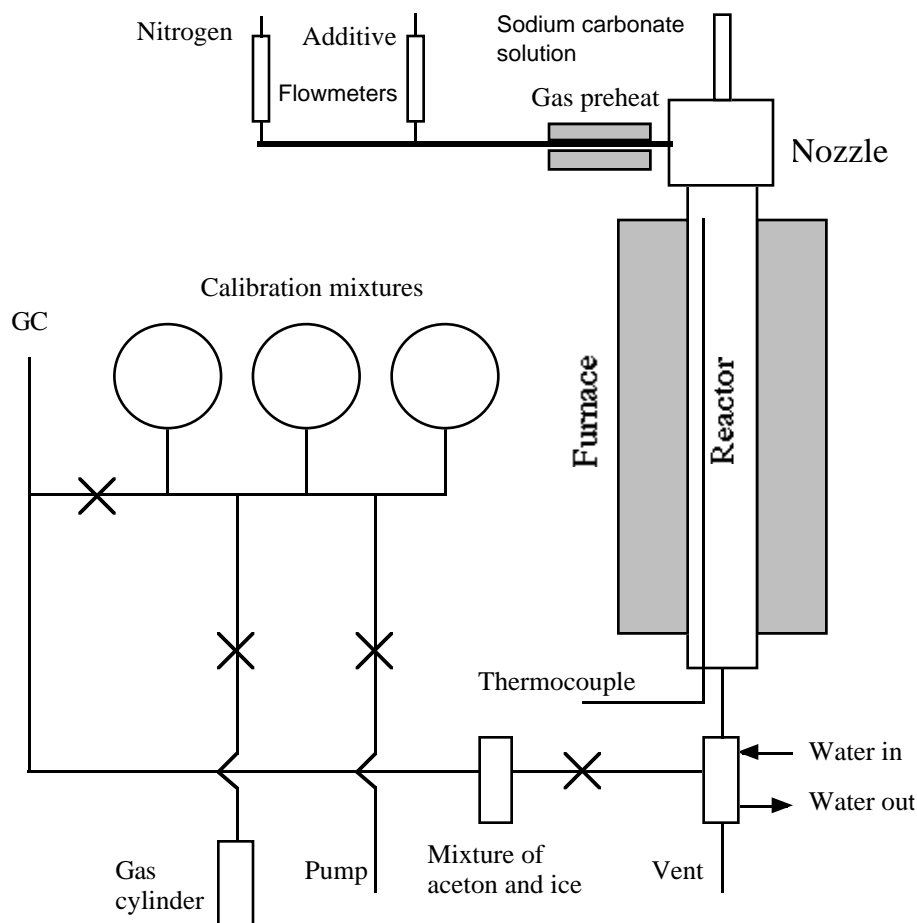


Figure 5.3.1 Flow system diagram.

Two drying systems were installed to dry gas after passing through the reactor. The first system was used to separate most of the water so as to prevent condensation in communication lines. The second system used acetone and dry ice to dry gas before taking a sample for GC analysis.

The second system protected the sensitive GC columns from being destroyed by the basic solution formed from Na_2CO_3 decomposition.

5.3.2 Mass Spectrometric Analysis

The products of Na_2CO_3 thermal decomposition were identified using a Finnigan MAT TSQ 70 mass spectrometer in thermal, electron bombardment and chemical ionization modes. Small amounts of aqueous Na_2CO_3 solution were heated on a Nichrome wire until the water evaporated and the solid or liquid Na_2CO_3 started to decompose. In electron ionization mode, used in most experiments, the gas phase was bombarded at electron ionization (EI) energies of 70, 25, 12 volts. In chemical ionization mode (CI), the gas pressure in the ion source was increased to typically 10^{-3} mbar of CH_4 ; the dominant initial CH_4^+ ions collide with molecules M and transfer a proton to give MH^+ ions with little excess initial energy and therefore little tendency to fragment. Thus, whereas the EI spectra contained peaks corresponding to both molecular and fragment ions, the CI spectra were simpler, mostly having predominantly parent ion peaks. Both EI and CI modes were used in our experiments. In auxiliary experiments the Nichrome wire was replaced by lower-melting metals in order to identify, by the melting temperature, the effective temperatures where changes in the ion patterns appeared.

5.4 Rate of Sodium Carbonate Decomposition

5.4.1 Sodium Carbonate Decomposition in Nitrogen

Experiments on Na_2CO_3 decomposition were done in quartz and stainless steel reactors. It was found that reactors made from different materials produced similar results. It is known, however, that sodium carbonate reacts with silicon oxide, the main component of quartz, to form silicates



Reaction (5.19) becomes spontaneous in the temperature range 500–600 K (Chase et al., 1985). That reaction (5.19) does occur for the conditions of our experiments is supported by the observation that after passing Na_2CO_3 -containing test gas through the quartz reactor for 18 to 20 hours the surface of the reactor roughened, and after running for still longer times the reactor was virtually destroyed. The observed rate of Na_2CO_3 decomposition was the same in a fresh reactor and in a reactor with surface exposed to Na_2CO_3 for several hours, which suggests that reaction (5.19) does not contribute significantly to CO_2 production on the time scale of our experiments. This observation is supported by a study of reaction (5.19) undertaken by Terai et al. (1968). Using thermogravimetry, x-ray diffraction, and radioactive tracing they studied the sodium carbonate-silica reaction in the temperature range from 1000 to 1100 K and reported that the reaction is not controlled by diffusion of Na in silica. The diffusion coefficient calculated from the penetration rate of Na into fused silica was determined to be $D = 5.0 \times 10^{-11} \text{ cm}^2/\text{s}$. This value of D actually shows how fast the reaction between sodium carbonate and silica is and can be used to estimate the rate of reaction (5.19), which then can be compared with rate of the reaction in the gas phase as follows. Since the gas volume in the reactor is $V = 100 \text{ cm}^3$ and typical concentrations of CO_2 were about $1 \times 10^{-7} \text{ mol}/\text{cm}^3$, the total amount of CO_2 produced is $1 \times 10^{-5} \text{ mol}$ per second. For a reactor with diameter 2.5 cm, length 40 cm and wall thickness 0.1 cm the total amount of silica in the reactor is 0.5 mol. From this data, the time required to produce $1 \times 10^{-5} \text{ mol}$ of CO_2 in reaction (5.19) can be computed and compared with typical residence time 0.5 second. Production of $1 \times 10^{-5} \text{ mol}$ of CO_2 results in consumption of $1 \times 10^{-5}/0.5 = 2 \times 10^{-5}$ volume of silica. For our reactor it gives penetration distance $l = 0.1 \times (2 \times 10^{-5}) = 2 \times 10^{-6} \text{ cm}$. Values of l and diffusion coefficient D give a simple estimation of reaction time t in the solid phase through the Einstein equation

$$t = l^2/D \tag{5.4.I}$$

Using $l = 2 \times 10^{-6}$ cm and the value of D measured by Terai et al. (1968), formula (5.4.I) gives $t = 8$ s, much larger than the 0.5 s characteristic times of our experiments.

An alternate line of reasoning leading to the same result is this. The entire reactor contains about 0.5 mol of silica; as the observed production rate of CO_2 is about 10^{-5} mol/s, the entire reactor would be lost to form sodium silicate in only 5×10^4 seconds (14 hours) if all of the CO_2 would originate in heterogeneous reaction (5.19) to form sodium silicate. Our observations show however that the lifetime of the quartz reactor is at least 30 hours. Thus reaction (5.19) does not contribute significantly to CO_2 production on the time scale of our experiments.

Experimental study of Na_2CO_3 decomposition at temperatures from 900 to 1300 K and pressure 1 atm was done in the flow system. Details of the experimental procedure are given below. An aqueous solution of Na_2CO_3 was sprayed into preheated flow of N_2 ; the mixture then passed through the quartz reactor and cooled. Sample taken from exhaust gases passed through additional cooling system to get rid of water traces and then analyzed by GC. The flow rate of N_2 and the rate of solution consumption were measured and used to calculate the residence time of the mixture in the reactor. These calculations were done assuming ideal behavior of N_2 and H_2O vapor formed upon evaporation of water in the reactor. Initial concentrations of Na_2CO_3 in the mixture were varied in the range from 300 to 1000 ppm. Since both reactions (5.12) and (5.13) give stoichiometric ratio $\text{CO}_2/\text{Na}_2\text{CO}_3 = 1$, this ratio can be used to determine degree of Na_2CO_3 decomposition. Concentrations of CO_2 measured in samples taken from the outlet of the reactor were used to compute the degree of Na_2CO_3 decomposition (Figure 5.4.1). Experiments in the flow system show that at temperatures above 900 K significant amounts of CO_2 are formed. The scatter of the data is significant, especially at short residence times, probably due to insufficiently controlled mixing. At residence times longer than 0.1 s a distinct temperature influence on CO_2 production can be observed. At temperatures around 900 K the maximum conversion of Na_2CO_3 to products is about 0.5 even at the longest residence times. As

temperature increases the reaction becomes faster and at 1190 K it takes only about 0.12 s for complete decomposition of Na_2CO_3 . The observations show a rate of reaction proportional to $[\text{Na}_2\text{CO}_3]^{1.5}$, indicating that reaction does not occur in one step but rather in a complex mechanism. Assuming that the rate of the total reaction has Arrhenius dependence on temperature, an effective energy of activation can be determined as follows. For fixed degree of Na_2CO_3 decomposition the time required for decomposition is a measure of the rate of the reaction, and effective energy of activation can be determined from the slope of the plot that shows dependence of this time on inverse temperature. Figure 5.4.2 shows the dependence of the time required for 30% decomposition on the reactor temperature. The effective energy of activation determined from this plot is 86 kJ/mol.

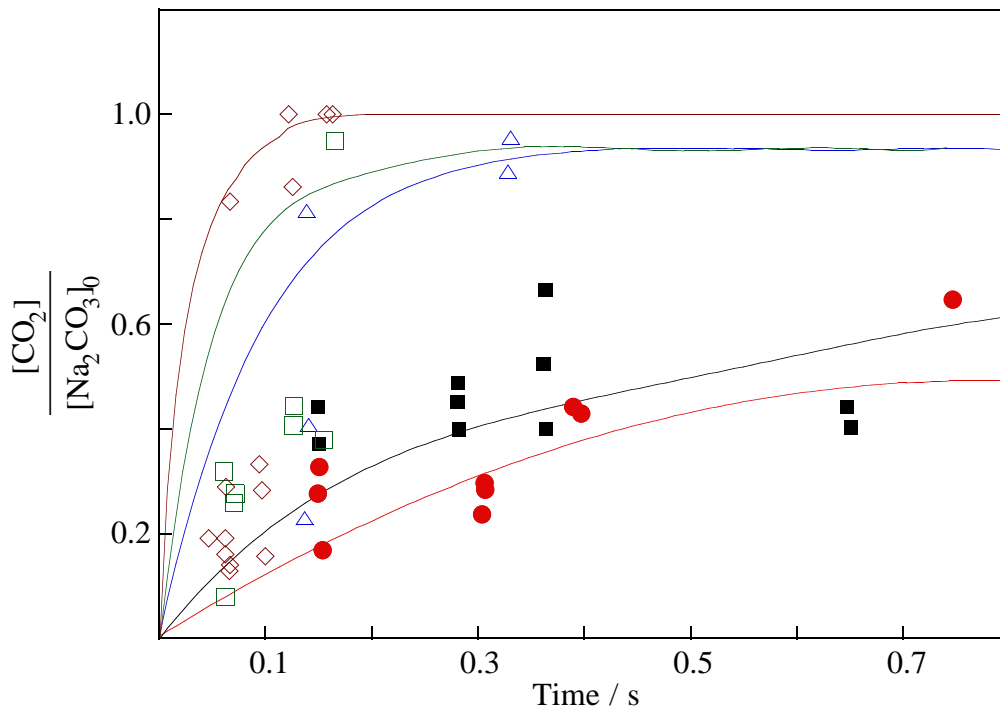


Figure 5.4.1 Comparison of experimental (symbols) and calculated (lines) Na_2CO_3 conversion profiles. Mixture 0.03% Na_2CO_3 + 20.00% H_2O + 79.97% N_2 at $P = 1$ atm.

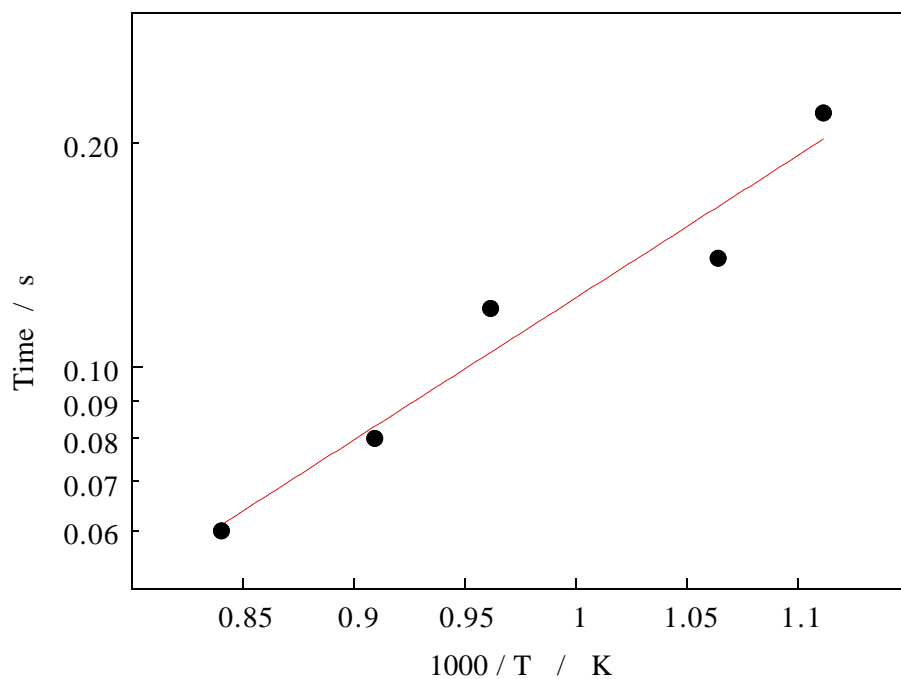


Figure 5.4.2 Temperature dependence of the decadic logarithm of time required for decomposition of 30% of the initial amount of Na_2CO_3 .

To model irreversible (see section 5.2) Na_2CO_3 conversion, we used reactions (5.16, 5.17) and



with reactions (5.16) and (5.17) being irreversible and reaction (5.20) being possible in both directions. The rate coefficient of reaction (5.20) was estimated as that of



measured by Cotton and Jenkins (1971) to be $9.18 \times 10^{12} \exp(-3120/RT)$. Estimates show that the characteristic lifetime of CaO in the reaction (5.21) at 1000 K, 1 atm and 20% H_2O is less than 1 μs , much less than the characteristic time of our experiments. This suggests that for the conditions of our experiments Na_2O is practically instantaneously converted to NaOH, and thus

the value of the rate coefficient of reaction (5.20) is not really important. All calculations were made using the Chemkin-II modeling program (Kee et al., 1992) under constant pressure and temperature constraints. Thermochemical data for all species but Na₂O were taken from Zamansky and Maly (January 1997); thermochemical data for Na₂O were taken from the NASA database (McBride et al., 1993).

Sensitivity calculations (Figure 5.4.3) show that the rate coefficient of reaction (5.16) affects both initial and equilibrium conversions of Na₂CO₃ to CO₂, while that of reaction (5.17) mainly affects the equilibrium value. The rate coefficients of reactions (5.16) and (5.17) were adjusted for the conditions of our experiments (0.03% Na₂CO₃ + 20.00% H₂O + 79.97% N₂ at 1 atm). The rate coefficient of reaction (5.16) was varied to match the initial part of the profiles at 900, 940, 1040, 1100 and 1190 K, while the rate coefficient of reaction (5.17) was changed until the final calculated conversion was equal to the experimental value. Figures 5.4.4 and 5.4.5 show the dependence of rate coefficient of reactions (5.16) and (5.17) on temperature as derived from matching the experimental conversion profiles. The rate coefficient of reaction (5.16) follows a simple Arrhenius dependence, while that of reaction (5.17) decreases with temperature, possibly due to limitation of the reaction rate by CO₂ transport. Least square fits to all data give next expressions for k_5 and k_6

$$k_{16} = 2.54 \times 10^6 \exp(-13040/T) \quad (5.4.II)$$

$$k_{17} = 1.11 \times 10^5 \exp(7580/T) \quad (5.4.III)$$

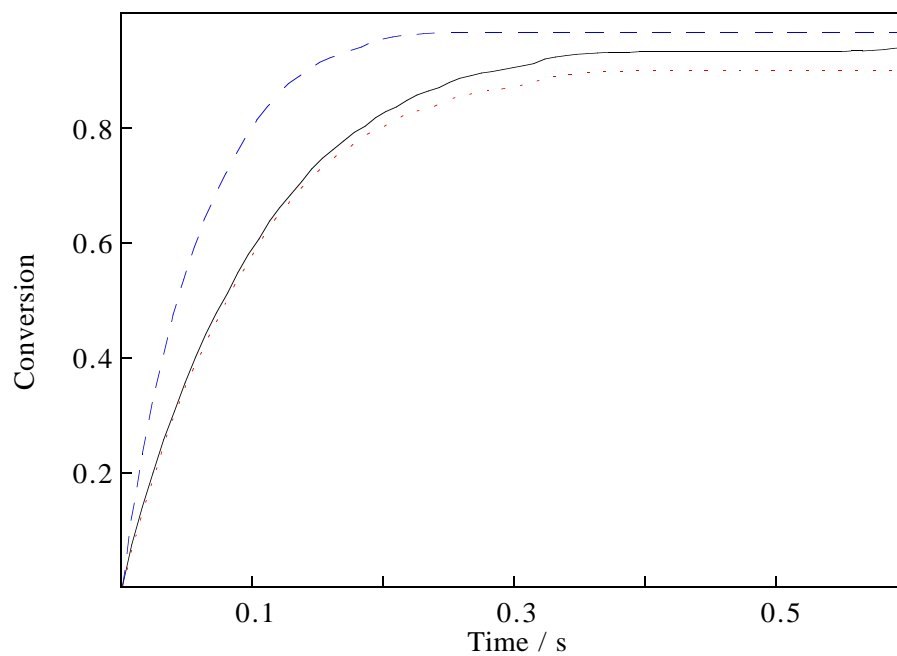


Figure 5.4.3 Sensitivity spectrum for decomposition of Na_2CO_3 . The dashed line represents calculations with a doubled rate coefficient of reaction (5.16), the dotted line a doubled rate coefficient of the reaction (5.17).

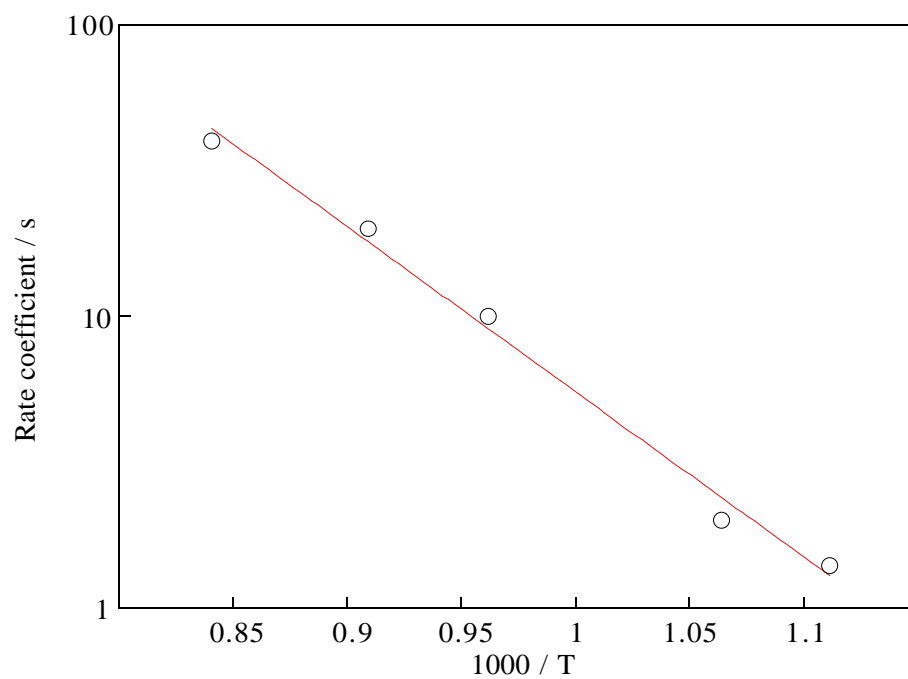


Figure 5.4.4 Rate coefficient inferred for $\text{Na}_2\text{CO}_3 \rightarrow \text{Na}_2\text{O} + \text{CO}_2$ (5.16).

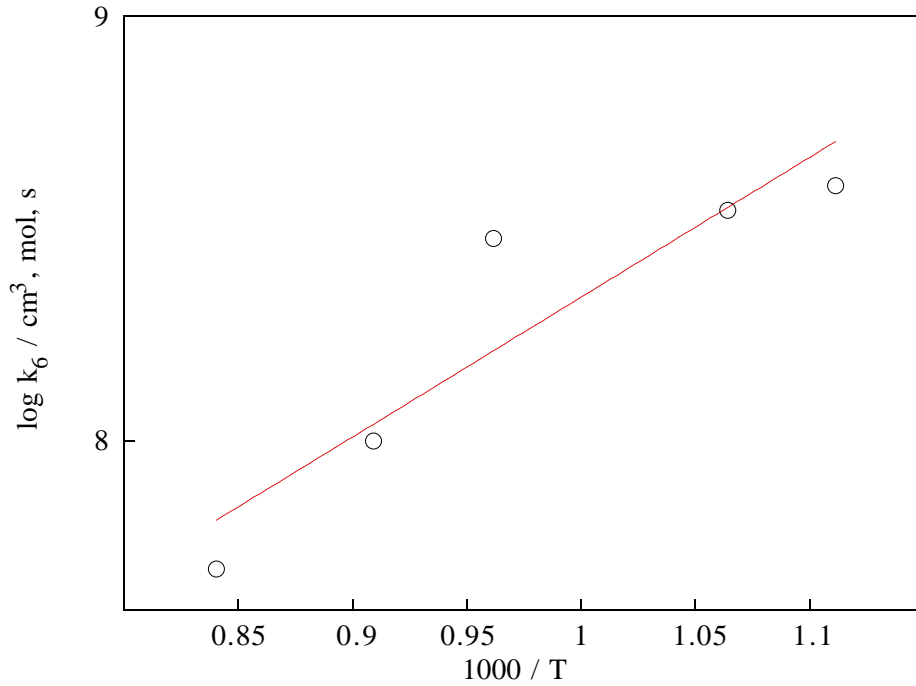


Figure 5.4.5 Rate coefficient inferred for $\text{Na}_2\text{O} + \text{CO}_2 \rightarrow \text{Na}_2\text{CO}_3$ (5.17).

The total uncertainties (TU) in rate coefficient of reactions (5.16) and (5.17) were determined through the formula

$$\text{TU}_i = ((a_i \times U_{\text{exp}})^2 + U_i^f)^{0.5}$$

where U_{exp} is the uncertainty of the experimental data (20%), a_i is the sensitivity of the rate coefficient of the reaction (i) to the experimental data, and U_i^f is the uncertainty associated with the least square fit to all data points for the rate coefficient of reaction (i). Sensitivity coefficients a_i were defined as $a_i = 1.4 \ln(C/C_0)$, where C and C_0 are computed conversions for doubled and for reference values of the rate coefficient of the reaction (i), and are equal to 0.46 for reaction (5.16) and 0.1 for reaction (5.17). The values of U_i^f were found to be 10 and 25% for k_{16} and k_{17} . Based on these data, values of TU_{16} and TU_{17} were calculated to be 14 and 25 %.

Figure 5.4.1 shows a comparison between experimental and calculated conversion profiles based

on the above expressions. At higher temperatures complete decomposition of Na_2CO_3 occurs within 0.2 s, while at low temperatures conversion at long times reaches a maximum value and then stays constant. Taking into account the significant scatter of the experimental data, the agreement between measured and calculated profiles is good.

These results for the rate of Na_2CO_3 decomposition thus show that at temperatures higher than 1400 K Na_2CO_3 decomposes relatively quickly to produce NaOH and CO_2 , suggesting that Na_2CO_3 and NaOH should have practically the same efficiencies as NO_x control agents.

5.4.2 Reactions of Sodium Carbonate with Components of Flue Gas

The flow system was used to measure the rate of reaction between the decomposition products of Na_2CO_3 and CH_4 , H_2 , CO, and NO. These experiments were done at 1150 K and a residence time of 2 s in mixtures containing $0.5\%\text{Na}_2\text{CO}_3 + 1.7\%\text{H}_2\text{O} + \text{N}_2$ with 0.5% additive. In each case the concentration of additive in the mixture after passing through the reactor was measured; measurements were done by GC for CH_4 , H_2 , CO, and O_2 additive and with the chemiluminescence analyzer for NO. In the first set of experiments pure water was sprayed through the nozzle while a mixture of additive and nitrogen passed through the reactor and the concentration of additive in the outlet gas was measured. In the second set of experiments the gas and liquid flow conditions were the same as in the first one except that the water was replaced with a solution containing 5% Na_2CO_3 by mass. Comparison of two runs showed no detectable changes in additive concentrations. We conclude that there is no chemical reaction with observable rate between the decomposition products of Na_2CO_3 and CH_4 , H_2 , CO, and NO under the conditions studied. It was also observed that the concentration of NO stayed constant when O_2 and Na_2CO_3 were injected into the mixture at the same time.

Experiments with ammonia injection to evaluate the reactions of NO and NH_3 in the presence of

Na are under way.

5.5 Mass Spectrometry of Decomposition Products

Mass spectrometric analysis was used to identify the species formed during decomposition of Na_2CO_3 . Figure 5.5.1 shows time histories of ions with mass/charge (m/z) ratios 44 (mostly CO_2^+) and 106 (Na_2CO_3^+) and total ion current for EI = 70 eV. The temperature during the run rises from room temperature (0 on the x-axis) to the final temperature, which corresponds to red hot nichrome. The first peak on the total ion current curve corresponds to the temperature at which all water evaporates. Peak heights are on a relative scale assuming the height of the largest one (in this case $m/z = 44$) to be 100. Figure 5.5.2 shows all detected ions for the moment when $m/z = 44$ reaches its maximum value (62 on the x-axis). It reveals the presence of H_2O^+ (18), Na^+ (23), CO_2^+ (44), very small amounts of NaOH^+ (40) and Na_2CO_3^+ (106). The peak with $m/z = 28$ corresponds to CO^+ and N_2^+ present as residual gas; the other peaks are difficult to identify. As the EI energy decreases (Figure 5.5.3) the contribution of Na^+ becomes more prominent compared to other ions because of its very low ionization energy: Figure 5.5.4 show a mass spectrometric analysis with EI = 0, i.e., with all ions arising from thermal ionization of Na_2CO_3 on the wire. This mass spectrum shows Na^+ (23) and a species with $m/z = 129$ (Na_3CO_3^+). (The species with $m/z = 39$ corresponds a background peak, probably K^+ (39), and always appear in analyses with low EI).

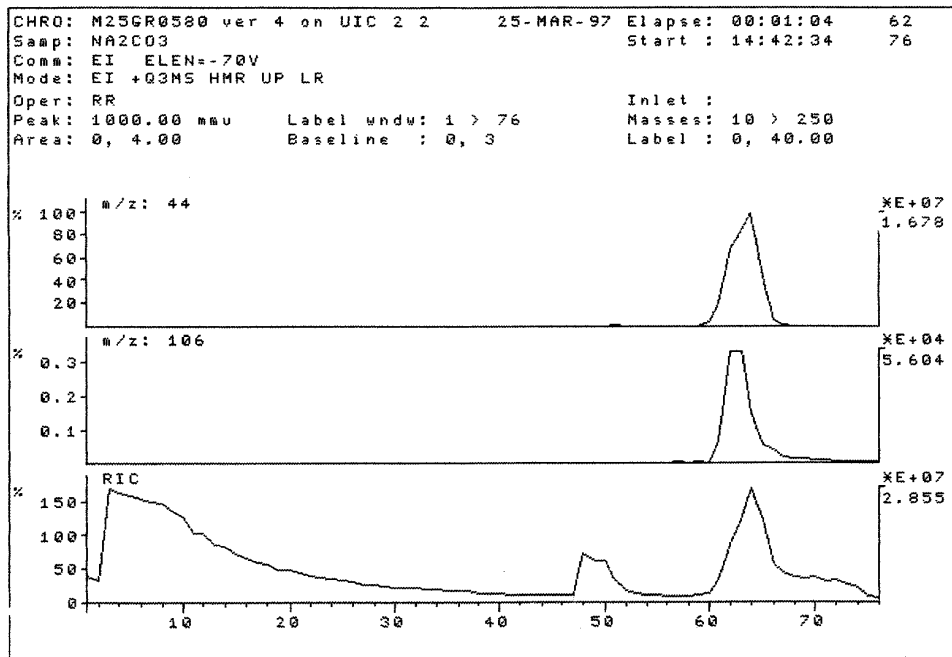


Figure 5.5.1 Time histories of ion currents at $m/z = 44$ and 106 and total ion current. EI = 70 eV, nichrome wire. The x-axis gives the heating time in seconds.

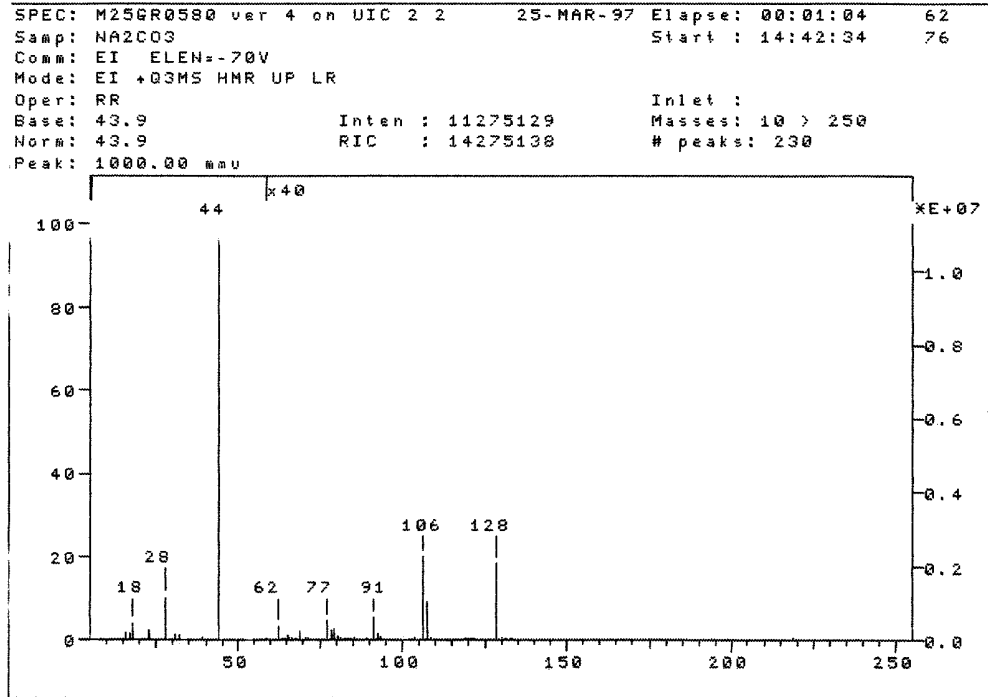


Figure 5.5.2 Mass spectrum at 62 s on the x-axis of Figure 5.5.1. $m/z = 18$ corresponds to H_2O^+ , 28 CO^+ to 44 CO_2^+ to 62 Na_2O^+ to 106 Na_2CO_3^+ and 128 to Na_3CO_3^+ .

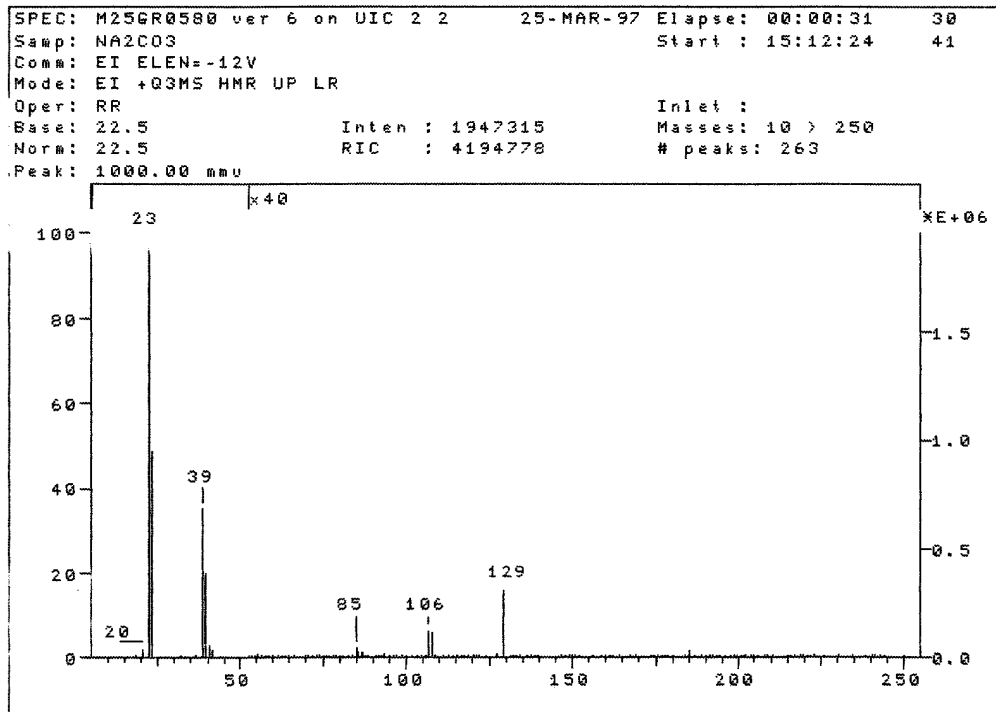


Figure 5.5.3 Mass spectrum at the time $m/z = 23$ reaches its maximum. EI = 12 eV.

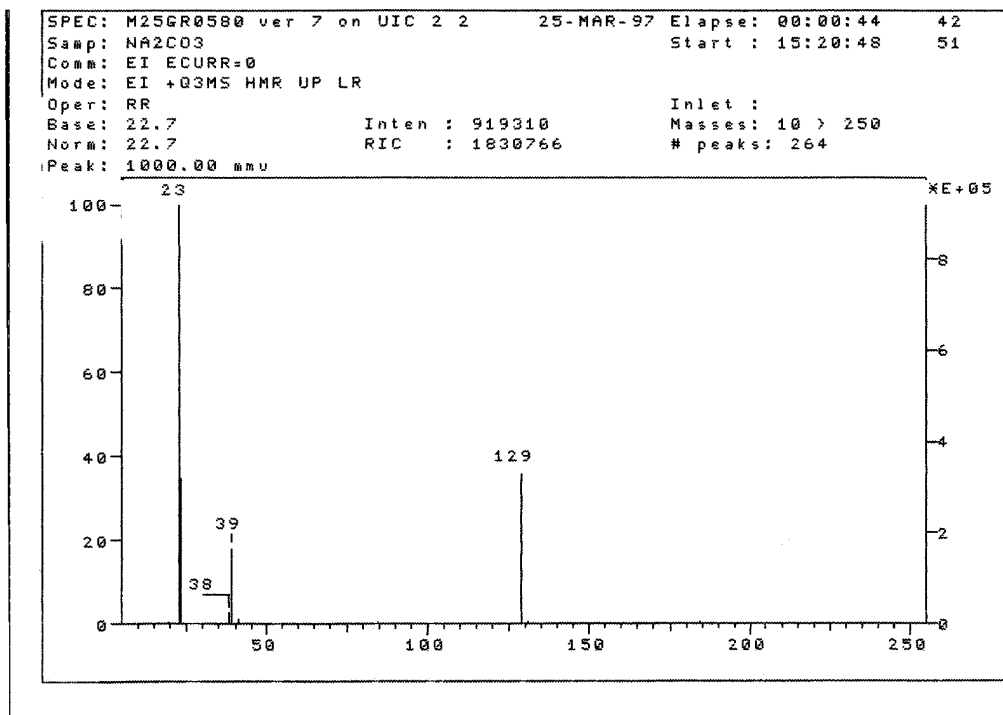


Figure 5.5.4 Mass spectrum at the time $m/z = 23$ reaches its maximum in thermal ionization mode.

Figure 5.5.5 shows results of mass spectrometric analysis of an Na_2CO_3 sample in chemical ionization mode. The product distribution (Na^+ , CO_2^+ , Na_2CO_3^+) is the same as in electron ionization mode with a few new species; among them $m/z = 53$ in greatest amount.

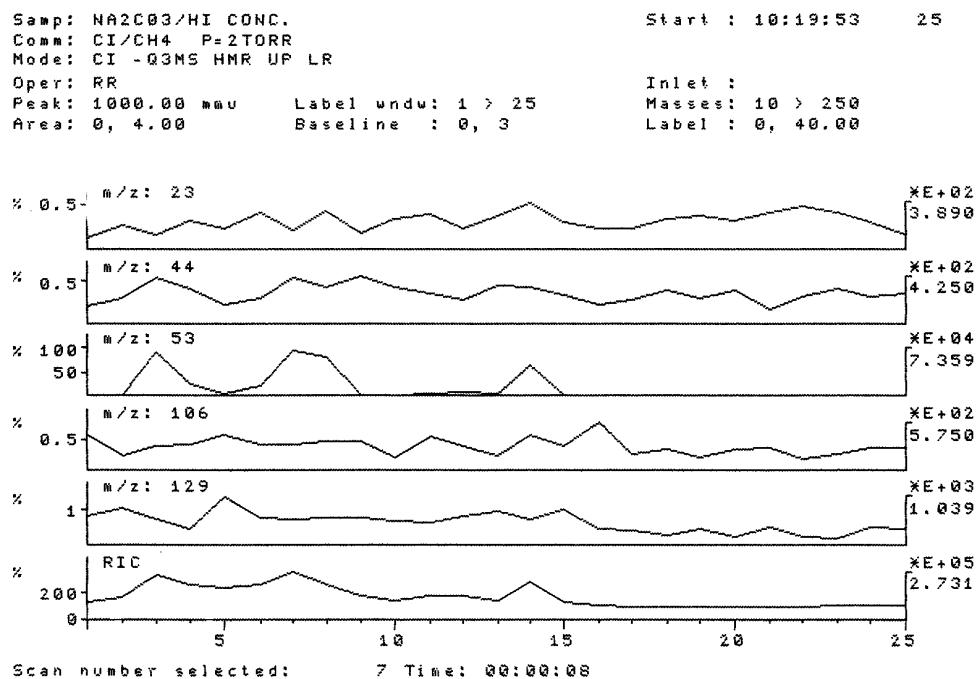


Figure 5.5.5 Time histories of ions with $m/z = 23$ (Na^+), 44 (CO_2^+), 53 ($\text{Na}_2\text{CO}_3^{++}$), 106 (Na_2CO_3^+), 129 (Na_3CO_3^+), and total ion current. Chemical ionization mode, Nichrome wire.

A general disadvantage of mass spectrometric measurements is that they do not provide continuous recording of the sample temperature. It is therefore not possible to correlate mass spectra closely with the temperature at which active species are formed and/or decomposition of Na_2CO_3 occurs. It is possible, however, to correlate some moments on the time scale with corresponding temperatures when in place of standard nichrome wire, which melts at very high temperature, wire made from a metal with lower melting temperature is used. The moment when such a wire melts is detected as a maximum in the total ion current and corresponds to the melting temperature of the metal. Since Ag has melting point of 1235 K, within the temperature range of our interest, we conducted some experiments using Ag wire instead of nichrome. These were done in EI mode with an ionization energy of 70 eV and in thermal ionization mode ($\text{EI} = 0$). The

time of Ag occurrence in the mass spectrum (Figure 5.5.6) (which also corresponds to the maximum in total current) corresponds to the moment of time when temperature of the wire is 1235 K (39 s). The mass spectrum (Figure 5.5.7) at this temperature shows CO_2^+ (44), NaOH^+ (40), Na_2CO_3^+ (106) and many other species. Some of them are easily identifiable (H_2O^+ and N_2^+), while secure identification of others requires additional (i.e., high-resolution) analysis. Figure 5.5.7 does not indicate the presence of Na atoms. To find out if Na atoms are present in the system at 1235 K we repeated experiments with an Ag wire in thermal ionization mode (Figs. 5.5.8 and 5.5.9). Figure 5.5.8 shows that one of the maximums in Ag^+ (109) concentration corresponds to the maximum in total ion current (22 s on x-axis) at the temperature 1235 K. The mass spectrum (Figure 5.5.9) at this temperature shows Na^+ (23) and species with $m/z = 39$ and 129.

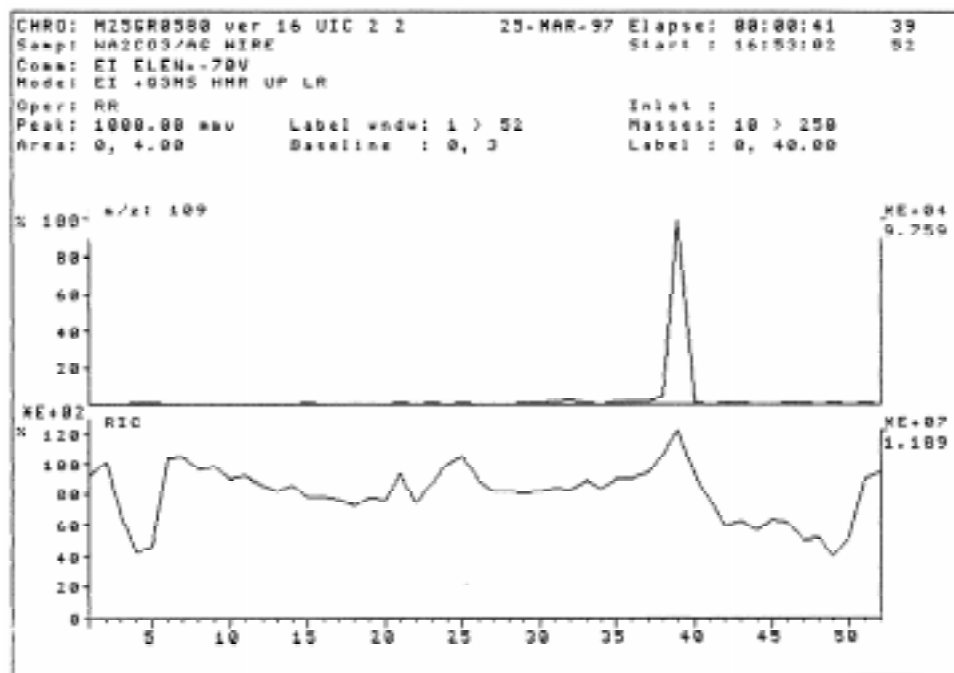


Figure 5.5.6 Time histories of Ag^+ (109) and total ion current for experiments with Ag wire. EI = 70 eV. Time 39 s corresponds to 1235 K.

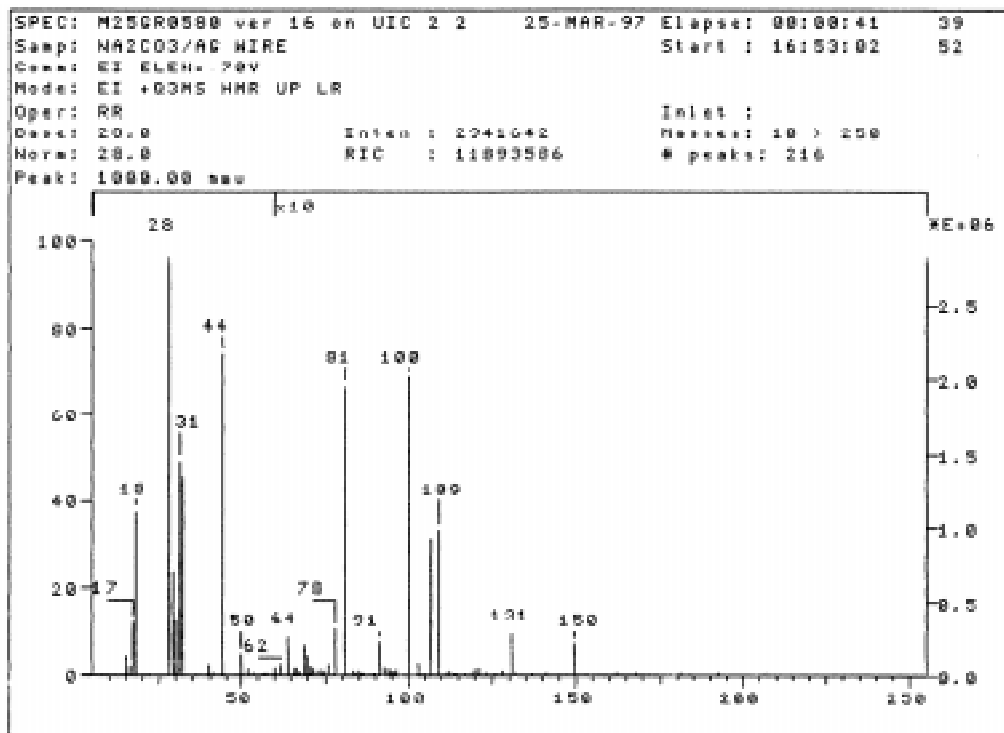


Figure 5.5.7 Mass spectrum at 1235 K. EI = 70 eV.

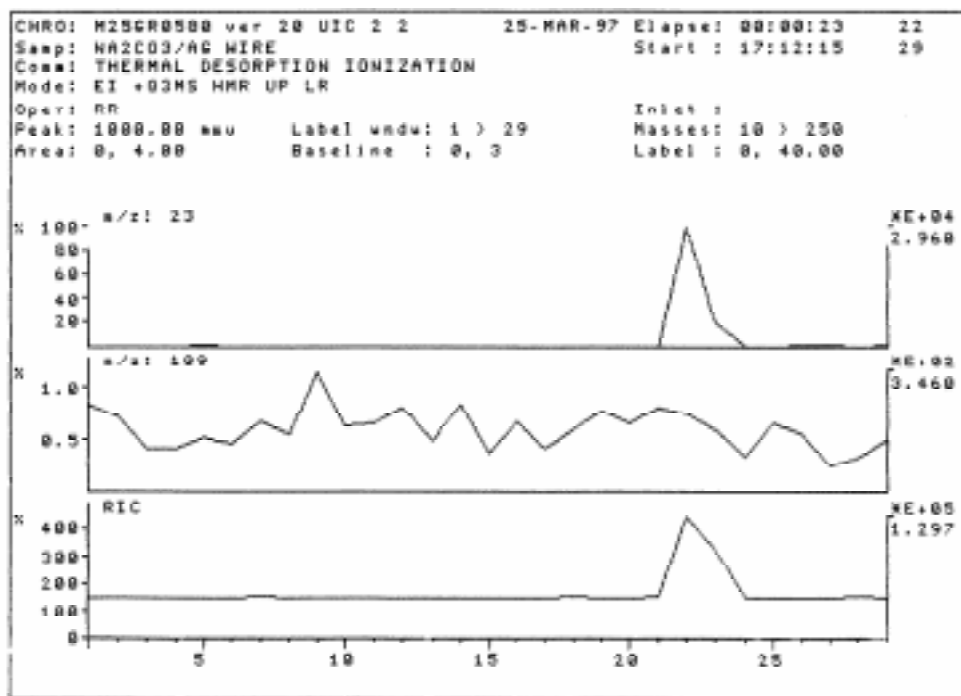


Figure 5.5.8 Time histories of ions with $m/z = 23$ (Na^+) and 109 (Ag^+), and total ion current through the detector for thermal ionization mode.

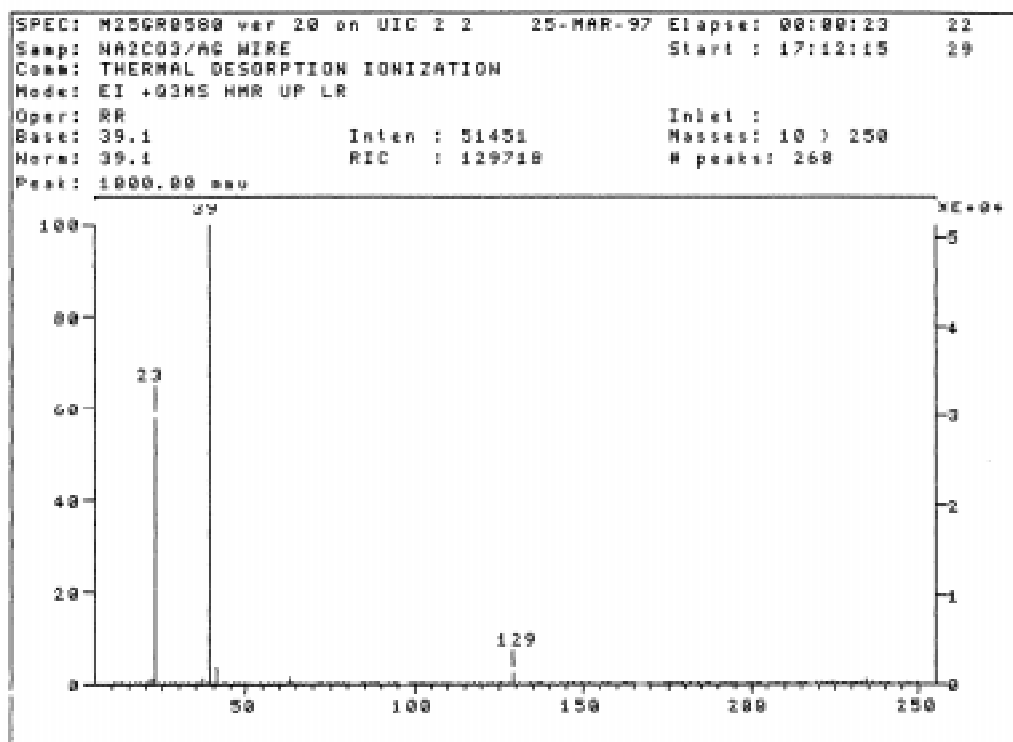


Figure 5.5.9 Mass spectrum corresponding to the moment of burnout of Ag wire for thermal ionization mode.

Mass spectrometric analysis of products of Na_2CO_3 decomposition thus confirms that the primary gas-phase decomposition products are Na, NaOH and CO_2 . Experiments with temperature control show formation of Na atoms at 1235 K.

5.6 Kinetics of Na_2CO_3 Reactions: Conclusions

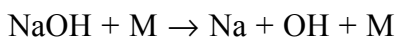
1. Decomposition of Na_2CO_3 was studied in a flow system over the temperature range from 900 to 1190 K. An aqueous solution of sodium carbonate was sprayed into a flow of N_2 such that the concentration of Na_2CO_3 injected into the test gas ranged from 100 to 500 ppm. The observed decomposition rate of Na_2CO_3 can be described kinetically in terms of two irreversible $\text{Na}_2\text{CO}_3 \rightarrow \text{Na}_2\text{O} + \text{CO}_2$ (5.16) and $\text{Na}_2\text{O} + \text{CO}_2 \rightarrow \text{Na}_2\text{CO}_3$ (5.17) and one reversible $\text{Na}_2\text{O} + \text{H}_2\text{O} \leftrightarrow$

2NaOH (5.20) chemical reactions. The corresponding rate coefficients k_{16} and k_{17} were adjusted to describe the measured rate of Na_2CO_3 decomposition, while the rate coefficient of reaction (5.20) was estimated from kinetic data for the similar reaction of CaO. Least square fits to all data gave $k_{16} = 2.54 \times 10^6 \exp(-13040/T)$, $k_{17} = 1.11 \times 10^5 \exp(7580/T)$ $\text{cm}^3 \text{mol}^{-1} \text{s}^{-1}$.

2. Mass spectrometric analysis of products of Na_2CO_3 decomposition confirms that the primary gas-phase products of decomposition are Na, NaOH and CO_2 . Experiments with temperature control show formation of Na atoms at temperature 1235 K.

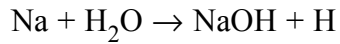
3. Extrapolating the results of our flow system experiments to higher temperatures shows that Na_2CO_3 decomposition at temperatures over 1400 K produces NaOH and CO_2 very quickly. NaOH then decomposes more slowly. According to Westley et al. (1994), the characteristic time of NaOH decomposition at 1500 K to produce Na and OH is 160 ms; extrapolation of our data for Na_2CO_3 decomposition to that temperature gives an Na_2CO_3 decomposition time of 2.3 ms. These observations suggest that Na_2CO_3 and NaOH should have practically the same efficiencies as pollution control agents.

4. Flow system experiments at 1150 K show no chemical reaction between Na_2CO_3 decomposition products and H_2 , CO, CH_4 or NO. This experiment indicates that the effect of NO removal by Na_2CO_3 is mainly due to promotional effect that Na_2CO_3 additive has on the concentrations of atoms and radicals already present in flue gas at high temperature, in particular OH and H. Enhancement of radical concentrations in the presence of Na_2CO_3 can occur through NaOH thermal decomposition

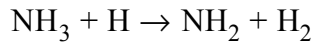
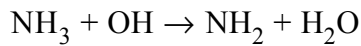


and in further reactions of Na atoms, which were observed among the products of Na_2CO_3

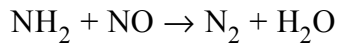
decomposition in mass spectrometric analysis. H-atoms, for example, are produced by



These two reactions provide for continuous flow of radicals into the system and thus account for high efficiency of Na_2CO_3 . Radicals then react with NH_3 which is injected to flue gas in SNCR process



such that the efficiency of NH_3 as NO removing agent through the reaction



in the conventional AR process is significantly enhanced in presence of Na_2CO_3 .

Our experiments indicate that other additives that have decomposition times similar to NaOH and produce active species that enhance production of OH and H radicals in flue gas should also be considered as potential NO control agents.

5. Completion of the Phase I research will include the following, as mentioned in the preceding sections. (a) Flow system experiments including ammonia and NO additives; (b) Translation of molecular electronic structure results into NASA-style thermochemical polynomials; and (c) Chemkin simulations with the expanded set of sodium species.

6.0 BENCH SCALE PROCESS OPTIMIZATION STUDIES

The Second Generation Advanced Reburning (SGAR) process includes different combinations of reburning, N-agent injection into the reburn zone, N-agent injection downstream of the reburn zone, and promoter injection. Bench scale tests were conducted at EER's Controlled Temperature Tower (CTT) to optimize each component of the technology individually and then to optimize overall performance of the combined process. Several nitrogen agents were tested. Sodium was used as the main promoter because its performance had been successfully demonstrated in previous tests. Specific test series included:

- Reburning alone
- Promoted AR-Lean
- Promoted AR-Rich
- Multiple injection advanced reburning

All tests were conducted in the CTT while firing natural gas at 20 kW (70,000 Btu/hr). The test facility and results of each test series are described in the following sections.

6.1 Controlled Temperature Tower

As shown in Figure 6.1, the CTT is a refractory lined, vertically down-fired combustion test facility designed to provide precise control of furnace temperature and gas composition. It consists of a variable swirl diffusion burner and a refractory furnace which is equipped with backfired heating channels. The furnace has an inside diameter of 8 inches. The backfired channels provide external heating to the refractory walls, allowing the rate of temperature decay to be controlled. Because of the relatively small size of the CTT, it is possible to use bottled gases (e.g. O₂, N₂, SO₂) to control furnace gas composition. In addition, characteristic mixing times in the CTT furnace are on the order of 100 ms, making it straightforward to separate zones and characterize individual processes.

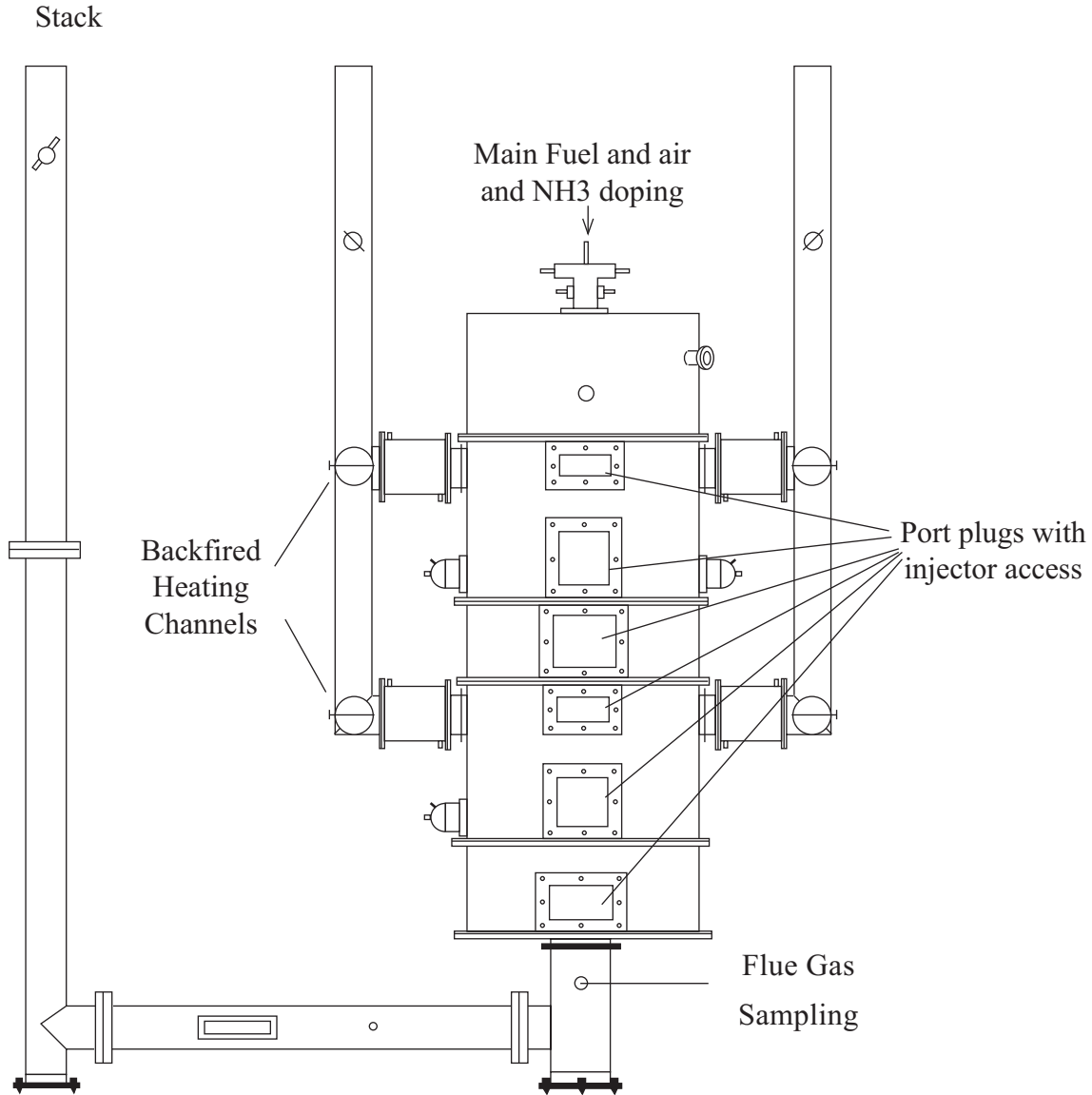


Figure 6.1 Controlled Temperature Tower (CTT).

Specific test equipment for the SGAR tests included injectors for the reburn fuel, N-agent/promoters, and overfire air. The reburn fuel and OFA were injected through radial injectors aligned upwards, i.e. countercurrent to the gas flow. The N-agents and promoters were injected through axial injectors aligned downwards. Delavan twin fluid nozzles were used for additive atomization, with bottled nitrogen as the atomization medium. Prior to the experiments, system temperature profiles were measured under various test configurations using a suction pyrometer. These profiles are presented in Figure 6.2.

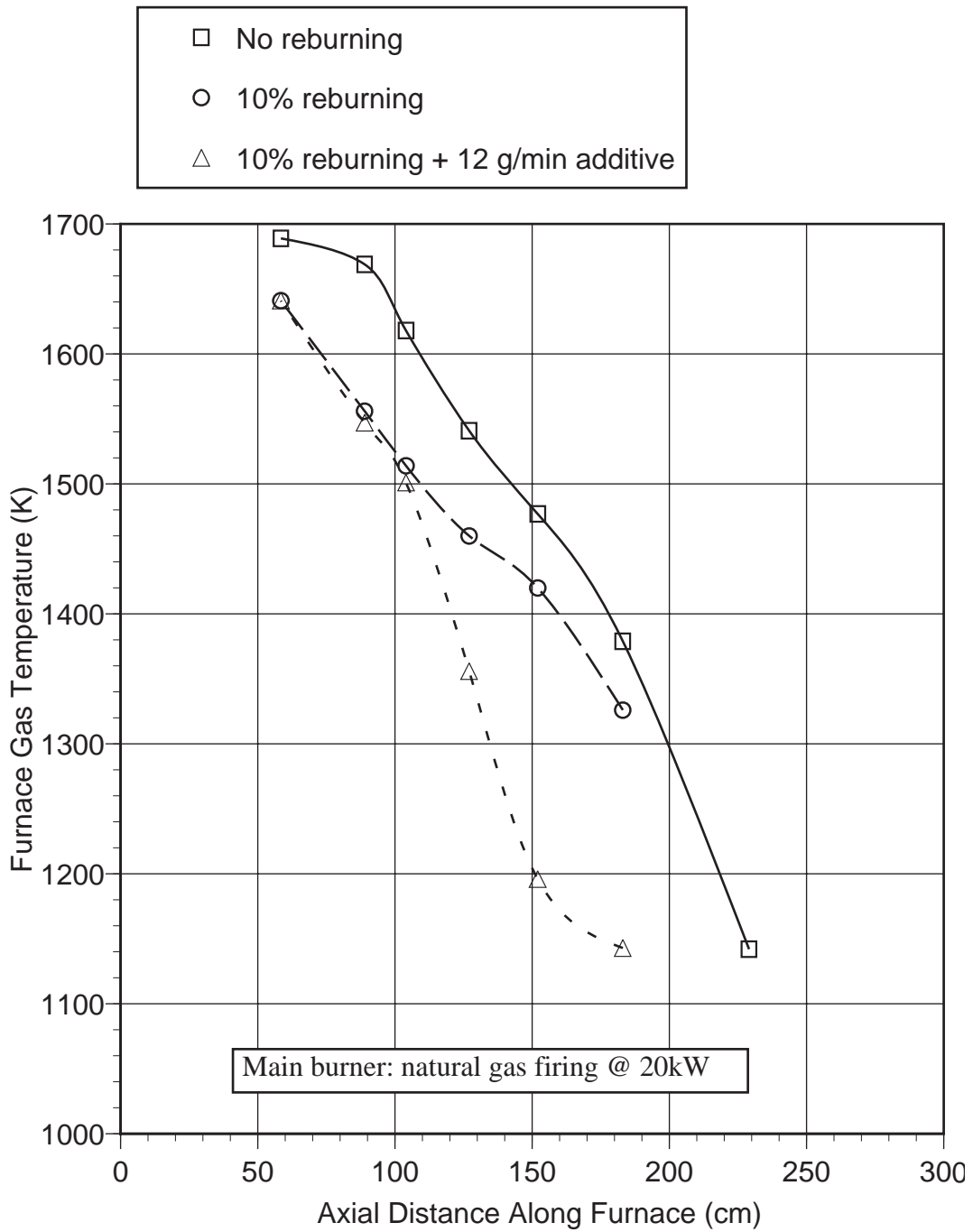


Figure 6.2 CTT temperature profiles.

Proper operation of system instrumentation was verified before the tests began, including thermocouples, pressure gauges, and the flue gas sample system. A continuous emissions monitoring system (CEMS) was used for on-line analysis of flue gas composition. The CEMS consisted of a heated sample line, sample conditioning system (to remove moisture and particulate), and gas analyzers. Species analyzed, detection principles, and detection limits were as follows:

- O₂: paramagnetism, 0.1%
- NO_x: chemiluminescence, 1 ppm
- CO: nondispersive infrared, 1 ppm
- CO₂: nondispersive infrared, 0.1%
- N₂O: nondispersive infrared, 1 ppm

Certified zero and span gases were used to calibrate the analyzers. A chart recorder was used to provide a hard copy of analyzer outputs.

6.2 Reburning Alone

The first series of tests was designed to define the nominal performance of gas reburning without additives. Test variables included reburn heat input (i.e. SR₂), reburn zone residence time, and reburn fuel transport medium (air or nitrogen). Baseline conditions were as follows:

- Reburn fuel injection temperature=1670 K
- SR₁=1.10, SR₃=1.15
- Overfire air injection temperature=1530 K
- Reburn zone residence time=350 msec
- NO_i=600 ppm as measured

Figure 6.3 shows the impact of varying reburn fuel heat input upon NO reduction. For both air and nitrogen transport, performance increased with increasing reburn heat input. Maximum NO reductions were 42% and 59% with air and nitrogen transport, respectively. On the basis of reburn heat input nitrogen transport gave greater NO reduction than air transport. However, this is primarily because nitrogen transport gives lower reburn zone stoichiometry than air. When compared on the basis of SR₂, results are nearly identical.

Main Fuel: Natural gas @ 20 kW
Reburn fuel: Natural gas
Reburn T=1670K
SR1=1.10
OFA T= 1530K
Reburn zone residence time = 0.35 sec
NO_i=600 ppm as meas

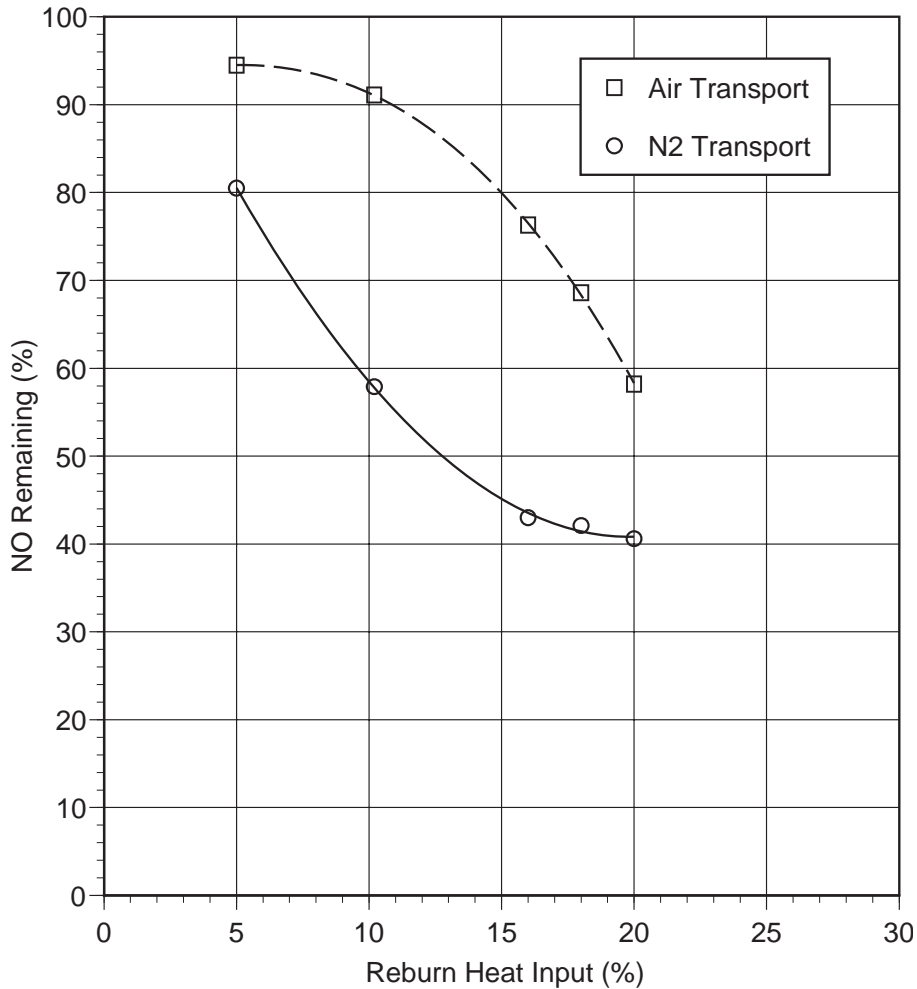


Figure 6.3 NO reduction vs. reburn heat input for CTT gas reburn: No additives or promoters.

Reburn zone residence time was varied by moving the OFA injector to different axial furnace positions. Reburn zone residence time was varied from 200 to 1600 msec at 10% reburn heat input. This corresponds to an overfire air injection temperature range of 1140 to 1590 K. As shown in Figure 6.4, with nitrogen transport NO control increased from 35 to 58% as reburn zone residence time increased from 200 to 1600 msec. With air transport NO control was not dependent upon residence time.

Main Fuel: Natural gas @ 20 kW
 Reburn fuel: Natural gas
 Reburn T=1670 K
 SR1=1.10
 10.2% Reburn
 SR2 (air)=1.10, SR2(N2)=0.99
 OFA T: varied
 NOi=600 ppm as meas

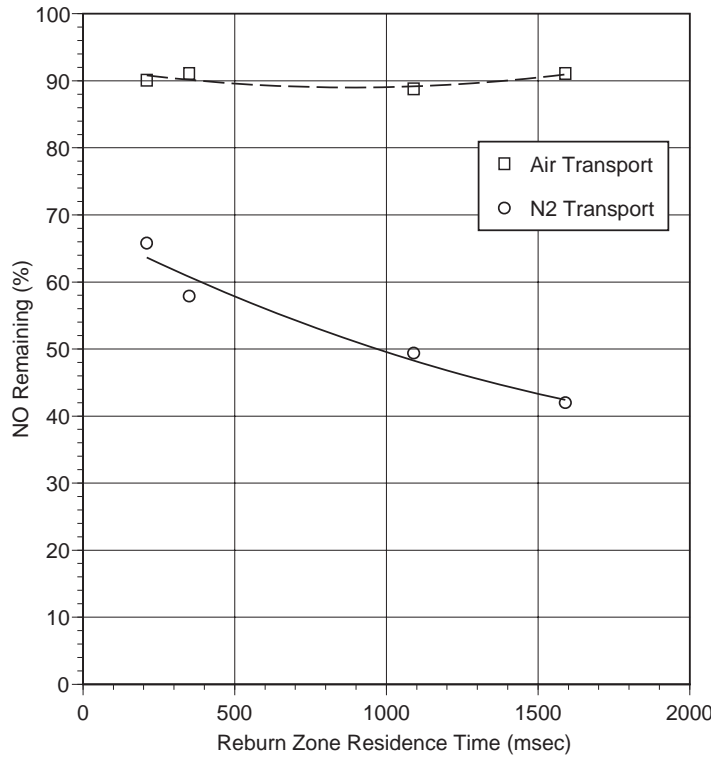


Figure 6.4 NO reduction vs. reburn zone residence time for gas reburn: No additives or promoters.

6.3 Promoted AR-Lean

In the AR-Lean tests, reburning was coupled with the injection of a single nitrogen agent, both with and without promoters. N-agent was injected with the overfire air. Reburn heat input was 10%. Figure 6.5 shows AR-Lean test results. The overfire air plus additive injection temperature was varied. This changed the reburn zone residence time, causing reburn performance to vary. Aqueous ammonia, urea, and ammonium sulfate were tested, each with and without 15 ppm of sodium carbonate promoter. The listed promoter concentration assumes complete conversion to the gas phase. Aqueous ammonia and urea performed somewhat better than ammonium sulfate. Sodium carbonate both expanded the optimum temperature window to the right (i.e. to higher temperatures) and increased maximum NO control. The highest NO reduction achieved was 87% with both promoted aqueous ammonia and promoted urea at an injection temperature of 1300 K.

Main Fuel: Natural gas @20 kW
 10% Reburn @ 1670 K, N2 transport
 Reburn zone res. time varies
 SR1=1.10, SR2=0.99, SR3=1.15
 NOi=600 ppm as meas, NSR=1.5
 N agent added with OFA

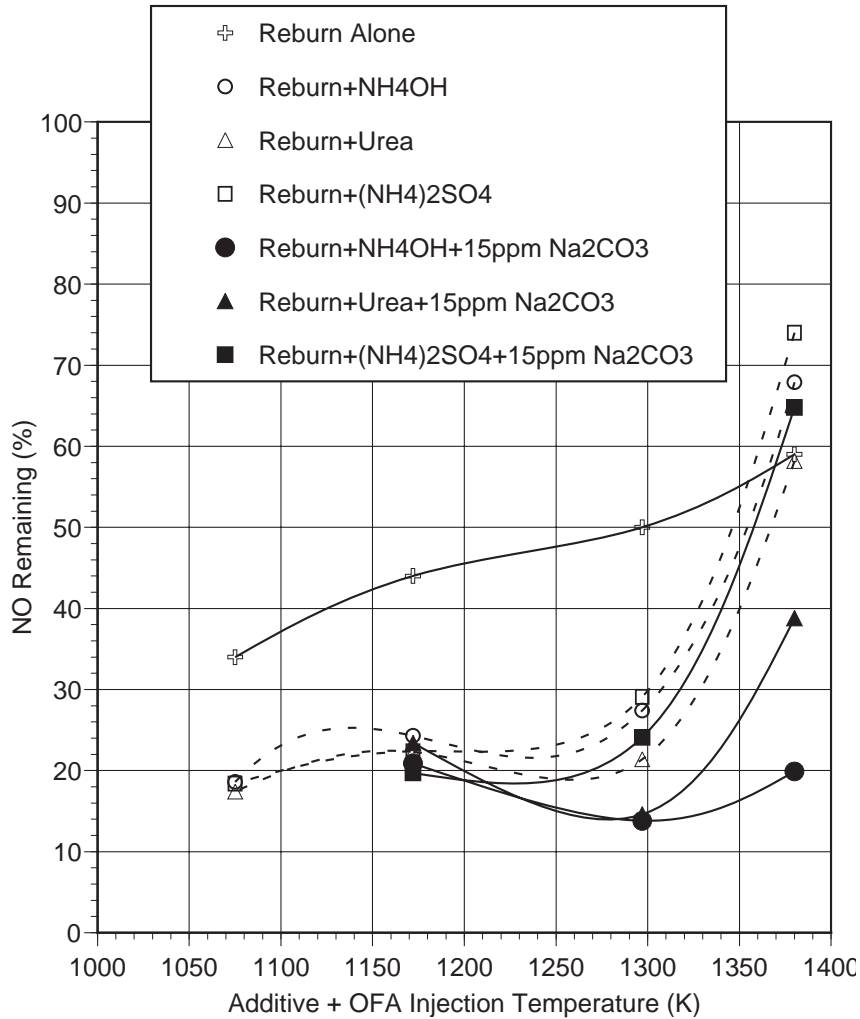


Figure 6.5 AR-Lean performance.

6.4 Promoted AR-Rich

In the AR-Rich tests aqueous ammonia and urea were injected into the fuel rich reburn zone. Overfire air was added at 1160 K. As shown in Figure 6.6, the impact of the promoter was pronounced for this test system. Sodium carbonate shifted the optimum temperature to the right and significantly widened the temperature window. Maximum NO reduction was 88%, obtained with both promoted aqueous ammonia and promoted urea at an injection temperature of 1470 K.

Main Fuel: Natural gas @20 kW
 10% Reburn @ 1670 K, N2 transport
 Reburn zone res. time=0.72 sec
 OFA added at 1160 K
 SR1=1.10, SR2=0.99, SR3=1.15
 NOi=600 ppm as meas, NSR=1.5
 N agent added in reburn zone

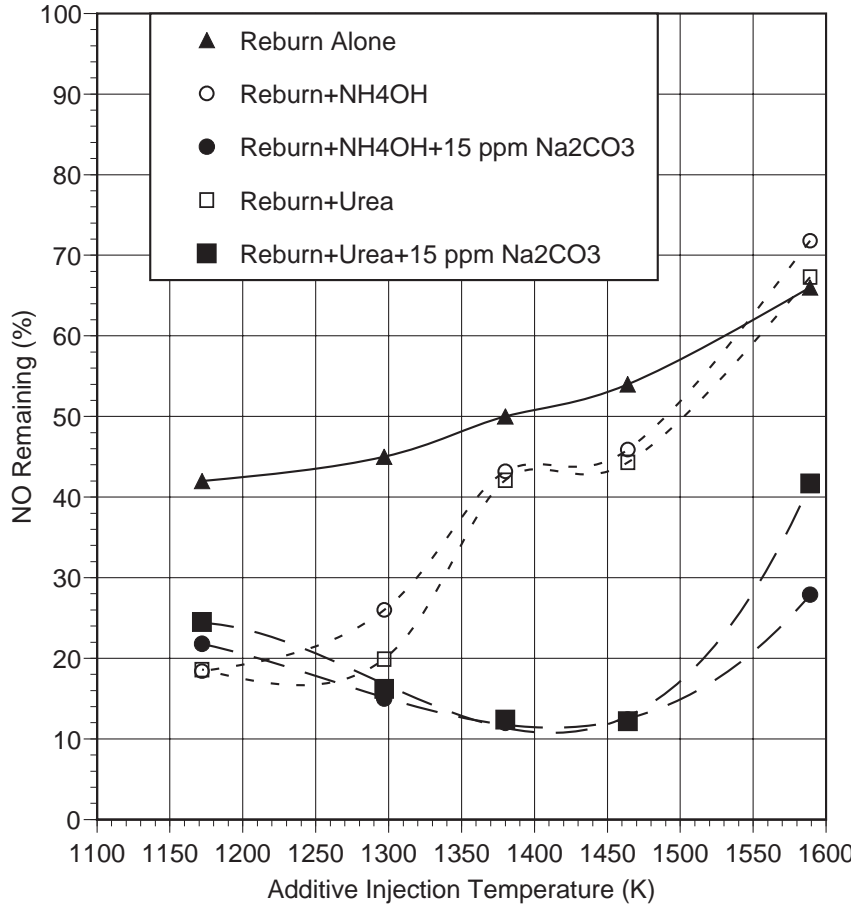


Figure 6.6 AR-Rich performance.

A series of screening tests was then conducted with different sodium promoter compounds. The promoters were injected along with aqueous ammonia into the reburn zone at 1460 K. Six different sodium compounds were characterized including Na_2CO_3 , NaHCO_3 , trona (a mineral product consisting of Na_2CO_3 and NaHCO_3), NaCl , NaNO_3 , and NaOH . As shown in Figure 6.7, reburning alone provided 47% NO control, which was increased to 57% by the addition of ammonia. All six sodium compounds significantly enhanced performance, although NaCl and NaNO_3 were somewhat less effective than the other four. Na_2CO_3 is effective, non-toxic, readily soluble in water, and is the least expensive compound on a unit-sodium basis, and thus was selected as the primary promoter compound for subsequent tests.

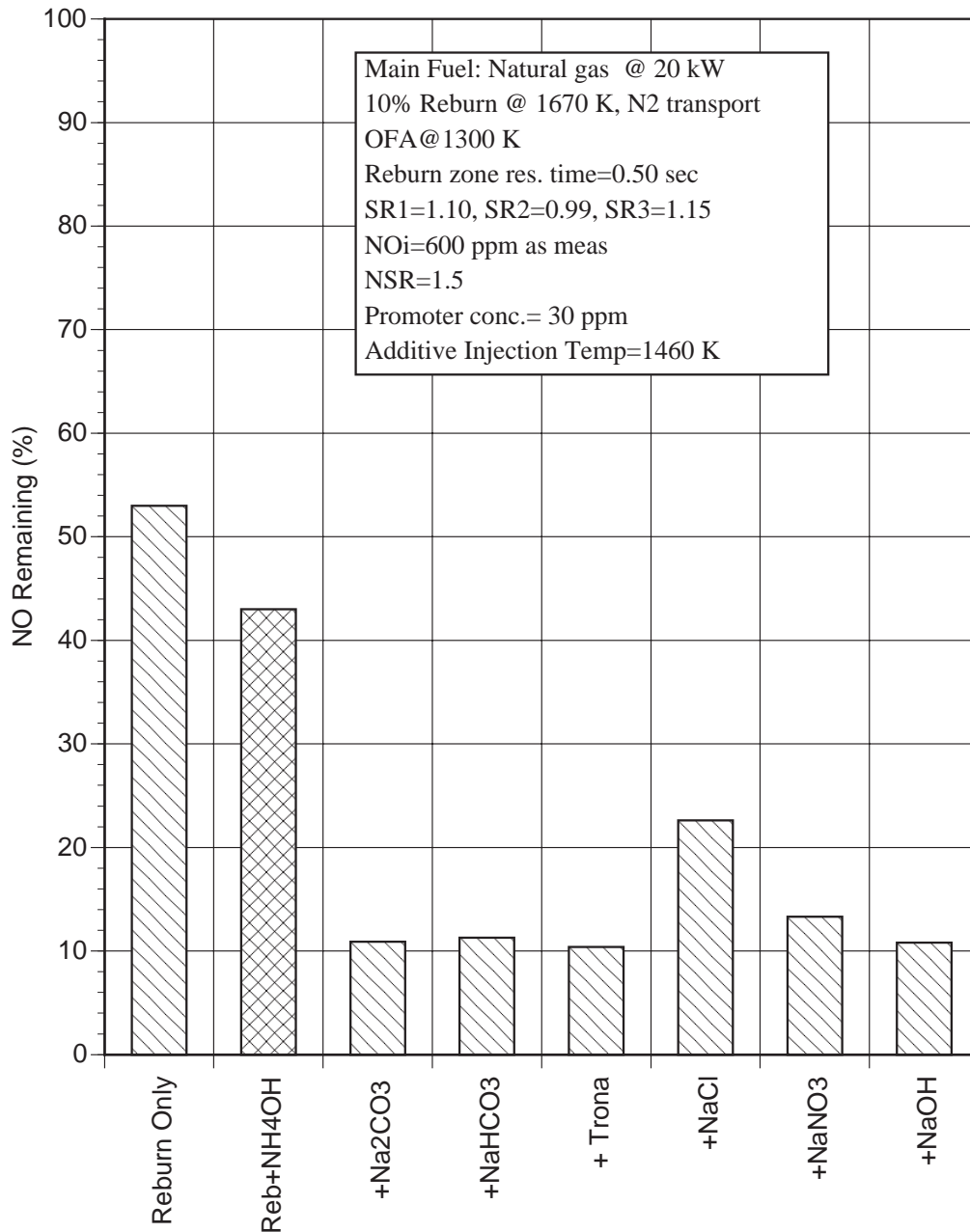


Figure 6.7 Alternative promoter screening test results.

Parametric studies were then conducted to evaluate the impact of three process variables: sodium concentration, initial NO concentration, and N-agent to NO stoichiometric ratio. Sodium concentration was varied during injection of aqueous ammonia and urea into the fuel rich zone with 10% reburning. As shown in Figure 6.8, NO control increased as sodium concentration increased from 0 to 30 ppm, and then levelled off as sodium concentration was further increased to over 100 ppm. Even 10 ppm Na (i.e. 5 ppm Na_2CO_3) reduced the remaining NO fraction by 21 percentage points, from 42 to 21%.

Main Fuel: Natural gas @ 20 kW
10% Reburn @ 1670 K, N₂ transport
Reburn zone res. time=0.72 sec
OFA added at 1160 K
SR1=1.10, SR2=0.99, SR3=1.15
NO_i=600 ppm as meas
NSR_i=1.5
Additive Injection Temp=1380 K

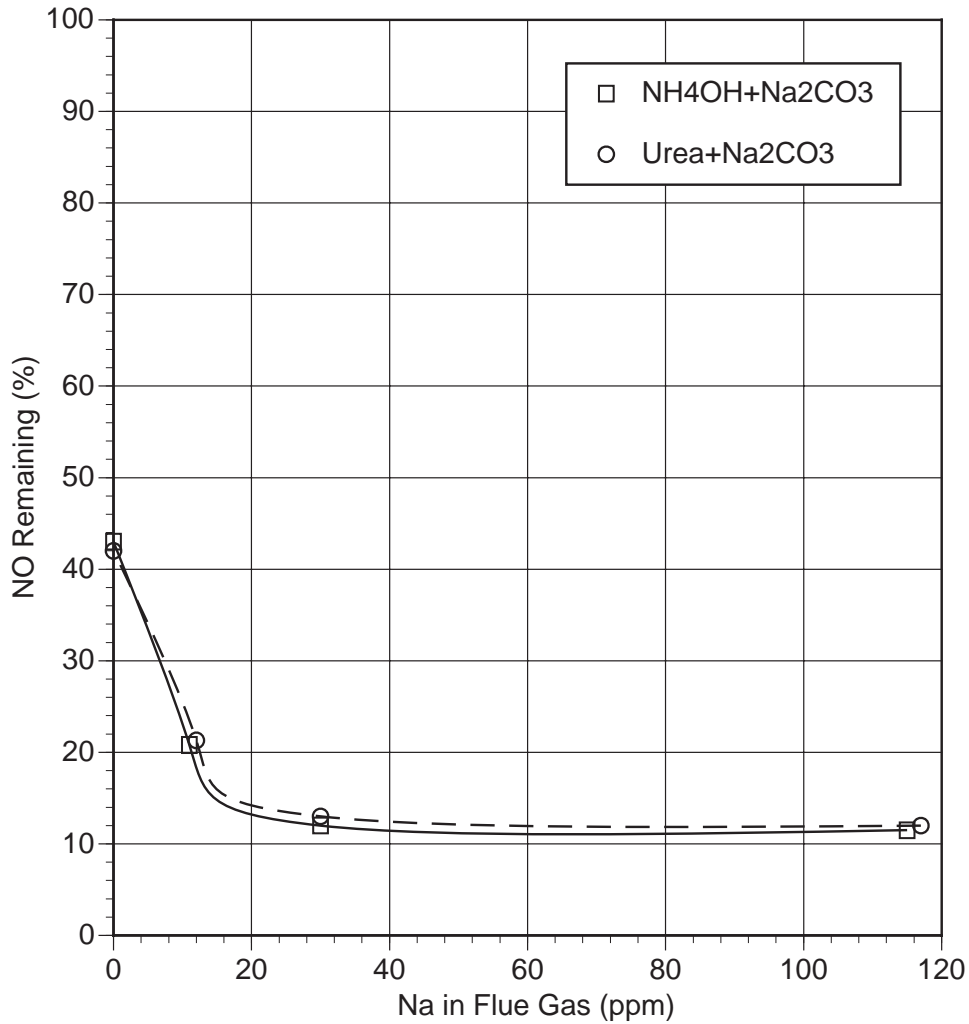


Figure 6.8 NO control vs. Na promoter concentration.

Initial NO concentration was varied from 150 to 950 ppm during tests with reburn alone and reburn plus injection of aqueous ammonia and sodium carbonate. As shown in Figure 6.9, NO reduction increased with increasing NO_i. For reburn plus injection of aqueous ammonia and sodium carbonate over 90% NO control was obtained at NO_i=950 ppm.

Main Fuel: Natural gas @ 20 kW
10% Reburn @ 1670 K
OFA @ 1300 K
Additive @ 1460 K
SR1=1.10, SR2=0.99, SR3=1.15
NSR=1.5

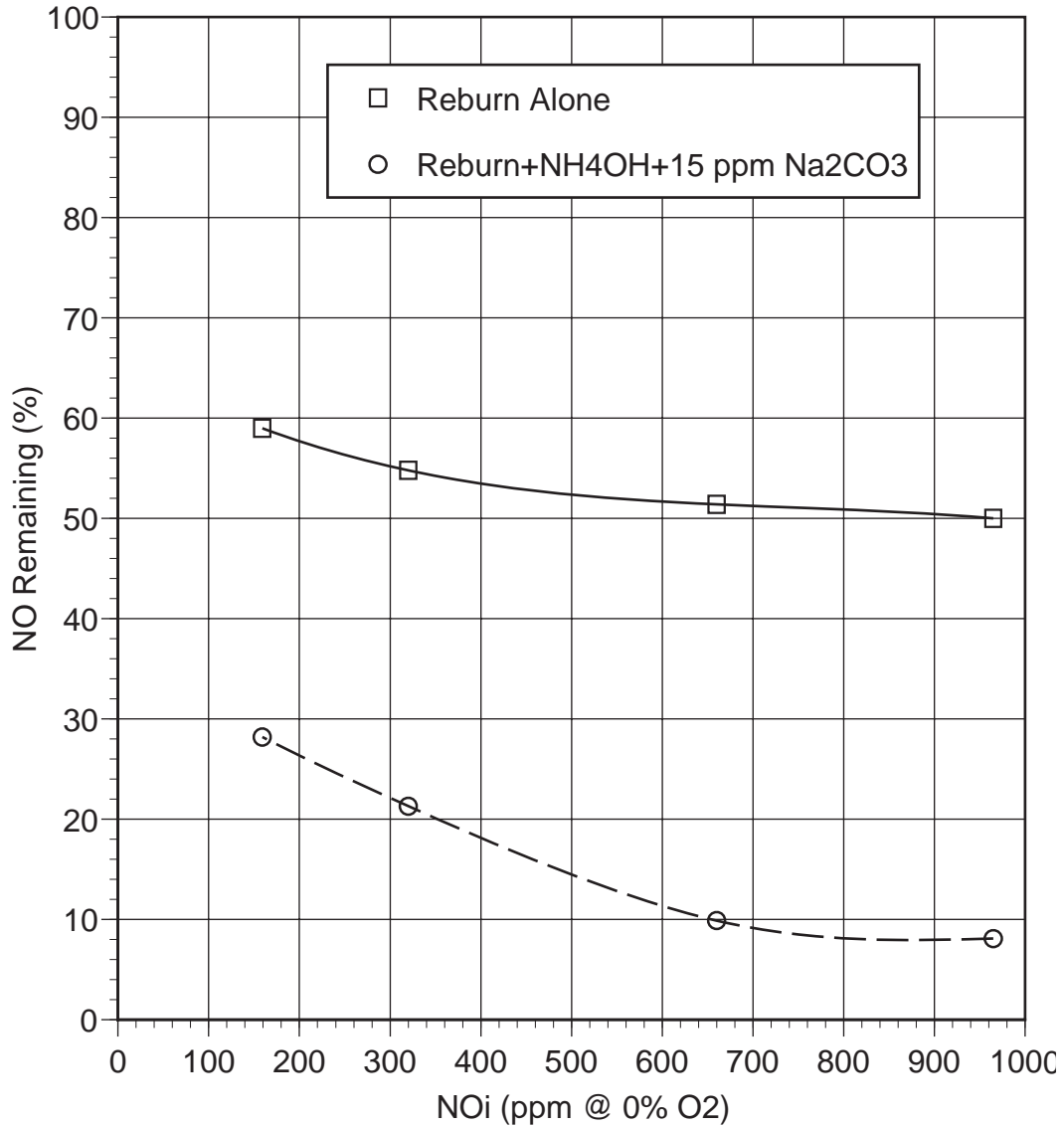


Figure 6.9 NO reduction vs. NO_i for rich side injection of NH₄OH + Na₂CO₃.

Nitrogen agent to NO_i stoichiometric ratio (NSR) was then varied from 0 to 2.0. As shown in Figure 6.10, NO reduction increased with increasing NSR. NO reduction was 93% at NSR=2.0.

Main Fuel: Natural gas @ 20 kW
 10% Reburn @ 1670 K
 OFA @ 1300 K
 Additive @ 1460 K
 SR1=1.10, SR2=0.99, SR3=1.15
 NOi=600 ppm as meas

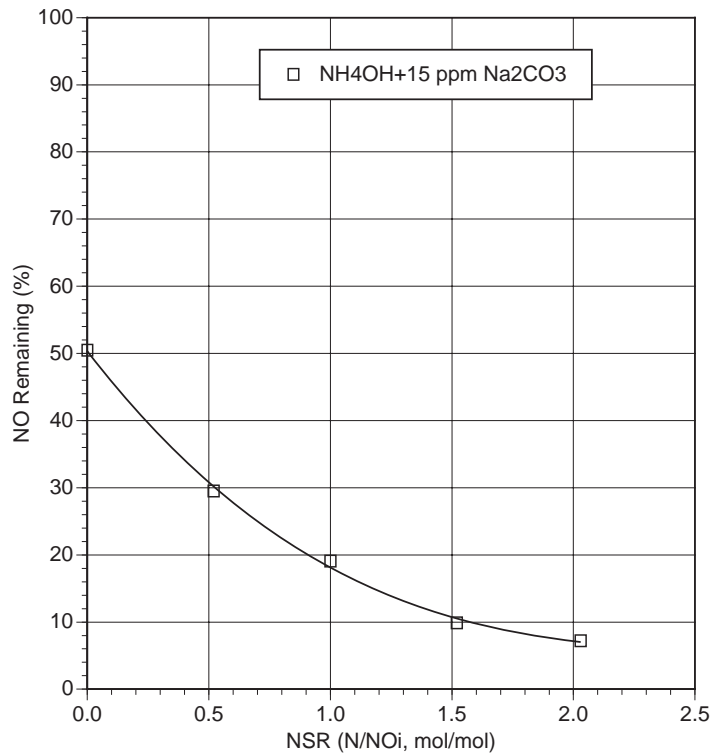


Figure 6.10 NO reduction vs. NSR for rich side injection of $\text{NH}_4\text{OH} + \text{Na}_2\text{CO}_3$.

6.5 Multiple Injection AR (MIAR)

In the MIAR process N-agents and promoters are injected both in the reburn zone and with the overfire air. CTT tests were conducted in which various combinations of rich and lean side additives were injected. Figure 6.11 shows MIAR results obtained with promoter added to the fuel rich zone. A maximum of 50% NO control was obtained by reburning alone. AR-Rich provided up to 67% NO control. Reburning plus both rich and lean side injection of aqueous ammonia with no promoter gave a maximum of 86% NO control. The best performance was obtained with reburning with rich side injection of N-agent plus promoter and lean side injection of N-agent alone. This system reduced NO emissions by over 90%. Reburning with rich side N-agent injection and lean side N-agent plus promoter injection also gave up to 90% NO control. Moreover, these systems were largely insensitive to injection temperature, with approximately 90% NO control obtained over the entire test range of 1380 to 1590 K.

Main Fuel: Natural gas @ 20 kW
 10% Reburn @ 1670 K, OFA @ 1300 K
 SR1=1.10, SR2=0.99, SR3=1.15
 NOi=600 ppm as meas
 First N-agent added in fuel rich zone: NSR=1.5
 Second N-agent added w/OFA: NSR=1.5
 Na₂CO₃ conc. in flue gas=15 ppm

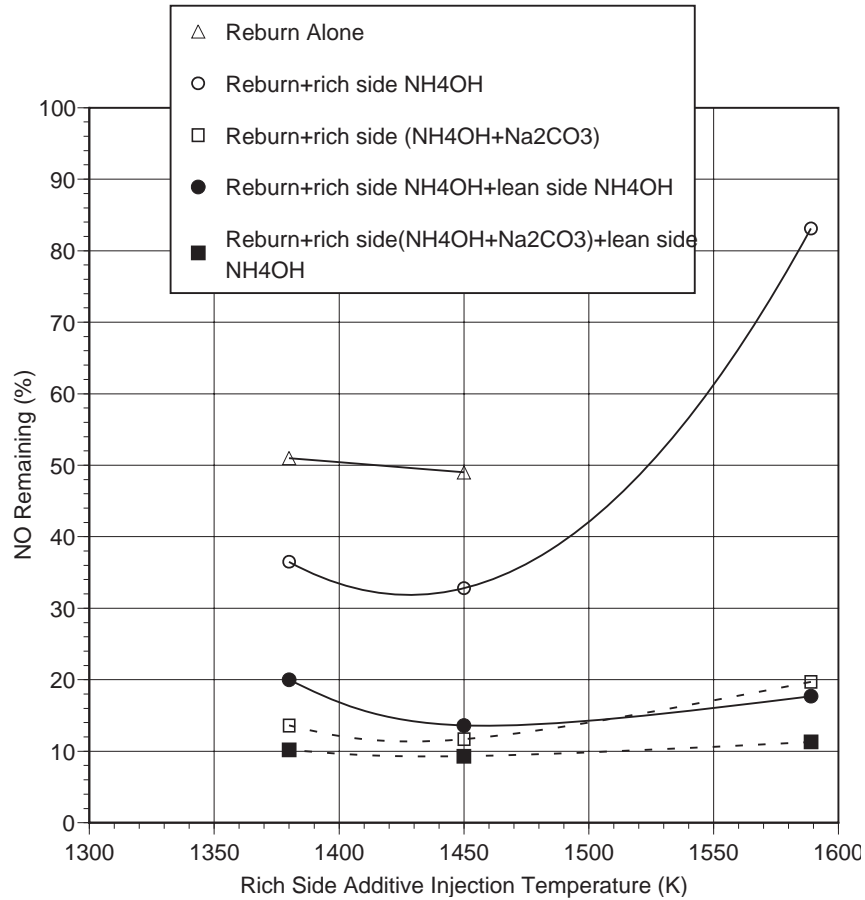


Figure 6.11 MIAR: NO reduction vs. additive injection temperature for reburn with both rich and lean side additives.

6.6 Bench Scale Combustion Tests: Conclusions

Under the closely-controlled process conditions obtained at the 20 kW combustion test facility, the following results were obtained:

1. Reburning alone achieved 50-60% NO reduction with SR₂=0.99-0.90 and high OFA injection temperature.

2. Promoted AR-Lean provided up to 86% NO reduction at 10% reburning heat input and 15 ppm Na₂CO₃ in the flue gas.
3. Promoted AR-Rich provided up to 88% NO reduction at 10% reburning heat input and 15 ppm Na₂CO₃ in the flue gas.
4. MIAR provided up to 91% NO removal, which is expected to increase at larger scale since the injectors will not affect the temperature profile.

7.0 PILOT SCALE DEVELOPMENT TESTS

Pilot scale tests were performed to build upon the bench scale results in a test facility more closely simulating the combustion conditions found in a full scale boiler. The test facility was first configured to match the residence time-temperature profile of a typical boiler, and then SGAR performance tests were conducted with both natural gas and coal as primary fuels. A series of sampling test runs was also performed to determine if the SGAR technologies caused concentrations of any byproduct species to increase.

7.1 Preparation of Pilot Scale Combustion Facility

The pilot scale test work was conducted in EER's Boiler Simulation Facility (BSF), which has a full load firing capacity of 300 kW (1 MMBtu/hr). The BSF is designed to provide an accurate subscale simulation of the flue gas temperatures and composition found in a full scale boiler. Prior to the tests the BSF was configured to provide access for all required reburn, additive, and overfire air injectors.

7.1.1 Boiler Simulator Facility

A schematic of the BSF is shown in Figure 7.1. The furnace is designed with a high degree of flexibility to produce combustion conditions typical of full scale utility boilers. The BSF consists of a burner, vertically down-fired radiant furnace, horizontal convective pass, and baghouse. A variable swirl diffusion burner with an axial fuel injector is used to simulate the approximate temperature and gas composition of a commercial burner in a full scale boiler. Primary air is injected axially, while the secondary air stream is injected radially through the swirl vanes to provide controlled fuel/air mixing. The swirl number can be controlled by adjusting the angle of the swirl vanes. Numerous ports located along the axis of the facility allow supplementary equipment such as reburn injectors, additive injectors, overfire air injectors, and sampling probes to be placed in the furnace.

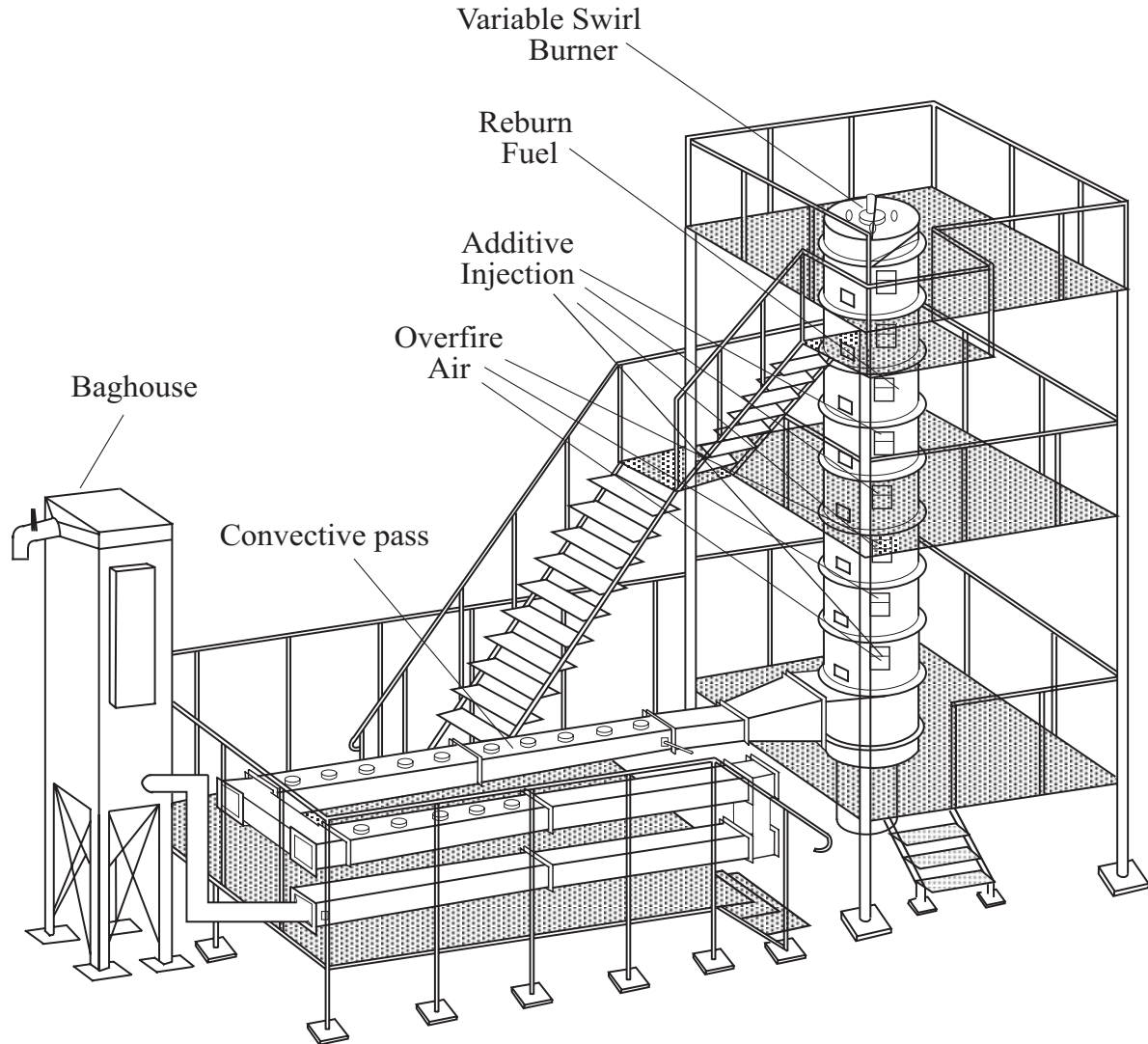


Figure 7.1 Boiler Simulator Facility (BSF).

The cylindrical furnace section is constructed of eight modular refractory lined sections with an inside diameter of 22 inches. The convective pass is also refractory lined, and contains air cooled tube bundles to simulate the superheater and reheater sections of a utility boiler. Heat extraction in the radiant furnace and convective pass can be controlled such that the residence time-temperature profile matches that of a typical full scale boiler. A suction pyrometer is used to measure furnace temperatures. Figure 7.2 shows the BSF temperature profile during natural gas firing with 10% reburning. Furnace temperatures are similar during coal firing.

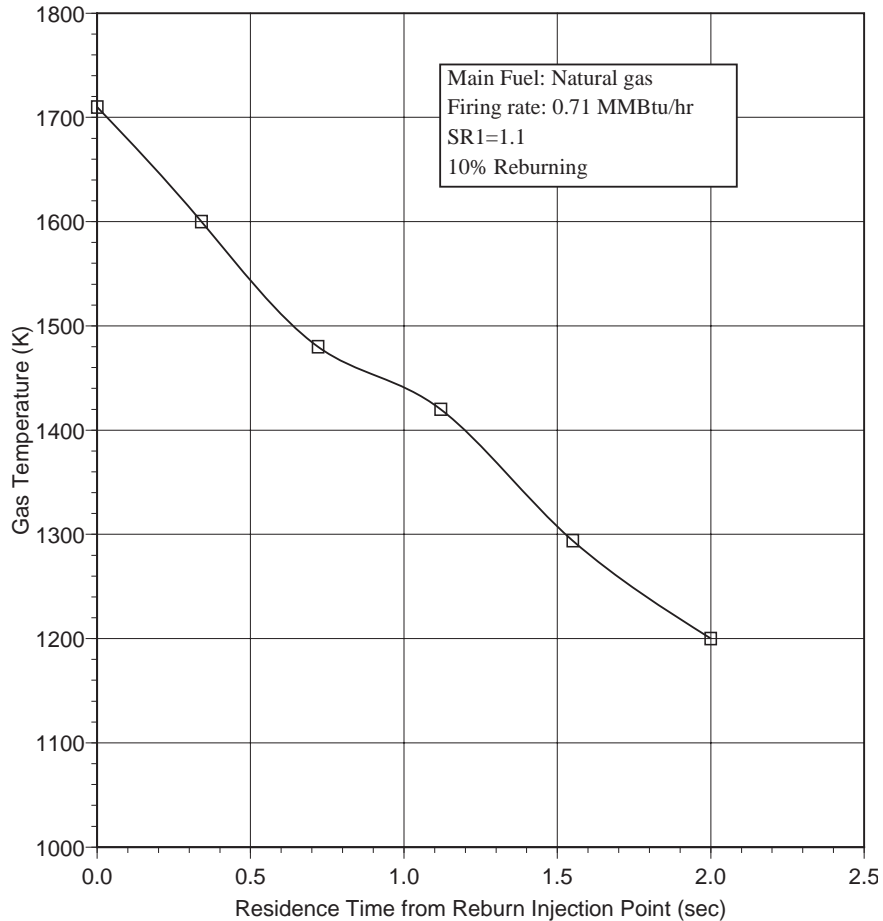


Figure 7.2 BSF temperature profile during 10% reburning.

Test fuels included natural gas and pulverized coal. Municipal natural gas was used, and was delivered by means of line pressure. Two test coals were employed, including a low sulfur bituminous Utah coal and a high sulfur bituminous Illinois coal. Each coal was pulverized such that 70% passed through a 200 mesh screen. Coal was metered using a twin screw feeder and was pneumatically transported to the burner.

7.1.2 Reburning and Additive Injection Systems

Natural gas was used as the reburn fuel. The reburn injector was elbow-shaped, and was installed along the centerline of the furnace, aligned in the direction of gas flow. A gaseous transport medium was added along with the reburn natural gas to provide sufficient momentum for good mixing with the furnace gas. Both air and bottled nitrogen were tested as transport media. Overfire air was injected through an elbow-shaped injector to burn out combustibles generated in the reburn zone. The OFA injection temperature was varied as required by the test plan.

Nitrogen agents and sodium promoters were injected as aqueous solutions. Twin fluid atomizers made by Delavan Corp. were used, employing both air and nitrogen as transport media. The additives were injected into the reburn zone and/or with the OFA. In the latter case, the OFA itself was used as the atomization medium.

7.1.3 Sampling and Analysis Methods

A continuous emissions monitoring system (CEMS) was used for on-line flue gas analysis. CEMS equipment and analyzers were identical to those for the bench scale tests, as described in Section 6.1. Manual method sampling was also performed for the following byproduct species:

- NH_3 and HCN: EPA Draft Method 206 with ion chromatography analysis
- SO_3 : controlled condensation
- Fly ash mass loading, size distribution, PM10, and PM2.5: EPA Method 5 and cascade impactors
- Carbon in ash: Extractive ash sampling with induction furnace analysis

7.2 Pilot Scale Combustion Tests with Natural Gas Firing

In the initial pilot scale tests, natural gas was used as the main and reburning fuel. The initial NO concentration, 600 ppm, was established by addition of ammonia to primary natural gas. The reburning fuel (10% of total heat input) provided slightly fuel-rich conditions in the reburn zone with $\text{SR}_2=0.99$. Processes characterized included promoted AR-Lean, promoted AR-Rich, hybrid AR-Lean/SNCR, hybrid AR-Rich/SNCR, and MIAR.

7.2.1 Promoted AR-Lean

AR-Lean includes the addition of reburning fuel followed by injection of OFA along with an N-agent. The N-agent can be injected with or without promoter which is dissolved in the aqueous N-agent solution. In all tests, the amount of N-agent corresponded to $\text{NSR}=1.5$.

Figures 7.3 and 7.4 demonstrate the performance of the AR-Lean process for injection of urea and aqueous ammonia, respectively. Reburning alone gave about 50% NO reduction, and depended slightly on the OFA injection location. At OFA injection temperatures of 1140 and 1530 K, NO was reduced by 52 and 47%, respectively. Injection of urea with OFA provided 53-82% NO reduction depending on the injection temperature. The performance of ammonia was slightly lower, i.e. 45-

81%. At an injection location of 1330 K, urea gave 78% NO reduction, while ammonia only 70%. The results with ammonia injection are qualitatively consistent with modeling (Section 8) taking into account the fact that ammonia appears in the gas mixture with a short delay time that is necessary for evaporation of the solution. Addition of sodium carbonate to the N-agent greatly improved NO reduction. Performance was about equal for ammonia and urea, in the range of 54-94% with optimum performance obtained between 1200 and 1370 K. These data are in agreement with the CTT results, although slightly higher NO reduction (by about 2-5 percentage points) was obtained in the BSE. As in the CTT tests, there is almost no difference in NO reduction between injection of 30 and 50 ppm Na.

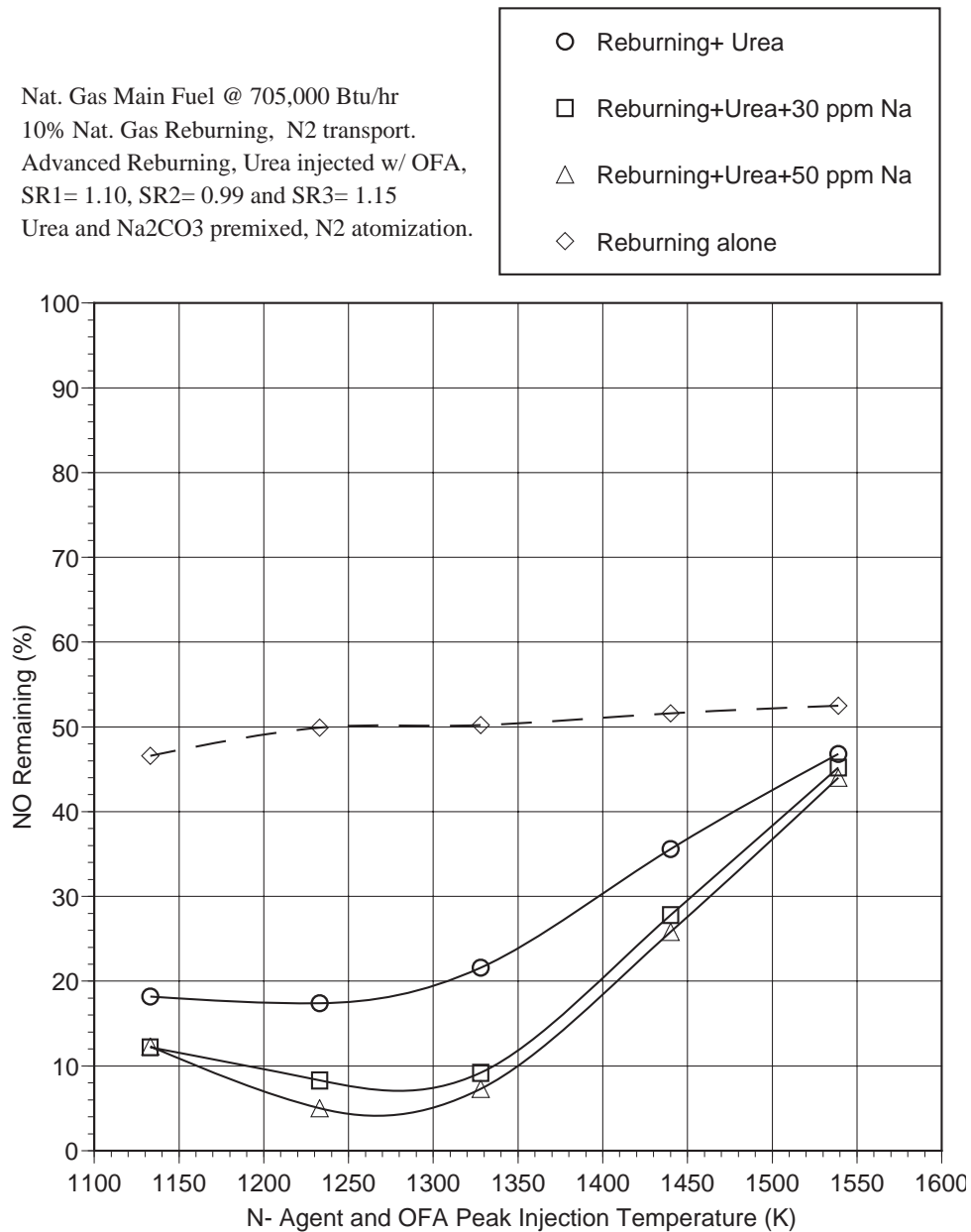


Figure 7.3 AR-Lean with aqueous urea/sodium injection.

Nat. Gas Main Fuel @ 705,000 Btu/hr
 10% Nat. Gas Reburning, N2 transport.
 Advanced Reburn, NH4OH injected w/ OFA,
 SR1= 1.10, SR2= 0.99 and SR3= 1.15
 NH4OH & Na2CO3 premixed, N2 atomization.

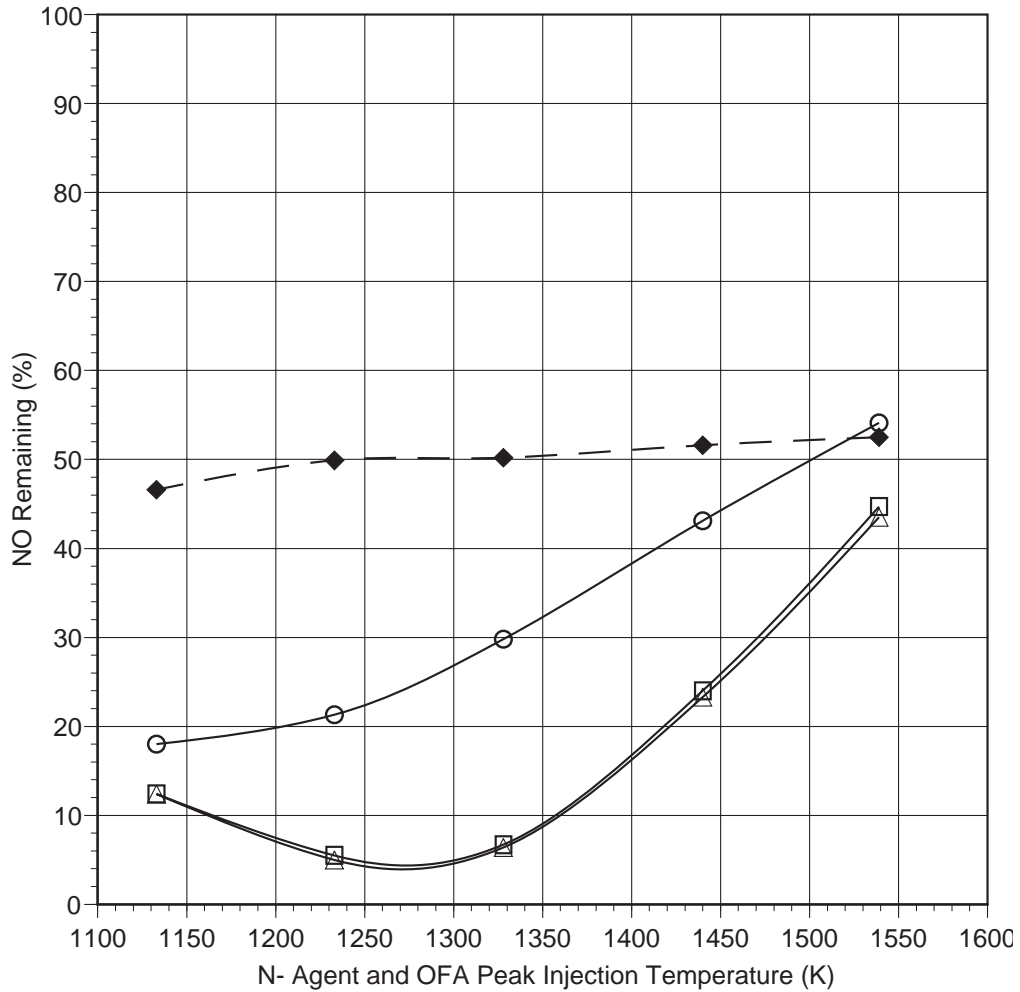
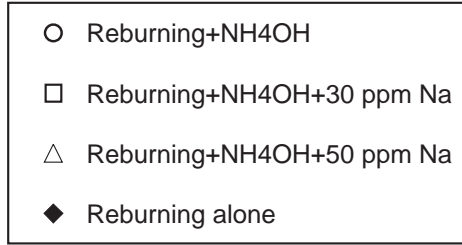


Figure 7.4 AR-Lean with aqueous ammonia/sodium injection.

Interestingly, the presence of small sodium amounts (30-50 ppm) affected CO emissions at low OFA injection temperatures. Without sodium, CO emissions were 20-60 ppm when OFA and N-agent were injected at 1230 K, and 100-120 ppm at 1130 K. In the presence of sodium, CO emissions were 60-100 ppm at 1230 K, and 120-320 ppm at 1130 K. At OFA injection temperatures higher than 1230 K, CO emissions were 20-30 ppm even in the presence of sodium. Thus, the optimum OFA/N-agent injection temperature is about 1260-1370 K. At these temperatures, NO can be reduced by 89-94% without increasing CO emissions.

7.2.2 Promoted AR-Rich

The AR-Rich process includes injection of reburning fuel, injection of N-agent into the reburning zone, and injection of OFA. The N-agent can be injected with or without promoter which is, as in AR-Lean, dissolved in an aqueous solution of the N-agent. In all tests the amount of N-agent corresponded to NSR=1.5.

The performance of AR-Rich greatly depends on the OFA injection temperature. Figures 7.5 and 7.6 show experimental results obtained with injection of urea and aqueous ammonia, respectively, for OFA injection at 1180 K. Each reagent provided 70-77% NO reduction, depending on injection temperature. However, addition of sodium carbonate at 30-50 ppm Na significantly improved NO reduction, up to 94-95%. Again, the reduction of NO in the BSF was a few percentage points better than that in the bench scale CTT.

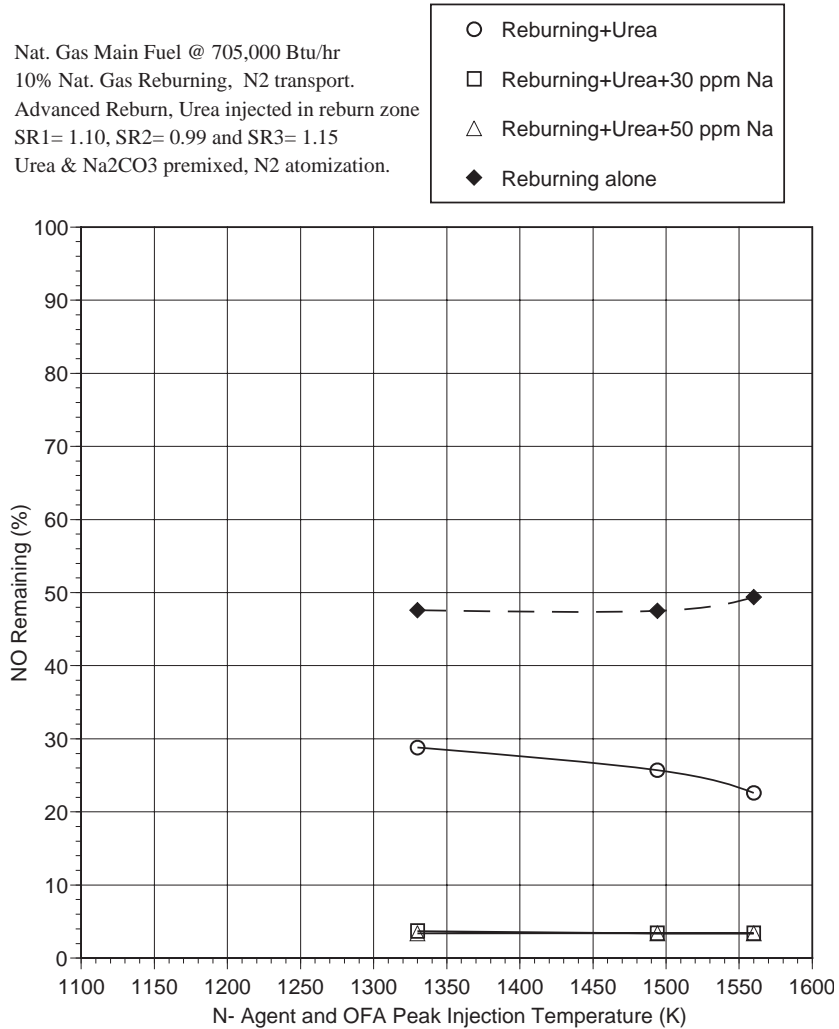


Figure 7.5 AR-Rich with urea/sodium injection. OFA is injected at 1180 K.

Nat. Gas Main Fuel @ 705,000 Btu/hr
 10% Nat. Gas Reburning, N2 transport.
 Advanced Reburn, NH4OH injected in reburn zone
 SR1= 1.10, SR2= 0.99 and SR3= 1.15
 NH4OH & Na2CO3 premixed, N2 atomization.

- Reburning+ NH4OH
- Reburning+NH4OH+30 ppm Na
- △ Reburning+NH4OH+50 ppm Na
- ◆ Reburning alone

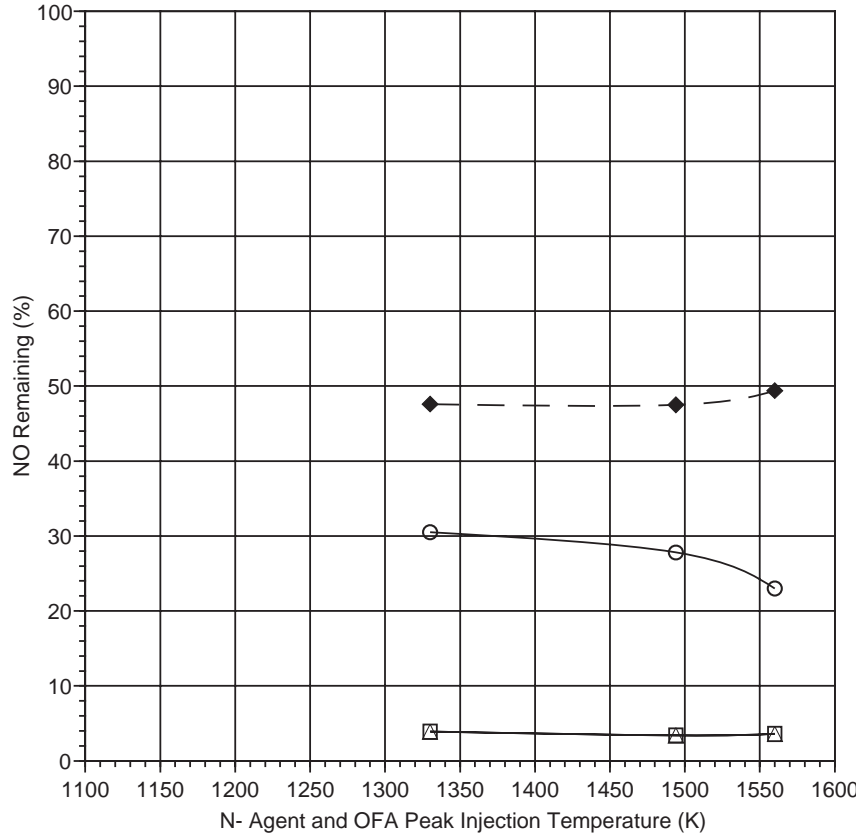
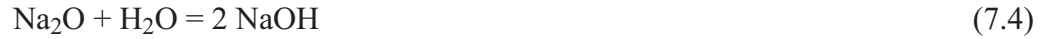


Figure 7.6 AR-Rich with ammonia/sodium injection. OFA is injected at 1180 K.

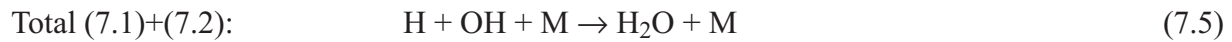
Surprisingly, injection of 30-50 ppm sodium resulted in much higher CO emissions (at low OFA injection temperatures) than in the AR-Lean process. Without sodium, CO emissions were within 10-25 ppm, but injection of sodium caused greater than 2500 ppm CO emissions. This effect (higher CO emissions after injection of sodium under fuel rich conditions) was noticed earlier in the CTT tests, but measurement accuracy was considered to be questionable. In the BSF tests, CO measurements were carefully checked and repeated. High CO emissions show that in the presence of sodium the process of CO oxidation is inhibited. This inhibition effect is stronger under fuel rich conditions. A possible explanation of this effect is the existence of the chain reaction involving sodium compounds, H atoms and OH radicals:



Sodium hydroxide, NaOH, can be formed via thermal decomposition of sodium carbonate followed by the reaction of sodium oxide with water vapor that is available in flue gas:



Then, NaOH reacts with H atoms via reaction (7.1) to form Na atoms and H₂O molecules. The Na atoms can then recombine with OH radicals to return NaOH (7.2). The total reaction (7.1)+(7.2) is just H and OH recombination into water:



Thus, under certain conditions, the total amount of H and OH radicals can be reduced, due to the presence of sodium compounds. As a result, CO can escape oxidation, since the main reaction of CO oxidation is the interaction with hydroxyl radicals:



Under fuel rich conditions, the total amount of radicals is typically lower than under fuel lean conditions. Therefore, this mechanism of radicals suppression can be more important under fuel rich conditions. The experimental effort at the University of Texas (Section 5) and the modeling study (Section 8) were conducted to model and better understand the reactions of Na in flue gas. A preliminary reaction mechanism with Na reactions was selected and is presented in Section 8.

Similar to AR-Lean, increasing the OFA temperature during AR-Rich can decrease CO emissions in the presence of sodium. AR-Rich tests were conducted with two higher OFA temperatures: 1380 and 1510 K. Figures 7.7 and 7.8 present the results. Injection of 20 g/min water in the reburning zone did not change NO reduction. When urea was added, 60-70% NO reduction was achieved. Sodium promoted the reaction up to 80-90% NO reduction, i.e. 10-20% NO remaining. CO emissions were also found to decrease to near baseline levels at these high OFA temperatures.

Main Fuel: Nat. gas @ 705,000 Btu/hr
 10% Reburn @ 1710 K, N2 transport
 SR1 = 1.10, SR2 = 0.99, SR3 = 1.15
 NOi = 600 ppm as measured
 OFA Temperature = 1380 K
 Na2CO3 Concentration = 15 ppm
 NSR = 1.5

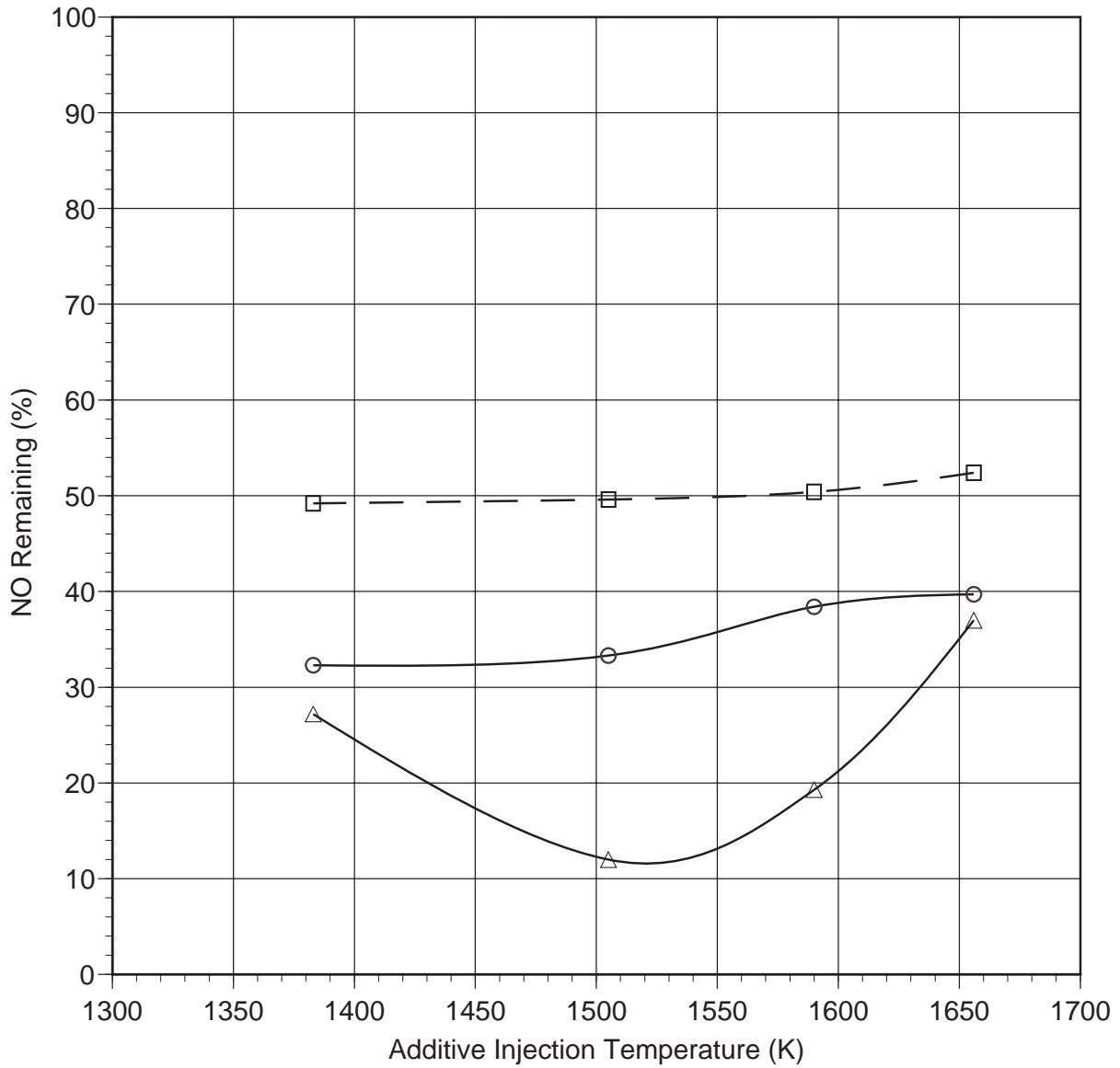
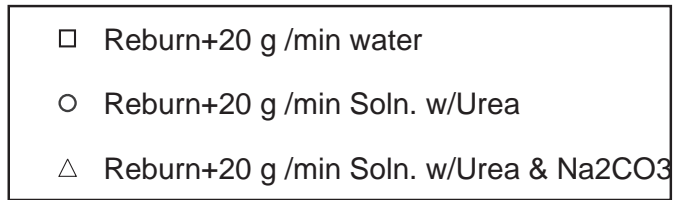


Figure 7.7 AR-Rich with urea/sodium injection. OFA is injected at 1380 K.

Main Fuel: Nat. gas @ 705,000 Btu/hr
 10% Reburn @ 1710 K, N2 transport
 SR1 = 1.10, SR2 = 0.99, SR3 = 1.15
 NO_i = 600 ppm as measured
 OFA Temperature = 1380 K
 Na₂CO₃ Concentration = 15 ppm
 NSR = 1.5

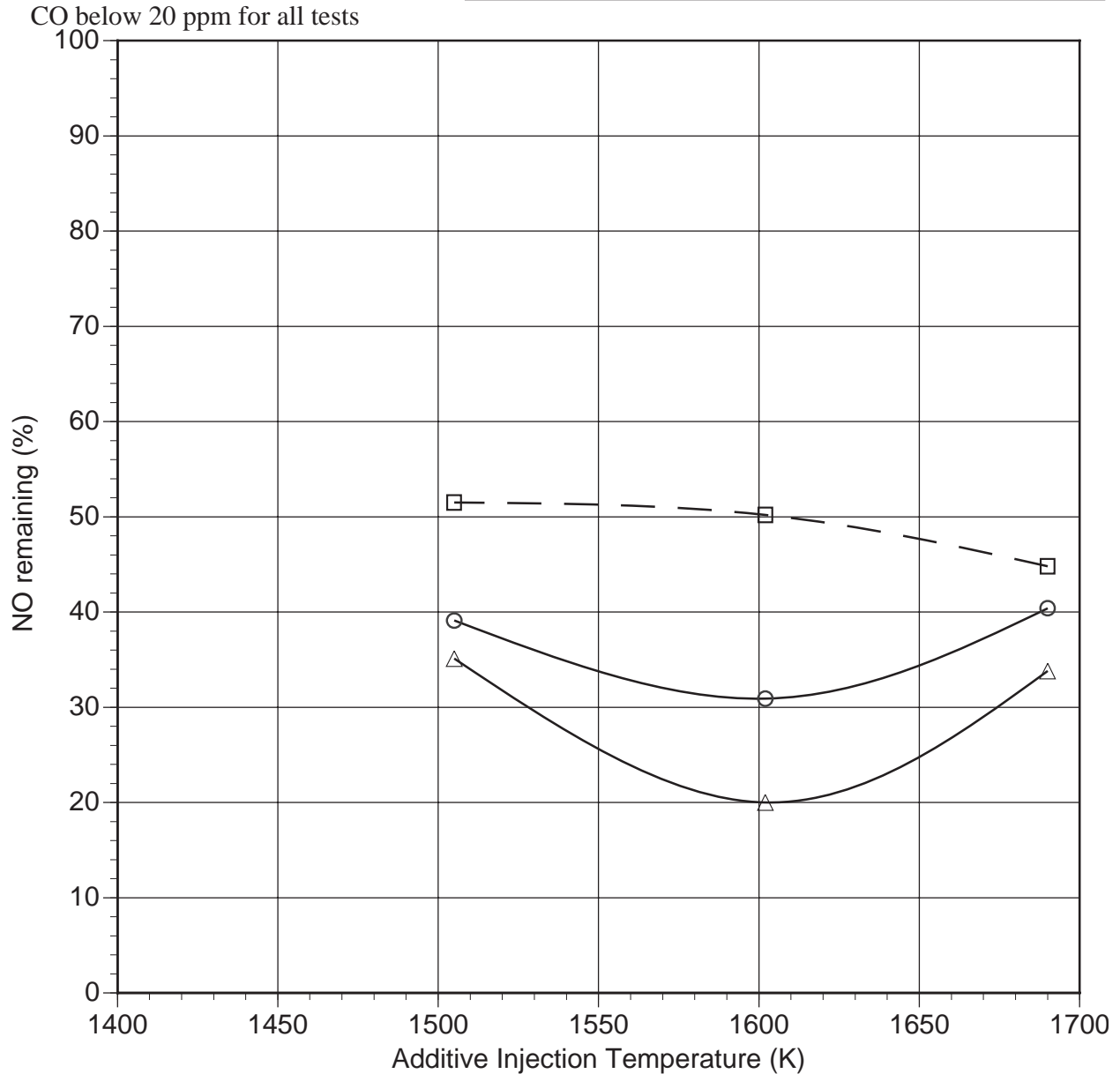
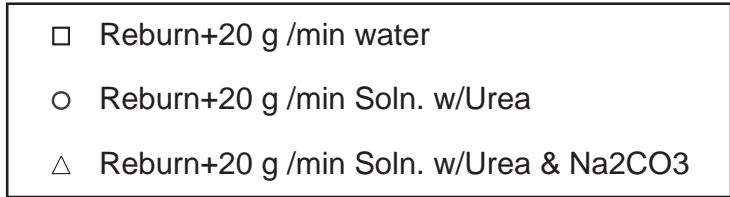


Figure 7.8 AR-Rich with urea/sodium injection. OFA is injected at 1510 K.

Figure 7.9 demonstrates the impact of sodium concentration on NO reduction for AR-Rich. In these tests, urea and sodium were injected at 1520 K and OFA at 1320 K. Increasing Na concentration

from 0 to 55 ppm resulted in improvement of NO reduction from 76 to 90%. However, the CO emissions increased from 20 ppm at Na=0 to 65 ppm at Na=22 ppm and to 500 ppm at Na=55 ppm. Thus, injection of sodium with a N-agent in the reburn zone requires a temperature of OFA injection higher than 1320 K to prevent CO formation. This result demonstrates the importance of sodium chemistry in NO control via reburning.

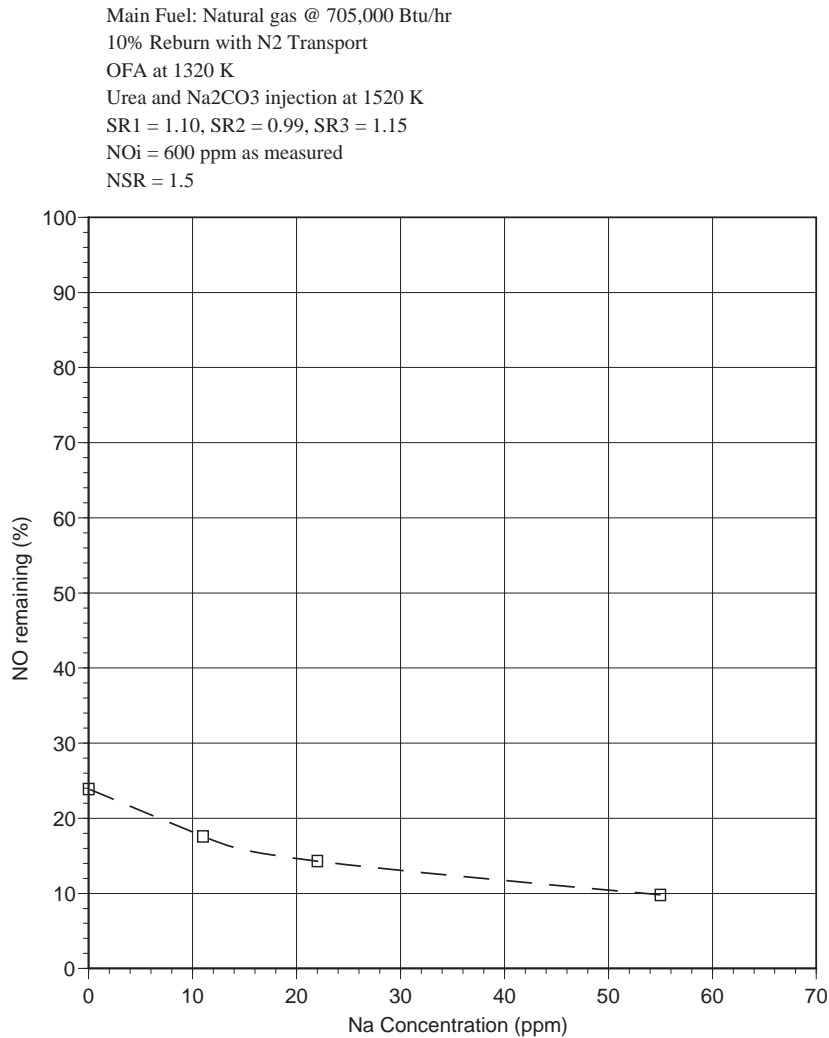


Figure 7.9 Effect of sodium on NO reduction in AR-Rich.

7.2.3 Hybrid AR-Lean/SNCR

Combined AR-Lean/SNCR tests were then conducted at the BSF. In these tests, the reburning fuel was injected at 1640 K and N-agent (aqueous ammonia or urea) was added with the OFA at 1370 K. Then, a second N-agent was injected under fuel lean conditions at 1160 K. Concentration of each N-agent corresponded to NSR=1.5. NO reduction was measured with and without addition of sodium

carbonate to each N-agent. The concentration of sodium was 100 ppm for each sodium carbonate addition. Figure 7.10 presents the results for the urea tests. Performance with urea was somewhat greater than that with ammonia.

Primary Fuel: Nat. gas @ 705,000 Btu/hr
 10.2% Natural Gas reburning
 SR1=1.10, SR2= 0.99, SR3= 1.15
 Location #1 is at 1370 K w/OFA, NSR=1.5
 Location #2 is at 1160 K, NSR=1.5
 Na₂CO₃ Promoter, 100 ppm Na

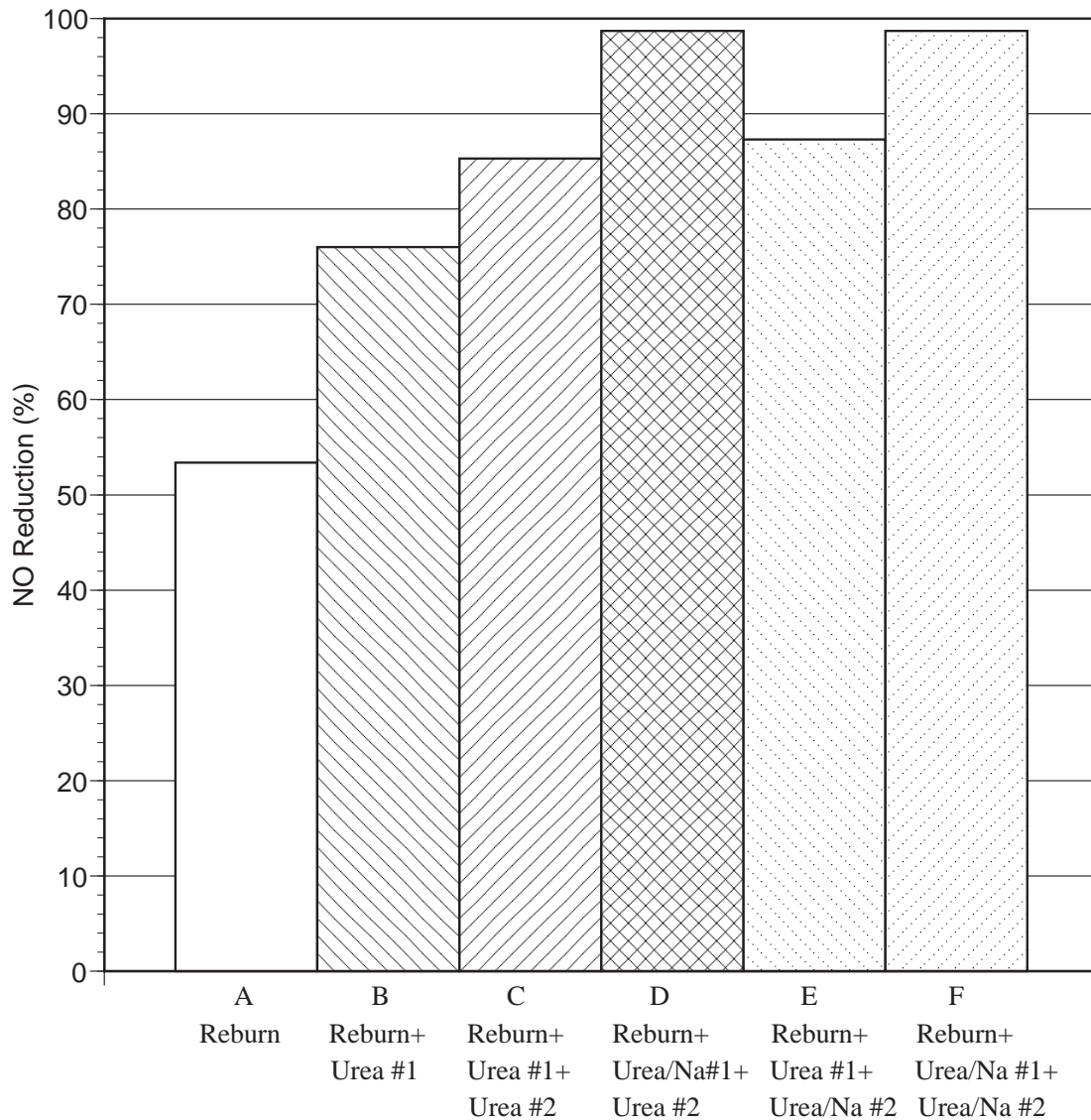


Figure 7.10 NO reduction during natural gas firing by combined AR-Lean/SNCR with urea injection at two locations.

Reburning alone (bar A) gave 53% NO reduction. Injection of urea with OFA, i.e. AR-Lean resulted in 76% NO removal, bar B. Injection of a second N-agent increased the NO_x control to 85%, bar C. The best result was achieved when sodium was injected with the first N-agent, bar D, for which NO removal increased from 85 to above 98%. Addition of sodium to the second N-agent was not effective, (see bars E and F). There is almost no difference in NO reduction for bars C and E, as well as for bars D and F. This would appear to imply that it is necessary to add the promoter with the high temperature N-agent for optimum performance.

7.2.4 MIAR

MIAR tests were conducted with natural gas as both the main and reburn fuels. N-agents and promoters were injected at rich and lean side locations. Rich and lean side additive injection temperatures and SR₂ were varied. In all tests urea was used as the N-agent and Na₂CO₃ was used as the promoter.

Tests were performed at SR₂ values of 0.99 (10% reburning) and 0.90 (18% reburning). In the first test series, rich side additive injection temperature was varied from 1370 to 1530 K, and lean side additives were injected along with the OFA at 1310 K. Figure 7.11 shows NO reduction as a function of rich side additive injection temperature at SR₂ = 0.99. The systems were fairly insensitive to temperature. Reburning alone gave 49% NO reduction. Reburning plus rich and lean side N-agents with no promoters gave 77 - 82% NO reduction. Addition of sodium promoter to the lean side additive improved NO reduction by about 4 percentage points at each temperature. When sodium promoter was added to the rich side N-agent, NO reduction increased to 95 - 97%. Addition of sodium to both N-agents also gave 95 - 97% NO reduction. These results indicate that for natural gas firing sodium is most effective when added to the rich side additive.

BSF, Firing Rate: 705,000 Btu/Hr
 Main Fuel: Nat.Gas, 10% Nat.Gas Reburn
 SR1=1.10, SR2=0.99 and SR3=1.15
 NOi=600 ppm @0%O2
 Rich side urea + Na2CO3 injection temperature varied
 Lean side urea + Na2CO3 injected w/OFA at 1310 K
 30 ppm Na

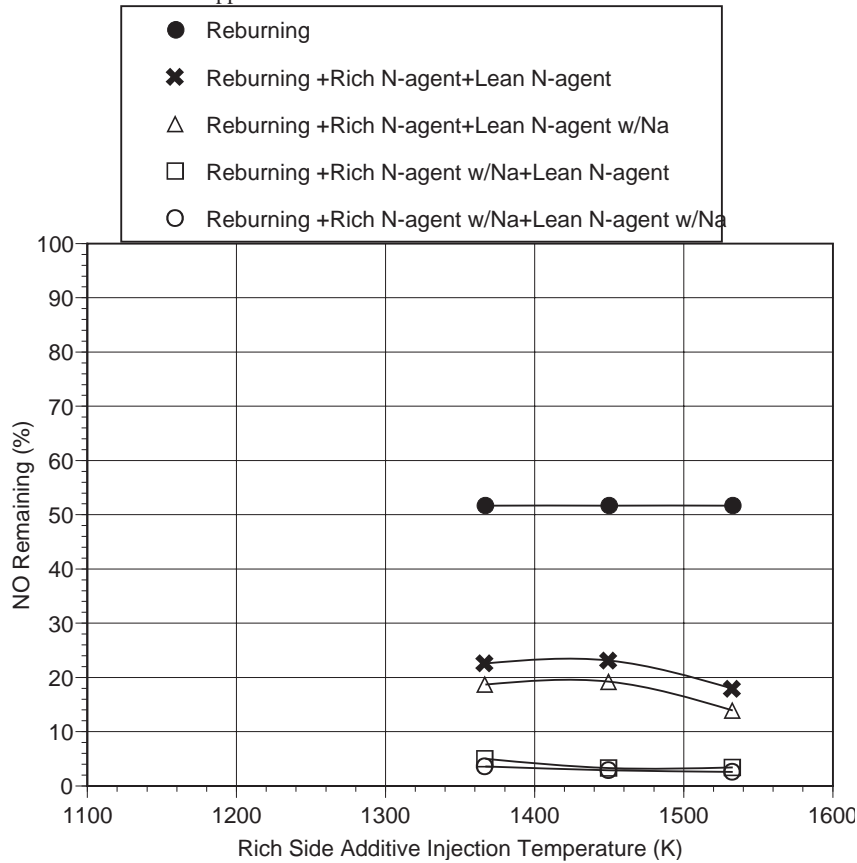


Figure 7.11 Effect of rich side additive injection temperature upon MIAR performance during natural gas firing at $SR_2 = 0.99$.

The promoters also demonstrated the ability to control N_2O emissions. When N-agents were injected without promoters, N_2O ranged from 80 ppm at 1370 K to 39 ppm at 1530 K. When sodium promoters were added with either N-agent, N_2O fell to near zero.

Figure 7.12 shows NO reduction as a function of rich side additive injection temperature at $SR_2 = 0.90$. Reburn alone provided 72% NO control. The N-agents provided limited additional NO control, and in some cases actually caused NO to increase. Sodium promoted addition improved performance, with the strongest effects seen when promoter was added in the rich zone. Maximum NO control was 90% at a rich side additive injection temperature of 1370 K. N_2O ranged from 13 to 32 ppm with N-agents but no promoter, and decreased to near zero when sodium was added.

BSF, Firing Rate: 705,000 Btu/Hr
 Main Fuel: Nat.Gas, 18% Nat.Gas Reburn
 SR1=1.10, SR2=0.90 and SR3=1.15
 NOi=600 ppm @0%O2
 Rich side urea + Na2CO3 injection temperature varied
 Lean side urea + Na2CO3 injected w/OFA at 1310 K
 30 ppm Na

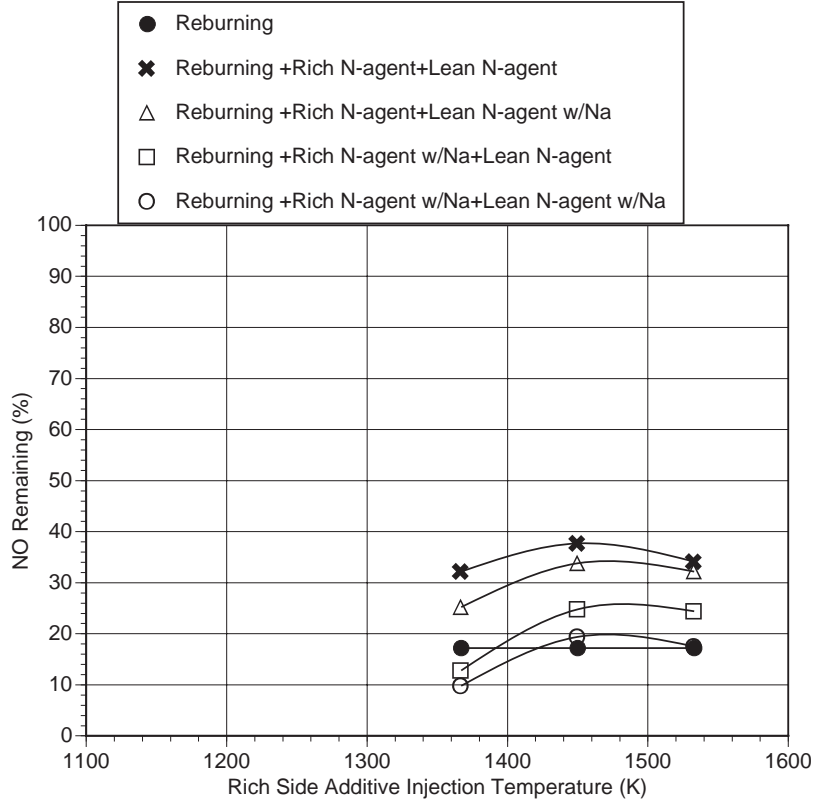


Figure 7.12 Effect of rich side additive injection temperature upon MIAR performance during natural gas firing at $SR_2 = 0.90$.

The test results indicate that optimum MIAR performance is obtained at $SR_2 = 0.99$ (10% reburning). This relatively low reburn heat input has several operational advantages. Specifically, the near-stoichiometric conditions serves to minimize high temperature boiler corrosion problems, and the low reburn heat input minimizes changes in boiler heat distribution and corresponding decreases in thermal efficiency.

7.3 Pilot Scale Combustion Tests with Coal Firing

Pilot scale tests were then conducted with coal as the primary fuel and natural gas as the reburning fuel. Both low sulfur Utah coal and high sulfur Illinois coal were tested. The initial NO concentration was 800-1000 ppm. Processes characterized included promoted AR-Lean, promoted AR-Rich, hybrid AR-Lean/SNCR, and MIAR. A series of byproduct sampling runs was also conducted while firing coal.

7.3.1 Promoted AR-Lean

In the first AR-Lean tests, low sulfur Utah coal was used as the main fuel and natural gas as the reburning fuel. Reburn fuel (10%) was injected at 1640 K, providing a reburn zone stoichiometry of 0.99. Aqueous urea and sodium carbonate were injected along with the OFA at varying temperatures. Figure 7.13 demonstrates that 55-60% NO reduction was achieved by 10% reburning alone. Performance strongly depended on the urea/OFA injection temperature. Injection of urea with the OFA had virtually no effect at high injection temperatures of 1480-1590 K. Under these conditions, emissions of CO were about 40 ppm without Na and 60 ppm in the presence of Na. At urea/OFA injection temperatures lower than 1480 K, NO is substantially reduced, by up to 90%. However, higher CO emissions were measured, i.e. 40-60 and 80-100 ppm CO in the absence and presence of sodium, respectively. The concentration of Na was varied from 0 to 200 ppm, equivalent to 0 to 100 ppm Na_2CO_3 in the flue gas. The effect of sodium on NO reduction was noticeable, 2-8 percentage points, but not as great as in the natural gas firing tests.

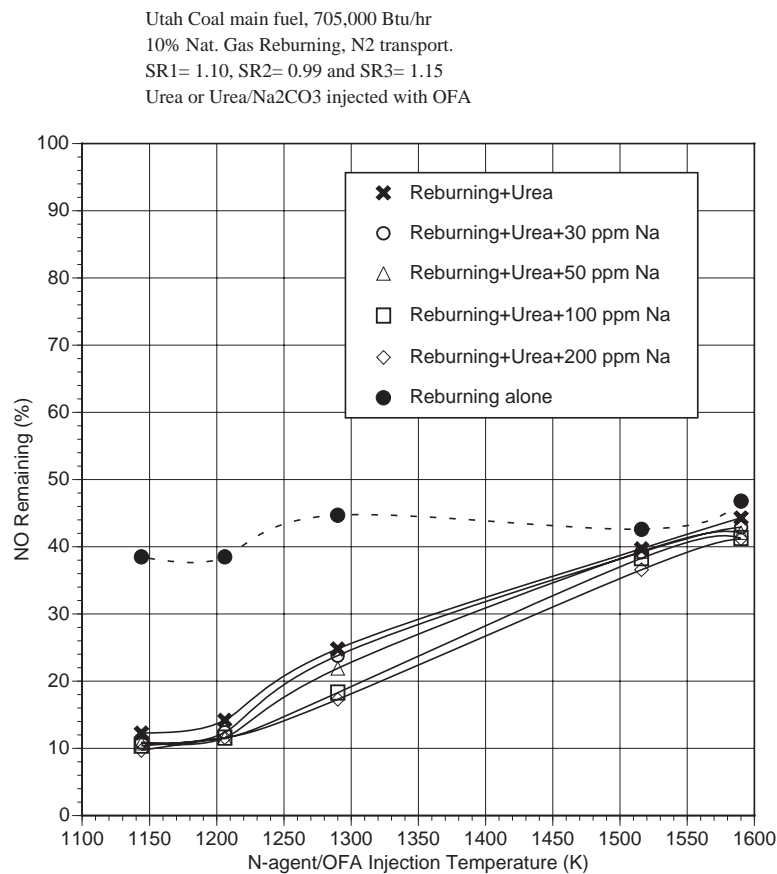


Figure 7.13 NO reduction by AR-Lean during coal firing.

Tests were then conducted with high sulfur Illinois coal as the primary fuel. Figure 7.14 shows NO reduction as a function of the N-agent/OFA injection temperature. Reburning alone gave 48% NO reduction. For both the promoted and unpromoted cases, optimum performance was obtained at 1310 K. Maximum NO reduction was 78% with no promoter and 84% with 150 ppm of Na. Sodium exhibited a greater promotional effect at the lower injection temperatures. Performance was slightly lower than that obtained with Utah coal, possibly because the higher SO₂ concentration generated by the Illinois coal partially deactivated the sodium promoter.

Firing Rate: 705,000 Btu/Hr
 Main Fuel : Illinois Coal
 9% Nat.Gas Reburn
 SR1=1.10, SR2=0.99, SR3=1.15
 NO level: 1000 ppm @0% O2 dry
 Additive co-injected with OFA, NSR=1.5

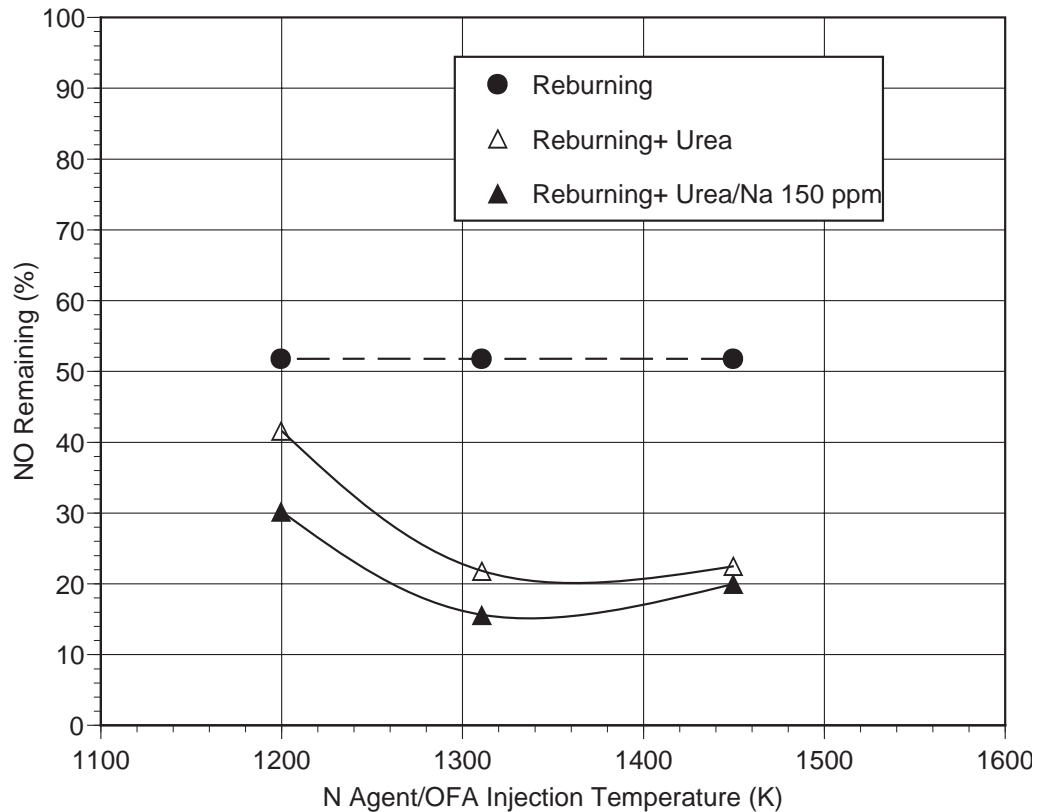


Figure 7.14 AR-Lean tests: Effect of N-agent/OFA injection temperature upon performance.

7.3.2 Promoted AR-Rich

Similar to natural gas firing, the performance of AR-Rich during coal firing depends strongly on the OFA injection temperature. Figures 7.15 and 7.16 demonstrate experimental results for injection

of OFA at 1170 and 1300 K, respectively. Utah coal was the main fuel. Urea (NSR=1.5) and different amounts of sodium (0-200 ppm) were injected at varying temperatures. Lower OFA injection temperature was found to provide better NO reduction. Reburning followed by urea injection in the reburn zone at different temperatures provided 78-88% NO control with OFA at 1170 K (Figure 7.13) and 70-77% NO control with OFA at 1300 K (Figure 7.15). With sodium addition, maximum NO reductions were 92% with OFA at 1170 K and 83% with OFA at 1300 K. The effect of sodium was less than for natural gas firing. A possible reason for this is interaction of sodium compounds with SO₂ and HCl in flue gas to form sodium sulfite, sodium sulfate or sodium chloride.

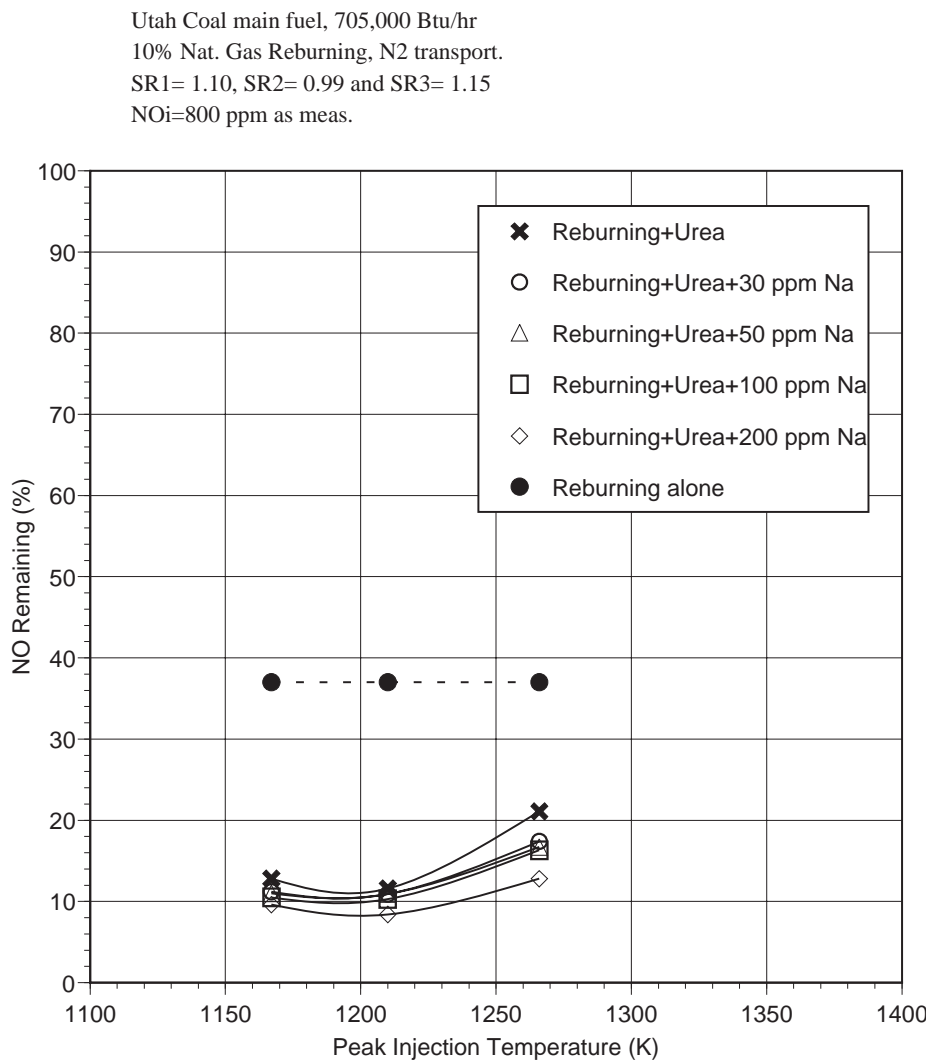


Figure 7.15 Effect of urea injection temperature and concentration of sodium on NO reduction in AR-Rich with coal firing. OFA injection temperature is 1170 K.

Utah Coal main fuel, 705,000 Btu/hr
 10% Nat. Gas Reburning, N2 transport.
 SR1= 1.10, SR2= 0.99 and SR3= 1.15
 NOi=800 ppm as meas.

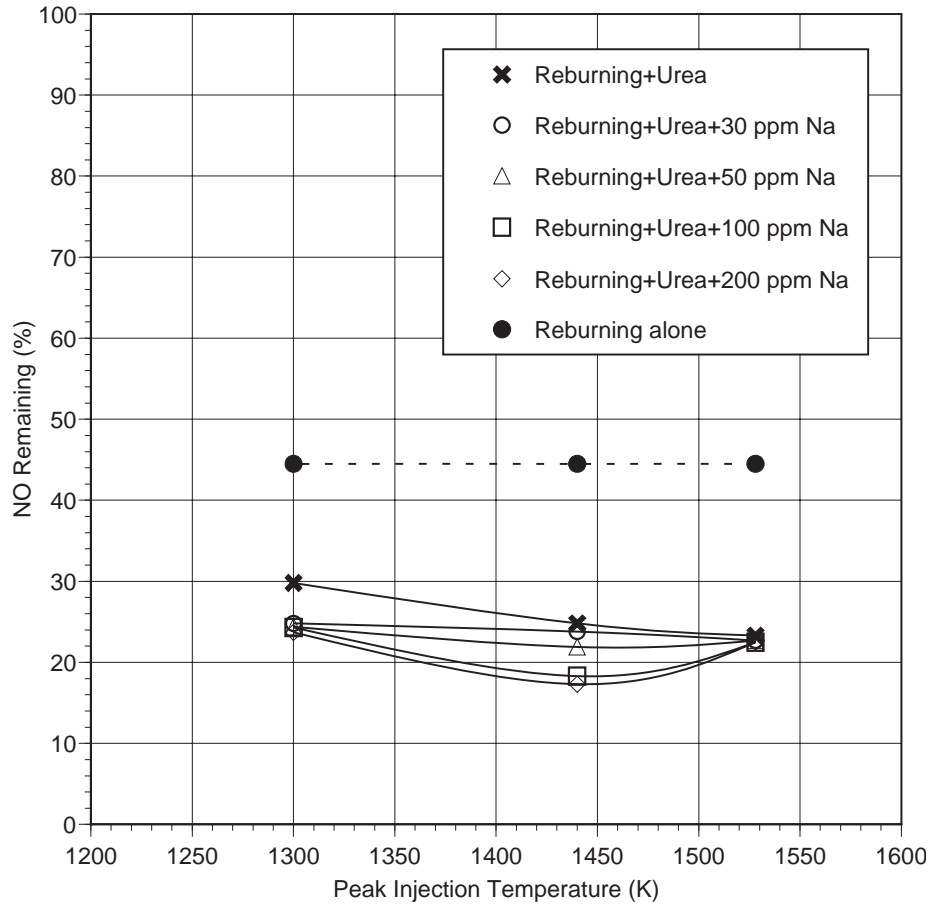


Figure 7.16 Effect of urea injection temperature and concentration of sodium on NO reduction in AR-Rich with coal firing. OFA injection temperature is 1300 K.

For injection of OFA at 1170 K, CO emissions were about 60 ppm without sodium and 100 ppm in the presence of sodium. Variation of the sodium concentration did not affect CO emissions. At an OFA injection temperature of 1300 K, CO emissions were about 40 and 60 ppm in the absence and in the presence of sodium, respectively.

AR-Rich tests were then conducted with high sulfur Illinois coal as the main fuel, with OFA added at 1310 K. Figure 7.17 shows NO reduction as a function of the N-agent injection temperature. Performance increased with decreasing injection temperature, with greatest NO reduction obtained at 1370 K. Maximum NO control was 86% with no promoter and 93% with 150 ppm sodium. The incremental benefit provided by the sodium promoter appeared to increase with decreasing temperature.

Firing Rate: 705,000 Btu/Hr
Main Fuel : Illinois Coal
9% Nat.Gas Reburn
SR1=1.10, SR2=0.99, SR3=1.15
NO level: 1000 ppm @0%O2 dry
OFA injected at 1310 K, NSR=1.5

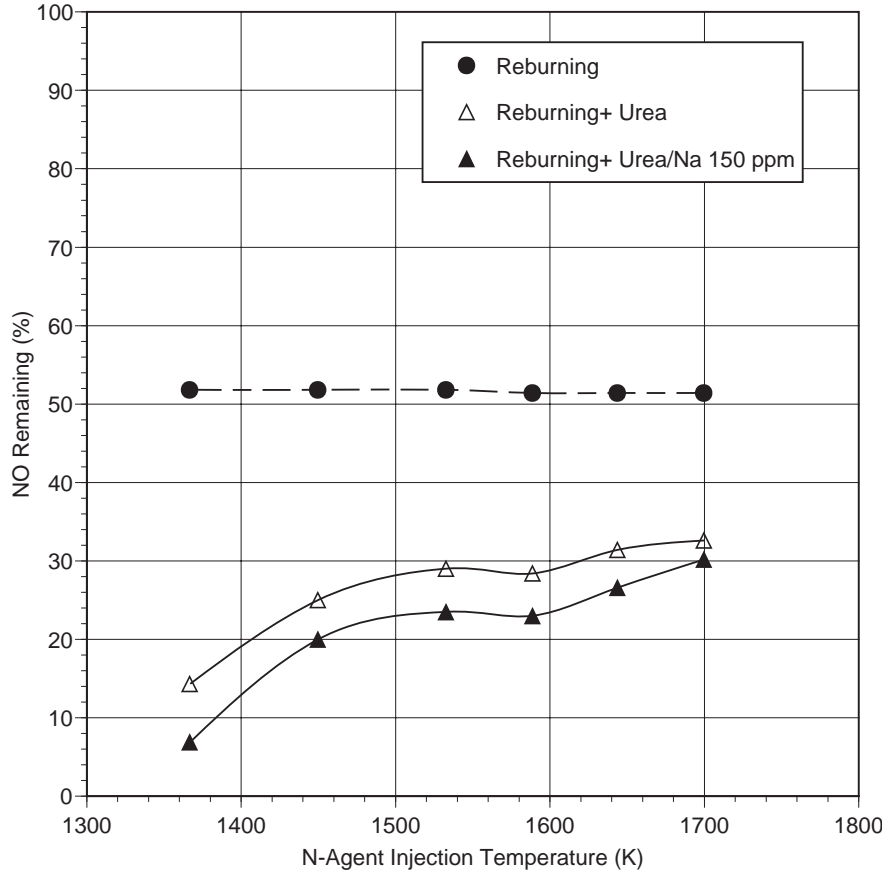


Figure 7.17 AR-Rich tests: Effect of N-agent injection temperature upon performance.

Illinois coal AR-Rich tests were then conducted in which the OFA injection temperature was varied, with the N-agent injection temperature held constant at 1530 K. This temperature is well above the optimum, but is of interest for boilers that have limited access at lower temperatures for liquid injectors. As shown in Figure 7.18, performance increased with decreasing OFA temperature. Sodium provided an incremental increase in NO reduction of about 6 percentage points at each temperature.

Firing Rate: 705,000 Btu/Hr
 Main Fuel : Illinois Coal
 9% Nat.Gas Reburn
 SR1=1.10, SR2=0.99, SR3=1.15
 NO level: 1000 ppm @0%O2 dry
 Additive injected at 1530 K, NSR=1.5

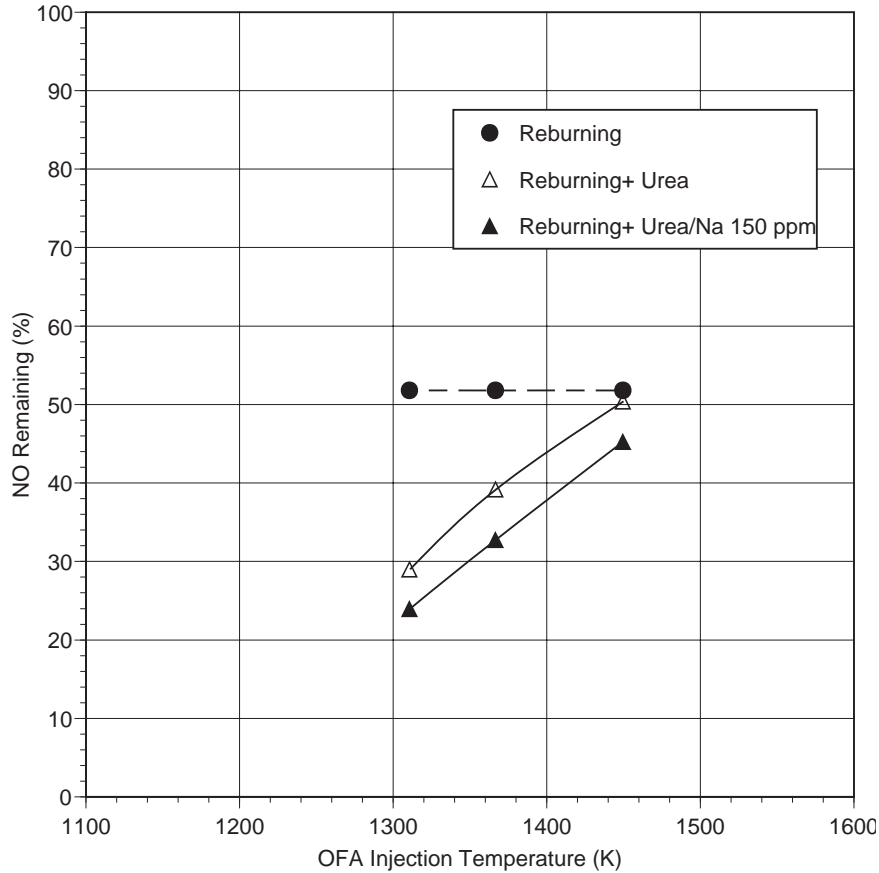


Figure 7.18 AR-Rich tests: Effect of OFA injection temperature upon performance.

Illinois coal AR-Rich tests were then conducted at high sodium concentrations to define the maximum achievable extent of NO reduction. Sodium promoter concentration was varied from 0 to 2000 ppm. Reburn zone SR was 0.99, additives were injected at 1450 K, and OFA was injected at 1370 K. As shown in Figure 7.19, NO reduction increased from 63% at 0 ppm sodium to 86% at 2000 ppm sodium. The main drawback of high sodium level is the potential for increased boiler fouling. A sodium concentration of 150 ppm was selected for most of the test work as a concentration providing significant promotion while being low enough to minimize fouling effects. As shown in Figure 7.19, this level of sodium addition can also provide a small degree of SO₂ control by reaction to form sodium sulfate.

Firing Rate: 705,000 Btu/Hr
 Main Fuel : Illinois Coal
 9% Nat.Gas Reburn
 SR1=1.10, SR2=0.99, SR3=1.15
 NO level: 1000 ppm @0%O2 dry
 Additive injected at 1450 K, OFA injected at 1370 K
 NSR=1.5

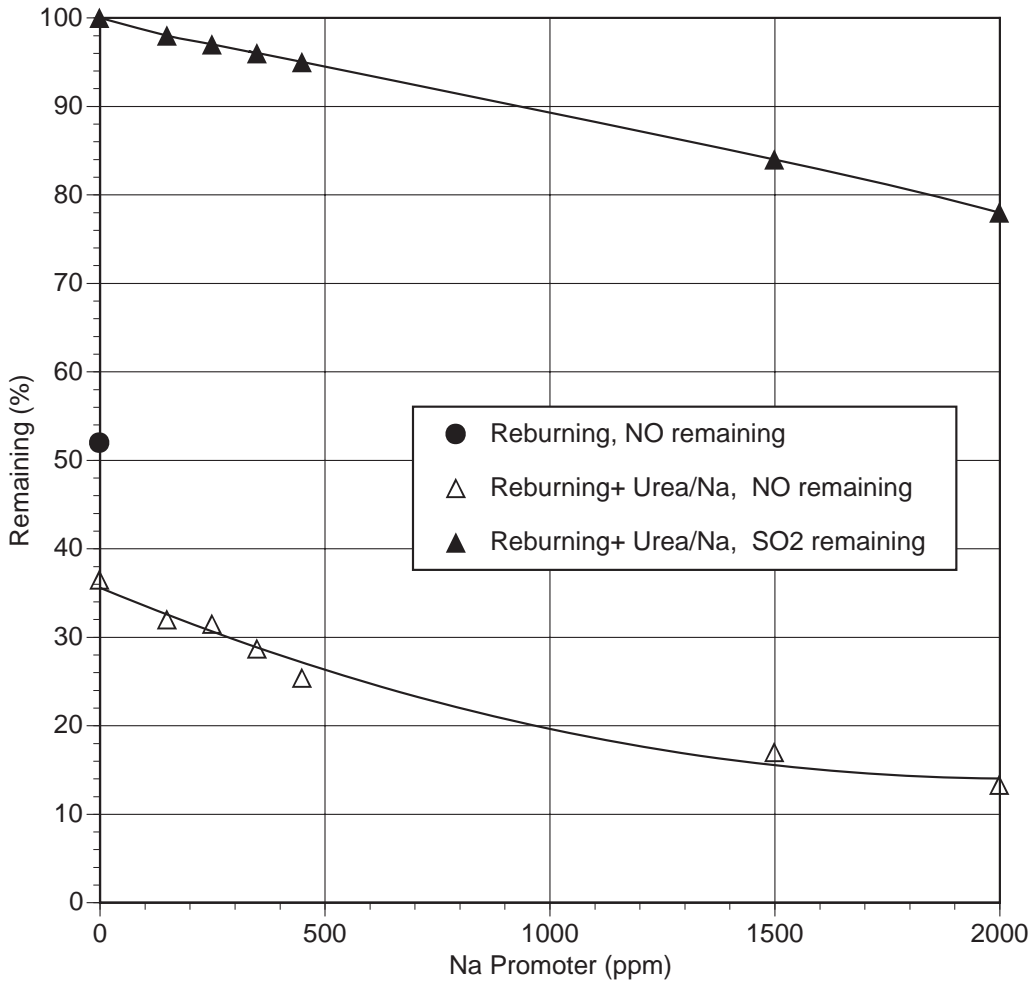


Figure 7.19 AR-Rich tests: Effect of sodium promoter concentration upon performance.

7.3.3 Hybrid AR-Lean/SNCR

Combined AR-Lean/SNCR tests were conducted with Utah coal as the main fuel. The conditions were similar to those for the natural gas tests: reburning fuel was injected at 1640 K, ammonia or urea was added at 1370 K, and 100 ppm Na was injected with each N-agent. NO reduction was measured with and without sodium. The second N-agent was injected under fuel lean conditions at 1200 K, a slightly higher temperature than in the natural gas firing tests. Figure 7.20 shows results for urea injection. Similar results were obtained with urea and ammonia.

Primary Fuel: Utah coal @ 705,000 Btu/hr
 10.2% Natural Gas reburning
 SR1=1.10, SR2= 0.99, SR3= 1.15
 Location #1 is at 1370 K w/OFA, NSR=1.5
 Location #2 is at 1200 K, NSR=1.5
 Na₂CO₃ Promoter, 100 ppm Na

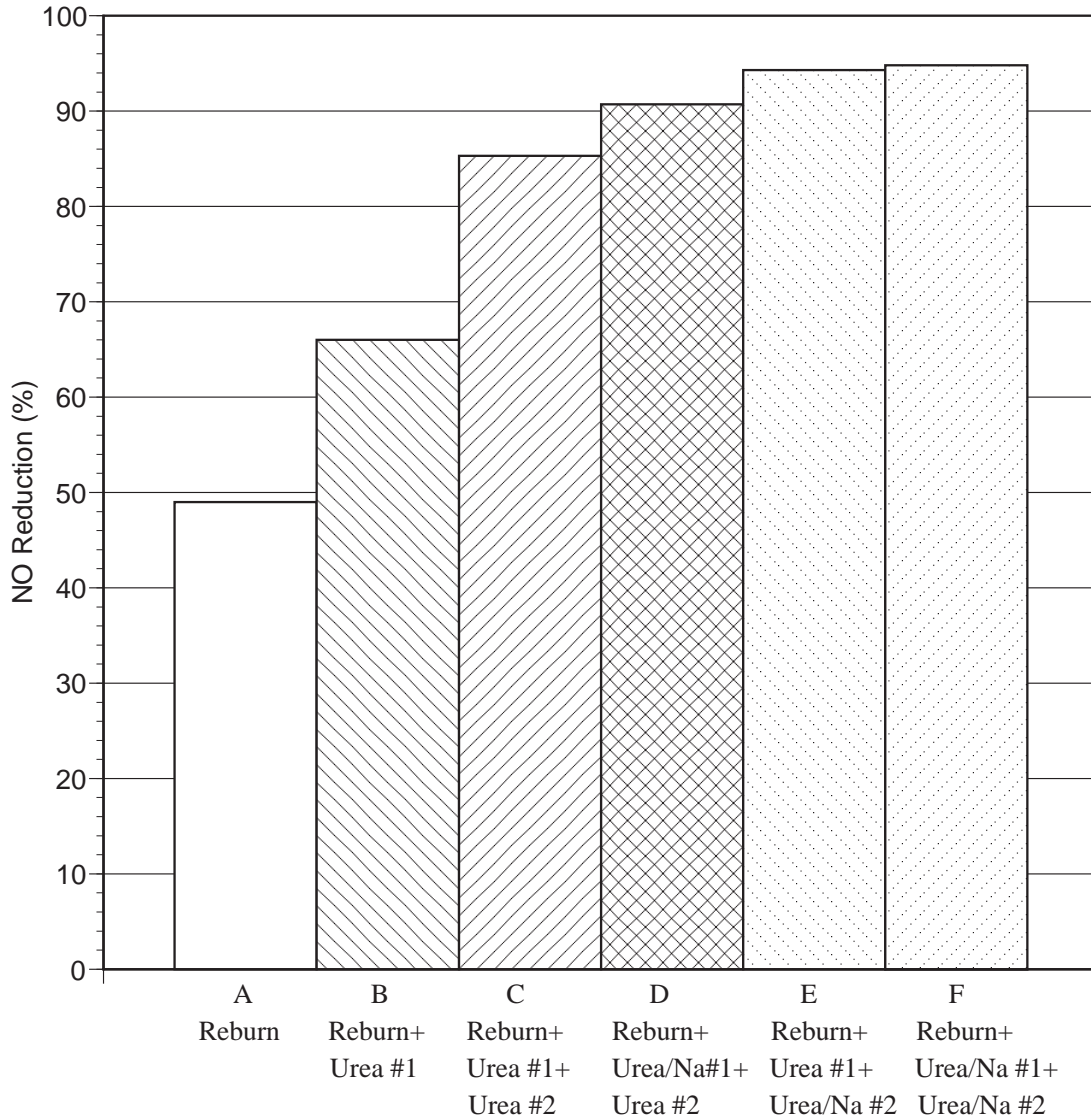


Figure 7.20 NO reduction during coal firing by combined AR-Lean/SNCR with urea injection at two locations.

It is of interest to compare the performance of the combined AR-Lean/SNCR process for natural gas and coal firing, as summarized in Table 7.1. Corresponding test conditions are shown in Figures 7.10 and 7.20 for gas and coal firing, respectively.

Table 7.1. Comparison of NO reduction (%) for hybrid AR-Lean/SNCR with gas and coal firing. Corresponding CO emissions in ppm are shown in parentheses.

Bar	Test Conditions	Natural Gas Firing		Coal Firing	
		Urea	Ammonia	Urea	Ammonia
A	10% Reburn @ 1640 K, OFA @ 1370 K	53(20)	53(20)	49(60)	49(60)
B	AR-Lean, OFA @ 1370 K	76(30)	58(30)	66(60)	62(60)
C	AR-Lean + SNCR	85(30)	73(30)	85(60)	84(60)
D	AR-Lean/Na + SNCR	98(190)	96(180)	91(60)	90(60)
E	AR-Lean + SNCR/Na	87(30)	78(30)	94(60)	93(60)
F	AR-Lean/Na + SNCR/Na	98(190)	96(180)	95(60)	94(60)

Reburning alone provided 53% NO reduction with natural gas firing and 49% NO reduction with coal firing. Mixed results were obtained for AR-Lean: 58-76% for natural gas and 62-66% for coal. AR-Lean + SNCR provided up to 85% NO reduction for both natural gas and coal firing. The best results for natural gas firing were achieved by addition of sodium to the first N-agent, 96-98% NO control. Under the same conditions, 90-91% NO was reduced in coal firing. Sodium can likely react with SO₂ and HCl in flue gas, and therefore the performance is not as great in the coal firing tests. Addition of sodium to the second N-agent can be considered as the best result for coal firing: 93-94% NO reduction. Surprisingly, the same arrangements with natural gas firing resulted in only 78-87% NO reduction. Coal flue gas includes vapors of some mineral compounds which can promote the reburning process, and therefore, the presence of the mineral matter in the reburn zone of coal combustion can improve NO reduction. Finally, addition of sodium to both N-agents shows that the second Na additive is not effective for natural gas firing, and the first Na additive has virtually no effect for coal firing.

Data on CO emissions are also presented in Table 7.1. The CO emissions increased in some tests with natural gas firing, but not with coal tests. Two important conclusions can be made based on these hybrid AR/SNCR tests:

1. The hybrid AR-Lean/SNCR process is very effective for NO_x control and can achieve up to 95 and 98% NO reduction for coal and natural gas firing, respectively.
2. Addition of sodium to the second N-agent is more effective for coal than for natural gas firing. The first Na additive is more effective for natural gas than for coal firing.

7.3.4 Hybrid AR-Rich/SNCR

A series of tests was conducted involving AR-Rich plus SNCR during Illinois coal combustion. The first N-agent was injected at 1590 K and OFA was added at 1530 K. The second N-agent was injected downstream of the reburn zone at temperatures ranging from 1230 to 1390 K. Four conditions were run, including no promoter, sodium addition to the first N-agent alone, sodium addition to the second N-agent alone, and sodium addition to both N-agents. As shown in Figure 7.21, performance increased with increasing second N-agent injection temperature. Adding 150 ppm sodium to both N-agents increased NO reduction by 4 to 6 percentage points at each temperature. Maximum NO reductions, obtained at 1390 K, were 88% with no promoter and 93% with sodium added to both N-agents.

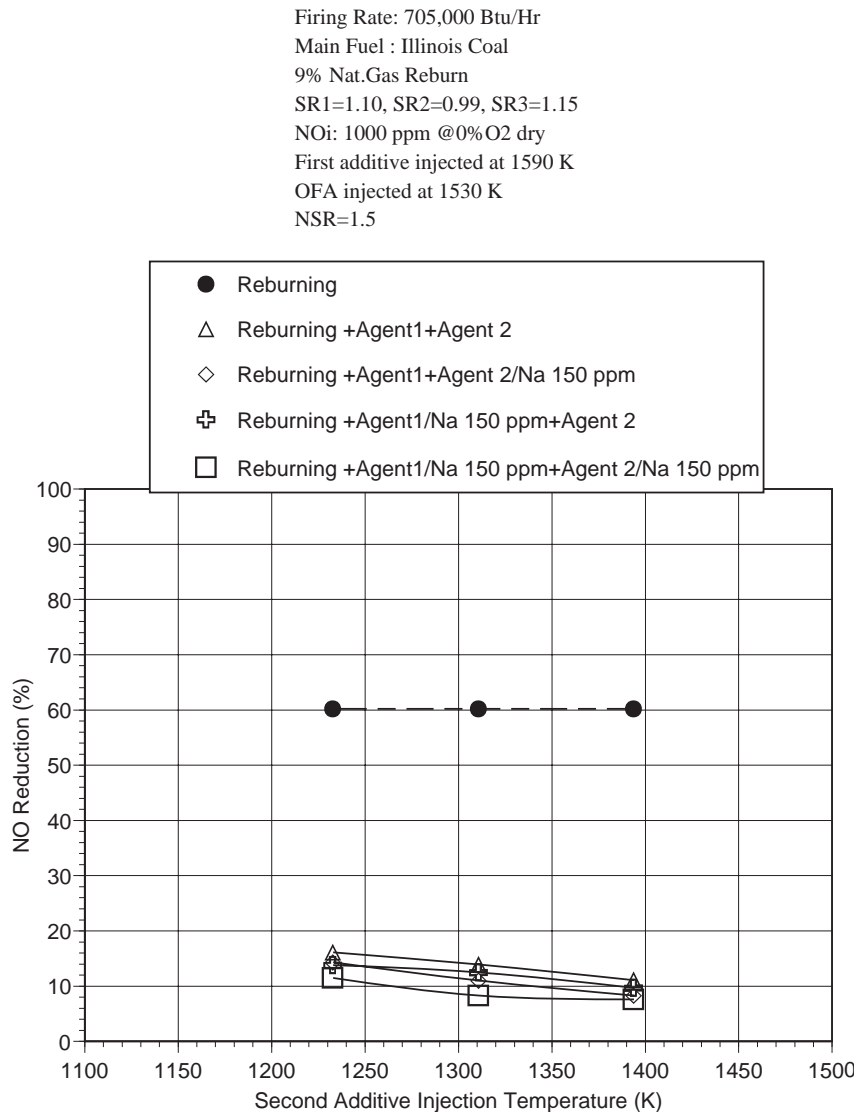


Figure 7.2.1 AR-Rich + SNCR tests: Effect of second additive injection temperature upon performance.

7.3.5 MIAR

Multiple injection advanced reburning (MIAR) components include reburning, AR-Rich, and AR-Lean (both with and without promoters). Test variables at the BSF included reburn heat input, AR-Rich injection temperature, AR-Lean injection temperature, and sodium promoter concentration. Illinois coal was used as the main fuel. Figure 7.22 shows NO reduction as a function of the AR-Rich injection temperature at reburn zone $SR_2=0.90$ (18% reburning heat input). OFA was injected at 1310 K. Reburning alone gave 74% NO reduction. Overall MIAR NO reduction was 80-82%, and was nearly constant as additive injection temperature was varied from 1370 to 1530 K. Addition of sodium promoter did not significantly impact performance. Because performance was relatively low at this SR_2 , temperatures above 1530 K were not tested. Thus, the effectiveness of N-agents and promoters is low at $SR_2 = 0.90$.

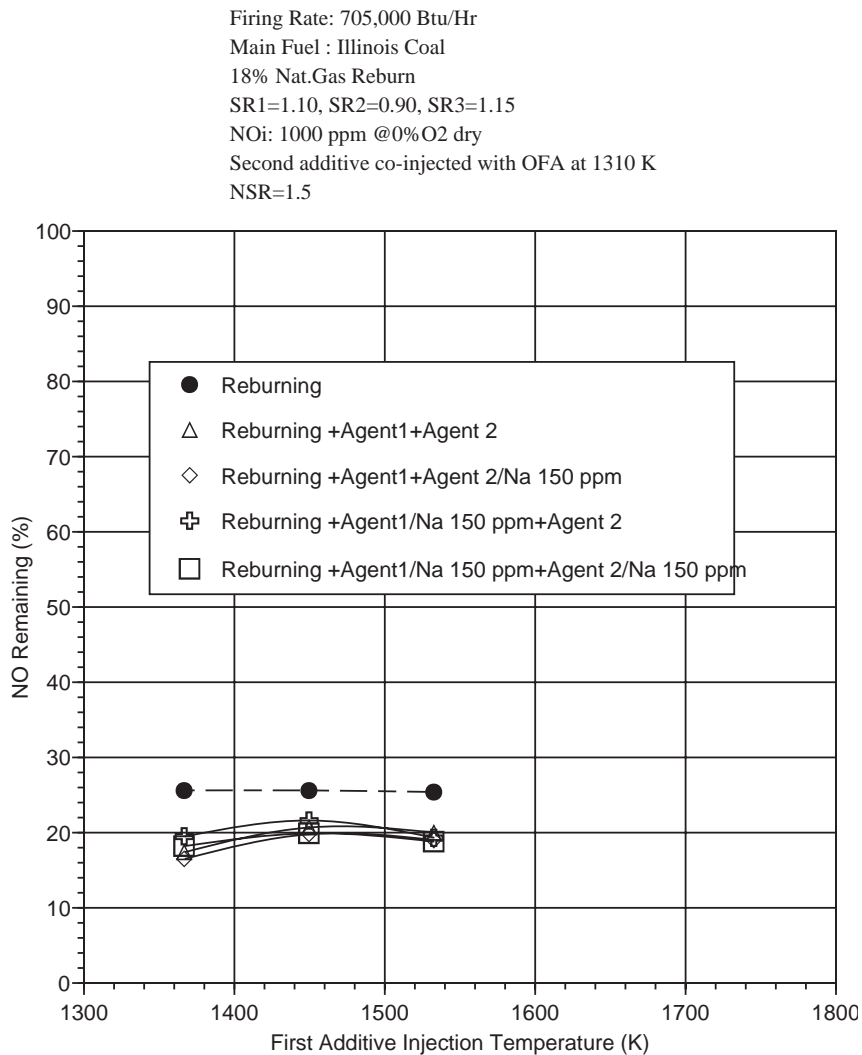


Figure 7.22 MIAR tests: Effect of first additive injection temperature upon performance at 18% reburning.

Similar tests were then conducted at $SR_2=0.99$ (9% reburning). Figure 7.23 shows performance as a function of AR-Rich additive injection temperature. Reburning alone gave 48% NO reduction. MIAR NO reduction increased with decreasing first additive injection temperature. Sodium promoter was added to each N-agent individually and to both agents. Adding promoter to both N-agents provided an incremental performance increase of about 5 percentage points at each temperature. Maximum NO reduction was 94%, obtained with promoter added to both N-agents at an AR-Rich injection temperature of 1370 K. It is also noteworthy that performance remained relatively good at high injection temperatures. NO reductions above 80% were obtained at injection temperatures below 1590 K. This insensitivity can provide greater flexibility for application to boilers with limited furnace access for injectors.

Firing Rate: 705,000 Btu/Hr
 Main Fuel : Illinois Coal
 9% Nat.Gas Reburn
 $SR_1=1.10$, $SR_2=0.99$, $SR_3=1.15$
 NOi: 1000 ppm @0%O2 dry
 Second additive co-injected with OFA at 1310 K
 NSR=1.5

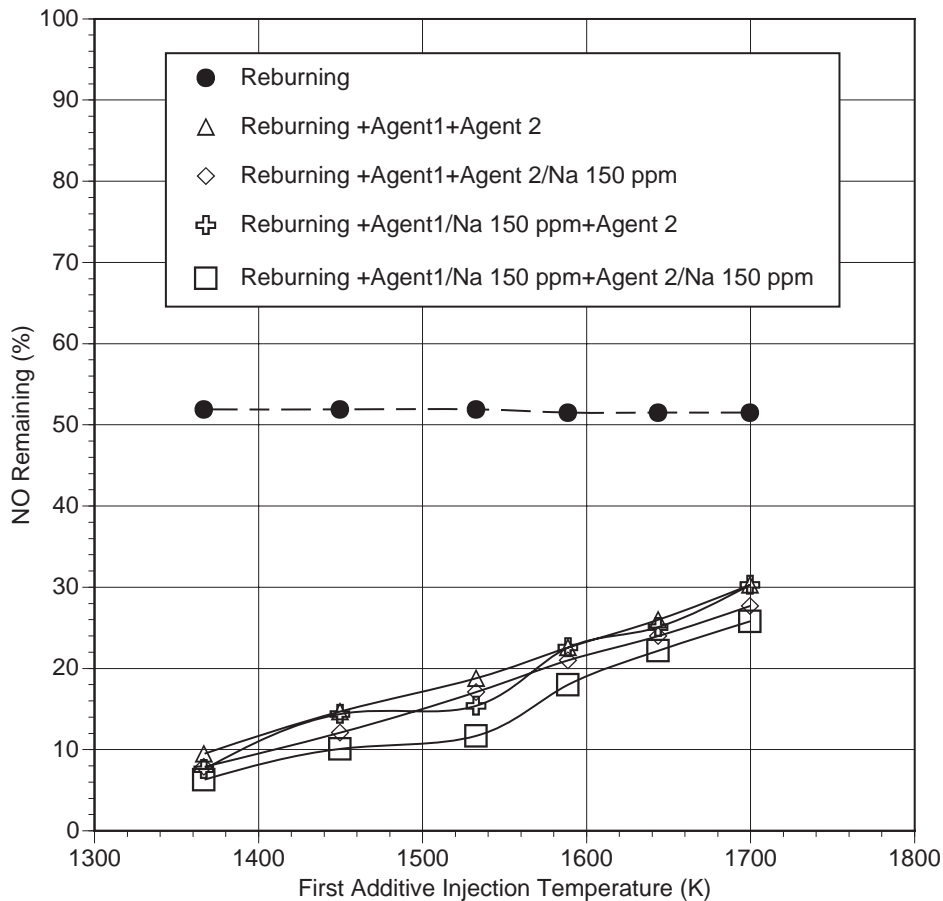


Figure 7.23 MIAR tests: Effect of first additive injection temperature upon performance at 9% reburning.

MIAR tests were then conducted in which the AR-Lean additive injection temperature was varied, with the AR-Rich temperature fixed at 1450 K. The AR-Lean additives were co-injected along with the OFA. Figure 7.24 shows results obtained at $SR_2=0.90$ (18% reburning heat input). Reburning alone gave 74% NO reduction. Overall MIAR NO reduction was 76-82%, and was nearly constant as additive injection temperature was varied from 1200 to 1370 K. Addition of sodium promoter to both N-agents increased NO reduction by 5 percentage points at 1200 K, but did not significantly impact performance at 1370 K. These tests confirmed that N-agents and Na promoters have relatively low effect at $SR_2 = 0.90$.

Firing Rate: 705,000 Btu/Hr
 Main Fuel : Illinois Coal
 18% Nat.Gas Reburn
 $SR_1=1.10$, $SR_2=0.90$, $SR_3=1.15$
 NOi: 1000 ppm @0%O₂ dry
 First additive injected at 1450 K
 Second additive co-injected with OFA
 NSR=1.5

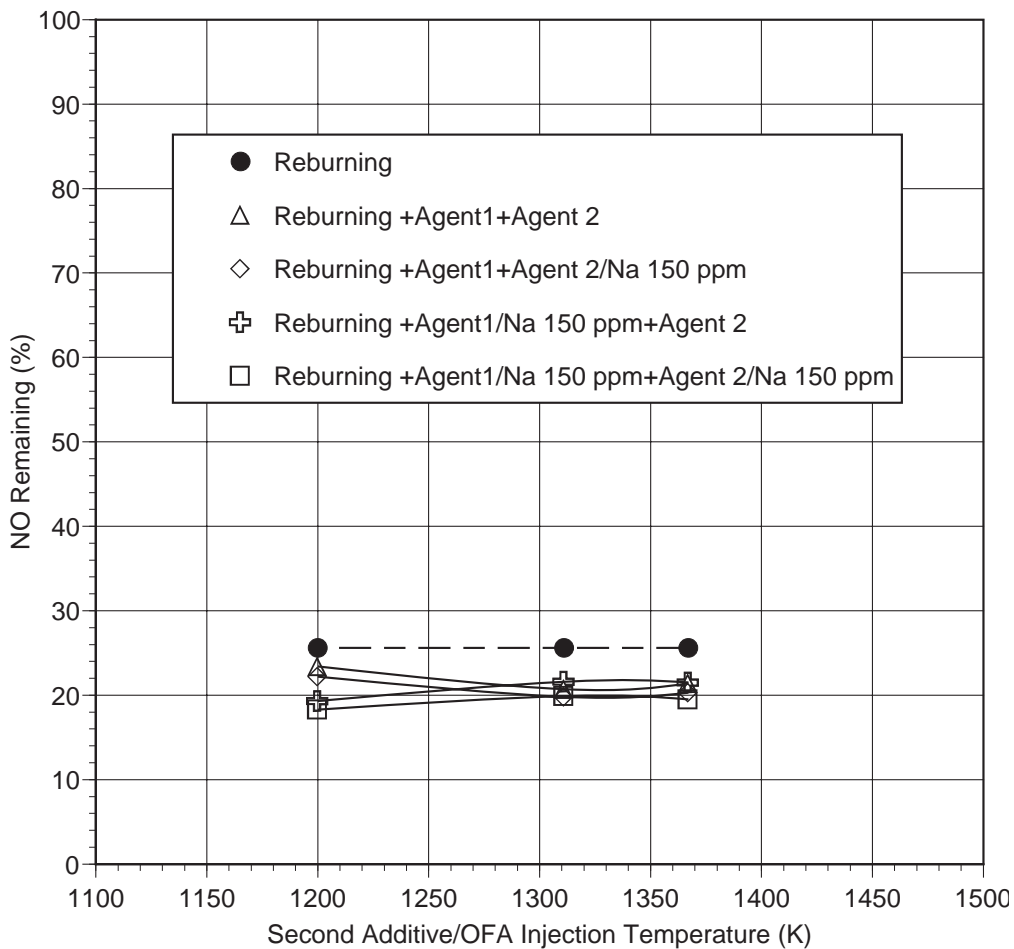


Figure 7.24 MIAR tests: Effect of second additive injection temperature upon performance at 18% reburning.

AR-Lean additive injection temperature was then varied at reburn zone SR=0.99 (9% reburning). As shown in Figure 7.25, reburning alone gave 48% NO reduction. With two N-agents with no promoters, a maximum of 86% NO reduction was obtained. The optimum temperature was 1310 K, and performance decreased as additive injection temperature increased to 1370 K. However, with 150 ppm sodium promoter added to the first N-agent, performance increased with increasing temperature. Highest NO reduction was 95%, obtained at an AR-Lean additive injection temperature of 1370 K. It is theorized that adding sodium with the first N-agent at higher temperatures makes it available to promote reduction of NO by the second N-agent.

Firing Rate: 705,000 Btu/Hr
 Main Fuel : Illinois Coal
 9% Nat.Gas Reburn
 SR1=1.10, SR2=0.99, SR3=1.15
 NOi: 1000 ppm @0%O2 dry
 First additive injected at 1450 K
 Second additive co-injected with OFA
 NSR=1.5

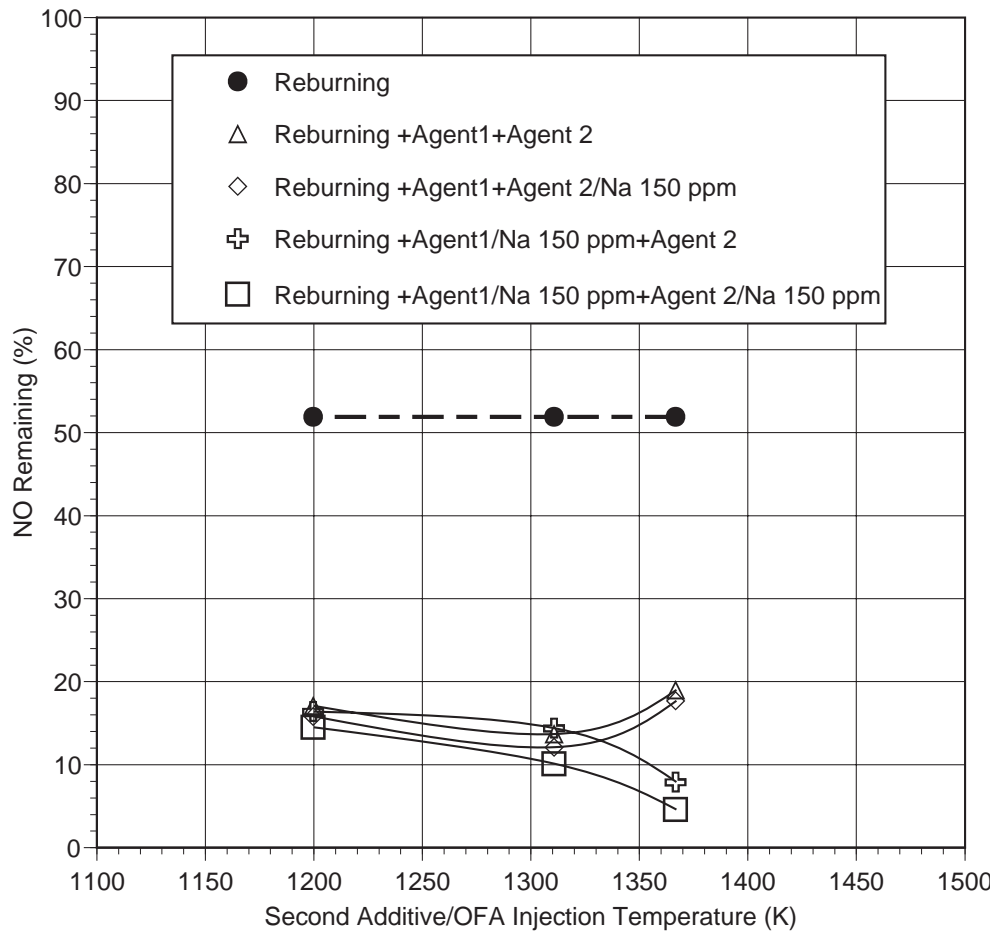


Figure 7.25 MIAR tests: Effect of second additive injection temperature upon performance at 9% reburning.

7.3.6 Byproduct Sampling Tests

While the AR technologies have shown the ability for effective NO_x control, another consideration is whether they generate any undesirable byproducts. Specifically, it was sought to determine whether the different variations of AR generate byproduct emissions greater than those of commercially accepted technologies such as SNCR and reburning. To answer this question, byproduct sampling tests were performed at the BSF. The following seven conditions were tested:

- Baseline coal firing
- SNCR
- Reburning
- AR-Rich
- AR-Lean
- Reburning plus SNCR
- MIAR

Test conditions, including reburn heat input, injection temperatures, promoter amounts and OFA temperatures, were selected as providing NO_x control in the 80 - 90% range and also being achievable in a typical utility boiler. For each condition, sampling included:

- CO, SO₂, N₂O, and total hydrocarbons
- NH₃ and HCN
- SO₃
- Fly ash mass loading, size distribution, PM10, and PM2.5
- Carbon in ash

Test conditions and sampling data are summarized in Table 7.2. The byproducts were measured at conditions which were preliminarily optimized for NO_x control. Additional optimization tests on byproduct emissions is planned for Phase II. However, even without significant byproduct optimization efforts, the AR technologies do not generate more byproducts than reburning or SNCR. Results for each of the byproduct compounds tested are described below.

Table 7.2 Byproduct sampling conditions and results.

Baseline configuration: Illinois coal @ 0.71 MMBtu/hr Test conditions: NSR=1.5
 NO_i=1000 ppm as measured N-agent: Urea
 SR1=1.10, SR3=1.15 Na promoter: Na₂CO₃

Parameter	Test Case						
	1. Baseline	2. SNCR	3. AR-Rich	4. MIAR	5. Reburn +SNCR	6. AR-Lean	7. Reburning
Test Conditions							
Reburn heat input (%)	None	None	10%	10%	10%	10%	20%
Rich side additive T (F)	None	None	2100	2000	None	None	None
Rich side Na (ppm)	None	None	150	150	None	None	None
OFA T (F)	None	None	1900	1900	2300	1900	2300
Lean side additive T (F)	None	1900	None	1900	1900	1900	None
Lean side Na (ppm)	None	None	None	0	None	150	None
Sampling Results							
CO (ppm @0% O ₂)	58	120	75	95	129	95	57
SO ₂ (ppm @0% O ₂)	3140	3011	3050	3012	3120	3045	3011
N ₂ O (ppm @0% O ₂)	1	73	1	38	98	69	1
THC (ppm @0% O ₂)	2	2	2	2	2	2	2
NH ₃ (ppm @0% O ₂)	0.0	47.3	0.0	4.4	50.1	0.0	0.0
HCN (ppm @0% O ₂)	0.0	0.0	1.1	1.2	1.6	1.0	0.5
SO ₃ (ppm @0% O ₂)	2.0	0.8	1.3	1.1	1.7	2.8	1.2
Particulate loading (gr/dscf)	2.0	2.3	1.8	1.9	2.2	2.3	2.1
Fly ash MMD (microns)	8.1	8.7	10.8	10.1	8.2	8.6	8.5
PM ₁₀ (%)	54.4	52.1	49.2	49.8	55.4	53.0	53.5
(gr/dscf)	1.09	1.21	0.88	0.93	1.24	1.23	1.10
PM _{2.5} (%)	10.5	10.1	9.4	13.6	14.3	11.2	12.6
(gr/dscf)	0.21	0.23	0.17	0.25	0.32	0.26	0.26
Carbon in ash (%)	0.08	0.03	0.17	0.26	0.07	0.10	0.08

CEMS Emissions

A continuous emissions monitoring system (CEMS) was used to sample for CO, SO₂, N₂O, and total hydrocarbons. SO₂ concentrations were in the range of 3010 to 3140 ppm (@ 0% O₂) for each condition, and were not affected by the AR technologies. Total hydrocarbon emissions were 2 ppm for each test condition. Figure 7.26 summarizes CO and N₂O emissions for each of the seven test conditions. CO and N₂O generally increased during application of the NO_x control technologies relative to baseline coal firing. The largest increases were associated with the low temperature N-agent injection technologies, i.e. SNCR and reburning + SNCR. For SNCR, CO increased from 58 to 120 ppm, and N₂O increased from 1 to 73 ppm. OFA was injected at 1310 K. Thus AR-Lean, AR-Rich, and MIAR generate lower concentrations of CO and N₂O than does SNCR under similar conditions. It is believed that CO and N₂O concentrations could be further reduced by injecting OFA at a higher temperature.

Main Fuel: Illinois Coal @ 705,000 Btu/hr
 SR1=1.10, SR3=1.15
 NOi=1000 ppm as measured

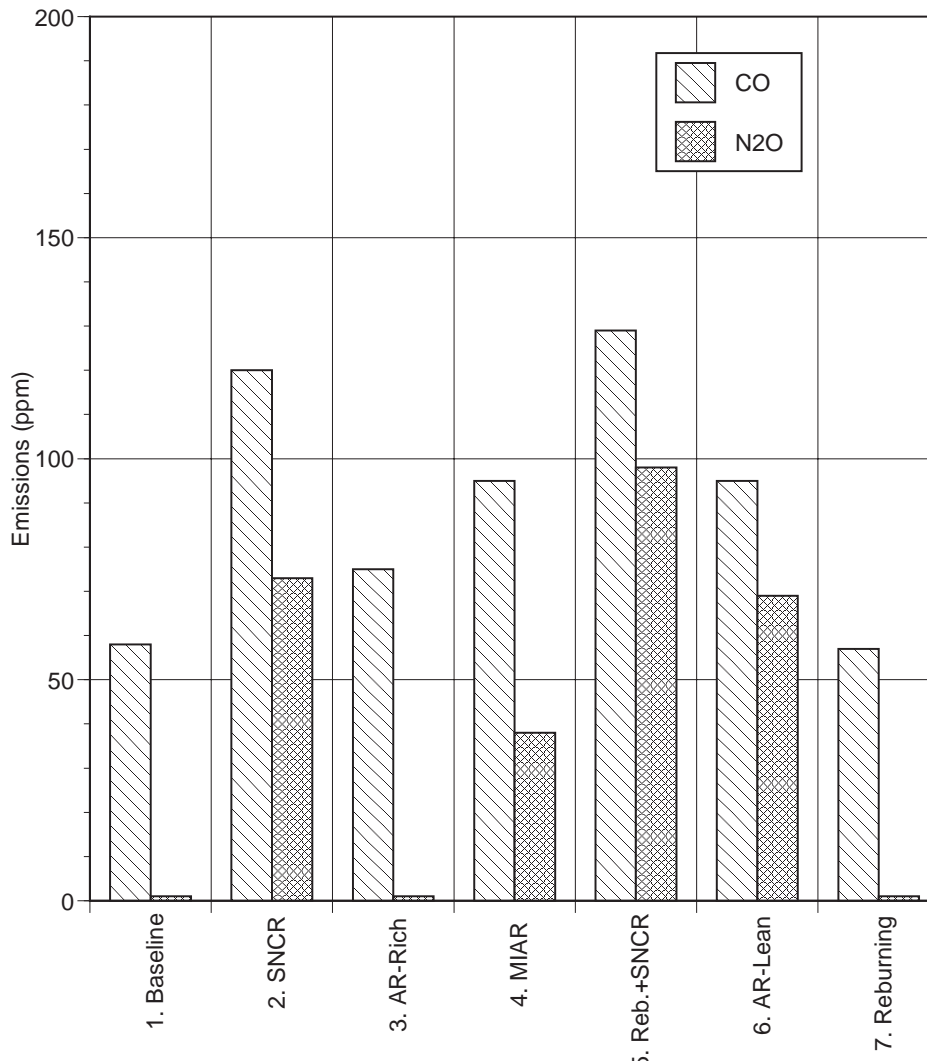


Figure 7.26 CO and N₂O emissions for AR technologies.

NH₃ and HCN Emissions

NH₃ and HCN emissions were measured by EPA Draft Method 206, using ion chromatography analysis. Results are shown in Figure 7.27. NH₃ emissions were fairly high (>40 ppm) for the two SNCR conditions, but were below 5 ppm for all other conditions (including MIAR). HCN emissions were below 2 ppm for baseline coal and all AR test conditions. Thus AR-Lean, AR-Rich, and MIAR generate significantly lower NH₃ emissions than does SNCR under similar conditions. These results would appear to indicate that as long as the N-agent(s) are added with or upstream of the OFA, NH₃ and HCN emissions can be minimized. For the SNCR cases, it is believed that a higher reagent injection temperature would reduce NH₃ emissions.

Main Fuel: Illinois Coal @ 705,000 Btu/hr
 SR1=1.10, SR3=1.15
 NOi=1000 ppm as measured

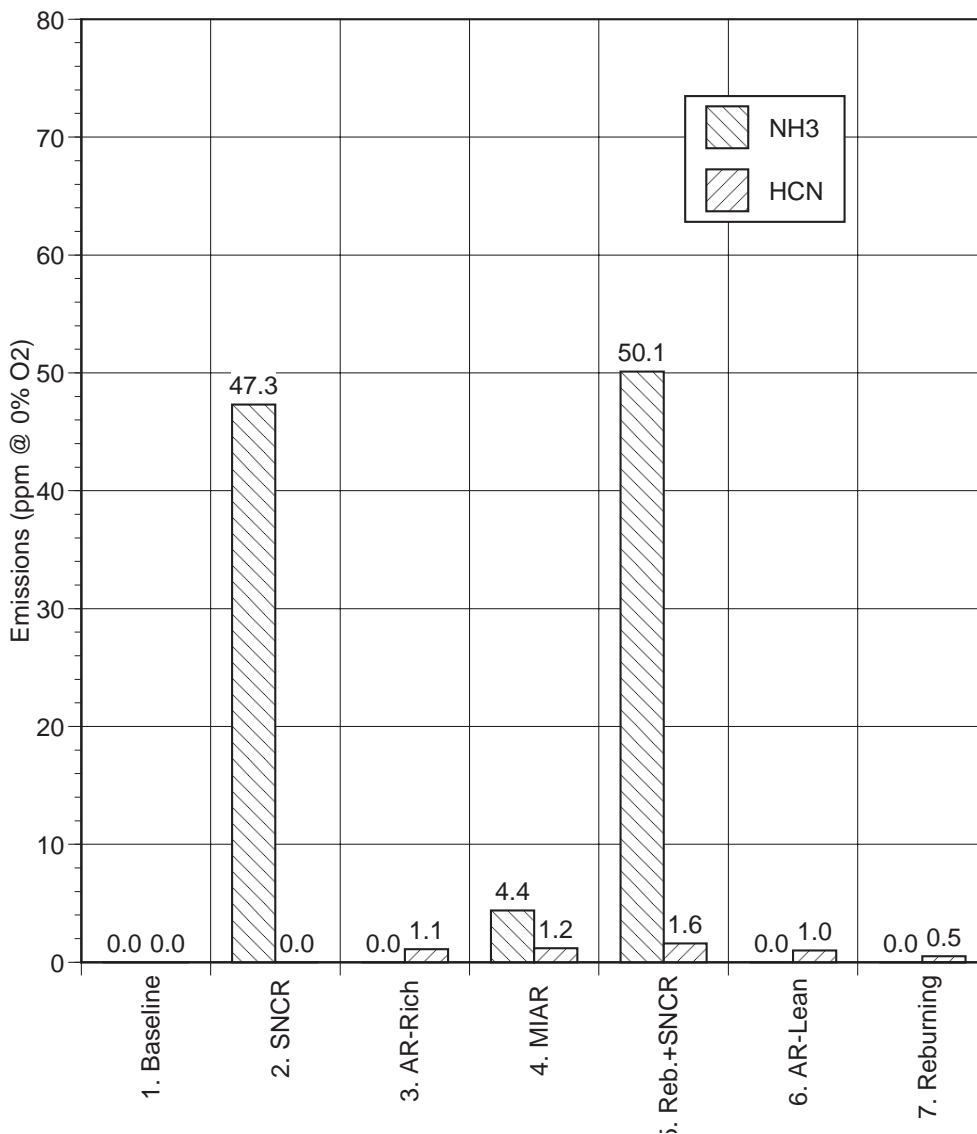


Figure 7.27 NH₃ and HCN emissions for AR technologies.

SO₃ Emissions

SO₃ emissions can impact electrostatic precipitator performance and, if present in high concentrations, cause boiler corrosion problems. SO₃ emissions were measured using the controlled condensation method, as detailed in the EPA's "Process Measurement Procedures - Sulfuric Acid Emissions" (1977). The sample probe was operated at a temperature of 590 K. Figure 7.28 shows SO₃ test results. The SO₃ concentration for baseline coal firing was about 2 ppm. For each of the NO_x control technologies, SO₃ remained below 3 ppm. It is concluded that none of the technologies cause a significant increase in SO₃ emissions.

Main Fuel: Illinois Coal @ 705,000 Btu/hr
SR1=1.10, SR3=1.15
NOi=1000 ppm as measured

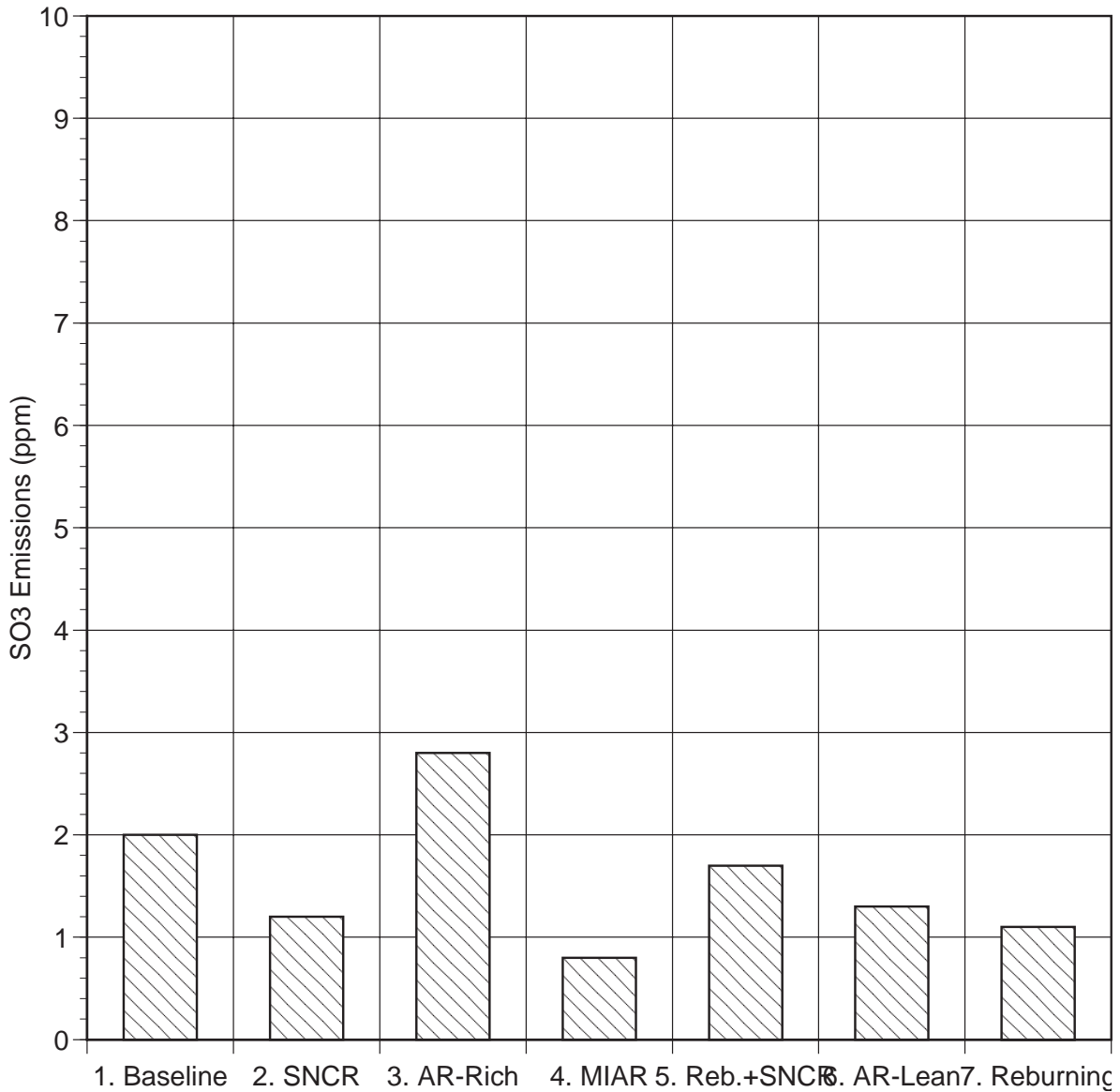


Figure 7.28 SO₃ emissions for AR technologies.

Particulate Size Distribution

Fly ash particle size can affect dust control equipment efficiency as well as causing respirability and health considerations. Particulate size distribution was measured using a cascade impactor. Figure 7.29 shows fly ash distributions for each of the seven test conditions. Fly ash mass mean diameter was between 8 and 11 microns for each condition. The AR technologies did not appear to significantly alter overall size distribution.

Main Fuel: Illinois Coal @ 705,000 Btu/hr
 SR1=1.10, SR3=1.15
 NOi=1000 ppm as measured

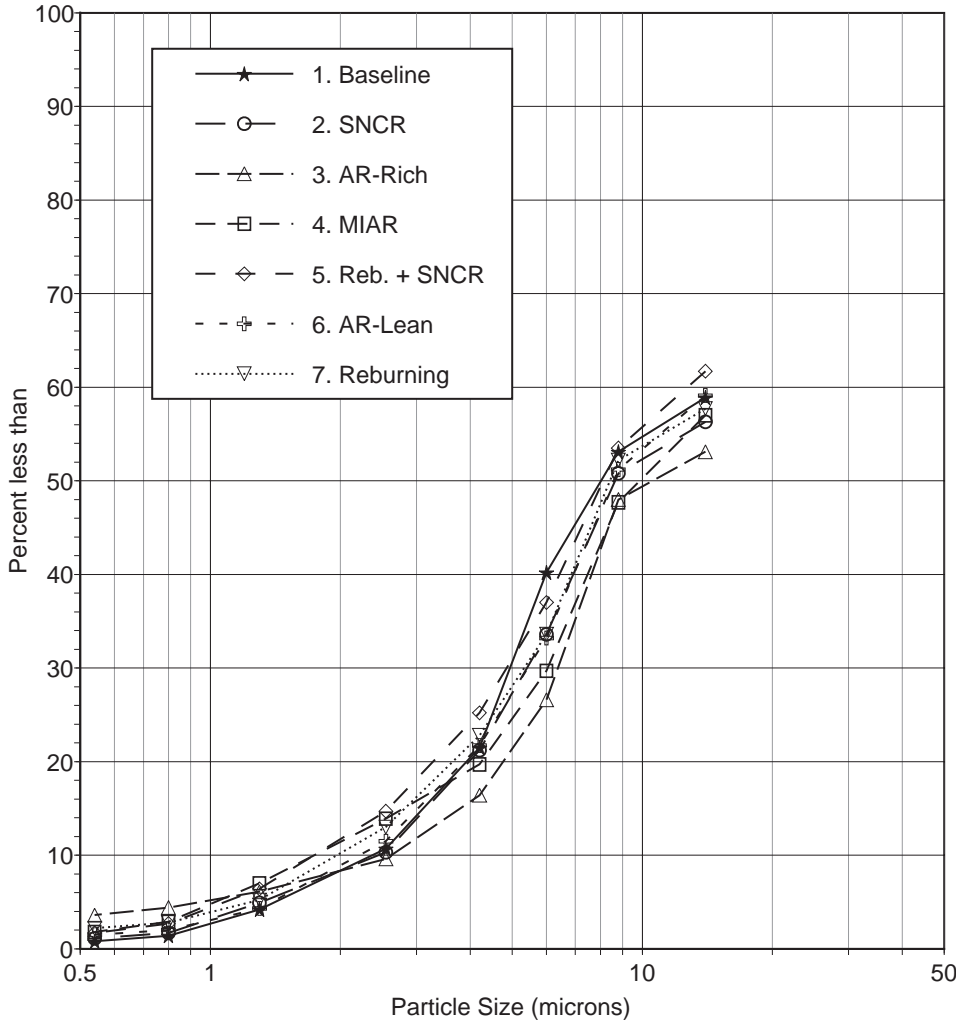
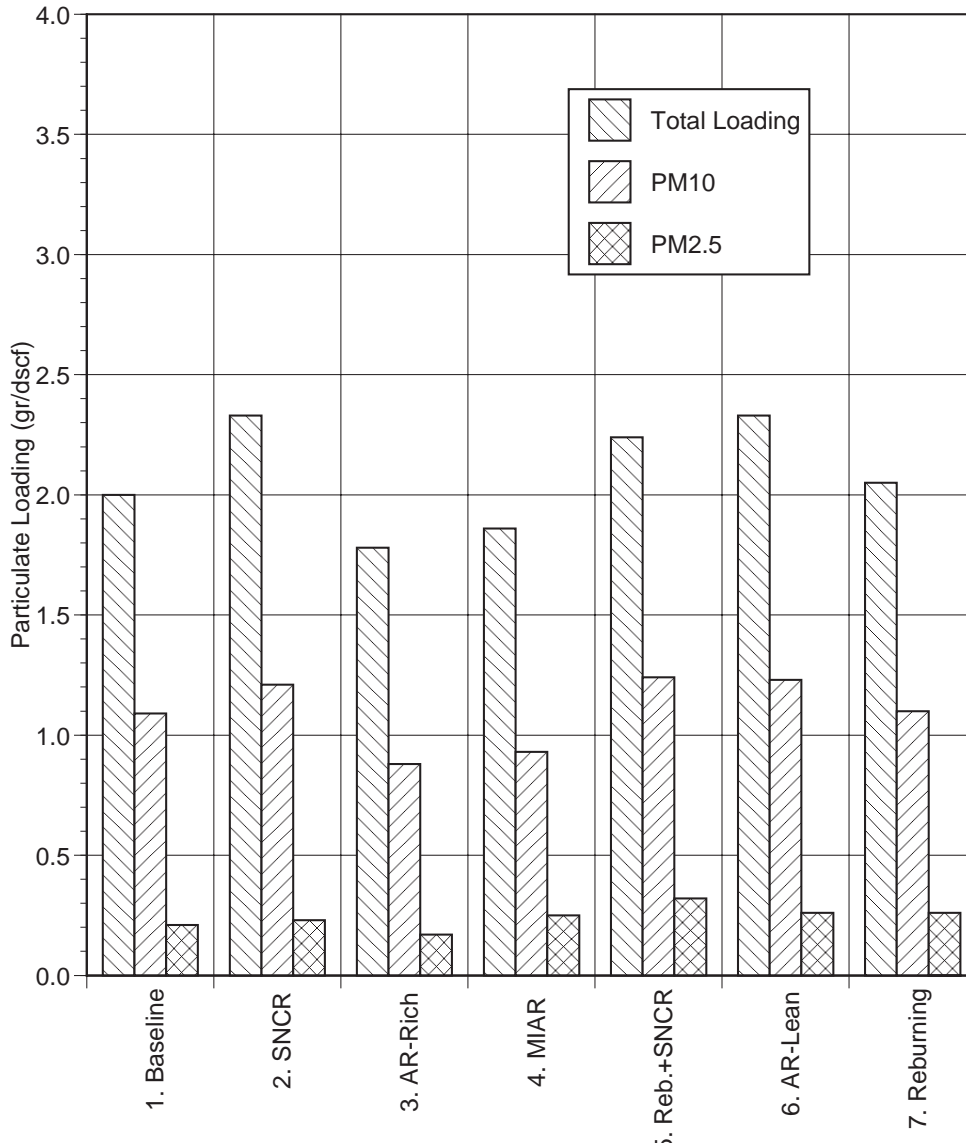


Figure 7.29 Fly ash size distribution.

Particulate Loading, PM10, and PM2.5

PM10 and PM2.5 are defined as the fraction of fly ash material of diameter less than 10 and 2.5 microns, respectively. EPA Method 5 and cascade impactors were used to determine total particle loading, PM10, and PM2.5. Results are shown in Figure 7.30. Total particulate loading was 2.0 gr/dscf for baseline coal firing, and ranged from 1.8 to 2.3 gr/dscf for the different NO_x control technologies. PM10 was about 1.1 gr/dscf for baseline coal firing, and ranged from 0.9 to 1.2 gr/dscf for the different technologies. PM2.5 was about 0.21 gr/dscf for baseline coal firing, and ranged from 0.17 to 0.32 gr/dscf for the different technologies. These results would appear to indicate that the AR NO_x control technologies do not significantly impact particulate loading, PM10, or PM2.5.

Main Fuel: Illinois Coal @ 705,000 Btu/hr
 SR1=1.10, SR3=1.15
 NOi=1000 ppm as measured



7.30 Fly ash total loading, PM 10, and PM 2.5.

Carbon in Ash

Poor carbon burnout can adversely impact boiler thermal performance, along with the commercial value of collected fly ash. Fly ash is generally salable to the construction industry if it contains less than 5% carbon. Ash samples were collected from the BSF convective pass using a volumetric sampler and were analyzed for carbon in an induction furnace. Figure 7.31 shows carbon in ash results. For all conditions, carbon in ash was well below 1%. Thus it is concluded, based on these tests, that the AR technologies do not significantly decrease carbon burnout.

Main Fuel: Illinois Coal @ 705,000 Btu/hr
SR1=1.10, SR3=1.15
NOi=1000 ppm as measured

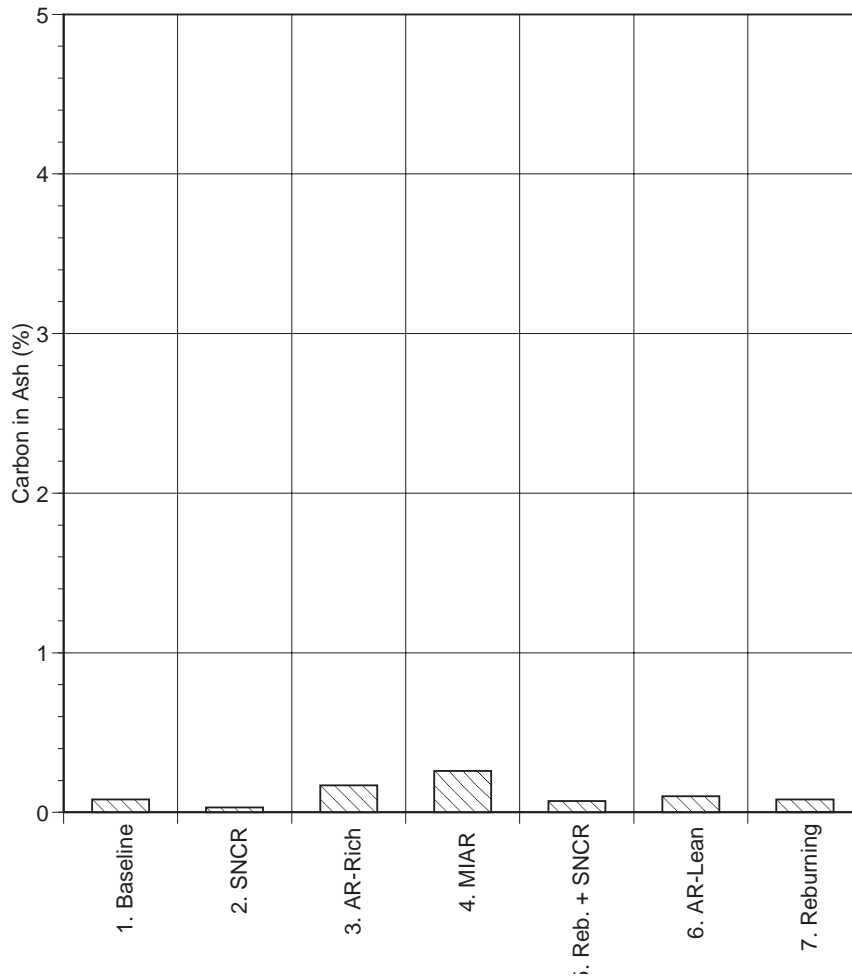


Figure 7.31 Carbon in ash results.

7.4 Pilot Scale Combustion Tests: Conclusions

In summary, the parametric tests showed that the AR technologies are able to provide effective NO_x control for a high-sulfur coal fired combustor. Three technologies were originally envisioned for development: AR-Lean, AR-Rich, and MIAR. Along with these, three additional technologies were identified during the course of the testing: Reburning plus SNCR, AR-Lean plus SNCR, and AR-Rich plus SNCR, where SNCR performance can be enhanced by addition of promoters.

Sodium was found to significantly promote performance more effectively during gas firing than coal firing. A possible reason for this is interaction of sodium compounds with fly ash, as well as reaction with SO₂ or HCl to form sodium sulfite, sodium sulfate or sodium chloride. Nevertheless,

even for high sulfur coal sodium was found to significantly improve performance when added at 150 ppm, which is a manageable level for most utility boilers.

Maximum NO reductions achieved by the promoted AR technologies during gas and coal firing were as follows:

	<u>Gas firing</u>	<u>Coal firing</u>
• AR-Lean:	95%	90%
• AR-Rich:	96%	93%
• AR-Lean + SNCR:	98%	94%
• AR-Rich + SNCR:	97%	93%
• MIAR:	98%	95%

These technologies have different optimum reburn heat input levels and furnace temperature requirements. For full scale application, an optimum technology can be selected on a boiler specific basis depending on furnace temperature profile and regions of injector access.

In terms of byproduct emissions, in some cases CO was observed to increase when sodium was added. This may be due to chain reactions involving sodium compounds, H atoms and OH radicals which allow CO to escape oxidation. However, it was found that CO could be controlled by increasing the OFA injection temperature. Emissions of N₂O and NH₃ showed the potential to increase under low-temperature SNCR conditions. Adding the second N-agent at higher temperature was found to minimize these emissions.

In summary, the promoted AR technologies demonstrated the ability to readily achieve NO reductions of 95+% during gas firing and 90+% during coal firing. Byproduct emissions were found to be manageable. Additional test work could be performed to further optimize variables such as N-agent stoichiometric ratio and additive-furnace gas mixing requirements, as well as to provide scale-up data for utility boiler application.

8.0 MECHANISM DEVELOPMENT AND KINETIC MODELING

The objective of this task is to develop a kinetic analytical model of the Advanced Reburning technologies. A high temperature reaction mechanism has been developed for use in this model, based on a standard natural gas combustion model (GRI-Mech) combined with nitrogen chemistry as well as reactions of sodium, sulfur, and chlorine. The chemical kinetic model has been implemented using chemical kinetics codes CHEMKIN-II and SENKIN, developed at Sandia National Laboratories, and EER's One Dimensional Flame (ODF) code. The experimentally validated model is used as a tool to investigate the process analytically.

The chemical kinetic model has been applied to an experimentally feasible range of conditions, with appropriate variations in controllable conditions including initial species concentrations, temperature, and residence time. Rate constants for the reactions in the mechanism have not been varied, and the model does not describe quantitatively the experimental data. However, the predicted exit concentrations do provide qualitative insight into expected performance trends. The predicted species histories also provide insight into internal details of the process which are not readily measured. In addition, sensitivity analysis has been applied to selected cases to identify the relative importance of specific reactions in the process as modeled. The mechanism development and modeling has extended the understanding of AR and provides a tool for future development and implementation of the process.

8.1 Mechanism Development

A high temperature kinetic mechanism has been developed and tested to model the AR systems process. This mechanism includes reactions of C-H-O species applicable to both rich and lean combustion chemistry. It also includes N-containing species reactions reflective of variations in stoichiometry (reburning), and the effect of additives (N-agents and/or promoters) on the species pool. To model the effect of promotion, the most important reactions of Na-containing compounds have been analyzed and incorporated. In addition, reactions of S- and Cl-containing compounds have been included to assist in future modeling of AR processes applied to coal combustion.

The resulting mechanism, which has been used in modeling, is presented in Appendix 1. The reaction numbers assigned there are used throughout this section for reference. Reversible rate data also requires thermodynamic properties for the participating species. To complete the description of the model mechanism, the thermodynamic database is presented in Appendix 2.

8.1.1 GRI-Mech

GRI-Mech (Bowman et al., 1995, and Frenklach, et. al., 1994) was selected for the basic C-H-O-N mechanism as it represents the current industry standard in natural gas combustion chemistry. The mechanism includes the elementary chemical reactions, the rate coefficients and parameters describing the thermodynamic properties of the included species. The basic combustion mechanism has been validated extensively against available experimental data, listed in the cited references.

The most current version as of the initiation of the modeling task is version 2.11, which contains 276 reactions with 49 species containing C, H, O, N, as well as Ar as a third body species. These are presented in Appendix 1 as reactions 1-278 (two duplicate reactions being added for compatibility with the kinetics software). Version 2.11 is an extension of the earlier Version 1.2, which was optimized specifically for accurate prediction of C, H, O combustions, in particular natural gas flames and ignition, with nitrogen included only as inert N₂. The nitrogen chemistry introduced in versions 2.11 is optimized specifically for natural gas flames and reburning. GRIMEch by itself has not yet been optimized for other NO_x control technologies. The authors also caution that the agreement with nitrogen chemistry and reburning data is not as close as for C-H-O chemistry, and therefore is subject to further development. Nevertheless, this mechanism represents the state of the art in these aspects of nitrogen chemistry, representing a significant improvement over previously published mechanisms such as Miller and Bowman (1989).

Due to these limitations in the current GRI-Mech, additional nitrogen reactions must be incorporated to obtain a mechanism capable of predicting AR processes which extend beyond conventional reburning, such as the SNCR chemistry inherent in N-agent addition.

8.1.2 SNCR Reactions

The analysis of available kinetic information resulted in preliminary selection of two reaction mechanisms for modeling the chemical behavior in the C-H-O-N system. Both mechanisms are based on GRI-Mech, with SNCR reactions added from other sources. The selection process is described in further detail in Zamansky and Maly (1996a).

Two variants of the C-H-O-N mechanism, denoted here as A and B, were considered. Mechanism A includes all GRI-Mech Version 2.11 reactions and reactions selected from the SNCR scheme suggested by Bowman, 1996. Mechanism B consists of the C-H-O system of GRI-Mech-1.2, N-chemistry reactions proposed by Glarborg et al., 1993, and reactions of CH_i radicals with nitrogenous

species (“C-N chemistry”) selected from GRI-Mech Version 2.11. Either scheme could be considered to be state of the art for C-H-O-N chemistry modeling.

The two selected mechanisms include the complete GRI-Mech Version 1.2, which was verified by its authors against multiple C-H-O experimental data from various sources. The N-chemistry from GRI-Mech-2.11 and the Glarborg’s N-mechanism were also verified against experimental data on reburning. However, because both mechanisms were broadened to include SNCR submechanisms, they required verification associated with the SNCR nitrogen chemistry. Calculations were performed based on available experimental data for the Thermal DeNOx process. Two sets of experiments were selected for comparison with modeling:

1. Laboratory-scale data presented by Lyon and Hardy, 1986. Conditions: flow system tests, variation of reactor temperature, residence time 0.1 s. Mixture composition: 225 ppm NO - 450 ppm NH₃ - balance He.
2. EER’s recent pilot-scale experimental data. Conditions: BSF natural gas combustion tests, variation of NH₃ injection temperature, quenching rate 167 K/s. Flue gas composition: 200 ppm NO - 300 ppm NH₃ - 3.8% O₂ (dry measure) - 8% CO₂ - 15% H₂O - balance N₂.

The CHEMKIN-II kinetic program developed at the Sandia National Laboratories (Kee et al., 1991) was used for modeling. Figure 8.1.1 demonstrates comparison of the experimental results and modeling by the use of the mechanisms A and B. Although both mechanisms show some difference from the experimental data and there is a shift in temperature, they both qualitatively model the temperature window of the Thermal DeNOx process. The differences can be explained by the values of rate constants, by errors in experimental temperature measurements, and by influence of mixing effects on NO removal. Calculations with both mechanisms were performed without any adjustments in rate constants taking into account an actual BSF temperature profile. Both models qualitatively described the most substantial feature of the SNCR process: the temperature window of NO reduction. However, this validation also shows that differences in quantitative comparison of modeling and AR experiments are to be expected.

Since both mechanisms show about the same performance in modeling experimental data, it is difficult to prefer one of them. Mechanism A was selected for further calculations since it includes less constituent parts (sub-mechanisms) and all of them were suggested by the same group of authors. The SNCR reactions which are added to GRI-Mech 2.11 are included in Appendix A as reactions 279-312.

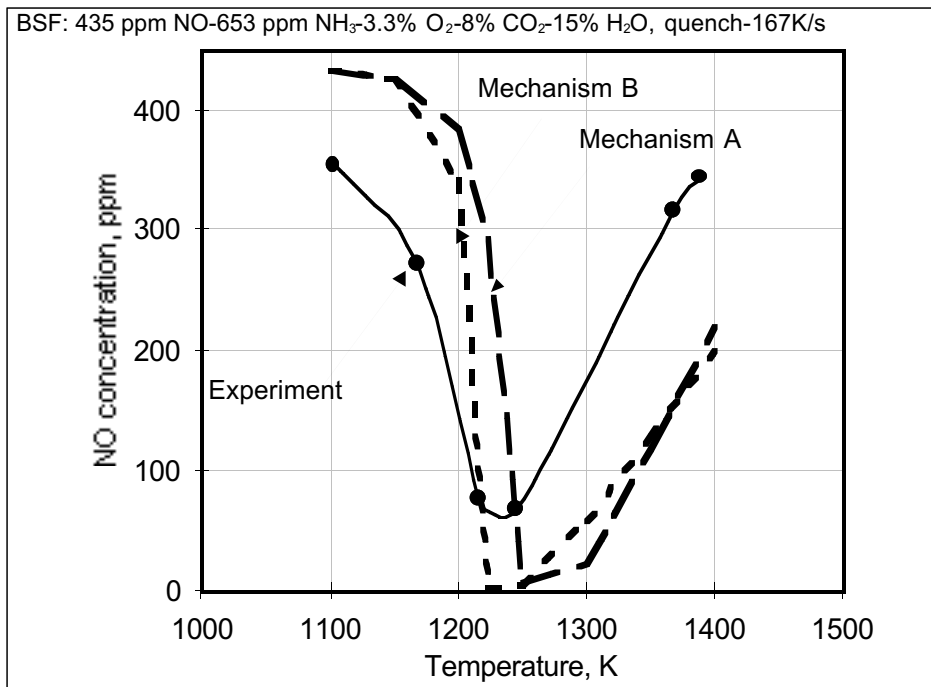
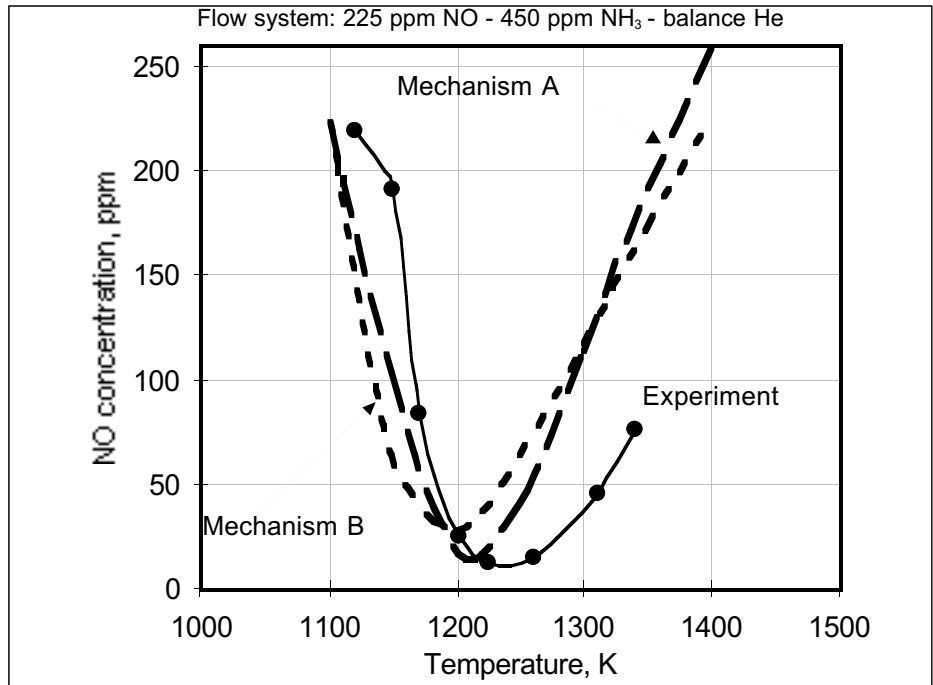


Figure 8.1.1 Comparison of experimental data and modeling with mechanisms A and B for the Thermal DeNO_x process.

8.1.3 Reactions of Sodium

Experimental data demonstrate that the addition of sodium compounds, such as sodium carbonate and sodium hydroxide, can increase reburning efficiency. However, the high temperature chemistry of sodium compounds is not well understood. Only a few rate constants have been measured directly, and kinetic information on many reactions is absent. However, estimates are available for several other rate constants.

Sodium carbonate was used as a promoter in most CTT and BSF experiments. It was also shown that sodium hydroxide has about the same efficiency as sodium carbonate. When sodium carbonate is injected into flue gas, it decomposes into oxides. The mechanism of Na_2CO_3 thermal decomposition and the corresponding rate constants are the subject of an experimental task at the University of Texas, as documented in Section 5.

Most likely, sodium carbonate dissociates at high temperatures to different oxides. The oxides react with water molecules which are available in flue gas to form sodium hydroxide. The specific reactions considered here (numbered corresponding to Appendix 1), based on the University of Texas study, are:



The conversion from Na_2CO_3 to NaOH is rapid, and it is most likely the reason for the equal promotion efficiency of Na_2CO_3 and NaOH .

Since the modeling effort was conducted in parallel with the University of Texas experimental effort, it was necessary to develop the modeling mechanism based on preliminary estimates of the reaction rates. For this reason, the rate constant used in modeling for Reaction 319 may not exactly match those reported for the experimental task (Section 5). For this reaction, rate expression used in modeling was $1.00\text{E}13 \exp(+35390/\text{RT})$, rather than the later experimental result of $9.18\text{E}12 \exp(-3120/\text{RT})$, which is now recommended. However, both versions of the rate constants predict rapid initial conversion of Na_2CO_3 to NaOH for example. The estimated rate constants in the model mechanism result in a characteristic decay time of 3 ms at 1400 K, while the University of Texas

rate constants predict less than 1 ms. In either case, the rates are sufficiently fast that the difference is not considered to be serious.

The additional 23 reactions (320 through 342) of sodium compounds with C-H-O-N species consider the reactions of NaOH and its decomposition products. The source for rate constants and expected behavior of some of the reactions follows:

- Reaction 320 is the most important for removing N_2O from flue gas. The rate constants for reaction 320 are from Plane, 1992, but several measurements of the rate constant agree rather well with each other (Mallard et al., 1994).
- Reactions 321-324 are important steps of NaO interaction with H_2O , O, NO and H_2 . Rate constant of these reactions have been measured; Reactions 321 and 324 rates are from Ager and Howard (1987), Reaction 322 from Plan and Husain (1986), and Reaction 323 from Ager et al. (1989).
- Reaction 325 represents oxidation of Na atoms by molecular oxygen. The rate constant of this reaction was measured several times and the most reliable value (Plane and Rajasekhar, 1989) was selected. Reaction 326 can be important for N_2O removal under fuel rich conditions. If the reaction proceeds as written to form Na atoms, they will react with N_2O via reaction 320. If reaction 320 is faster in reverse direction, it will be not effective.
- Reaction 327 is probably important for defining the processes of radicals formation and removal. Indeed, if the recombination reaction 327 of sodium atoms and hydroxyl radicals is fast enough, the efficiency of the promoter will be low. Measurements by Jensen and Jones, 1982 were accepted as rate constants for reactions 327 and 328.
- Other reactions of sodium, 329-341, were recently estimated by Perry and Miller, 1996.
- Reaction 342 represents a process of sodium-ammonia interaction. It was observed in experiments that sodium promoters are effective mainly in the presence of N-agents. However, no kinetic data on sodium-ammonia interaction was found in the literature. The rate constant was estimated to be close to the collision frequency.

To complete these mechanism enhancements, the thermodynamic database was updated to include the thermodynamic data for the sodium compounds. The value of the Na-O₂ bond energy was

selected to be $D_0 = 37.2$ kcal/mol as was determined theoretically by Partridge et al., 1992 and recommended by Perry and Miller, 1996.

Additional sodium reactions include interactions with sulfur-containing species (reactions 343 through 346) and chlorine-containing species (374 through 350).

8.1.4 Reactions of Sulfur and Chlorine

It has been found that sodium promoters are less effective in flue gas from coal combustion flue gas compared to that from natural gas. Coal includes sulfur and chlorine compounds which can react with sodium, decreasing its efficiency. The submechanisms for reactions of S- and Cl- compounds with Na-O-H species have been added to the mechanism for future modeling of the effect of sulfur and chlorine compounds on reburning efficiency and to understand the chemistry of sodium promotion under different conditions. All selected reactions are presented in Appendix 1 as reactions 312-316 and 343-355.

Rate constants for SO_2/SO_3 reactions, 312-316, were taken from the literature review by Atkinson et al., 1992 and direct measurements by Armitage and Cullis, 1971 (for reaction 312) and Smith et al., 1982 (for reaction 316). Though many kinetic measurements of these reactions were reported in the literature, most of them were performed at relatively low temperatures, mainly below 400 K. Therefore, there is a significant uncertainty in high temperature kinetic data for SO_2/SO_3 interaction.

Reactions 343-346 represent interaction of sodium and sulfur compounds. Reaction 343 was suggested by Fenimore, 1973; the rate constant for this reaction was estimated to be $k = 10^{13} \exp(-17700/T)$ $\text{cm}^3/\text{mol}\cdot\text{s}$ where the activation energy is equal to the reaction endothermicity. A single rate constant measurement for reaction 344 was reported by Shi and Marshall, 1991. Rate constants for reactions 345 and 346 were assumed to be close to that measurement.

During the combustion process, most chlorinated compounds are converted into HCl. Therefore, to model the effect of chlorine on reburning efficiency and Na promotion, it is logical to perform modeling using the initial concentration of HCl in flue gas corresponding the amount of chlorine in coal. For this reason, chlorine reactions have been added which address the reactions of HCl and its products.

Nine reactions of chlorine were included in the mechanism. The first four, 347-350, represent the reactions of sodium compounds (Na, NaO, NaO_2 , and NaOH) with HCl. All these reactions are

fast, and available experimental measurements of the rate constants were selected (Silver et al., 1984; Husain and Marshall, 1986; DeMore et al., 1987; and Silver and Kolb et al., 1986, respectively). Five other chlorine reactions, 351-355, include the well known steps of $\text{Cl}_2\text{-H}_2$ interaction. Their rate constants were taken from kinetic tables by Baulch et al., 1981.

The thermodynamic database was updated to include data for the sulfur and chlorine containing compounds. Thermodynamic data for NaSO_2 were calculated by using the Na-SO_2 bond energy $D_0 = 47.1$ kcal/mol defined by Steinberg and Schofield, 1990. This value corresponds to the heat of formation of NaSO_2 , $\Delta H_{f,0} = -92$ kcal/mol.

Thermodynamic analysis. To verify which species are important to include in the sulfur and chlorine mechanisms, an analysis of equilibrium flue gas compositions was performed. This predicts the species concentrations if the thermodynamic state of the gas (*e.g.*, temperature, pressure) were held uniform indefinitely. Although actual conditions are far from invariant, the analysis is still useful. Species participating in reactions which are fast relative to the rate of change in temperature (*e.g.* natural gas combustion) may establish a partial equilibrium in the mixture, and thermodynamic analysis can indicate the relative amounts to expect. Furthermore, products which are favored thermodynamically are important to include in the reaction mechanism so that all likely products are considered.

The calculations were performed using the latest version of the NASA Chemical Equilibrium program, CET93 (McBride et al., 1994). To ensure that all potentially important species are considered, the completeness of the code's species database (which identifies species to consider and their thermodynamic properties) is crucial. The standard CET93 database includes over 1000 compounds mostly from the JANAF tables, including combustion products as well as alkali metals. EER has extended this by adding data from other sources, including the Barin (1989) tables and current research at Lawrence Livermore National Laboratories (Ebbinghaus, 1993). Several metals and radionuclides are thus incorporated, as well as their oxides, hydroxides, oxyhydroxides, chlorides, metal-sulfur compounds, and other species. A list of sodium compounds included in the updated CET93 thermodynamic database, and sample properties, is presented in Appendix 3.

CET93 was used to predict concentrations of sodium compounds in the reburning and overfire air zones at various conditions, including different temperatures, stoichiometries, quantities of sodium, and the presence of sulfur and chlorine. Equilibrium was calculated for each composition for a range of temperatures from 1100 to 1900 K. Zamansky et al. (1997a) provides further details of the calculations.

For stoichiometric ratios ranging from 0.9 to 1.25, with 10 ppm Na in the mixture, the most favored sodium species are NaOH and Na, with all other sodium species at less than 0.1 ppm. The same species dominate with 50 ppm Na at an SR of 0.99. The major species as a function of temperature are shown in Figure 8.1.2(a) for 10 ppm Na and SR=0.99. When 2000 ppm SO₂ is included in this mixture, the presence of sulfur does not result in formation of significant amounts of sodium sulfate over the temperature range considered, as shown in Figure 8.1.2(b). However, Na₂SO₄ increases as temperature is reduced and could be significant in modeling the interaction between sodium and sulfur. If 50 ppm Cl₂ is included instead of sulfur, sodium chloride becomes the most stable sodium compound, as shown in Figure 8.1.2(c). It must be cautioned, however, that thermodynamic data for gaseous sodium salts are not considered reliable, and so these results should not be considered conclusive without future validation. Nevertheless, these results establish NaOH, Na, Na₂SO₄ and NaCl as potentially important species in a C-H-O-N-Na-S-Cl mechanism. Appropriately, reactions involving these species have been included in the current mechanism.

8.1.5 Mechanism Development: Summary

The mechanism developed based on the above considerations consists of 355 reactions and 66 species. It has been developed based on the best existing data for mechanisms and individual reactions as of the time of its development. The core of the mechanism is based on the industry standard for natural gas combustion and reburning, GRI-Mech 2.11. The mechanism was then extended to include reactions for the prediction of N-agent chemistry.

The resulting C-H-O-N mechanism was further extended to include Na compounds in order to model processes involving sodium carbonate or sodium hydroxide promoters. The sodium reactions were developed in parallel with the experimental effort at the University of Texas.

The addition of sulfur and chlorine reactions enable predictions of the behavior of promoted AR in coal combustion. Thermodynamic analysis shows that the most significant species for interaction of S and Cl with Na have been included. The rates for reactions involving S and Cl species were estimated based on published data, and have not yet been tested against experimental results.

8.2 Modeling with Instantaneous Mixing Times

Initial modeling focused on the chemistry of individual AR processes after premixing the combustion gases with the reactant stream being introduced. This approximation represents instantaneous mixing of the reactants, thus removing the details of the physical mixing process from the model. Once

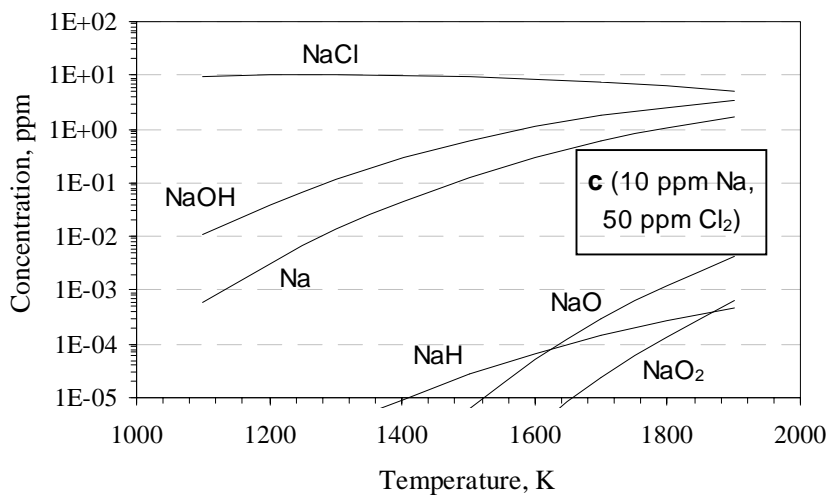
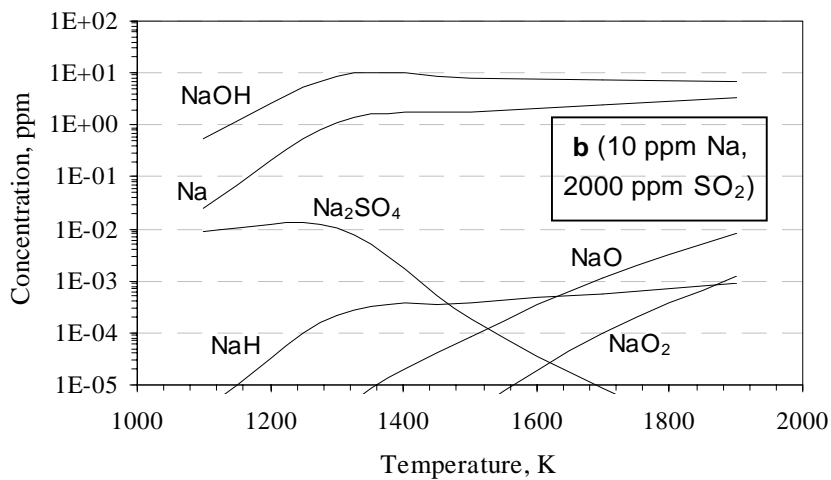
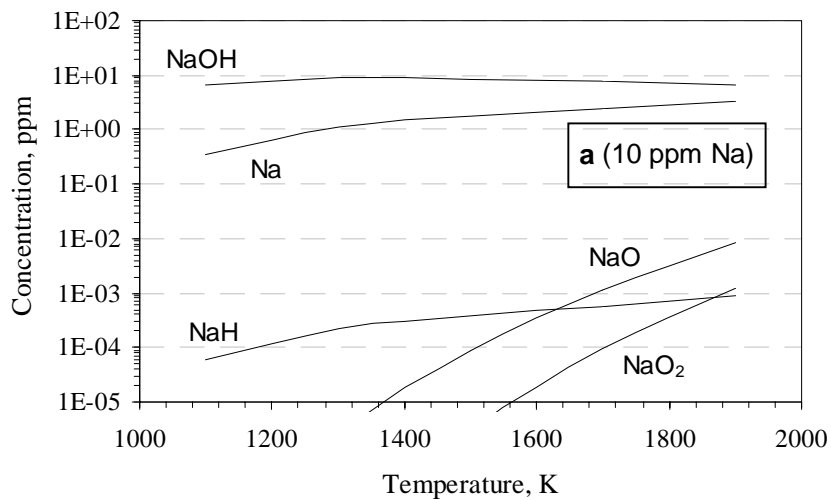


Figure 8.1.2. Effect of sulfur and chlorine on equilibrium concentrations of sodium species in flue gas.

premixed, the reactions proceed along a one-dimensional (plug flow) reactor, which again allows the reactions to proceed in time without any fluid dynamic effects. Thus, this approach focuses on the chemistry of the process.

Individual AR injection processes include reburning, N-agent injection in the reburning zone (ARRich) or with OFA (AR-Lean), addition of promoters with the N-agent, and OFA addition. Each injection involves different parameters which affect its performance. One of these parameters is the location of injection, characterized either by time from the point of reburn fuel or OFA injection, or by temperature at the point of injection. Another is the amount of added reactants, characterized by concentration, stoichiometric ratio following addition (for fuel or air addition), or NSR (for N-agent addition).

In these modeling studies, the reburning fuel is CH_4 , the N-agent is NH_3 , and the promoter is Na_2CO_3 . In all cases the pressure is held constant at 1 atm. The temperature profile was specified at a constant quench rate of 300 K/s, reflective of the actual reburning zone environment in the BSF.

The CHEMKIN-II kinetic program developed at the Sandia National Laboratories (Kee et al., 1991) was used for most instantaneous modeling. CHEMKIN-II is used to predict the kinetic curves of major components in the reaction zone (concentration vs. time) for comparison with experimental data. However, the kinetic curves do not provide information about the importance of specific elementary reactions with respect to increasing or decreasing concentrations of certain components. The next step, sensitivity analysis, was done to obtain this information. Sensitivity analysis is a procedure to quantitatively determine the dependence of the model solution on the elementary reaction rate constants. It provides insight about how important certain reactions are to the model's predictions. The sensitivity analysis was performed with the use of the SENKIN code developed by Sandia National Laboratory (Lutz et al., 1987). SENKIN is a FORTRAN computer program for predicting the species and temperature histories and for calculating the first order sensitivity coefficients of each species with respect to the elementary reaction rate parameters.

In addition to species mole fraction histories (kinetic curves) which are also available from Chemkin-II, Senkin provides information about contribution and sensitivity factors. Contribution factors for a selected species show the effect of elementary reactions with participation of the species on its concentration. Sensitivity factors for a selected species show the effect of each elementary reaction in the mechanism on the concentration of the species.

The chief difference between these two parameters is that contribution factors show the direct influence of specific reactions on a given species. Sensitivity factors show indirect influences hidden in the complex reaction mechanism, to show how a change in the rate for a given reaction would affect the production or removal of a given species. Both measures are important. While contribution factors show the reactions directly involved in formation and destruction, often groups of reactions work rapidly and in opposition to each other, masking the net influence of another reaction which is driving them. Sodium promotion, in which injected sodium species significantly affect NO but have very little direct interaction with it, is an example of a process where sensitivity analysis is particularly useful. By ranking reactions with respect to these factors, the most important direct and indirect influences on a given species can be determined, along the length of the reactor.

The contribution factor $c_{i,k}$ is defined as the contribution of reaction i to the net production rate of species k at a given instant, and may be calculated as:

$$c_{i,k} = v_{k,i} q_i$$

$v_{k,i}$ is the net stoichiometric coefficient of species k in reaction i (the number of molecules of species k on the right side of the reaction minus the number of molecules on the left side, the net number of molecules of k produced as the reaction proceeds to the right). q_i is the rate of progress variable, calculated as:

$$q_i = k_{f,i} \prod_k [x_k]^{v'_{k,i}} - k_{r,i} \prod_k [x_k]^{v''_{k,i}}$$

where $k_{f,i}$ is the forward rate constant and $k_{r,i}$ is the reverse rate constant for reaction i , $v'_{k,i}$ and $v''_{k,i}$ are the stoichiometric coefficients of species k on the left and right hand side of reaction i , respectively, and x_k is the mole fraction of species k . Note that $v_{k,i} = v''_{k,i} - v'_{k,i}$.

The sensitivity of species k to reaction i is defined as

$$(dx_k / dA_i) (A_i / x_{k,max})$$

where A_i is the frequency factor from the Arrhenius rate expression for reaction i , and $x_{k,max}$ is the maximum value of x_k over all points in time which are processed by Senkin. (In other words, the normalizing value of $x_{k,max}$ is somewhat dependent on the timestep resolution of the Senkin calculation if the species undergoes a very rapid transient).

The histories of concentration, contribution factors, and sensitivities provide information useful for understanding chemistry of the processes under investigation. This is a valuable tool in optimizing NO removal while ensuring that other emissions such as NH₃ remain low.

8.2.1 Modeling of the Basic Reburning Process

Stoichiometric ratio SR₁ in the primary zone was kept at SR₁=1.1 for all calculations. This SR₁ corresponds to methane combustion with the following mixture composition:

8.72% CH₄ - 19.18% O₂ - balance N₂

If the combustion process in the primary zone is complete, it generates about 8% CO₂ and 15% H₂O. At the same time, 1.74% O₂ is left which is available for oxidation of the reburning fuel. Therefore, the premixed reactants for reburning can be described as:

[CH₄] - 1.74% O₂ - 600 ppm NO - 8% CO₂ - 15% H₂O - balance N₂,

where [CH₄] is the molar percent of reburning fuel. For example, [CH₄] is 1.94% for reburning zone stoichiometry SR₂=0.90, 1.37% for SR₂=0.95, and 0.967% for SR₂=0.99.

An initial NO concentration NO_i = 600 ppm was used for calculations. Figures 8.2.1-8.2.3 demonstrate concentration profiles of main species in the reburning zone at an injection temperature T₁ = 1700 K and SR₂ equals 0.99, 0.95, and 0.90, respectively. Comparison of these graphs shows that CH₄ is rapidly converted to CO and H₂. Only at SR₂=0.90, about 300 ppm CH₄ is present in the mixture. At SR₂=0.99 and 0.95, the amount of CH₄ is lower than 1 ppm.

At SR₂ = 0.99 (Figure 8.2.1), NO concentration drops during a very short period of time from 600 ppm to about 540 ppm and then, slowly decreases to 502 ppm. Concentrations of NH₃ and HCN are lower than 1 ppm, though some O₂ is still present.

At SR₂ = 0.95 (Figure 8.2.2), oxygen disappears within 0.05 s, and NH₃ concentration slowly increases. NO again rapidly drops to about 430 ppm and decay slowly to 330 ppm. Total Fixed Nitrogen (mole fraction of N in species other than N₂, approximated by NO+NH₃+HCN) is a measure of the total unreacted nitrogen in the mixture. In this case, TFN concentration is 332 ppm by 0.5 s.

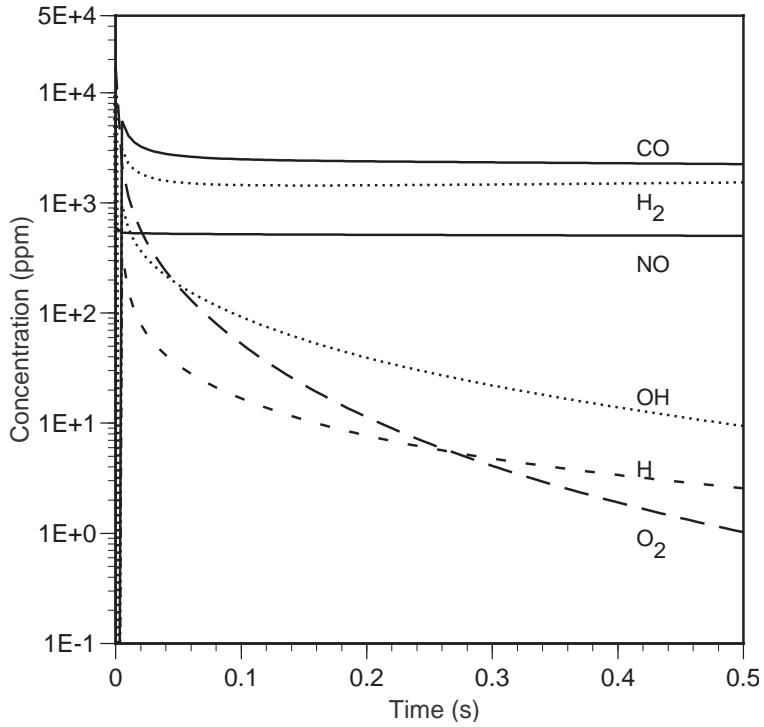


Figure 8.2.1. Kinetic curves of the main species in the reburning zone at $SR_2 = 0.99$ and injection temperature $T_1 = 1700$ K.

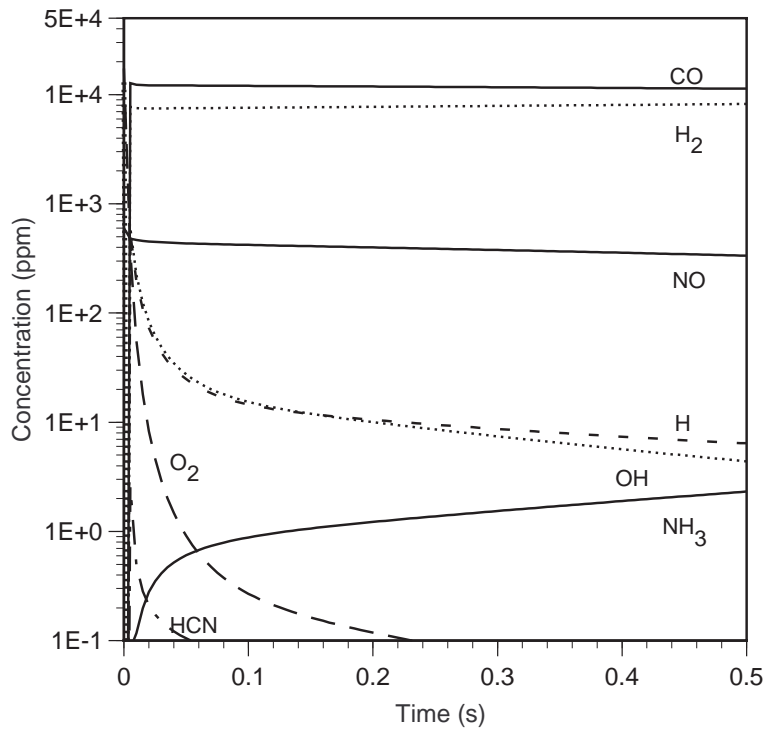


Figure 8.2.2. Kinetic curves of the main species in the reburning zone at $SR_2 = 0.95$ and injection temperature $T_1 = 1700$ K.

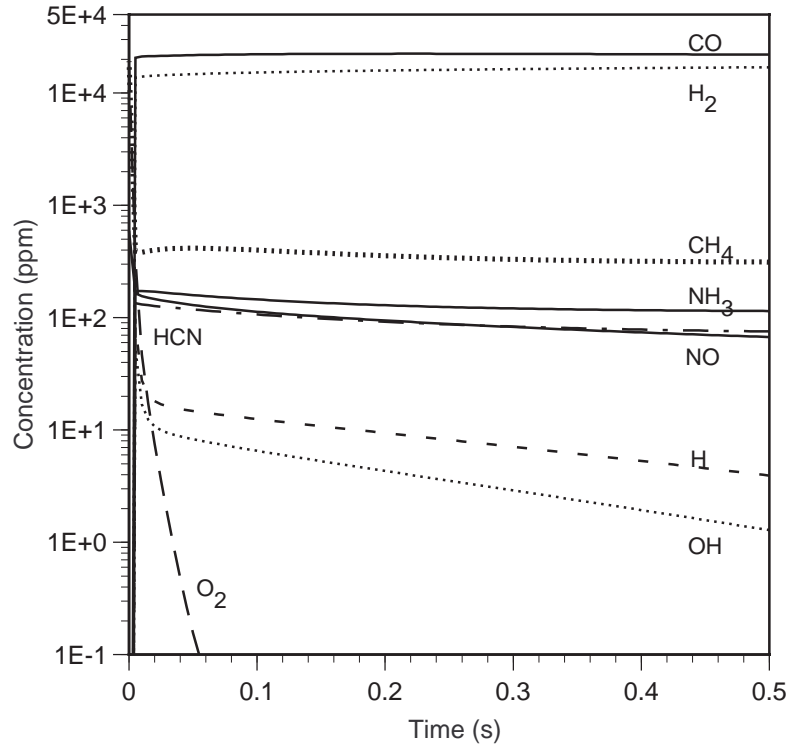


Figure 8.2.3. Kinetic curves of the main species in the reburning zone at $SR_2 = 0.90$ and injection temperature $T_1 = 1700$ K.

At $SR_2 = 0.90$ (Figure 8.2.3), NO rapidly and more efficiently decreases from 600 to 160 ppm, and then slowly to 67 ppm. However, in this case, the mixture contains 75 ppm HCN and 115 ppm NH_3 at $t = 0.5$ s. Hence, TFN equals 257 ppm.

Chemistry at Short Time Scales. The results show that there are two steps of NO reduction in the reburning process: the first very fast step and the second slow step. The cause of these fast and slow decreases in NO concentration is of primary interest for understanding the reburning phenomenon. To clarify the main processes in the fast NO reduction zone, calculations were carried out over a reaction time interval of 5 msec for $SR_2 = 0.99$ and 0.90. Figures 8.2.4 and 8.2.5 represent the results.

Figure 8.2.4 demonstrates kinetic curves in the reburning zone at $SR_2 = 0.99$, $T_1 = 1700$ K, and $t = 5$ ms. The NO concentration has a little minimum at about 2 ms. This minimum is explained by reactions of NO with C-containing radicals: CH_3 , CH_2 , HCCO, $CH_2(S)$, CH, and C. The radicals are formed from CH_3 which, in turn, is formed from CH_4 . The radicals participate also in recombination reactions with each other and in reactions with oxygen and other species. As a result of these processes, concentrations of the radicals increase within 2 ms, and then, since all CH_4 is

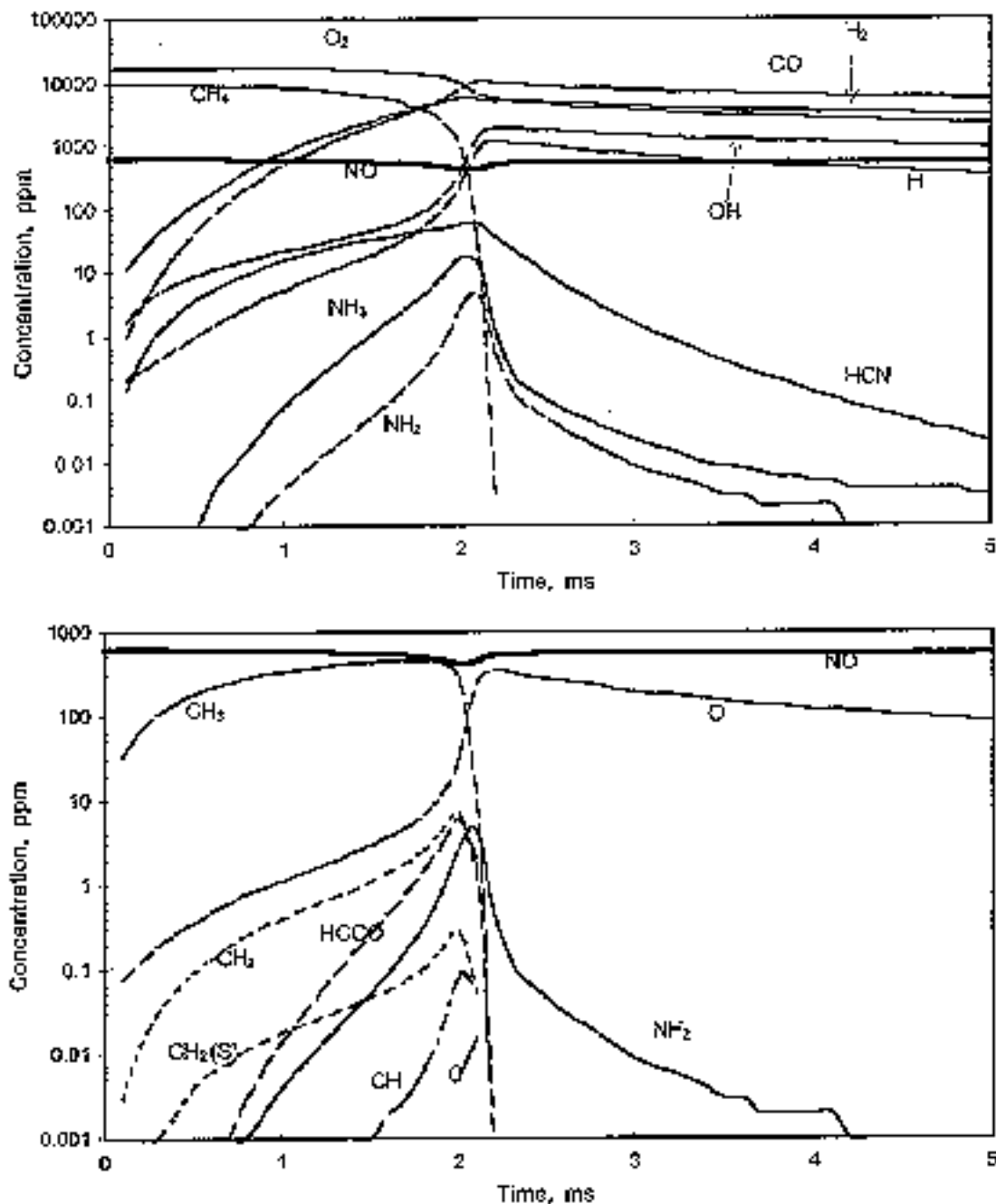


Figure 8.2.4. Kinetic curves in the reburning zone at $SR_2 = 0.99$, $T_1 = 1700$ K, and $t = 5$ ms.

consumed and there is no more feed, the concentration of C-radicals reduces, due to recombination and oxidation, by several orders of magnitude. Concentrations of HCN and NH_3 rise simultaneously with C-radicals because HCN and NH_3 are the main molecules formed due to reactions of the radicals with NO. At about 2 ms, both HCN and NH_3 are oxidized by existing oxygen into NO. Therefore, the NO concentration slightly increases. It is of interest to note that concentrations of

CH₂ and HCCO reach 8-9 ppm, though CH concentration does not exceed 0.1 ppm. Main reactions of NO removal can be compared by considering their rates at the maximum point of radical concentrations. Table 8.2.1 presents the NO reactions with C-radicals and their rates in arbitrary units at 2 ms.

This comparison shows that HCCO radicals, followed by CH₂ radicals, are the most important species depleting NO concentration. Thus, the reactions of HCCO and CH₂ radicals are dominant pathways (in the scope of the assumed mechanism) for NO consumption during the initial fast NO removal after reburn fuel injection under the conditions examined.

Table 8.2.1. Comparison of NO reaction rates with C-radicals at SR₂ = 0.99, T₁=1700K and t = 2 ms.

C-radical	Reaction	Rate, arb. units	Total rate, a. u.	Rank
C	C + NO = CN + O	1	2.6	6
	= CO + N	1.6		
CH	CH + NO = HCN + O	25	51	4
	= H + NCO	10		
	= N + HCO	16		
CH ₂	CH ₂ + NO = H + HNCO	560	900	2
	= OH + HCN	140		
	= H + HCNO	200		
CH ₂ (S)	CH ₂ (S) + NO = H + HNCO	14	22.6	5
	= OH + HCN	3.6		
	= H + HCNO	5		
CH ₃	CH ₃ + NO = HCN + H ₂ O	71	76.6	3
	= H ₂ CN + OH	5.6		
HCCO	HCCO + NO = HCNO + CO	1860	1860	1

Figure 8.2.5 shows kinetic curves in the reburning zone within first 5 ms at SR₂ = 0.90 and T₁ = 1700 K. NO concentration decreases from 600 to 165 ppm, and this is explained by reactions of NO with the same C-containing radicals. Concentrations of the radicals also have a maximum, in this case at about 3 ms, but they are removed not so rapidly since CH₄ concentration is much higher, and the source of the radicals (CH₄ and CH₃) still exists within 5 ms. Concentrations of HCN and NH₃ again rise simultaneously with C-radicals, but, in this case, HCN and NH₃ are almost not oxidized since O₂ concentration drops rapidly (only 1 ppm O₂ exists in the mixture in 30 ms).

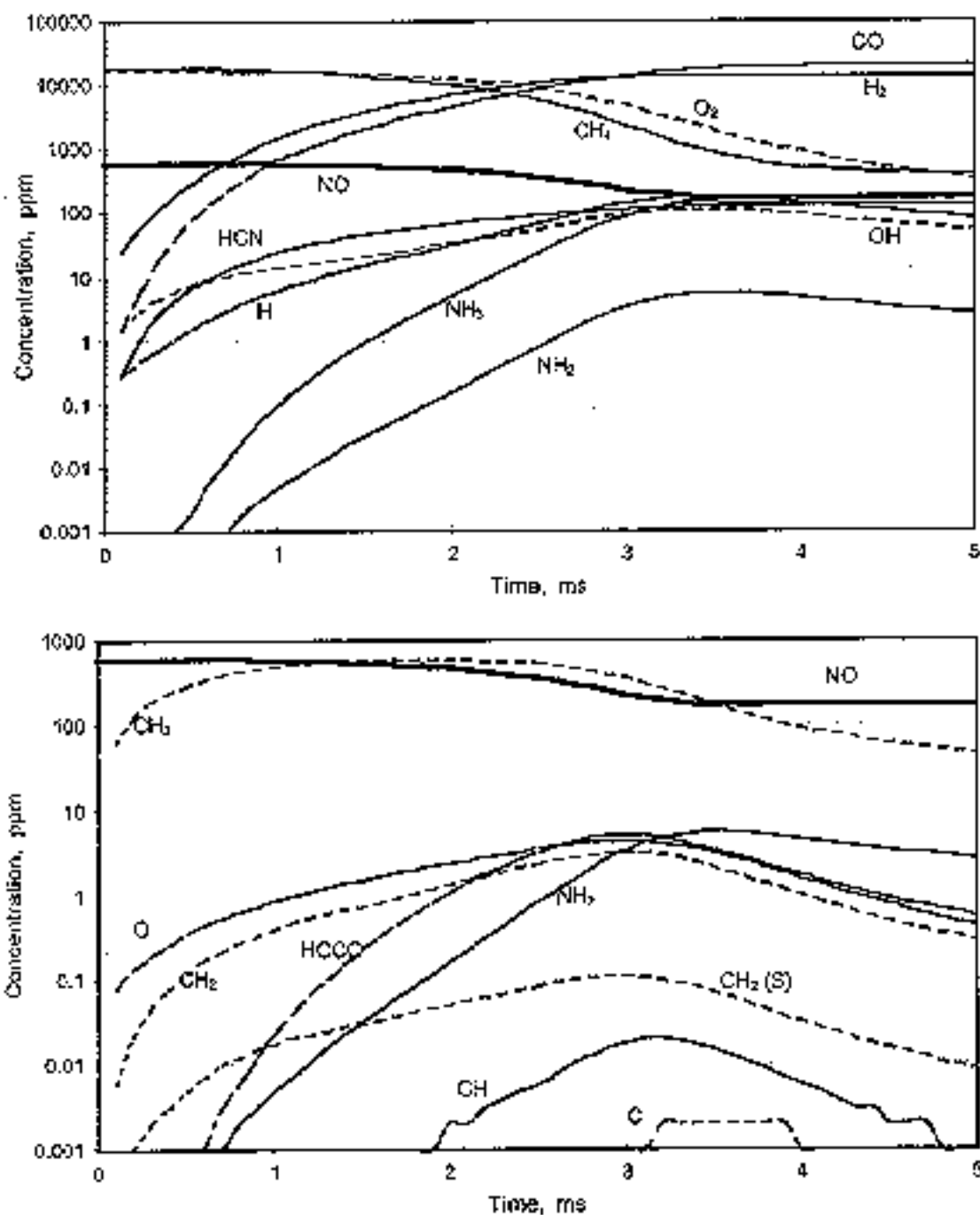


Figure 8.2.5. Kinetic curves in the reburning zone at $SR_2 = 0.90$, $T_1 = 1700$ K, and $t = 5$ ms.

Analysis of reaction rates for the NO reactions with C-radicals at $SR_2 = 0.90$ has been performed at the maximum point of radical concentrations (3 ms). The same conclusion can be made as for $SR_2 = 0.99$: the primary NO-removing radicals in decreasing order of importance is HCCO, CH_2 , CH_3 , CH, $CH_2(S)$, and C.

Dependence on Reburn Zone Stoichiometry. Figure 8.2.6 compares modeling and experimental data on concentrations of NO, NH₃, HCN, and TFN in the reburning zone ($t = 0.5$ s) at $T_1 = 1700$ K for different reburn fuel concentrations (various SR_2). The main difference between the experimental and modeling data sets is observed at low SR_2 where modeling predicts higher NH₃ concentration, but experiment demonstrates higher HCN level.

However, at $SR_2 = 0.90-0.99$, experimental and modeling concentrations are close to each other. It worth noting that experimental data can, of course, be affected by the rate of mixing. For this reason, mixing rates will be introduced as a variable in Section 8.3. However, Figure 8.2.6 demonstrates the current level of confidence in kinetic mechanisms developed for modeling of reburning. Even for the simplified treatment of mixing, the model can predict major reaction trends and can help to find prospective conditions of NO removal, for verification by experiment.

Dependence on Reburn Fuel Injection Temperature. Figure 8.2.7 compares performance of the reburning process at different temperatures for $SR_2 = 0.99, 0.95,$ and 0.90 . Under conditions close to stoichiometry, $SR_2 = 0.99$, concentrations of NH₃ and HCN in the reburning zone are less than 1 ppm, and all TFN is in the form of NO. TFN concentration in the reburning zone is decreased by 20-30%, and it is smaller at lower temperatures where C-radicals exist longer. Since they do not disappear too fast, more C-radicals are available for the reactions with NO. For instance, as shown in Figure 8.2.4, the first, fast reburning stage proceeds within 5 ms at $T = 1700$ K, mainly within 2 ms. At 1500 K, C-radicals do not disappear so fast, and the first stage proceeds longer, within about 20 ms. As a result, NO concentration drops in this fast stage from 600 to 535 ppm at 1700 K, but at 1500 K the process is more efficient: NO decreases from 600 to 450 ppm.

At $SR_2 = 0.95$ (Figure 8.2.7), only small amounts of NH₃ and HCN are formed at about 1500 K, and most of TFN exists in the form of NO. TFN concentration again lower at low temperatures, and it is within 40-65% TFN reduction range. At $T_1 = 1500$ K, the fast reburning stage proceeds in about 30-40 ms, much slower than at 1700 K (5 ms). The slower reactions of C-radicals cause more efficient first reburning stage: NO concentration decreases from 600 to 475 ppm and from 600 to 300 ppm at 1700 and 1500 K, respectively.

At higher reburn fuel injection rate (Figure 8.2.7, $SR_2 = 0.90$) most of NO is converted to NH₃ and HCN. Efficiency of TFN removal is 20-55%, and, in the contrary to the previous cases, TFN removal is more efficient at higher temperatures. Explanation of this effect is straightforward. At $SR_2 = 0.90$, the efficiency of NO removal continues to increase, as seen in Figure 8.2.7, and NO level is smaller at low temperatures. However, concentrations of NH₃ and HCN are much higher

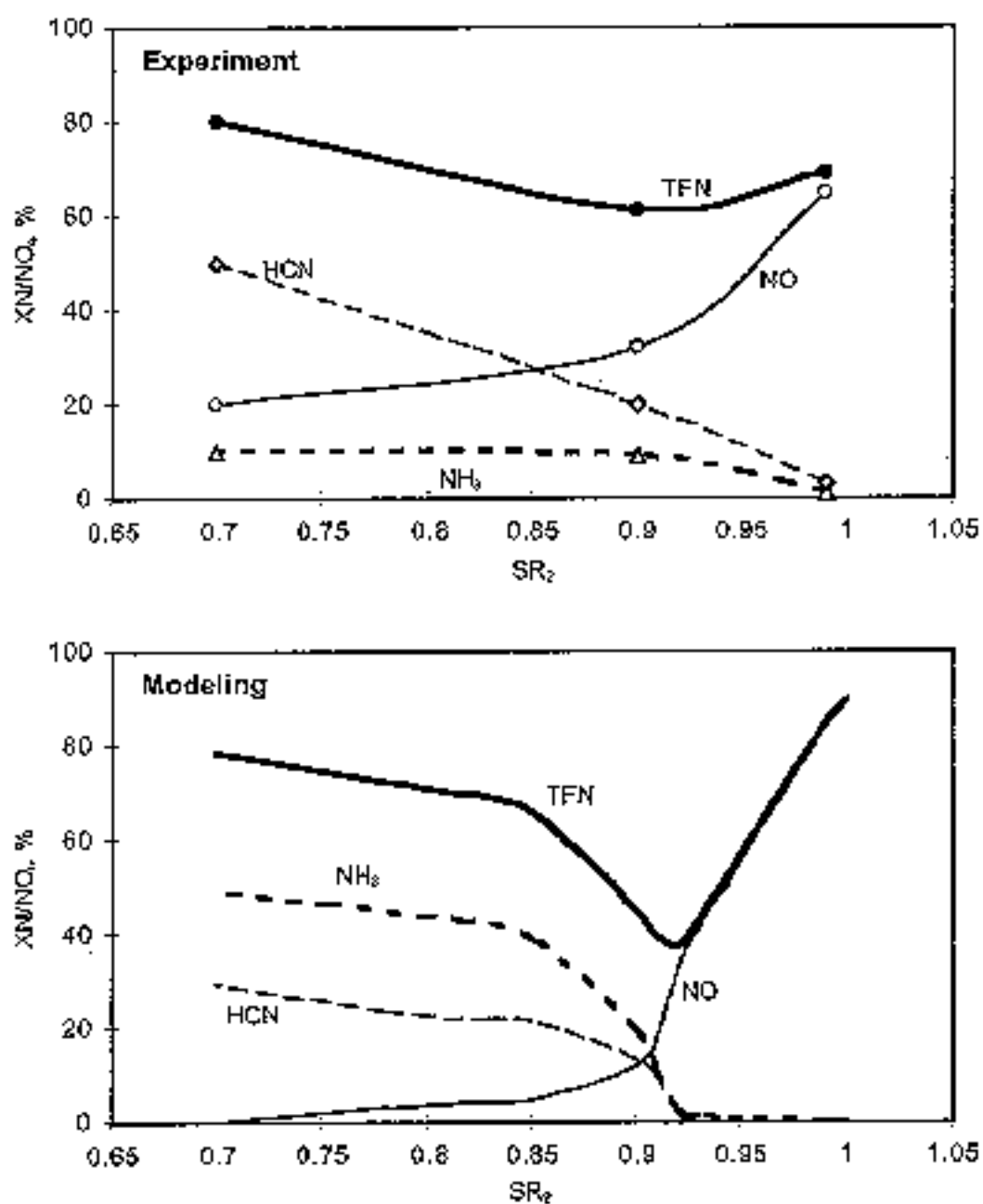


Figure 8.2.6. Modeling and experimental data on concentrations of NO, NH_3 , HCN, and TFN in the reburning zone ($t = 0.5$ s) at $T_1 = 1700$ K for different concentrations of reburning fuel, SR_2 .

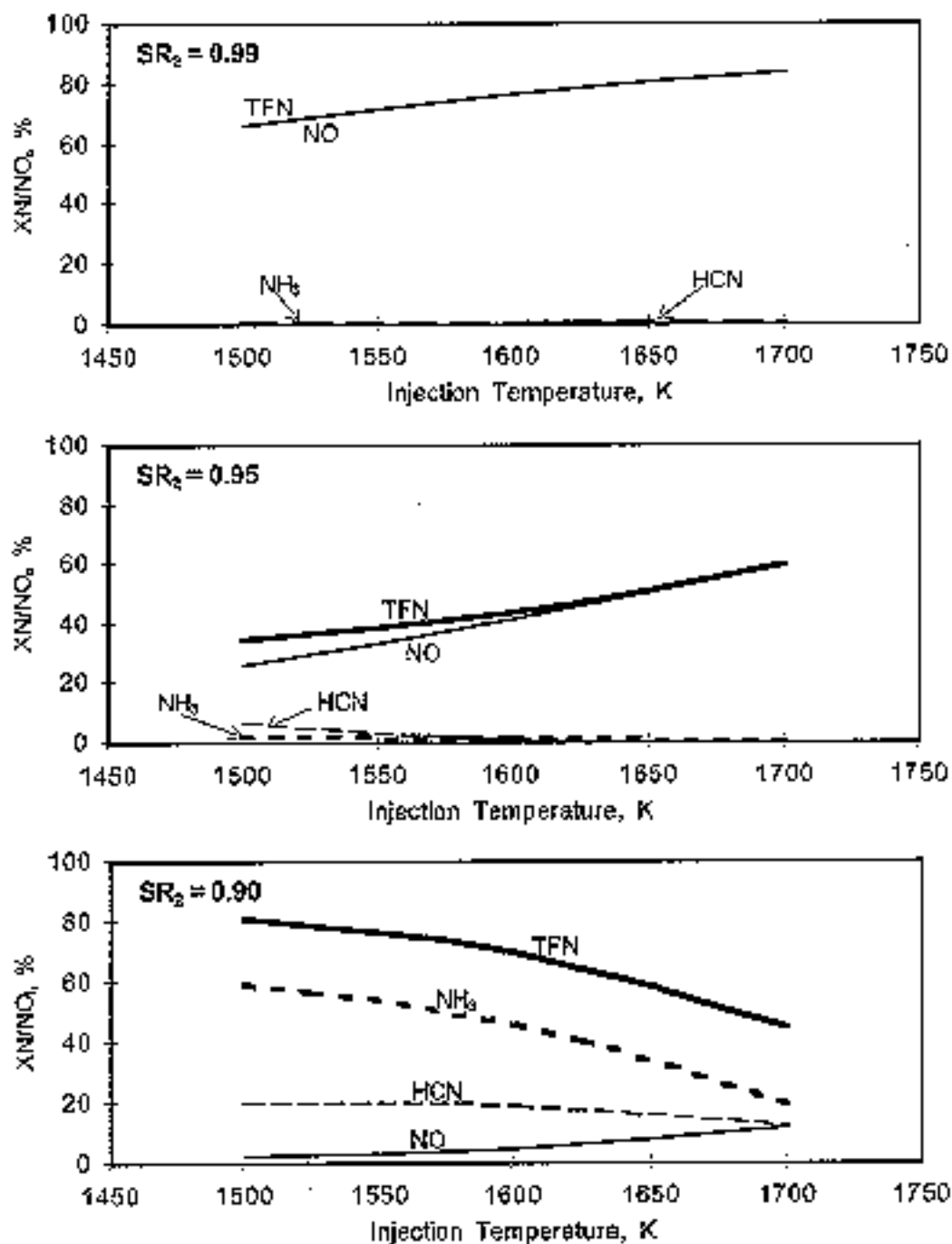


Figure 8.2.7. Modeling data on concentrations of NO, NH₃, HCN, and TFN in the reburning zone ($t = 0.5$ s) at $T_1 = 1500$ - 1700 K for different concentrations of reburning fuel, SR_2 .

than NO, and they decrease at higher temperatures since they react faster. Therefore, TFN decreases at $T = 1700$ K.

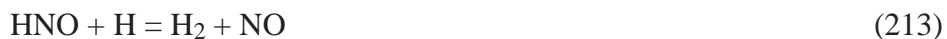
Thus, modeling shows that at higher reburn fuel mass flow rates (SR_2 at about 0.90), higher temperatures results in higher efficiency of TFN removal. At lower injection rates ($SR_2 = 0.950.99$), reburning efficiency is higher at lower temperatures.

Sensitivity Analysis at $SR_2=0.99$. Sensitivity analysis was performed for reburn fuel injection at 1700 K, for $SR_2=0.99$ and 0.90, to better understand the important reactions for these conditions. The following is a summary of the reburn zone analysis. A more detailed analysis appears in Zamansky et al. (1997a). Results for $SR_2=0.99$ will be addressed first, followed by those for $SR_2=0.90$.

The kinetic curves for $SR_2=0.99$ are presented in Figure 8.2.1. As previously discussed, there are two regions of NO reduction: the initial fast decrease (from 600 to 540 ppm) which lasts for a very short period of time (about 2-3 ms), followed by a slow decrease (to 502 ppm). Figures 8.2.8 and 8.2.9 present reactions which contribute to NO reduction during the fast and slow NO reduction regions, respectively. (In these and other plots which follow, some curve labels overlap near the y-axis. Note that the reactions of interest are those with large positive or negative contribution or sensitivity factors; it is not important to read values close to the axis.) The most important steps of NO reduction in the fast region (Figure 8.2.8) are reactions (273) and (248):

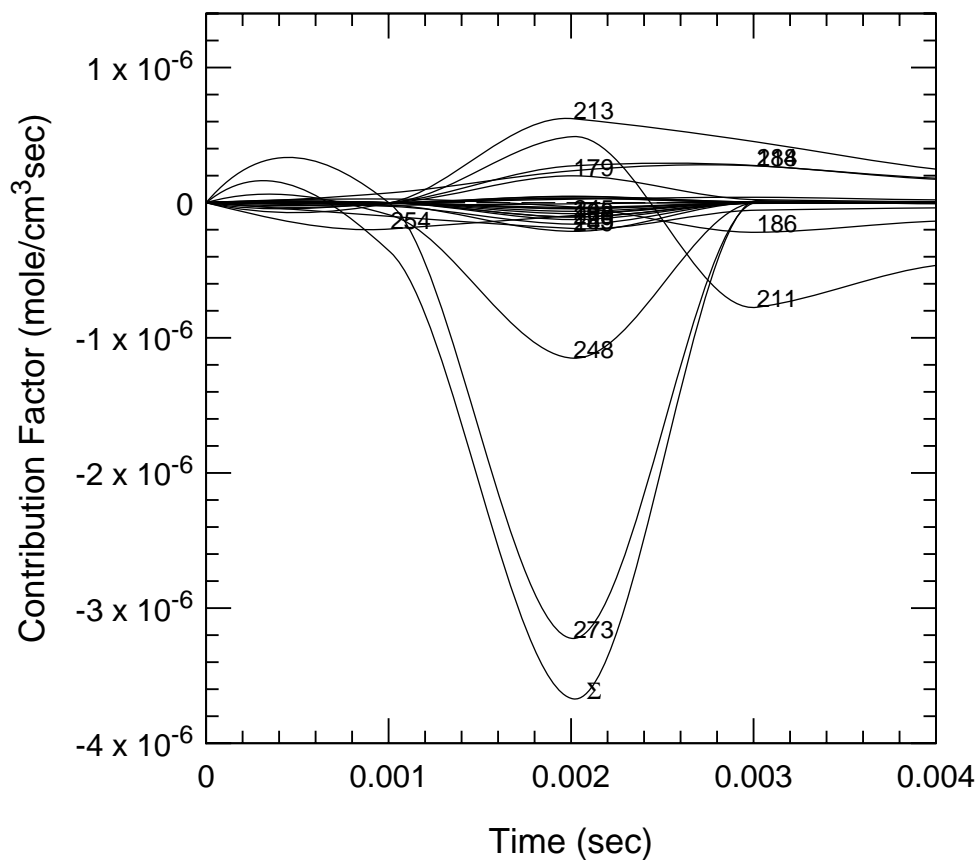


Simultaneously, some HNO and NO_2 are formed which can contribute to both NO formation



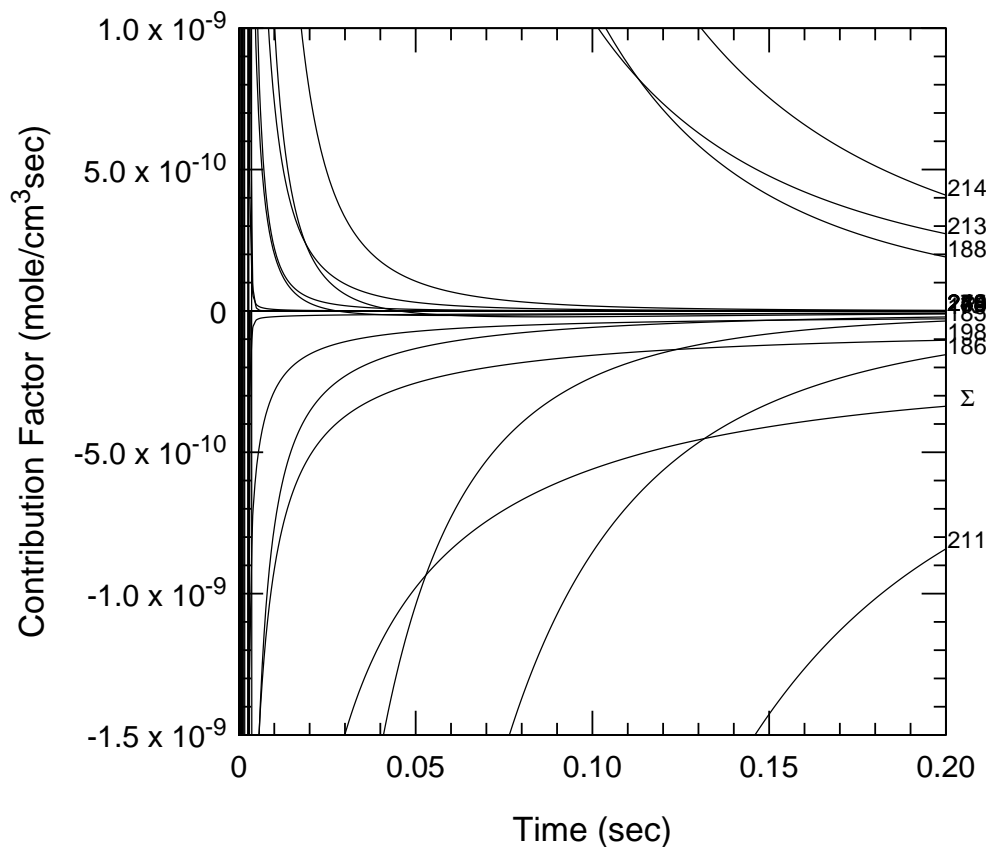
and NO reduction via reaction (211) and (186):





273	$\text{HCCO} + \text{NO} \rightleftharpoons \text{HCNO} + \text{CO}$	249	$\text{CH}_2 + \text{NO} \rightleftharpoons \text{OH} + \text{HCN}$
248	$\text{CH}_2 + \text{NO} \rightleftharpoons \text{H} + \text{HNCO}$	179	$\text{N} + \text{OH} \rightleftharpoons \text{NO} + \text{H}$
211	$\text{H} + \text{NO} + \text{M} \rightleftharpoons \text{HNO} + \text{M}$	254	$\text{CH}_3 + \text{NO} \rightleftharpoons \text{HCN} + \text{H}_2\text{O}$
213	$\text{HNO} + \text{H} \rightleftharpoons \text{H}_2 + \text{NO}$	185	$\text{HO}_2 + \text{NO} \rightleftharpoons \text{NO}_2 + \text{OH}$
214	$\text{HNO} + \text{OH} \rightleftharpoons \text{NO} + \text{H}_2\text{O}$	250	$\text{CH}_2 + \text{NO} \rightleftharpoons \text{H} + \text{HCNO}$
188	$\text{NO}_2 + \text{H} \rightleftharpoons \text{NO} + \text{OH}$	198	$\text{NH} + \text{NO} \rightleftharpoons \text{N}_2\text{O} + \text{H}$
186	$\text{NO} + \text{O} + \text{M} \rightleftharpoons \text{NO}_2 + \text{M}$	245	$\text{CH} + \text{NO} \rightleftharpoons \text{HCN} + \text{O}$

Figure 8.2.8. NO contribution factors at $\text{SR}_2 = 0.99$ in the fast NO decrease region.



273 $\text{HCCO} + \text{NO} \rightleftharpoons \text{HCNO} + \text{CO}$	249 $\text{CH}_2 + \text{NO} \rightleftharpoons \text{OH} + \text{HCN}$
248 $\text{CH}_2 + \text{NO} \rightleftharpoons \text{H} + \text{HNCO}$	179 $\text{N} + \text{OH} \rightleftharpoons \text{NO} + \text{H}$
211 $\text{H} + \text{NO} + \text{M} \rightleftharpoons \text{HNO} + \text{M}$	254 $\text{CH}_3 + \text{NO} \rightleftharpoons \text{HCN} + \text{H}_2\text{O}$
213 $\text{HNO} + \text{H} \rightleftharpoons \text{H}_2 + \text{NO}$	185 $\text{HO}_2 + \text{NO} \rightleftharpoons \text{NO}_2 + \text{OH}$
214 $\text{HNO} + \text{OH} \rightleftharpoons \text{NO} + \text{H}_2\text{O}$	250 $\text{CH}_2 + \text{NO} \rightleftharpoons \text{H} + \text{HCNO}$
188 $\text{NO}_2 + \text{H} \rightleftharpoons \text{NO} + \text{OH}$	198 $\text{NH} + \text{NO} \rightleftharpoons \text{N}_2\text{O} + \text{H}$
186 $\text{NO} + \text{O} + \text{M} \rightleftharpoons \text{NO}_2 + \text{M}$	245 $\text{CH} + \text{NO} \rightleftharpoons \text{HCN} + \text{O}$

Figure 8.2.9 NO contribution factors at $\text{SR}_2 = 0.99$ in the slow NO decrease region.

Reactions (211) and (186) are mainly responsible for the slow NO decrease as shown in Figure 8.2.9. The NO decrease is slow since these reactions compete with NO formation via (188), (213), and (214).

Figures 8.2.10 and 8.2.11 show sensitivity coefficients for NO formation and reduction in the reburning zone with $SR_2=0.99$ in the fast and slow NO reduction regions, respectively. Figure 8.2.10 clearly demonstrates that the chain branching steps



are responsible for the boost of radicals. In these reactions, each H atom and CH_3 radical forms several active species. Reaction (159) is also a chain branching step since C_2H_5 instantly decomposes into C_2H_4 and H. The increased radical pool generates carbon-containing radicals (HCCO and CH_2) which reduce NO via reactions (273) and (248).

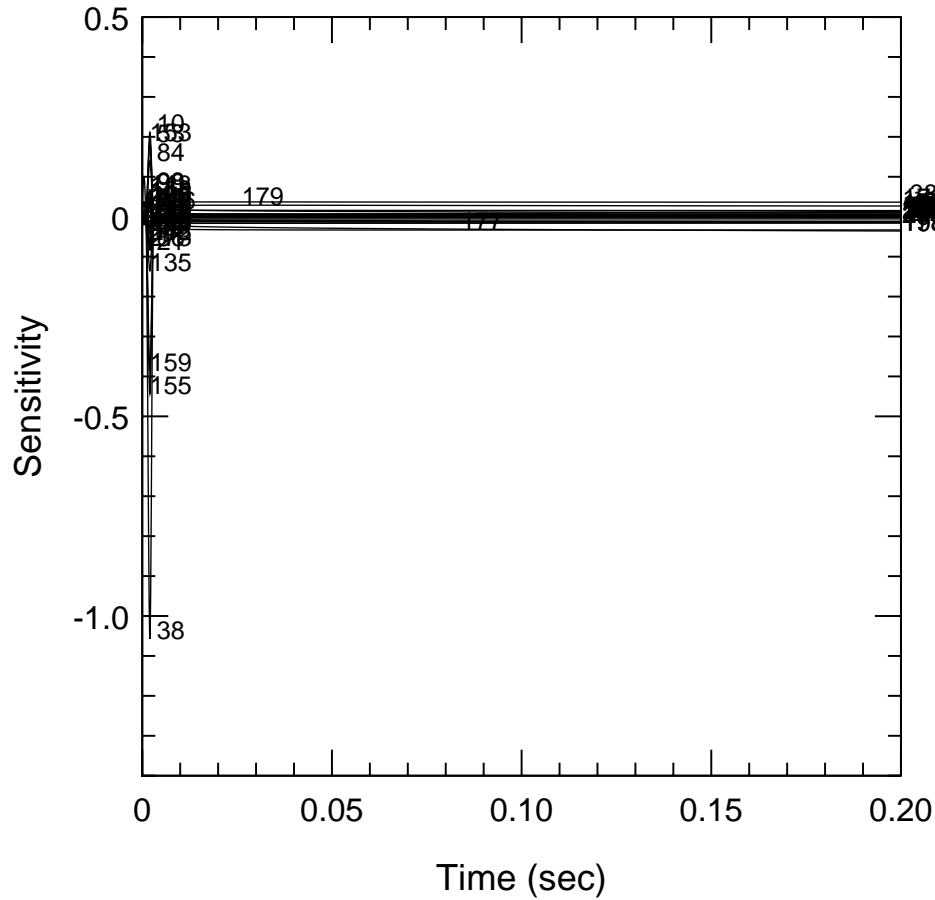
Figure 8.2.11 shows that two reactions



primarily contribute to NO removal in the slow region. Reaction (177) competes with reaction



Interestingly, the major chain branching step, reaction (38), behaves differently in the fast and slow reduction regions. In the fast region, this reaction supports formation of the radical pool and increases concentrations of carbon-containing radicals, such as HCCO, CH_2 , etc. As a result, the radicals react with NO, and its concentration decreases. At a certain point, concentrations of carbon-containing radicals decrease since all methane is oxidized, and NO removal becomes slow. However, in this slow region, concentrations of N and NH are relatively high, and reactions (177) and (198) are responsible for NO reduction. The decrease of NO concentration is slow since reaction (38) results in an increase of the OH level that causes acceleration of NO formation via (179).



38	$\text{H} + \text{O}_2 \rightleftharpoons \text{O} + \text{OH}$	135	$\text{CH}_2 + \text{O}_2 \rightleftharpoons \text{OH} + \text{HCO}$
155	$\text{CH}_3 + \text{O}_2 \rightleftharpoons \text{O} + \text{CH}_3\text{O}$	21	$\text{O} + \text{C}_2\text{H}_2 \rightleftharpoons \text{H} + \text{HCCO}$
159	$2\text{CH}_3 \rightleftharpoons \text{H} + \text{C}_2\text{H}_5$	273	$\text{HCCO} + \text{NO} \rightleftharpoons \text{HCNO} + \text{CO}$
10	$\text{O} + \text{CH}_3 \rightleftharpoons \text{H} + \text{CH}_2\text{O}$	86	$2\text{OH} \rightleftharpoons \text{O} + \text{H}_2\text{O}$
153	$\text{CH}_2(\text{S}) + \text{CO}_2 \rightleftharpoons \text{CO} + \text{CH}_2\text{O}$	98	$\text{OH} + \text{CH}_4 \rightleftharpoons \text{CH}_3 + \text{H}_2\text{O}$
53	$\text{H} + \text{CH}_4 \rightleftharpoons \text{CH}_3 + \text{H}_2$	11	$\text{O} + \text{CH}_4 \rightleftharpoons \text{OH} + \text{CH}_3$
84	$\text{OH} + \text{H}_2 \rightleftharpoons \text{H} + \text{H}_2\text{O}$	99	$\text{OH} + \text{CO} \rightleftharpoons \text{H} + \text{CO}_2$

Figure 8.2.10. NO sensitivity coefficients at $\text{SR}_2=0.99$ in the fast NO decrease region. Graph shows important reactions at early reaction times. Sensitivities for long reaction times (over lapping here) are shown in Figure 8.2.11.

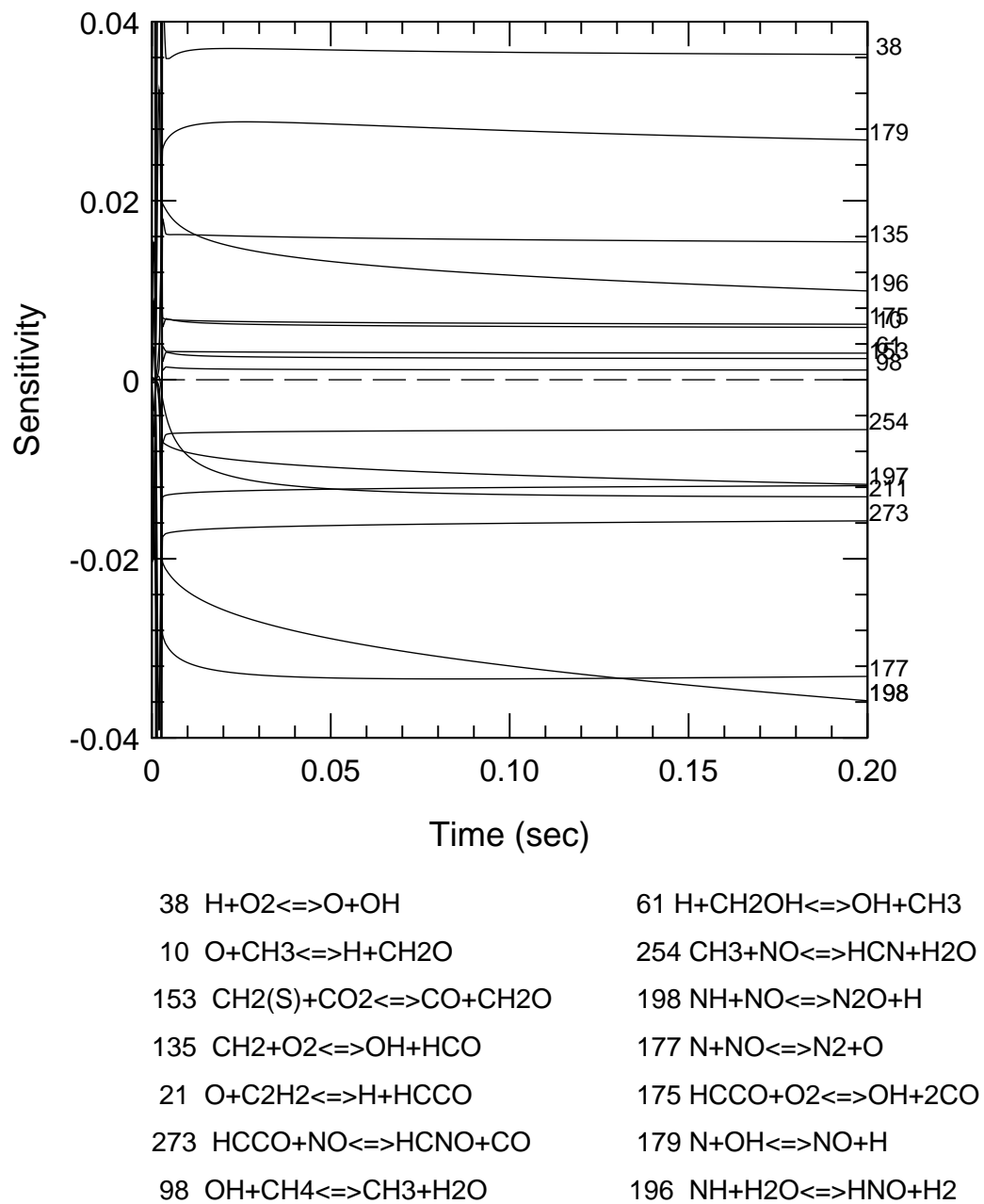


Figure 8.2.11. NO sensitivity coefficients at $\text{SR}_2=0.99$ in the slow NO decrease region.

Sensitivity Analysis at SR₂=0.90. The kinetic curves for SR₂=0.90 are presented in Figure 8.2.3. In this case, the NO concentration decreases from 600 to 160 ppm, and then slowly to 67 ppm. At t=0.5 s, the mixture contains 75 ppm HCN and 115 ppm NH₃. Methane is even more rapidly converted to CO and H₂. Again there are two steps of NO reduction: the fast short and slow long regions.

Figures 8.2.12 and 8.2.13 show NO contribution coefficients for the fast and slow NO reduction regions, respectively, at SR₂=0.90. The same as at SR₂=0.99, the most important step of NO reduction in the fast region (Figure 8.2.12) is reaction (273). Reactions (248) and:



are less important, and some NO is formed from HNO via (-211).

At longer reaction times (Figure 8.2.13), reaction (281) is of primary importance for NO reduction



followed by reactions (254) and (273). In this region, the NO is also formed from HNO (-211).

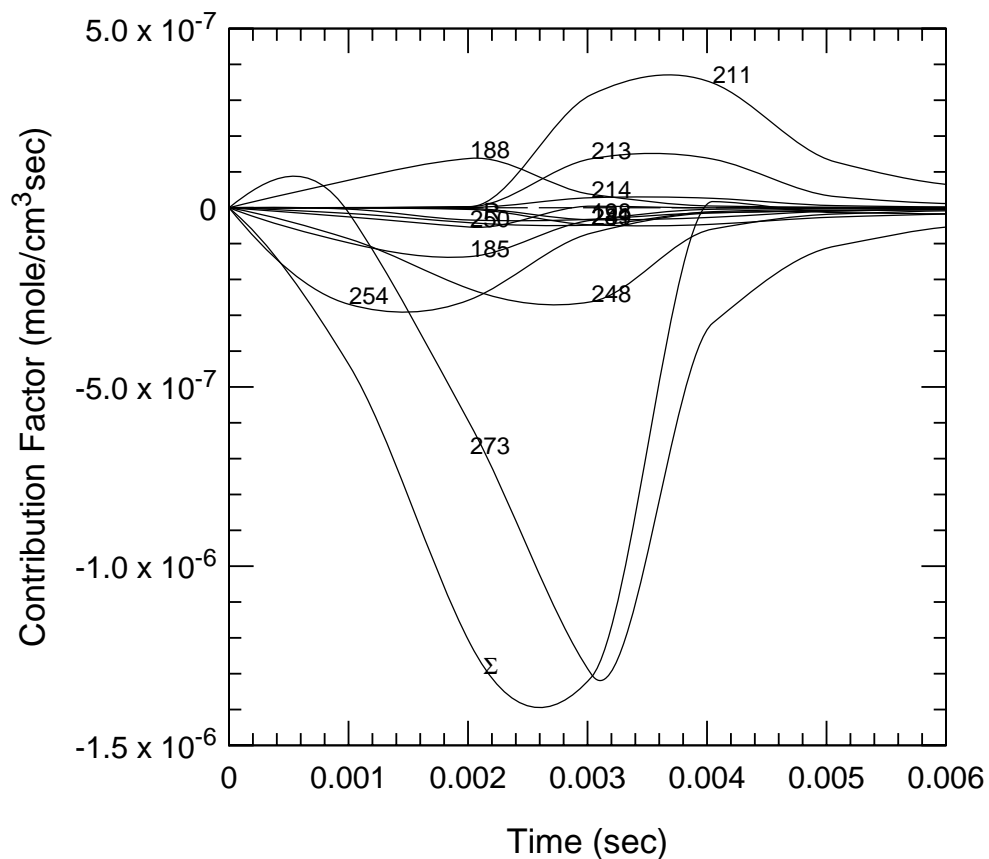
Sensitivity coefficients in the reburning zone at SR₂=0.90 in the fast NO reduction regions shows that chain branching reactions (38), (155), and (159) are primarily responsible for increasing the radical pool and initially reducing NO, the same as for SR₂=0.99.

In the slow region (Figure 8.2.14), there are many elementary processes which affect the NO concentration. The main NO reducing reactions include interaction of NO with NH₂ and HCCO radicals, via (281) and (273), and reaction (281) becomes increasingly important at longer times. Reaction



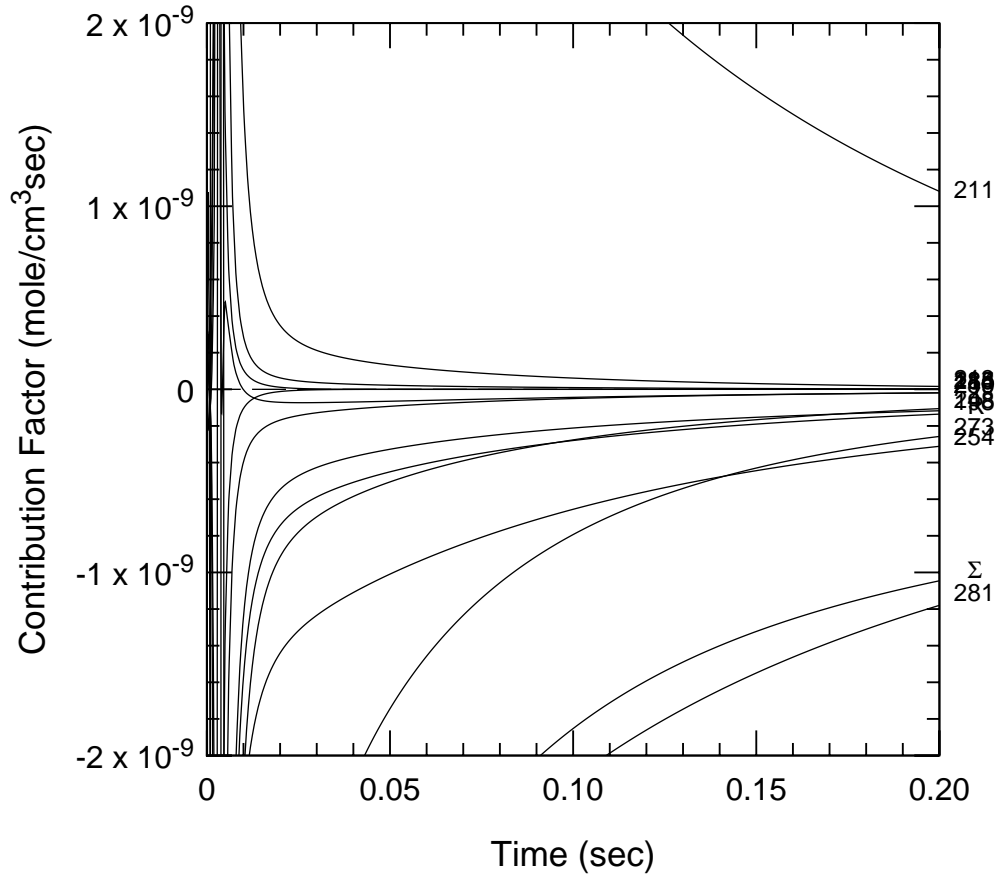
decreases the NH₂ concentration and consequently contributes to increasing NO.

Contribution and sensitivity factors have also been calculated at SR₂=0.90 for NH₃, HCN, and HNO. Contribution factors are dominated by transients occurring in about the first 10 ms. Reverse reactions



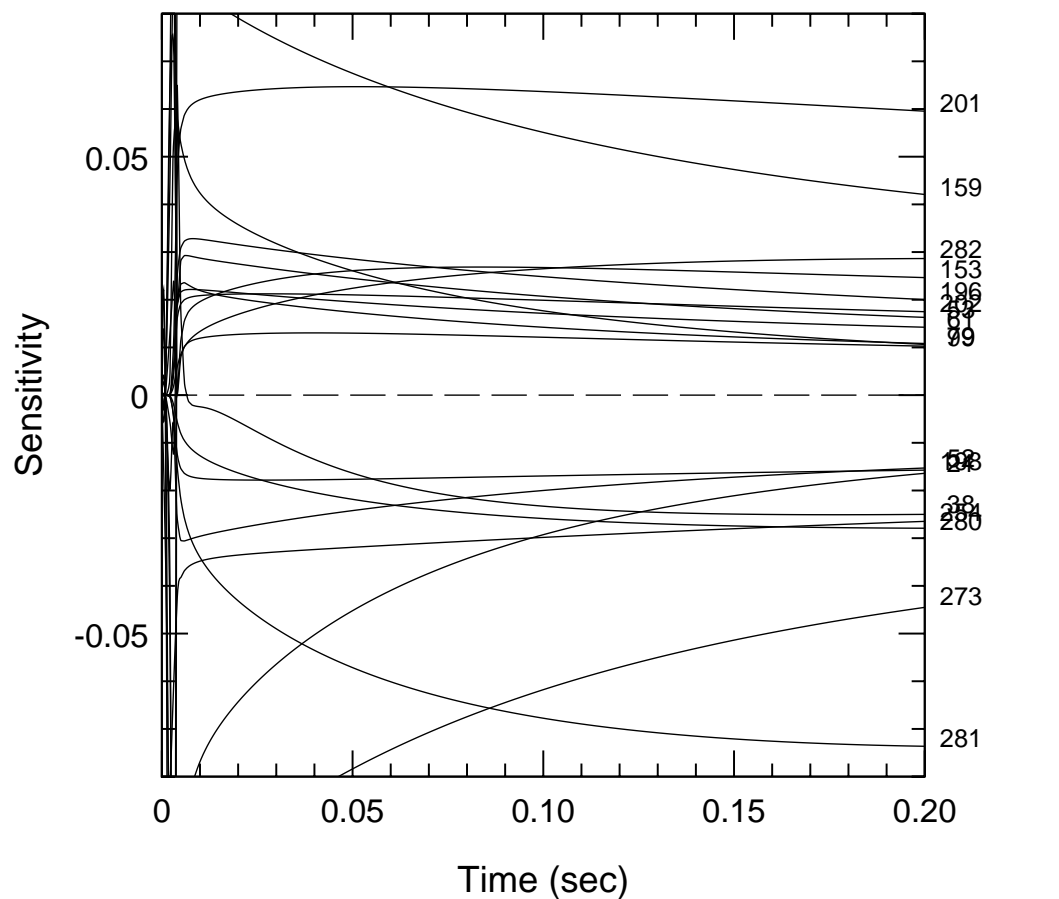
273	$\text{HCCO} + \text{NO} \rightleftharpoons \text{HCNO} + \text{CO}$	250	$\text{CH}_2 + \text{NO} \rightleftharpoons \text{H} + \text{HCNO}$
211	$\text{H} + \text{NO} + \text{M} \rightleftharpoons \text{HNO} + \text{M}$	249	$\text{CH}_2 + \text{NO} \rightleftharpoons \text{OH} + \text{HCN}$
254	$\text{CH}_3 + \text{NO} \rightleftharpoons \text{HCN} + \text{H}_2\text{O}$	281	$\text{NH}_2 + \text{NO} \rightleftharpoons \text{N}_2 + \text{H}_2\text{O}$
248	$\text{CH}_2 + \text{NO} \rightleftharpoons \text{H} + \text{HNCO}$	198	$\text{NH} + \text{NO} \rightleftharpoons \text{N}_2\text{O} + \text{H}$
188	$\text{NO}_2 + \text{H} \rightleftharpoons \text{NO} + \text{OH}$	214	$\text{HNO} + \text{OH} \rightleftharpoons \text{NO} + \text{H}_2\text{O}$
213	$\text{HNO} + \text{H} \rightleftharpoons \text{H}_2 + \text{NO}$	R	Remainder
185	$\text{HO}_2 + \text{NO} \rightleftharpoons \text{NO}_2 + \text{OH}$	Σ	Summation

Figure 8.2.12. NO contribution factors at $\text{SR}_2 = 0.90$ in the fast NO decrease region.



273	$\text{HCCO} + \text{NO} \rightleftharpoons \text{HCNO} + \text{CO}$	250	$\text{CH}_2 + \text{NO} \rightleftharpoons \text{H} + \text{HCNO}$
211	$\text{H} + \text{NO} + \text{M} \rightleftharpoons \text{HNO} + \text{M}$	249	$\text{CH}_2 + \text{NO} \rightleftharpoons \text{OH} + \text{HCN}$
254	$\text{CH}_3 + \text{NO} \rightleftharpoons \text{HCN} + \text{H}_2\text{O}$	281	$\text{NH}_2 + \text{NO} \rightleftharpoons \text{N}_2 + \text{H}_2\text{O}$
248	$\text{CH}_2 + \text{NO} \rightleftharpoons \text{H} + \text{HNCO}$	198	$\text{NH} + \text{NO} \rightleftharpoons \text{N}_2\text{O} + \text{H}$
188	$\text{NO}_2 + \text{H} \rightleftharpoons \text{NO} + \text{OH}$	214	$\text{HNO} + \text{OH} \rightleftharpoons \text{NO} + \text{H}_2\text{O}$
213	$\text{HNO} + \text{H} \rightleftharpoons \text{H}_2 + \text{NO}$	R	Remainder
185	$\text{HO}_2 + \text{NO} \rightleftharpoons \text{NO}_2 + \text{OH}$	Σ	Summation

Figure 8.2.13. NO contribution factors at $\text{SR}_2 = 0.90$ in the slow NO decrease region.



38 $\text{H} + \text{O}_2 \rightleftharpoons \text{O} + \text{OH}$	53 $\text{H} + \text{CH}_4 \rightleftharpoons \text{CH}_3 + \text{H}_2$
159 $2\text{CH}_3 \rightleftharpoons \text{H} + \text{C}_2\text{H}_5$	281 $\text{NH}_2 + \text{NO} \rightleftharpoons \text{N}_2 + \text{H}_2\text{O}$
273 $\text{HCCO} + \text{NO} \rightleftharpoons \text{HCNO} + \text{CO}$	201 $\text{NH}_2 + \text{H} \rightleftharpoons \text{NH} + \text{H}_2$
21 $\text{O} + \text{C}_2\text{H}_2 \rightleftharpoons \text{H} + \text{HCCO}$	79 $\text{H} + \text{HCCO} \rightleftharpoons \text{CH}_2(\text{S}) + \text{CO}$
10 $\text{O} + \text{CH}_3 \rightleftharpoons \text{H} + \text{CH}_2\text{O}$	282 $\text{NH}_2 + \text{NO} \rightleftharpoons \text{N}_2 + \text{H}_2\text{O}$
153 $\text{CH}_2(\text{S}) + \text{CO}_2 \rightleftharpoons \text{CO} + \text{CH}_2\text{O}$	280 $\text{NH}_2 + \text{NO} \rightleftharpoons \text{NNH} + \text{OH}$
254 $\text{CH}_3 + \text{NO} \rightleftharpoons \text{HCN} + \text{H}_2\text{O}$	99 $\text{OH} + \text{CO} \rightleftharpoons \text{H} + \text{CO}_2$

Figure 8.2.14. NO sensitivity coefficients at $\text{SR}_2=0.90$ in the slow NO decrease region.



are important contributors to NH_3 formation. HCN is mainly formed via (254) and



HNO radicals are important intermediate species in the fast reaction region. They are rapidly formed from NH



and decompose via reaction (211).

Sensitivity analysis for NH_3 at $\text{SR}=0.90$ show an initial fast transient where the same chain branching steps (38, 155, 159) which influence NO also result in a higher NH_2 level and a faster rate of NH_3 formation via reverse reactions (-276) and (-277). In the slow region, NH_3 removal is enhanced by reactions (159), (281), and



The HCN concentration is initially increased due to reactions (254) and (38), and then reduced mainly due to reaction



8.2.2 Injection of Ammonia into the Reburning Zone (AR-Rich)

When fuel is added into the reburning zone, the oxygen disappears very fast in the reaction with the fuel to form CO and H_2 . If N-agents (ammonia, urea, etc.) are injected into the reburning zone, they form NH_i radicals (NH_2 , NH , N) which are active in NO removal reactions. The NH_i radicals can react either with O_2 into NO or with NO into N_2 . The NO reduction process is effective if the NH_i precursors (N-agents) appear in the gas mixture when concentration of oxygen has been significantly depleted by the reburning fuel, thus preventing oxidation of N-agents into NO . Calculated characteristic times for O_2 disappearance after reburn fuel injection are less than 0.01 s at 1700 K

and about 0.1 s at 1450 K. The delay time between reburn fuel injection and the formation of NH_i species should be close to these times for effective NO reduction.

Results of calculations which demonstrate the effect of the delayed ammonia injection on NO reduction by CH_4 reburning are presented in Figure 8.2.15. The first graph shows concentrations of NO, NH_3 , HCN, and TFN after 0.5 s as a function of SR_2 for injection of 600 ppm NH_3 without delay, i.e. co-injection with the reburning fuel. At $\text{SR}_2 = 0.90$, ammonia co-injection causes a decrease in TFN from 1200 ppm (600 ppm NO and 600 ppm NH_3) to 327 ppm. At $\text{SR}_2 = 0.90$, the concentration of the reburning fuel is high, and its reaction with the oxygen forms a large radical pool. The radicals initiate a rapid reaction between NH_3 and NO, and the TFN concentration is depleted. This reaction requires a small amount of oxygen to support the radical pool, and this amount is available in the mixture during the first rapid reaction stage. The concentration of ammonia decreases slowly at $\text{SR}_2 = 0.90$ since most of the oxygen reacts with the high concentration of CH_4 . Some CH_4 (about 400 ppm) remains unreacted in the reburning zone. At $\text{SR}_2 = 0.99$, all NH_3 and CH_4 are instantly oxidized since the concentration of O_2 is the same, but the $[\text{CH}_4]$ level is much lower. In this oxidation process, ammonia forms some additional NO, and this NO cannot be decreased in the reaction with ammonia since it is no longer present in the mixture. Therefore, $\text{TFN} = \text{NO} = 742$ ppm, i.e. the NO concentration increases.

The picture is completely different if ammonia is injected with a 0.1 s delay time, as shown in the second graph in Figure 8.2.15. In this case, at $\text{SR}_2 = 0.90$, ammonia is injected when the O_2 concentration is already very low (about 0.01 ppm). Concentration of NO is reduced in the first rapid reburning stage within the delay time of 0.1 s and it decreases further utilizing some ammonia. However, in 0.5 s the NH_3 concentration is still high, about 420 ppm, and it does not react rapidly with NO since there is no oxygen to feed the radical pool. At $\text{SR}_2 = 0.99$, NH_3 is injected when the O_2 concentration is about 50 ppm (see Figure 8.2.1) and the OH concentration is still high. Therefore, in the presence of this oxygen level, NH_3 and NO are capable of reacting with each other, and TFN concentration efficiently decreases. Thus, at the right conditions, delayed ammonia injection can result in more effective NO removal. These conditions require the presence of both reagents and some oxygen, and so is most effective under near-stoichiometric conditions.

Parametric Dependencies. The effect of the delayed ammonia injection depends on many factors, including the value of SR_2 , the delay time, ammonia concentration, oxygen concentration, etc. Figure 8.2.16 presents concentrations of fuel-N species in the reburning zone at $\text{SR}_2 = 0.99$ as a function of ammonia injection delay time. If ammonia is injected along with the reburning fuel, it rapidly disappears in the reaction with the high amount of oxygen and causes some NO formation.

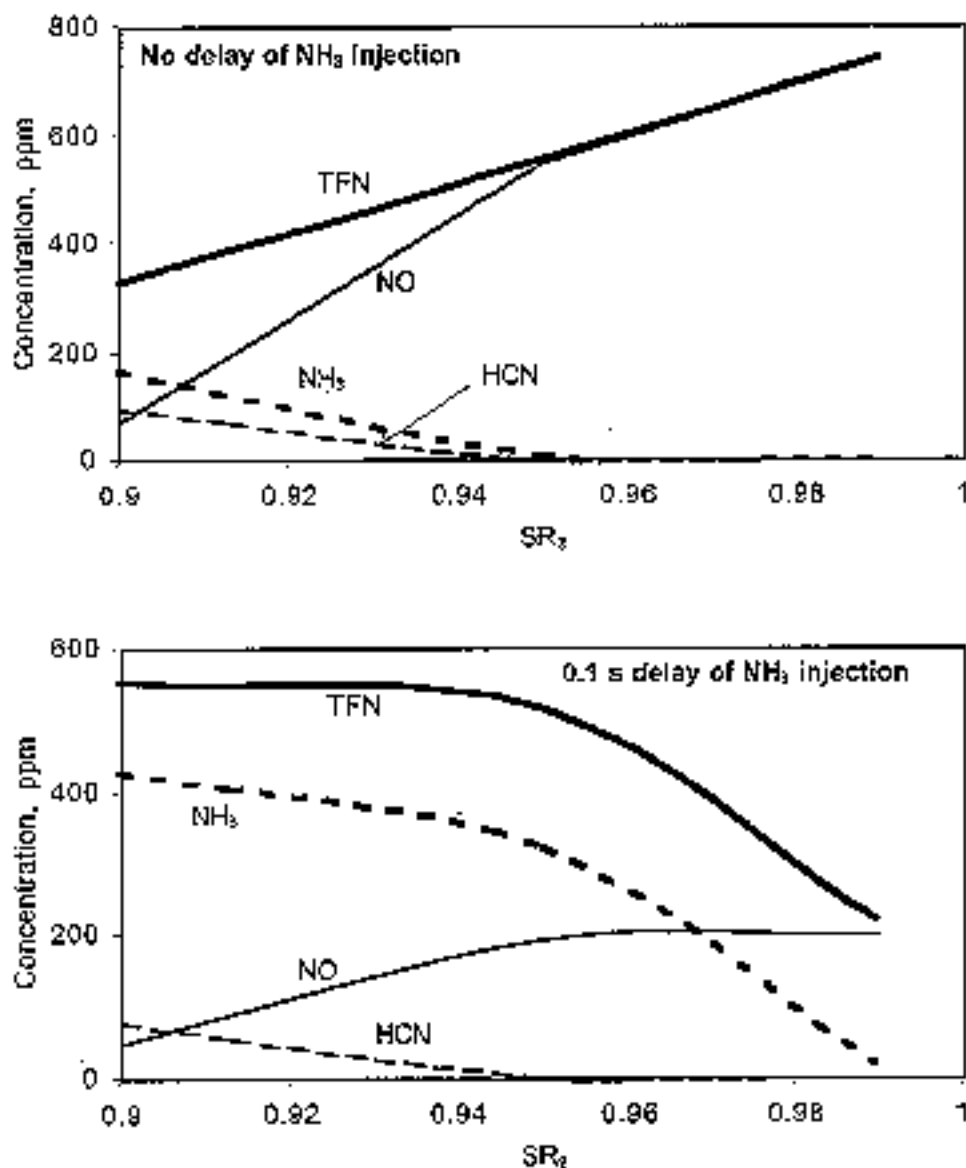


Figure 8.2.15. Effect of ammonia co-injection with the reburning fuel and 0.1 s delayed NH_3 injection on fuel-N species in the reburning zone. $[NH_3] = 600$ ppm, $NO_i = 600$ ppm, $T_3 = 1700$ K.

As previously discussed, the initial stage of reburning is fast and forms high concentrations of radicals. Therefore, injection of ammonia with a short delay time results in NH_3-O_2 interaction in the presence of the radicals and small amounts of oxygen. This interaction efficiently reduces concentrations of NO and TFN. If ammonia is injected with a longer delay time, NH_3 and NO interact with lower radical (and O_2) concentrations, and so the efficiency of NO and TFN removal is lower.

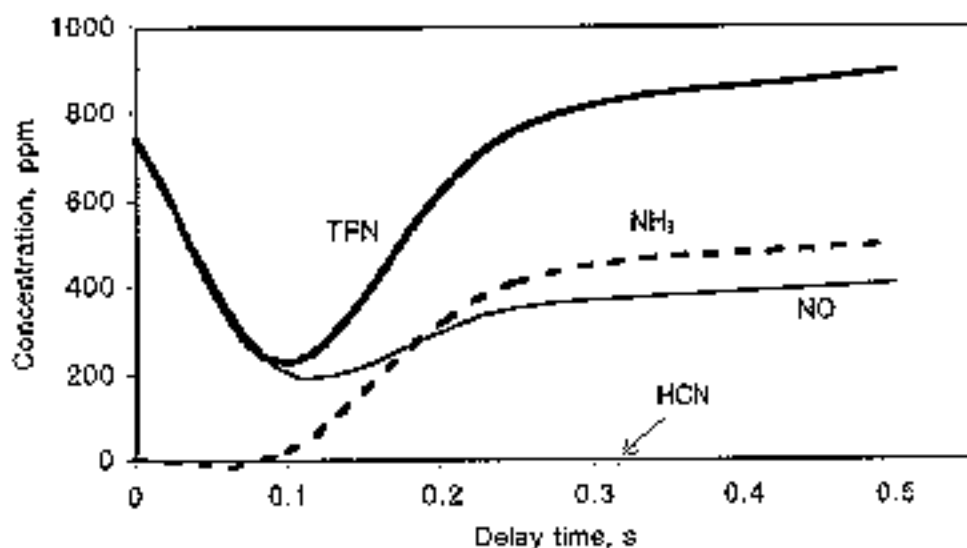


Figure 8.2.16. Effect of the delay time of NH_3 injection into the reburning zone at $\text{SR}_2 = 0.99$. Other conditions are the same as in Figure 8.2.15.

Figure 8.2.17 shows the dependence of NO and TFN on the quantity of NH_3 injected with a 0.1 s delay time at $\text{SR}_2 = 0.99$. As injected $[\text{NH}_3]$ increases, the resulting NO concentration decreases, but the residual $[\text{NH}_3]$ increases. The TFN concentration has a minimum which approximately corresponds to equimolecular amounts of NO and NH_3 in the gas mixture ($\text{NSR} = 1.0 - 1.3$).

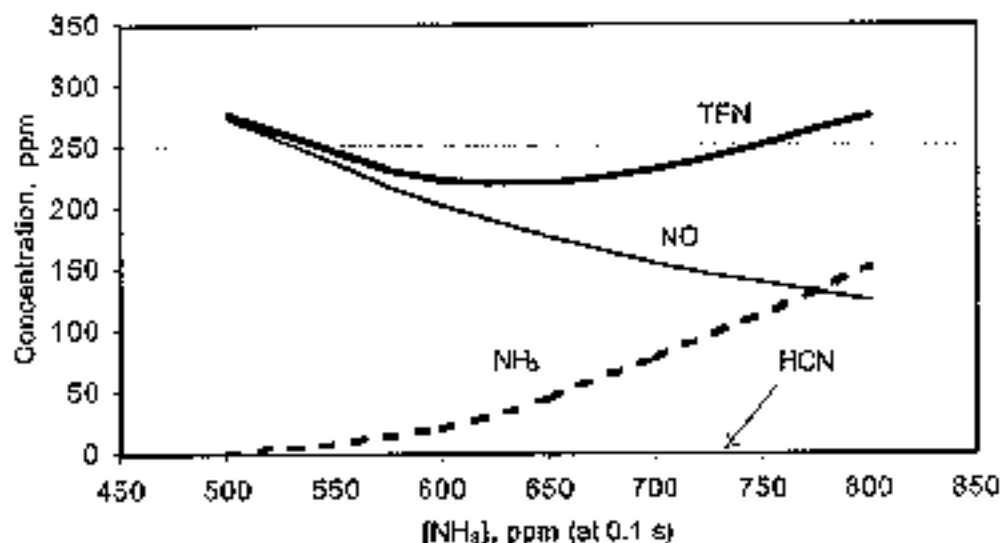
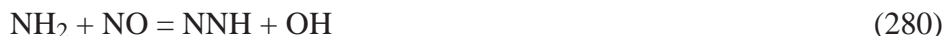


Figure 8.2.17. Effect of the NH_3 concentration injected into the reburning zone at $\text{SR}_2 = 0.99$ and 0.1 s delay time. Other conditions are the same as in Figure 8.2.15.

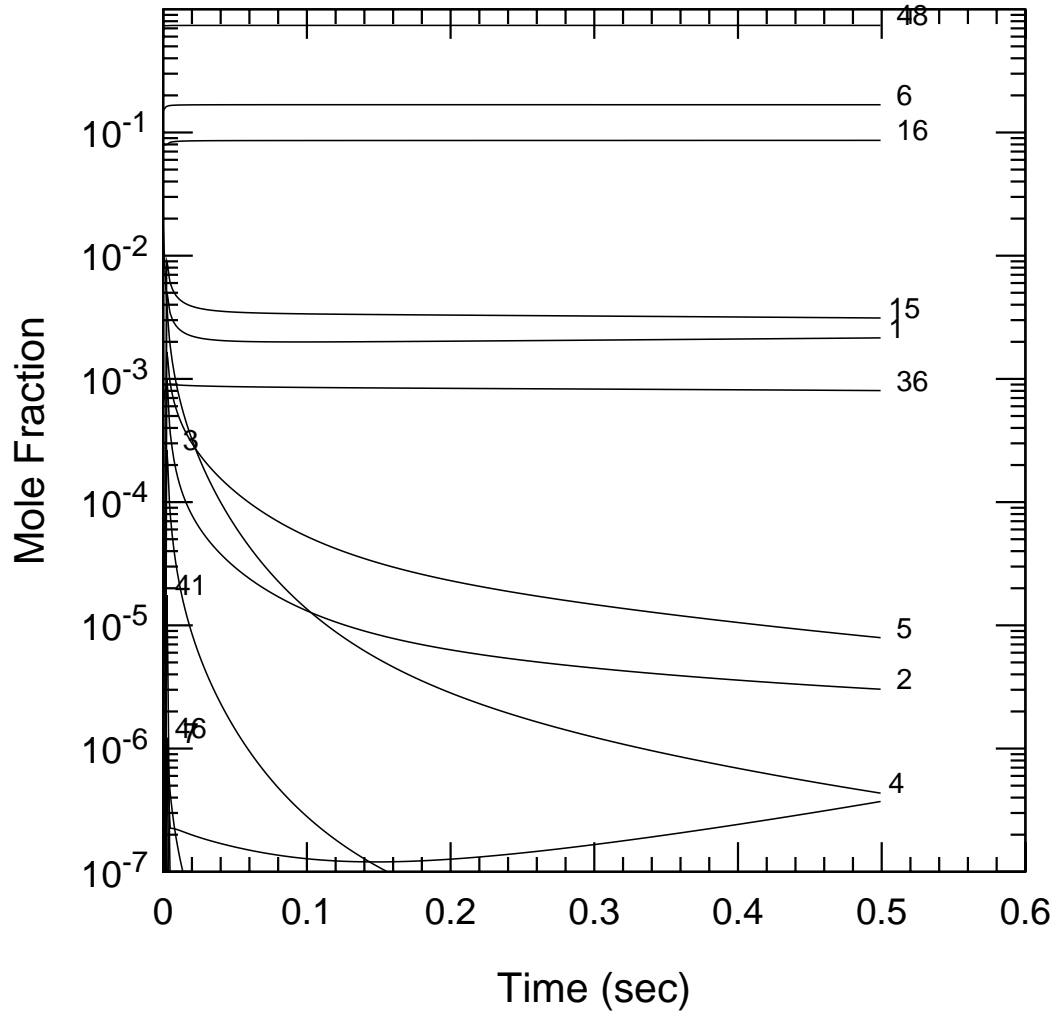
Although the concentrations in the reburn zone are presented here, post-burnout concentrations remain consistent with this observation. Zamansky (1996b) includes further discussion and comparison of the concentration histories for different ammonia injection scenarios.

Sensitivity Analysis. Figure 8.2.18 shows kinetic curves of major components for injection of 800 ppm ammonia with the reburning fuel at $SR_2=0.99$ and $T_1=1700$ K. The predictions are similar to those for reburning without ammonia injection (Figure 8.2.1) except that NO concentration jumps from 600 to about 900 ppm and then slowly decreases to 800 ppm. Thus, part of the ammonia is converted to molecular nitrogen and another part to NO. Figure 8.2.19 presents NO contribution factors for the first 10 ms at these conditions. Reaction (211) is primarily responsible for the NO decrease, but the NO is formed via reaction (213) and to lesser extent via (214) and (188). Sensitivity analysis shows that as for reburning without N-agent (Figure 8.2.11), reaction (38) accelerates NO formation by increasing the radical pool. Reactions of NH_i radicals with NO ((198), (281), and (177)) decrease the NO level. The most notable difference from conventional reburning is the increased importance of reaction 281, which involves NH_2 , compared to those involving NH and N.

Figure 8.2.20 shows the concentration curves for the same conditions as in Figure 8.2.18, but with the 800 ppm NH_3 injected with a 0.1 s delay after the reburning fuel. This delay dramatically changed the NO concentration as well as concentrations of other species. NO was reduced to slightly above 100 ppm and about 150 ppm NH_3 is present in the mixture at $t=0.5$ s. Significant amounts of H₂CO and O_2 are present at $t=0.5$ s. Figure 8.2.21 shows the main reactions contributing to NO formation and reduction in the first 0.10 s under these conditions. Reactions (281) and (282) represent one elementary step which was formally written as two reactions in the mechanism. The code calculated the sum of these reactions which result in NO reduction. Another important NO reducing step is the reaction

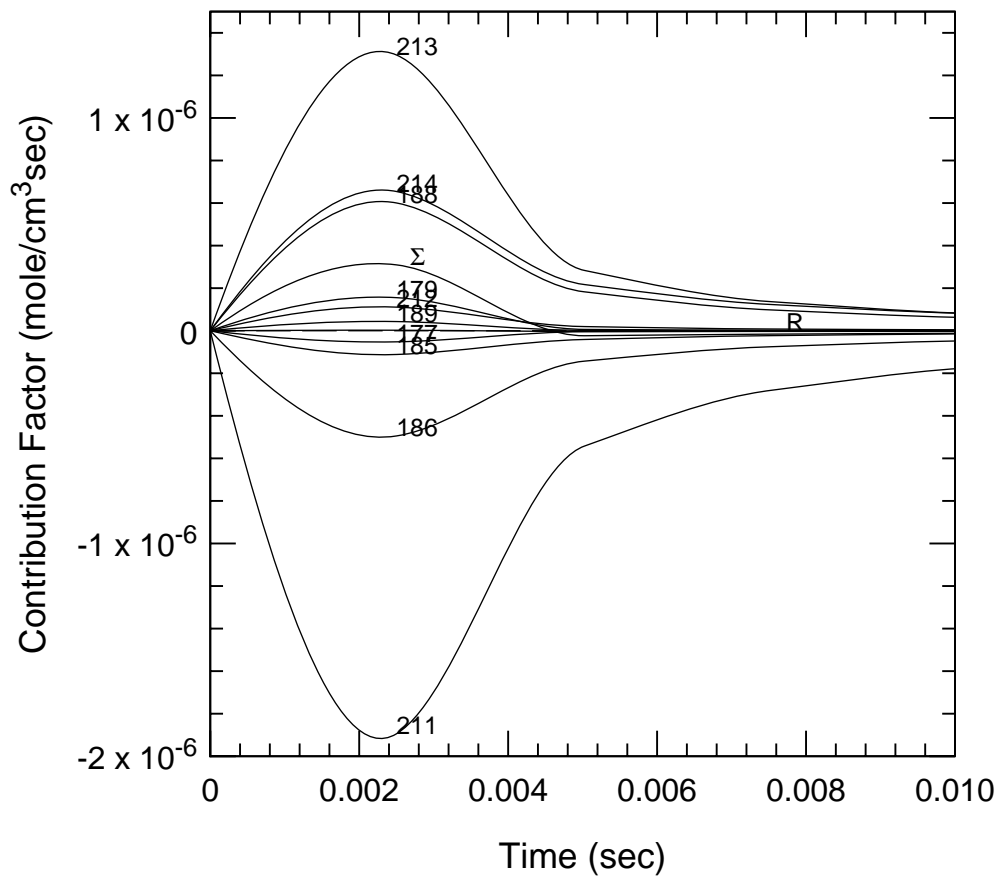


NO formation is largely via reaction (-211). Figure 8.2.22 presents NO sensitivity coefficients which also demonstrate the importance of the sum (281+282). Interestingly, this reaction reduces NO at early reaction stages ($t<0.03$ s), then increases the NO concentration at about 0.04-0.16 s, and finally reduces NO again. The reason for this “strange” behavior is that reaction (280) includes the same reagents, NH_2 and NO, and it is a single process which is mainly responsible for NO reduction under these conditions. Indeed, though reaction (281+282) forms molecular nitrogen from NO, it removes the NH_2 radical from the reaction media thus decreasing the radical pool.



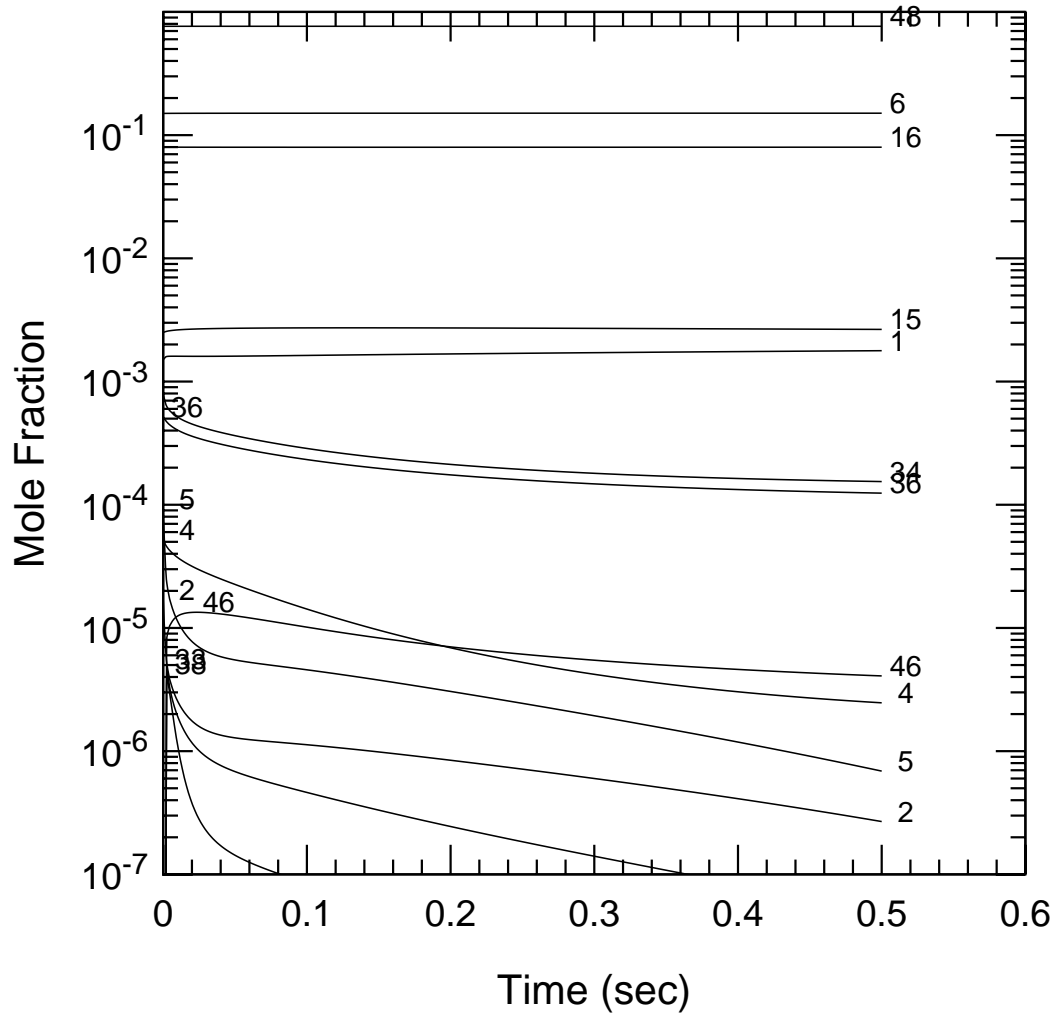
48 N ₂	5 OH
6 H ₂ O	2 H
16 CO ₂	36 NO
4 O ₂	34 NH ₃
14 CH ₄	3 O
15 CO	41 HCN
1 H ₂	46 HNCO

Figure 8.2.18. Kinetic curves of species in the reburning zone at $SR_2 = 0.99$ for injection of 800 ppm ammonia along with the reburning fuel at 1700 K.



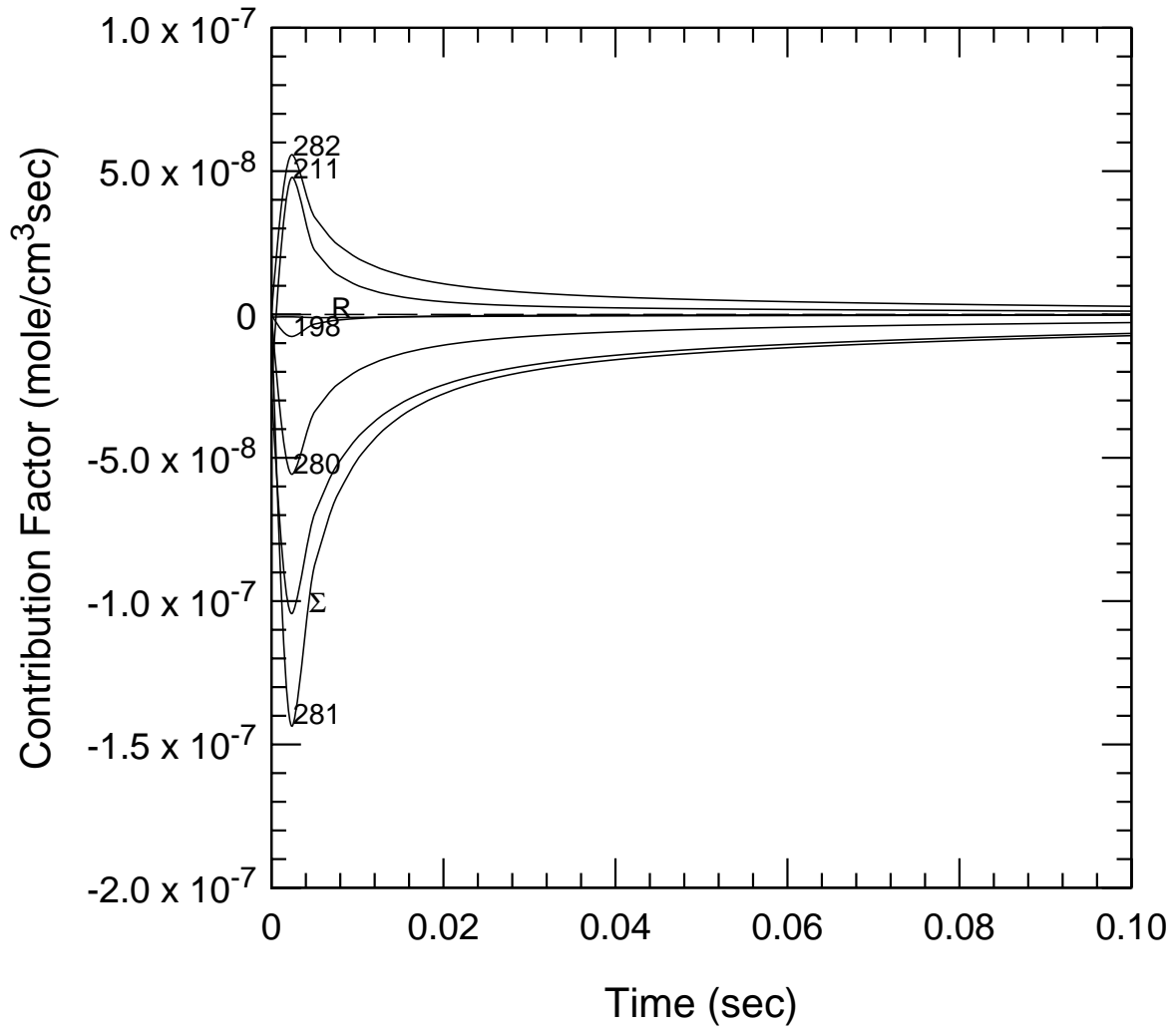
211	$\text{H} + \text{NO} + \text{M} \rightleftharpoons \text{HNO} + \text{M}$	212	$\text{HNO} + \text{O} \rightleftharpoons \text{NO} + \text{OH}$
213	$\text{HNO} + \text{H} \rightleftharpoons \text{H}_2 + \text{NO}$	177	$\text{N} + \text{NO} \rightleftharpoons \text{N}_2 + \text{O}$
214	$\text{HNO} + \text{OH} \rightleftharpoons \text{NO} + \text{H}_2\text{O}$	189	$\text{NH} + \text{O} \rightleftharpoons \text{NO} + \text{H}$
188	$\text{NO}_2 + \text{H} \rightleftharpoons \text{NO} + \text{OH}$	R	Remainder
186	$\text{NO} + \text{O} + \text{M} \rightleftharpoons \text{NO}_2 + \text{M}$	Σ	Summation
179	$\text{N} + \text{OH} \rightleftharpoons \text{NO} + \text{H}$		
185	$\text{HO}_2 + \text{NO} \rightleftharpoons \text{NO}_2 + \text{OH}$		

Figure 8.2.19. NO contribution factors for conditions of Figure 8.2.18.



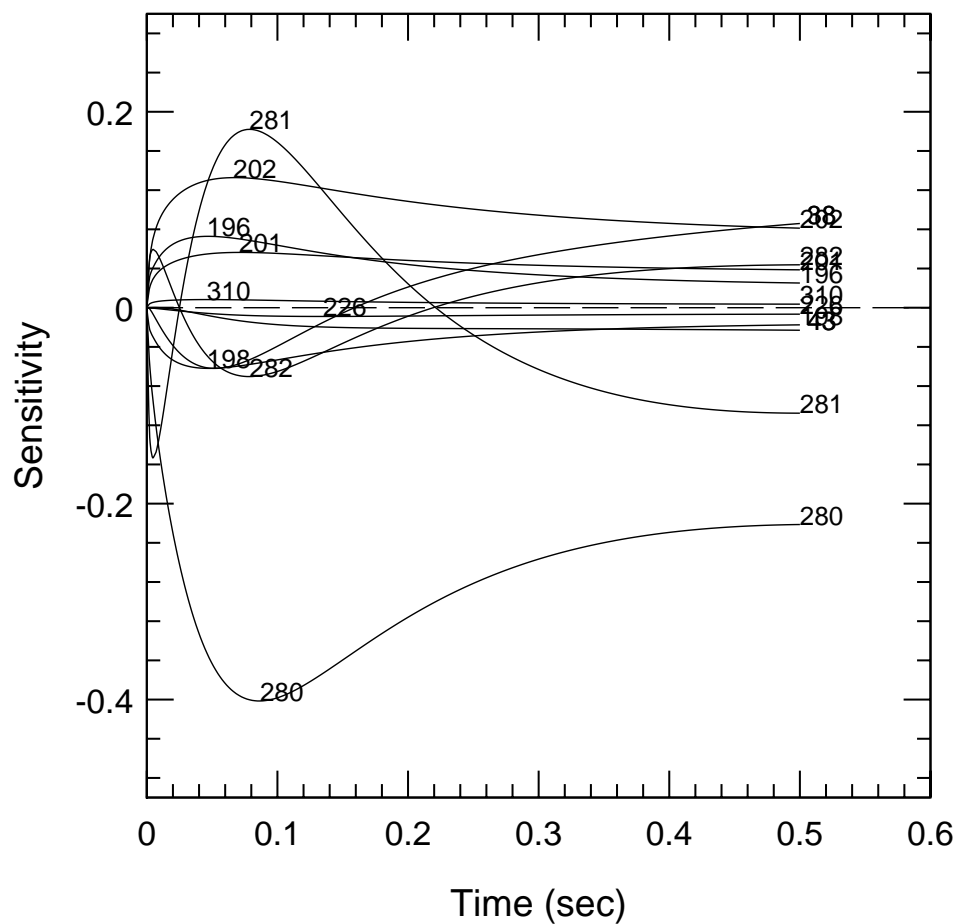
48 N ₂	5 OH
6 H ₂ O	4 O ₂
16 CO ₂	2 H
15 CO	46 HNCO
1 H ₂	33 NH ₂
34 NH ₃	38 N ₂ O
36 NO	

Figure 8.2.20. Kinetic curves of species in the reburning zone at $SR_2 = 0.99$ for injection of 800 ppm ammonia with a 0.1 s delay after the reburning fuel injected at 1700 K.



- 281 $\text{NH}_2 + \text{NO} \rightleftharpoons \text{N}_2 + \text{H}_2\text{O}$
- 282 $\text{NH}_2 + \text{NO} \rightleftharpoons \text{N}_2 + \text{H}_2\text{O}$
- 280 $\text{NH}_2 + \text{NO} \rightleftharpoons \text{NNH} + \text{OH}$
- 211 $\text{H} + \text{NO} + \text{M} \rightleftharpoons \text{HNO} + \text{M}$
- 198 $\text{NH} + \text{NO} \rightleftharpoons \text{N}_2\text{O} + \text{H}$
- R Remainder
- Σ Summation

Figure 8.2.21. NO contribution factors for conditions of Figure 8.2.20.



280	$\text{NH}_2 + \text{NO} \rightleftharpoons \text{NNH} + \text{OH}$	201	$\text{NH}_2 + \text{H} \rightleftharpoons \text{NH} + \text{H}_2$
281	$\text{NH}_2 + \text{NO} \rightleftharpoons \text{N}_2 + \text{H}_2\text{O}$	43	$\text{H} + \text{OH} + \text{M} \rightleftharpoons \text{H}_2\text{O} + \text{M}$
202	$\text{NH}_2 + \text{OH} \rightleftharpoons \text{NH} + \text{H}_2\text{O}$	226	$\text{NCO} + \text{M} \rightleftharpoons \text{N} + \text{CO} + \text{M}$
38	$\text{H} + \text{O}_2 \rightleftharpoons \text{O} + \text{OH}$	310	$2\text{NH}_2 \rightleftharpoons \text{NH} + \text{NH}_3$
196	$\text{NH} + \text{H}_2\text{O} \rightleftharpoons \text{HNO} + \text{H}_2$		
282	$\text{NH}_2 + \text{NO} \rightleftharpoons \text{N}_2 + \text{H}_2\text{O}$		
198	$\text{NH} + \text{NO} \rightleftharpoons \text{N}_2\text{O} + \text{H}$		

Figure 8.2.22. NO sensitivity coefficients for conditions of Figure 8.2.20.

Reaction (280) also removes NO and one NH₂ radical, but it forms NNH radical which is unstable and decomposes with returning active species (H atoms) via reactions



8.2.3 Promotion of the NO-NH₃ Interaction in the Reburning Zone

Consideration of the kinetic curves of the reburning process (Figures 8.2.1 to 8.2.3) demonstrates that after the initial fast reaction stage, concentrations of main components in the reburning zone (CO, H₂ and NO at SR₂ = 0.99-0.95 and CO, H₂, CH₄, HCN, NH₃, NO at SR₂ = 0.90) remain almost constant, and, simultaneously, concentrations of radicals (OH and H) and O₂ decrease. The goal of modeling is to find conditions under which NO and TFN concentrations will further decrease in the reburning zone. As previously discussed, delayed injection of ammonia can reduce NO and TFN concentrations under certain conditions. The effectiveness of the NO-NH₃ interaction in the reburning zone can be further improved in the presence of promoters. The influence of different promoter species on NO/TFN removal is analyzed in the following. The initial analysis focuses on the effect of boosting the concentration of specific species upon NO. In some cases (e.g. radicals) direct injection of the species is not intended. Rather, the goal is to find target species whose increase is beneficial; the next step is to find injectable species which will have the desired effect.

The analysis focuses on the later part of the reburning zone in which NO reduction is relatively slow. Parameters affecting the NO/TFN level are varied to find optimum conditions of NO/TFN removal. These parameters include the stoichiometric ratio in the reburning zone (SR₂); reburn fuel injection temperature (T₁); concentrations of ammonia, oxygen, radicals, and other compounds capable of promoting the NO-NH₃ interaction. It is clear that the influence of ammonia is different at various values of SR₂. Variation of process parameters was performed for SR₂ = 0.99 and 0.90 at a constant temperature gradient of 300 K/s. For all conditions, concentrations are shown at a reaction time of 1 s, for injection with 0.1 s delay after reburn fuel injection. This injection point is after the fast reaction stage, at which point all CH₄ was consumed, and concentrations of CO, H₂ and NO stabilized on a certain level. The composition at SR₂ = 0.99 and at the NH₃/promoter injection point (mixture I) is:

500 ppm NO - 0.16% H₂ - 0.23% CO - 8% CO₂ - 15% H₂O - balance N₂.

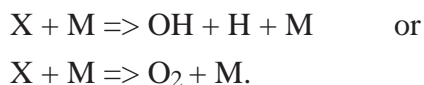
The effect of ammonia addition alone to mixture I is shown in Figure 8.2.23. Without NH₃ injection (the upper graph), NO is slightly reduced at lower temperatures. Injections of 500 and 800 ppm NH₃ cause an increase in TFN at lower temperatures and significant NO/TFN reduction at higher temperatures.

Performance of candidate promoter species was modeled by co-injection with ammonia in different amounts into mixture I at 1600 K. Figure 8.2.24 compares effect of different additives: O₂, OH, H, O, O₂+OH, and O₂+H₂O₂. Different promoters show different degrees of TFN removal, some with a clear optimum.

Carbon-containing compounds can also provide radicals which promote the NO-NH₃ interaction in the reburning zone. Effect of different potential promoters on concentrations of NO, NH₃ and TFN is shown in Figure 8.2.25. This graph compares the effect of 500 ppm NH₃ injection into mixture I at 1600 K with co-injection of 100 ppm promoter: oxygen, methanol, methane, ethylene or ethane. Of the hydrocarbons considered, only ethane results in much TFN reduction beyond the original NO level. This screening of hydrocarbon promoters does not reveal a significant performance benefit.

Of the promoters considered in figures 8.2.24 and 8.2.25, the best performance is shown for O₂ injection. Oxygen participates in formation of different radicals via reactions with CO, H₂ and NH₃, shows better or about the same performance as the other additives tested. The next section will discuss the effect of oxygen in some additional detail.

All promotive additives presented so far were co-injected with ammonia and appeared instantly in the gas phase. However, under real conditions, the promoter species may be formed in the mixture with a certain rate constant. As has been proven by Zamansky and Borisov, 1992, the rate of promoter formation may be optimum, i.e. formation of promoters with a certain optimum rate constant results in maximum promotion effect. It was assumed for modeling that a hypothetical promoter X dissociates with formation of radicals or oxygen in the gas mixture. The following reaction was added to the mechanism:



These equations simulate fast interaction of the hypothetical promoter X with water molecules or other species in flue gas with formation of OH, H, and O₂. The initial concentration of X was

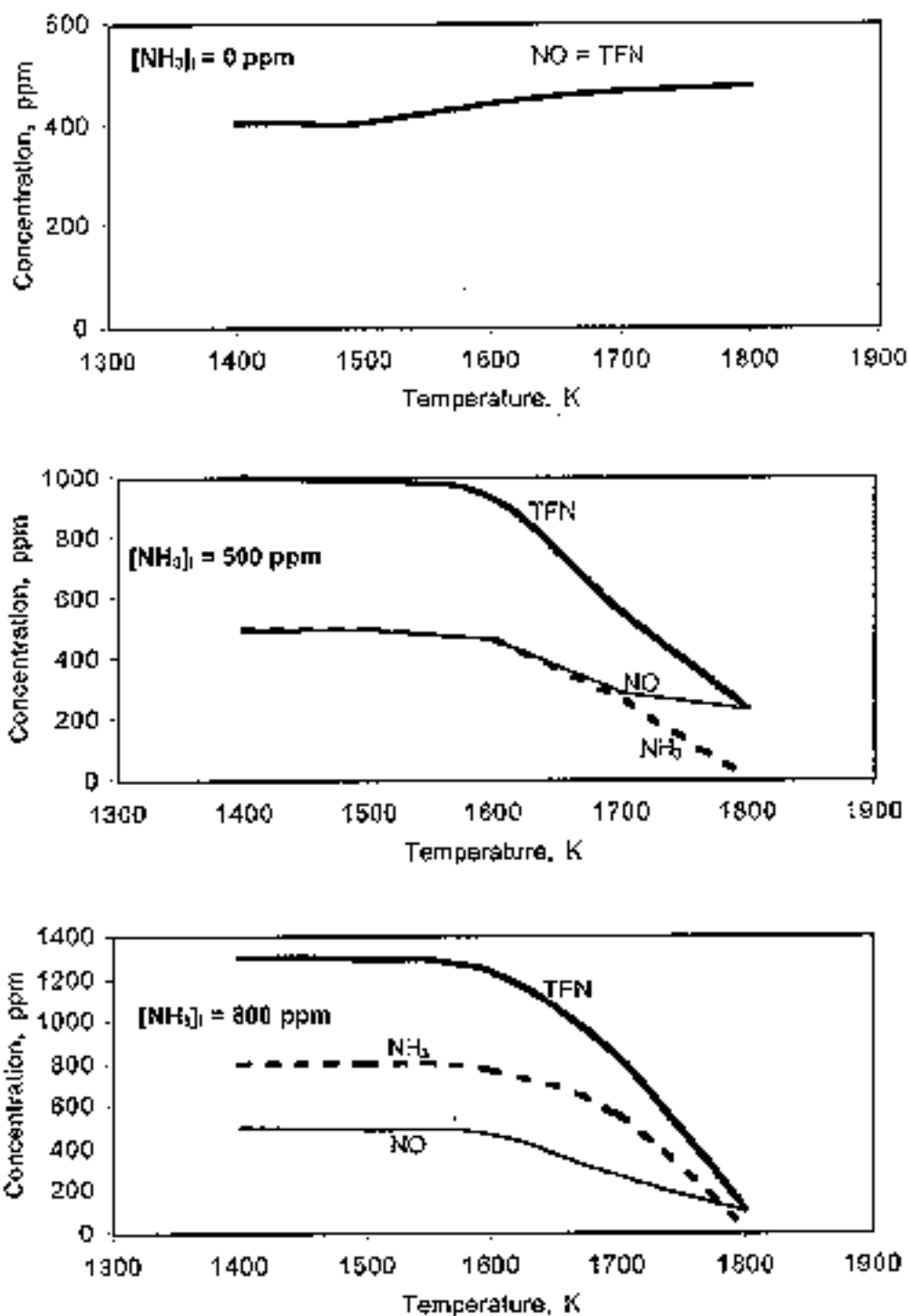


Figure 8.2.23. Effect of NH_3 injection temperature and NH_3 concentration in mixture I on NO/TFN reduction.

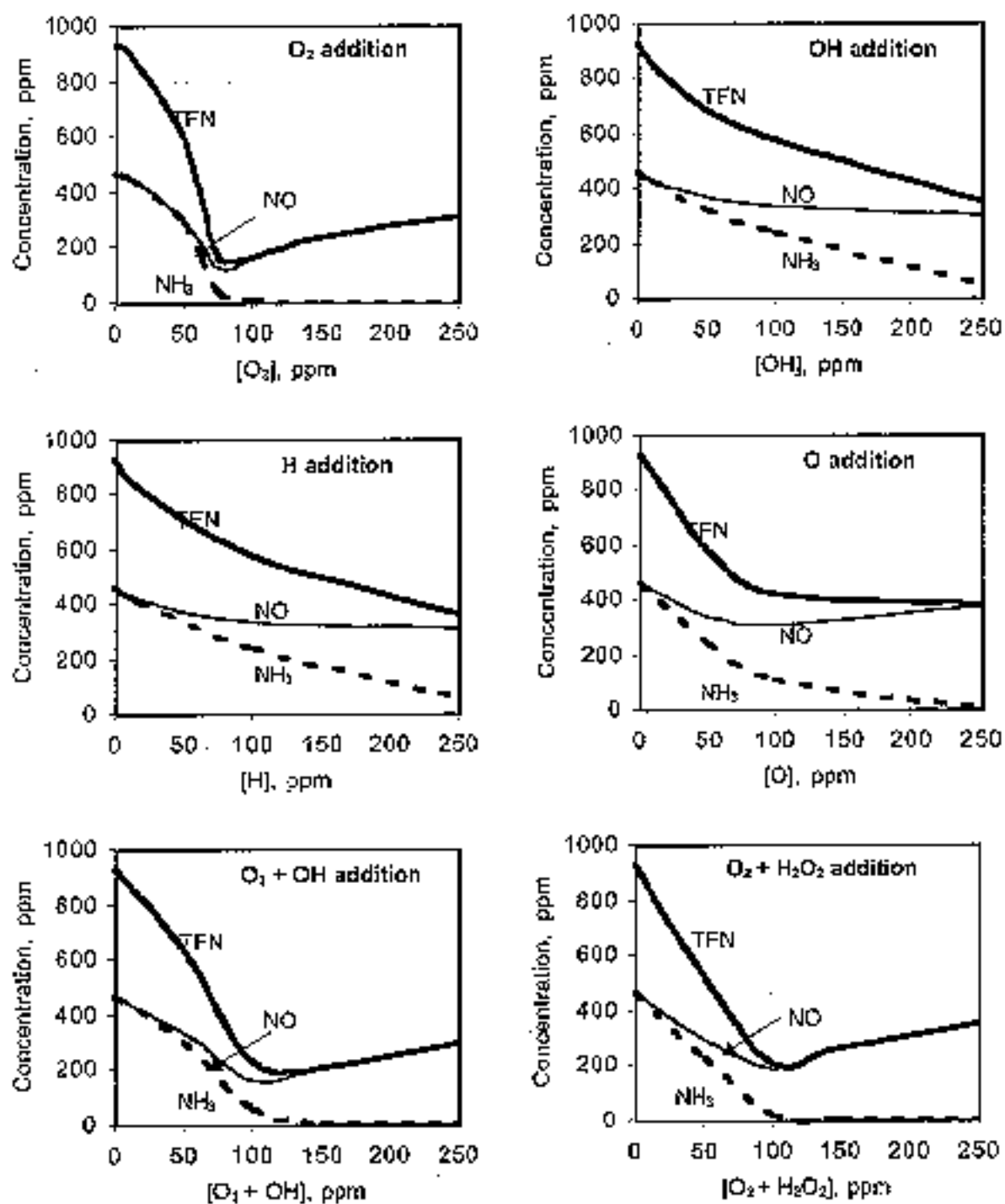


Figure 8.2.24. Effect of radicals co-injection with 500 ppm NH₃ into mixture I, T₃ = 1600 K.

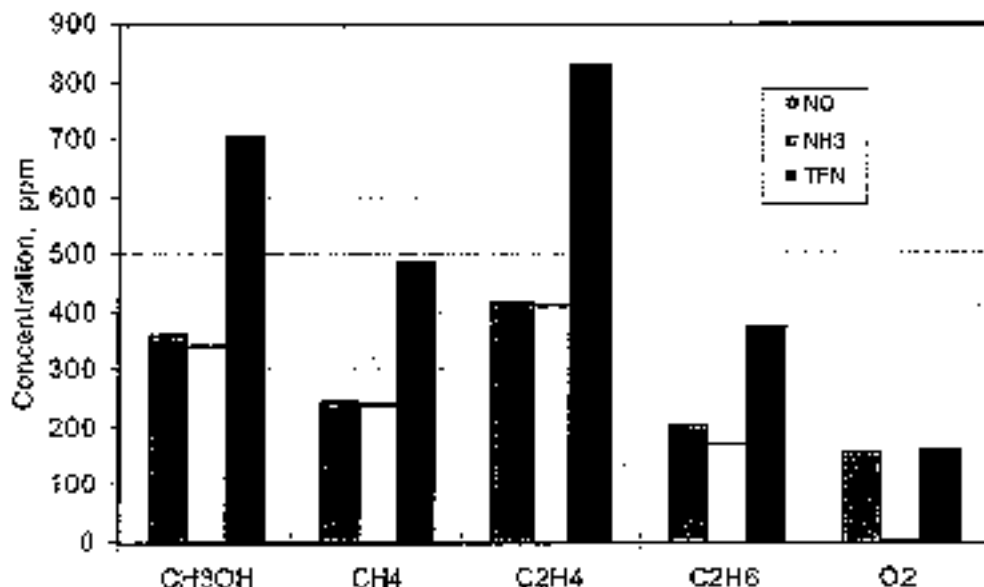


Figure 8.2.25. Comparison of the promotion effect of different compounds. The promoter (100 ppm) is co-injected with 500 ppm NH_3 into mixture I at $T_1 = 1600 \text{ K}$ and $SR_2 = 0.99$.

assumed to be 50 ppm in modeling. The rate constant for X decomposition was selected in the Arrhenius form

$$k = A \cdot \exp(-20,000/T) \text{ cm}^3/\text{mole}\cdot\text{s}$$

where the preexponential factor A was varied in the range from 10^9 to 10^{13} . These values of the rate constant provided formation of radicals and O_2 with characteristic times between approximately 0.1 and 100 s.

Figure 8.2.26 compares the results of modeling NO, NH_3 and TFN concentrations at different values of the factor A (i.e. depending on the rate of active species formation in the mixture) for three different cases: formation of OH+H radicals, formation of O_2 , and formation of the OH/H radicals with co-injection of NH_3 and 75 ppm O_2 . In a wide range of the promoter decomposition rate, NO and TFN concentrations are substantially lower than their values without promoter. In all cases, an optimum rate constant exists which results in minimum TFN concentration. The optimum factor A is in the range $\log A = 10.5-12.0$. Oxygen formation and co-injection present the most attractive cases because the TFN minimum is lower.

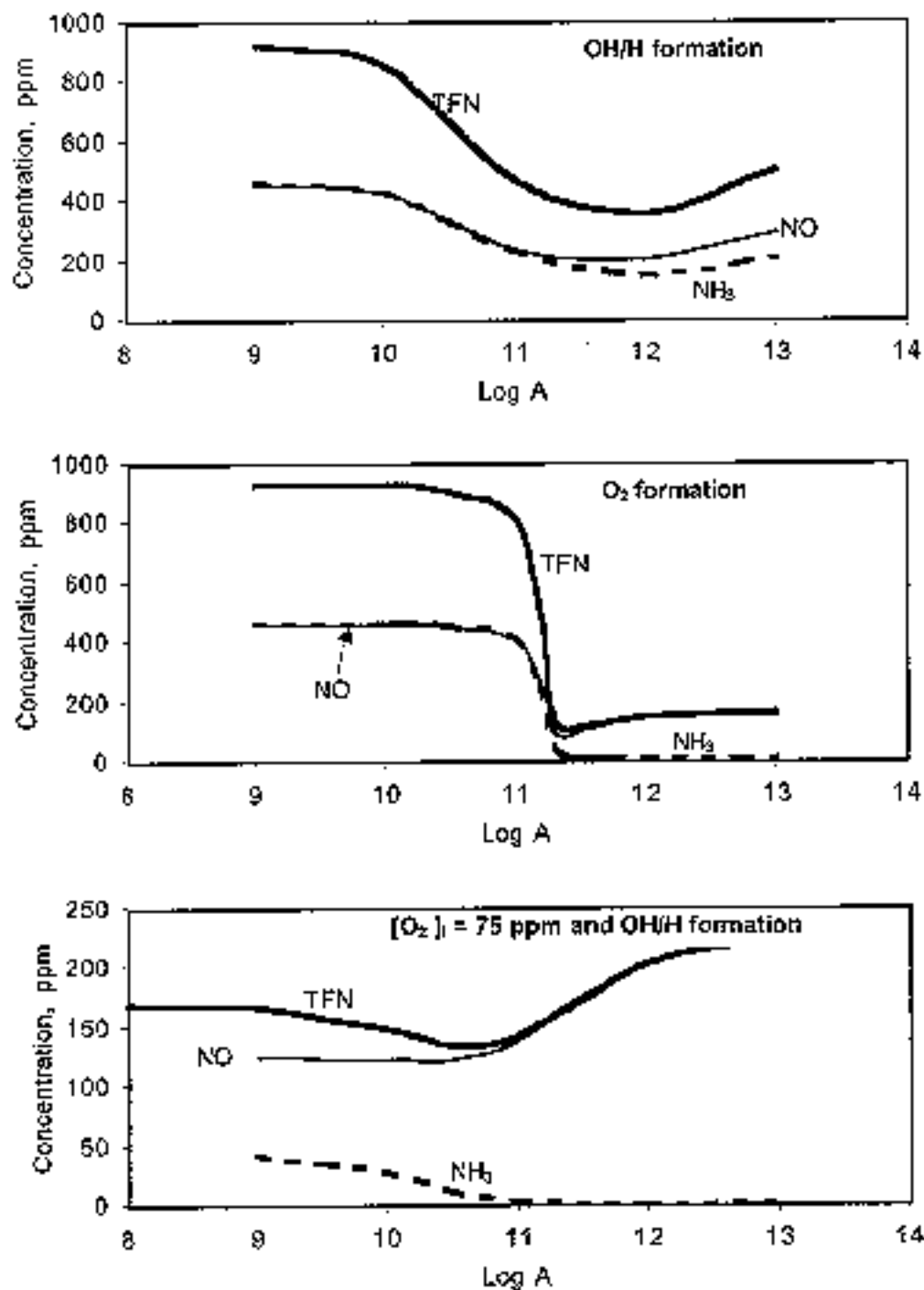


Figure 8.2.26. Modeling of the promotion effect at different preexponential factors A. The promoter appears with different rate constants in mixture I + 500 ppm NH₃ at T₁ = 1600 K.

8.2.4 Effect of Different Factors on the NO-NH₃ Interaction in the Reburn Zone

Effect of Oxygen. Performance of ammonia in the reburning zone greatly depends on the level of oxygen. If the oxygen concentration is high, NH₃ is partially converted to NO. If oxygen concentration is low, active radicals are not formed in oxidation processes. Thus, a maximum performance of NO/TFN removal should correspond to a certain optimum O₂ concentration. When sufficient O₂ is available, CO and H₂ react with O₂ via chain branching reactions producing radicals, which in turn participate in reactions with ammonia to form NH₂ followed by the reaction of NH₂ and NO.

To determine the optimum O₂ concentration, calculations were performed with injection of 500 ppm NH₃ with various amounts of oxygen into mixture I, as shown in Figure 8.2.27. The optimum O₂ amounts, and the resulting TFN removal performance, increase as injection temperature decreases. O₂ promotion provides a means for promoting the NH₃-NO interaction at lower temperatures in the reburning zone, where it would normally not be effective due to low oxygen and radical concentrations.

At lower temperatures, there is a certain threshold level of oxygen below which NO does not react with NH₃. This threshold depends on temperature, CO/H₂ concentrations, and initial NO and NH₃ concentrations. At [O₂] above the optimum, the efficiency of NO removal decreases slowly. At sufficiently high O₂ concentrations the NO level will actually increase.

Effect of CO and H₂. NO reduction efficiency is controlled by active radicals formed in CO and H₂ interaction with oxygen. Therefore, concentrations of CO and H₂ are important factors affecting NO-NH₃ interaction. The amounts of CO and H₂ in the mixture depend on composition of the main and reburning fuels and on the stoichiometric ratios, SR₁ and SR₂. For the current modeling study, with natural gas as both the primary and reburning fuel, the dependence is only on SR₂. Variations in SR₂ for 500 ppm NH₃ injection into Mixture I at 1300-1500 K, accompanied by the optimum level of O₂, show that there is an optimum SR₂ in the neighborhood of 0.99 to 1.0 (depending on injection temperature) for TFN reduction. Both CO and H₂ generate radicals in the oxidation process and help to reduce NO. The relative importance of each compound depends on conditions: temperature and concentrations of main components. For example, CO is more efficient than H₂ in reducing NO concentration at 1500 K, but H₂ has higher efficiency at 1300 K. Thus, modeling predicts that at the low temperature end of the reburning zone, NO/TFN removal is more efficient at lower temperatures with an optimum CO/H₂ level in the mixture as well as oxygen.

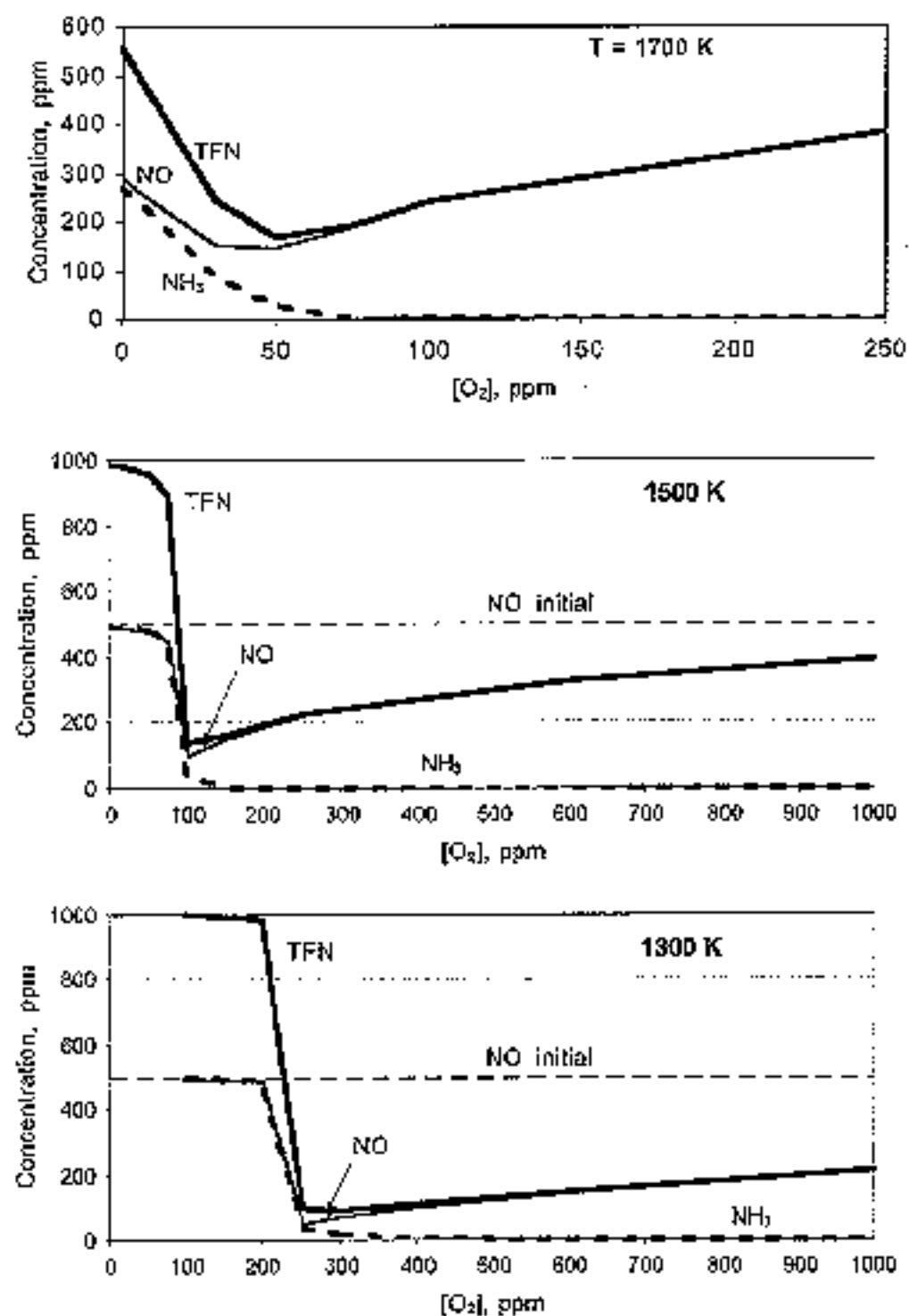


Figure 8.2.27. Effect of O₂ co-injection with 500 ppm NH₃ into mixture I at different injection temperatures.

Effect of Initial NO. Modeling suggests that injection of ammonia and oxygen into the reburning zone is less efficient at lower initial NO concentrations. This has been confirmed by modeling with 200 ppm NO and 200 ppm NH₃ in the reburning zone at SR₂ = 0.99 and T₂ = 1300-1000 K. Comparing performance with previous results at 500 ppm, a substantial decrease was noted in both the NO removal efficiency (from 80% to 50%) and in the range of effective O₂ concentrations. It was also found that a decrease in the injection temperature is capable of widening the O₂ window, but the NO removal efficiency is about the same.

8.2.5 Injection of Ammonia into the Burnout Zone (AR-Lean)

Modeling suggests that injection of OFA at different values of SR₂, SR₃, and temperature results in a final NO concentration which is near the TFN level in the mixture before OFA injection. Only at relatively high values of SR₂ (about 0.9) and at low OFA injection temperatures (about 1250 K), a small decrease of final NO concentration was observed (about 15%) compared with the TFN concentration upstream of OFA injection.

If ammonia is injected along with OFA in the reburning zone at SR₂ = 0.99, the NO reduction process is not effective at injection temperatures above 1100 K. Figure 8.2.28 (Curve 1) demonstrates the effect of OFA injection at different locations with co-injection of ammonia at NSR₂ = 1.0 on the final NO concentration. The initial NO concentration (100%, i.e. 350-500 ppm depending on the residence time in the reburning zone) increases when OFA is injected at 1120 K or higher. At these temperatures, some ammonia reacts with NO, but some is converted to NO, resulting in a final NO concentration (NO_f) higher than the initial NO concentration at the point of OFA injection. The concentration of NH₃ decreases to less than 1 ppm after the OFA/NH₃ injection. In the temperature range of 950-1050 K, the NO concentration is decreased, but this range is too low for OFA injection since all CO from the reburning zone remains unreacted.

Curve 1 represents the conditions of NO removal via the Thermal DeNO_x process in the presence of high concentrations of CO and H₂. It is well known (for instance, Lyon and Hardy, 1986) that the presence of CO and/or H₂ shifts the temperature window of NO removal by the SNCR process to lower temperatures. In order to avoid that shift, ammonia can be injected into flue gas with a short delay after injection of the OFA or in the aqueous form to allow some time for evaporation of the water. In this case, the OFA rapidly reacts with CO and H₂, and the NH₃ appears in the gas mixture when all CO and H₂ are already oxidized. Modeling shows that a delay time of about 0.1 s is enough for complete CO and H₂ removal. The results of calculations are shown in Figure 8.2.28,

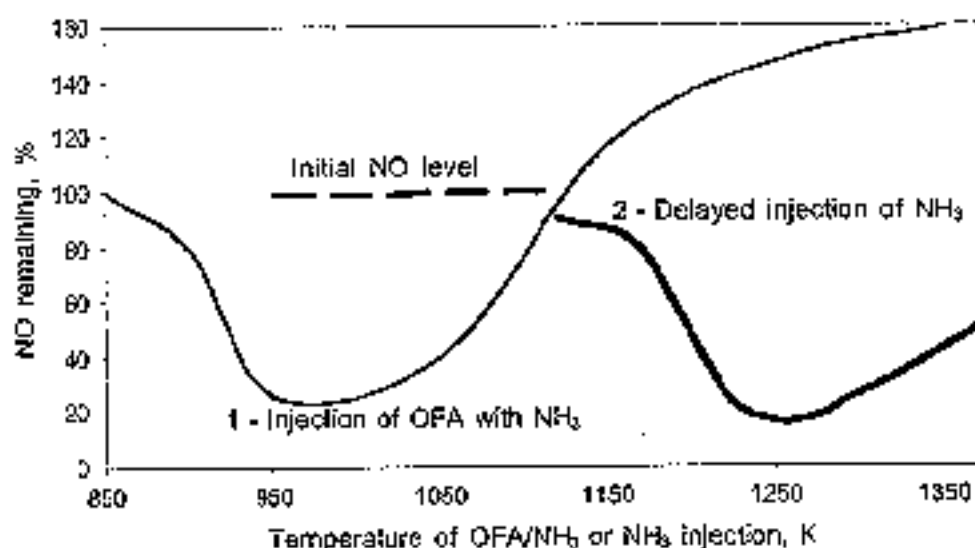


Figure 8.2.28. Effect OFA co-injection with NH_3 on the final NO concentration. $\text{NSR} = 1.0$.

Curve 2 which represents the effect of NH_3 injection temperature (NH_3 is injected with a 0.1 s delay time after the OFA) on NO concentrations. Under these conditions, the ammonia reacts with NO in the presence of oxygen and in the absence of CO and H_2 , and the optimum temperature for NH_3 injection is about 1200 K, which is typical for the Thermal DeNO_x process.

If the reburning fuel is injected with $\text{SR}_2 = 0.90$ at $T_1 = 1700$ K, modeling shows that the concentration of ammonia in the reburning zone is higher than the NO concentration. For example, at $T_3 = 1400$ K, concentrations of fuel-N species are: 71 ppm HCN, 50 ppm NO, and 113 ppm NH_3 . Injection of OFA converts all fuel-N species to NO. Therefore, co-injection of gaseous ammonia with OFA does not make sense for these conditions either. Variation of the O_2 concentration in OFA does not change the final NO level.

8.2.6 Modeling with Instantaneous Mixing Times: Summary

The performance of individual AR processes has been considered using a time-dependent chemistry calculation, putting aside the influence of finite-rate mixing effects. Some of the most important points are summarized here.

Reburning zone chemistry has been examined over the range of stoichiometric ratios from 0.90 to 0.99. It has been shown that there is a short, fast initial reduction in NO followed by slower reduction over the remainder of the reburning zone. This effect is linked to the disappearance of oxygen and radicals, and highlights an opportunity for introduction of species which can reestablish optimum concentrations for NO removal.

Injection of N-agents is effective at reducing NO when temperatures and concentrations of oxygen and other radicals are conducive. Conditions are more favorable at reburn SRs close to stoichiometric. Mixing of the N-agent with flue gas must occur in a window downstream of reburn fuel injection to encounter the correct environment for effective NO reduction. This delay may be achieved by locating injectors downstream of fuel injectors, or by use of aqueous N-agent solutions with associated evaporation delays.

Introduction of promoter species along with the N-agent may enhance its performance by making the reactant mixture more favorable to NO reduction by NH_3 and associated species. Injection of ammonia with small amounts of oxygen upstream of the OFA improves NO reduction. The efficiency of NO removal depends mainly on SR_2 and concentrations of oxygen, CO/H_2 , and NO. The optimal oxygen concentration depends on the injection temperature. The efficiency is lower at lower NO initial concentrations. Radical species also exhibit a promotion effect, calling for the injection of species which provide them in the proper amounts and at the proper rates.

Injection of OFA into the fuel-rich reburning zone converts all fuel-nitrogen species into NO as long as the temperature of OFA injection is adequately high.

Co-injection of ammonia with the OFA significantly shifts the temperature window of the Thermal DeNOx process to lower temperatures because of the CO and H_2 present. To avoid this shift, ammonia should be injected after a short delay time relatively to the OFA location. This delay can be provided by evaporation of aqueous ammonia or urea co-injected with OFA.

8.3 Evaluation of Mixing Effects

8.3.1 Approach

The modeling discussed above treated the AR process as a one-dimensional plug flow reactor with instantaneous mixing at each injection point. This approach simplifies the analysis by focusing on chemistry, but puts aside the effect of finite rate mixing. The results demonstrated qualitative trends

but did not quantitatively reproduce experimental data. Indeed, quantitative predictions are challenging even in the most sophisticated (and computationally demanding) three dimensional model coupling chemistry and fluid dynamic effects, as ongoing research continues to develop understanding of chemical reaction mechanisms and turbulent mixing. However, the basic one dimensional model which has already proven useful may be incrementally improved by incorporating a simplified treatment of finite-rate mixing of an injected stream into the main flow.

The tool chosen for this study is a one dimensional chemical kinetics code developed at EER. This program is known as “ODF,” for “One Dimensional Flame,” although the code is applicable to any gas phase system. ODF contains the same basic capabilities as Chemkin, including the evaluation of pressure-dependent and reversible Arrhenius rate expressions, and the specification of time-dependent profiles of temperature and pressure. Most importantly for the current study, the solution algorithm has been formulated to allow for the introduction of an arbitrary profile of mass injection along the length of the reactor.

ODF has been applied to basic and advanced reburning scenarios. The reburning system is treated as a plug flow reactor, beginning with the introduction of reburning fuel into primary combustion products at 1700 K. The reacting flow is cooled at a uniform rate of -300 K/s. Overfire air and (for AR) gaseous ammonia are introduced at different locations along this temperature ramp, and the reactions continue until the system reaches a temperature of about 600 K, at which point the reaction rates may be considered negligible.

The primary mixture is at a stoichiometric ratio of about 1.1, with initial (wet) concentrations of 600 ppm NO, 1.74% O₂, 8% CO₂, 15% H₂O, after mixing with methane which is the reburn fuel. The two reburning stoichiometries are nominally 0.90 (1.94% CH₄), and 0.99 (0.967% CH₄). The OFA is added for a final stoichiometry of 1.15. Unless otherwise noted, OFA injection is at 1300 K, based on previous modeling suggesting that this is a good temperature for effective NO reduction as well as burnout of other fixed nitrogen species and incomplete combustion products. Some cases were also run with OFA introduced at 1200 K or 1400 K for comparison.

In each AR case presented here, the ammonia addition was adjusted to NSR=1.0, matching the concentration of added NH₃ to the concentration of NO at the start of N-agent injection. Because NO varied with injection location, the quantity of added ammonia varied. Additional calculations with a uniform quantities of ammonia, with NSRs greater than equal to 1.0, is discussed in Zamansky et al. (1997a and 1997b).

To evaluate the effect of mixing time, three mixing scenarios were applied to each basic or advanced reburning condition modeled: instantaneous mixing, 30 ms mixing, and 300 ms mixing. The same mixing time was applied to all external streams (reburn fuel, N-agent, and OFA), and mixing over 30 or 300 ms was applied at a uniform rate of mass addition. The instantaneous mixing case is the limiting case corresponding to the approach in earlier Chemkin modeling. 30 ms mixing may be considered fast, corresponding to bench and small pilot scale systems such as EER's combustion facilities CTT and BSF. 300 ms mixing is more typical of large pilot-scale systems such as EER's Tower Furnace (10 MMBTU/hr) and full-scale industrial combustion systems.

8.3.2 Effect of Mixing Times on Basic Reburning

The kinetic behavior of the model during and after reburning fuel addition was examined closely to determine the effects of finite mixing time on kinetic behavior in the reburning zone. Figures 8.3.1 through 8.3.4 show the concentrations of important species as a function of time from the start of the reburning fuel injection, for nominal reburning stoichiometries of 0.99 and 0.90, and for the finite rate mixing scenarios (30 ms, and 300 ms mixing). In addition to the individual species concentrations, there is also a curve for TFN (total fixed nitrogen), which in these four figures includes not only NO, NH₃, and HCN, but all sources of N-atom except N₂.

The case with instantaneous mixing was also run, and results correspond to those already presented in Figures 8.2.1 (for SR₂=0.99) and 8.2.3 (for SR₂=0.90). Comparison with the figures generated by Chemkin shows that the same trends are predicted. This serves to validate the ODF model setup against the equivalent modeling previously done in Chemkin. However, note that Figures 8.2.1 and 8.2.3 cover a different range of time and concentration than the other plots presented here.

As mixing time is increased to 30 ms (Figure 8.3.1) and to 300 ms (Figure 8.3.2) for a nominal reburn stoichiometry of 0.99, the behavior in the mixing zone is modified by the slower rate of fuel addition and the accompanying slower rate of stoichiometry change. At 30 ms, distributed mixing of the reburn fuel results in a spike in CH₄ concentration along with other species, which persists on about the same time scale as the mass addition interval. Also present but less obvious are increases in the concentrations of other species including O₂, OH, and H for a couple of hundred milliseconds following the end of reburn fuel injection. These species are then more available for the reactions involved in reburning and so NO reduction is more effective as mixing time is increased. In Figure 8.3.2, the 0.3 injection interval is now more obvious and reflects a more dramatic impact on all species concentrations. Several species, including O₂, HCN and NH₃ persist in higher quantities throughout the reburning zone. The net effect is a decrease in NO.

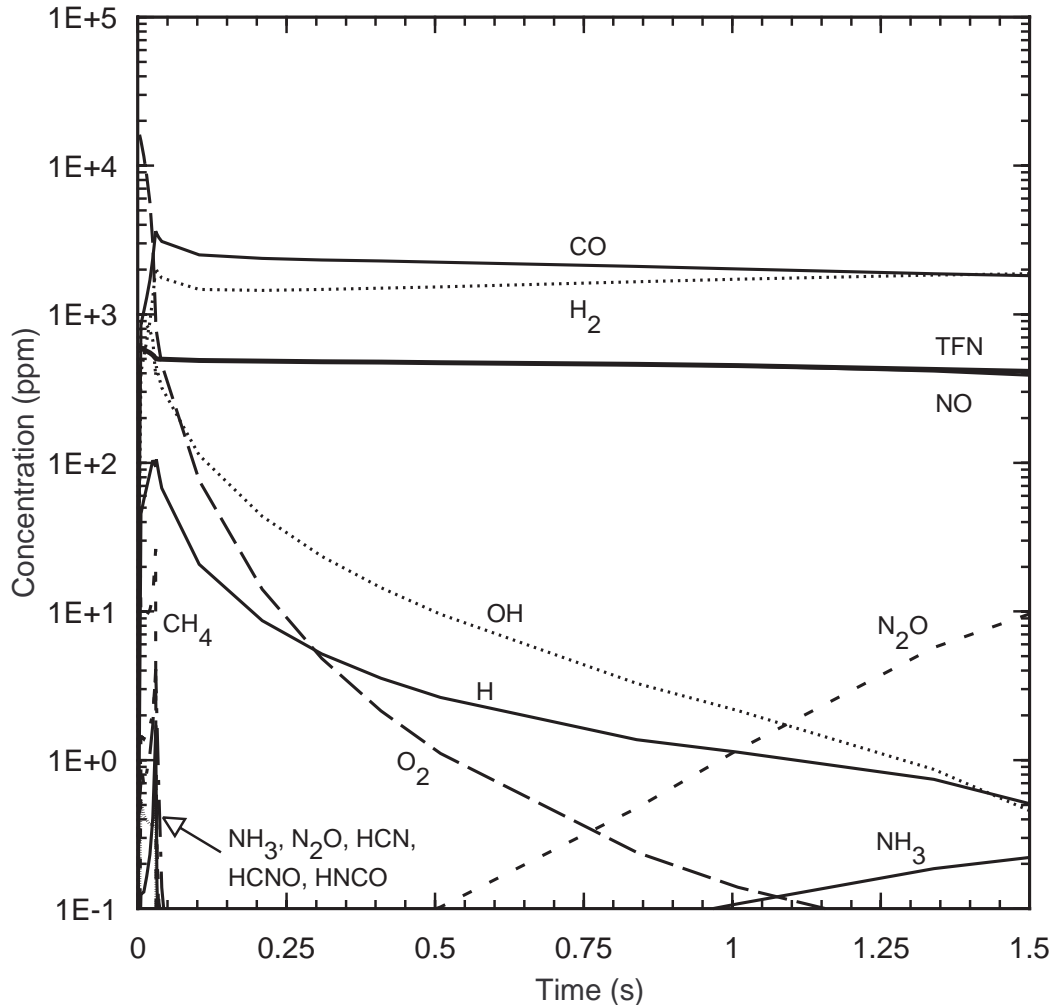


Figure 8.3.1. Kinetic curves of important species in the reburning zone at $SR_2 = 0.99$ and with mixing of the reburning fuel over an interval of 30 ms.

The same trends are found for a nominal reburn stoichiometry of 0.90 as mixing is varied from instantaneous (Figure 8.2.3) to 30 ms (Figure 8.3.3) to 300 ms (Figure 8.3.4). The impact on the kinetic curve for NO is similar but more obvious than at $SR_2=0.99$ since the magnitude of NO reduction due to reburn fuel addition alone is more pronounced at the more fuel rich condition. Even at 30 ms mixing time, O_2 persists for a longer time. It is interesting to note that most of the decrease in NO is on roughly the same time scale as the decrease in O_2 in all cases. The result is a clear improvement in NO reduction as mixing time is increased.

8.3.3 Effect of Mixing Times on AR-Rich

The AR-Rich cases were run with either co-injection of ammonia with reburn fuel (“no delay”) or with the start of ammonia injection delayed by a specified time after the beginning of reburn fuel

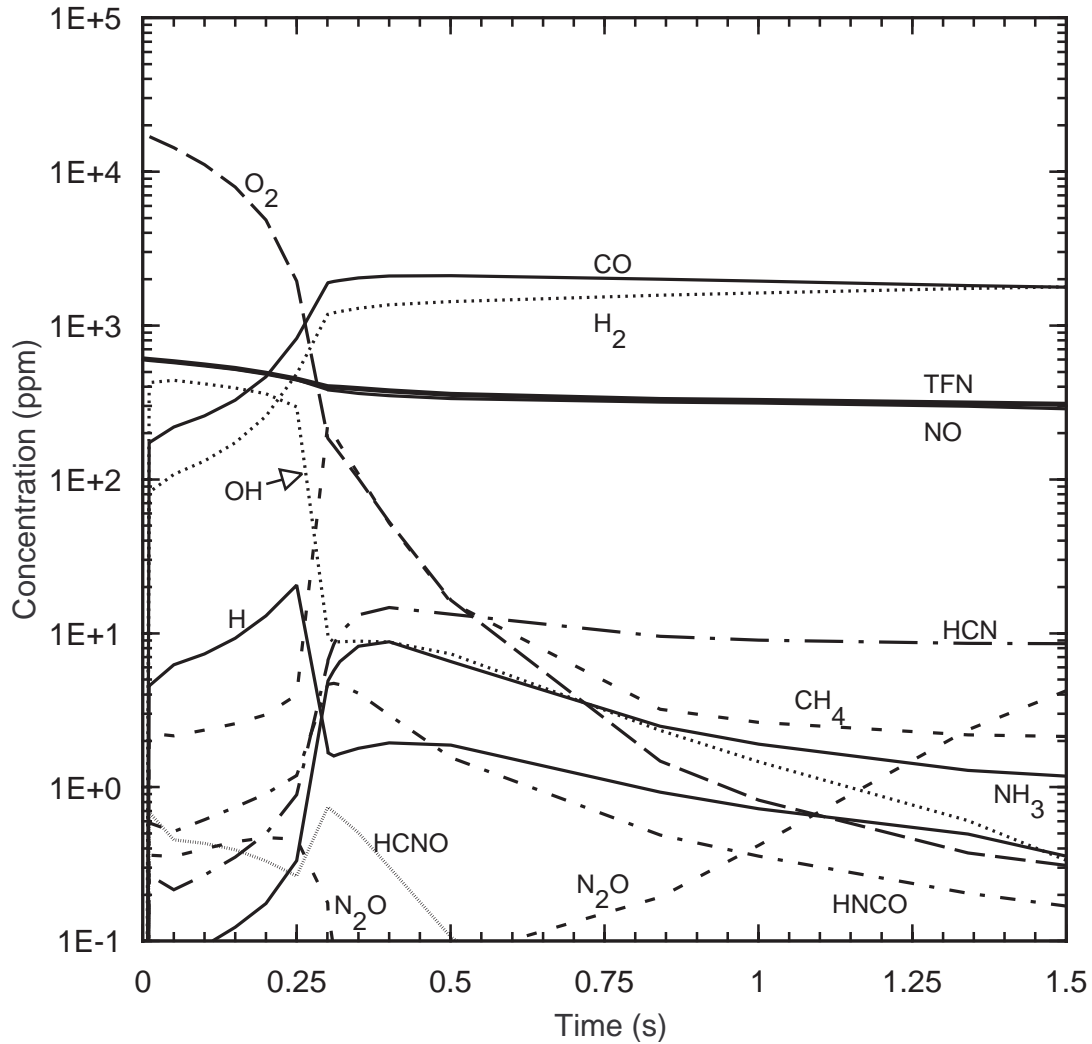


Figure 8.3.2. Kinetic curves of important species in the reburning zone at $SR_2 = 0.99$ and with mixing of the reburning fuel over an interval of 300 ms.

injection. Since the same mixing time is used for every stream in this simulation, some cases with short delay times (e.g. 0.1 s) and long mixing times (e.g. 0.3 s) included an overlap between the end of reburn fuel mixing and the beginning of ammonia mixing.

In all of the basic reburning and AR-Rich cases presented here, OFA was injected at 1300 K. However, some cases were run at 1200 K and 1400 K which verified earlier modeling conclusions that 1300 K gives better overall results in terms of NO reduction and destruction of other nitrogen containing species.

Figure 8.3.5 shows the NO reduction for basic reburning and AR-Rich at a nominal reburning zone stoichiometry of 0.99. Co-injecting ammonia with the reburn fuel increases the final NO compared

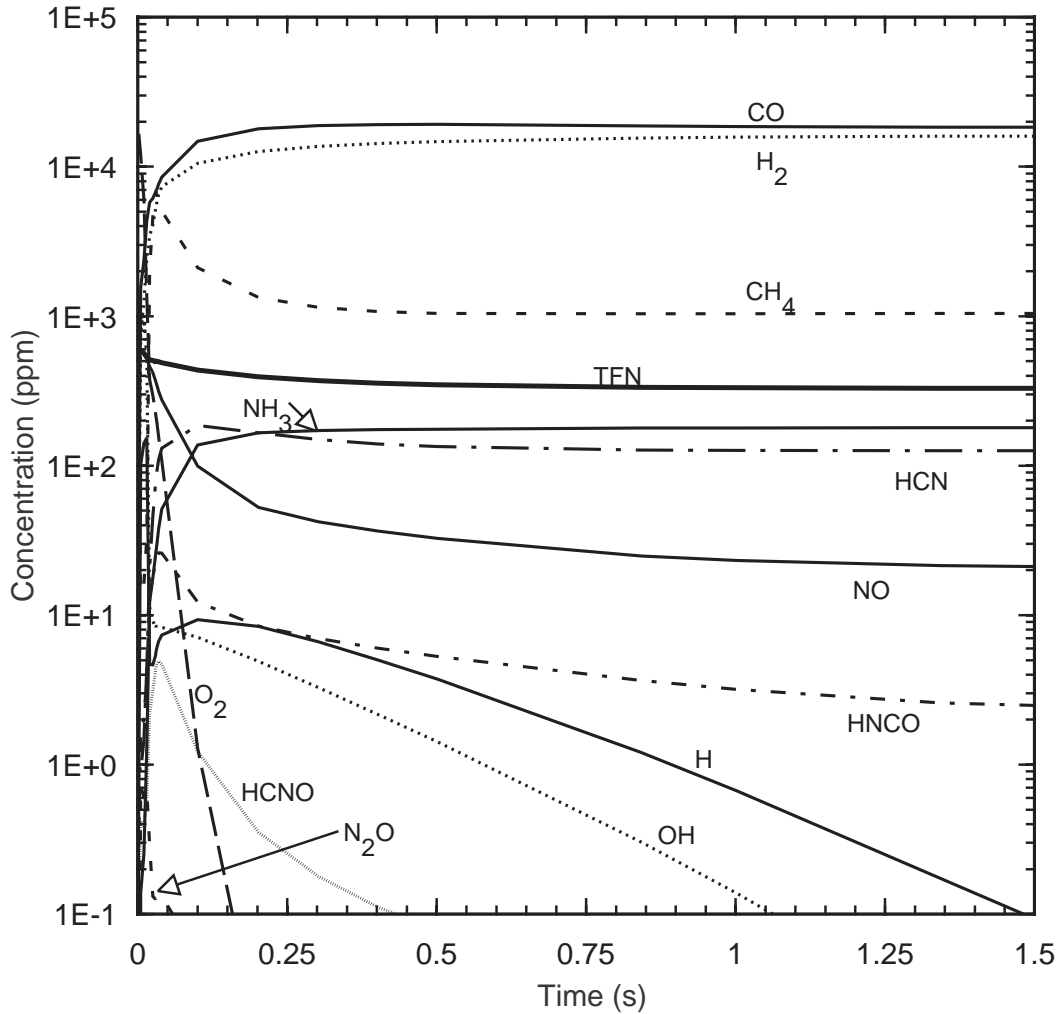


Figure 8.3.3. Kinetic curves of important species in the reburning zone at $SR_2 = 0.99$ and with mixing of the reburning fuel over an interval of 30 ms.

to basic reburning, but a delay of 0.1 s causes the final NO to decrease substantially. An additional condition with a longer delay time (0.833 s) returns to the higher final NO concentrations. These results show that there is clearly an optimum delay time for ammonia injection, in the neighborhood of 0.1 s. This optimum delay time effect is shown in Figure 8.2.16; note that the results there are before burnout, for which TFN is the best indicator of postburnout NO. At 0.1 s delay time, shorter mixing times actually yield slightly better results than longer mixing times, but the difference is small. These results also make it clear that there is a distinction between delay of the start of injection and the duration of mixing, underscoring the importance of both parameters in this system.

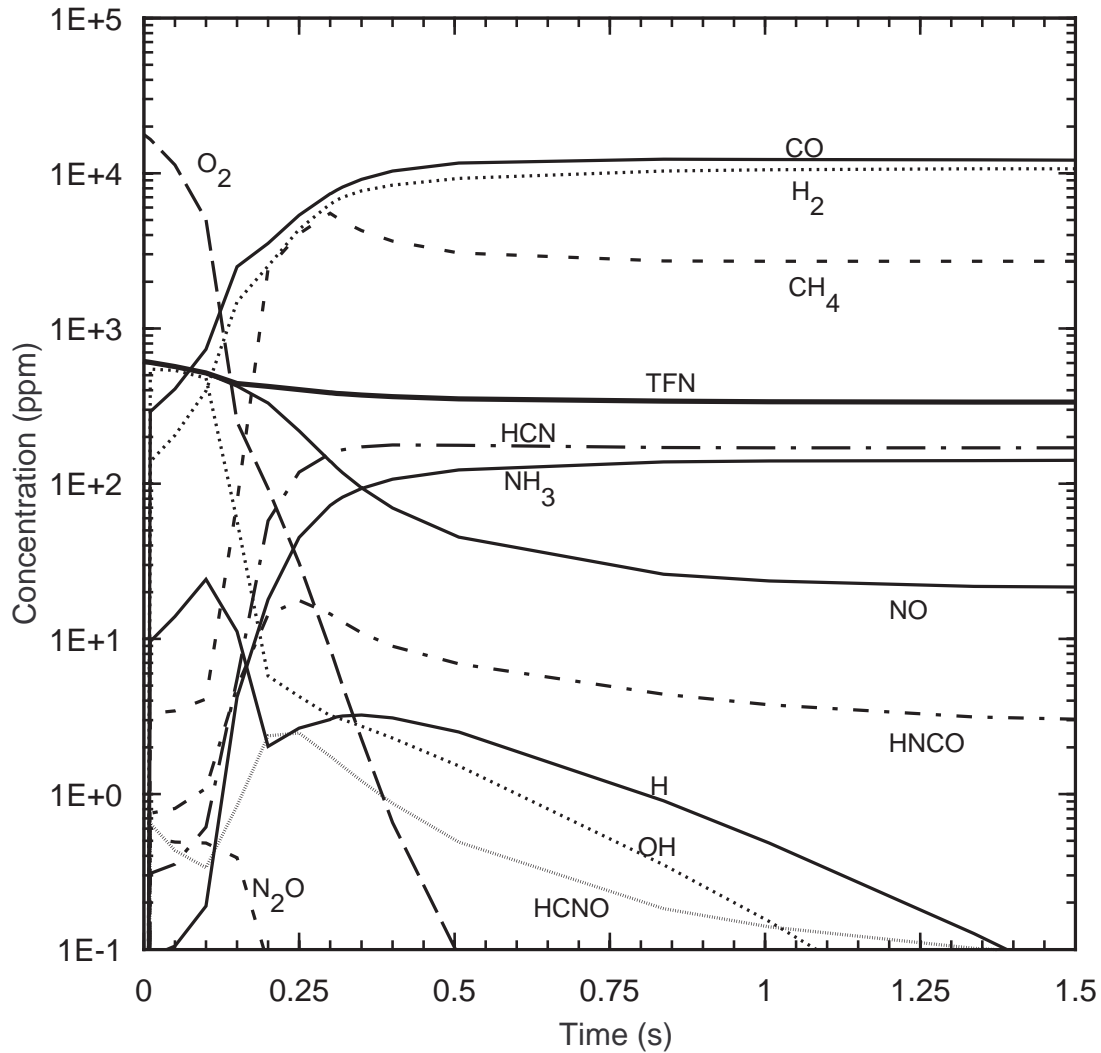


Figure 8.3.4. Kinetic curves of important species in the reburning zone at $SR_2 = 0.99$ and with mixing of the reburning fuel over an interval of 300 ms.

8.3.4 Effect of Mixing Times on AR-Lean

Further modeling addressed the injection of ammonia into the burnout zone (AR-Lean), either co-injected with the OFA or introduced with a short delay time (0.1 s). All cases were run for a nominal reburning zone stoichiometry of 0.99 only as this is the condition of greatest interest for AR. The location of OFA addition was varied between 1200, 1300, and 1400 K. The same three mixing scenarios (instantaneous, 30 ms, and 300 ms) were applied to each condition.

Figure 8.3.6 shows the NO reduction as a function of mixing time for OFA injection at 1300 and 1400 K when ammonia is co-injected. As mixing time increases, NO decreases at both temperatures. For the temperature range considered, NO reduction is better at 1300 K for short mixing times, but

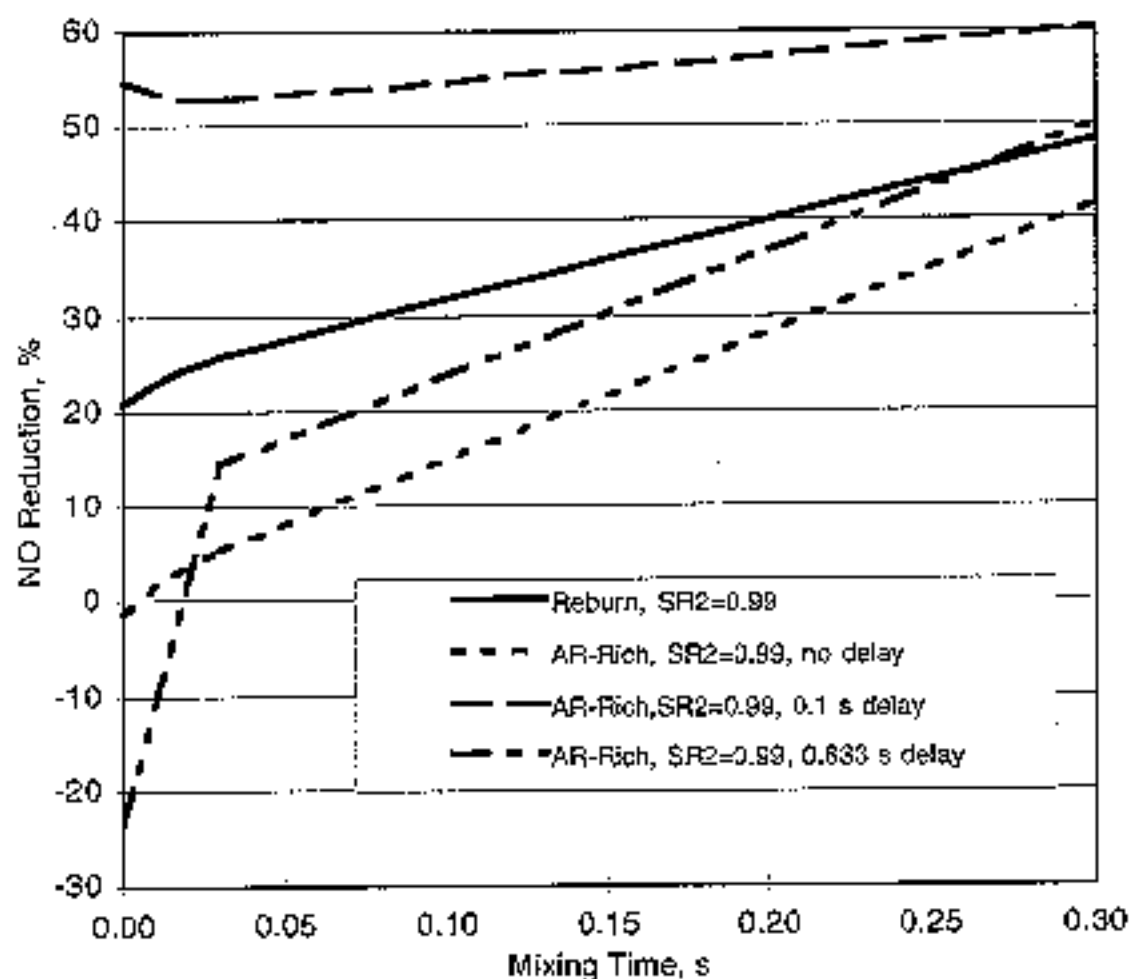


Figure 8.3.5. AR-Rich NO emissions, for $SR_2 = 0.99$ and NH_3 added at $NSR = 1$.

for longer (300 ms) mixing, 1400 K is preferable as it provides good NO reduction with a minimum of other fixed nitrogen species.

Figure 8.3.7 shows the corresponding cases when ammonia injection is delayed by 0.1 s after the beginning of OFA injection. Longer mixing time leads to lower NO in most cases, but there is less difference in NO between instantaneous mixing and 30 ms mixing in this case. This implies that the kinetics is less sensitive to mixing time for the introduction of ammonia at lean conditions, than for ammonia when introduced at initially rich conditions.

Figure 8.3.7 shows that final NO is lower for 1300 K than for 1400 K at all mixing times. However, at 300 ms mixing times, 1300 K OFA injection also results in significant TFN in addition to NO, about 69 ppm NH_3 . Therefore, 1300 K injection gives the best performance for fast mixing conditions, and 1400 K is better for slower mixing conditions due to the lower TFN.

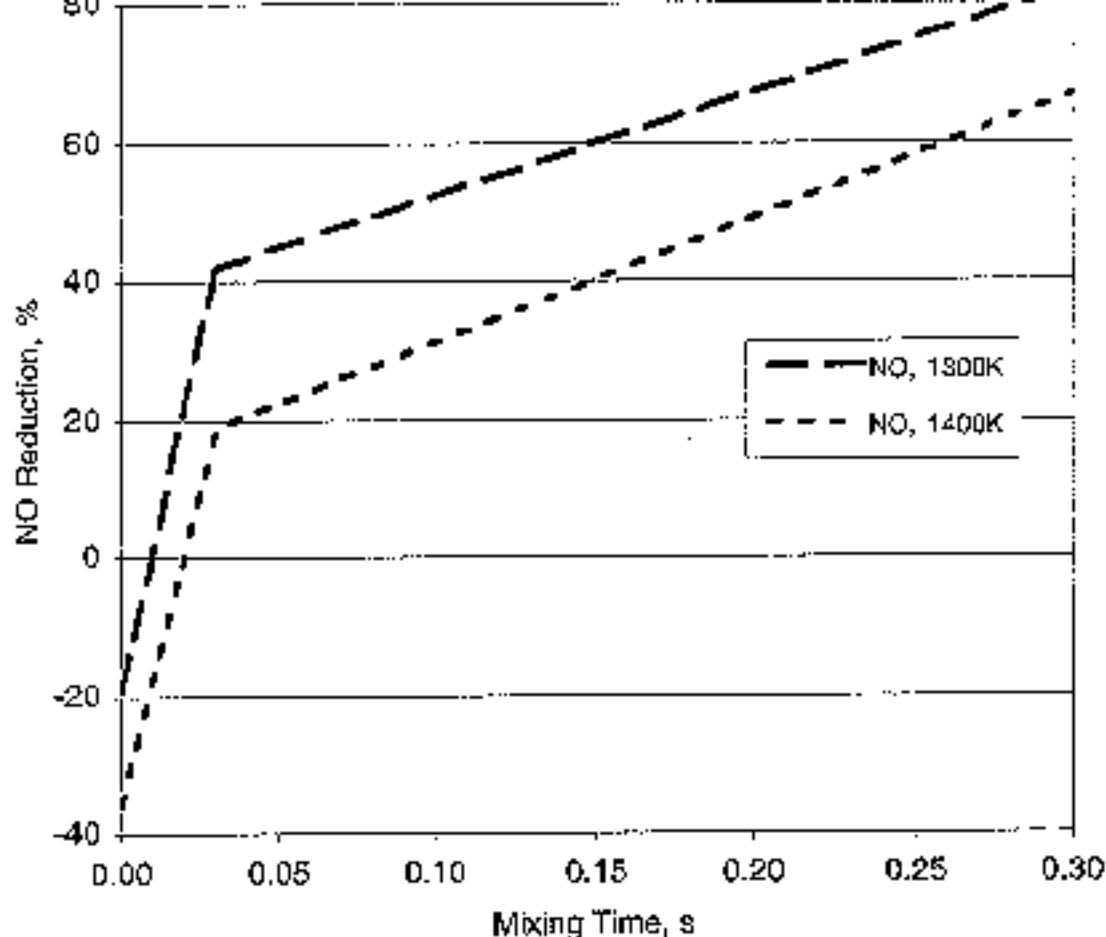


Figure 8.3.6. AR-Lean NO emissions, for $SR_2 = 0.99$ and NH_3 added at the same time as overfire air, at $NSR = 1$.

8.3.5 Mixing Studies: Summary

These studies demonstrate that the rate of mixing of injected streams may have a significant impact on basic or advanced reburning performance. A simplified one-dimensional chemical reactor model is significantly amplified in its scope of prediction by incorporating a simple mass injection model.

In the design of AR systems, the predicted impacts of mixing time may provide guidance in selecting injection nozzles for a given installation. In an experimental study such as this one, however, the most important issue is the prediction of trends which guide in the interpretation of experimental results from reduced scale furnaces, to anticipate the results to be expected for fullscale implementation.

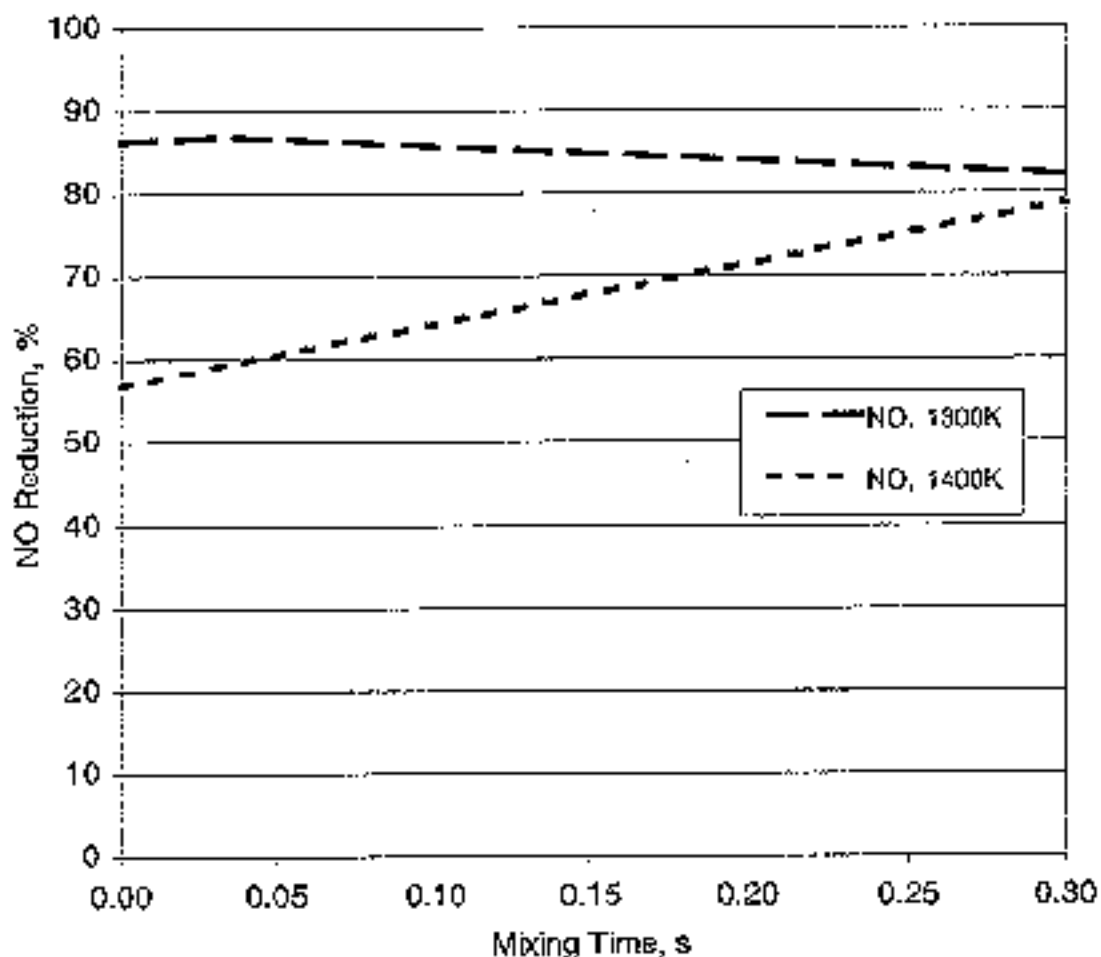


Figure 8.3.7. AR-Lean NO emissions, for $SR_2 = 0.99$ and NH_3 added 0.1 s after burnout air at $NSR = 1$.

For the basic and advanced reburning conditions considered here, four major parameters were varied: the reburn zone stoichiometry, the OFA injection temperature, the location of ammonia injection, and the mixing time. In general, good results were obtained with longer mixing times and with about 0.1 s delay in ammonia injection for both AR-Rich and AR-Lean systems. Very long delays in ammonia injection led to poor performance.

8.4 Effect of Sodium

Of immediate interest is gas-fired AR with sodium promotion. As discussed in Section 8.1.3, the kinetic mechanism has been extended to include reactions of sodium so that this process may be examined.

8.4.1 Effect of Sodium Promotion in AR-Rich

Effect of Mixing Time. The cases considered here for AR-Rich conditions are based on the reactor model with finite-rate mixing, described in Section 8.3 above. The first results examine the effect of mixing time, similarly to Section 8.3.2.

As before, the stoichiometric ratios are nominally 1.10 in the primary zone, 0.99 in the reburn zone, and 1.15 in the burnout zone. Reburn fuel is injected at 1700 K, after which the gas cools at a constant rate of 300 K/s. N-agent and sodium promoter, if any, are co-injected at 0.1 s after the beginning of reburn fuel injection (this condition was selected for initial screening as it showed promise in the earlier AR-Rich studies). When included, the sodium promoter is 50 ppm of Na_2CO_3 .

Figures 8.4.1 through 8.4.3 show the kinetic curves for the AR-Rich reburning zone with and without promotion, for $\text{NSR}=1.0$. The curves start at the point at which the injection of reburn fuel begins (1700 K), and continues for 1.0 s of reactor time (to a temperature of 1400 K).

Figure 8.4.1 shows the kinetic curves with and without sodium promoter, respectively, for the reactor with instantaneous mixing. The discontinuity at 0.1 s is due to the sudden premixing of the additives at that location. For these conditions, there is little net impact of sodium promotion. The greatest change is that O_2 disappears more rapidly in the presence of the promoter. Correspondingly, the radicals H and OH also decrease more quickly for the case with sodium. The net impact is that the final concentrations of NO and NH_3 are actually somewhat lower in the case without promoter. However, the differences are relatively small.

Figure 8.4.2 shows the corresponding behavior for 30 ms mixing. The kinetic curves are similar to those for instantaneous mixing, again with promotion causing a more rapid decline in O_2 , OH, and H. With the distributed mixing, however, the sudden change in concentrations at the addition points is smoothed over the mixing time. 30 ms is relatively fast in terms of the overall reaction time, but at the given conditions the chemical reactions are faster. Therefore, the distributed mixing does change the shape of the curves and affect the downstream composition. In this case the net effect of the sodium promoter is a slight decrease in the NO concentrations near the end of the zone shown.

Figure 8.4.3 shows the kinetic curves for 300 ms mixing, with and without promoter. Here the mixing is distributed over such a long time that the chemistry is definitely affected. The long mixing times result in slow progression through a range of stoichiometries and local NSR's as the reburn fuel, N-agent, and overfire air are slowly introduced. Since the mixing time is longer than the delay

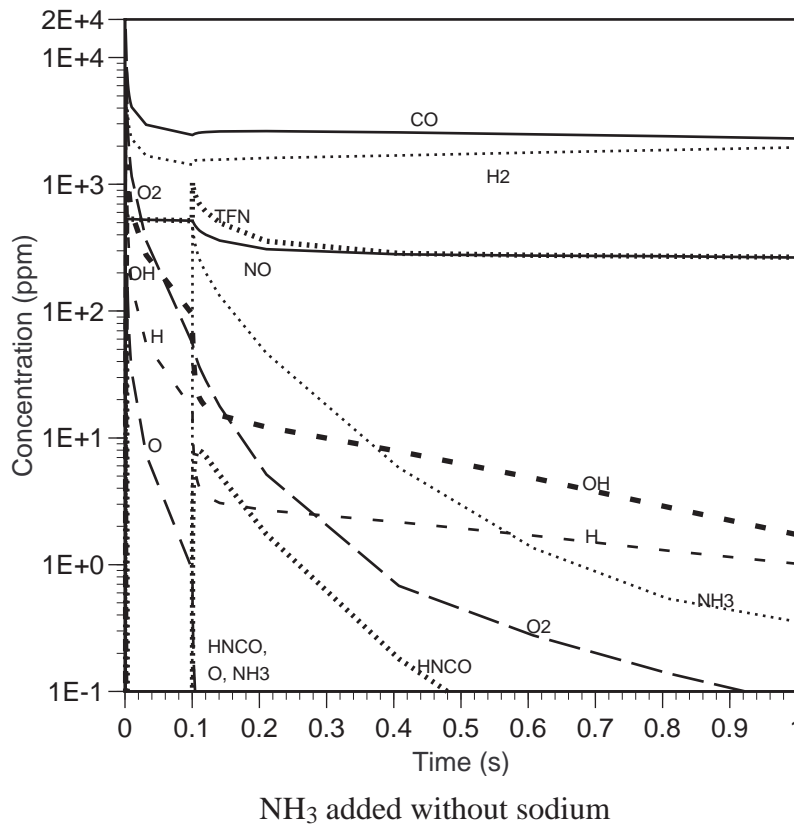
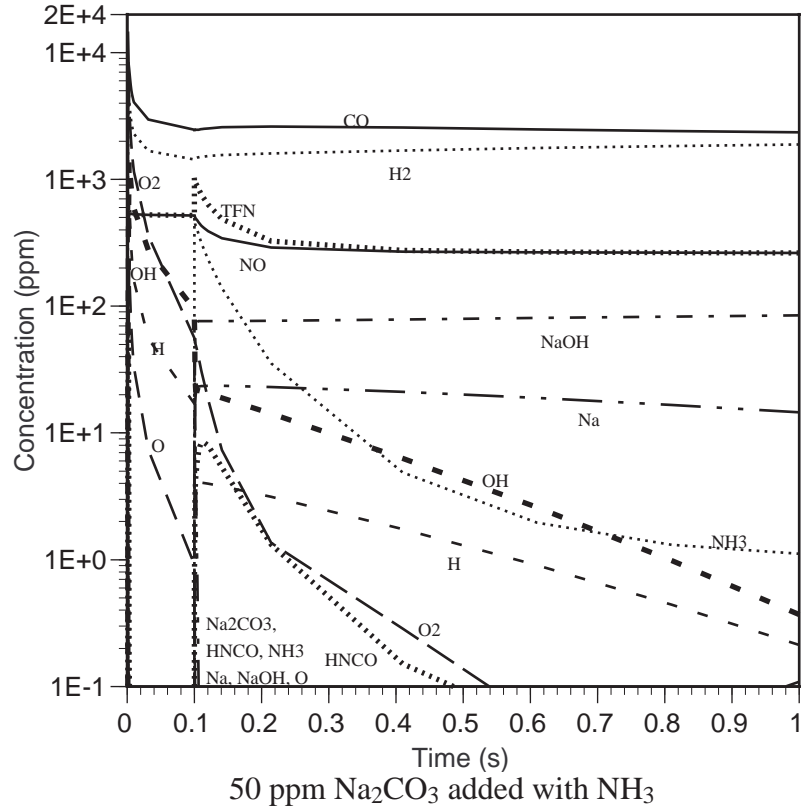


Figure 8.4.1. AR-Rich kinetic curves with instantaneous mixing, from the point of reburn fuel injection with NH_3 (NSR = 1) injected after 0.1 s.

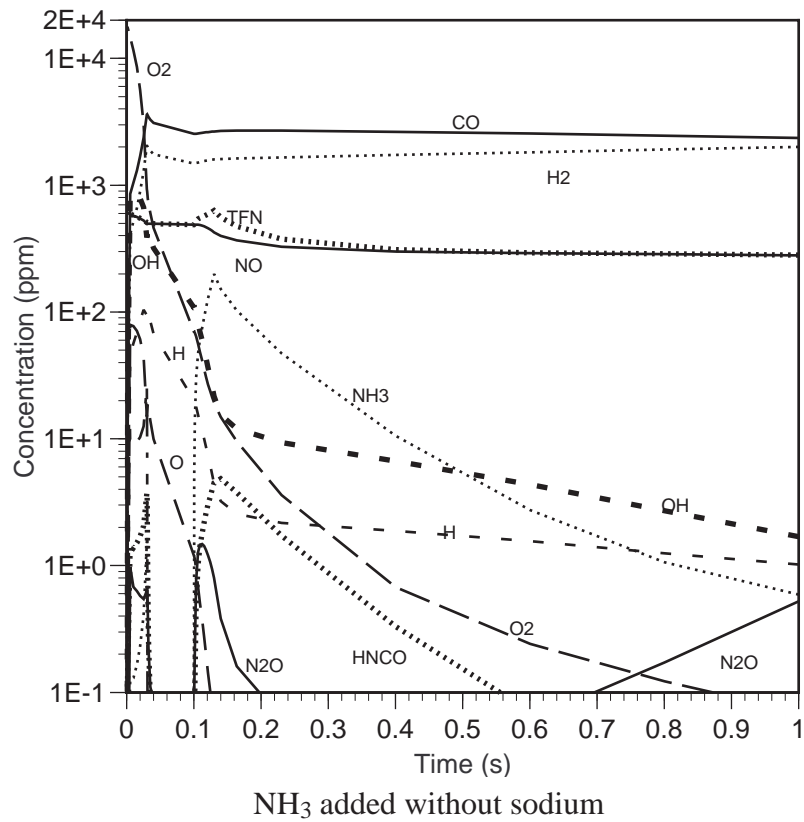
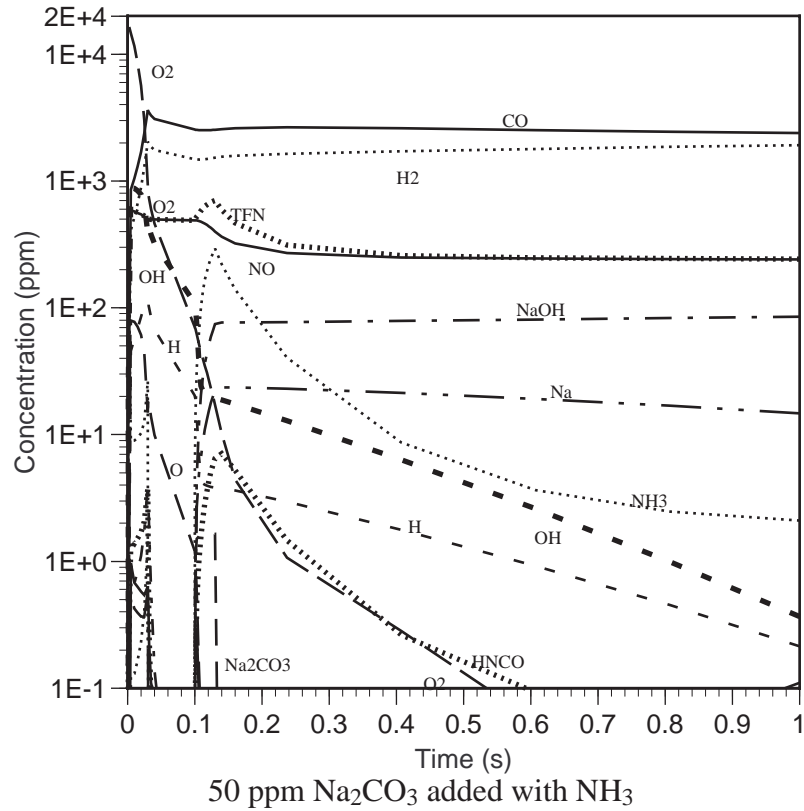


Figure 8.4.2. AR-Rich kinetic curves with 30 ms mixing, from the point of reburn fuel injection with NH_3 ($\text{NSR} = 1$) injected after 0.1 s.

between reburn fuel and N-agent addition, these two mixing zones actually overlap. At 0.3 s, the supply of reburn fuel is out and the pool of radicals and unburned fuel that it helps to sustain now begins to disappear, changing the direction of the kinetic curves at that point. With sodium promotion, even this transition is spread out, suggesting that in this case the sodium promoter helps to sustain the radical pool and has a definite beneficial effect on NO and TFN emissions.

The net impact of promotion is illustrated in Figure 8.4.4, which shows the concentration of NO and TFN in the reburn zone at 1300 K (1.33 s after the start of reburn fuel injection), with and without sodium promotion. At instantaneous mixing, the promoter has a very slight negative effect on emissions. However, for mixing times as short as 30 ms, promotion begins to show a beneficial effect. For longer mixing times representative of industrial installations, the effect is quite pronounced. Longer mixing times also show very large TFN concentrations aside from NO, but it should be remembered that this is before burnout.

As discussed before, the quantity of N-agent can have a significant impact on system performance. To illustrate this, Figure 8.4.5 shows the results of AR-Rich calculations with the same conditions as for Figure 8.4.4, except that the injected N-agent is 800 ppm in all cases. This guarantees an NSR greater than 1 since the initial NO is 600 ppm. The actual NSR is approximately 1.5 based on NO at the point of injection. As would be expected, the NO concentration decreases as more N-agent is added, but note that the effect is non-linear. For instant mixing, the adverse effect of the sodium promoter within the reburning zone increases, but systems with finite mixing times still perform better with sodium promotion. The differences in the effect of promotion at different mixing times reflect the difference in kinetic behavior with mixing time, as illustrated in Figures 8.4.1 through 8.4.3. These changes in characteristic behavior are due to the effect of distributing mass addition, and at long mixing times the shift in temperature due to gas cooling also has an impact. Figures 8.4.4 and 8.4.5 demonstrate the potential improvement in NO and TFN reduction due to the inclusion of a promoter at finite mixing times characteristic of real combustion systems.

Effect of Delay Time. To better understand the temperature dependence of promoted AR-Rich, variations were run varying the delay time with a fixed mixing time of 30 ms and NSR=1.0. Cases were run with NH₃ only, with NH₃+50 ppm Na₂CO₃, with 50 ppm Na₂CO₃ only, and with no additives (basic reburning). The delay time was varied from 0 s (co-injection with the reburning fuel) to 1 s.

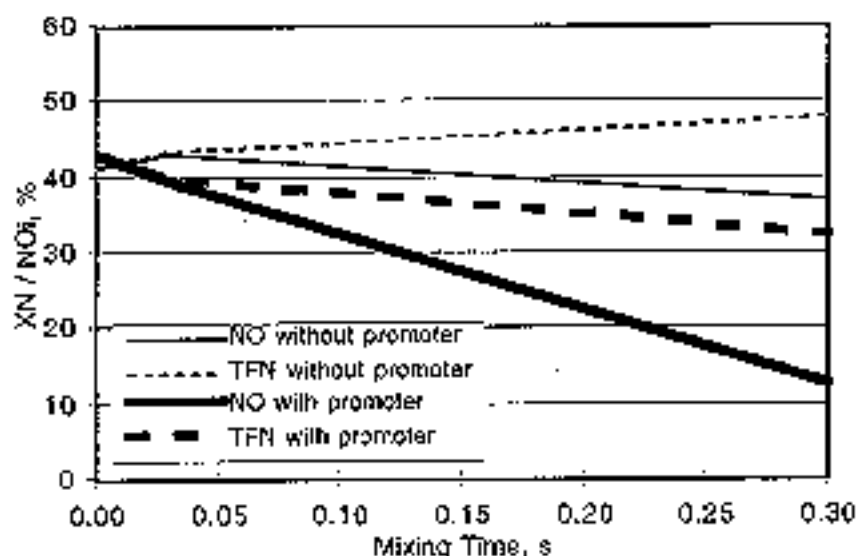


Figure 8.4.4. NO and total fuel nitrogen before burnout for AR-Rich vs. mixing time. NH_3 added at NSR = 1.0 with and without 50 ppm Na_2CO_3 promoter.

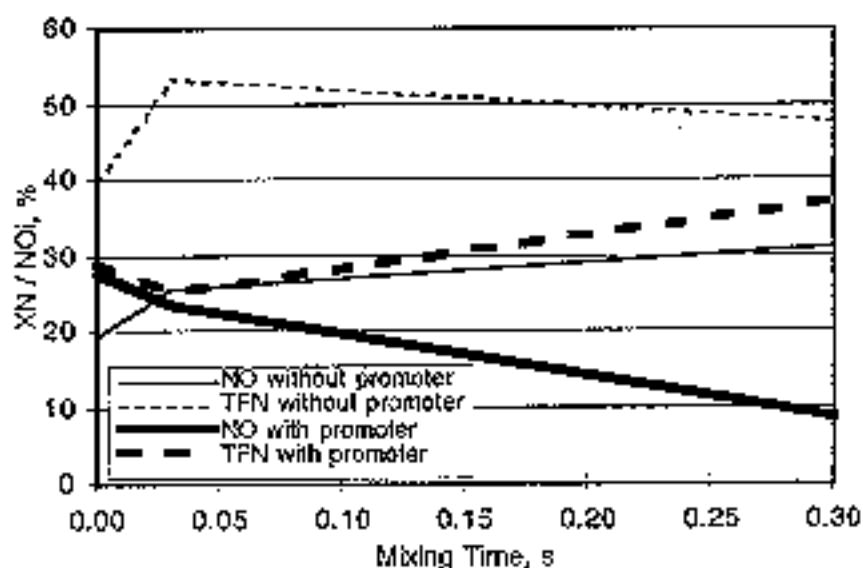


Figure 8.4.5. NO and total fuel nitrogen before burnout for AR-Rich vs. mixing time. 800 ppm NH_3 added (NSR approximately 1.5), with and without 50 ppm Na_2CO_3 promoter.

Figure 8.4.6 and 8.4.7 respectively show the NO and TFN concentration just before the addition of OFA at 1300 K. TFN includes all nitrogen-containing species except N_2 , weighted by the number of N-atoms. From these curves there is an obvious difference due to the addition of promoter along with NH_3 , considerably broadening the interval over which high levels of NO_x reduction are achieved. Figure 8.4.8 shows the final concentration of NO after OFA addition and completion of burnout, at 600 K. There is very little TFN other than NO at this point, so a TFN plot would appear the same. Comparing with Figure 8.4.6, it is seen that NO has improved for the case with N-agent and promoter added, particularly at late delay times. However, there is relatively less improvement due to burnout for the case in which N-agent is added without promoter.

Figure 8.4.8 indicates a very broad optimum for delayed addition of $NH_3+Na_2CO_3$. The optimum delay time for NO reduction is at about 0.4 s. However, the maximum effect of Na addition (that is, the greatest difference between Reburn+ NH_3 and Reburn+ $NH_3+Na_2CO_3$ results) is at somewhat higher delay times. To better understand the role of sodium promotion at a condition where the effect is maximized, the cases with delay times of 0.5 s were selected for further analysis. The kinetic curves for 0.5 s delay, with and without Na promoter, are shown in Figure 8.4.9.

Results at 0.5 s delay (shown in Figure 8.4.8), compared with those at 0.1 s delay (shown in Figure 8.4.2) provide a picture of the effect of sodium under conditions where it has a significant impact (at 0.5 s) versus conditions where the impact is minor (0.1 s), consistent with results in Figures 8.4.6 through 8.4.8. At 0.5 s, Figure 8.4.8 shows that the NH_3 concentration stays high in the AR-Rich zone, compared with its fairly rapid decline at 0.1s. This may be attributed to the reduced temperature at which the NH_3 is added. Without promoter present, the radical populations at 0.5 s are also very low, and so NH_3 and NO coexist without reacting. The addition of promoter at these conditions increases the radical population, allowing NH_3 to react with NO while the radicals persist in adequate concentrations.

Table 8.4.1 provides a summary of the parameters and results of the promoted and unpromoted AR-Rich cases at 0.1 s and 0.5 s delay time. These conditions have been labeled as Cases 1 through 4, and are analyzed for further insight into the chemical basis for the differences between them. Table 8.4.1, in conjunction with Figures 8.4.2 and 8.4.9 with the corresponding kinetic curves, shows an important correlation between TFN species (NO and NH_3) and radicals (OH and H). All cases have similar NO concentrations just prior to N-agent injection.

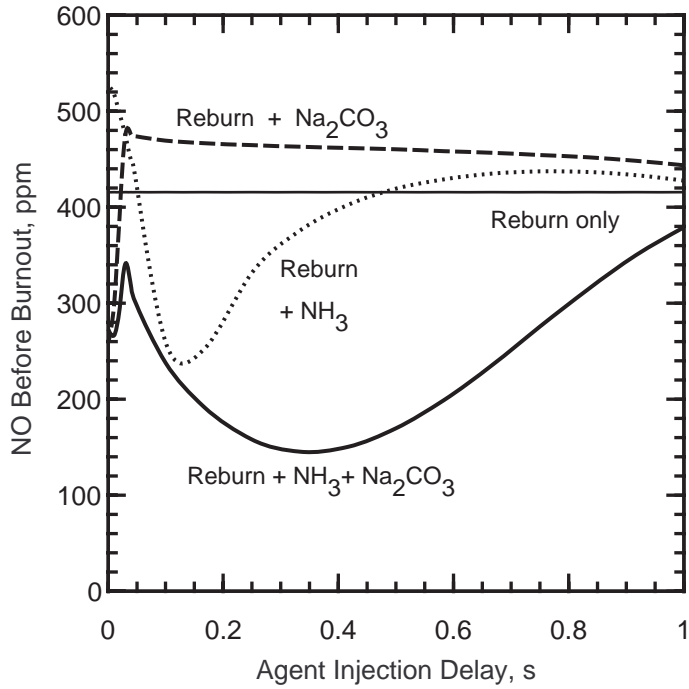


Figure 8.4.6. NO concentration prior to start of overfire air injection at 1300 K, as a function of N-agent/promoter injection delay time.

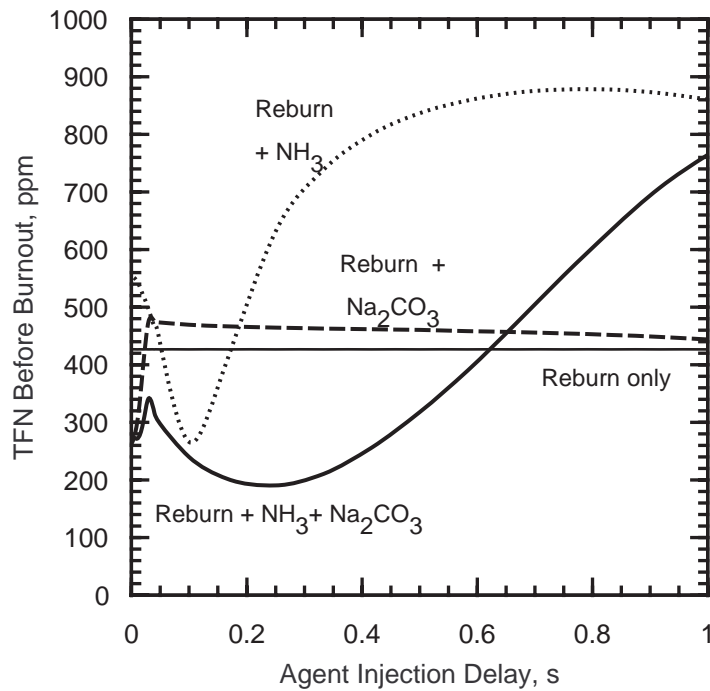


Figure 8.4.7. TFN concentration prior to start of overfire air injection at 1300 K, as a function of N-agent/promoter injection delay time.

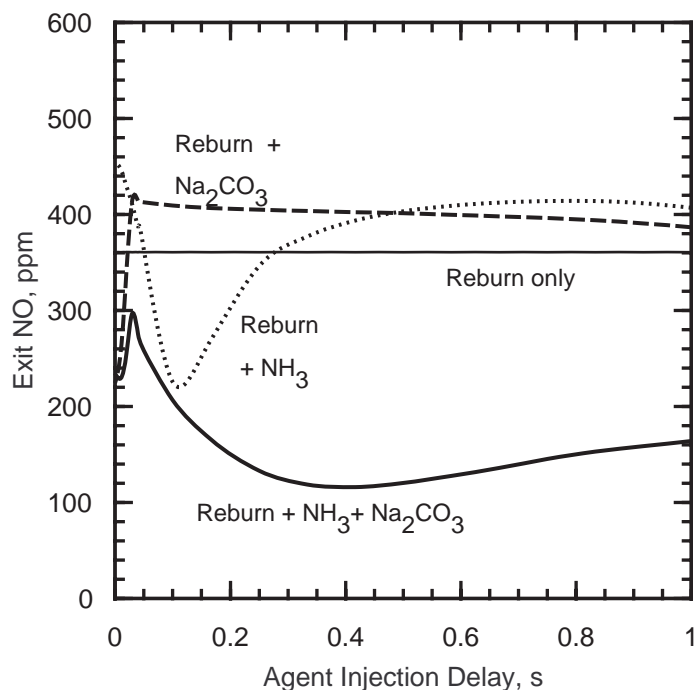


Figure 8.4.8. Final NO concentration at 600 K, as a function of N-agent/promoter injection delay time.

Cases 1 and 2 represent a delay of 0.1 s between the injection of reburn fuel and N-agent, with and without sodium added to the NH₃. For these cases, the OH and H concentrations are relatively high before injection, and are still several ppm at 0.1 s after N-agent injection, but have dropped an order of magnitude from the pre-injection values and are rapidly declining. NH₃, which is added in the same amount as NO at the point of injection (so that NSR=1.0), is also rapidly declining. As a result, these species are only available to react with NO over a limited time, and by 0.1 s after the start of injection most of the ultimate NO reduction is achieved. The remaining rich zone residence time is not as effectively utilized because the necessary reactants are not available in the proper quantities.

The presence of sodium (Case 1) appears to enhance this trend somewhat, compared to the same conditions without sodium (Case 2). After 0.1 s, somewhat higher concentrations of OH, H and NH₃ are present for Case 1 than at the same point in Case 2, and NO reduction is more effective in this interval. As shown in Figure 8.4.2, in the remainder of the rich zone OH and H decline more rapidly and NH₃ less rapidly with sodium than without. However, sodium is unable to provide any

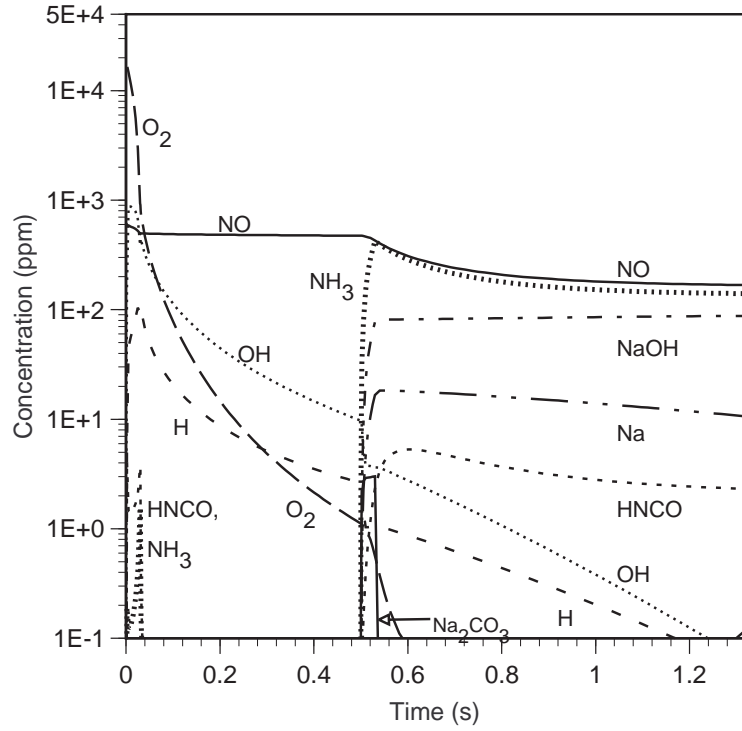
Table 8.4.1. Results of AR-Rich at Different Delay Times.

Case	1	2	3	4
Injection Conditions				
Delay time (s)	0.1	0.1	0.5	0.5
Temperature (K)	1670	1670	1550	1550
Na ₂ CO ₃ added (ppm)	50	0	50	0
Concentrations (ppm)				
Just Before NH₃ added				
NO	490.	490.	473.	473.
OH	111.4	111.4	9.7	9.7
H	20.3	20.3	2.6	2.6
0.1 s after start of NH₃ Addition				
NO	284.	342.	309.	429.
NH ₃	59.	52.	287.	423.
OH	15.	11.	2.8	0.06
H	3.2	2.4	0.9	0.02
Before OFA added				
NO	243.	274.	168.	420.
NH ₃	1.3	0.3	140.2	413.8
After burnout				
NO	210.	237.	121.	403.
NH ₃	<0.001	<0.001	0.02	<0.001

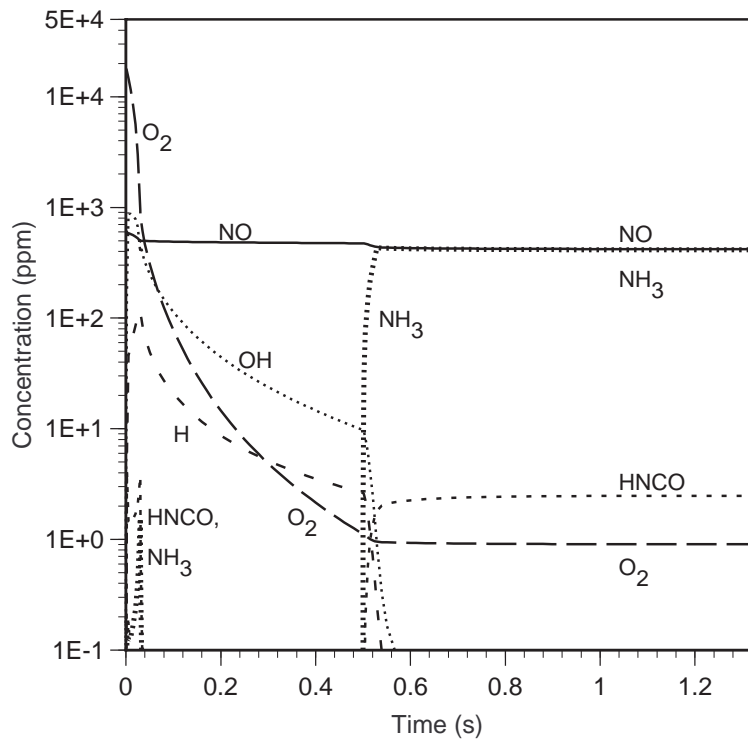
Notes: Delay time is defined as time from start of Reburn Fuel injection to the start of NH₃ injection
 For all cases, mixing time is 30 ms for all injected streams, and SR2 = 0.99.
 NSR = 1.0 based on NO concentration at point of NH₃ injection.
 Na₂CO₃, when added, is always premixed with the added NH₃.
 Temperature profile is -300 K/s from start of reburn fuel addition at 1700 K.
 Initial (primary zone) NO before reburn fuel injection is 606 ppm for all cases.
 OFA is added at 1300 K in all cases.

beneficial effect without a sufficient amount of NH₃. The resulting NO reduction in the last part of the reburning zone (after 0.1 s) is less with sodium than without. The net effect of sodium promotion in this case, however, is a modest improvement of 30 ppm in NO removal, by increasing NO destruction rates at earlier times, where the reaction is most effective.

These results imply that at the high temperature conditions of Case 1, that increasing the quantity of NH₃ added would be beneficial, particularly in the presence of sodium. The more N-agent present in



50 ppm Na_2CO_3 added with NH_3



NH_3 added without sodium

Figure 8.4.9. AR-Rich kinetic curves with 30 ms mixing from the point of reburn fuel injection with NH_3 ($\text{NSR} = 1$) injected after 0.5 s.

the initial, fast-reaction interval, the more NO reduction may be expected. Further, under these conditions, particularly with sodium added, NH_3 is effectively destroyed in the last part of the reburning zone, so that little ammonia slip would be expected even at higher NSR's. This approach provides a means of improving AR-Rich performance at higher injection temperatures. Comparison of Figures 8.4.4 and 8.4.5 supports this hypothesis and also indicates that it is true over a wide range of mixing times as well.

Cases 3 and 4 represent a delay of 0.5 s between the injection of reburn fuel and N-agent, with and without sodium added to the NH_3 . In these cases, the OH and H concentrations are not as high before injection as in Cases 1 and 2. In Case 3, in which sodium is included, OH and H have decreased after 0.1 s, but not as quickly as in Cases 1 and 2, and are still present in quantities on the order of 1 ppm. After 0.1 s in the presence of sodium, NH_3 has not declined as much as in Case 1. NO also declines somewhat less in the first 0.1 s, but continues to decline over the remainder of the rich zone and achieves a lower final concentration (168 ppm) than for Case 1 (243 ppm). The TFN at the end of the rich zone for Case 3 is high because NH_3 is still present in substantial quantities. However, this TFN is effectively burned out when OFA is added at 1300 K, as indicated by Figures 8.4.7 and 8.4.8.

In Case 4, OH and H decrease to very low concentrations (0.06 and 0.02 ppm) in the first 0.1 s from the start of NH_3 injection, while NO and NH_3 have declined only by about 50 ppm. In the remainder of the rich zone, NO and NH_3 decline by only about another 10 ppm. Apparently the concentration of radicals was inadequate to sustain reactions of NO and NH_3 in the rich zone. Although burnout does reduce the high level of rich zone TFN, the final NO is still on the order of 400 ppm as shown in Figure 8.4.8.

These results show the importance of maintaining the proper concentrations of important reactants for effective NO reduction. High initial levels of NH_3 and radicals promote rapid initial reduction, but the NO reduction rate is not sustained if the NH_3 concentration declines too quickly, as in Cases 1 and 2. In Case 4, it is seen that a sustained high level of NH_3 is also ineffective if radicals are not sustained in sufficient quantities. Case 3 represents the most desirable situation: even though the initial radical levels are the same as for Case 4, in the presence of sodium the radicals are sustained

at those levels for a longer time. Even though the initial reaction rate is slower in Case 3 than Case 1, it is effective for a longer time and results in better overall performance.

The implication of these observations is that NO reduction is optimized by sustaining radical populations at the proper concentrations to maintain a steady rate of reaction of NO with NH₃ and its decomposition products. In these cases, sodium is only partially successful at short delay times/higher temperatures, but is very successful at longer delay times/lower temperatures.

Sensitivity Analysis. The results shown so far strongly imply a correlation between radical concentrations and NO-NH₃ chemistry, but do not show what specific reactions are involved. Analysis of sensitivity and contribution factors, as discussed in Section 8.2, provides specific information about the relative importance of different reactions in the mechanism. This analysis has been performed for Cases 1 through 4 defined in Table 8.4.1, examining the rich zone from the end of NH₃/Na₂CO₃ injection to just before OFA injection at 1300 K.

Contribution factors for all four cases show the same predominant reactions involving NO as discussed earlier (see Figure 8.2.21). Reaction (280) and the combined Reaction (281+282) dominate NO removal:



Opposing these, the reverse of Reaction (211) is the predominant source of NO formation during the fast reaction stage:



At the lower temperatures corresponding to longer delay times (Cases 3 and 4), Reaction (-211) has smaller effect relative to Reactions (280-282) than at higher temperatures. This indicates that NO formation reactions, which compete with the NO removal process, are less effective at lower temperatures.

Sensitivity analysis for the four cases shows that Reactions (280-282) are also among the most important from a sensitivity perspective. The net effect of Reaction (281-282) generally dominates, with a net negative impact on NO (that is, an increase in the rates of reactions (281-282) increases the rate of NO reduction).

In Case 1, the sensitivity impact of Reactions (280-282) is opposed significantly, particularly after the initial fast NO reduction period, by Reaction (202):



This reaction acts as a chain termination step because it converts NH_2 to NH , which is less reactive in NO reduction.

A review of sensitivity coefficients for several species in the mechanism, under conditions where sodium is added (Cases 1 and 3), indicate that Reaction (327) has the most significant effect among the reactions involving sodium, and that Reaction (326) is important as well. This combination of reactions is believed to be especially significant because of its impact on the radical pool:



The net effect of these two reactions acting together is $\text{H} + \text{OH} \rightleftharpoons \text{H}_2\text{O}$. If both reactions proceed forward, they are removing OH and H radicals, and if both proceed in reverse they contribute these radicals. While these reactions are significant among the reactions of sodium whose presence has a significant impact on NO reduction, they do not show the largest sensitivity factors. This reflects the nature of these reactions as moderating the fast-reacting radical species, rather than reacting directly with the high concentration, slowly reacting species such as NO and NH_3 .

In both Cases 1 and 3, Reactions (326-327) both proceed in the reverse direction, thus boosting the radical pool by converting H_2O to OH and H. In Case 1, their rates diminish rapidly after about 0.1 s following the end of N-agent addition, while in Case 3 they also diminish with time but less

rapidly, as is the case for most of the other significant reactions. These observations are consistent with the correlations between radical and NO/NH₃ histories discussed above.

8.4.2 Effect of Sodium Promotion in AR-Lean

Effect of Injection Temperature. To better understand the effect of co-injecting sodium with Nagent in AR-Lean, the kinetic models (ODF and SENKIN) have been used to predict behavior at different injection locations with and without sodium. The modeling approach for these calculations are similar to those for the results just presented for AR-Rich. Many of the input parameters are the same: SR₂=0.99, and mixing time 0.03 s for all injections. The temperature profile is -300 K/s to a final exit temperature of about 600 K. The chief difference is that in this case the OFA injection location is varied, and the delay time for the start of NH₃ injection is 0.1 s after the start of OFA injection in all cases. This is consistent with results shown earlier (for example, Figure 8.2.16) which indicate an optimum delay time at about 0.1 s.

The amount of NH₃ added was fixed at 394 ppm for all cases presented here. This corresponds to NSR=1.0 for OFA injection at 1400 K. At higher injection temperatures, the resulting NSR will be slightly lower, and vice versa, due to the corresponding change in NO at the injection point. Over the range of OFA injection temperatures considered, NSR ranges between 0.9 and 1.5. Adjusting the NH₃ injection to a uniform NSR would not be expected to change the trends in the results presented here.

Figure 8.4.10 shows the impact of promotion on the exit NO for each case. The predominant effect of sodium injection is a horizontal shift in the curves. For temperatures higher than about 1330 K, including the promoter has a beneficial effect on final NO, but at lower temperatures the addition of sodium actually increased NO relative to AR-Lean at the same conditions without sodium.

The trend in exit NH₃ is similar to that for SNCR. For injection temperatures higher than a few degrees above the optimum for NO reduction, exit NH₃ is negligible. As injection temperature decreases to temperatures just below the optimum, NH₃ increases rapidly, asymptotically approaching the injected concentration. As for SNCR, practical AR-Lean systems should be designed to ensure temperatures on the high side of the optimum value for NO reduction alone, to avoid ammonia slip.

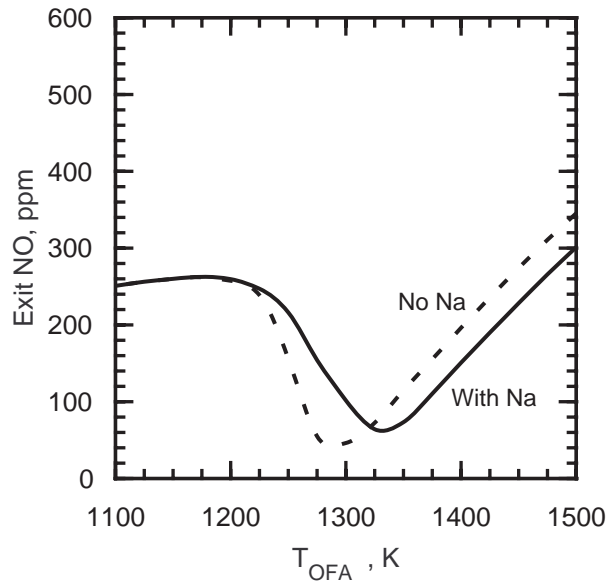


Figure 8.4.10. Effect of promoter on NO exit concentrations for AR-Lean.

The next step is to understand why this upward temperature shift is predicted. For this purpose, four cases were selected for additional analysis, for two injection temperatures with and without promoter. The two conditions selected are designed to maximize the difference due to promotion, negative in one case (lower injection temperature) and positive in the other. The cases selected are presented in Table 8.4.2, along with predicted concentrations at specific locations. Cases 1 and 2 represent OFA injection at 1280 K (near the optimum for unpromoted AR-Lean). Cases 3 and 4 represent OFA injection at 1380 K (near the optimum for promoted AR-Lean). Cases 1 and 3 inject 50 ppm Na_2CO_3 with the NH_3 , which Cases 2 and 4 add no sodium.

Figure 8.4.11 shows the kinetic curves for some of the most important species for Cases 1 and 2, to show the effect of sodium for OFA injection at 1280 K. The most notable difference between these two cases is the faster initial decay rates in the presence of sodium for a number of species including NO, NH_3 , CO, OH, NO_2 , and N_2O (the latter two decaying substantially with promoter but persisting in ppm levels without it). On the other hand, NO, NH_3 , and H_2 persist in higher levels in the presence of promoter, consistent with the reduced performance predicted for 1280 K OFA injection. Furthermore, note that after initial conversion to NaOH, sodium is reconverted to Na_2CO_3 in Case 1, effectively eliminating its effectiveness for reactions involving radicals.

Table 8.4.2. Results of AR-Lean at Different Injection Temperatures, with and without sodium.

Case	1	2	3	4
Injection Conditions				
T at start of OFA injection (K)	1280	1280	1380	1380
T at start of NH ₃ injection (K)	1250	1250	1350	1350
Na ₂ CO ₃ added (ppm)	50	0	50	0
Concentrations (ppm)				
Just Before NH ₃ added				
NO	353.	353.	388.	388.
OH	9.4	9.4	17.8	17.8
H	0.001	0.001	0.003	0.003
0.03 s after start of NH ₃ Addition (End of Mixing Zone)				
NO	269.	254.	242.	232.
NH ₃	303.	290.	187.	160.
OH	2.	3.2	15.	22.
H	0.007	0.015	0.033	0.068
0.1 s after start of NH ₃ Addition				
NO	196.	119.	141.	167.
NH ₃	224.	141.	27.	2.
OH	0.8	2.9	10.	18.
H	0.002	0.005	0.003	0.004
Exit (at 600 K)				
NO	146.	52.	121.	165.
NH ₃	173.	64.	0.02	0.
NO ₂	0.01	7.	1.	1.
N ₂ O	<0.001	7.	0.01	4.

Notes: Delay time is 0.1s from start of OFA injection in all cases.
 For all cases, mixing time is 30 ms for all injected streams, and $SR_2 = 0.99$.
 394 ppm NH₃ added in all cases (NSR = 1.0 to 1.1)
 Na₂CO₃, when added, is always premixed with the added NH₃.
 Temperature profile is -300 K/s from start of reburn fuel addition at 1700 K.
 Initial (primary zone) NO before reburn fuel injection is 606 ppm for all cases.

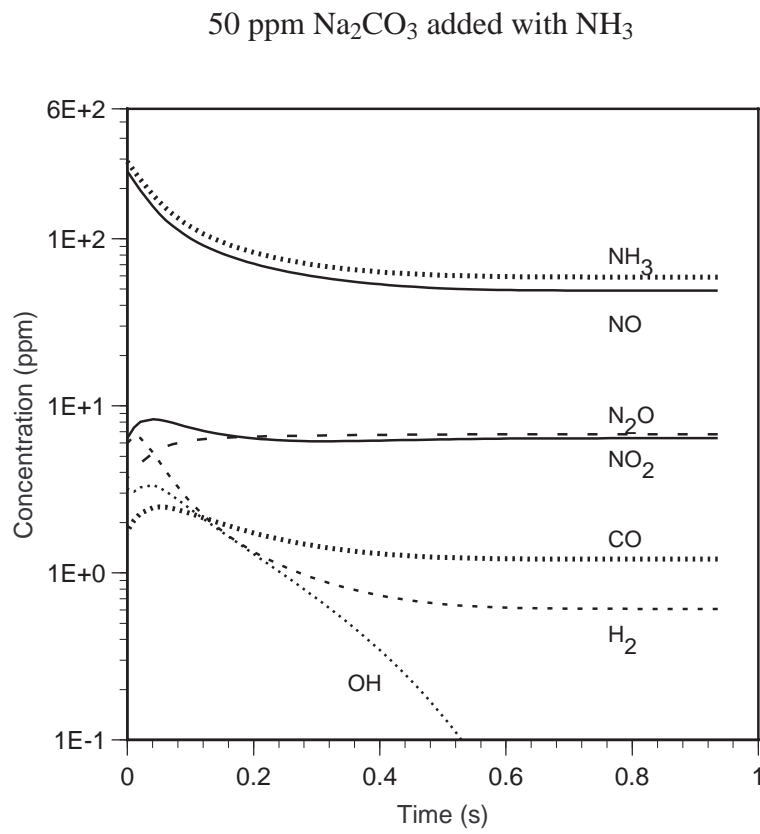
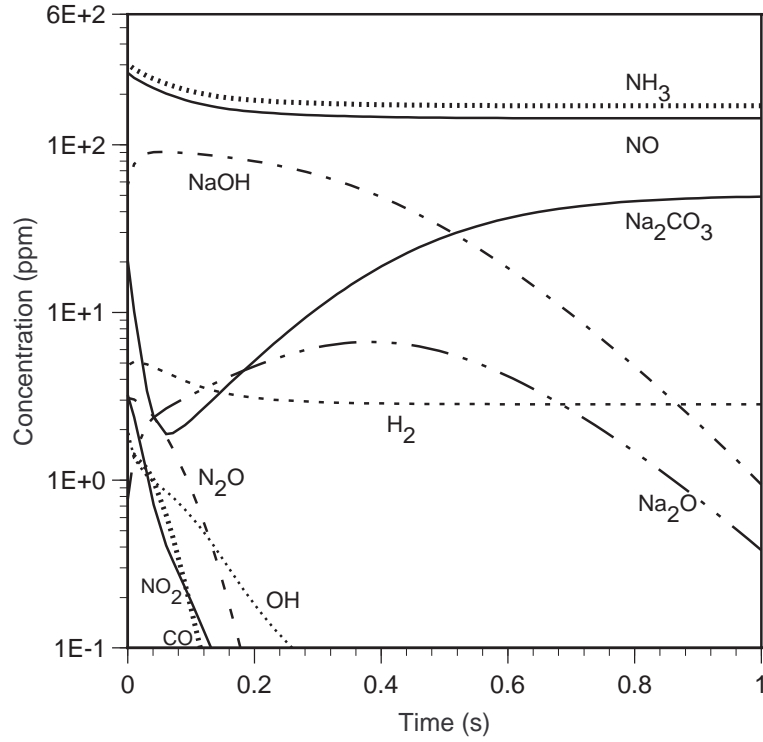


Figure 8.4.11. AR-Lean kinetic curves with 30 ms mixing from the point of NH₃ injection, which is 0.1 s after OFA injection at 1280 K.

Figure 8.4.12 shows the kinetic curves for Cases 3 and 4, to show the effect of sodium for OFA injection at 1380 K. These curves show faster decay for many species (notably excepting NH₃ and H₂) in the presence of promoter. The initial decay rate for NO appears to be similar with and without promoter for about the first 20 ms. The difference in NO appears to occur over the time span from about 20 to 200 ms, during which NO decay continues (albeit at a reduced rate) with promoter, but essentially stops without it. These time scales appear to reflect the difference in decay time of NH₃. As previously discussed for AR-Rich, an important element in the sodium promotion mechanism is persistence in the availability of the N-agent (or intermediate species generated by it).

The NO concentration immediate after the end of N-agent injection (0.03 s) is better without promoter, for both injection temperatures. At the lower temperature, the gap widens, while at the higher temperature the promoter eventually results in lower NO and TFN at the exit. As for the optimum case in AR-Rich, the beneficial effect in sodium addition lies in the prolonging of significant NO reduction rates over a longer interval in the NH₃ reaction zone.

Sensitivity Analysis. The ODF results immediately following the end of N-agent mass addition was used as the initial condition for SENKIN sensitivity calculations. This analysis provides further insight into the source of the differences between these cases.

Comparing the NO contribution and sensitivity factors, it is seen that reactions 280, 281 and 282 are the most significant reactions in all cases. All of these reactions involve NH₂+NO, with final products NNH+OH for Reaction (280) and N₂+H₂O for Reactions (281-282).

Other reactions with significant sensitivity effects include reaction (38) and (202):



Reaction (38) has a negative influence at the lower temperature and (after an initial negative transient) a positive influence on NO at the higher temperature. Reaction (202) has a notable positive sensitivity effect on NO at the higher temperature, as it competes with other NH₂ reactions (280-282) which

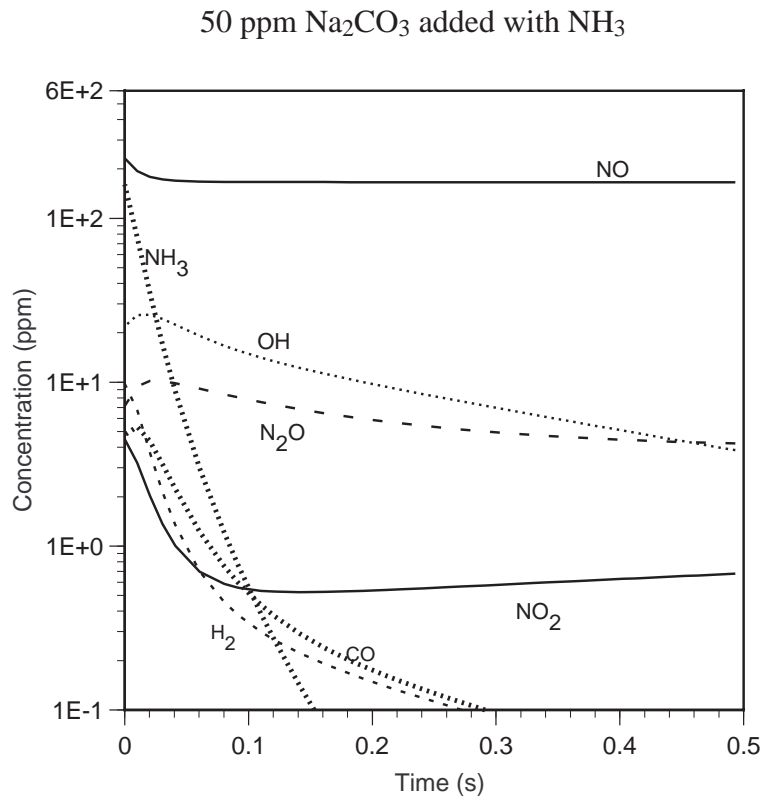
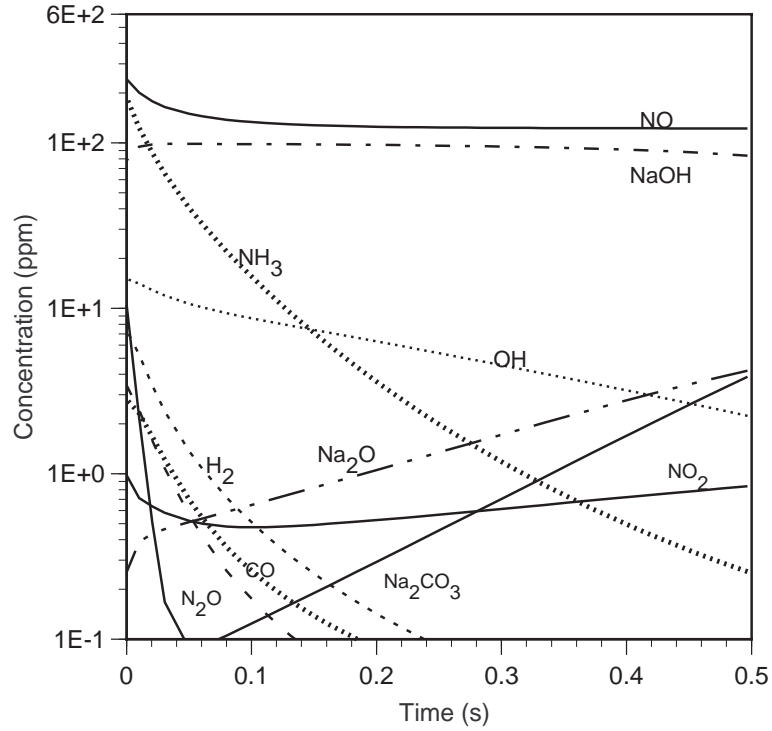


Figure 8.4.12. AR-Lean kinetic curves with 30 ms mixing from the point of NH_3 injection, which is 0.1 s after OFA injection at 1380 K.

remove NO, and at the same time converts NH₂ to less reactive NH.

The importance of radicals in the NO removal mechanism begins with the removal of NH₃, which is dominated by Reaction (277):



Therefore, the availability of OH controls the rate of NH₃ reaction. It is NH₂ which predominates in reactions (280-281) which remove NO, and so control of the rate of NH₃ affects the availability of NH₂.

For both cases with sodium, the Na reactions with the largest contribution effect for NO is (323)



The contribution to NO is positive, indicating that the reaction is proceeding in reverse. The sodium reaction with the greatest sensitivity is (326)



. In fact, reaction (326) is also the most significant sodium reaction for several other species, including NH₃ and NH₂. Reaction (326) shows positive sensitivity for NO at all times in Case 1, while for Case 3, it peaks positive at about 20 ms, then declines and goes negative. In other words, NO formation is favored by Reaction (326) in Case 1, but NO destruction is favored by Reaction (326) for most of Case 3. This is consistent with the positive and negative influence of the presence of sodium in those cases.

Having identified reactions with major contribution and sensitivity influences, a more complete picture of the role of sodium may be drawn. The initial steps of the sodium mechanism can be summarized by Reactions (317-319):





Since Reaction (317) is the only one involving Na_2CO_3 , it is seen that Na_2CO_3 is ineffective at managing the radical pool, adding to the ineffectiveness of sodium at later times in Case 1, when Na_2CO_3 is the dominant species.

When NaOH is available, it reacts predominantly through Reaction (326) to remove H:



If reaction (327)



is running in the same direction, it works with Reaction (326) to either recombine $\text{H} + \text{OH}$ into H_2O , or in reverse to increase these radicals. In Case 3, both reactions move forward, while in Case 1 they oppose each other. In both cases, the rate of (326) is larger in magnitude. Its main importance may lie in the indirect influence of the OH concentration through other reactions such as Reaction (38):



By reducing the concentration of H, Reaction (326) slows Reaction (38) and therefore reduces the availability of OH. Other sodium reactions affect the radical pool, but to a lesser extent than (326). However, at the higher temperature the OH concentration is much higher, resulting in more rapid and complete NH_3 destruction than at the lower temperature, where a significant NH_3 concentration persists.

When NH_3 removal is incomplete (as for 1280 K OFA injection), the reduction of NH_3 at early times is all that contributes to NO removal, so faster NH_3 removal during that time period is more beneficial to NO reduction. When NH_3 removal is complete (as for 1380 K OFA injection), then

spreading it out over a longer time provides a more consistent stream of reactants to reduce NO, and so is able to do so more effectively. The role of sodium in slowing NH₃ removal rates appears to be the primary difference in the behavior for 1280 K versus 1380 K OFA injection.

8.5 Summary of Modeling Studies

The GRI-Mech combustion mechanism has been extended based on literature and experimental data to include SNCR chemistry, as well as reactions involving compounds of Na, S, and Cl. The sodium mechanism has been used to evaluate the performance of AR-Rich and AR-Lean scenarios, promoted by Na₂CO₃.

The individual AR injection processes have been investigated using one-dimensional chemical kinetics models, to determine their behavior over time and as a result of parametric variations. Analysis of sensitivity and contribution factors identifies specific reactions in the mechanism which affect the results.

Analysis of the basic reburning process revealed an initial fast NO reduction zone followed by a longer, slower NO reduction zone. This provides an opportunity for improvement through AR-Rich, by enhancing the rate of reaction in the latter zone.

The effect of ammonia in both AR-Rich and AR-Lean was investigated. In both cases, it is possible to optimize NO reduction with respect to the injection temperature and/or delay time of N-agent injection. Optimization of the amount of N-agent is also important to system performance. The quantity must be adequate for the degree of NO reduction but more is not necessarily better. Designing the injection system to promote uniform mixing should help minimize the quantity of N-agent needed but the performance also depends on the characteristic time of mixing. The NSR and mixing time both affect the net NO reduction as well as the net concentration of other TFN species. In most cases, the trend is toward better performance at longer mixing times, which implies that the results at full scale should be able to at least match pilot scale experimental results. The chief drawback of larger scales is increased potential unmixedness of the reburn fuel, as well as N-agents with flue gas. This may create zones with too high and too low SR₂ that will reduce AR performance.

The effect of promoters was also investigated. First, the effect and influence of various types of promoting species, including radicals, was considered. Later, more attention was paid to the use of specific promoters of current interest for field implementation, notably Na_2CO_3 . In AR-Rich the effect of Na_2CO_3 is to broaden the range of injection locations with good NO reduction performance. In AR-Lean, the primary effect is to shift the optimum in NO reduction to higher temperatures.

Sodium promotion can improve AR-Rich performance by sustaining the radical pool when it is needed. As for unpromoted AR, this effect is most pronounced in systems with long characteristic mixing times, and so promoted advanced reburning continues to show promise for commercial implementation. Similarly, sodium promotion can improve AR-Lean, in this case by limiting the radical pool to moderate the reaction rate of NH_3 .

In both AR-Rich and AR-Lean, it should be noted that optimization involves managing both the concentrations of important species (such as NH_3 and OH), and their rate of removal. Generally, concentrations and rates which are too high are undesirable as well as those which are too low. In general, optimum solutions tend to be those with slow but steady NO removal using as much of the reaction zone as possible.

9.0 DESIGN METHODOLOGY AND APPLICATION

This task was included in the project to provide a conduit for translation of the analytical and experimental SGAR configurations into practical full scale designs. The task includes the extension of EER's reburning design methodology to AR and SGAR configurations and the evaluation of SGAR economics and market potential for US utility boilers. The original work scope for this task was based on use of a hypothetical case study. However, it was hoped that an initial AR demonstration could be developed in parallel with Phase I (outside the scope of this DOE project) and could be used to evaluate some of the elements of SGAR during the later portion of Phase I and in Phase II.

EER has been successful in developing an initial AR demonstration project. In 1995 EER installed the original AR configuration (now termed AR-Lean) on a 105 MW tangentially fired boiler. Accordingly, this unit was used as the basis for extending the design methodology. Testing is being conducted in three phases during the summer of 1996, 97, and 98. In this task, this unit was used as a case study for extending the reburn design methodology to SGAR. It also was used to test some elements of the various SGAR configurations during summer 1997. If the project proceeds through Phase II, additional elements will be tested in 1998.

The following section describes the extension of EER's reburning design methodology to AR and SGAR. The general approach is outlined and then applied to the 105 MW tangentially fired demonstration unit. Section 9.2 discusses the application of AR-Lean to this unit which was conducted as part of a separate project, and the initial testing of some SGAR elements. Finally, Section 9.3 discusses the application of SGAR to the US utility industry including the regulatory drivers, economics and market potential.

9.1 AR Design Methodology

9.1.1 General Approach

EER's general methodology for application of AR technologies to utility boilers is shown in Figure 9.1.1. The design methodology uses various experimental and analytical tools to develop the injector specifications and operating characteristics of the AR system with the objective of meeting specific process requirements for optimum emissions control performance while maintaining boiler operation and performance at normal levels. The primary elements of the methodology consist of:

- Collection of system design and operating data to quantify the characteristics of the

full-scale system, and to obtain data for use in model set up and calibration. This information typically includes the range of typical operation, specific unit limitations that should be taken into account in the design, and emissions controls requirements.

- Heat transfer modelling of the unit to predict the boiler's thermal characteristics as functions of various input and operational variables. This analysis is focussed on studying the impacts of the process on boiler performance, and on identification of possible remedies for any adverse impacts which are expected to occur.
- Isothermal flow modelling of the unit to simulate the full-scale furnace flow field, and to optimize the injection parameters of the reburning/AR systems. A key objective of the flow model studies is to develop injection systems which provide rapid and uniform mixing of the reburning fuel, OFA, and N-agents.
- Development of performance predictions for full-scale applications of the reburning process using process and kinetic models developed from the results of subscale tests and the fundamental chemistry involved in the process. Model predictions under ideal mixing conditions are used in conjunction with the results of isothermal model mixing studies to assess the impacts of mixing on reburning/AR performance.

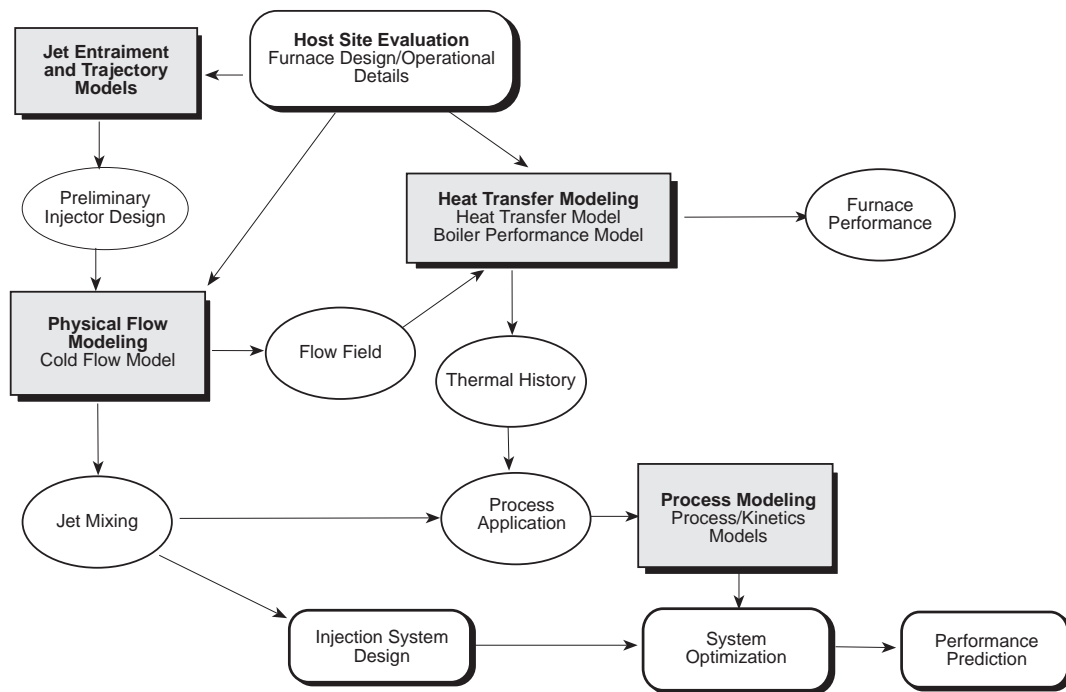


Figure 9.1.1 Generalized design methodology for AR technologies.

This design methodology has been used to scale up and apply reburning and AR technologies to utility boilers. In this task of the project, the methodology was updated to take into account the specific requirements of the AR systems. To demonstrate the applicability of the final methodology, it was applied to a typical 100 MW coal-fired utility boiler with tangentially firing burners, resulting in development of conceptual designs for several second generation AR systems, and predictions of their impacts on boiler NO_x emissions and operating performance.

9.1.2 Case Study Boiler Characteristics

The boiler used for the case study analysis was NYSEG's Greenridge 105 MWe unit manufactured by Combustion Engineering. The boiler is a tangentially fired, radiant, single drum unit typical of pre-NSPS boilers. A schematic detailing the major components of the boiler is shown in Figure 9.2.1. The boiler is rated for 97.52 kg/s of superheated steam and 73.21 kg/s of reheat steam. Superheated steam temperature control is provided by means of burner tilt control and desuperheater sprays. Reheat outlet steam temperature is primarily maintained by means of burner tilt control.

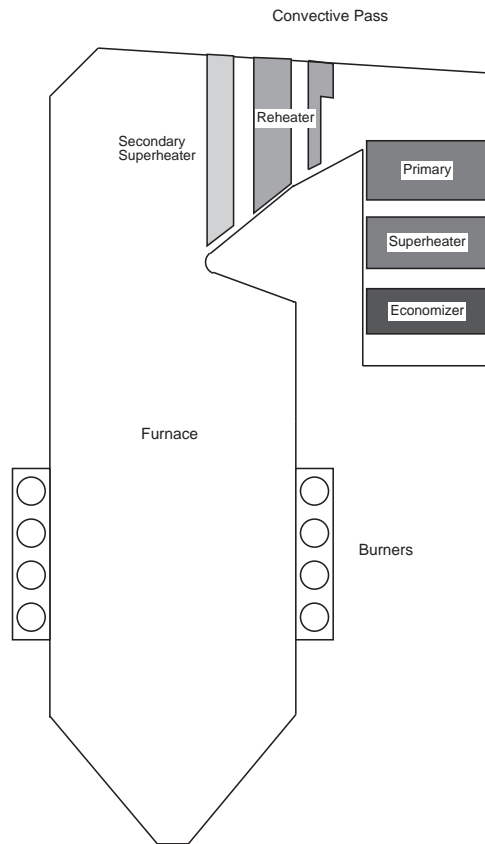


Figure 9.1.2 Schematic of case study boiler.

The unit is currently fired with the eastern bituminous coal which has a higher heating value of 29.94 J/kg. Four bowl type mills pulverize the coal to a maximum fineness of 83 percent through a #200 U.S.S. sieve. The pulverized coal is transported by heated primary air at a temperature of 344 K to one of four rows of coal burners on each corner of the boiler. Each pulverizer serves a row of burners for a total of sixteen burners on the unit. The burners have tilting mechanisms with a maximum range of $\pm 27^\circ$ from the horizontal. Heated secondary air at a temperature of 533 K is supplied to the furnace windbox which distributes the air to the burner air registers. At each corner, the fuel and air nozzles are directed along lines tangent to an imaginary circle located in the center of the furnace. The fuel and air streams combine to form a single swirling “fireball” in the furnace area. The resulting swirl action effectively mixes the fuel and air, resulting in near complete combustion of the fuel. Exiting the furnace, the hot combustion gases pass through a secondary superheater, reheater, primary superheater, economizer, and two regenerative air heaters.

For baseline operation of the unit at full load (104 MW), NO_x emissions are 512 ppm, dry, corrected to 3% O_2 . Corresponding CO emissions at these conditions are 4 ppm, dry, corrected to 3% O_2 . As boiler load drops, the firing intensity of each level of burners is reduced resulting in lower NO_x with a slight increase in CO emissions. As the boiler load is reduced further, the top row of burners are taken out of service resulting in increased firing rate for the remaining burners and the excess air is increased, resulting in an increase in NO_x emissions. Unburned carbon-in-ash is less than 4 percent over this load range.

9.1.3 Heat Transfer Analysis

A heat transfer analysis of the case study boiler was performed to identify appropriate locations for injection of the streams involved in SGAR processes (i.e, reburning fuel, OFA, and N-agents), and to assess the impacts of the process on unit performance. The heat transfer analysis consisted of setting up a two-dimensional heat transfer model simulation of the radiant furnace and a one-dimensional model simulation of the convective pass sections. The model was calibrated against available field data and design and operating data. The results of the furnace predictions for baseline operating conditions was used to identify appropriate locations for the reburning fuel, OFA, and reagent streams associated with the SGAR processes. Next, a parametric study of the impacts of the SGAR processes on boiler performance was performed. The models used in the analysis and the results of the study are summarized below.

For this study, EER’s two-dimensional furnace combustion and heat transfer code (2DHT) was applied to evaluate thermal characteristics in a radiation-dominated boiler furnace. A key element

of this code is the radiation submodel for calculating radiative heat exchange between all volume and surface zones in the boiler furnace. This submodel is based on a semi-stochastic method derived from pure Monte-Carlo techniques, and considers radiative species of CO₂, H₂O, ash, char, and soot as non-gray components. The furnace code has submodels to handle coal devolatilization, as well as char and fuels (gas, liquid, volatiles) combustion. Coal particles are divided into ten different classes of size, and devolatilized according to a one-step Arrhenius rate law. Volatile packets are assigned statistically distributed lifetimes, and each packet reacts completely at the end of its assigned lifetime. Char oxidation is described by a global rate equation which considers diffusion and chemical reaction rates.

Other unique features of the furnace code include: (a) Directly calculates radiative heat exchange between upper-furnace radiant heat exchangers and the lower-furnace flame zones; (b) Handles complicated boundary conditions as usually occurs in large-scale utility boilers or combustors, such as variation of ash deposition, steam temperature, and wall emissivity. The code is decoupled from the solution of the momentum conservation equation. Therefore, the flow field is prescribed by the user, based on the results of isothermal flow modeling, experience in modeling boilers of similar design, or from computational fluid dynamics codes. The furnace code can handle furnaces fired with gas, liquid, and solid fuels with the option of introducing over- and under-fired air streams. The furnace code has built-in submodels to simulate various forms of burner fuel co-firing and reburning with gaseous, liquid and solid fuels.

EER's boiler performance model (BPM) was used to calculate boiler steam-side heat balance for all heat exchanger surfaces in the flue gas pass of the boiler. For boiler sections not modeled by the furnace code, such as the backpass convective tube-banks and the air heater, the boiler performance model calculated a heat balance for both the steam or air and the gas sides. For sections that were included in the domain of the furnace code, it is not necessary for the boiler performance model to recalculate the gas-side heat balance.

The boiler performance model is basically a one-dimensional heat transfer model which solves the coupled energy balance equations of the boiler steam and gas sides. The model uses computerized functions for enthalpy calculations of all flue gas components and steam/water, and is coupled with the outputs of the furnace heat transfer code, which in turn incorporates the input of boilerspecific information such as heat fluxes and gas temperatures for the boiler performance model. The boiler performance model predicts steam and gas sides properties including steam temperatures, steam flow rates, attemperation flows and flue gas temperatures for a given set of feedwater inlet temperatures, boundary conditions and steam-cycle pressure distributions throughout the boiler.

The boiler efficiency is calculated based on the ASME heat loss method.

To set up the furnace code to simulate the boiler performance under baseline operation and with retrofit of the SGAR processes, the furnace was first divided into a computational grid for input to the model. Figure 9.1.3 illustrates how the three-dimensional boiler is represented in the furnace code as an axisymmetric cylindrical grid, and how the boiler furnace was divided into 26 layers in the direction of the gas flow. The length and radius of each section up to the nose plane were chosen such that the volume, furnace height, and cross-sectional area were matched to those of the corresponding section in the full-scale unit. For the sections above the nose plane until the exit of the low temperature reheater section, the ratio of heat sink surface to zonal volume was preserved. This geometric transformation was performed to maintain the heat transfer similarity between the model and the actual boiler. Since the momentum conservation equation was not solved in the furnace heat transfer code, the flow field was prescribed using flow patterns acquired from an isothermal flow modeling study.

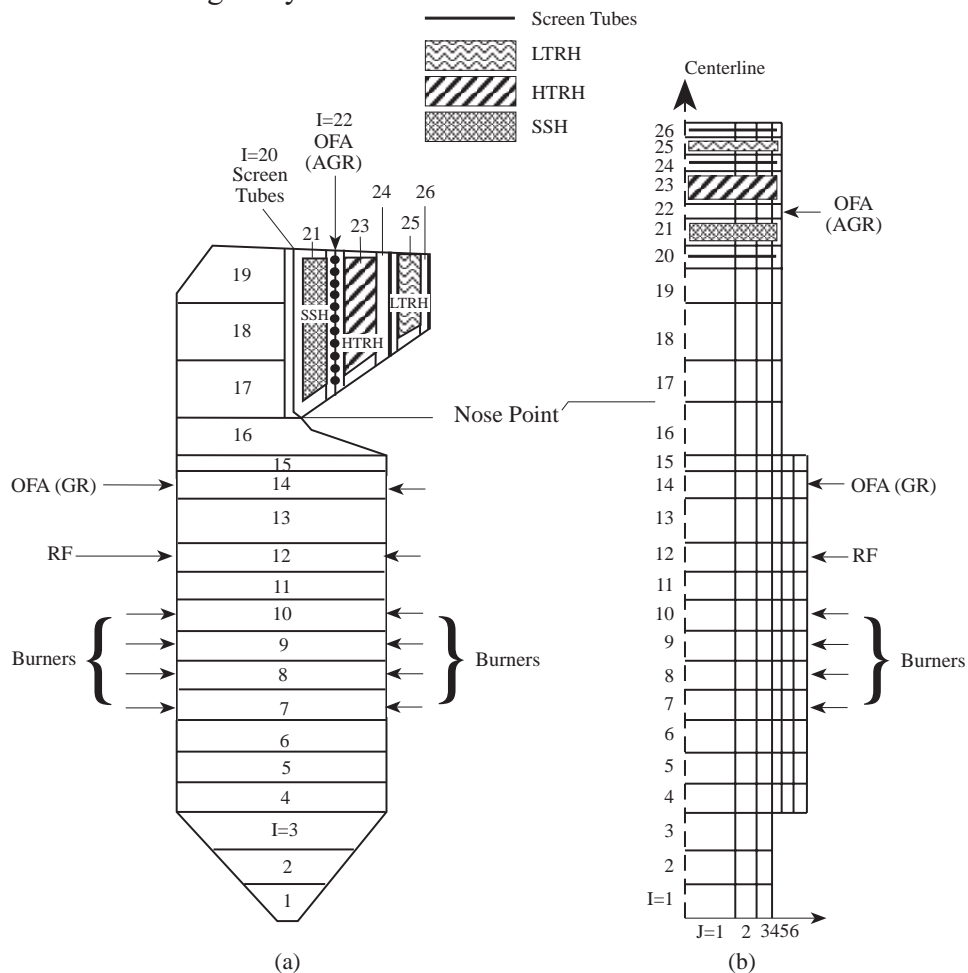


Figure 9.1.3 Furnace heat transfer model set up.

Since it is not possible to fully describe a complicated three-dimensional object using only two dimensions, and since some model parameters cannot be easily assessed without comprehensive boiler data, the model was initially calibrated against existing data to verify that the models were properly simulating the boiler performance at full load with two levels of tilt. The model was calibrated against field data collected by EER in a previous project and boiler design data provided by the boiler owner. The field data include flue gas temperatures, unburned fixed carbon-in-ash value, steam generation, attemperation flows, and water/steam temperatures for the major heat transfer components.

Mean gas temperatures predicted by the furnace code for the furnace section before the exit of low-temperature reheater section are shown in Figure 9.1.4, where burner locations, nose plane and upper-furnace heat exchanger sections are labeled. The plot identifies the first few banks of the convective pass simulated in the furnace code: secondary superheater (SSH), hightemperature reheater (HTRH), and low-temperature reheater (LTRH). The predicted mean gas temperatures basically fall in the range of the measured data, except for the temperatures at the nose plane. The differences between predicted gas temperatures and measurement at the nose plane are believed to be primarily due to the temperature stratification, since no measurement close to the center of the plane was taken. Therefore, these differences are considered within the prediction accuracy.

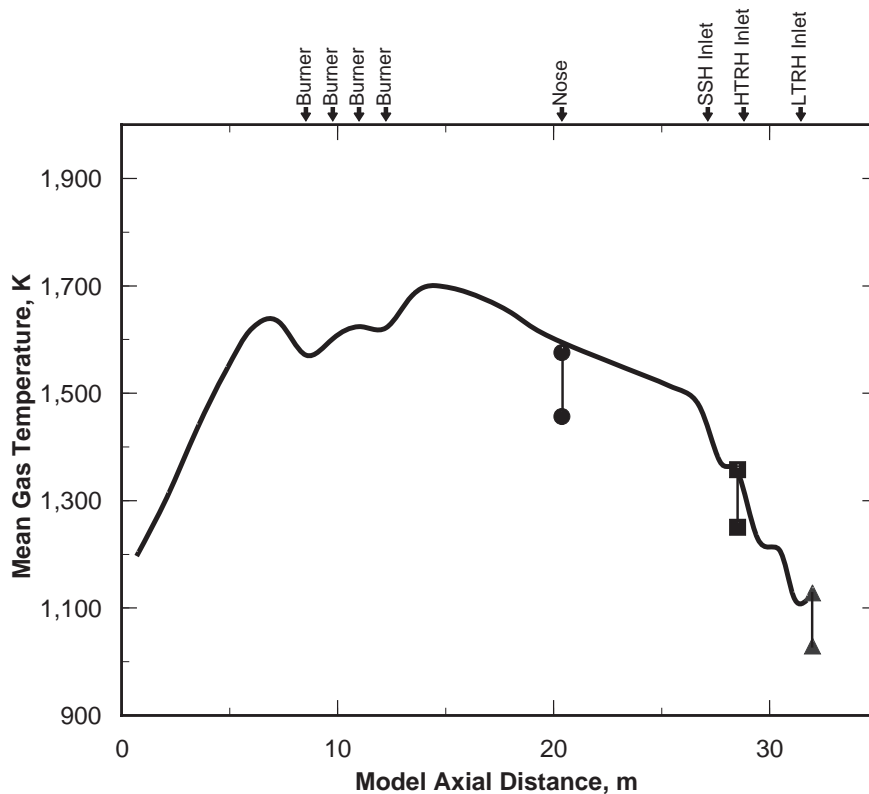


Figure 9.1.4 Comparison of predicted and measured furnace gas temperatures.

Three processes are being considered for application to the case study boiler: AR-Lean, AR-Rich, and MIAR. The results of the pilot scale studies (Section 7) indicate that optimum performance of the AR-Lean process requires injection of the OFA and N-agent at approximately 1300 K. For the AR-Rich process, the OFA is injected at this temperature, but the N-agent is injected upstream at a temperature of about 1370 K. For optimum performance of the MIAR process, the OFA is again injected at close to 1300 K, but the N-agent is divided into two streams and injected at temperatures of 1300 K and 1370 K, which correspond to the point of OFA introduction and to a plane upstream of the overfire air. In each of these processes, the reburning fuel is injected in the lower furnace above the main burners.

Figure 9.1.5 shows the bulk mean temperatures predicted in the upper furnace of the case study boiler by the heat transfer model. As shown in this figure, the optimum location for overfire air injection for each of the AR processes occurs within the first tube bank of the reheater, and the optimum location for reagent injection for AR-Rich and MIAR occurs between the secondary superheater and the reheater. Therefore, one approach for implementation of these processes on this boiler would be to inject the fuel-rich reagent into the cavity between the secondary superheater and reheater and the overfire air into the cavity between the reheater tube banks. As shown in Figures 9.1.4 and 9.1.5, the temperature in the reheater cavity is on the order of 1,120 K, which is expected to be too cold for overfire air injection and for injection of reagent in the AR-Lean and MIAR processes. Installation of OFA/N-agent injection systems in this region would also interfere with the plant sootblowing equipment in this region.

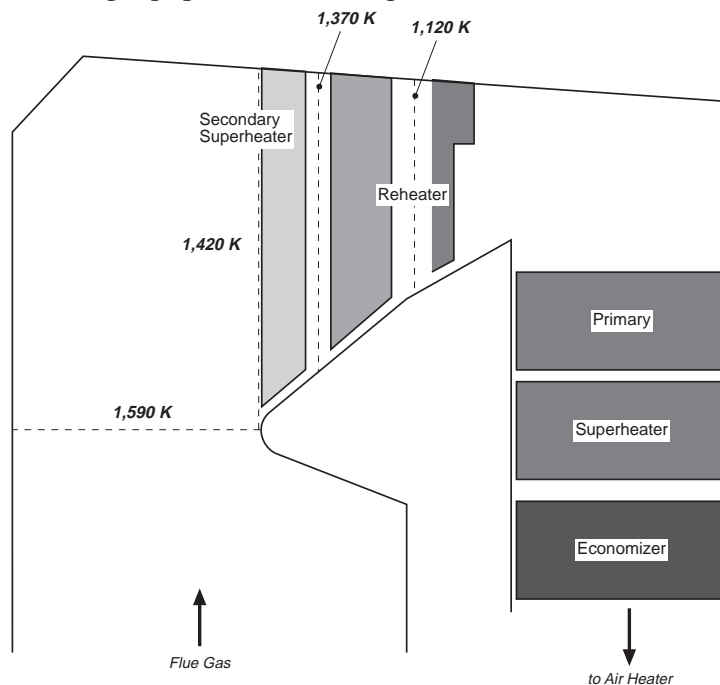


Figure 9.1.5 Predicted bulk mean temperatures in upper furnace of case study boiler.

The preferred approach for implementation of the OFA and N-agents stages of the AR processes on the case study boiler is shown in Figure 9.1.6. For the AR-Lean process, natural gas is injected in the furnace, and OFA and N-agent are injected into the cavity in between the secondary superheater platen and the first reheater platen. This location is on the high side of the optimum temperature, but should be adequate to ensure burnout of the carbon monoxide in the flue gases during AR-Lean operation. For the AR-Rich process, natural gas is injected in the furnace, Nagent is injected upstream of the secondary superheater, and OFA is injected into the cavity in between the secondary superheater platen and the first reheater platen. Injection of both of these streams at a higher than optimum temperature represents a compromise between practical implementation of the process on the case study boiler, and achieving optimum performance. Implementation of the MIAR process on the case study boiler consists of natural gas injection into the furnace, reagent injection upstream of the secondary superheater, and OFA and N-agent injection into the cavity in between the secondary superheater platen and the first reheater platen.

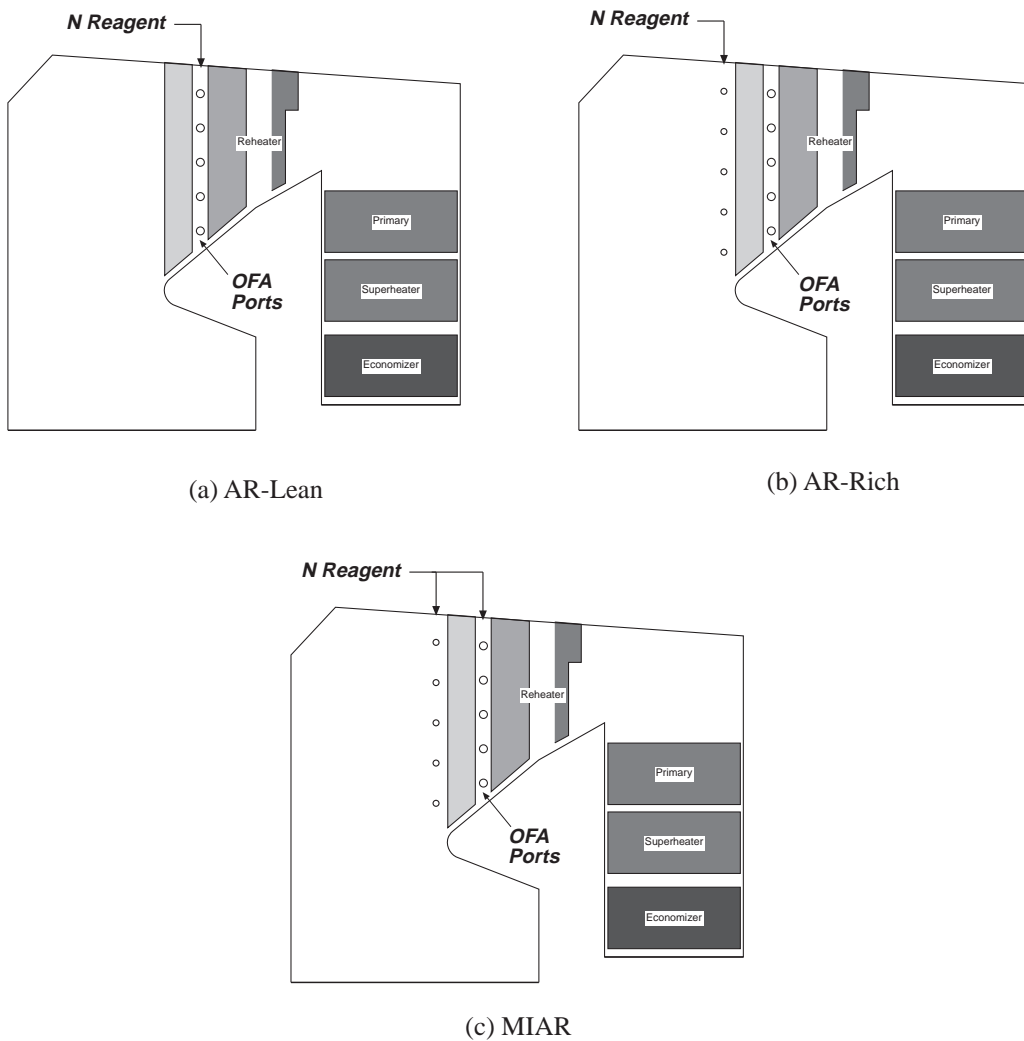


Figure 9.1.6 Implementation of AR technologies on case study boiler.

To study the impacts of the AR process configurations shown in Figure 9.1.6 on unit performance and efficiency, a parametric study was performed using the heat transfer models. Injection of the N-agent was assumed to have a negligible impact on boiler performance, therefore, the analysis was concentrated on evaluating the effects of stoichiometric ratio changes in conjunction with OFA injection into the secondary superheater/reheater cavity. In the analysis, the reburning fuel was assumed to be natural gas. The primary operating variables under study were the zone stoichiometries and the burner tilt settings. Two sets of zone stoichiometries were evaluated. The first set of zone stoichiometries consisted of using stoichiometric ratios (SR) of 1.1, 0.99, and 1.15 for, respectively, the primary (SR₁), reburning (SR₂), and burnout zones (SR₃). This set of zone stoichiometries represents assumed operating conditions for optimum NO_x reduction performance with each of the AR processes. The second set of zone stoichiometries consisted of using stoichiometric ratios of 1.2, 1.05, and 1.2 for, respectively, the primary, reburning, and burnout zones. This set of zone stoichiometries represents operating conditions assumed to reduce the impacts of AR on carbon in ash and boiler thermal performance. Both of these cases were run with the burner tilt at its baseline or normal setting. A final case was run with the burner tilt set higher than the normal setting to assess the ability to minimize the impacts of the AR processes on boiler performance by modifying boiler operation. For comparison, the model was also used to predict the impacts of basic reburning on boiler performance as well. The thermal performance impacts evaluated in this study include furnace exit gas temperature (FEGT), unburned fixed carbon in ash, main and reheat steam temperatures, and attemperation requirements. The FEGT is defined as the mean flue gas temperature located at the nose plane.

Figures 9.1.7 and 9.1.8 show the predicted impacts of gas reburning and advanced reburning processes on furnace exit gas temperature and carbon in ash. For implementation of gas reburning, the model predicts a slight decrease in furnace exit gas temperature, and an increase in carbon loss. The change in furnace exit gas temperature with reburning is due to a slight modification of the boiler heat absorption distribution. Carbon loss is expected to increase by close to 3.5% over baseline conditions with reburning due to operation of the burners at a lower than baseline excess air level. In the proposed AR process configurations, the overfire air is injected into the secondary superheater/reheater cavity. This reduces the mass loading to the furnace at the nose plane by approximately 20% in comparison to basic reburning. As shown in Figure 9.1.7, the reduction in mass loading in the furnace results in an increase in furnace exit gas temperatures with AR operation. For baseline AR operation (i.e, primary SR ~ 1.1, reburning SR ~ 0.99), delaying the addition of OFA until the convective pass is predicted to increase carbon loss by approximately 9% over normal reburning operation. Increasing the primary zone stoichiometry from 1.1 to 1.2 while maintaining close to 10% reburning fuel, results in an increase in furnace exit gas temperature, but reduces the impact of

OFA injection into the convective pass on carbon loss. For the case of AR operation with 20% excess air in the burners, carbon loss is expected to increase by only 1.5% over reburning operation.

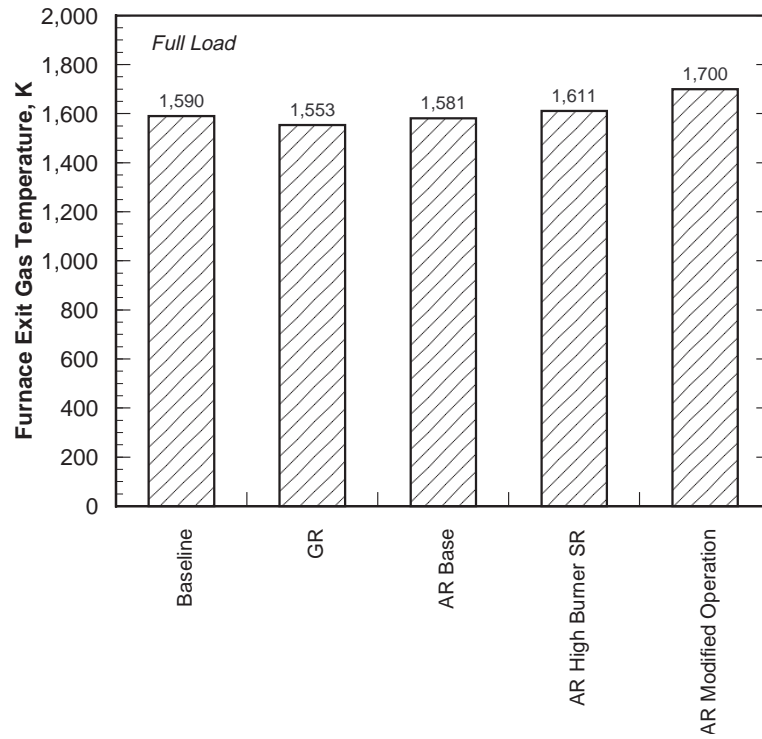


Figure 9.1.7 Projected impacts of AR processes on furnace exit gas temperature.

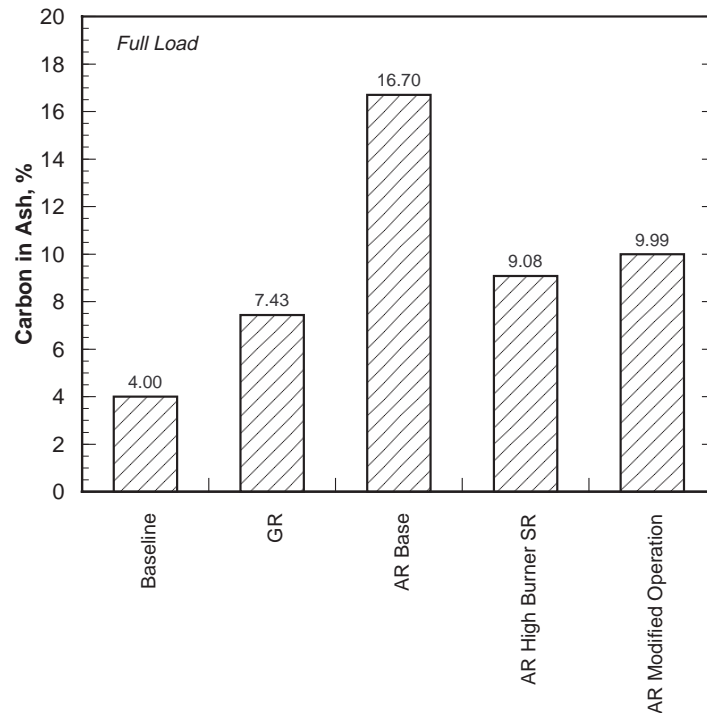


Figure 9.1.8 Projected impacts of AR processes on carbon in ash.

For baseline AR process operation, carbon loss is expected to increase over basic reburning operation, however, the impact of the additional carbon loss on boiler efficiency is small, as shown in Figure 9.1.9, in comparison to the effects of basic gas reburning alone. The use of gas reburning is expected to reduce boiler efficiency by close to 1.25%. This reduction is primarily due to the change in hydrogen/carbon ratio of the fuel. The use of natural gas increases the boiler heat loss efficiency due to an increase in water vapor in the flue gas in comparison to operation with coal. For operation with AR, Figure 9.1.9 shows that the heat loss efficiency is close to that for operation with basic reburning and is higher or lower depending upon the process and boiler operating conditions.

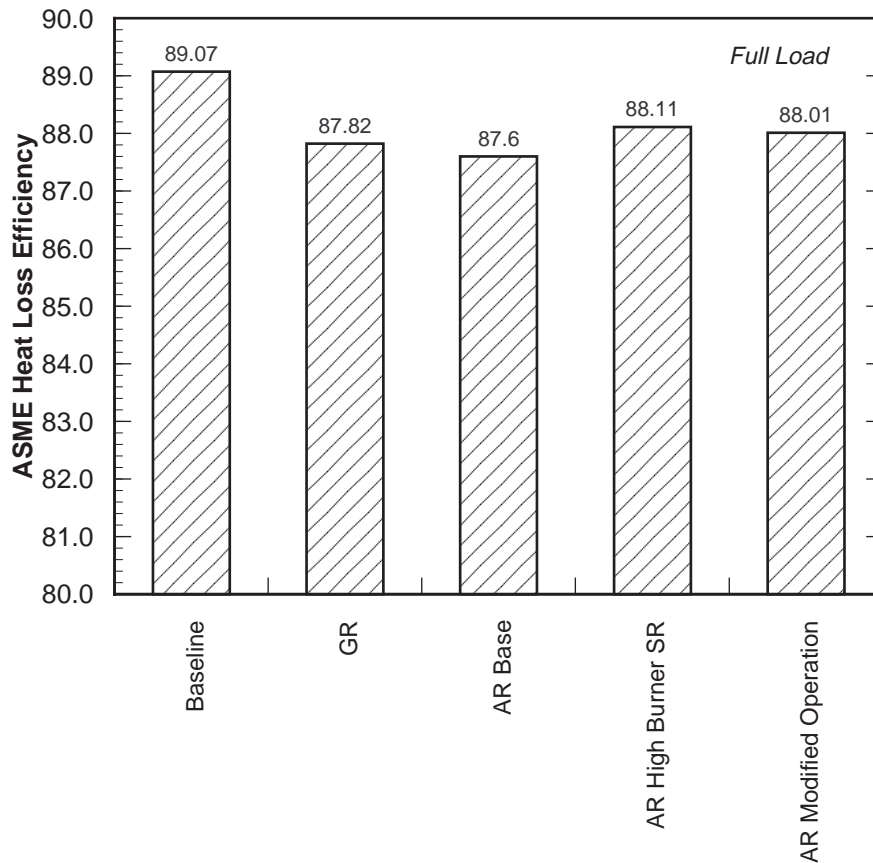


Figure 9.1.9 Projected impacts of AR processes on ASME heat loss efficiency.

The impacts of operation with basic reburning and AR processes on main and reheat steam temperatures at full load are shown in Figure 9.1.10. For the gas reburning case, the model main and reheat steam temperatures can be maintained close to normal levels using the same degree of burner tilt as that used for normal operation. For baseline AR process operation, the predicts that main and reheat steam temperatures will decrease below normal operation when burner tilt is maintained at its normal full load set point. This decrease is primarily due to the reduced mass loading across the secondary superheater section, as compared to the mass loading with basic

reburning. Although the mass loading after the OFA ports is restored close to that for basic reburning, the reheat steam temperatures for AR process operation are still lower than those for basic reburning due to the quenching effect of the overfire air that is introduced into the secondary superheater/reheater cavity. As shown in Figure 9.1.10, increasing the primary zone stoichiometry improves the main and reheat steam temperatures. This improvement is due to slight increases in furnace exit gas temperature and overall mass loading to the boiler. Alternatively, increasing the burner tilt when operating the AR system would also be expected to restore main and reheat steam temperatures back to normal conditions, as shown by the AR Modified Operation case in Figure 9.1.10.

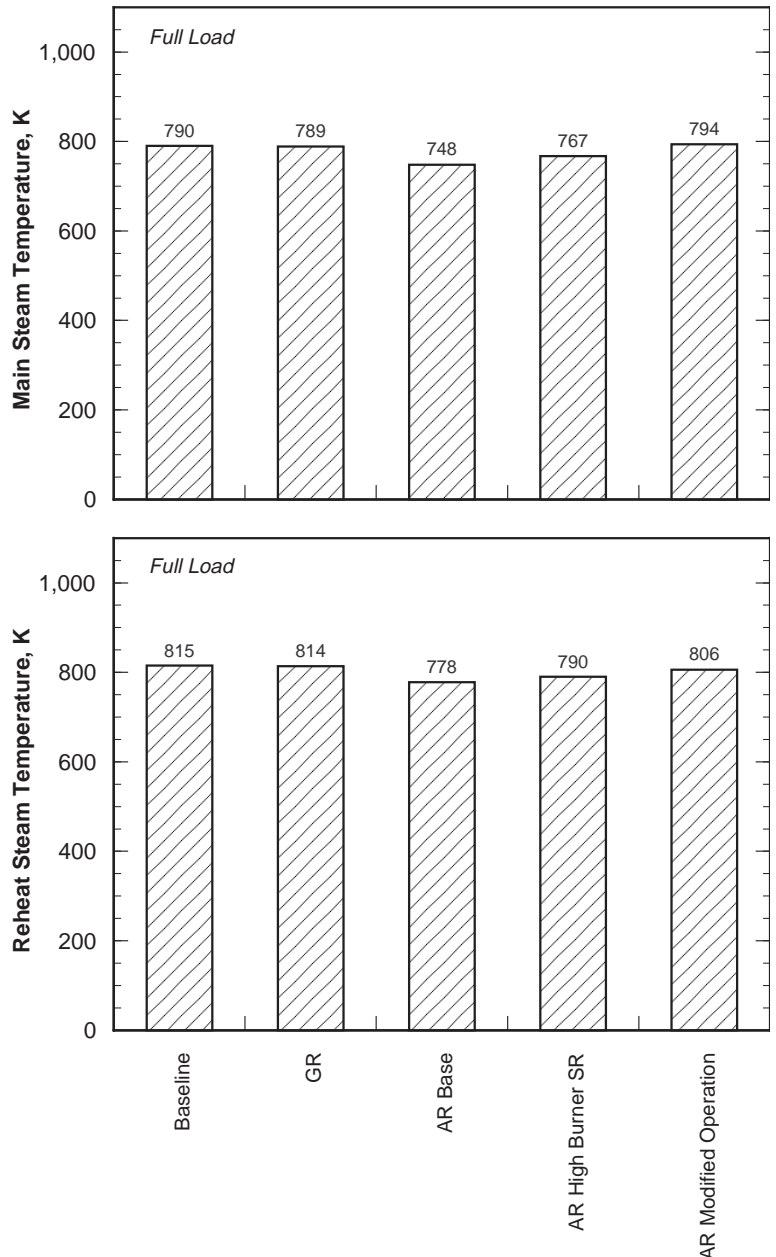


Figure 9.1.10 Projected impacts of AR processes on steam temperatures.

In summary, thermal performance models were used to evaluate the impacts of implementing AR processes on the thermal performance of a nominally 100 MW tangentially fired boiler. For implementation of AR-Lean, AR-Rich, or MIAR processes on this boiler, the reburning fuel would be injected into the lower furnace and the overfire air would be injected into the upper furnace in a cavity between the first two tube banks of the convective pass. The model results indicate that this configuration is expected to increase carbon loss and reduce main and reheat steam temperatures in comparison to baseline or gas reburning operation. Changes in the operating settings of the AR process can be used to mitigate some of the increase in carbon loss. However, the overall boiler efficiency for operation with an AR system is similar to that for operation with a basic gas reburning system. Changes in the operating settings of the AR process or in the boiler operating settings can be used to mitigate the impacts of AR on main and reheat steam temperatures. It should be noted that the results of this analysis are specific to the boiler configuration evaluated and should not be generalized to other boiler designs.

9.1.4 Injection System Studies

To assist in the design of injection systems for the reburning fuel and overfire air used in implementation of the AR processes, a physical model of the case study boiler was constructed. The model was a 1:12 geometric scale replica of the boiler furnace from the hopper to the primary superheater. Following construction of the model, flow visualization was performed to study the characteristics of the furnace flow field. Next, simulated injection systems were installed on the model. Jet penetration and mixing studies were performed to develop injection systems which resulted in optimum dispersion of the advanced reburning process streams. The results of these studies are summarized below.

The major characteristics of the case study boiler flow field under baseline conditions are shown in Figure 9.1.11. During baseline operation, the burners are tilted -15° with respect to the horizontal. It should be noted that the natural swirl for the tangentially fired unit is counter clockwise. The two planes represented in the figure are with respect to the right-hand side wall. Flow in the near field is front to back and is supplied from the left-hand side burner packs. As the flow approaches the nose elevation, gases flow from the front wall and enter the convective sections without contributing much mass to the recirculations zones in the upper furnace. Flow in the far plane is supplied from the right-hand side burner packs. The flow field on the far plane is more heavily effected by the nose and provides some mass in the upper furnace recirculation zones. From the right-hand side, gases flow under the nose and enter the far plane from back to front. Gases are then distributed into the center and left side portions of the convective pass entrance. Some mass is entrained into the

upper furnace recirculation zone. The characteristics of the flow field are typical of a tangentially fired boiler. Because of the firing orientation, the flow entering the superheater is biased toward the upper right-hand side wall. This is also considered typical of tangentially fired boilers.

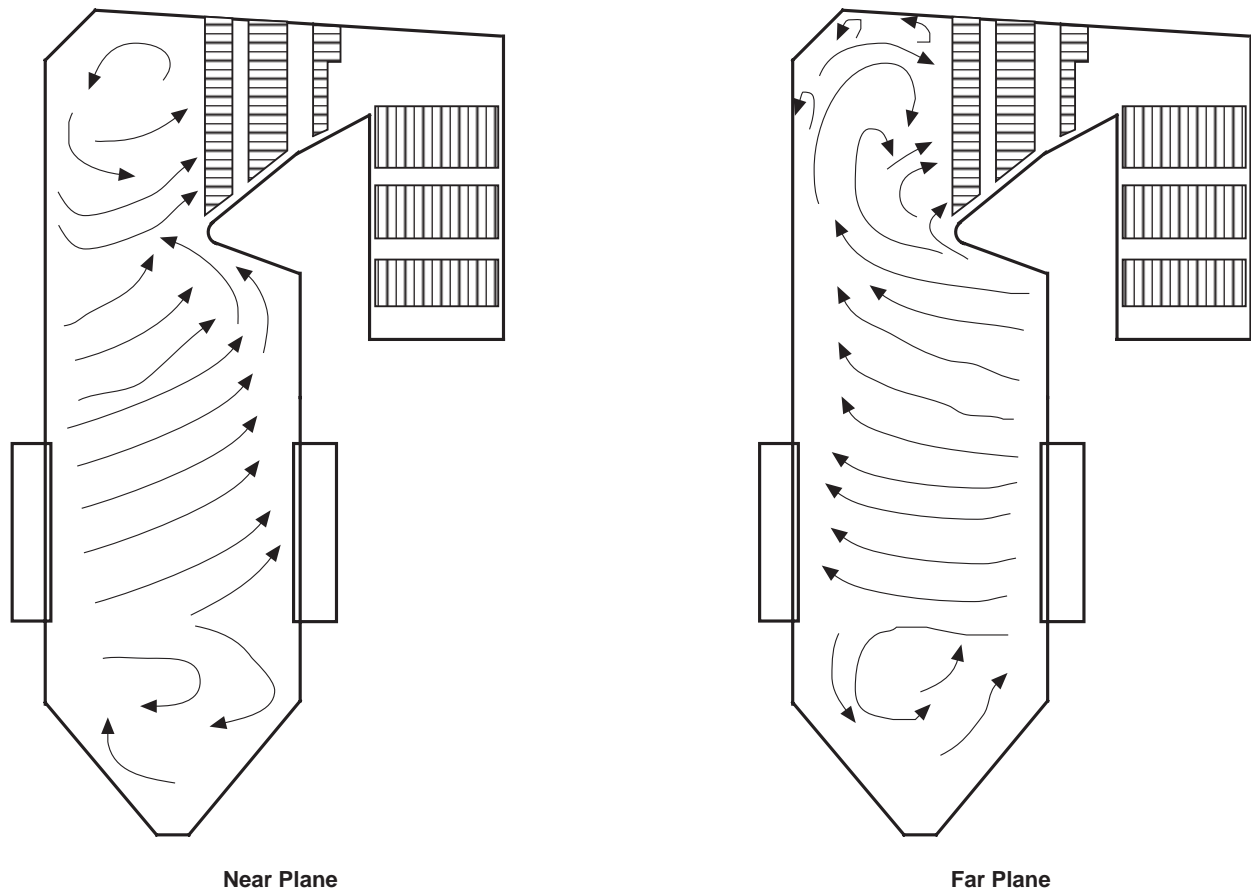


Figure 9.1.11 Baseline flow field characteristics.

Next, the flow model was used to study the design of injection systems for effective distribution of the reburning fuel into the lower furnace and overfire air into the convective pass. Various configurations were valuated for both systems. The configurations were first screened using smoke visualization to determine jet penetration and dispersion of the smoke fluid throughout the furnace. The more promising design options were then selected for more detailed characterization using tracer dispersion measurements. In this technique, a small amount of tracer gas was added to the stream of interest and the extent of dispersion of the tracer evaluated across a plane downstream of the injection location. The results were then evaluated in terms of the local stoichiometric ratio at full scale to determine how effectively the system was mixing the stream of interest into the flue gas. Various injector configurations were tested until an optimum configuration was identified. The

optimum configurations identified for the reburning fuel and overfire air within the constraints of the boiler geometry are described below.

For the reburning fuel, the nozzles in the optimum configuration were arranged with two highvelocity natural gas injectors in each corner. The firing circle of the reburning fuel jets was set opposite that of the burners. This allowed the jets to penetrate into the flue gas at a steeper angle and increased the mixing rate of the reburning fuel. The dispersion profile for this configuration is shown in Figure 9.1.12. The contour lines represent constant reburning zone stoichiometry. The figure shows that reasonably good distribution of the reburning fuel into the flue gas was achieved over most of the boiler cross section without the reburning fuel jets over penetrating into the center recirculation zone. Coverage near the corners was reduced, but this is not expected to greatly influence the performance of the injection system.

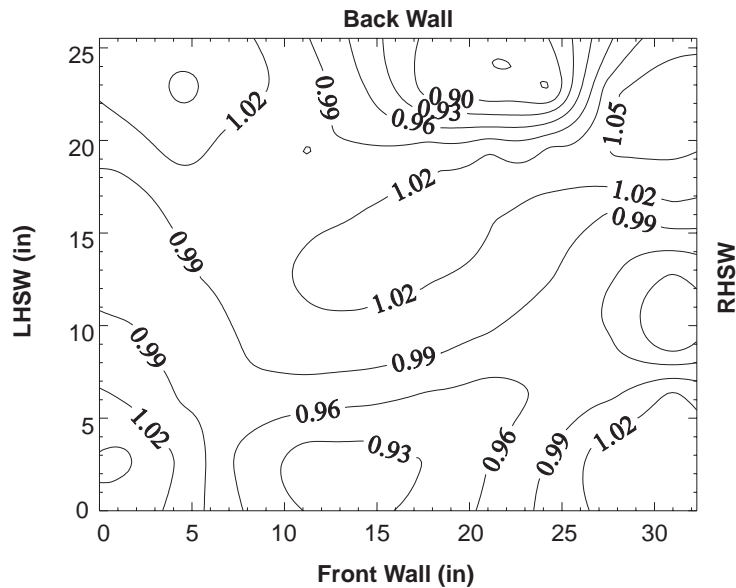


Figure 9.1.12 Dispersion pattern for preferred reburning fuel injector configuration.

For the overfire air, the injector arrangement in the optimum configuration consisted of ports located on the sidewalls of the furnace designed to effectively distributed overfire air across the width and height of plane at the entrance to the reheater, and a centrally located lance designed to cover the center portion of the plane. Measurements without this lance showed that the center region was poorly treated. The dispersion profile for this configuration is shown in Figure 9.1.13. The contour lines represent constant burnout zone stoichiometry. As shown in this figure, this injection configuration provides for good distribution of the overfire air at this location.

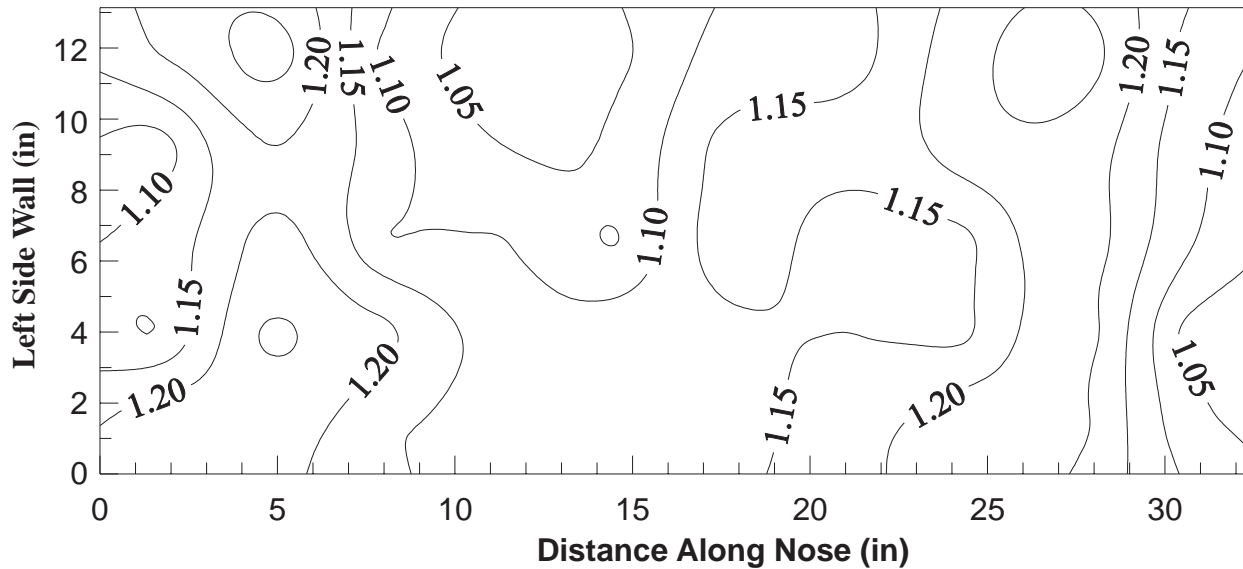


Figure 9.1.13 Dispersion pattern for preferred overfire air port configuration.

For injection of the nitrogen-based reagent in the AR processes, the approach used to inject the reagent depends upon the process used. For the AR-Lean process, the preferred approach would be to inject the reagent with the overfire air stream thereby allowing the momentum of the air jets to transport and mix the reagent with the flue gas. For the AR-Rich process, the reagent would need to be injected in front of the secondary superheater either from lances placed into the gas flow or from high-velocity wall jets. For the MIAR process, a portion of the reagent would be injected with the overfire air, and a portion would be injected using lances or wall jets. For the case study boiler, injection of the reagent along with the overfire air would be an effective means of mixing the reagent into the flue gas. As shown in Figure 9.1.13, good mixing of the overfire air can be achieved with a design that consists of wall injectors and an in-furnace distribution header. Therefore, it is expected that any reagent injected with the overfire air would be mixed well into the flue gas.

Effective distribution of reagent into the flue gases entering the secondary superheater on the case study boiler is complicated by the complex structure of the flue gas flow in this region. Although wall jets have been effectively used for injection of SNCR agents on utility boilers, it is not believed that this approach is applicable to the features of the flow field shown in Figure 9.1.11. In addition, the use of air to assist with injection of the reagent would be detrimental to the process and the use of steam would be undesirable from a boiler performance standpoint. Therefore, for this application, the use of lances inserted into the flow would be the preferred means of injecting reagent for the AR-Rich and MIAR processes. It should be noted that lance-based SNCR systems have been used successfully in a number of utility applications. For the case study boiler, design calculations suggest that a lance system consisting of five lances inserted into the gas flow from each sidewall in front of

the secondary superheater could achieve adequate distribution of the reagent. Each lance would be equipped with approximately six nozzles for reagent atomization. The nozzles would need to generate droplets with a size less than 100 microns in order to ensure rapid droplet evaporation.

In summary, the results of injection system analysis indicate that good mixing of the process streams necessary to implement advanced reburning (AR-Lean, AR-Rich, and MIAR) on the case study boiler can be achieved. Natural gas can be injected from each wall in a pattern which achieves good distribution of the reburning fuel. Overfire air injection into a cavity in the convective pass, needed for implementation of each of the AR processes under consideration, can be achieved using high pressure wall jets. For the AR-Lean and MIAR processes, these ports can also be used to inject the reagent. Injection of reagent into the upper furnace, needed for the AR-Rich and MIAR processes, can be achieved using a lance-based system.

9.1.5 Full Scale Performance Prediction

This section of the report presents the results of an analysis of the potential NO_x reduction levels which are expected to be achievable by the application of the SGAR processes to the case study boiler. The NO_x projections presented herein were developed based upon the boiler emissions characteristics (i.e., sensitivity towards load, excess air and boiler operating conditions), the results of the flow model studies, and the estimated thermal characteristics of the boiler. These projections were developed by applying EER's process models and database on performance of SGAR processes at pilot scale to the information generated in this study. The NO_x projections attempt to take into account all of the various parameters (temperature, residence time, stoichiometry, initial NO_x level, reburning fuel and reagent mixing, etc.) which are believed to have the most significant influence on the performance of the reburning process.

Baseline NO_x emissions for the case study boiler at full load are approximately 340 ppm, 3% O₂. For the use of 10% natural gas as a reburning fuel, NO_x emissions could be reduced to 187 ppm, which represents a reduction in baseline emissions of 45%. By applying AR-Lean, EER projects that NO_x emissions could be reduced to approximately 74 ppm, which represents a reduction in baseline emissions of 78%. The use of AR-Rich and MIAR on this unit is expected to result in NO_x emissions levels of respectively, 45 and 30 ppm. For AR-Rich, this emissions level corresponds to 87% control from baseline conditions, and for MIAR, it corresponds to 91% control. Additional NO_x reduction can be achieved with the use of promoters. These estimates of the potential NO_x control levels achievable with the implementation of AR processes on the case study boiler are expected to be representative of the levels which could potentially be achieved with a properly designed and operating reburning system on the unit used in the study. The performance achievable

on other units would be sensitive to the NO_x emissions and operating characteristics of the boiler, and would need to be evaluated on a site specific basis.

9.2 AR Application

This subsection discusses the conversion of the process design presented in the previous subsection into retrofit hardware for the AR-Lean system and discusses the results of initial AR-Lean tests as well as tests of some of the SGAR components.

The unit is Greenidge Unit 4, which is owned and operated by New York State Electric and Gas (NYSEG). All of NYSEG's units are located within the North East Ozone Transport Region (NEOTR) and as a result are subject to Title 1 NO_x control requirements. (See subsection 9.3 for additional information on the regulations.) NYSEG's compliance plan involves a system-wide daily cap on NO_x emissions. After considering a number of alternatives, NYSEG decided to utilize reburning and AR-Lean for NO_x control at Greenidge. EER installed the gas reburning system as part of a commercial project with guaranteed performance. The upgrade to AR-Lean was conducted as a cooperatively funded demonstration project with the support of NYSEG and a number of cofunding organizations including the Electric Power Research Institute, Empire State Electric Energy Research Corporation, Gas Research Institute, Gaz de France, New York State Energy Research & Development Authority, and Orange & Rockland Utilities.

The AR-Lean process design specifications for the location and size of the reburning gas, furnace overfire air, and convective pass overfire air (discussed in the previous section) were utilized to prepare an engineering retrofit design. Figure 9.2.1 is an isometric view of the unit showing the arrangement of the gas reburning and AR-Lean components external to the furnace.

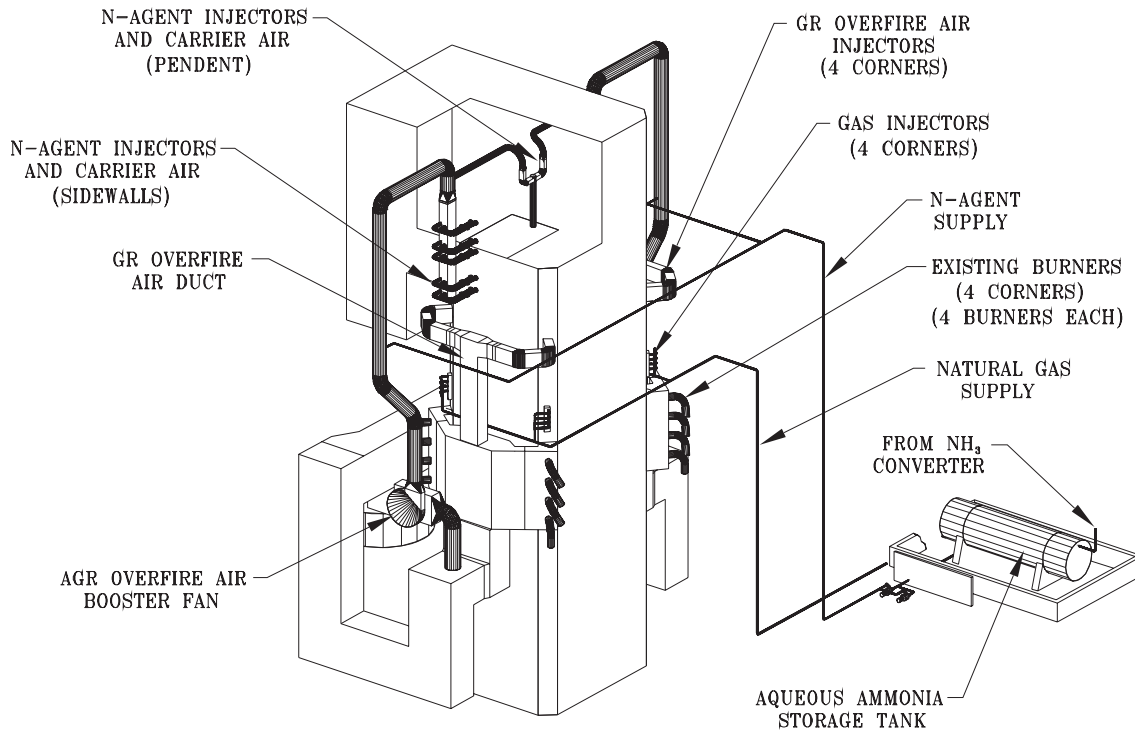


Figure 9.2.1 Isometric view of Greenridge Unit 4 showing gas reburning and AR-Lean components external to the boiler.

The gas injectors were corner mounted and consisted of multiple injectors in each corner with a surrounding cooling air passage. The multiple gas injector approach allows independent control of the quantity of reburn fuel and the injection velocity. The natural gas valve train included pressure reduction, double block and bleed shutoff control, and flowrate control valves.

The furnace OFA ports were corner mounted above the reburn injectors but below the furnace nose. The OFA for these ports was supplied by takeoffs from the top of the burner windbox. Although this tangentially fired unit operates at a relatively low windbox to furnace pressure differential, the differential was sufficient to achieve the design air injection velocities. The overfire air flow was controlled by dampers.

To achieve the required rapid and complete mixing of the convective pass OFA with the furnace gases in the narrow space between the convective surfaces, air was injected from side wall ports as well as a header in the center extending downward from the boiler penthouse. The windbox to furnace pressure differential was insufficient to produce the design point velocity. To boost the pressure, two fans were installed between the windbox and the convective pass overfire air supply headers.

Aqueous ammonia was used for the N-agent. It was produced on site from anhydrous ammonia. A variable speed positive displacement pump provided flow control. The N-agent was piped to pressure atomizers located in the convective pass overfire air headers on each side of the unit downstream of the booster fans. To provide enhanced control of the N-agent injection distribution, this system was subsequently modified with separate injectors in each wall port and in each air supply duct feeding the central header.

The gas reburning and AR-Lean components were integrated with the unit's WDPF Level 4 control system. This includes 140 input/outputs fully integrated with the combustion control system. The gas reburning and AR-Lean systems can be controlled remotely from the boiler control room and are fully automated. A series of permissives and trips ensure safe operation.

The gas reburning and AR-Lean systems were designed to provide the flexibility to adjust NO_x to meet NYSEG's system-wide NO_x cap. The initial NO_x reduction is from leakage air through the furnace and convective pass overfire air ports which provides a degree of staging.

The gas reburning system is brought into operation for the second increment of NO_x reduction. This involves, (1) ramping up the gas injection rate, (2) reducing the coal firing rate to compensate for the gas, (3) decreasing the combustion air supplied to the burners to maintain lower furnace stoichiometry, and (4) injecting combustion air through the furnace overfire air ports to maintain the overall stoichiometry at near baseline. The gas injection rate is the primary variable controlling NO_x reduction. The coal firing rate and air flows are adjusted to the design point burner and overall stoichiometries. NO_x is decreased as the gas injection rate is ramped up.

A transition is made to AR-Lean for the final increment of NO_x reduction. This involves (1) decreasing the gas injection rate, (2) increasing the coal firing rate, (3) increasing the combustion air supplied to the burners to maintain lower furnace stoichiometry, (4) switching the OFA from the furnace to the convective pass ports, (5) adjusting the OFA flowrate to maintain the overall stoichiometry at near baseline, and (6) injecting the N-agent through the convective pass overfire air ports. The N-agent injection rate is the primary variable controlling NO_x reduction. The gas, coal and combustion air flowrates are adjusted to produce near stoichiometric conditions in the reburn zone and design point burner and overall stoichiometries. NO_x is decreased as the N-agent injection rate is ramped up.

NO_x emissions for gas reburning and AR-Lean are shown in Figure 9.2.2 as a function of the reburning gas percentage. The baseline NO_x emissions for the unit prior to the equipment retrofit

were 0.62 lb/106 Btu. Leakage air through the furnace and convective pass overfire air ports provided air staging and reduced NO_x to 0.46 lb/106 Btu. In the normal gas reburning mode, additional overfire air was added through the furnace overfire air ports as the reburning gas was injected. As shown in Figure 9.2.2, NO_x decreased as the gas injection rate increased down to 0.22 lb/106 Btu which represents a NO_x control level of 62 percent. CO emissions were typically under 30 ppm.

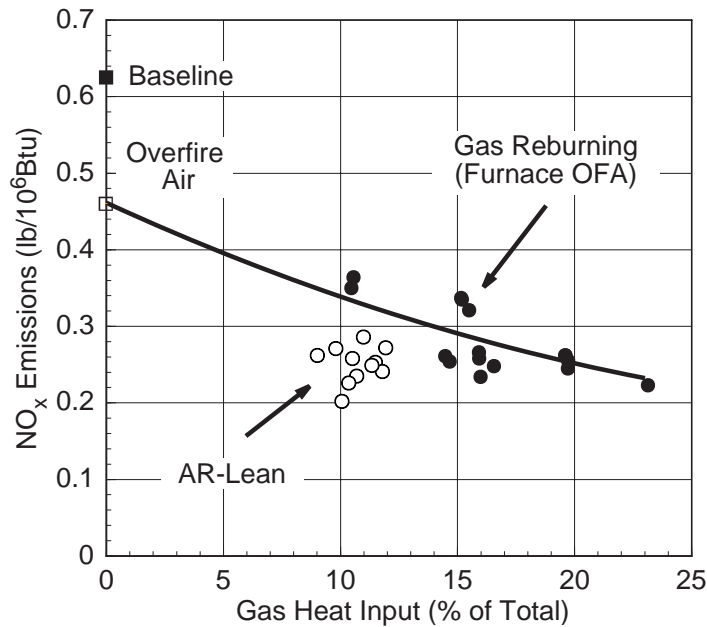


Figure 9.2.2 Gas reburning and AR-Lean NO_x data, Greenridge Unit 4.

Since the gas reburning portion of the system was a commercial system, a guarantee test was conducted with the following result at 15% gas injection.

Parameter	Measured Performance	Commercial Guarantee	Units
NO _x	0.286	0.300	lb/106 Btu
CO	17	60	ppm

Initial testing of AR-Lean was conducted in summer 1996. The initial tests focused on establishing the operating conditions without ammonia injection. This involved the first five steps listed above. The system was set up to control the CO level at the point of convective pass overfire air introduction. Under these conditions, NO_x was reduced slightly to about 0.30 lb/106 Btu. This was a consequence of the moving the overfire air injection to the convective pass which extended the reburning zone. The convective pass overfire air system was effective in controlling stack CO emissions to levels comparable to baseline.

The next test series involved ramping up the N-agent injection (step six in the list above). As the N-agent injection was increased, NO_x decreased, as expected. Figure 9.2.2 shows the AR-Lean NO_x data superimposed on the gas reburning data illustrating the lower NO_x emissions achieved at nominally 10% gas firing. In these AR-Lean tests, minimum NO_x was constrained by NH_3 emissions to 0.19 lb/106 Btu. This was unexpected and was traced to non-uniform conditions in the reburning zone as discussed below.

In conventional N-agent injection without reburning, the temperature window is narrow: injection within the window reduces NO_x with minimum NH_3 emissions; injection on the hot side of the temperature window may increase NO_x but with minimal NH_3 emissions; injection on the cold side of the temperature window achieves less NO_x reduction and produces NH_3 emissions. With AR-Lean, CO oxidation occurs in parallel with the NH_3 reactions effectively broadening the temperature window on the cold side. During these AR-Lean tests, the CO level in the reburning zone was in the range expected to broaden the temperature window to lower temperatures, on the order of several thousand ppm. CO measured in the boiler exhaust was typically less than 50 ppm indicating excellent CO burnout. While the overall CO levels and burnout were on design, probe measurements in the upper furnace showed considerable CO stratification. In some regions the furnace gases had low CO and excess O_2 . In other areas while CO was on design, O_2 was also present indicating streamwise stratification or poor micro-mixing. This stratification accounts for the NO_x emission reduction and NH_3 emissions. That portion of the furnace flow with low CO and excess O_2 was not producing the temperature window broadening and this resulted in excess NH_3 emissions limiting the maximum NH_3 injection rate and hence NO_x reduction.

These Greenidge tests have revealed an important AR issue: the uniformity of conditions in the reburning zone is important to the optimization of the AR process. In small scale tests, the furnace flow is fairly well mixed so that this stratification effect is not significant. However, stratification may be the limiting factor in full scale applications.

Once this stratification effect was understood, additional tests were conducted at Greenidge to improve performance. The focus of testing in summer 1997 was on adjusting the AR-Lean system to provide more uniform reburn zone conditions. This included: (1) burner balancing, (2) modification of the gas injectors to reduce stratification and enhance the micro-mixing of the fuel and air so as to avoid regions of excessively rich or lean conditions, and (3) reduction of leakage air through the furnace overfire air ports. In addition, the N-agent injectors were modified to allow the tailoring of the distribution of the N-agent among the convective pass overfire air injectors. These changes have resulted in improved performance and additional NO_x reduction with lower NH_3 slip.

In addition to these AR-Lean tests, opportunity was taken to obtain larger scale data on several of the SGAR components. It should be noted that the Greenidge unit was set up only for AR-Lean and the furnace penetrations available in the unit were not optimum for the other SGAR configurations. A series of tests were conducted in Summer 1997 to evaluate the following SGAR components:

- N-agent injection downstream of the overfire air In these tests, the gas reburning system was operated in the normal mode using the furnace overfire air. The N-agent was injected through a series of lances on the front wall above the overfire air ports. Based on the process design studies, it was expected that these temporary N-agent injectors would not produce a uniform distribution of N-agent across the furnace and that the furnace temperature would be too hot for effective SNCR operation. The tests confirmed these predictions. Only modest NO_x reduction was achieved and NH_3 slip was minimal.
- N-agent Injection into the reburn zone This SGAR component was tested by operating the system in the AR-Lean configuration using the convective pass overfire air ports. The N-agent was injected through the same furnace lances described above. While this injection location was not optimum, it provided some initial data on AR-Rich conditions. These tests will continue through fall 1997.
- Multiple N-agent injection Limited tests were also conducted with injection both through the furnace lances and through the convective pass injectors. Again, the tests do not represent an optimum MIAR configuration. However, they allow a preliminary evaluation of multiple injection and the ability to stratify the N-agent injection for the stratified furnace flow conditions.

If this project proceeds to Phase II, these large scale tests will continue in summer 1998. Alternate injection arrangements and promoters are expected to be tested.

9.3 Economic and Market Analysis

This section discusses the economics of NO_x control via AR and the potential market for the AR technologies in the US for compliance under the 1990 CAAA. The following subsection 9.3.1 discusses the market drivers and the nominal NO_x control requirements to meet existing and projected regulations (see also Section 3.1). Then, Section 9.3.2 outlines an economic methodology for comparing cost effectiveness of conventional and AR technologies and defines two representative

applications, cyclone and wall-fired boilers. The methodology was used to compare the costs of conventional NO_x controls (SNCR, SCR and OFA) with the costs of reburning based technologies including basic reburning and the full range of AR technologies being developed in this project. Subsection 9.3.3 discusses the cost and performance of each NO_x control technology and Subsection 9.3.4 presents the results. The results show a considerable economic advantage for the AR technologies particularly for deep NO_x control with cost savings in the range of 50%. The resulting market for these AR technologies is discussed in Subsection 9.3.5.

9.3.1 NO_x Control Drivers

The Clean Air Act Amendment of 1990 (CAAA), established the framework for NO_x emission regulations to mitigate ozone non-attainment areas and acid rain. Over the last seven years, EPA has developed most of the specific NO_x regulations authorized by the CAAA. The most stringent NO_x controls are required in ozone non-attainment areas or areas which transport pollutants into ozone non-attainment areas. In the Northeast, EPA has defined the Northeast Ozone Transport Region (NEOTR) consisting of Pennsylvania and the States North and East. In that zone, NO_x reductions of up to 75% are required by 2003 with the potential for even deeper controls depending on the results of modeling over the next few years. EPA is now considering expanding the NEOTR to include Texas and all states North and East. In this 37 state region, it is projected that NO_x emissions may need to be reduced by as much as 85%.

As these specific regulations have developed, the trend has been towards cost effective emission controls. Rather than setting specific limits for each plant, in many areas the regulations have been established to provide the flexibility to over-control on some units and under-control on others if that approach is cost effective. This can be of considerable advantage since the cost of NO_x control for some units (particularly smaller units) may be much higher than for others, on a \$/ton basis. This bubbling approach depends on the availability of NO_x control technologies which can achieve NO_x reductions greater than the nominal control levels (75-85%) with low costs.

The NO_x control requirements developed by EPA to date were based on the current National Ambient Air Quality Standards (NAAQS). EPA has issued revised NAAQS for ozone and fine particulate which are substantially lower. Since NO_x is a precursor of both pollutants, achieving the new NAAQS will require even greater NO_x reductions.

Therefore, the goal established by DOE for this project, 95% NO_x control down to 0.06 lb/10⁶ Btu, is appropriate. NO_x control technologies which meet this goal will only be employed if their costs

are competitive with conventional controls on a \$/ton basis. At present, the only commercial NO_x control technology capable of achieving such deep NO_x control is SCR. The advantage of the AR technologies being developed on this project is that they can provide the deep NO_x control of SCR at a considerable cost reduction.

9.3.2 Methodology and Cases Evaluated

To evaluate the cost effectiveness of the AR technologies, an economic analysis has been conducted using the EPRI Technology Assessment Guide (TAG) methodology, which is widely used in the utility industry to evaluate advanced emission control technologies. The TAG methodology calculates the total levelized annual costs including capital and operating cost components. This can be expressed in terms of \$/ton of NO_x controlled. The total installed cost (capital cost) of the NO_x control technology is estimated and distributed over the operating life in a series of uniform annual costs by applying a Capital Recovery Factor (CRV). The CRV depends on the operating life, time value of money, depreciation, etc. In this analysis, a CRV of 0.131 was utilized. This is equivalent to simple amortization at an annual interest rate of 10% over a 15 year operating life. The annual operating costs for the technology are calculated for the first year and then levelized over the life of the technology by applying an annual levelization factor. In this TAG analysis, a constant dollar approach was utilized so that the levelization factor is 1.0.

AR technologies can be applied to all types of combustion systems including the three most common utility boilers (wall, tangential and cyclone fired). Two applications have been selected for the economic evaluation: A cyclone fired boiler and a dry bottom wall fired unit equipped with low NO_x burners.

Reburning applications on cyclones are particularly attractive for several reasons:

1. The baseline NO_x levels are high. Since NO_x is a reactant in the reburning reactions, high baseline NO_x increases the rate of NO_x reduction. Thus, the cost of NO_x control for units with high baseline NO_x is low for reburning based technologies.
2. Furnace temperatures are high. High furnace temperatures improve reburning NO_x control since the reduction reactions are kinetically limited.
3. No other combustion modification NO_x controls. Low NO_x burners and OFA ports cannot be used with cyclones. This makes reburning based controls SNCR, and SCR the only alternatives.

In contrast to the cyclone application, dry bottom wall fired units can be equipped with low NO_x burners and OFA. In fact, Title 4 of the CAAA mandates that “Low NO_x Burner Technology” be applied to all dry bottom wall fired units by 2000 with a NO_x requirement of 0.46 lb/10⁶ Btu.

The assumptions utilized in the analysis and those specific to the two applications (cyclone and wall-fired) are summarized in Table 9.3.1.

Table 9.3.1. Economic data.

Parameter	Units		
Unit Specifications			
Unit Capacity	MW		200
Capacity Factor	%		65
Heat Rate	Btu/KWH		10,000
Fuels data			
Coal Sulfur	lb/10 ⁶ Btu		1.2
Coal Heating Value	Btu/lb		12,000
Coal cost	\$/10 ⁶ Btu		1.50
Gas cost	\$/10 ⁶ Btu		2.5
Coal ash content	%		10
Unit costs			
Value of SO ₂ Reduction	\$/ton		125
Ash Disposal Cost	\$/ton		10
Economic Factors			
Capital Recovery Factor			0.131
Escalation	Constant dollar		
Boiler Data			
Firing Configuration		Cyclone	Wall-Fired
Baseline NO _x controls		None	Low NO _x Burners
Baseline NO _x	lb/10 ⁶ Btu	1.2	0.46

9.3.3 Technology Specific Inputs

The NO_x control technologies selected for evaluation are presented in Table 9.3.2. The reburning technologies were evaluated using both gas and coal as reburning fuels. The key technology specific

assumptions are presented in Table 9.3.3 and are discussed further below.

The performance of SNCR is highly site specific. A typical performance in full scale applications with modest ammonia slip is in the range of 40% NO_x reduction with injection of an N-agent at NSR=1.5. The capital cost was based on discussions with SNCR vendors. The N-agent was Nalco Fuel Tech NO_xOut A, a commercially available aqueous urea solution.

Table 9.3.2. Evaluated NO_x control technologies.

Technology	NO _x Reduction (%)	Application	
		Cyclone	Wall
Conventional NO _x Controls			
Overfire Air	25		X
Selective Non-Catalytic Reduction (SNCR)	40	X	X
Selective Catalytic Reduction (SCR)	80	X	X
Selective Catalytic Reduction (SCR)	90	X	X
Reburning NO _x Controls			
Basic Reburning	60	X	X
Advanced Reburning—Rich (AR-Rich)	80	X	X
Advanced Reburning—Lean (AR-Lean)	80	X	X
Promoted Advanced Reburning—Lean (PAR-Lean)	90	X	X
Promoted Advanced Reburning—Rich (PAR-Rich)	90	X	X
Multiple Injection Advanced Reburning (MIAR)	95	X	X

Table 9.3.3. NO_x control technology data.

	Units	OFA	SNCR	Basic Reburn	AR R/L	PAR R/L	MIAR	SCR 80%	SCR 95%
NO _x									
NO _x Reduction	%		40	60	80	90	95	80	95
Cyclone Final NO _x	lb/10 ⁶		0.72	0.48	0.24	0.12	0.06	0.24	0.06
Wall Fired Final NO _x		0.35	0.28	0.18	0.09	0.05	0.02	0.05	0.02
SO ₂ Control (via gas)	%	0	0	15	10	10	10	0	0
Capital Cost									
Gas Reburning	\$/kw			15	20/22	20/22	27		
Coal Reburning	\$/kw			25	30/32	30/32	37		
Conventional	\$/kw	10	5					80	109
Reburning fuel firing	%			15	10	10	10		
Catalyst Life	Years							4	4

Costs and performance for SCR were obtained from an EPA report (Phase II NO_x Control, 1996) which presented DOE estimates for a high sulfur coal fired unit of 200 MW capacity with initial NO_x of 1.0 lb/10⁶ Btu and 80% NO_x reduction. These conditions were scaled to those utilized here. Reburning costs and performance were based on EER's extensive data base and the projected performance of AR systems developed in this project. For the coal reburning systems, costs were included for the pulverizers to produce the fine-grind (micronized) coal necessary to minimize carbon loss. There is no incremental fuel cost (except for efficiency penalty) since the normal plant coal is used for reburning. For gas reburning systems, no pulverizers are required, but the gas cost is greater than coal. A differential of 1.00 \$/10⁶ Btu was assumed. It is assumed that coal and gas reburning technologies can achieve comparable NO_x reduction.

9.3.4 Economic Results

Figures 9.3.1 and 9.3.2 show the results of the economic comparison as plots of the total annual cost of NO_x reduction versus percentage NO_x reduction. Lines of constant unit cost of NO_x control (\$/ton of NO_x reduced) are also plotted as fans. As discussed above, the unit cost of NO_x control is the appropriate figure of merit since utilities will apply controls to a number of units, bubbling to achieve the lowest total cost.

Figure 9.3.1 shows the cyclone results. The conventional NO_x controls, SNCR and SCR have the highest unit cost of NO_x control in the range of 800-1100 \$/ton. The reburning based technologies are considerably lower in cost. Based on the assumptions used for this study, the costs for coal as the reburning fuel are lower than for gas. However, it should be noted that site specific considerations may favor gas in some situations. Factors favoring gas include a low gas-coal cost differential, problems related to carbon loss which are more significant with coal as the reburning fuel, and space limitations which make pulverizer installation expensive, difficult or impossible.

Figure 9.3.2 shows the wall fired results. Since the baseline NO_x is lower than for the cyclone application (0.46 versus 1.2 lb/10⁶ Btu), the unit cost of NO_x control is higher. As with the cyclone results, the reburn technologies have a considerable cost advantage. OFA has been included for this application (it cannot be applied to cyclone fired units). While the total annual cost of OFA is low, the low NO_x reduction (25%) results in higher unit cost of NO_x control than all except the SCR technologies. The lower baseline NO_x for this application reduces the amount of N-agent required improving the unit cost of NO_x control for SNCR.

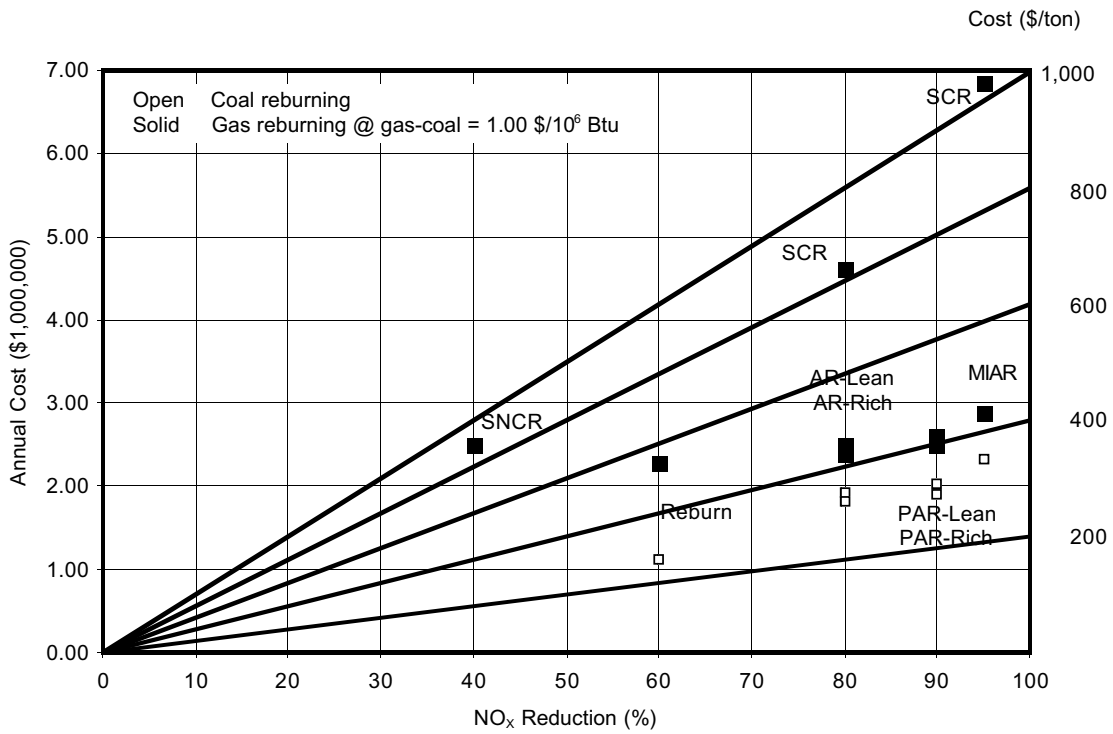


Figure 9.3.1. Cyclone fired boiler NO_x economics.

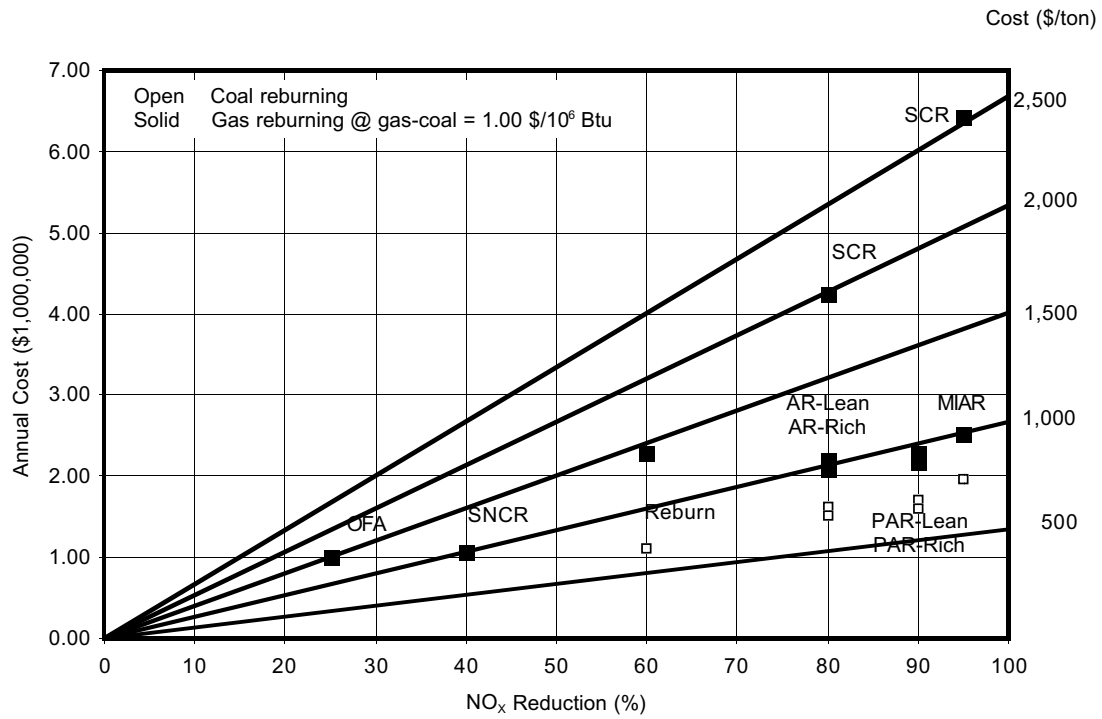


Figure 9.3.2. Wall fired boiler NO_x economics.

These results show the significant economic advantage of the technologies developed on this project for the projected NO_x control market characterized by deep NO_x control and the potential for bubbling. For example, in the cyclone application, the total annual cost of SNCR is comparable to MIAR, but MIAR provides more than twice the NO_x reduction.

Table 9.3.4 compares the deep control techniques for 80 and 95% NO_x reduction. Both the coal and gas reburning based AR technologies have considerable cost advantages over SCR in the range of 48 to 69%. Under conditions of this analysis, 80% NO_x reduction via AR is 1.9-2.9 times less expensive than SCR, and 95% AR NO_x reduction is 2.0-3.2 times less expensive than SCR.

Table 9.3.4. Comparing cost effectiveness for deep NO_x control.

		Cyclone, Baseline NO _x 1.2 lb/10 ⁶ Btu				Wall, Baseline NO _x 0.46 lb/10 ⁶ Btu			
NO _x Control		80%		95%		80%		95%	
AR Technology		AR-Rich		MIAR		AR-Rich		MIAR	
		10 ⁶ \$/yr	\$/ton NO _x	10 ⁶ \$/yr	\$/ton NO _x	10 ⁶ \$/yr	\$/ton NO _x	10 ⁶ \$/yr	\$/ton NO _x
Costs									
	SCR	4.61	836	6.84	1,034	4.26	2,011	6.41	2,527
	AR (gas reburning)	2.39	433	2.88	440	2.08	986	2.52	1,000
	AR (coal reburning)	1.81	328	2.33	355	1.51	712	1.96	780
Cost Reduction									
	AR (gas reburning)	48		58		51		61	
	AR (coal reburning)	61		66		65		69	

9.3.5 Market Assessment

The size of the market for AR technologies has been estimated by considering the existing and projected CAAA regulations, the power plants affected by the regulations, and industry projections for the mix of NO_x control technologies necessary for cost effective compliance with these regulations. The results are presented in Table 9.3.5 and are discussed below.

Table 9.3.5. Estimated market for AR technologies.

	Units	NEOTR	OTAG Expansion	Total
States		10	27	37
Boiler Capacity				
Total	1,000 MW	70.40	305.70	376.10
Coal Fired Portion	%	36.93	50.00	
Coal Fired Capacity	1,000 MW	26.00	152.85	178.85
Projected Deep Controls				
Portion of Coal Fired		38.00	67.00	
Total Capacity To Be Retrofitted	1,000 MW	9.88	102.41	112.29
AGR Market				
Unit AGR Cost	\$/kw	30.00	30.00	
Total Market (100% penetration)				
Capacity	1,000 MW	9.88	102.41	112.29
Installed Cost	\$1,000,000	296.40	3,072.29	3,368.69
Potential Penetration				
Estimated Penetration	%	50.00	50.00	
Capacity	1,000 MW	4.94	51.20	56.14
Installed Cost	\$1,000,000	148.20	1,536.14	1,684.34

At present, NO_x control regulations requiring reductions of up to 75% have been established in the NEOTR. A recent study conducted by ICF Kaiser evaluated the alternatives for cost effective NO_x control compliance in this region. It was projected that 9,880 MW of coal fired units will be retrofitted for deep NO_x control, assumed to be SCR. This is the AR market potential and corresponds to \$296 million at the mean installed cost for AR of 30 \$/kw (range 22-37 \$/kw). Although AR is projected to be considerably more cost effective than SCR, a number of factors will reduce AR's market penetration such as the lack of full scale operating experience at the time the retrofit decision is required. If the market is shared equally between SCR and AR, AR will be installed on 4,900 MW at a total cost of \$148 million.

EPA is now considering expanding the NEOTR to the 37 state OTAG region. NO_x reductions as high as 85% are being discussed for units in this region. A recent study of NO_x control alternatives in this area was conducted by Hewson and Stamberg (1995) using an approach similar the ICF Kaiser study. Using similar assumptions, the total market for deep NO_x control in the expansion region is 102,000 MW corresponding to \$3.07 billion. If the market is shared equally between SCR and AR, AR will be installed on 51,000 MW at a total cost of \$1.54 billion. The total market is the sum of the NEOTR and expansion region.

The total market is the sum of the NEOTR and expansion region and is as shown in Table 9.3.6.

Table 9.3.6. Total estimated AR market.

	Capacity (1,000 MW)	Installed Cost (\$ billion)
Total Market	112	3.4
Projected Penetration, 50%	56	1.7

Economic analysis demonstrates a considerable economic advantage for the AR technologies. In particular, for deep NO_x control in the 80-95% range the cost savings are at least 50% in comparison with SCR. NO_x reduction efficiency of 80% via AR is 1.9-2.9 times less expensive than SCR, and 95% AR NO_x reduction is 2.0-3.2 times less expensive than SCR. The resulting market for AR technologies is estimated to be about \$1.7 billion.

9.4 Design Methodology and Application: Conclusions

In this task, a design methodology, which consists of various computational and analytical models, was generalized for use with SGAR technologies. This methodology was then applied to develop conceptual designs for application of three AR concepts—AR-Lean, AR-Rich, and MIAR to a typical 100 MW tangentially fired utility boiler, and to predict the impacts of the AR systems on boiler performance and NO_x emissions.

The design methodology uses various experimental and analytical tools to develop the injector specifications and operating characteristics of the AR system with the objective of meeting specific process requirements for optimum emissions control performance while maintaining boiler operation and performance at normal levels.

Thermal performance models were used to evaluate the impacts of implementing AR processes on the thermal performance of a nominally 100 MW tangentially fired boiler. For implementation of AR-Lean, AR-Rich, or MIAR processes on this boiler, the reburning fuel would be injected into the lower furnace and the overfire air would be injected into the upper furnace in a cavity between the first two tube banks of the convective pass. The model results indicate that this configuration is expected to increase carbon loss and reduce main and reheat steam temperatures in comparison to baseline or gas reburning operation. Changes in the operating settings of the AR process can be used to mitigate some of the increase in carbon loss. However, the overall boiler efficiency for operation with an AR system is similar to that for operation with a basic gas reburning system. Changes in the operating settings of the AR process or in the boiler operating settings can be used

to mitigate the impacts of AR on main and reheat steam temperatures. It should be noted that the results of this analysis are specific to the boiler configuration evaluated and should not be generalized to other boiler designs. The results of injection system analysis indicate that good mixing of the process streams necessary to implement advanced reburning (AR-Lean, AR-Rich, and MIAR) on the case study boiler can be achieved. Natural gas can be injected from each wall in a pattern which achieves good distribution of the reburning fuel. Overfire air injection into a cavity in the convective pass, needed for implementation of each of the AR processes under consideration, can be achieved using high pressure wall jets. For the AR-Lean and MIAR processes, these ports can also be used to inject the reagent. Injection of reagent into the upper furnace, needed for the AR-Rich and MIAR processes, can be achieved using a lance-based system. The overall boiler efficiency for operation with AR systems is similar to that for operation with a basic gas reburning system. Full scale NO_x reduction level is predicted to be above 90% and can be additionally increased with the use of promoters.

The original work scope was based on applying the design methodology to a hypothetical case study; however, it was hoped that an initial AR demonstration could be developed in parallel with Phase I (outside the scope of this DOE project) to allow application to a real unit and evaluation of some of the SGAR elements. EER was successful in developing an initial AR demonstration project. In 1995 EER installed AR-Lean on a 105 MW tangentially fired boiler. Initial AR testing was conducted in 1996-97 and will continue through 1998. This unit was used as the basis for extending the design methodology. AR-Lean tests on the boiler showed that stratification within the reburn zone could adversely affect the performance. Regions of inadequate CO in the reburning zone reduced the N-agent NO_x control and caused NH₃ slip. While modifications were successful in reducing stratification, this experience shows the importance of mixing and scale up, two factors to be evaluated in Phase II. In addition to these AR-Lean tests, opportunity was taken to obtain preliminary larger scale data on several of the SGAR components, including N-agent injection into the reburning zone, N-agent injection downstream of the reburning zone in an SNCR mode, and N-agent injection into the reburning zone and with the overfire air.

Economic analysis demonstrates a considerable economic advantage of AR technologies in comparison with existing commercial NO_x control techniques, such as basic reburning, SNCR, and SCR. Particularly for deep NO_x control, AR results in 2-3 times lower costs (in \$/ton of NO_x removed) than SCR for the same level of NO_x control. The market for AR technologies is estimated to be above \$1.5 billion.

10.0 CONCLUSIONS

1. This project is developing novel AR concepts for high efficiency and low cost NO_x control from coal fired utility boilers. AR technologies are based on a combination of basic reburning and N-agent/promoter injection. All Phase I project objectives have been met or exceeded, and it was demonstrated that the AR technologies can provide effective NO_x control for coal fired combustors. Three technologies were originally envisioned for development: AR-Lean, AR-Rich, and MIAR. Along with these, three additional technologies were identified during the project: reburning plus promoted SNCR, AR-Lean plus promoted SNCR, and AR-Rich plus promoted SNCR. These six SGAR configurations differ primarily in the N-agent/promoter injection components. Various components can be selected to tailor the SGAR system to site specific boiler design and NO_x control requirements.

2. Bench scale combustion tests in the 20 kW facility demonstrated NO_x reduction of 86%, 88%, and 91% for AR-Lean, AR-Rich, and MIAR, respectively. These levels of NO_x control can be achieved with only 15 ppm Na₂CO₃ in flue gas. Pilot scale studies in the 200 kW combustion facility demonstrated the ability of the AR technologies to achieve NO_x reductions of 95+% during gas firing and 90+% during coal firing. Byproduct emissions were found to be lower than those generated by commercial reburning and SNCR technologies. Sodium compounds promote NO_x reduction more effectively during gas firing than coal firing; however, NO_x control without sodium addition is more effective for coal than for gas firing. The maximum NO_x reductions achieved by the SGAR configurations were 95-98% during gas firing and 90-95% during coal firing.

3. A flow system decomposition study revealed that the primary gas-phase decomposition products of Na₂CO₃ are Na atoms, NaOH and CO₂. The observed decomposition rate of Na₂CO₃ can be described kinetically in terms of two irreversible Na₂CO₃

→ $\text{Na}_2\text{O} + \text{CO}_2$ and $\text{Na}_2\text{O} + \text{CO}_2 \rightarrow \text{Na}_2\text{CO}_3$ and one reversible $\text{Na}_2\text{O} + \text{H}_2\text{O} \rightleftharpoons 2\text{NaOH}$ chemical reactions. The corresponding rate coefficients were measured or estimated to describe the rate of Na_2CO_3 decomposition in the temperature range of 900-1190 K. Extrapolating the results to higher temperatures shows that Na_2CO_3 decomposition at temperatures over 1400 K produces NaOH and CO_2 very quickly. NaOH then decomposes more slowly. Experiments show no chemical reaction between Na_2CO_3 decomposition products and H_2 , CO, CH_4 or NO at 1150 K. This confirms that sodium has little or no reactivity with major flue gas components in the absence of ammonia.

4. A detailed reaction mechanism was developed to model the AR chemical processes. The mechanism (355 reactions of 65 species) includes the following submechanisms: GRI-Mech-2.11, SNCR chemistry, sodium chemistry with Na_2CO_3 decomposition reactions, SO_2/SO_3 reactions, and interaction of HCl with flue gas components. Kinetic modeling provided insight into the controlling factors of the process and qualitatively described the observed reaction trends. The following factors mainly define the efficiency of AR systems: equivalence ratio in the reburning zone, process streams injection temperatures (reburning fuel, N-agents, promoters, and OFA), concentrations of N-agents and promoters, delay times for injection of N-agents into the reburning and burnout zones, and characteristic mixing times of the injection streams with flue gas. The modeling predicted and explained the NO_x reduction enhancement of sodium promotion under both fuel-rich and fuel-lean conditions. The promotion effect is most pronounced in systems with long characteristic mixing times which are typical of full scale industrial and utility boilers. A sensitivity analysis revealed the most significant elementary reactions affecting formation and destruction of NO and other N-containing compounds in the reburning and burnout zones.

5. The AR design methodology was upgraded by using experiments and analytical models to include the second generation improvements. This work took advantage of a full scale application of the original AR configuration in progress on a 105 MW tangentially fired boiler

outside the scope of this project. The upgraded methodology was used to prepare process designs for three SGAR concepts on the 105 MW boiler and to predict the impacts of the SGAR systems on boiler performance and NO_x emissions. Some elements of SGAR were tested in the boiler. These tests showed that the large scale stratification in the furnace gases affected the NO_x reduction and ammonia slip associated with N-agent injection. These mixing-related issues will be addressed in Phase II in the 10 x 10⁶ Btu/hr tests and limited additional boiler tests.

6. An economic analysis was conducted to compare the cost effectiveness of SGAR and SCR using the EPRI Technology Assessment Guide methodology for two representative Title 1 CAAA applications: a cyclone fired boiler and a wall fired boiler equipped with low NO_x burners. The total cost of NO_x control (combining capital and operating cost components) for the SGAR systems was 48-69% less than for SCR depending on the specific application. The requirements for NO_x control under the CAAA were evaluated. The key drivers are the current ozone non-attainment areas, the potential to expand those regions to the eastern half of the US and the recent tightening of the National Ambient Air Quality Standards for ozone and fine particulate which will require additional NO_x control nationwide. The market for AR technologies was estimated to be above \$1.5 billion.

7. Additional work is needed in Phase II to move the technology to a demonstration stage. In particular, the following steps are necessary to optimize and scale up the SGAR technologies:

- Identify alternative promoters based on the promotion mechanisms developed in Phase I.
- Identify and test coal mineral compounds responsible for the increased NO_x reduction in AR-Rich and MIAR with coal firing (about 10% higher than for gas firing).
- Optimize mixing (reburn fuel, N-agents, OFA) via combined chemistry/mixing models.
- Optimize N-agent injection to maximize NO_x reduction with negligible ammonia slip.
- Evaluate the effect of N-agent/promoter mixing times representative of full scale.

- Optimize SGAR with new promoters and mixing regimes at 1×10^6 Btu/hr scale.
- Scale up and confirm the design methodology via 10×10^6 Btu/hr Proof-of- Concept tests and limited component tests during the ongoing boiler AR tests.
- Update the economic and market analysis to confirm the advantages of SGAR.

11.0 ACKNOWLEDGMENTS

The authors of this report would like to acknowledge the input and support of FETC Contracting Officer's Representatives, Lori D. Gould, William P. Barnett, and current COR Thomas J. Feeley. We appreciate the effort of EER engineers (Don Engelhardt, Quang Nguyen and Bruce Li) and the dedication of EER combustion research technicians (Brian Jacobs, Andy Furlong, Robert Elliot, Sr. and Robert Elliot, Jr.) who significantly contributed to this project by generating high quality combustion test data. A continuing support of EER secretaries, Laura Rogers and Jody Reeder, is also gratefully acknowledged.

12.0 REFERENCES

- Ager, J.W., III and Howard, C.J. (1987). Gas Phase Kinetics of the Reactions of NaO with H₂, D₂, H₂O, and D₂O, J. Chem. Phys., V. 87, p. 921.
- Ager, J.W., III and Talcott, C.L., Howard, C.J. (1986). Gas Phase Kinetics of the Reactions of Na and NaO with O₃ and N₂O, J. Chem. Phys., V. 85, p. 5584.
- Arand, J.K., Muzio, L.J. and Sotter, J.G., U.S. Patent 4,208,386, June 17, 1980.
- Armitage, J. W. and Cullis, C. F. (1971). Studies of the Reaction between Nitrogen Dioxide and Sulfur Dioxide, Combust. Flame, V. 16, p. 125.
- Atkinson, R., Baulch, D.L., Cox, R.A., Hampson, R.F., Jr., Kerr, J.A. and Troe, J. (1992). Evaluated Kinetic and Photochemical Data for Atmospheric Chemistry, J. Phys. Chem. Ref. Data, V. 21, pp. 1125-1568.
- Bailar, J.C. Jr., Emeleus, H.J. Nyholm, R. and Trotman-Dickenson, A.F. (1973). Comprehensive Inorganic Chemistry, Pergamon Press.
- Ball, M.C., Snelling, C.M., Strachan, A.N. and Strachan, R.M. (1992). Thermal Decomposition of Solid Sodium Sesquicarbonate, Na₂CO₃.NaHCO₃.2H₂O. J. Chem. Soc. Faraday Trans. 88, pp. 631-636.
- Barin, I. (1989). Thermodynamic Data of Pure Substances, VCH Verlagsgesellschaft mbH, D-6940 Weinheim, Germany.
- Baulch, D.L., Duxbury, J., Grant, S.J. and Montague, D.C. (1981). Evaluated Kinetic Data for High Temperature Reactions. Volume 4. Homogeneous Gas Phase Reactions of Halogen- and Cyanide-Containing Species, J. Phys. Chem. Ref. Data, V. 10, Suppl. 1, 1-1.
- Bowman, C.T. (1996). In Physical and Chemical Aspects of Combustion: A Tribute to Irvine Glassman (F.L. Dryer, R.F. Sawyer, Eds), Gordon and Breach.
- Bowman, C.T., Hanson, R.K., Davidson, D.F., Gardiner, W.C.Jr., Lissianski, V.V., Smith, G.P., Golden, D.M., Frenklach, M., Wang, H. and Goldenberg, M. (1995). <http://www.gri.org>.
- Carabetta, R. and Kaskan, W.E. (1968). The Oxidation of Sodium, Potassium, and Cesium in Flames. J. Phys. Chem. 72, No. 7, pp. 2483-2489.

Chase, M.W. Jr., Davies, C.A., Downey, J.R. Jr., Frurip, D.J., McDonald, R.A. and Syverud, A.N. (1985). JANAF Thermochemical Tables, Third Edition. Journal of Physical and Chemical Reference Data, 14, Suppl. 1.

Chen, S.L., Ho, L., Cole, J.A and Seeker, W.R., 1989, "An Investigation to Define the Physical/Chemical Constraints Which Limit NO_x Emission Reduction Achievable by Reburning", EER Final Report, DOE contract No. DE-AC22-86PC91025.

Chen, S.L., Lyon, R.K. and Seeker, W.R. (1991). Environ. Progress, V. 10, P. 182, August, 1991.

Chen, S.L., Seeker, W.R., Lyon, R.K. and Ho, L. (1993). N₂O Decomposition Catalyzed in the Gas Phase by Sodium, 205th ACS National Meeting, Denver, CO, March 28 - April 2, 1993.

Cohen, N. (1996) J. Phys. Chem. Ref. Data 25, 1411.

Cotton, D.H. and Jenkins, D.R. (1971). Trans. Faraday Soc. 67, 730, 1971.

DeMore, W.B., Golden, D.M., Hampson, R.F., Howard, C.J., Kurylo, M.J., Molina, M.J., Ravishankara, A.R. and Sander, S.P. (1987). Chemical Kinetics and Photochemical Data for Use in Stratospheric Modeling, Evaluation Number 8, JPL Publication 87-41, 1.

Ebbinghaus, B.B. (1993). Thermodynamics of Gas Phase Chromium Species, Combust. Flame, 93, pp. 119-137.

Feitelberg, A.S. (1994). CET89 for the Macintosh: A Chemical Equilibrium and Transport Properties Calculator. General Electric Company.

Fenimore, C.P. (1973). Two Modes of Interaction of NaOH and SO₂ in Gases From Fuel-Lean H₂-Air Flames, 14th Symposium (Intern.) on Combustion, The Combustion Institute, Pittsburgh, pp. 955-963.

Frenklach, M., Wang, H., Bowman, C.T., Hanson, R.K., Smith, G.P., Golden, D.M., Gardiner, W.C., and Lissianski, V. (1994). An Optimized Kinetics Model for Natural Gas Combustion, 25th International Symposium on Combustion, Irvine, California, Work-In-Progress Poster Session 3, Number 26.

Galwey, A.K. and Hood, W.J. (1979). Thermal Decomposition of Sodium Carbonate Perhydrate in the Solid State. J. Phys. Chem. 83, pp. 1810-1815.

Gardiner, W.C. Jr., Walker, B.F. and Wakefield, C.B. (1981). In Shock Waves in Chemistry, A. Lifshitz., Ed.; Marcel Dekker: New York; p. 319.

Glarborg, P., Dam-Johansen, K. and Kristensen, P.G. (1993). Reburning Rich-Lean Kinetics, Final Report to GRI, Contract No. 5091-260-2126.

Heda, P.K. Dollimore, D., Alexander, K.S., Chen, D., Law, E. and Bicknell, P. (1995). A Method of Assessing Solid State Reactivity Illustrated by Thermal Decomposition Experiments on Sodium Bicarbonate. *Thermochimica Acta* 255, pp. 255-272.

Hewson, T.A. and Stamberg, J.B. (1995) Evaluation of Proposed 37 State Seasonal NO_x Control Program. Compliance Costs and Issues, Report by Energy Ventures Analysis, Inc., Arlington, VA.

Hildenbrand, D.L. And Murad, E. (1970). Dissociation Energy of NaO(g) and the Heat of Atomization of Na₂O(g), *J. Chem. Phys.* 53, 3403-3408.

Ho, L. Chen, S.L., Seeker, W.R. and Maly, P.M. (1993). U.S. Patent No. 5,270,025.

Husain, D. and Plane, J.M.C. (1982). Kinetic Investigation of the Reaction Between Na + O₂ + M by Time-Resolved Atomic Resonance Absorption Spectroscopy. *J. Chem. Soc. Faraday Trans. 2* 78, pp. 163-178.

Husain, D. and Marshall, P. (1986). Determination of Absolute Rate Data for the Reactions of Atomic Sodium with CH₃F, CH₃Cl, CH₃Br, HCl, and HBr as a Function of Temperature by Time-Resolved Atomic Resonance Spectroscopy, *Int. J. Chem. Kinet.*, V. 18, p. 83.

Hynes, A.J., Steinberg, M. and Schofield, K., The Chemical Kinetics and Thermodynamics of Sodium Species in Oxygen-Rich Hydrogen Flames, *J. Chem. Phys.* 80, 1984, pp. 2585-2597.

Jensen, D.E. and Jones, G.A. (1982). Kinetics of Flame Inhibition by Sodium, *J. Chem. Soc. Faraday Trans. 1*, V. 78, p. 2843.

Kaskan, W.E. (1971). The Reaction of Alkali Atoms in Lean Flames. 10th Symposium (International) on Combustion, The Combustion Institute, pp.4 1-45.

Kee, R.J., Rupley, F.M. and Miller, J.A. (1992). Chemkin II: a Fortran Chemical Kinetics Package for the Analysis of Gas Phase Chemical Kinetics, Sandia National Laboratories, Report SAND89-8009.

Lay, T.H., Bozzelli, J.W., Dean, A.M., and Ritter, E.R. (1995) *J. Phys. Chem.* 99, 14514.

Lutz, A.E., Kee, R.J. and Miller, J.A. (1987). SENKIN: a Fortran Program for Predicting Gas Phase Chemical Kinetics with Sensitivity Analysis, Sandia National Laboratories Report No.

SAND87-8248.

Lyon, R. K. U.S. Patent 3,900,554, August 19, 1975.

Lyon, R.K. and Hardy, J.E. (1986). *Ind. Eng. Chem. Fundam.* 25, 19.

Mallard, W.G., Westley, F., Herron, J.T., Hampson, R.F., and Frizzell, D.H. (1994). NIST Chemical Kinetics Database: Version 6.0, National Institute of Standards and Technology, Gaithersburg, MD.

Marshall, P., Narayan, A.S., and Fontijn, A. (1990) *J. Phys. Chem.* 94, 2998.

McBride, B.J., Gordon, S., and Reno, M.A. (1993). Coefficients for Calculating Thermodynamic and Transport Properties of Individual Species, NASA Technical Memorandum 4513, October, 1993.

McBride, B.J., M.A. Reno, and S. Gordon (1994), CET93 and CETPC: An Interim Updated Version of the NASA Lewis Computer Program for Calculating Complex Chemical Equilibria with Applications, NASA Lewis Research Center, Cleveland, Ohio, NASA technical Memorandum 4557; program distributed by COSMIC, NASA's Software Technology Center, The University of Georgia, GA.

McEwan, M.J. and Phillips, L.F. (1965). *Trans. Faraday Soc.* 62, p. 1717.

Miller, J.A. and Bowman, C.T. (1989). Mechanism and Modeling of Nitrogen Chemistry in Combustion, *Progr. Energy Combust. Sci.*, 15, 287-338.

Mitani, T. and Nioka, T. (1984). Extinction Phenomenon of Premixed Flames with Alkali Metal Compounds. *Combust. Flame* 55, pp. 13-21.

Partridge, H., Bauschlichter, C.W., Jr., Sodupe, M. and Langhoff, S.R. (1992). *Chem. Phys. Lett.*, V. 195, p. 200.

Perry, R.A. and Miller, J.A. (1995). An Exploratory Investigation of the Use of Alkali Metals in Nitrous Oxide Control. *Int. J. Chem. Kinetics* 28, pp. 217-234.

Phase II NO_x Controls for the MARAMA and NESCAUM Regions, EPA-453/R-96-002, 1996.

Plane, J.M.C. and Rajasekhar, B. (1989). Kinetic Study of the Reactions Na + O₂ and Na + N₂O over an Extended Temperature Range, *J. Phys. Chem.*, V. 93, p. 3135.

Plane, J.M.C. and Husain, D. (1986). Determination of the Absolute Rate Constant for the

Reaction $O+NaO = Na+O_2$ by Time-Resolved Atomic Chemiluminescence, *J. Chem. Soc. Faraday Trans. 2*, V. 82, p. 2047.

Plane, J.M.C. (1991) *Int. Reviews Phys. Chem.* 10, 55.

Plane, J.M.C. (1992). A Comparison Between the Oxidation Reactions of the Alkali and Alkaline Earth Atoms, *Gas-Phase Metal Reactions*, ed. A. Fontijn, Elsevier Science Publ., Amsterdam, Netherlands, pp. 29-56.

Schofield, K., and Steinberg, M. (1992) *J. Phys. Chem.* 96, 715.

Seeker, W.R., Proc. of the Reburning Workshop, Orenas Slott, Sweden, Nov. 26-27, 1990.

Seeker, W.R., Chen, S.L. and Kramlich, J.C., 1992, "Advanced Reburning for Reduction of NO_x Emissions in Combustion Systems", U.S. Patent 5,139,755.

Shi, Y. and Marshall, P. (1991). A Kinetic Study of the Recombination Reaction $Na + SO_2 + Ar$, *J. Phys. Chem.*, V. 95, p. 1654.

Silver, J.A. and Kolb, C.E. (1986). Gas-Phase Reaction Rate of Sodium Superoxide with Hydrochloric Acid, *J. Phys. Chem.*, V. 90, p. 3267.

Silver, J.A., Stanton, A.C., Zahniser, M.S. and Kolb, C.E. (1984). Gas-Phase Reaction Rate of Sodium Hydroxide with Hydrochloric Acid, *J. Phys. Chem.*, V. 88, p. 3123.

Smith, O. I., Tseregounis, S. and Wang, S-N. (1982). High-Temperature Kinetics of the Reactions of SO_2 and SO_3 with Atomic Oxygen, *Int. J. Chem. Kinet.*, V. 14, p. 679.

Srinivasachar, S., Helble, J.J., Ham, D.O. and Domazetis, G. (1990). A Kinetic Description of Vapor Phase Alkali Transformations in Combustion Systems. *Progr. Energy Combust. Sci.* 16, pp. 303-309.

Steinberg, M. and Schofield, K. (1990). The Chemistry of Sodium with Sulfur in Flames, *Prog. Energy Combust. Sci.*, Vol. 16, pp. 311-317.

Terai, R., Sugae, I., Hayami, R. (1968). Kinetics and Mechanism of the Solid State Reaction of Alkali Carbonate and Silica. *Zairyo*, 17(177) 527.

United States Environmental Protection Agency. (1977). Process Measurement Procedures - Sulfuric Acid Emissions.

Wendt, J.O.L., Sterling, C.V. and Matovich, M.A. (1973). 14th Symposium (International) on

Combustion, P. 897, 1973.

Westley, F., Frizzell, D.H., Herron, J.T., Hampson, R.F. and Mallard, W.G. (1994). NIST Chemical Kinetics Database, version 5.0. NIST.

Wu, Y.-L. and Shih, S.-M. (1993). Intrinsic Kinetics of the Thermal Decomposition of Sodium Bicarbonate. *Thermochimica Acta* 223, pp. 177-186.

Zamansky, V.M. and Borisov, A.A. (1992). Promotion of High-Temperature Self-Ignition, *Prog. Energy Combust. Sci.*, V. 18, pp. 297-325.

Zamansky, V.M. and Maly, P.M. (1996a). Second Generation Advanced Reburning for High Efficiency NOx Control, EER 1st Quarterly Report, DOE Contract No. DE-AC22-95PC95251, January, 1996.

Zamansky, V.M. (1996). Second Generation Advanced Reburning for High Efficiency NOx Control, EER 2nd Quarterly Report, DOE Contract No. DE-AC22-95PC95251, April, 1996.

Zamansky, V.M. and Maly, P.M. (1996b). Second Generation Advanced Reburning for High Efficiency NOx Control, EER 3d Quarterly Report, DOE Contract No. DE-AC22-95PC95251, July, 1996.

Zamansky, V.M. and Maly, P.M. (1996c). Second Generation Advanced Reburning for High Efficiency NOx Control, EER 4th Quarterly Report, DOE Contract No. DE-AC22-95PC95251, October, 1996.

Zamansky, V.M. and Maly, P.M. (1997a). Second Generation Advanced Reburning for High Efficiency NOx Control, EER 5th Quarterly Report, DOE Contract No. DE-AC22-95PC95251, January, 1997.

Zamansky, V.M. et al. (1997b). Second Generation Advanced Reburning for High Efficiency NOx Control, EER 6th Quarterly Report, DOE Contract No. DE-AC22-95PC95251, April, 1997.

Appendix 1. Reaction Mechanism in Chemkin/Senkin Interpreter Format

CHEMKIN INTERPRETER OUTPUT: CHEMKIN-II Version 3.1 Feb. 1993; DOUBLE PRECISION

ELEMENTS CONSIDERED	ATOMIC WEIGHT
1. O	15.9994
2. H	1.00797
3. C	12.0112
4. N	14.0067
5. AR	39.9480
6. S	32.0640
7. NA	22.9898
8. CL	35.4530

SPECIES CONSIDERED	C P H A R S G	MOLECULAR WEIGHT	TEMPERATURE		ELEMENT COUNT									
			LOW	HIGH	O	H	C	N	AR	S	NA	CL		
1. H2	G 0	2.01594	200.0	3500.0	0	2	0	0	0	0	0	0	0	0
2. H	G 0	1.00797	200.0	3500.0	0	1	0	0	0	0	0	0	0	0
3. O	G 0	15.99940	200.0	3500.0	1	0	0	0	0	0	0	0	0	0
4. O2	G 0	31.99880	200.0	3500.0	2	0	0	0	0	0	0	0	0	0
5. OH	G 0	17.00737	200.0	3500.0	1	1	0	0	0	0	0	0	0	0
6. H2O	G 0	18.01534	200.0	3500.0	1	2	0	0	0	0	0	0	0	0
7. HO2	G 0	33.00677	200.0	3500.0	2	1	0	0	0	0	0	0	0	0
8. H2O2	G 0	34.01474	200.0	3500.0	2	2	0	0	0	0	0	0	0	0
9. C	G 0	12.01115	200.0	3500.0	0	0	1	0	0	0	0	0	0	0
10. CH	G 0	13.01912	200.0	3500.0	0	1	1	0	0	0	0	0	0	0
11. CH2	G 0	14.02709	200.0	3500.0	0	2	1	0	0	0	0	0	0	0
12. CH2 (S)	G 0	14.02709	200.0	3500.0	0	2	1	0	0	0	0	0	0	0
13. CH3	G 0	15.03506	200.0	3500.0	0	3	1	0	0	0	0	0	0	0
14. CH4	G 0	16.04303	200.0	3500.0	0	4	1	0	0	0	0	0	0	0
15. CO	G 0	28.01055	200.0	3500.0	1	0	1	0	0	0	0	0	0	0
16. CO2	G 0	44.00995	200.0	3500.0	2	0	1	0	0	0	0	0	0	0
17. HCO	G 0	29.01852	200.0	3500.0	1	1	1	0	0	0	0	0	0	0
18. CH2O	G 0	30.02649	200.0	3500.0	1	2	1	0	0	0	0	0	0	0
19. CH2OH	G 0	31.03446	200.0	3500.0	1	3	1	0	0	0	0	0	0	0
20. CH3O	G 0	31.03446	300.0	3000.0	1	3	1	0	0	0	0	0	0	0
21. CH3OH	G 0	32.04243	200.0	3500.0	1	4	1	0	0	0	0	0	0	0
22. C2H	G 0	25.03027	200.0	3500.0	0	1	2	0	0	0	0	0	0	0
23. C2H2	G 0	26.03824	200.0	3500.0	0	2	2	0	0	0	0	0	0	0
24. C2H3	G 0	27.04621	200.0	3500.0	0	3	2	0	0	0	0	0	0	0
25. C2H4	G 0	28.05418	200.0	3500.0	0	4	2	0	0	0	0	0	0	0
26. C2H5	G 0	29.06215	200.0	3500.0	0	5	2	0	0	0	0	0	0	0
27. C2H6	G 0	30.07012	200.0	3500.0	0	6	2	0	0	0	0	0	0	0
28. HCCO	G 0	41.02967	300.0	4000.0	1	1	2	0	0	0	0	0	0	0
29. CH2CO	G 0	42.03764	200.0	3500.0	1	2	2	0	0	0	0	0	0	0
30. HCCOH	G 0	42.03764	300.0	5000.0	1	2	2	0	0	0	0	0	0	0
31. N	G 0	14.00670	200.0	6000.0	0	0	0	1	0	0	0	0	0	0
32. NH	G 0	15.01467	200.0	6000.0	0	1	0	1	0	0	0	0	0	0
33. NH2	G 0	16.02264	200.0	6000.0	0	2	0	1	0	0	0	0	0	0
34. NH3	G 0	17.03061	200.0	6000.0	0	3	0	1	0	0	0	0	0	0
35. NNH	G 0	29.02137	200.0	6000.0	0	1	0	2	0	0	0	0	0	0
36. NO	G 0	30.00610	200.0	6000.0	1	0	0	1	0	0	0	0	0	0
37. NO2	G 0	46.00550	200.0	6000.0	2	0	0	1	0	0	0	0	0	0
38. N2O	G 0	44.01280	200.0	6000.0	1	0	0	2	0	0	0	0	0	0
39. HNO	G 0	31.01407	200.0	6000.0	1	1	0	1	0	0	0	0	0	0
40. CN	G 0	26.01785	200.0	6000.0	0	0	1	1	0	0	0	0	0	0
41. HCN	G 0	27.02582	200.0	6000.0	0	1	1	1	0	0	0	0	0	0
42. H2CN	G 0	28.03379	300.0	4000.0	0	2	1	1	0	0	0	0	0	0
43. HCNN	G 0	41.03252	300.0	5000.0	0	1	1	2	0	0	0	0	0	0
44. HCNO	G 0	43.02522	300.0	5000.0	1	1	1	1	0	0	0	0	0	0
45. HOCN	G 0	43.02522	300.0	5000.0	1	1	1	1	0	0	0	0	0	0
46. HNCO	G 0	43.02522	300.0	5000.0	1	1	1	1	0	0	0	0	0	0
47. NCO	G 0	42.01725	200.0	6000.0	1	0	1	1	0	0	0	0	0	0
48. N2	G 0	28.01340	300.0	5000.0	0	0	0	2	0	0	0	0	0	0
49. AR	G 0	39.94800	300.0	5000.0	0	0	0	0	1	0	0	0	0	0
50. N2H2	G 0	30.02934	300.0	5000.0	0	2	0	2	0	0	0	0	0	0
51. SO2	G 0	64.06280	300.0	5000.0	2	0	0	0	0	1	0	0	0	0
52. SO3	G 0	80.06220	300.0	5000.0	3	0	0	0	0	0	1	0	0	0
53. HSO3	G 0	81.07017	300.0	2000.0	3	1	0	0	0	1	0	0	0	0

SPECIES CONSIDERED (cont'd)	S E	G W	MOLECULAR WEIGHT	TEMPERATURE		ELEMENT COUNT								
				LOW	HIGH	O	H	C	N	AR	S	NA	CL	
54. HCL	G	0	36.46097	300.0	2000.0	0	1	0	0	0	0	0	0	1
55. CL	G	0	35.45300	300.0	2000.0	0	0	0	0	0	0	0	0	1
56. CL2	G	0	70.90600	300.0	2000.0	0	0	0	0	0	0	0	0	2
57. NAO2	G	0	54.98860	300.0	2000.0	2	0	0	0	0	0	0	1	0
58. NASO2	G	0	87.05260	300.0	2000.0	2	0	0	0	0	0	1	1	0
59. NA2SO3	L	0	126.04180	300.0	2000.0	3	0	0	0	0	0	1	2	0
60. NA2SO4	G	0	142.04120	300.0	2000.0	4	0	0	0	0	0	1	2	0
61. NAACL	G	0	58.44280	300.0	2000.0	0	0	0	0	0	0	0	1	1
62. NAOH	G	0	39.99717	300.0	2000.0	1	1	0	0	0	0	0	1	0
63. NA	G	0	22.98980	300.0	2000.0	0	0	0	0	0	0	0	1	0
64. NAO	G	0	38.98920	300.0	2000.0	1	0	0	0	0	0	0	1	0
65. NA2CO3	G	0	105.98895	300.0	2000.0	3	0	1	0	0	0	0	2	0
66. NA2O	S	0	61.97900	300.0	2000.0	1	0	0	0	0	0	0	2	0

(k = A T**b exp(-E/RT))

REACTIONS	A	b	E
NOTE: A units mole-cm-sec-K, E units cal/mole			
IGRI-Mech 2.11			
1. 2O+M<=>O2+M	1.20E+17	-1.0	0.0
H2	Enhanced by	2.400E+00	
H2O	Enhanced by	1.540E+01	
CH4	Enhanced by	2.000E+00	
CO	Enhanced by	1.750E+00	
CO2	Enhanced by	3.600E+00	
C2H6	Enhanced by	3.000E+00	
AR	Enhanced by	8.300E-01	
2. O+H+M<=>OH+M	5.00E+17	-1.0	0.0
H2	Enhanced by	2.000E+00	
H2O	Enhanced by	6.000E+00	
CH4	Enhanced by	2.000E+00	
CO	Enhanced by	1.500E+00	
CO2	Enhanced by	2.000E+00	
C2H6	Enhanced by	3.000E+00	
AR	Enhanced by	7.000E-01	
3. O+H2<=>H+OH	5.00E+04	2.7	6290.0
4. O+HO2<=>OH+O2	2.00E+13	0.0	0.0
5. O+H2O2<=>OH+H2O	9.63E+06	2.0	4000.0
6. O+CH<=>H+CO	5.70E+13	0.0	0.0
7. O+CH2<=>H+HCO	8.00E+13	0.0	0.0
8. O+CH2(S)<=>H2+CO	1.50E+13	0.0	0.0
9. O+CH2(S)<=>H+HCO	1.50E+13	0.0	0.0
10. O+CH3<=>H+CH2O	8.43E+13	0.0	0.0
11. O+CH4<=>OH+CH3	1.02E+09	1.5	8600.0
12. O+CO+M<=>CO2+M	6.02E+14	0.0	3000.0
H2	Enhanced by	2.000E+00	
O2	Enhanced by	6.000E+00	
H2O	Enhanced by	6.000E+00	
CH4	Enhanced by	2.000E+00	
CO	Enhanced by	1.500E+00	
CO2	Enhanced by	3.500E+00	
C2H6	Enhanced by	3.000E+00	
AR	Enhanced by	5.000E-01	
13. O+HCO<=>OH+CO	3.00E+13	0.0	0.0
14. O+HCO<=>H+CO2	3.00E+13	0.0	0.0
15. O+CH2O<=>OH+HCO	3.90E+13	0.0	3540.0
16. O+CH2OH<=>OH+CH2O	1.00E+13	0.0	0.0
17. O+CH3O<=>OH+CH2O	1.00E+13	0.0	0.0
18. O+CH3OH<=>OH+CH2OH	3.88E+05	2.5	3100.0
19. O+CH3OH<=>OH+CH3O	1.30E+05	2.5	5000.0
20. O+C2H<=>CH+CO	5.00E+13	0.0	0.0
21. O+C2H2<=>H+HCCO	1.02E+07	2.0	1900.0
22. O+C2H2<=>OH+C2H	4.60E+19	-1.4	28950.0
23. O+C2H2<=>CO+CH2	1.02E+07	2.0	1900.0
24. O+C2H3<=>H+CH2CO	3.00E+13	0.0	0.0
25. O+C2H4<=>CH3+HCO	1.92E+07	1.8	220.0
26. O+C2H5<=>CH3+CH2O	1.32E+14	0.0	0.0
27. O+C2H6<=>OH+C2H5	8.98E+07	1.9	5690.0
28. O+HCCO<=>H+2CO	1.00E+14	0.0	0.0

REACTIONS				(k = A T**b exp(-E/RT))		
			A	b	E	
29.	O+CH2CO<=>OH+HCCO		1.00E+13	0.0	8000.0	
30.	O+CH2CO<=>CH2+CO2		1.75E+12	0.0	1350.0	
31.	O2+CO<=>O+CO2		2.50E+12	0.0	47800.0	
32.	O2+CH2O<=>HO2+HCO		1.00E+14	0.0	40000.0	
33.	H+O2+M<=>HO2+M		2.80E+18	-0.9	0.0	
	O2	Enhanced by	0.000E+00			
	H2O	Enhanced by	0.000E+00			
	CO	Enhanced by	7.500E-01			
	CO2	Enhanced by	1.500E+00			
	C2H6	Enhanced by	1.500E+00			
	N2	Enhanced by	0.000E+00			
	AR	Enhanced by	0.000E+00			
34.	H+2O2<=>HO2+O2		3.00E+20	-1.7	0.0	
35.	H+O2+H2O<=>HO2+H2O		9.38E+18	-0.8	0.0	
36.	H+O2+N2<=>HO2+N2		3.75E+20	-1.7	0.0	
37.	H+O2+AR<=>HO2+AR		7.00E+17	-0.8	0.0	
38.	H+O2<=>O+OH		8.30E+13	0.0	14413.0	
39.	2H+M<=>H2+M		1.00E+18	-1.0	0.0	
	H2	Enhanced by	0.000E+00			
	H2O	Enhanced by	0.000E+00			
	CH4	Enhanced by	2.000E+00			
	CO2	Enhanced by	0.000E+00			
	C2H6	Enhanced by	3.000E+00			
	AR	Enhanced by	6.300E-01			
40.	2H+H2<=>2H2		9.00E+16	-0.6	0.0	
41.	2H+H2O<=>H2+H2O		6.00E+19	-1.2	0.0	
42.	2H+CO2<=>H2+CO2		5.50E+20	-2.0	0.0	
43.	H+OH+M<=>H2O+M		2.20E+22	-2.0	0.0	
	H2	Enhanced by	7.300E-01			
	H2O	Enhanced by	3.650E+00			
	CH4	Enhanced by	2.000E+00			
	C2H6	Enhanced by	3.000E+00			
	AR	Enhanced by	3.800E-01			
44.	H+HO2<=>O+H2O		3.97E+12	0.0	671.0	
45.	H+HO2<=>O2+H2		2.80E+13	0.0	1068.0	
46.	H+HO2<=>2OH		1.34E+14	0.0	635.0	
47.	H+H2O2<=>HO2+H2		1.21E+07	2.0	5200.0	
48.	H+H2O2<=>OH+H2O		1.00E+13	0.0	3600.0	
49.	H+CH<=>C+H2		1.10E+14	0.0	0.0	
50.	H+CH2(+M)<=>CH3(+M)		2.50E+16	-0.8	0.0	
	Low pressure limit:	0.32000E+28	-0.31400E+01	0.12300E+04		
	TROE centering:	0.68000E+00	0.78000E+02	0.19950E+04	0.55900E+04	
	H2	Enhanced by	2.000E+00			
	H2O	Enhanced by	6.000E+00			
	CH4	Enhanced by	2.000E+00			
	CO	Enhanced by	1.500E+00			
	CO2	Enhanced by	2.000E+00			
	C2H6	Enhanced by	3.000E+00			
	AR	Enhanced by	7.000E-01			
51.	H+CH2(S)<=>CH+H2		3.00E+13	0.0	0.0	
52.	H+CH3(+M)<=>CH4(+M)		1.27E+16	-0.6	383.0	
	Low pressure limit:	0.24770E+34	-0.47600E+01	0.24400E+04		
	TROE centering:	0.78300E+00	0.74000E+02	0.29410E+04	0.69640E+04	
	H2	Enhanced by	2.000E+00			
	H2O	Enhanced by	6.000E+00			
	CH4	Enhanced by	2.000E+00			
	CO	Enhanced by	1.500E+00			
	CO2	Enhanced by	2.000E+00			
	C2H6	Enhanced by	3.000E+00			
	AR	Enhanced by	7.000E-01			
53.	H+CH4<=>CH3+H2		6.60E+08	1.6	10840.0	
54.	H+HCO(+M)<=>CH2O(+M)		1.09E+12	0.5	-260.0	
	Low pressure limit:	0.13500E+25	-0.25700E+01	0.14250E+04		
	TROE centering:	0.78240E+00	0.27100E+03	0.27550E+04	0.65700E+04	
	H2	Enhanced by	2.000E+00			
	H2O	Enhanced by	6.000E+00			
	CH4	Enhanced by	2.000E+00			
	CO	Enhanced by	1.500E+00			
	CO2	Enhanced by	2.000E+00			
	C2H6	Enhanced by	3.000E+00			
	AR	Enhanced by	7.000E-01			
55.	H+HCO<=>H2+CO		7.34E+13	0.0	0.0	
56.	H+CH2O(+M)<=>CH2OH(+M)		5.40E+11	0.5	3600.0	

REACTIONS		(k = A T**b exp(-E/RT))			
		A	b	E	
Low pressure limit:	0.12700E+33	-0.48200E+01	0.65300E+04		
TROE centering:	0.71870E+00	0.10300E+03	0.12910E+04	0.41600E+04	
H2	Enhanced by	2.000E+00			
H2O	Enhanced by	6.000E+00			
CH4	Enhanced by	2.000E+00			
CO	Enhanced by	1.500E+00			
CO2	Enhanced by	2.000E+00			
C2H6	Enhanced by	3.000E+00			
57. H+CH2O(+M)<=>CH3O(+M)			5.40E+11	0.5	2600.0
Low pressure limit:	0.22000E+31	-0.48000E+01	0.55600E+04		
TROE centering:	0.75800E+00	0.94000E+02	0.15550E+04	0.42000E+04	
H2	Enhanced by	2.000E+00			
H2O	Enhanced by	6.000E+00			
CH4	Enhanced by	2.000E+00			
CO	Enhanced by	1.500E+00			
CO2	Enhanced by	2.000E+00			
C2H6	Enhanced by	3.000E+00			
58. H+CH2O<=>HCO+H2			2.30E+10	1.1	3275.0
59. H+CH2OH(+M)<=>CH3OH(+M)			1.80E+13	0.0	0.0
Low pressure limit:	0.30000E+32	-0.48000E+01	0.33000E+04		
TROE centering:	0.76790E+00	0.33800E+03	0.18120E+04	0.50810E+04	
H2	Enhanced by	2.000E+00			
H2O	Enhanced by	6.000E+00			
CH4	Enhanced by	2.000E+00			
CO	Enhanced by	1.500E+00			
CO2	Enhanced by	2.000E+00			
C2H6	Enhanced by	3.000E+00			
60. H+CH2OH<=>H2+CH2O			2.00E+13	0.0	0.0
61. H+CH2OH<=>OH+CH3			1.20E+13	0.0	0.0
62. H+CH2OH<=>CH2(S)+H2O			6.00E+12	0.0	0.0
63. H+CH3O(+M)<=>CH3OH(+M)			5.00E+13	0.0	0.0
Low pressure limit:	0.86000E+29	-0.40000E+01	0.30250E+04		
TROE centering:	0.89020E+00	0.14400E+03	0.28380E+04	0.45569E+05	
H2	Enhanced by	2.000E+00			
H2O	Enhanced by	6.000E+00			
CH4	Enhanced by	2.000E+00			
CO	Enhanced by	1.500E+00			
CO2	Enhanced by	2.000E+00			
C2H6	Enhanced by	3.000E+00			
64. H+CH3O<=>H+CH2OH			3.40E+06	1.6	0.0
65. H+CH3O<=>H2+CH2O			2.00E+13	0.0	0.0
66. H+CH3O<=>OH+CH3			3.20E+13	0.0	0.0
67. H+CH3O<=>CH2(S)+H2O			1.60E+13	0.0	0.0
68. H+CH3OH<=>CH2OH+H2			1.70E+07	2.1	4870.0
69. H+CH3OH<=>CH3O+H2			4.20E+06	2.1	4870.0
70. H+C2H(+M)<=>C2H2(+M)			1.00E+17	-1.0	0.0
Low pressure limit:	0.37500E+34	-0.48000E+01	0.19000E+04		
TROE centering:	0.64640E+00	0.13200E+03	0.13150E+04	0.55660E+04	
H2	Enhanced by	2.000E+00			
H2O	Enhanced by	6.000E+00			
CH4	Enhanced by	2.000E+00			
CO	Enhanced by	1.500E+00			
CO2	Enhanced by	2.000E+00			
C2H6	Enhanced by	3.000E+00			
AR	Enhanced by	7.000E-01			
71. H+C2H2(+M)<=>C2H3(+M)			5.60E+12	0.0	2400.0
Low pressure limit:	0.38000E+41	-0.72700E+01	0.72200E+04		
TROE centering:	0.75070E+00	0.98500E+02	0.13020E+04	0.41670E+04	
H2	Enhanced by	2.000E+00			
H2O	Enhanced by	6.000E+00			
CH4	Enhanced by	2.000E+00			
CO	Enhanced by	1.500E+00			
CO2	Enhanced by	2.000E+00			
C2H6	Enhanced by	3.000E+00			
AR	Enhanced by	7.000E-01			
72. H+C2H3(+M)<=>C2H4(+M)			6.08E+12	0.3	280.0
Low pressure limit:	0.14000E+31	-0.38600E+01	0.33200E+04		
TROE centering:	0.78200E+00	0.20750E+03	0.26630E+04	0.60950E+04	
H2	Enhanced by	2.000E+00			
H2O	Enhanced by	6.000E+00			
CH4	Enhanced by	2.000E+00			
CO	Enhanced by	1.500E+00			
CO2	Enhanced by	2.000E+00			
C2H6	Enhanced by	3.000E+00			
AR	Enhanced by	7.000E-01			
73. H+C2H3<=>H2+C2H2			3.00E+13	0.0	0.0

		(k = A T**b exp(-E/RT))		
REACTIONS		A	b	E
74.	H+C2H4(+M)<=>C2H5(+M)	1.08E+12	0.5	1820.0
	Low pressure limit:	0.12000E+43	-0.76200E+01	0.69700E+04
	TROE centering:	0.97530E+00	0.21000E+03	0.98400E+03
	H2	Enhanced by	2.000E+00	
	H2O	Enhanced by	6.000E+00	
	CH4	Enhanced by	2.000E+00	
	CO	Enhanced by	1.500E+00	
	CO2	Enhanced by	2.000E+00	
	C2H6	Enhanced by	3.000E+00	
	AR	Enhanced by	7.000E-01	
75.	H+C2H4<=>C2H3+H2	1.32E+06	2.5	12240.0
76.	H+C2H5(+M)<=>C2H6(+M)	5.21E+17	-1.0	1580.0
	Low pressure limit:	0.19900E+42	-0.70800E+01	0.66850E+04
	TROE centering:	0.84220E+00	0.12500E+03	0.22190E+04
	H2	Enhanced by	2.000E+00	
	H2O	Enhanced by	6.000E+00	
	CH4	Enhanced by	2.000E+00	
	CO	Enhanced by	1.500E+00	
	CO2	Enhanced by	2.000E+00	
	C2H6	Enhanced by	3.000E+00	
	AR	Enhanced by	7.000E-01	
77.	H+C2H5<=>H2+C2H4	2.00E+12	0.0	0.0
78.	H+C2H6<=>C2H5+H2	1.15E+08	1.9	7530.0
79.	H+HCCO<=>CH2(S)+CO	1.00E+14	0.0	0.0
80.	H+CH2CO<=>HCCO+H2	5.00E+13	0.0	8000.0
81.	H+CH2CO<=>CH3+CO	1.13E+13	0.0	3428.0
82.	H+HCCOH<=>H+CH2CO	1.00E+13	0.0	0.0
83.	H2+CO(+M)<=>CH2O(+M)	4.30E+07	1.5	79600.0
	Low pressure limit:	0.50700E+28	-0.34200E+01	0.84350E+05
	TROE centering:	0.93200E+00	0.19700E+03	0.15400E+04
	H2	Enhanced by	2.000E+00	
	H2O	Enhanced by	6.000E+00	
	CH4	Enhanced by	2.000E+00	
	CO	Enhanced by	1.500E+00	
	CO2	Enhanced by	2.000E+00	
	C2H6	Enhanced by	3.000E+00	
	AR	Enhanced by	7.000E-01	
84.	OH+H2<=>H+H2O	2.16E+08	1.5	3430.0
85.	2OH(+M)<=>H2O2(+M)	7.40E+13	-0.4	0.0
	Low pressure limit:	0.23000E+19	-0.90000E+00	-0.17000E+04
	TROE centering:	0.73460E+00	0.94000E+02	0.17560E+04
	H2	Enhanced by	2.000E+00	
	H2O	Enhanced by	6.000E+00	
	CH4	Enhanced by	2.000E+00	
	CO	Enhanced by	1.500E+00	
	CO2	Enhanced by	2.000E+00	
	C2H6	Enhanced by	3.000E+00	
	AR	Enhanced by	7.000E-01	
86.	2OH<=>O+H2O	3.57E+04	2.4	-2110.0
87.	OH+HO2<=>O2+H2O	2.90E+13	0.0	-500.0
88.	OH+H2O2<=>HO2+H2O	1.75E+12	0.0	320.0
	Declared duplicate reaction...			
89.	OH+H2O2<=>HO2+H2O	5.80E+14	0.0	9560.0
	Declared duplicate reaction...			
90.	OH+C<=>H+CO	5.00E+13	0.0	0.0
91.	OH+CH<=>H+HCO	3.00E+13	0.0	0.0
92.	OH+CH2<=>H+CH2O	2.00E+13	0.0	0.0
93.	OH+CH2<=>CH+H2O	1.13E+07	2.0	3000.0
94.	OH+CH2(S)<=>H+CH2O	3.00E+13	0.0	0.0
95.	OH+CH3(+M)<=>CH3OH(+M)	6.30E+13	0.0	0.0
	Low pressure limit:	0.27000E+39	-0.63000E+01	0.31000E+04
	TROE centering:	0.21050E+00	0.83500E+02	0.53980E+04
	H2	Enhanced by	2.000E+00	
	H2O	Enhanced by	6.000E+00	
	CH4	Enhanced by	2.000E+00	
	CO	Enhanced by	1.500E+00	
	CO2	Enhanced by	2.000E+00	
	C2H6	Enhanced by	3.000E+00	
96.	OH+CH3<=>CH2+H2O	5.60E+07	1.6	5420.0
97.	OH+CH3<=>CH2(S)+H2O	2.50E+13	0.0	0.0
98.	OH+CH4<=>CH3+H2O	1.00E+08	1.6	3120.0
99.	OH+CO<=>H+CO2	4.76E+07	1.2	70.0
100.	OH+HCO<=>H2O+CO	5.00E+13	0.0	0.0
101.	OH+CH2O<=>HCO+H2O	3.43E+09	1.2	-447.0
102.	OH+CH2OH<=>H2O+CH2O	5.00E+12	0.0	0.0

REACTIONS		(k = A T**b exp(-E/RT))		
		A	b	E
103.	OH+CH3O<=>H2O+CH2O	5.00E+12	0.0	0.0
104.	OH+CH3OH<=>CH2OH+H2O	1.44E+06	2.0	-840.0
105.	OH+CH3OH<=>CH3O+H2O	6.30E+06	2.0	1500.0
106.	OH+C2H<=>H+HCCO	2.00E+13	0.0	0.0
107.	OH+C2H2<=>H+CH2CO	2.18E-04	4.5	-1000.0
108.	OH+C2H2<=>H+HCCOH	5.04E+05	2.3	13500.0
109.	OH+C2H2<=>C2H+H2O	3.37E+07	2.0	14000.0
110.	OH+C2H2<=>CH3+CO	4.83E-04	4.0	-2000.0
111.	OH+C2H3<=>H2O+C2H2	5.00E+12	0.0	0.0
112.	OH+C2H4<=>C2H3+H2O	3.60E+06	2.0	2500.0
113.	OH+C2H6<=>C2H5+H2O	3.54E+06	2.1	870.0
114.	OH+CH2CO<=>HCCO+H2O	7.50E+12	0.0	2000.0
115.	2HO2<=>O2+H2O2	1.30E+11	0.0	-1630.0
	Declared duplicate reaction...			
116.	2HO2<=>O2+H2O2	4.20E+14	0.0	12000.0
	Declared duplicate reaction...			
117.	HO2+CH2<=>OH+CH2O	2.00E+13	0.0	0.0
118.	HO2+CH3<=>O2+CH4	1.00E+12	0.0	0.0
119.	HO2+CH3<=>OH+CH3O	2.00E+13	0.0	0.0
120.	HO2+CO<=>OH+CO2	1.50E+14	0.0	23600.0
121.	HO2+CH2O<=>HCO+H2O2	1.00E+12	0.0	8000.0
122.	C+O2<=>O+CO	5.80E+13	0.0	576.0
123.	C+CH2<=>H+C2H	5.00E+13	0.0	0.0
124.	C+CH3<=>H+C2H2	5.00E+13	0.0	0.0
125.	CH+O2<=>O+HCO	3.30E+13	0.0	0.0
126.	CH+H2<=>H+CH2	1.11E+08	1.8	1670.0
127.	CH+H2O<=>H+C2H2O	1.71E+13	0.0	-755.0
128.	CH+CH2<=>H+C2H2	4.00E+13	0.0	0.0
129.	CH+CH3<=>H+C2H3	3.00E+13	0.0	0.0
130.	CH+CH4<=>H+C2H4	6.00E+13	0.0	0.0
131.	CH+CO(+M)<=>HCCO(+M)	5.00E+13	0.0	0.0
	Low pressure limit:	0.26900E+29	-0.37400E+01	0.19360E+04
	TROE centering:	0.57570E+00	0.23700E+03	0.16520E+04 0.50690E+04
	H2	Enhanced by	2.000E+00	
	H2O	Enhanced by	6.000E+00	
	CH4	Enhanced by	2.000E+00	
	CO	Enhanced by	1.500E+00	
	CO2	Enhanced by	2.000E+00	
	C2H6	Enhanced by	3.000E+00	
	AR	Enhanced by	7.000E-01	
132.	CH+CO2<=>HCO+CO	3.40E+12	0.0	690.0
133.	CH+CH2O<=>H+CH2CO	9.46E+13	0.0	-515.0
134.	CH+HCCO<=>CO+C2H2	5.00E+13	0.0	0.0
135.	CH2+O2<=>OH+HCO	1.32E+13	0.0	1500.0
136.	CH2+H2<=>H+CH3	5.00E+05	2.0	7230.0
137.	2CH2<=>H2+C2H2	3.20E+13	0.0	0.0
138.	CH2+CH3<=>H+C2H4	4.00E+13	0.0	0.0
139.	CH2+CH4<=>2CH3	2.46E+06	2.0	8270.0
140.	CH2+CO(+M)<=>CH2CO(+M)	8.10E+11	0.5	4510.0
	Low pressure limit:	0.26900E+34	-0.51100E+01	0.70950E+04
	TROE centering:	0.59070E+00	0.27500E+03	0.12260E+04 0.51850E+04
	H2	Enhanced by	2.000E+00	
	H2O	Enhanced by	6.000E+00	
	CH4	Enhanced by	2.000E+00	
	CO	Enhanced by	1.500E+00	
	CO2	Enhanced by	2.000E+00	
	C2H6	Enhanced by	3.000E+00	
	AR	Enhanced by	7.000E-01	
141.	CH2+HCCO<=>C2H3+CO	3.00E+13	0.0	0.0
142.	CH2(S)+N2<=>CH2+N2	1.50E+13	0.0	600.0
143.	CH2(S)+AR<=>CH2+AR	9.00E+12	0.0	600.0
144.	CH2(S)+O2<=>H+OH+CO	2.80E+13	0.0	0.0
145.	CH2(S)+O2<=>CO+H2O	1.20E+13	0.0	0.0
146.	CH2(S)+H2<=>CH3+H	7.00E+13	0.0	0.0
147.	CH2(S)+H2O(+M)<=>CH3OH(+M)	2.00E+13	0.0	0.0
	Low pressure limit:	0.27000E+39	-0.63000E+01	0.31000E+04
	TROE centering:	0.15070E+00	0.13400E+03	0.23830E+04 0.72650E+04
	H2	Enhanced by	2.000E+00	
	H2O	Enhanced by	6.000E+00	
	CH4	Enhanced by	2.000E+00	
	CO	Enhanced by	1.500E+00	
	CO2	Enhanced by	2.000E+00	
	C2H6	Enhanced by	3.000E+00	
148.	CH2(S)+H2O<=>CH2+H2O	3.00E+13	0.0	0.0
149.	CH2(S)+CH3<=>H+C2H4	1.20E+13	0.0	-570.0

REACTIONS		(k = A T**b exp(-E/RT))		
		A	b	E
150.	CH2(S)+CH4<=>2CH3	1.60E+13	0.0	-570.0
151.	CH2(S)+CO<=>CH2+CO	9.00E+12	0.0	0.0
152.	CH2(S)+CO2<=>CH2+CO2	7.00E+12	0.0	0.0
153.	CH2(S)+CO2<=>CO+CH2O	1.40E+13	0.0	0.0
154.	CH2(S)+C2H6<=>CH3+C2H5	4.00E+13	0.0	-550.0
155.	CH3+O2<=>O+CH3O	2.68E+13	0.0	28800.0
156.	CH3+O2<=>OH+CH2O	3.60E+10	0.0	8940.0
157.	CH3+H2O2<=>HO2+CH4	2.45E+04	2.5	5180.0
158.	2CH3(+M)<=>C2H6(+M)	2.12E+16	-1.0	620.0
	Low pressure limit:	0.17700E+51	-0.96700E+01	0.62200E+04
	TROE centering:	0.53250E+00	0.15100E+03	0.10380E+04 0.49700E+04
	H2	Enhanced by	2.000E+00	
	H2O	Enhanced by	6.000E+00	
	CH4	Enhanced by	2.000E+00	
	CO	Enhanced by	1.500E+00	
	CO2	Enhanced by	2.000E+00	
	C2H6	Enhanced by	3.000E+00	
	AR	Enhanced by	7.000E-01	
159.	2CH3<=>H+C2H5	4.99E+12	0.1	10600.0
160.	CH3+HCO<=>CH4+CO	2.65E+13	0.0	0.0
161.	CH3+CH2O<=>HCO+CH4	3.32E+03	2.8	5860.0
162.	CH3+CH3OH<=>CH2OH+CH4	3.00E+07	1.5	9940.0
163.	CH3+CH3OH<=>CH3O+CH4	1.00E+07	1.5	9940.0
164.	CH3+C2H4<=>C2H3+CH4	2.27E+05	2.0	9200.0
165.	CH3+C2H6<=>C2H5+CH4	6.14E+06	1.7	10450.0
166.	HCO+M<=>H+CO+M	1.87E+17	-1.0	17000.0
	H2	Enhanced by	2.000E+00	
	H2O	Enhanced by	1.120E+01	
	CH4	Enhanced by	2.000E+00	
	CO	Enhanced by	1.500E+00	
	CO2	Enhanced by	2.000E+00	
	C2H6	Enhanced by	3.000E+00	
167.	HCO+O2<=>HO2+CO	7.60E+12	0.0	400.0
168.	CH2OH+O2<=>HO2+CH2O	1.80E+13	0.0	900.0
169.	CH3O+O2<=>HO2+CH2O	4.28E-13	7.6	-3530.0
170.	C2H+O2<=>HCO+CO	5.00E+13	0.0	1500.0
171.	C2H+H2<=>H+C2H2	4.07E+05	2.4	200.0
172.	C2H3+O2<=>HCO+CH2O	3.98E+12	0.0	-240.0
173.	C2H4(+M)<=>H2+C2H2(+M)	8.00E+12	0.4	88770.0
	Low pressure limit:	0.70000E+51	-0.93100E+01	0.99860E+05
	TROE centering:	0.73450E+00	0.18000E+03	0.10350E+04 0.54170E+04
	H2	Enhanced by	2.000E+00	
	H2O	Enhanced by	6.000E+00	
	CH4	Enhanced by	2.000E+00	
	CO	Enhanced by	1.500E+00	
	CO2	Enhanced by	2.000E+00	
	C2H6	Enhanced by	3.000E+00	
	AR	Enhanced by	7.000E-01	
174.	C2H5+O2<=>HO2+C2H4	8.40E+11	0.0	3875.0
175.	HCCO+O2<=>OH+2CO	1.60E+12	0.0	854.0
176.	2HCCO<=>2CO+C2H2	1.00E+13	0.0	0.0
177.	N+NO<=>N2+O	3.50E+13	0.0	330.0
178.	N+O2<=>NO+O	2.65E+12	0.0	6400.0
179.	N+OH<=>NO+H	7.33E+13	0.0	1120.0
180.	N2O+O<=>N2+O2	1.40E+12	0.0	10810.0
181.	N2O+O<=>2NO	2.90E+13	0.0	23150.0
182.	N2O+H<=>N2+OH	4.40E+14	0.0	18880.0
183.	N2O+OH<=>N2+HO2	2.00E+12	0.0	21060.0
184.	N2O(+M)<=>N2+O(+M)	1.30E+11	0.0	59620.0
	Low pressure limit:	0.62000E+15	0.00000E+00	0.56100E+05
	H2	Enhanced by	2.000E+00	
	H2O	Enhanced by	6.000E+00	
	CH4	Enhanced by	2.000E+00	
	CO	Enhanced by	1.500E+00	
	CO2	Enhanced by	2.000E+00	
	C2H6	Enhanced by	3.000E+00	
	AR	Enhanced by	7.000E-01	
185.	HO2+NO<=>NO2+OH	2.11E+12	0.0	-480.0

REACTIONS				(k = A T**b exp(-E/RT))		
			A	b	E	
186.	NO+O+M<=>NO2+M		1.06E+20	-1.4	0.0	
	H2	Enhanced by	2.000E+00			
	H2O	Enhanced by	6.000E+00			
	CH4	Enhanced by	2.000E+00			
	CO	Enhanced by	1.500E+00			
	CO2	Enhanced by	2.000E+00			
	C2H6	Enhanced by	3.000E+00			
	AR	Enhanced by	7.000E-01			
187.	NO2+O<=>NO+O2		3.90E+12	0.0	-240.0	
188.	NO2+H<=>NO+OH		1.32E+14	0.0	360.0	
189.	NH+O<=>NO+H		5.00E+13	0.0	0.0	
190.	NH+H<=>N+H2		3.20E+13	0.0	330.0	
191.	NH+OH<=>HNO+H		2.00E+13	0.0	0.0	
192.	NH+OH<=>N+H2O		2.00E+09	1.2	0.0	
193.	NH+O2<=>HNO+O		4.61E+05	2.0	6500.0	
194.	NH+O2<=>NO+OH		1.28E+06	1.5	100.0	
195.	NH+N<=>N2+H		1.50E+13	0.0	0.0	
196.	NH+H2O<=>HNO+H2		2.00E+13	0.0	13850.0	
197.	NH+NO<=>N2+OH		2.16E+13	-0.2	0.0	
198.	NH+NO<=>N2O+H		4.16E+14	-0.5	0.0	
199.	NH2+O<=>OH+NH		7.00E+12	0.0	0.0	
200.	NH2+O<=>H+HNO		4.60E+13	0.0	0.0	
201.	NH2+H<=>NH+H2		4.00E+13	0.0	3650.0	
202.	NH2+OH<=>NH+H2O		9.00E+07	1.5	-460.0	
203.	NNH<=>N2+H		3.30E+08	0.0	0.0	
	Declared duplicate reaction...					
204.	NNH+M<=>N2+H+M		1.30E+14	-0.1	4980.0	
	H2	Enhanced by	2.000E+00			
	H2O	Enhanced by	6.000E+00			
	CH4	Enhanced by	2.000E+00			
	CO	Enhanced by	1.500E+00			
	CO2	Enhanced by	2.000E+00			
	C2H6	Enhanced by	3.000E+00			
	AR	Enhanced by	7.000E-01			
	Declared duplicate reaction...					
205.	NNH+O2<=>HO2+N2		5.00E+12	0.0	0.0	
206.	NNH+O<=>OH+N2		2.50E+13	0.0	0.0	
207.	NNH+O<=>NH+NO		7.00E+13	0.0	0.0	
208.	NNH+H<=>H2+N2		5.00E+13	0.0	0.0	
209.	NNH+OH<=>H2O+N2		2.00E+13	0.0	0.0	
210.	NNH+CH3<=>CH4+N2		2.50E+13	0.0	0.0	
211.	H+NO+M<=>HNO+M		8.95E+19	-1.3	740.0	
	H2	Enhanced by	2.000E+00			
	H2O	Enhanced by	6.000E+00			
	CH4	Enhanced by	2.000E+00			
	CO	Enhanced by	1.500E+00			
	CO2	Enhanced by	2.000E+00			
	C2H6	Enhanced by	3.000E+00			
	AR	Enhanced by	7.000E-01			
212.	HNO+O<=>NO+OH		2.50E+13	0.0	0.0	
213.	HNO+H<=>H2+NO		4.50E+11	0.7	660.0	
214.	HNO+OH<=>NO+H2O		1.30E+07	1.9	-950.0	
215.	HNO+O2<=>HO2+NO		1.00E+13	0.0	13000.0	
216.	CN+O<=>CO+N		7.70E+13	0.0	0.0	
217.	CN+OH<=>NCO+H		4.00E+13	0.0	0.0	
218.	CN+H2O<=>HCN+OH		8.00E+12	0.0	7460.0	
219.	CN+O2<=>NCO+O		6.14E+12	0.0	-440.0	
220.	CN+H2<=>HCN+H		2.10E+13	0.0	4710.0	
221.	NCO+O<=>NO+CO		2.35E+13	0.0	0.0	
222.	NCO+H<=>NH+CO		5.40E+13	0.0	0.0	
223.	NCO+OH<=>NO+H+CO		2.50E+12	0.0	0.0	
224.	NCO+N<=>N2+CO		2.00E+13	0.0	0.0	
225.	NCO+O2<=>NO+CO2		2.00E+12	0.0	20000.0	
226.	NCO+M<=>N+CO+M		8.80E+16	-0.5	48000.0	
	H2	Enhanced by	2.000E+00			
	H2O	Enhanced by	6.000E+00			
	CH4	Enhanced by	2.000E+00			
	CO	Enhanced by	1.500E+00			
	CO2	Enhanced by	2.000E+00			
	C2H6	Enhanced by	3.000E+00			
	AR	Enhanced by	7.000E-01			
227.	NCO+NO<=>N2O+CO		2.85E+17	-1.5	740.0	
228.	NCO+NO<=>N2+CO2		5.70E+18	-2.0	800.0	

REACTIONS				(k = A T**b exp(-E/RT))		
				A	b	E
229.	HCN+M<=>H+CN+M			1.04E+29	-3.3	126600.0
	H2	Enhanced by	2.000E+00			
	H2O	Enhanced by	6.000E+00			
	CH4	Enhanced by	2.000E+00			
	CO	Enhanced by	1.500E+00			
	CO2	Enhanced by	2.000E+00			
	C2H6	Enhanced by	3.000E+00			
	AR	Enhanced by	7.000E-01			
230.	HCN+O<=>NCO+H			1.11E+04	2.6	4980.0
231.	HCN+O<=>NH+CO			2.77E+03	2.6	4980.0
232.	HCN+O<=>CN+OH			2.13E+09	1.6	26600.0
233.	HCN+OH<=>HOCN+H			1.10E+06	2.0	13370.0
234.	HCN+OH<=>HNCO+H			4.40E+03	2.3	6400.0
235.	HCN+OH<=>NH2+CO			1.60E+02	2.6	9000.0
236.	H+HCN+M<=>H2CN+M			1.40E+26	-3.4	1900.0
	H2	Enhanced by	2.000E+00			
	H2O	Enhanced by	6.000E+00			
	CH4	Enhanced by	2.000E+00			
	CO	Enhanced by	1.500E+00			
	CO2	Enhanced by	2.000E+00			
	C2H6	Enhanced by	3.000E+00			
	AR	Enhanced by	7.000E-01			
237.	H2CN+N<=>N2+CH2			6.00E+13	0.0	400.0
238.	C+N2<=>CN+N			6.30E+13	0.0	46020.0
239.	CH+N2<=>HCN+N			2.86E+08	1.1	20400.0
240.	CH+N2(+M)<=>HCNN(+M)			3.10E+12	0.1	0.0
	Low pressure limit:	0.13000E+26	-0.31600E+01	0.74000E+03		
	TROE centering:	0.66700E+00	0.23500E+03	0.21170E+04	0.45360E+04	
	H2	Enhanced by	2.000E+00			
	H2O	Enhanced by	6.000E+00			
	CH4	Enhanced by	2.000E+00			
	CO	Enhanced by	1.500E+00			
	CO2	Enhanced by	2.000E+00			
	C2H6	Enhanced by	3.000E+00			
	AR	Enhanced by	7.000E-01			
241.	CH2+N2<=>HCN+NH			1.00E+13	0.0	74000.0
242.	CH2(S)+N2<=>NH+HCN			1.00E+11	0.0	65000.0
243.	C+NO<=>CN+O			1.90E+13	0.0	0.0
244.	C+NO<=>CO+N			2.90E+13	0.0	0.0
245.	CH+NO<=>HCN+O			5.00E+13	0.0	0.0
246.	CH+NO<=>H+NCO			2.00E+13	0.0	0.0
247.	CH+NO<=>N+HCO			3.00E+13	0.0	0.0
248.	CH2+NO<=>H+HNCO			3.10E+17	-1.4	1270.0
249.	CH2+NO<=>OH+HCN			2.90E+14	-0.7	760.0
250.	CH2+NO<=>H+HCNO			3.80E+13	-0.4	580.0
251.	CH2(S)+NO<=>H+HNCO			3.10E+17	-1.4	1270.0
252.	CH2(S)+NO<=>OH+HCN			2.90E+14	-0.7	760.0
253.	CH2(S)+NO<=>H+HCNO			3.80E+13	-0.4	580.0
254.	CH3+NO<=>HCN+H2O			9.60E+13	0.0	28800.0
255.	CH3+NO<=>H2CN+OH			1.00E+12	0.0	21750.0
256.	HCNN+O<=>CO+H+N2			2.20E+13	0.0	0.0
257.	HCNN+O<=>HCN+NO			2.00E+12	0.0	0.0
258.	HCNN+O2<=>O+HCO+N2			1.20E+13	0.0	0.0
259.	HCNN+OH<=>H+HCO+N2			1.20E+13	0.0	0.0
260.	HCNN+H<=>CH2+N2			1.00E+14	0.0	0.0
261.	HNCO+O<=>NH+CO2			9.80E+07	1.4	8500.0
262.	HNCO+O<=>HNO+CO			1.50E+08	1.6	44000.0
263.	HNCO+O<=>NCO+OH			2.20E+06	2.1	11400.0
264.	HNCO+H<=>NH2+CO			2.25E+07	1.7	3800.0
265.	HNCO+H<=>H2+NCO			1.05E+05	2.5	13300.0
266.	HNCO+OH<=>NCO+H2O			4.65E+12	0.0	6850.0
267.	HNCO+OH<=>NH2+CO2			1.55E+12	0.0	6850.0
268.	HNCO+M<=>NH+CO+M			1.18E+16	0.0	84720.0
	H2	Enhanced by	2.000E+00			
	H2O	Enhanced by	6.000E+00			
	CH4	Enhanced by	2.000E+00			
	CO	Enhanced by	1.500E+00			
	CO2	Enhanced by	2.000E+00			
	C2H6	Enhanced by	3.000E+00			
	AR	Enhanced by	7.000E-01			
269.	HCNO+H<=>H+HNCO			2.10E+15	-0.7	2850.0
270.	HCNO+H<=>OH+HCN			2.70E+11	0.2	2120.0
271.	HCNO+H<=>NH2+CO			1.70E+14	-0.8	2890.0
272.	HOCN+H<=>H+HNCO			2.00E+07	2.0	2000.0
273.	HCCO+NO<=>HCNO+CO			2.35E+13	0.0	0.0

REACTIONS		(k = A T**b exp(-E/RT))		
		A	b	E
274.	CH3+N<=>H2CN+H	6.10E+14	-0.3	290.0
275.	CH3+N<=>HCN+H2	3.70E+12	0.1	-90.0
276.	NH3+H<=>NH2+H2	5.40E+05	2.4	9915.0
277.	NH3+OH<=>NH2+H2O	5.00E+07	1.6	955.0
278.	NH3+O<=>NH2+OH	9.40E+06	1.9	6460.0
!End GRI-Mech 2.1				
!Bowman's SNCR mechanism				
279.	NH2+O=NO+H2	5.00E+12	0.0	0.0
280.	NH2+NO=NNH+OH	2.80E+13	-0.6	0.0
281.	NH2+NO=N2+H2O	1.30E+16	-1.2	0.0
Declared duplicate reaction...				
282.	NH2+NO=N2+H2O	-2.80E+13	-0.6	0.0
Declared duplicate reaction...				
283.	NNH+NO=N2+HNO	5.00E+13	0.0	0.0
284.	NNH+NH2=N2+NH3	5.00E+13	0.0	0.0
285.	NNH+NH=N2+NH2	5.00E+13	0.0	0.0
286.	NNH+O=N2O+H	1.00E+14	0.0	0.0
287.	HNO+NH2=NH3+NO	2.00E+13	0.0	1000.0
288.	HNO+HNO=N2O+H2O	3.95E+12	0.0	5000.0
289.	HNO+NO=N2O+OH	2.00E+12	0.0	26000.0
290.	NH2+NH=N2H2+H	1.50E+15	-0.5	0.0
291.	NH+NH=N2+H+H	2.50E+13	0.0	0.0
292.	NH2+N=N2+H+H	7.20E+13	0.0	0.0
293.	N2H2+M=NNH+H+M	5.00E+16	0.0	50000.0
	H2O	Enhanced by	1.500E+01	
	O2	Enhanced by	2.000E+00	
	N2	Enhanced by	2.000E+00	
	H2	Enhanced by	2.000E+00	
294.	N2H2+H=NNH+H2	5.00E+13	0.0	1000.0
295.	N2H2+O=NH2+NO	1.00E+13	0.0	0.0
296.	N2H2+O=NNH+OH	2.00E+13	0.0	1000.0
297.	N2H2+OH=NNH+H2O	1.00E+13	0.0	1000.0
298.	N2H2+NO=N2O+NH2	3.00E+12	0.0	0.0
299.	N2H2+NH=NNH+NH2	1.00E+13	0.0	1000.0
300.	N2H2+NH2=NH3+NNH	1.00E+13	0.0	1000.0
301.	NH2+NH2=N2H2+H2	5.00E+11	0.0	0.0
302.	NH2+O2=HNO+OH	4.50E+12	0.0	25000.0
303.	NCO+NO2=N2O+CO2	5.80E+14	-0.7	0.0
304.	NH+HNCO=NH2+NCO	3.00E+13	0.0	23700.0
305.	NH2+HNCO=NH3+NCO	1.00E+12	0.0	6955.0
306.	HO2+HNCO=NCO+H2O2	3.00E+11	0.0	29000.0
307.	NH3+HO2=NH2+H2O2	3.00E+11	0.0	22000.0
308.	NH2+NO2=N2O+H2O	2.84E+18	-2.2	0.0
309.	NH+NO2=N2O+OH	1.00E+13	0.0	0.0
310.	NH2+NH2=NH+NH3	5.00E+13	0.0	10000.0
311.	NH2+HO2=NH3+O2	4.30E+13	0.0	0.0
312.	NO2+SO2=NO+SO3	6.31E+12	0.0	27000.0
!End of Bowman's SNCR mechanism				
!Reactions of sulfur oxides				
313.	SO2+O+M=SO3+M	1.45E+16	0.0	2000.0
314.	SO2+OH+M=HSO3+M	2.12E+25	-3.3	0.0
315.	HSO3+O2=HO2+SO3	7.83E+11	0.0	656.0
316.	O+SO3=SO2+O2	1.32E+12	0.0	6100.0
!Reactions of sodium				
317.	NA2CO3=>NA2O+CO2	2.54E+06	0.0	25820.0
318.	NA2O+CO2=>NA2CO3	1.11E+05	0.0	-15000.0
319.	NA2O+H2O<=>2NAOH	9.18E+12	0.0	3120.0
320.	NA+N2O=NAO+N2	1.69E+14	0.0	3159.0
321.	NAO+H2O=NAOH+OH	1.32E+13	0.0	0.0
322.	NAO+O=NA+O2	2.23E+14	0.0	0.0
323.	NAO+NO=NA+NO2	9.04E+13	0.0	0.0
324.	NAO+H2=NAOH+H	1.25E+13	0.0	0.0
325.	NA+O2+M=NAO2+M	1.74E+21	-1.3	0.0
	H2O	Enhanced by	5.000E+00	
	CO2	Enhanced by	3.000E+00	
	CO	Enhanced by	2.000E+00	
	H2	Enhanced by	2.000E+00	
326.	NAOH+H=NA+H2O	5.00E+13	0.0	0.0
327.	NA+OH+M=NAOH+M	1.82E+21	-1.0	0.0
328.	NAO+OH=NAOH+O	2.00E+13	0.0	0.0
329.	NAO+HO2=NAOH+O2	5.00E+13	0.0	0.0
330.	NAO+H2=NA+H2O	3.13E+12	0.0	0.0

		(k = A T**b exp(-E/RT))		
REACTIONS		A	b	E
331.	NAO+CO=NA+CO2	1.00E+14	0.0	0.0
332.	H+NAO2=HO2+NA	2.00E+14	0.0	0.0
333.	NAO+H=NA+OH	2.00E+14	0.0	0.0
334.	NAO+OH=NA+HO2	3.00E+13	0.0	0.0
335.	NA+HO2=NAOH+O	1.00E+14	0.0	0.0
336.	NAO2+H=NAO+OH	5.00E+13	0.0	0.0
337.	NAO2+OH=NAOH+O2	2.00E+13	0.0	0.0
338.	NAO+HO2=NAO2+OH	5.00E+13	0.0	0.0
339.	NAO2+H=NAOH+O	1.00E+14	0.0	0.0
340.	NAO2+CO=NAO+CO2	1.00E+14	0.0	0.0
341.	NAO2+O=NAO+O2	1.00E+14	0.0	0.0
342.	NAO+NH3=NAOH+NH2	1.00E+13	0.0	0.0
343.	NAOH+SO2=NASO2+OH	1.00E+13	0.0	35400.0
344.	NA+SO2=NASO2	1.21E+14	0.0	0.0
345.	NASO2+NAO2=NA2SO4	1.00E+14	0.0	0.0
346.	NASO2+NAO=NA2SO3	1.00E+14	0.0	0.0
!Reactions of chlorine				
347.	NAO+HCL=NACL+OH	1.69E+14	0.0	0.0
348.	NA+HCL=NACL+H	2.41E+14	0.0	130.0
349.	NAOH+HCL=NACL+H2O	1.69E+14	0.0	0.0
350.	NAO2+HCL=NACL+HO2	1.39E+14	0.0	0.0
351.	CL+H2=HCL+H	1.45E+13	0.0	4370.0
352.	H+CL2=CL+HCL	8.59E+13	0.0	1170.0
353.	CL+CL+M=CL2+M	2.23E+14	0.0	-1800.0
354.	O+HCL=CL+OH	6.87E+12	0.0	6697.0
355.	CL+H2O=OH+HCL	1.68E+13	0.0	17230.0

Appendix 2. Thermodynamic database for Reaction Mechanism in Chemkin Format

Nomenclature (from Kee et al., 1991):

Thermodynamic properties for each species are calculated from polynomial fits to the specific heat at constant pressure:

$$C_{p/R} = a_1 + a_2T + a_3T^2 + a_4T^3 + a_5T^4$$

$$H_0/RT = a_1 + (a_2/2)T + (a_3/3)T^2 + (a_4/4)T^3 + (a_5/5)T^4 + (a_6/T)$$

$$S/R = a_1 \ln(T) + a_2T + (a_3/2)T^2 + (a_4/3)T^3 + (a_5/4)T^4 + a_7$$

These coefficients are stored for two temperature intervals, one between a low temperature and a common temperature, the second between the common temperature and the high temperature. The second line of the database (before any species data) contains the lowest, highest, and default common temperatures. The data for each species occupies four lines (with the line number at the right margin, in column 80) and contains the following information (see Kee et al., 1991 for detailed format information):

Line 1: Species Name
 Date (not used in the code)
 up to four atomic symbols and formula
 phase of species (S, L, or G for solid, liquid, or gas, respectively)
 low temperature
 high temperature
 common temperature (or blank for default)
 fifth atomic symbols and formula (if needed)

Line 2: Coefficients a1 through a5, for the upper temperature interval

Line 3: Coefficients a6, a7 for the upper temperature interval and
 a1, a2, a3 for the lower temperature interval

Line 4: Coefficients a4, a5, a6, a7 for the lower temperature interval

```

THERMO
300.      5000.      1000.
NA2O      81092NA  2O  1      S  0300.00  2000.00  1000.00      1
0.08804423E+02 0.03253428E-01-0.03530522E-05-0.04324117E-08 0.01394574E-11      2
-0.05257507E+06-0.04209654E+03 0.04776964E+02 0.01483269E+00-0.01052247E-03      3
0.01278469E-07 0.01046187E-10-0.05155651E+06-0.02156737E+03      4
NAO2      D=37.2NA  1O  2  0  G  300.000  2000.000  1000.00      1
.24373729D+01 .11708054D-01 -.12465450D-04 .60394798D-08 -.10877028D-11      2
-.68349080D+04 .15175355D+02 .24373729D+01 .11708054D-01 -.12465450D-04      3
.60394798D-08 -.10877028D-11 -.68349080D+04 .15175355D+02      4
HCL      42189CL  1H  1  G  300.000  2000.000  1000.00      1
.37039792D+01 -.12852596D-02 .24168090D-05 -.12493998D-08 .21730232D-12      2
-.12167451D+05 .16516317D+01 .37039792D+01 -.12852596D-02 .24168090D-05      3
-.12493998D-08 .21730232D-12 -.12167451D+05 .16516317D+01      4
CL      42189CL  1  G  300.000  2000.000  1000.00      1
.21819488D+01 .23933914D-02 -.34824719D-05 .19618096D-08 -.38542551D-12      2
.13858705D+05 .68500574D+01 .21819488D+01 .23933914D-02 -.34824719D-05      3
.19618096D-08 -.38542551D-12 .13858705D+05 .68500574D+01      4
CL2      42189CL  2  G  300.000  2000.000  1000.00      1
.33474856D+01 .35465402D-02 -.41020340D-05 .21051260D-08 -.39180420D-12      2
-.11234604D+04 .68564007D+01 .33474856D+01 .35465402D-02 -.41020340D-05      3
.21051260D-08 -.39180420D-12 -.11234604D+04 .68564007D+01      4
NASO2     EST-VZNA  1S  1O  2  OG  300.000  2000.000  1000.00      1
.10564578D+02 .12021251D-02 .23902747D-05 -.21589178D-08 .52044716D-12      2
-.49517463D+05 -.45542840D+02 .10564578D+02 .12021251D-02 .23902747D-05      3
-.21589178D-08 .52044716D-12 -.49517463D+05 -.45542840D+02      4
NA2SO4    80792NA  2O  4S  1  G  300.000  2000.000  1000.00      1
.45889397D+01 .38040129D-01 -.41096543D-04 .20017107D-07 -.36046429D-11      2
-.12705639D+06 .58915156D+01 .45889397D+01 .38040129D-01 -.41096543D-04      3
.20017107D-07 -.36046429D-11 -.12705639D+06 .58915156D+01      4
NA2SO3    BAR 77NA  2S  1O  3  OL  300.000  2000.000  1000.00      1
.21890427D+02 .00000000D+00 .00000000D+00 .00000000D+00 .00000000D+00      2
-.13847832D+06 -.11136788D+03 .21890427D+02 .00000000D+00 .00000000D+00      3
.00000000D+00 .00000000D+00 -.13847832D+06 -.11136788D+03      4
NACL      81092CL  1NA  1  G  300.000  2000.000  1000.00      1
.38609970D+01 .21586897D-02 -.25630874D-05 .13632700D-08 -.26045355D-12      2
-.23047048D+05 .50924911D+01 .38609970D+01 .21586897D-02 -.25630874D-05      3
.13632700D-08 -.26045355D-12 -.23047048D+05 .50924911D+01      4
NAOH      J12/70NA  1O  1H  100  OG  300.000  2000.000  1000.00      1
.45711116D+01 .61346093D-02 -.76237353D-05 .43706135D-08 -.89064713D-12      2
-.25359026D+05 -.95321963D-01 .45711116D+01 .61346093D-02 -.76237353D-05      3
.43706135D-08 -.89064713D-12 -.25359026D+05 -.95321963D-01      4
NA        L 4/93NA  10O  000  000  OG  300.000  2000.000  1000.00      1
.25010442D+01 .00000000D+00 .00000000D+00 .00000000D+00 .00000000D+00      2
.12157060D+05 .42385793D+01 .25010442D+01 .00000000D+00 .00000000D+00      3
.00000000D+00 .00000000D+00 .12157060D+05 .42385793D+01      4
  
```

NAO	J12/67NA	10	100	000	OG	300.000	2000.000	1000.00	1	
.36192660D+01	.29441938D-02	-.35206654D-05	.18827273D-08	-.36198896D-12					2	
.88821327D+04	.62033018D+01	.36192660D+01	.29441938D-02	-.35206654D-05					3	
.18827273D-08	-.36198896D-12	.88821327D+04	.62033018D+01						4	
NA2CO3(S)	J 3/66NA	2C	10	3	OS	300.000	2000.000	1000.00	1	
.12014036D+02	-.50536347D-02	.25519440D-04	-.13688606D-07	.27714728D-11					2	
-.13815566D+06	-.48715125D+02	.12014036D+02	-.50536347D-02	.25519440D-04					3	
-.13688606D-07	.27714728D-11	-.13815566D+06	-.48715125D+02						4	
NA2CO3(L)	J 3/66NA	2C	10	3	OL	300.000	2000.000	1000.00	1	
.22796238D+02	.00000000D+00	.00000000D+00	.00000000D+00	.00000000D+00					2	
-.14229112D+06	-.11622189D+03	.22796238D+02	.00000000D+00	.00000000D+00					3	
.00000000D+00	.00000000D+00	-.14229112D+06	-.11622189D+03						4	
NA2CO3	BENSONNA	2C	10	3	OG	300.000	2000.000	1000.00	1	
.56157861D+01	.25916438D-01	.25963740D-05	-.15866667D-07	.51192999D-11					2	
-.13627651D+06	-.21019356D+02	.56157861D+01	.25916438D-01	.25963740D-05					3	
-.15866667D-07	.51192999D-11	-.13627651D+06	-.21019356D+02						4	
HSO3	T 3/96H	1S	10	3	OG	300.000	2000.00	1000.00	1	
.29221355D+01	.24537632D-01	-.28258748D-04	.14728290D-07	-.28007910D-11					2	
-.48042084D+05	.12532987D+02	.29221355D+01	.24537632D-01	-.28258748D-04					3	
.14728290D-07	-.28007910D-11	-.48042084D+05	.12532987D+02						4	
SO2	121286S	10	2		G	0300.00	5000.00	1000.00	1	
0.05254498E+02	0.01978545E-01	0.08204226E-05	0.15763830E-09	0.11204512E-13					2	
-0.03756885E+06	-0.11460563E+01	0.02911438E+02	0.08103022E-01	0.06906710E-04					3	
0.03329015E-07	0.08777121E-11	0.03687881E+06	0.11117403E+02						4	
SO3	121286S	10	3		G	0300.00	5000.00	1000.00	1	
0.07050668E+02	0.03246560E-01	0.14088974E-05	0.02721535E-08	0.01942364E-12					2	
-0.05020667E+06	-0.11064426E+02	0.02575282E+02	0.15150916E-01	0.12298717E-04					3	
0.04240257E-07	-0.05266812E-11	0.04894410E+06	0.12195116E+02						4	
CH3O2	L184	C	1H	30	2	G	300.000	5000.00	1000.00	1
0.66812963E 01	0.80057271E-02	0.27188507E-05	0.40631365E-09	0.21927725E-13					2	
0.52621851E 03	-0.99423847E 01	0.20986490E 01	0.15786357E-01	0.75683261E-07					3	
-0.11274587E-07	0.56665133E-11	0.20695879E 04	0.15007068E 02						4	
CH3O2H	BENSON/Vit C	1H	40	2	G	300.000	2000.000	1000.00	1	
.70880631D+02	-.34336913D+00	.54005126D-03	-.32136525D-06	.65219886D-10					2	
-.24541521D+05	-.29072672D+03	.70880631D+02	-.34336913D+00	.54005126D-03					3	
-.32136525D-06	.65219886D-10	-.24541521D+05	-.29072672D+03						4	
CH2*	L S/93C	1H	2	00	00G	200.000	3500.000	1000.000	1	
2.29203842E+00	4.65588637E-03	-2.01191947E-06	4.17906000E-10	-3.39716365E-14					2	
0.9259997E+04	8.62650169E+00	4.19860411E+00	-2.36661419E-03	8.23296220E-06					3	
-6.68815981E-09	1.94314737E-12	5.04968163E+04	-7.69118967E-01	9.93967200E+03					4	
HNO2	120186H	1N	10	2	G	0200.00	6000.00	1000.00	1	
0.57900059E+01	0.36505061E-02	0.12902803E-05	0.20751067E-09	0.12300051E-13					2	
-0.11563080E+05	-0.40550308E+01	0.32100428E+01	0.81300665E-02	0.16621031E-05					3	
-0.95328431E-08	0.48700696E-11	0.10700764E+05	0.98200995E+01						4	
HNO3	121286H	1N	10	3	G	0300.00	5000.00	1000.00	1	
0.07003844E+02	0.05811493E-01	0.02333788E-04	0.04288814E-08	0.02959385E-12					2	
-0.01889952E+06	-0.10478628E+02	0.13531850E+01	0.02220024E+00	0.01978811E-03					3	
0.08773908E-07	-0.16583844E-11	0.01738562E+06	0.01851868E+03						4	
H2O2+	120186H	2O	2		G	0300.00	5000.00	1000.00	1	
0.04573167E+02	0.04336136E-01	0.14746888E-05	0.02348903E-08	0.14316536E-13					2	
0.01800696E+06	0.05011369E+01	0.03388753E+02	0.06569226E-01	0.14850125E-06					3	
-0.04625805E-07	0.02471514E-10	0.01766314E+06	0.06785363E+02						4	
O	L 1/90O	1	00	00	00G	200.000	3500.000	1000.000	1	
2.56942078E+00	-8.59741137E-05	4.19484589E-08	-1.00177799E-11	1.22833691E-15					2	
2.92175791E+04	4.78433864E+00	3.16826710E+00	-3.27931884E-03	6.64306396E-06					3	
-6.12806624E-09	2.11265971E-12	2.91222592E+04	2.05193346E+00	6.72540300E+03					4	
O2	TPIS89O	2	00	00	00G	200.000	3500.000	1000.000	1	
3.28253784E+00	1.48308754E-03	-7.57966669E-07	2.09470555E-10	-2.16717794E-14					2	
-1.08845772E+03	5.45323129E+00	3.78245636E+00	-2.99673416E-03	9.84730201E-06					3	
-9.68129509E-09	3.24372837E-12	-1.06394356E+03	3.65767573E+00	8.68010400E+03					4	
H	L 7/88H	1	00	00	00G	200.000	3500.000	1000.000	1	
2.50000001E+00	-2.30842973E-11	1.61561948E-14	-4.73515235E-18	4.98197357E-22					2	
2.54736599E+04	-4.46682914E-01	2.50000000E+00	7.05332819E-13	-1.99591964E-15					3	
2.30081632E-18	-9.27732332E-22	2.54736599E+04	-4.46682853E-01	6.19742800E+03					4	
H2	TPIS78H	2	00	00	00G	200.000	3500.000	1000.000	1	
3.33727920E+00	-4.94024731E-05	4.99456778E-07	-1.79566394E-10	2.00255376E-14					2	
-9.50158922E+02	-3.20502331E+00	2.34433112E+00	7.98052075E-03	-1.94781510E-05					3	
2.01572094E-08	-7.37611761E-12	-9.17935173E+02	6.83010238E-01	8.46810200E+03					4	

OH	RUS 780	1H	1	00	00G	200.000	3500.000	1000.000	1
3.09288767E+00	5.48429716E-04	1.26505228E-07	-8.79461556E-11	1.17412376E-14					2
3.85865700E+03	4.47669610E+00	3.99201543E+00	-2.40131752E-03	4.61793841E-06					3
-3.88113333E-09	1.36411470E-12	3.61508056E+03	-1.03925458E-01	8.81310600E+03					4
H2O	L 8/89H	20	1	00	00G	200.000	3500.000	1000.000	1
3.03399249E+00	2.17691804E-03	-1.64072518E-07	-9.70419870E-11	1.68200992E-14					2
-3.00042971E+04	4.96677010E+00	4.19864056E+00	-2.03643410E-03	6.52040211E-06					3
-5.48797062E-09	1.77197817E-12	-3.02937267E+04	-8.49032208E-01	9.90409200E+03					4
HO2	L 5/89H	10	2	00	00G	200.000	3500.000	1000.000	1
4.01721090E+00	2.23982013E-03	-6.33658150E-07	1.14246370E-10	-1.07908535E-14					2
1.11856713E+02	3.78510215E+00	4.30179801E+00	-4.74912051E-03	2.11582891E-05					3
-2.42763894E-08	9.29225124E-12	2.94808040E+02	3.71666245E+00	1.00021620E+04					4
H2O2	L 7/88H	20	2	00	00G	200.000	3500.000	1000.000	1
4.16500285E+00	4.90831694E-03	-1.90139225E-06	3.71185986E-10	-2.87908305E-14					2
-1.78617877E+04	2.91615662E+00	4.27611269E+00	-5.42822417E-04	1.67335701E-05					3
-2.15770813E-08	8.62454363E-12	-1.77025821E+04	3.43505074E+00	1.11588350E+04					4
C	L11/88C	1	00	00	00G	200.000	3500.000	1000.000	1
2.49266888E+00	4.79889284E-05	-7.24335020E-08	3.74291029E-11	-4.87277893E-15					2
8.54512953E+04	4.80150373E+00	2.55423955E+00	-3.21537724E-04	7.33792245E-07					3
-7.32234889E-10	2.66521446E-13	8.54438832E+04	4.53130848E+00	6.53589500E+03					4
CH	TPIS79C	1H	1	00	00G	200.000	3500.000	1000.000	1
2.87846473E+00	9.70913681E-04	1.44445655E-07	-1.30687849E-10	1.76079383E-14					2
7.10124364E+04	5.48497999E+00	3.48981665E+00	3.23835541E-04	-1.68899065E-06					3
3.16217327E-09	-1.40609067E-12	7.07972934E+04	2.08401108E+00	8.62500000E+03					4
CH2	L S/93C	1H	2	00	00G	200.000	3500.000	1000.000	1
2.87410113E+00	3.65639292E-03	-1.40894597E-06	2.60179549E-10	-1.87727567E-14					2
4.62636040E+04	6.17119324E+00	3.76267867E+00	9.68872143E-04	2.79489841E-06					3
-3.85091153E-09	1.68741719E-12	4.60040401E+04	1.56253185E+00	1.00274170E+04					4
CH2(S)	L S/93C	1H	2	00	00G	200.000	3500.000	1000.000	1
2.29203842E+00	4.65588637E-03	-2.01191947E-06	4.17906000E-10	-3.39716365E-14					2
5.09259997E+04	8.62650169E+00	4.19860411E+00	-2.36661419E-03	8.23296220E-06					3
-6.68815981E-09	1.94314737E-12	5.04968163E+04	-7.69118967E-01	9.93967200E+03					4
CH3	L11/89C	1H	3	00	00G	200.000	3500.000	1000.000	1
2.28571772E+00	7.23990037E-03	-2.98714348E-06	5.95684644E-10	-4.67154394E-14					2
1.67755843E+04	8.48007179E+00	3.67359040E+00	2.01095175E-03	5.73021856E-06					3
-6.87117425E-09	2.54385734E-12	1.64449988E+04	1.60456433E+00	1.03663400E+04					4
CH4	L 8/88C	1H	4	00	00G	200.000	3500.000	1000.000	1
7.46514950E-02	1.33909467E-02	-5.73285809E-06	1.22292535E-09	-1.01815230E-13					2
-9.46834459E+03	1.84373180E+01	5.14987613E+00	-1.36709788E-02	4.91800599E-05					3
-4.84743026E-08	1.66693956E-11	-1.02466476E+04	-4.64130376E+00	1.00161980E+04					4
CO	TPIS79C	10	1	00	00G	200.000	3500.000	1000.000	1
2.71518561E+00	2.06252743E-03	-9.98825771E-07	2.30053008E-10	-2.03647716E-14					2
-1.41518724E+04	7.81868772E+00	3.57953347E+00	-6.10353680E-04	1.01681433E-06					3
9.07005884E-10	-9.04424499E-13	-1.43440860E+04	3.50840928E+00	8.67100000E+03					4
CO2	L 7/88C	10	2	00	00G	200.000	3500.000	1000.000	1
3.85746029E+00	4.41437026E-03	-2.21481404E-06	5.23490188E-10	-4.72084164E-14					2
-4.87591660E+04	2.27163806E+00	2.35677352E+00	8.98459677E-03	7.12356269E-06					3
-1.04532012E-09	-1.43699548E-13	-4.83719697E+04	9.90105222E+00	9.36546900E+03					4
HCO	L12/89H	1C	10	1	00G	200.000	3500.000	1000.000	1
2.77217438E+00	4.95695526E-03	-2.48445613E-06	5.89161778E-10	-5.33508711E-14					2
4.01191815E+03	9.79834492E+00	4.22118584E+00	-3.24392532E-03	1.37799446E-05					3
-1.33144093E-08	4.33768865E-12	3.83956496E+03	3.39437243E+00	9.98945000E+03					4
CH2O	L 8/88H	2C	10	1	00G	200.000	3500.000	1000.000	1
1.76069008E+00	9.20000082E-03	-4.42258813E-06	1.00641212E-09	-8.83855640E-14					2
-1.39958323E+04	1.36563230E+01	4.79372315E+00	-9.90833369E-03	3.73220008E-05					3
-3.79285261E-08	1.31772652E-11	-1.43089567E+04	6.02812900E-01	1.00197170E+04					4
CH2OH	GUNL93C	1H	30	1	00G	200.000	3500.000	1000.000	1
3.69266569E+00	8.64576797E-03	-3.75101120E-06	7.87234636E-10	-6.48554201E-14					2
-3.24250627E+03	5.81043215E+00	3.86388918E+00	5.59672304E-03	5.93271791E-06					3
-1.04532012E-08	4.36967278E-12	-3.19391367E+03	5.47302243E+00	1.18339080E+04					4
CH3O	L12/88C	1H	30	1	00G	300.000	3000.000	1000.000	1
0.03770799E+02	0.07871497E-01	-0.02656384E-04	0.03944431E-08	-0.02112616E-12					2
0.12783252E+03	0.02929575E+02	0.02106204E+02	0.07216595E-01	0.05338472E-04					3
-0.07377636E-07	0.02075610E-10	0.09786011E+04	0.13152177E+02						4
CH3OH	L 8/88C	1H	40	1	00G	200.000	3500.000	1000.000	1
1.78970791E+00	1.40938292E-02	-6.36500835E-06	1.38171085E-09	-1.17060220E-13					2
-2.53748747E+04	1.45023623E+01	5.71539582E+00	-1.52309129E-02	6.52441155E-05					3
-7.10806889E-08	2.61352698E-11	-2.56427656E+04	-1.50409823E+00	1.14352770E+04					4
C2H	L 1/91C	2H	1	00	00G	200.000	3500.000	1000.000	1
3.16780652E+00	4.75221902E-03	-1.83787077E-06	3.04190252E-10	-1.77232770E-14					2
6.71210650E+04	6.63589475E+00	2.88965733E+00	1.34099611E-02	-2.84769501E-05					3
2.94791045E-08	-1.09331511E-11	6.68393932E+04	6.22296438E+00	1.04544720E+04					4
C2H2	L 1/91C	2H	2	00	00G	200.000	3500.000	1000.000	1
4.14756964E+00	5.96166664E-03	-2.37294852E-06	4.67412171E-10	-3.61235213E-14					2
2.59359992E+04	-1.23028121E+00	8.08681094E-01	2.33615629E-02	-3.55171815E-05					3
2.80152437E-08	-8.50072974E-12	2.64289807E+04	1.39397051E+01	1.00058390E+04					4
C2H3	L 2/92C	2H	3	00	00G	200.000	3500.000	1000.000	1
3.01672400E+00	1.03302292E-02	-4.68082349E-06	1.01763288E-09	-8.62607041E-14					2
3.46128739E+04	7.78732378E+00	3.21246645E+00	1.51479162E-03	2.59209412E-05					3
-3.57657847E-08	1.47150873E-11	3.48598468E+04	8.51054025E+00	1.05750490E+04					4

C2H4	L 1/91C	2H	4	00	00G	200.000	3500.000	1000.000	1
2.03611116E+00	1.46454151E-02	-6	71077915E-06	1.47222923E-09	-1	25706061E-13			2
4.93988614E+03	1.03053693E+01	3	95920148E+00	-7.57052247E-03	5	70990292E-05			3
-6.91588753E-08	2.69884373E-11	5	08977593E+03	4.09733096E+00	1	05186890E+04			4
C2H5	L12/92C	2H	5	00	00G	200.000	3500.000	1000.000	1
1.95465642E+00	1.73972722E-02	-7	98206668E-06	1.75217689E-09	-1	49641576E-13			2
1.28575200E+04	1.34624343E+01	4	30646568E+00	-4.18658892E-03	4	97142807E-05			3
-5.99126606E-08	2.30509004E-11	1	28416265E+04	4.70720924E+00	1	21852440E+04			4
C2H6	L 8/88C	2H	6	00	00G	200.000	3500.000	1000.000	1
1.07188150E+00	2.16852677E-02	-1	00256067E-05	2.21412001E-09	-1	90002890E-13			2
-1.14263932E+04	1.51156107E+01	4	29142492E+00	-5.50154270E-03	5	99438288E-05			3
-7.08466285E-08	2.68685771E-11	-1	15222055E+04	2.66682316E+00	1	18915940E+04			4
CH2CO	L 5/90C	2H	20	1	00G	200.000	3500.000	1000.000	1
4.51129732E+00	9.00359745E-03	-4	16939635E-06	9.23345882E-10	-7	94838201E-14			2
-7.55105311E+03	6.32247205E-01	2	13583630E+00	1.81188721E-02	-1	73947474E-05			3
9.34397568E-09	-2.01457615E-12	-7	04291804E+03	1.22156480E+01	1	17977430E+04			4
HCCO	SRIC91H	1C	20	1	00G	300.000	4000.000	1000.000	1
0.56282058E+01	0.40853401E-02	-0	15934547E-05	0.28626052E-09	-0	19407832E-13			2
0.19327215E+05	-0.39302595E+01	0	22517214E+01	0.17655021E-01	-0	23729101E-04			3
0.17275759E-07	-0.50664811E-11	0	20059449E+05	0.12490417E+02					4
HCCOH	SR191C	20	1H	2	00G	300.000	5000.000	1000.000	1
0.59238291E+01	0.67923600E-02	-0	25658564E-05	0.44987841E-09	-0	29940101E-13			2
0.72646260E+04	-0.76017742E+01	0	12423733E+01	0.31072201E-01	-0	50866864E-04			3
0.43137131E-07	-0.14014594E-10	0	80316143E+04	0.13874319E+02					4
H2CN	41687H	2C	1N	1	00G	300.000	4000.000	1000.000	1
0.52097030E+01	0.29692911E-02	-0	28555891E-06	-0.16355500E-09	0	30432589E-13			2
0.27677109E+05	-0.44444780E+01	0	28516610E+01	0.56952331E-02	0	10711400E-05			3
-0.16226120E-08	-0.23511081E-12	0	28637820E+05	0.89927511E+01	0	00000000E+00			4
HCN	L 7/88H	1C	1N	1	00G	200.000	6000.000	1000.000	1
0.38022392E+01	0.31464228E-02	-0	10632185E-05	0.16619757E-09	-0	97997570E-14			2
0.14910512E+05	0.15754601E+01	0	22589886E+01	0.10051170E-01	-0	13351763E-04			3
0.10092349E-07	-0.30089028E-11	0	15215853E+05	0.89164419E+01	0	16236675E+05			4
HNO	And93 H	1N	10	1	00G	200.000	6000.000	1000.000	1
0.29792509E+01	0.34944059E-02	-0	78549778E-06	0.57479594E-10	-0	19335916E-15			2
0.11750582E+05	0.86063728E+01	0	45334916E+01	-0.56696171E-02	0	18473207E-04			3
-0.17137094E-07	0.55454573E-11	0	11548297E+05	0.17498417E+01	0	12271667E+05			4
N	L 6/88N	1	00	00	00G	200.000	6000.000	1000.000	1
0.24159429E+01	0.17489065E-03	-0	11902369E-06	0.30226245E-10	-0	20360982E-14			2
0.56133773E+05	0.46496096E+01	0	25000000E+01	0.00000000E+00	0	00000000E+00			3
0.00000000E+00	0.00000000E+00	0	56104637E+05	0.41939087E+01	0	56850012E+05			4
NNH	T07/93N	2H	1	00	00G	200.000	6000.000	1000.000	1
0.37667544E+01	0.28915082E-02	-0	10416620E-05	0.16842594E-09	-0	10091896E-13			2
0.28650697E+05	0.44705067E+01	0	43446927E+01	-0.48497072E-02	0	20059459E-04			3
-0.21726464E-07	0.79469539E-11	0	28791973E+05	0.29779410E+01	0	30009828E+05			4
N2O	L 7/88N	20	1	00	00G	200.000	6000.000	1000.000	1
0.48230729E+01	0.26270251E-02	-0	95850874E-06	0.16000712E-09	-0	97752303E-14			2
0.80734048E+04	-0.22017207E+01	0	22571502E+01	0.11304728E-01	-0	13671319E-04			3
0.96819806E-08	-0.29307182E-11	0	87417744E+04	0.10757992E+02	0	98141680E+04			4
NH	And94 N	1H	1	00	00G	200.000	6000.000	1000.000	1
0.27836928E+01	0.13298430E-02	-0	42478047E-06	0.78348501E-10	-0	55044470E-14			2
0.42120848E+05	0.57407799E+01	0	34929085E+01	0.31179198E-03	-0	14890484E-05			3
0.24816442E-08	-0.10356967E-11	0	41880629E+05	0.18483278E+01	0	40758266E+05			4
NH2	And89 N	1H	2	00	00G	200.000	6000.000	1000.000	1
0.28347421E+01	0.32073082E-02	-0	93390804E-06	0.13702953E-09	-0	79206144E-14			2
0.22171957E+05	0.65204163E+01	0	42040029E+01	-0.21061385E-02	0	71068348E-05			3
-0.56115197E-08	0.16440717E-11	0	21885910E+05	-0.14184248E+00	0	22851617E+05			4
NH3	J 6/77N	1H	3	00	00G	200.000	6000.000	1000.000	1
0.26344521E+01	0.56662560E-02	-0	17278676E-05	0.23867161E-09	-0	12578786E-13			2
-0.65446958E+04	0.65662928E+01	0	42860274E+01	-0.46605230E-02	0	21718513E-04			3
-0.22808887E-07	0.82638046E-11	-0	67417285E+04	-0.62537277E+00	-0	55202866E+04			4
NO	RUS 78N	10	1	00	00G	200.000	6000.000	1000.000	1
0.32606056E+01	0.11911043E-02	-0	42917048E-06	0.69457669E-10	-0	40336099E-14			2
0.99209746E+04	0.63693027E+01	0	42184763E+01	-0.46389760E-02	0	11041022E-04			3
-0.93361354E-08	0.28035770E-11	0	98446230E+04	0.22808464E+01	0	10976594E+05			4
NO2	L 7/88N	10	2	00	00G	200.000	6000.000	1000.000	1
0.48847542E+01	0.21723956E-02	-0	82806906E-06	0.15747510E-09	-0	10510895E-13			2
0.23164983E+04	-0.11741695E+00	0	39440312E+01	-0.15854290E-02	0	16657812E-04			3
-0.20475426E-07	0.78350564E-11	0	28966179E+04	0.63119917E+01	0	41124702E+04			4
HCNO	BDEA94H	1N	1C	10	1G	300.000	5000.000	1382.000	1
6.59860456E+00	3.02778626E-03	-1	07704346E-06	1.71666528E-10	-1	01439391E-14			2
1.79661339E+04	-1.03306599E+01	2	64727989E+00	1.27505342E-02	-1	04794236E-05			3
4.41432836E-09	-7.57521466E-13	1	92990252E+04	1.07332972E+01					4
HOCN	BDEA94H	1N	1C	10	1G	300.000	5000.000	1368.000	1
5.89784885E+00	3.16789393E-03	-1	11801064E-06	1.77243144E-10	-1	04339177E-14			2
-3.70653331E+03	-6.18167825E+00	3	78604952E+00	6.88667922E-03	-3	21487864E-06			3
5.17195767E-10	1.19360788E-14	-2	82698400E+03	5.63292162E+00					4
HNCO	BDEA94H	1N	1C	10	1G	300.000	5000.000	1478.000	1
6.22395134E+00	3.17864004E-03	-1	09378755E-06	1.70735163E-10	-9	95021955E-15			2
-1.66599344E+04	-8.38224741E+00	3	63096317E+00	7.30282357E-03	-2	28050003E-06			3
-6.61271298E-10	3.62235752E-13	-1	55873636E+04	6.19457727E+00					4

NCO	EA 93 N	1C	10	1	00G	200.000	6000.000	1000.000	1
	0.51521845E+01	0.23051761E-02	-0.88033153E-06	0.14789098E-09	-0.90977996E-14				2
	0.14004123E+05	-0.25442660E+01	0.28269308E+01	0.88051688E-02	-0.83866134E-05				3
	0.48016964E-08	-0.13313595E-11	0.14682477E+05	0.95504646E+01	0.21347373E+05				4
CN	HBH92 C	1N	1	00	00G	200.000	6000.000	1000.000	1
	0.37459805E+01	0.43450775E-04	0.29705984E-06	-0.68651806E-10	0.44134173E-14				2
	0.51536188E+05	0.27867601E+01	0.36129351E+01	-0.95551327E-03	0.21442977E-05				3
	-0.31516323E-09	-0.46430356E-12	0.51708340E+05	0.39804995E+01	0.52954172E+05				4
HCNN	SRI/94C	1N	2H	1	00G	300.000	5000.000	1000.000	1
	0.58946362E+01	0.39895959E-02	-0.15982380E-05	0.29249395E-09	-0.20094686E-13				2
	0.53452941E+05	-0.51030502E+01	0.25243194E+01	0.15960619E-01	-0.18816354E-04				3
	0.12125540E-07	-0.32357378E-11	0.54261984E+05	0.11675870E+02					4
N2	121286N	2			00G	300.000	5000.000	1000.000	1
	0.02926640E+02	0.14879768E-02	-0.05684760E-05	0.10097038E-09	-0.06753351E-13				2
	-0.09227977E+04	0.05980528E+02	0.03298677E+02	0.14082404E-02	-0.03963222E-04				3
	0.05641515E-07	-0.02444854E-10	-0.10208999E+04	0.03950372E+02					4
AR	120186AR	1			00G	300.000	5000.000	1000.000	1
	0.02500000E+02	0.00000000E+00	0.00000000E+00	0.00000000E+00	0.00000000E+00				2
	-0.07453750E+04	0.04366000E+02	0.02500000E+02	0.00000000E+00	0.00000000E+00				3
	0.00000000E+00	0.00000000E+00	-0.07453750E+04	0.04366000E+02					4
N2H2	121286N	2H	2		00G	300.000	5000.000	1000.000	1
	0.03371185E+02	0.06039968E-01	-0.02303853E-04	0.04062789E-08	-0.02713144E-12				2
	0.02418172E+06	0.04980585E+02	0.16179994E+01	0.13063122E-01	-0.01715711E-03				3
	0.16056079E-07	-0.06093638E-10	0.02467526E+06	0.13794670E+02					4
C2N2	121286C	2N	2		00G	300.000	5000.000	1000.000	1
	0.06548002E+02	0.03984707E-01	-0.16342164E-05	0.03038596E-08	-0.02111069E-12				2
	0.03490716E+06	-0.09735790E+02	0.04265459E+02	0.11922569E-01	-0.13420142E-04				3
	0.09192297E-07	-0.02778941E-10	0.03547887E+06	0.01713212E+02					4
H2NO	102290H	2N	10	1	00G	300.000	4000.000	1500.000	1
	0.05673346E+02	0.02298837E-01	-0.01774446E-05	-0.01103482E-08	0.01859762E-12				2
	0.05569325E+05	-0.06153540E+02	0.02530590E+02	0.08596035E-01	-0.05471030E-04				3
	0.02276249E-07	-0.04648073E-11	0.06868030E+05	0.01126651E+03					4
END									

Appendix 3. Thermodynamic database for sodium compounds.

(Heats of formation, entropies, and thermal conductivities at different temperatures in kcal/cal/mol/K Units)

SPECIES	HF(298)	S (298)	CP300	CP500	CP800	CP1000	CP1500	CP2000	COMMENTS
ELEMENTS									
Na2CO3	-265.20	37.14	26.31	34.89	43.69	46.46	45.11	45.33	BENSON
NA 2 C 1 O 3		0 G							
NAO2	-11.30	63.69	9.90	11.65	12.86	13.18	13.57	13.72	D=37.2
NA 1 O 2		0 G							
NASO2	-92.00	30.00	22.03	22.90	24.17	24.88	26.02	27.00	EST-VZ
NA 1 S 1 O 2		0 G							
Na	25.64	36.74	4.97	4.97	4.97	4.97	4.97	4.97	L 4/93
NA 1.	0.	0. G							
Na+	145.63	35.36	4.97	4.97	4.97	4.97	4.97	4.97	J12/83
NA 1. E -1.	0.	0. G							
NaAlF4	-439.99	82.44	24.91	28.56	30.37	30.86	31.36	31.58	J12/79
NA 1. AL 1. F 4.		0. G							
NaBO2	-155.00	68.66	13.96	16.07	17.72	18.32	19.06	19.43	J 6/71
NA 1. B 1. O 2.		0. G							
NaBr	-34.40	57.65	8.69	8.92	9.04	9.10	9.21	9.31	J 9/64
NA 1. BR 1.	0.	0. G							
NaCN	22.53	58.17	12.01	12.71	13.40	13.75	14.26	14.53	J3/66
NA 1. C 1. N 1.		0. G							
NaCl	-43.36	54.92	8.56	8.85	9.00	9.06	9.17	9.26	J12/64
NA 1. CL 1.	0.	0. G							
NaF	-69.42	52.01	8.19	8.68	8.92	9.01	9.14	9.25	J12/68
NA 1. F 1.	0.	0. G							
NaF2-	-160.00	59.92	13.14	14.13	14.57	14.69	14.80	14.85	J12/68
NA 1. F 2. E 1.		0. G							
NaH	29.70	45.02	7.24	7.91	8.54	8.77	9.09	9.30	J 3/63
NA 1. H 1.	0.	0. G							
NaI	-21.30	59.52	8.77	8.95	9.06	9.12	9.23	9.34	L 6/72
NA 1. I 1.	0.	0. G							
NaO	20.00	54.77	8.41	8.80	9.00	9.08	9.21	9.33	J12/67
NA 1. O 1.	0.	0. G							
NaO-	-29.00	51.98	8.39	8.79	9.00	9.08	9.22	9.34	J12/67
NA 1. O 1. E 1.		0. G							
NaOH	-47.26	54.60	11.59	12.39	12.82	13.07	13.63	14.03	J12/70
NA 1. O 1. H 1.		0. G							
NaOH+	162.00	57.99	11.80	12.48	12.86	13.11	13.66	14.05	J12/71
NA 1. O 1. H 1. E -1.		0. G							
Na2	33.95	55.03	8.98	9.16	9.38	9.41	8.43	7.91	J12/83
NA 2.	0.	0. G							
Na2C2N2	-2.10	82.97	25.78	27.35	28.77	29.48	30.50	31.05	J 3/66
NA 2. C 2. N 2.		0. G							
Na2CL2	-135.29	77.78	18.85	19.49	19.72	19.77	19.83	19.85	J12/64
NA 2. CL 2.	0.	0. G							
Na2F2	-202.30	68.69	16.99	18.69	19.38	19.56	19.72	19.80	J12/68
NA 2. F 2.	0.	0. G							
Na2O	-9.90	62.43	13.27	14.19	14.60	14.71	14.81	14.86	L10/74
NA 2. O 1.	0.	0. G							
Na2O2H2	-145.20	73.47	18.99	22.24	25.16	26.38	28.36	29.56	J12/70
NA 2. O 2. H 2.		0. G							
Na2SO4	-247.04	82.90	25.32	31.12	34.64	35.67	36.76	37.25	J 6/78
NA 2. S 1. O 4.		0. G							
Na(cr)	.00	12.26	6.76	11.32	45.19	100.09	.00	.00	CODA89
NA 1.	0.	0. C							
Na(L)	.58	13.80	7.77	7.32	6.92	6.88	7.62	9.58	CODA89
NA 1.	0.	0. C							
NaALO2(b)	-271.02	15.93	21.70	22.39	23.60	24.45	26.59	28.62	J 3/63
NA 1. AL 1. O 2.		0. C							
NaBr(s)	-86.38	20.75	12.31	13.11	13.99	14.60	16.57	19.63	J 9/64
NA 1. BR 1.	0.	0. C							
NaBr(L)	-81.10	24.94	14.90	14.90	14.90	14.90	14.90	14.90	J 9/64
NA 1. BR 1.	0.	0. C							
NaCN(s)	-21.67	28.31	16.39	16.44	16.51	16.37	11.78	-10.59	J 3/66
NA 1. C 1. N 1.		0. C							
NaCN(L)	-20.94	28.20	19.00	19.00	19.00	19.00	19.00	19.00	J 3/66
NA 1. C 1. N 1.		0. C							
NaCL(s)	-98.26	17.24	12.08	12.88	14.17	15.50	12.44	-23.81	J 9/64
NA 1. CL 1.	0.	0. C							
NaCL(L)	-95.37	16.07	21.34	19.72	17.95	17.14	16.04	15.79	J 9/64
NA 1. CL 1.	0.	0. C							
NaF(s)	-137.52	12.25	11.23	12.26	13.31	14.22	17.00	13.15	J12/68
NA 1. F 1.	0.	0. C							
NaF(L)	-134.21	10.30	20.07	19.14	18.00	17.41	16.38	15.85	J12/68
NA 1. F 1.	0.	0. C							
NaI(s)	-68.80	23.54	12.50	13.16	13.98	14.51	15.46	13.65	J 9/63

NA 4. V 2. O 7.	0. S										
NA6SI207(S)-856.30	83.32	73.34	83.73	94.75	101.60	118.20	134.60				BAR 73
NA 6. SI 2. O 7.	0. S										
NA6V208(S)-845.10	90.63	82.69	94.62	101.35	104.62	111.51	117.91				BAR 73
NA 6. V 2. O 8.	0. S										

Appendix B. Reaction Mechanism of C-H-O-N Species in Chemkin Format

ELEMENTS

H O C N AR

END

SPECIES

NO O2 CO CO2 CH4 NH3

C2H6 NO2 N2O H2O C2H4 C2H2

HCN N2 AR

H O OH HO2 H2 H2O2

CH2O HCO

CH3 CH2 CH2(S) CH C

CH3OH CH3O CH2OH

C2H5 C2H3 C2H C2

CH3HCO CH2HCO CH3CO C2H2OH OCHCHO CH2CO HCCOH HCCO C2O

C2H5CHO C2H5CO

NO3 HNO HONO H2NO

NH2 NH N N2H2 NNH

CN NCO HNCO HOCN HCNO C2N2 NCN CH3CN CH2CN H2CN

END

REACTIONS

! $k = A \times T^n \exp(-E/RT)$

! Units: A mole-cm-sec-K; E cal/mole

! *****

! * H2/O2 Subset *

! *****

! **Reactions**

	A	n	E
O+OH=O2+H	2.0E14	-0.40	0
O+H2=OH+H	5.0E04	2.67	6290
OH+H2=H2O+H	2.1E08	1.52	3450
2OH=O+H2O	4.3E03	2.70	-2486
H+H+M=H2+M	1.0E18	-1.00	0
H2O/0/			
H+H+H2O=H2+H2O	6.0E19	-1.25	0
H+O+M=OH+M	6.2E16	-0.60	0
H2O/5/			
H+OH+M=H2O+M	1.6E22	-2.00	0
H2O/5/			
O+O+M=O2+M	1.9E13	0.00	-1788
H2O/5/			
H+O2+M=HO2+M	2.1E18	-1.00	0
H2O/10/ N2/0/			
H+O2+N2 = HO2+N2	6.7E19	-1.42	0
H+HO2=H2+O2	4.3E13	0.00	1411
H+HO2=2OH	1.7E14	0.00	874
H+HO2=O+H2O	3.0E13	0.0	1721
O+HO2=O2+OH	3.3E13	0.0	0
OH+HO2=H2O+O2	1.9E16	-1.0	0
HO2+HO2=H2O2+O2	4.2E14	0.0	11982
DUP			
HO2+HO2=H2O2+O2	1.3E11	0.0	-1629
DUP			
H2O2+M=OH+OH+M	1.3E17	0.0	45500
H2O/5/			
H2O2+H=HO2+H2	1.7E12	0.0	3755

Reactions	A	n	E
H2O2+H=OH+H2O	1.0E13	0.0	3576
H2O2+O=OH+HO2	6.6E11	0.0	3974
H2O2+OH=H2O+HO2	7.8E12	0.0	1330
DUP			
H2O2+OH=H2O+HO2	5.8E14	0.0	9560
DUP			
!			
! *****			
! * CO Subset *			
! *****			
!			
CO+O+M=CO2+M	6.2E14	0.0	3000
H2O/5/			
CO+OH=CO2+H	1.5E07	1.3	-758
CO+O2=CO2+O	2.5E12	0.0	47700
HO2+CO=CO2+OH	5.8E13	0.0	22934
!			
! *****			
! * CH2O/HCO Subset *			
! *****			
!			
CH2O+M=HCO+H+M	3.3E16	0.0	81000
H2O/5/			
CH2O+H = HCO+H2	1.3E08	1.62	2166
CH2O+O=HCO+OH	1.8E13	0.00	3080
CH2O+OH=HCO+H2O	3.4E09	1.18	-447
CH2O+HO2 = HCO+H2O2	3.0E12	0.00	13000
CH2O+O2 = HCO+HO2	6.0E13	0.00	40660
HCO+M=H+CO+M	1.9E17	-1.0	17000
H2O/5/			
HCO+H=CO+H2	1.2E13	0.25	0
HCO+O=CO+OH	3.0E13	0.000	0
HCO+O=CO2+H	3.0E13	0.000	0
HCO+OH=H2O+CO	1.0E14	0.00	0
HCO+O2=HO2+CO	7.6E12	0.0	400
!			
! *****			
! * CH4/CH3/CH2/CH/C Subset *			
! *****			
!			
CH3+H(+M)=CH4(+M)	1.3E16	-0.63	383
LOW/1.75E33 -4.76 2440.0/			
TROE/0.783 74.0 2941.0 6964.0/			
H2O/8.57/ N2/1.43/			
CH4+H=CH3+H2	1.3E04	3.00	8040
CH4+O=CH3+OH	1.0E09	1.5	8600
CH4+OH=CH3+H2O	1.6E06	2.10	2460
CH4+HO2=CH3+H2O2	1.8E11	0.00	18700
CH4+O2=CH3+HO2	7.9E13	0.00	56000
CH3+H=CH2+H2	9.0E13	0.00	15100
CH2(S)+H2=CH3+H	7.2E13	0.0	0
CH3+O=CH2O+H	8.4E13	0.0	0
CH3+OH=CH2+H2O	7.5E06	2.0	5000
CH2(S)+H2O=CH3+OH	3.0E15	-0.6	0
CH2OH+H=CH3+OH	1.0E14	0.0	0
CH3O+H=CH3+OH	1.0E14	0.0	0

Reactions	A	n	E
CH3+OH(+M)=CH3OH(+M) LOW/1.89E38 -6.3 3100/ TROE/0.2105 83.5 5398 8370/ N2/1.43/ H2O/8.58/	6.3E13	0.0	0
CH3+HO2 = CH3O+OH	8.0E12	0.00	0
CH3+O2=CH3O+O	2.9E13	0.0	30480
CH3+O2=CH2O+OH	1.9E12	0.0	20315
CH3+CH3(+M)=C2H6(+M) LOW /1.26E50 -9.67 6220/ TROE/ 0.5325 151 1038 4970 / N2/1.43/ H2O/8.59/ H2/2/ CO/2/ CO2/3/	2.1E16	-0.97	620
CH3+CH2O = CH4+HCO	7.8E-8	6.10	1967
CH3+HCO = CH4+CO	1.2E14	0.00	0
CH2+H=CH+H2	1.0E18	-1.56	0
CH2+O=CO+H+H	5.0E13	0.0	0
CH2+O=CO+H2	3.0E13	0.0	0
CH2+OH=CH+H2O	1.1E07	2.0	3000
CH2+OH=CH2O+H	2.5E13	0.0	0
CH2+O2=CO+H2O	2.2E22	-3.3	2867
CH2+O2=CO2+H+H	3.3E21	-3.3	2867
CH2+O2=CH2O+O	3.3E21	-3.3	2867
CH2+O2=CO2+H2	2.6E21	-3.3	2867
CH2+O2=CO+OH+H	1.6E21	-3.3	2867
CH2+CO2=CH2O+CO	1.1E11	0.0	1000
CH2+CH4 = CH3+CH3	4.3E12	0.0	10030
CH2+CH3=C2H4+H	4.2E13	0.0	0
CH2+CH2=C2H2+H+H	4.0E13	0.0	0
CH2+HCCO=C2H3+CO	3.0E13	0.00	0
CH2(S)+M=CH2+M H/0/ H2O/0/ N2/0/ AR/0/	1.0E13	0.0	0
CH2(S)+N2=CH2+N2	1.3E13	0.0	430
CH2(S)+AR=CH2+AR	1.5E13	0.0	884
CH2(S)+H=CH2+H	2.0E14	0.0	0
CH2(S)+H2O=CH2+H2O	3.0E13	0.0	0
CH2(S)+H=CH+H2	3.0E13	0.0	0
CH2(S)+O=CO+H+H	3.0E13	0.0	0
CH2(S)+OH=CH2O+H	3.0E13	0.0	0
CH2(S)+O2=CO+OH+H	7.0E13	0.0	0
CH2(S)+CO2=CH2O+CO	3.0E12	0.0	0
CH2(S)+CH4=CH3+CH3	4.3E13	0.0	0
CH2(S)+CH3=C2H4+H	2.0E13	0.0	0
CH2(S)+CH2CO=C2H4+CO	1.6E14	0.0	0
CH2(S)+C2H6=CH3+C2H5	1.2E+14	0.0	0
CH+H=C+H2	1.5E14	0.0	0
CH+O=CO+H	5.7E13	0.0	0
CH+OH=HCO+H	3.0E13	0.0	0
CH+OH=C+H2O	4.0E7	2.0	3000
CH+O2=HCO+O	3.3E13	0.0	0
CH+H2O=CH2O+H	5.7E12	0.0	-751
CH+CO2=HCO+CO	3.4E12	0.0	690
CH+CH4=C2H4+H	6.0E13	0.0	0
CH+CH3=C2H3+H	3.0E13	0.0	0
CH+CH2=C2H2+H	4.0E13	0.0	0
CH+CH2O=CH2CO+H	9.5E13	0.00	-515
CH+HCCO=C2H2+CO	5.0E13	0.00	0
C+OH=CO+H	5.0E13	0.00	0

Reactions	A	n	E
C+O2=CO+O	2.0E13	0.00	0
C+CH3=C2H2+H	5.0E13	0.00	0
C+CH2=C2H+H	5.0E13	0.00	0
!			
! *****			
! * CH3OH/CH2OH/CH2O subset *			
! *****			
!			
CH3OH+H=CH2OH+H2	1.7E7	2.1	4868
CH3OH+H=CH3O+H2	4.2E6	2.1	4868
CH3OH+O=CH2OH+OH	3.9E5	2.5	3080
CH3OH+OH=CH2OH+H2O	5.30E4	2.53	960
CH3OH+OH=CH3O+H2O	1.32E4	2.53	960
CH3OH+HO2=CH2OH+H2O2	9.6E10	0.0	12578
CH2O+H(+M)=CH3O(+M)	5.4E11	0.454	2600
LOW/1.54E30 -4.8 5560 /			
TROE/ 0.758 94 1555 4200/			
N2/1.43/ H2O/8.58/			
CH3O+H=CH2O+H2	2.0E13	0.00	0
CH3O+O=CH2O+OH	1.0E13	0.00	0
CH3O+OH=CH2O+H2O	1.0E13	0.00	0
CH3O+O2=CH2O+HO2	6.3E10	0.00	2600
H+CH2O(+M)=CH2OH(+M)	5.4E11	0.454	3600
LOW/.91E32 -4.82 6530/			
TROE/0.7187 103 1291 4160/			
N2/1.43/ H2O/8.58/ CO/2/ CO2/3/ H2/2/			
CH2OH+H=CH2O+H2	2.0E13	0.00	0
CH2OH+O=CH2O+OH	1.0E13	0.00	0
CH2OH+OH=CH2O+H2O	1.0E13	0.00	0
CH2OH+O2=CH2O+HO2	1.6E15	-1.0	0
DUP			
CH2OH+O2=CH2O+HO2	7.2E13	0.0	3577
DUP			
!			
! *****			
! * C2H6/C2H5/C2H4/C2H3/C2H2/C2H/C2 subset *			
! *****			
!			
C2H6+H=C2H5+H2	5.4E02	3.50	5210
C2H6+O=C2H5+OH	3.0E07	2.00	5115
C2H6+OH=C2H5+H2O	7.2E6	2.0	864
C2H6+HO2 = C2H5+H2O2	1.3E13	0.00	20460
C2H6+O2=C2H5+HO2	5.0E13	0.0	55000
C2H6+CH3=C2H5+CH4	5.5E-1	4.00	8300
C2H4+H(+M)=C2H5(+M)	1.1E12	0.454	1822
LOW/1.112E34 -5.0 4448.0/			
TROE/0.5 95.0 95.0 200./			
H2O/5/			
C2H5+H(+M) = C2H6(+M)	5.2E17	-0.99	1580 ! GR
LOW / 2.0E41 -7.08 6685/			
TROE/ 0.8422 125 2219 6882 /			
N2/1.0/ H2O/6/ AR/0.7/			
C2H5+H=CH3+CH3	4.9E12	0.35	0
C2H5+O = CH3+CH2O	4.2E13	0.00	0
C2H5+O = CH3HCO+H	5.3E13	0.00	0
C2H5+O = C2H4+OH	3.0E13	0.00	0

Reactions	A	n	E
C2H5+OH = C2H4+H2O	2.4E13	0.00	0
C2H5+O2 = C2H4+HO2	1.0E10	0.00	-2190
C2H5+CH2O = C2H6+HCO	5.5E03	2.81	5860
C2H5+HCO = C2H6+CO	1.2E14	0.00	0
C2H5+CH3 = C2H4+CH4	1.1E12	0.00	0
C2H5+C2H5 = C2H6+C2H4	1.5E12	0.00	0
C2H3+H(+M)=C2H4(+M)	6.1E12	0.27	280
LOW /0.98E30 -3.86 3320./			
TROE /0.7820 207.50 2663.00 6095.00/			
H2/2.85/ CO/2.1/ CO2/2.85/ H2O/7.14/ CH4/2.85/ C2H6/4.29/ N2/1.43/			
C2H4+M=C2H2+H2+M	3.5E16	0.0	71500
N2/1.5/ H2O/10/			
C2H4+H=C2H3+H2	5.4E14	0.0	14900
C2H4+O = CH2HCO+H	4.7E06	1.88	180
C2H4+O = CH3+HCO	8.1E06	1.88	180
C2H4+O = CH2CO+H2	6.8E05	1.88	180
C2H4+OH=C2H3+H2O	2.0E13	0.00	5940
C2H4+HO2=CH3HCO+OH	2.2E12	0.0	17200
C2H4+O2=CH2HCO+OH	2.0E8	1.5	39000
C2H4+CH3 = C2H3+CH4	5.0E11	0.00	15000
H+C2H2(+M)=C2H3(+M)	3.1E11	0.58	2590
LOW/2.254E40 -7.269 6577./			
TROE/0.5 675. 675./			
H2/2/ CO/2/ CO2/3/ H2O/5/			
C2H3+H=C2H2+H2	4.0E13	0.00	0
C2H3+O=CH2CO+H	3.0E13	0.000	0
C2H3+OH=C2H2+H2O	2.0E13	0.0	0
C2H3+O2 = CH2O+HCO	1.1E23	-3.29	3890
C2H3+O2 = CH2HCO+O	2.5E15	-0.78	3135
C2H3+O2=C2H2+HO2	5.2E15	-1.26	3310
C2H3+CH2O = C2H4+HCO	5.4E03	2.81	5860
C2H3+HCO = C2H4+CO	9.0E13	0.00	0
C2H3+CH3 = C2H2+CH4	2.1E13	0.00	0
C2H3+C2H3 = C2H4+C2H2	1.5E13	0.00	0
C2H2+M=C2H+H+M	9.1E30	-3.7	127138
H2/2/ CO/2/ CO2/3/ H2O/5/			
H2+C2H=C2H2+H	4.1E05	2.39	864
C2H2+O=CH2+CO	6.1E6	2.00	1900
C2H2+O=HCCO+H	1.4E7	2.00	1900
C2H2+O=C2H+OH	3.2E15	-0.60	15000
OH+C2H2=C2H+H2O	3.4E7	2.0	14000
OH+C2H2=HCCOH+H	5.0E5	2.3	13500
OH+C2H2=CH2CO+H	2.2E-4	4.5	-1000
OH+C2H2=CH3+CO	4.8E-4	4.0	-2000
OH+C2H2(+M)=C2H2OH(+M)	1.5E8	1.7	1000
LOW/1.81E23 -2.0 0.0 /			
H2/2/ CO/2/ CO2/3/ H2O/5/			
HO2+C2H2=CH2HCO+O	1.0E12	0.0	10000
HO2+C2H2=CH2O+HCO	1.0E12	0.0	10000
C2H2+O2=HCO+HCO	2.0E08	1.5	30100
C2+H2=C2H+H	4.0E5	2.4	1000
C2H+O=CH+CO	5.0E13	0.00	0
C2H+OH=HCCO+H	2.0E13	0.00	0
C2H+OH=C2+H2O	4.0E7	2.0	8000
C2H+O2=CO+CO+H	2.5E13	0.0	0
C2H+CH4=CH3+C2H2	7.2E12	0.0	976

Reactions	A	n	E
C2+OH=C2O+H	5.0E13	0.0	0
C2+O2=CO+CO	5.0E13	0.0	0
!			
! *****			
! * CH3HCO/CH2HCO/CH3CO/CH2CO/HCCOH/HCCO/C2O subset *			
! *****			
!			
CH3HCO = CH3+HCO	7.1E15	0.00	81280
CH3HCO+H = CH3CO+H2	4.1E09	1.16	2400
CH3HCO+O = CH3CO+OH	5.8E12	0.00	1800
CH3HCO+OH=CH3CO+H2O	2.3E10	0.73	-1110
CH3HCO+HO2 = CH3CO+H2O2	3.0E12	0.00	12000
CH3HCO+O2 = CH3CO+HO2	3.0E13	0.00	39000
CH3HCO+CH3=CH3CO+CH4	2.0E-6	5.6	2464
CH2HCO=CH3+CO	1.0E13	0.0	42000
!CH2HCO+M=CH3+CO+M	2.0E16	0.0	42000
! H2/2/ CO/2/ CO2/3/ H2O/5/			
CH2HCO+H=CH3+HCO	1.0E14	0.0	0
CH2HCO+H=CH3CO+H	3.0E13	0.0	0
CH2HCO+O=CH2O + HCO	5.0E13	0.0	0
CH2HCO+OH=CH2CO+H2O	2.0E13	0.0	0
CH2HCO+OH=CH2OH+HCO	1.0E13	0.0	0
CH2HCO+O2 = CH2O+CO+OH	2.2E11	0.0	1500
CH2HCO+CH3=C2H5CHO	5.0E13	0.0	0
CH2HCO+CH2=C2H4+HCO	5.0E13	0.0	0
CH2HCO+CH =C2H3+HCO	1.0E14	0.0	0
C2H5+HCO = C2H5CHO	1.8E13	0.0	0
C2H5CHO+H = C2H5CO+H2	8.0E13	0.0	0
C2H5CHO+O = C2H5CO+OH	7.8E12	0.0	1730
C2H5CHO+OH = C2H5CO+H2O	1.2E13	0.0	0
C2H5+CO = C2H5CO	1.5E11	0.0	4800
C2H2OH+H=CH2HCO+H	5.0E13	0.0	0
C2H2OH+O=OCHCHO+H	5.0E13	0.0	0.0
C2H2OH+O2=OCHCHO+OH	1.0E12	0.0	5000
CH3CO(+M)=CH3+CO(+M)	2.8E13	0.0	17100
LOW/2.1E15 0.0 14000./			
TROE/ 0.5 1.0E-30 1.0E30 /			
H2/2/ CO/2/ CO2/3/ H2O/5/			
CH3CO+H = CH3+HCO	2.1E13	0.00	0
CH3CO+H = CH2CO+H2	1.2E13	0.00	0
CH3CO+O = CH3+CO2	1.5E14	0.00	0
CH3CO+O = CH2CO+OH	4.0E13	0.00	0
CH3CO+OH = CH2CO+H2O	1.2E13	0.00	0
CH2+CO(+M)=CH2CO(+M)	8.1E11	0.5	4510
LOW/ 1.88E33 -5.11 7095./			
TROE/ 0.5907 275 1226 5185/			
H2/2/ CO/2/ CO2/3/ H2O/8.58/ N2/1.43/			
CH2CO+H=CH3+CO	5.9E6	2.0	1300
CH2CO+H=HCCO+H2	3.0E7	2.0	10000
CH2CO+O=CO2+CH2	1.8E12	0.0	1350
CH2CO+O=HCCO+OH	2.0E7	2.0	10000
CH2CO+OH=HCCO+H2O	1.0E7	2.0	3000
CH2CO+OH=CH2OH+CO	7.2E12	0.0	0
CH2CO+OH=CH3+CO2	3.0E12	0.0	0
HCCOH+H=HCCO +H2	3.0E7	2.0	1000
HCCOH+OH=HCCO+H2O	1.0E7	2.0	1000

Reactions	A	n	E
HCCOH+O=HCCO+OH	2.0E7	3.0	1900
OCHCHO+M=HCO+HCO+M	1.0E17	0.0	58000
OCHCHO+H=CH2O+HCO	3.0E13	0.0	0
CH+CO(+M)=HCCO(+M)	5.0E13	0.0	0
LOW/ 1.88E28 -3.74 1936 /			
TROE/ 0.5757 237 1652 5069 /			
N2/1.43/ H2O/8.58/ CO/2/ CO2/3/ H2/2/			
H+HCCO=CH2(S)+CO	1.0E14	0.0	0
O+HCCO=H+CO+CO	1.0E14	0.0	0
HCCO+OH=C2O+H2O	6.0E13	0.0	0
HCCO+O2=CO2+CO+H	1.4E7	1.7	1000
HCCO+O2=CO +CO +OH	2.9E7	1.7	1000
HCCO+HCCO=C2H2+CO+CO	1.0E13	0.00	0
C2O+H=CH+CO	1.0E13	0.0	0
C2O+O=CO+CO	5.0E13	0.0	0
C2O+OH=CO+CO+H	2.0E13	0.0	0
C2O+O2=CO+CO+O	2.0E13	0.0	0
!			
! *****			
! * H/N/O subset *			
! * taken from [nh2no2] except where noted *			
! *****			
!			
H+NO+M=HNO+M	2.7E15	0.0	-600
H2O/10/ O2/1.5/ H2/2/ CO2/3/ N2/0.0/			
H+NO+N2=HNO+N2	7.0E19	-1.50	0
NO+O+M=NO2+M	7.5E19	-1.41	0
N2/1.7/ O2/1.5/ H2O/10/			
OH+NO+M=HONO+M	5.1E23	-2.51	-68
H2O/5/			
HO2+NO=NO2+OH	2.1E12	0.00	-479
NO2+H=NO+OH	8.4E13	0.0	0
NO2+O=NO+O2	3.9E12	0.0	-238
NO2+O(+M)=NO3(+M)	1.3E13	0.0	0
LOW/1.0E28 -4.08 2470./			
N2/1.5/ O2/1.5/ H2O/18.6/			
NO2+NO2=NO+NO+O2	1.6E12	0.0	26123
NO2+NO2=NO3+NO	9.6E09	0.73	20900
NO3+H=NO2+OH	6.0E13	0.0	0
NO3+O=NO2+O2	1.0E13	0.0	0
NO3+OH=NO2+HO2	1.4E13	0.0	0
NO3+HO2=NO2+O2+OH	1.5E12	0.0	0
NO3+NO2=NO+NO2+O2	5.0E10	0.0	2940
HNO+H=H2+NO	4.5E11	0.72	655
HNO+O=NO+OH	1.0E13	0.0	0
HNO+OH=NO+H2O	3.6E13	0.0	0
HNO+O2=HO2+NO	1.0E13	0.0	25000
HNO+NO2=HONO+NO	6.0E11	0.0	2000
HNO+HNO=N2O+H2O	9.0E08	0.0	3100
HNO+NH2=NH3+NO	3.63E6	1.63	-1252
H2NO+M=HNO+H+M	2.5E15	0.0	50000
H2O/5/ N2/2/			
H2NO+H=HNO+H2	3.0E7	2.0	2000
H2NO+H=NH2+OH	5.0E13	0.0	0
H2NO+O=HNO+OH	3.0E7	2.0	2000
H2NO+O = NH2+O2	2.0E14	0	0

Reactions	A	n	E
H2NO+OH=HNO+H2O	2.0E7	2.0	1000
H2NO+NO=HNO+HNO	2.0E04	2.0	13000
H2NO+NO2=HNO+HONO	6.0E11	0.0	2000
HONO+H=H2+NO2	1.2E13	0.0	7352
HONO+O=OH+NO2	1.2E13	0.0	5961
HONO+OH=H2O+NO2	4.0E12	0.0	0
NH3+M = NH2+H+M	2.2E16	0	93470
NH3+H=NH2+H2	6.4E05	2.39	10171
NH3+O=NH2+OH	9.4E06	1.94	6460
NH3+OH=NH2+H2O	2.0E06	2.04	566
NH3+HO2=NH2+H2O2	3.0E11	0.0	22000
NH2+H=NH+H2	4.0E13	0.00	3650
NH2+O=HNO+H	6.6E14	-0.50	0
NH2+O=NH+OH	6.8E12	0.	0
NH2+OH=NH+H2O	4.0E06	2.	1000
NH2+HO2=H2NO+OH	5.0E13	0.0	0
NH2+HO2=NH3+O2	1.0E13	0.0	0
NH2+NO=NNH+OH	8.9E12	-0.35	0
NH2+NO=N2+H2O	1.3E16	-1.25	0
DUP			
NH2+NO=N2+H2O	-8.9E12	-0.35	0
DUP			
NH2+NO2=N2O+H2O	3.2E18	-2.2	0
NH2+NO2=H2NO+NO	3.5E12	0.	0
NH2+H2NO=NH3+HNO	3.0E12	0.0	1000
HONO+NH2=NO2+NH3	71.1	3.02	-4941
NH2+NH2=N2H2+H2	8.5E11	0.	0
NH2+NH=N2H2+H	5.0E13	0.	0
NH2+N=N2+H+H	7.2E13	0.	0
NH+H=N+H2	3.0E13	0.	0
NH+O=NO+H	9.2E13	0.	0
NH+OH=HNO+H	2.0E13	0.	0
NH+OH=N+H2O	5.0E11	0.50	2000
NH+O2=HNO+O	4.6E05	2.	6500
NH+O2=NO+OH	1.3E06	1.5	100
NH+NO=N2O+H	2.9E14	-0.4	0
DUP			
NH+NO=N2O+H	-2.2E13	-0.23	0
DUP			
NH+NO=N2+OH	2.2E13	-0.23	0
NH+NO2=N2O+OH	1.0E13	0.	0
NH+NH=N2+H+H	2.5E13	0.	0
NH+N=N2+H	3.0E13	0.	0
N+OH=NO+H	3.8E13	0.	0
N+O2=NO+O	6.4E09	1.	6280
N+NO=N2+O	3.3E12	0.30	0
N2H2+M=NNH+H+M	5.0E16	0.	50000
H2O/15/ O2/2/ N2/2/ H2/2/			
N2H2+H=NNH+H2	5.0E13	0.	1000
N2H2+O=NH2+NO	1.0E13	0.	0
N2H2+O=NNH+OH	2.0E13	0.	1000
N2H2+OH=NNH+H2O	1.0E13	0.	1000
N2H2+NO=N2O+NH2	3.0E12	0.	0
N2H2+NH2=NH3+NNH	1.0E13	0.	1000
N2H2+NH=NNH+NH2	1.0E13	0.	1000
NNH=N2+H	1.0E7	0.	0

Reactions	A	n	E
NNH+H=N2+H2	1.0E14	0.	0
NNH+O=N2+OH	8.0E13	0.	0
NNH+O=N2O+H	1.0E14	0.	0
NNH+O=NH+NO	5.0E13	0.	0
NNH+OH=N2+H2O	5.0E13	0.	0
NNH+O2=N2+HO2	2.0E14	0.	0
NNH+O2=N2+O2+H	5.0E13	0.	0
NNH+NO=N2+HNO	5.0E13	0.	0
NNH+NH2=N2+NH3	5.0E13	0.	0
NNH+NH=N2+NH2	5.0E13	0.	0
N2O+M=N2+O+M	4.0E14	0.	56100
N2/1.7/ O2/1.4/ H2O/12/ CO/1.5/ CO2/3/			
N2O+H=N2+OH	3.3E10	0.	4729
DUP			
N2O+H=N2+OH	4.4E14	0.	19254
DUP			
N2O+O=NO+NO	6.6E13	0.	26630
N2O+O=N2+O2	1.0E14	0.	28000
N2O+OH=N2+HO2	1.3E-2	4.72	36561
N2O+OH=HNO+NO	1.2E-4	4.33	25081
N2O+NO=NO2+N2	5.3E05	2.23	46281
!			
! *****			
! * cyanide subset *			
! *****			
!			
CN+H2=HCN+H	3.0E05	2.45	2237
HCN+O=NCO+H	1.4E04	2.64	4980
HCN+O=NH+CO	3.5E03	2.64	4980
HCN+O=CN+OH	2.7E09	1.58	29200
HCN+OH = CN+H2O	3.9E06	1.83	10300
HCN+OH=HOCN+H	5.9E04	2.40	12500
HCN+OH=HNCO+H	2.0E-3	4.	1000
HCN+OH=NH2+CO	7.8E-4	4.	4000
HCN+CN=C2N2+H	1.5E07	1.71	1530
CN+O=CO+N	7.7E13	0.	0
CN+OH=NCO+H	4.0E13	0.	0
CN+O2=NCO+O	7.5E12	0.	-389
CN+CO2=NCO+CO	3.7E06	2.16	26884
CN+NO2=NCO+NO	5.3E15	-0.752	344
CN+NO2=CO+N2O	4.9E14	-0.752	344
CN+NO2=N2+CO2	3.7E14	-0.752	344
CN+HNO=HCN+NO	1.8E13	0.00	0
CN+HONO=HCN+NO2	1.2E13	0.00	0
CN+N2O=NCN+NO	3.9E03	2.6	3696
CN+HNCO=HCN+NCO	1.5E13	0.	0
CN+NCO=NCN+CO	1.8E13	0.	0
HNCO+M=NH+CO	1.1E16	0.	86000
HNCO+H=NH2+CO	2.2E07	1.7	3800
HNCO+O=HNO+CO	1.5E08	1.57	44012
HNCO+O=NH+CO2	9.8E7	1.41	8524
HNCO+O=NCO+OH	2.2E6	2.11	11425
HNCO+OH=NCO+H2O	6.4E05	2.	2563
HNCO+HO2=NCO+H2O2	3.0E11	0.	22000
HNCO+O2=HNO+CO2	1.0E12	0.	35000
HNCO+NH2=NH3+NCO	5.0E12	0.	6200

Reactions	A	n	E
HNCO+NH=NH2+NCO	3.0E13	0.	23700
HOCN+H=NCO+H2	2.0E07	2.	2000
HOCN+O=NCO+OH	1.5E04	2.64	4000
HOCN+OH=NCO+H2O	6.4E05	2.	2563
HCNO+H=HCN+OH	1.0E14	0	12000
HCNO+O=HCO+NO	2.0E14	0.	0
HCNO+OH=CH2O+NO	4.0E13	0.	0
NCO+M=N+CO+M	3.1E16	-0.50	48000
NCO+H=NH+CO	5.0E13	0.	0
NCO+O=NO+CO	4.7E13	0.	0
NCO+OH=NO+HCO	5.0E12	0.	15000
NCO+O2=NO+CO2	2.0E12	0.	20000
NCO+H2=HNCO+H	7.6E02	3.	4000
NCO+HCO=HNCO+CO	3.6E13	0.	0
NCO+NO=N2O+CO	6.2E17	-1.73	763
NCO+NO=N2+CO2	7.8E17	-1.73	763
NCO+NO2=CO+NO+NO	2.5E11	0.	-707
NCO+NO2=CO2+N2O	3.0E12	0.	-707
NCO+HNO=HNCO+NO	1.8E13	0.	0
NCO+HONO=HNCO+NO2	3.6E12	0.	0
NCO+N=N2+CO	2.0E13	0.	0
NCO+NCO=N2+CO+CO	1.8E13	0.	0
C2N2+O=NCO+CN	4.6E12	0.	8880
C2N2+OH=HOCN+CN	1.9E11	0.	2900
NCN+O=CN+NO	1.0E14	0.	0
NCN+OH=HCN+NO	5.0E13	0.	0
NCN+H=HCN+N	1.0E14	0.	0
NCN+O2=NO+NCO	1.0E13	0.	0
H+CH3CN=HCN+CH3	4.0E7	2.	2000
H+CH3CN=CH2CN+H2	3.0E7	2.	1000
O+CH3CN=NCO+CH3	1.5E4	2.64	4980
OH+CH3CN=CH2CN+H2O	2.0E7	2.	2000
CH2CN+O=CH2O+CN	1.0E14	0.	0.
CN+CH2OH=CH2CN+OH	5.0E13	0.	0
H2CN+M=HCN+H+M	3.0E14	0.	22000
!			
! *****			
! * subset for CxHyOz+nitrogen species reactions *			
! * (see paper for refs) *			
! *****			
!			
CO+NO2 = CO2+NO	9.0E13	0.	33779
CO+N2O=N2+CO2	3.2E11	0.	20237
CO2+N=NO+CO	1.9E11	0.	3400
CH2O+NCO=HNCO+HCO	6.0E12	0.	0
CH2O+NO2 = HCO+HONO	8.0E02	2.77	13730
HCO+NO=HNO+CO	7.2E12	0.	0
HCO+NO2 = CO+HONO	1.2E23	-3.29	2355
HCO+NO2 = H+CO2+NO	8.4E15	-0.75	1930
HCO+HNO=CH2O+NO	6.0E11	0.	2000
CH4+CN=CH3+HCN	6.2E04	2.64	-437
NCO+CH4 = CH3+HNCO	9.8E12	0.00	8120
CH3+NO=HCN+H2O	1.5E-1	3.523	3950
CH3+NO=H2CN+OH	1.5E-1	3.523	3950
CH3+NO2=CH3O+NO	1.4E13	0.	0
CH3+N=H2CN+H	7.1E13	0.	0

Reactions	A	n	E
CH ₃ +CN=CH ₂ CN+H	1.0E14	0.	0
CH ₃ +HOCN=CH ₃ CN+OH	5.0E12	0.	2000
CH ₂ +NO=HCN+OH	2.2E12	0.	-378
CH ₂ +NO=HCNO+H	1.3E12	0.	-378
CH ₂ +NO ₂ =CH ₂ O+NO	5.9E13	0.	0
CH ₂ +N=HCN+H	5.0E13	0.	0
CH ₂ +N ₂ =HCN+NH	1.0E13	0.	74000
H ₂ CN+N=N ₂ +CH ₂	2.0E13	0.	0
CH ₂ (S)+NO=HCN+OH	2.0E13	0.	0
CH ₂ (S)+NO=CH ₂ +NO	1.0E14	0.	0
CH ₂ (S)+HCN=CH ₃ +CN	5.0E13	0.	0
CH+NO ₂ =HCO+NO	1.0E14	0.	0
CH+NO = HCN+O	4.8E13	0.00	0
CH+NO = HCO+N	3.4E13	0.00	0
CH+NO = NCO+H	1.9E13	0.00	0
CH+N=CN+H	1.3E13	0.	0
CH+N ₂ =HCN+N	3.7E07	1.42	20723
CH+N ₂ O=HCN+NO	1.9E13	0.	-511
C+NO=CN+O	2.0E13	0.	0
C+NO=CO+N	2.8E13	0.	0
C+N ₂ =CN+N	6.3E13	0.	46019
C+N ₂ O=CN+NO	5.1E12	0.	0
C ₂ H ₆ +CN=C ₂ H ₅ +HCN	1.2E05	2.77	-1788
C ₂ H ₆ +NCO = C ₂ H ₅ +HNCO	1.5E-9	6.89	-2910
C ₂ H ₄ +CN = C ₂ H ₃ +HCN	5.9E14	-0.24	0
C ₂ H ₃ +NO=C ₂ H ₂ +HNO	1.0E12	0.	1000
C ₂ H ₃ +N=HCN+CH ₂	2.0E13	0.	0
C ₂ H ₂ +NCO = HCCO+HCN	1.4E12	0.00	1815
C ₂ H+NO=CN+HCO	2.1E13	0.	0
CH ₂ CO+CN=HCCO+HCN	2.0E13	0.	0
HCCO+NO=HCNO+CO	7.2E12	0.	0
HCCO+NO=HCN+CO ₂	1.6E13	0.	0
HCCO+NO ₂ =HCNO+CO ₂	1.6E13	0.	0
HCCO+N=HCN+CO	5.0E13	0.	0
END			

Appendix C. Thermodynamic Database for C-H-O-N Species in Chemkin Format

Thermodynamic properties for each species are calculated from polynomial fits to the specific heat at constant pressure:

$$C_p^o/R = a_1 + a_2T + a_3T^2 + a_4T^3 + a_5T^4$$

$$H^o/RT = a_1 + (a_2/2)T + (a_3/3)T^2 + (a_4/4)T^3 + (a_5/5)T^4 + (a_6/T)$$

$$S/R = a_1 \ln(T) + a_2T + (a_3/2)T^2 + (a_4/3)T^3 + (a_5/4)T^4 + a_7$$

These coefficients are stored for two temperature intervals, one between a low temperature and a common temperature, the second between the common temperature and the high temperature. The second line of the database (before any species data) contains the lowest, highest, and default common temperatures. The data for each species occupies four lines (with the line number at the right margin, in column 80) and contains the following information:

Line 1: Species Name

Date (not used in the code)
up to four atomic symbols and formula
phase of species (S, L, or G for solid, liquid, or gas, respectively)
low temperature
high temperature
common temperature (or blank for default)
fifth atomic symbols and formula (if needed)

Line 2: Coefficients a_1 through a_5 , for the upper temperature interval

Line 3: Coefficients a_6 , a_7 for the upper temperature interval and a_1 , a_2 , a_3 for the lower temperature interval

Line 4: Coefficients a_4 , a_5 , a_6 , a_7 for the lower temperature interval

```

THERMO
  200.000  1500.000  6000.000
C2H5      83194H  5C  2  0  0G  300.000  4000.000  1400.00  0  1
  0.87349157E+01  0.54537677E-02-0.37647177E-06-0.31297920E-09  0.52844000E-13  2
  0.10265269E+05-0.23104086E+02  0.24398923E+01  0.13747212E-01-0.85500653E-06  3
-0.31469924E-08  0.93754355E-12  0.13158588E+05  0.13099146E+02  4
C2H3      83194H  3C  2  0  0G  300.000  4000.000  1400.00  0  1
  0.71861677E+01  0.34552682E-02-0.29435373E-06-0.20681942E-09  0.36797774E-13  2
  0.32229627E+05-0.15977573E+02  0.24955740E+01  0.10269993E-01-0.10226917E-05  3
-0.27594382E-08  0.96919825E-12  0.34232813E+05  0.10614626E+02  4
C2H       83194H  1C  2  0  0G  300.000  4000.000  1400.00  0  1
  0.52086663E+01  0.12875765E-02-0.10398387E-06-0.67526325E-10  0.11751871E-13  2
  0.64697773E+05-0.53721781E+01  0.39396334E+01  0.32114412E-02-0.39412765E-06  3
-0.74782530E-09  0.27493521E-12  0.65224684E+05  0.17814000E+01  4
CH2(S)    83194H  2C  1  0  0G  300.000  4000.000  1400.00  0  1
  0.40752106E+01  0.15779120E-02-0.10806129E-06-0.84592437E-10  0.14033284E-13  2
  0.50007492E+05-0.15480316E+01  0.35932946E+01  0.13151238E-02  0.30756846E-06  3
  0.42637904E-09-0.34178712E-12  0.50451547E+05  0.17780241E+01  4
CH2       83194H  2C  1  0  0G  300.000  4000.000  1400.00  0  1
  0.39737520E+01  0.16097502E-02-0.10785119E-06-0.86399922E-10  0.14301196E-13  2
  0.45608973E+05  0.75549729E-01  0.36872995E+01  0.15066403E-02  0.69679857E-07  3
  0.23537297E-09-0.19397147E-12  0.45863672E+05  0.20267601E+01  4
CH3CN     111596H  3C  2N  1  0G  300.000  3000.000  1000.00  0  1
  0.23924046E+01  0.15618873E-01-0.79120497E-05  0.19372333E-08-0.18611956E-12  2
  0.84999377E+04  0.11145236E+02  0.25197531E+01  0.13567523E-01-0.25764077E-05  3
-0.30893967E-08  0.14288692E-11  0.85533762E+04  0.10920868E+02  4
CH2CN     111596H  2C  2N  1  0G  300.000  3000.000  1000.00  0  1
  0.46058146E+01  0.94485160E-02-0.47116329E-05  0.11389957E-08-0.10828942E-12  2
  0.29171486E+05  0.10084415E+01  0.25296724E+01  0.18114138E-01-0.18960575E-04  3
  0.11944583E-07-0.32544142E-11  0.29592293E+05  0.10993441E+02  4
OCHCHO    120596H  2C  2O  2  0G  300.000  3000.000  1000.00  0  1
  0.49087462E+01  0.13182673E-01-0.71416730E-05  0.18461316E-08-0.18525858E-12  2

```

-0.27116386E+05	0.59148768E+00	0.25068862E+01	0.18899139E-01	-0.10302623E-04	3					
0.62607508E-09	0.88114253E-12	-0.26427374E+05	0.13187043E+02		4					
C2H2OH HCCO TRAN	121196H	3C	2O	1	OG	300.000	3000.000	1000.00	0	1
0.57206843E+01	0.10704185E-01	-0.50358494E-05	0.11324499E-08	-0.10086621E-12	2					
0.12849424E+05	-0.47081776E+01	0.81498282E-01	0.31640644E-01	-0.34085361E-04	3					
0.18978838E-07	-0.41950165E-11	0.14060783E+05	0.22908977E+02		4					
C2H5CO burcat	T 9/92C	3H	5O	1	OG	298.150	5000.000	1000.00		1
0.30445698E+01	0.23236429E-01	-0.86317936E-05	0.14799550E-08	-0.96860829E-13	2					
-0.61787211E+04	0.13122302E+02	0.67368294E+01	-0.26945299E-02	0.49927017E-04	3					
-0.50025808E-07	0.15011503E-10	-0.65703366E+04	-0.23398732E+01	-0.43321855E+04	4					
C2H5CHO burcat	T 9/92C	3H	6O	1	OG	273.150	5000.000	1000.00		1
0.33137982E+01	0.26619606E-01	-0.10475596E-04	0.18815334E-08	-0.12761310E-12	2					
-0.25459603E+05	0.96608447E+01	0.76044596E+01	-0.86403564E-02	0.73930097E-04	3					
-0.79687398E-07	0.28004927E-10	-0.25489789E+05	-0.67643691E+01	-0.23097645E+05	4					
CH3CN	111596H	3C	2N	1	OG	300.000	3000.000	1000.00	0	1
0.23924046E+01	0.15618873E-01	-0.79120497E-05	0.19372333E-08	-0.18611956E-12	2					
0.84999377E+04	0.11145236E+02	0.25197531E+01	0.13567523E-01	-0.25764077E-05	3					
-0.30893967E-08	0.14288692E-11	0.85533762E+04	0.10920868E+02		4					
CH2CN	111596H	2C	2N	1	OG	300.000	3000.000	1000.00	0	1
0.46058146E+01	0.94485160E-02	-0.47116329E-05	0.11389957E-08	-0.10828942E-12	2					
0.29171486E+05	0.10084415E+01	0.25296724E+01	0.18114138E-01	-0.18960575E-04	3					
0.11944583E-07	-0.32544142E-11	0.29592293E+05	0.10993441E+02		4					
HNO	pg9601H	1N	1O	1	G	0300.00	5000.00	1000.00		1
0.03615144E+02	0.03212486E-01	-0.01260337E-04	0.02267298E-08	-0.01536236E-12	2					
0.11769108E+05	0.04810264E+02	0.02784403E+02	0.06609646E-01	-0.09300223E-04	3					
0.09437980E-07	-0.03753146E-10	0.12025976E+05	0.09035629E+02		4					
HCN	110193H	1C	1N	1	G	0300.00	4000.00	1000.00		1
0.03426457E+02	0.03924190E-01	-0.01601138E-04	0.03161966E-08	-0.02432850E-12	2					
0.01485552E+06	0.03607795E+02	0.02417787E+02	0.09031856E-01	-0.01107727E-03	3					
0.07980141E-07	-0.02311141E-10	0.01501044E+06	0.08222891E+02		4					
HNCO	110193H	1C	1N	1O	1G	0300.00	4000.00	1400.00		1
0.06545307E+02	0.01965760E-01	-0.01562664E-05	-0.01074318E-08	0.01874680E-12	2					
-0.01664773E+06	-0.01003880E+03	0.03858467E+02	0.06390342E-01	-0.09016628E-05	3					
-0.01898224E-07	0.07651380E-11	-0.01562343E+06	0.04882493E+02		4					
HOCN	110193H	1C	1N	1O	1G	0300.00	4000.00	1400.00		1
0.06022112E+02	0.01929530E-01	-0.01455029E-05	-0.01045811E-08	0.01794814E-12	2					
-0.04040321E+05	-0.05866433E+02	0.03789424E+02	0.05387981E-01	-0.06518270E-05	3					
-0.01420164E-07	0.05367969E-11	-0.03135335E+05	0.06667052E+02		4					
NCO	110193C	1N	1O	1	G	0300.00	4000.00	1400.00		1
0.06072346E+02	0.09227829E-02	-0.09845574E-06	-0.04764123E-09	0.09090445E-13	2					
0.01359820E+06	-0.08507293E+02	0.03359593E+02	0.05393239E-01	-0.08144585E-05	3					
-0.01912868E-07	0.07836794E-11	0.01462809E+06	0.06549694E+02		4					
NO	J 6/63N	1O	1	0	OG	300.000	5000.000	1397.000		01
3.30616438E+00	0.105880379E-03	-3.35101565E-07	4.84712126E-11	-2.66276333E-15	2					
9.80488610E+03	6.14537840E+00	3.18302768E+00	1.26159588E-03	-4.40480253E-07	3					
6.32411494E-11	-1.29137488E-15	9.85926748E+03	6.84194428E+00		4					
NO2	J 9/64N	1O	2	0	OG	300.000	5000.000	1502.000		01
5.25702679E+00	1.59120496E-03	-5.75149303E-07	9.26518589E-11	-5.51558940E-15	2					
1.98171367E+03	-2.31252539E+00	2.83832558E+00	6.42094110E-03	-3.71675448E-06	3					
7.13464440E-10	2.36187798E-14	2.88065438E+03	1.09303839E+01		4					
N2O	J12/64N	2O	1	0	OG	300.000	5000.000	1389.000		01
5.34204014E+00	1.90604176E-03	-6.74838906E-07	1.07237509E-10	-6.32392655E-15	2					
7.86113134E+03	-5.23705883E+00	2.69094434E+00	8.36738233E-03	-6.74046569E-06	3					
2.71424228E-09	-4.38174973E-13	8.74933506E+03	8.89673234E+00		4					
NH3	J 9/65N	1H	3	0	OG	300.000	5000.000	1389.000		01
2.97970284E+00	5.36649578E-03	-1.72269060E-06	2.55767504E-10	-1.43684720E-14	2					
-6.74869189E+03	4.46279267E+00	3.24695599E+00	3.11219422E-03	1.94311272E-06	3					
-1.94660247E-09	4.40577561E-13	-6.64082103E+03	3.66779173E+00		4					
N2	J 9/65N	2	0	0	OG	300.000	5000.000	1651.000		01
2.99595342E+00	1.23650804E-03	-3.70307892E-07	5.05346628E-11	-2.62980307E-15	2					
-9.13275945E+02	5.68044094E+00	3.26021755E+00	5.91317615E-04	2.24046981E-07	3					
-1.95572855E-10	3.61873253E-14	-9.99926028E+02	4.27471775E+00		4					
CH4	L 8/88C	1H	4	00	00G	200.000	3500.000	1000.000		1
7.48514950E-02	1.33909467E-02	-5.73285809E-06	1.22292535E-09	-1.01815230E-13	2					

-9.46834459E+03	1.84373180E+01	5.14987613E+00	-1.36709788E-02	4.91800599E-05	3				
-4.84743026E-08	1.66693956E-11	-1.02466476E+04	-4.64130376E+00	1.00161980E+04	4				
CO	TPIS79C	10	1	00	00G	200.000	3500.000	1000.000	1
2.71518561E+00	2.06252743E-03	-9.98825771E-07	2.30053008E-10	-2.03647716E-14	2				
-1.41518724E+04	7.81868772E+00	3.57953347E+00	-6.10353680E-04	1.01681433E-06	3				
9.07005884E-10	-9.04424499E-13	-1.43440860E+04	3.50840928E+00	8.67100000E+03	4				
CO2	L 7/88C	10	2	00	00G	200.000	3500.000	1000.000	1
3.85746029E+00	4.41437026E-03	-2.21481404E-06	5.23490188E-10	-4.72084164E-14	2				
-4.87591660E+04	2.27163806E+00	2.35677352E+00	8.98459677E-03	-7.12356269E-06	3				
2.45919022E-09	-1.43699548E-13	-4.83719697E+04	9.90105222E+00	9.36546900E+03	4				
O2	TPIS89O	2	00	00	00G	200.000	3500.000	1000.000	1
3.28253784E+00	1.48308754E-03	-7.57966669E-07	2.09470555E-10	-2.16717794E-14	2				
-1.08845772E+03	5.45323129E+00	3.78245636E+00	-2.99673416E-03	9.84730201E-06	3				
-9.68129509E-09	3.24372837E-12	-1.06394356E+03	3.65767573E+00	8.68010400E+03	4				
H2O	L 8/89H	20	1	00	00G	200.000	3500.000	1000.000	1
3.03399249E+00	2.17691804E-03	-1.64072518E-07	-9.70419870E-11	1.68200992E-14	2				
-3.00042971E+04	4.96677010E+00	4.19864056E+00	-2.03643410E-03	6.52040211E-06	3				
-5.48797062E-09	1.77197817E-12	-3.02937267E+04	-8.49032208E-01	9.90409200E+03	4				
C2H2	L 1/91C	2H	2	00	00G	200.000	3500.000	1000.000	1
4.14756964E+00	5.96166664E-03	-2.37294852E-06	4.67412171E-10	-3.61235213E-14	2				
2.59359992E+04	-1.23028121E+00	8.08681094E-01	2.33615629E-02	-3.55171815E-05	3				
2.80152437E-08	-8.50072974E-12	2.64289807E+04	1.39397051E+01	1.00058390E+04	4				
C2H4	L 1/91C	2H	4	00	00G	200.000	3500.000	1000.000	1
2.03611116E+00	1.46454151E-02	-6.71077915E-06	1.47222923E-09	-1.25706061E-13	2				
4.93988614E+03	1.03053693E+01	3.95920148E+00	-7.57052247E-03	5.70990292E-05	3				
-6.91588753E-08	2.69884373E-11	5.08977593E+03	4.09733096E+00	1.05186890E+04	4				
C2H6	L 8/88C	2H	6	00	00G	200.000	3500.000	1000.000	1
1.07188150E+00	2.16852677E-02	-1.00256067E-05	2.21412001E-09	-1.90002890E-13	2				
-1.14263932E+04	1.51156107E+01	4.29142492E+00	-5.50154270E-03	5.99438288E-05	3				
-7.08466285E-08	2.68685771E-11	-1.15222055E+04	2.66682316E+00	1.18915940E+04	4				
O	L 1/90O	1	00	00	00G	200.000	3500.000	1000.000	1
2.56942078E+00	-8.59741137E-05	4.19484589E-08	-1.00177799E-11	1.22833691E-15	2				
2.92175791E+04	4.78433864E+00	3.16826710E+00	-3.27931884E-03	6.64306396E-06	3				
-6.12806624E-09	2.11265971E-12	2.91222592E+04	2.05193346E+00	6.72540300E+03	4				
H	L 7/88H	1	00	00	00G	200.000	3500.000	1000.000	1
2.50000001E+00	-2.30842973E-11	1.61561948E-14	-4.73515235E-18	4.98197357E-22	2				
2.54736599E+04	-4.46682914E-01	2.50000000E+00	7.05332819E-13	-1.99591964E-15	3				
2.30081632E-18	-9.27732332E-22	2.54736599E+04	-4.46682853E-01	6.19742800E+03	4				
OH	RUS 78O	1H	1	00	00G	200.000	3500.000	1000.000	1
3.09288767E+00	5.48429716E-04	1.26505228E-07	-8.79461556E-11	1.17412376E-14	2				
3.85865700E+03	4.47669610E+00	3.99201543E+00	-2.40131752E-03	4.61793841E-06	3				
-3.88113333E-09	1.36411470E-12	3.61508056E+03	-1.03925458E-01	8.81310600E+03	4				
H2	TPIS78H	2	00	00	00G	200.000	3500.000	1000.000	1
3.33727920E+00	-4.94024731E-05	4.99456778E-07	-1.79566394E-10	2.00255376E-14	2				
-9.50158922E+02	-3.20502331E+00	2.34433112E+00	7.98052075E-03	-1.94781510E-05	3				
2.01572094E-08	-7.37611761E-12	-9.17935173E+02	6.83010238E-01	8.46810200E+03	4				
HO2	L 5/89H	10	2	00	00G	200.000	3500.000	1000.000	1
4.01721090E+00	2.23982013E-03	-6.33658150E-07	1.14246370E-10	-1.07908535E-14	2				
1.11856713E+02	3.78510215E+00	4.30179801E+00	-4.74912051E-03	2.11582891E-05	3				
-2.42763894E-08	9.29225124E-12	2.94808040E+02	3.71666245E+00	1.00021620E+04	4				
H2O2	L 7/88H	20	2	00	00G	200.000	3500.000	1000.000	1
4.16500285E+00	4.90831694E-03	-1.90139225E-06	3.71185986E-10	-2.87908305E-14	2				
-1.78617877E+04	2.91615662E+00	4.27611269E+00	-5.42822417E-04	1.67335701E-05	3				
-2.15770813E-08	8.62454363E-12	-1.77025821E+04	3.43505074E+00	1.11588350E+04	4				
HCO	L12/89H	1C	10	1	0G	200.000	3500.000	1000.000	1
2.77217438E+00	4.95695526E-03	-2.48445613E-06	5.89161778E-10	-5.33508711E-14	2				
4.01191815E+03	9.79834492E+00	4.22118584E+00	-3.24392532E-03	1.37799446E-05	3				
-1.33144093E-08	4.33768865E-12	3.83956496E+03	3.39437243E+00	9.98945000E+03	4				
CH2O	L 8/88H	2C	10	1	0G	200.000	3500.000	1000.000	1
1.76069008E+00	9.20000082E-03	-4.42258813E-06	1.00641212E-09	-8.83855640E-14	2				
-1.39958323E+04	1.36563230E+01	4.79372315E+00	-9.90833369E-03	3.73220008E-05	3				
-3.79285261E-08	1.31772652E-11	-1.43089567E+04	6.02812900E-01	1.00197170E+04	4				
CH3	L11/89C	1H	3	00	0G	200.000	3500.000	1000.000	1
2.28571772E+00	7.23990037E-03	-2.98714348E-06	5.95684644E-10	-4.67154394E-14	2				

1.67755843E+04	8.48007179E+00	3.67359040E+00	2.01095175E-03	5.73021856E-06	3				
-6.87117425E-09	2.54385734E-12	1.64449988E+04	1.60456433E+00	1.03663400E+04	4				
C	L11/88C	1	00	00	OG	200.000	3500.000	1000.000	1
2.49266888E+00	4.79889284E-05	-7.24335020E-08	3.74291029E-11	-4.87277893E-15	2				
8.54512953E+04	4.80150373E+00	2.55423955E+00	-3.21537724E-04	7.33792245E-07	3				
-7.32234889E-10	2.66521446E-13	8.54438832E+04	4.53130848E+00	6.53589500E+03	4				
CH	TPIS79C	1H	1	00	OG	200.000	3500.000	1000.000	1
2.87846473E+00	9.70913681E-04	1.44445655E-07	-1.30687849E-10	1.76079383E-14	2				
7.10124364E+04	5.48497999E+00	3.48981665E+00	3.23835541E-04	-1.68899065E-06	3				
3.16217327E-09	-1.40609067E-12	7.07972934E+04	2.08401108E+00	8.62500000E+03	4				
CH2OH	GUNL93C	1H	30	1	OG	200.000	3500.000	1000.000	1
3.69266569E+00	8.64576797E-03	-3.75101120E-06	7.87234636E-10	-6.48554201E-14	2				
-3.24250627E+03	5.81043215E+00	3.86388918E+00	5.59672304E-03	5.93271791E-06	3				
-1.04532012E-08	4.36967278E-12	-3.19391367E+03	5.47302243E+00	1.18339080E+04	4				
CH3O	121686C	1H	30	1	OG	300.00	3000.00	1000.000	1
0.03770799E+02	0.07871497E-01	-0.02656384E-04	0.03944431E-08	-0.02112616E-12	2				
0.12783252E+03	0.02929575E+02	0.02106204E+02	0.07216595E-01	0.05338472E-04	3				
-0.07377636E-07	0.02075610E-10	0.09786011E+04	0.13152177E+02		4				
CH3OH	L 8/88C	1H	40	1	OG	200.000	3500.000	1000.000	1
1.78970791E+00	1.40938292E-02	-6.36500835E-06	1.38171085E-09	-1.17060220E-13	2				
-2.53748747E+04	1.45023623E+01	5.71539582E+00	-1.52309129E-02	6.52441155E-05	3				
-7.10806889E-08	2.61352698E-11	-2.56427656E+04	-1.50409823E+00	1.14352770E+04	4				
CH2CO	L 5/90C	2H	20	1	OG	200.000	3500.000	1000.000	1
4.51129732E+00	9.00359745E-03	-4.16939635E-06	9.23345882E-10	-7.94838201E-14	2				
-7.55105311E+03	6.32247205E-01	2.13583630E+00	1.81188721E-02	-1.73947474E-05	3				
9.34397568E-09	-2.01457615E-12	-7.04291804E+03	1.22156480E+01	1.17977430E+04	4				
HCCO	SRIC91H	1C	20	1	OG	300.00	4000.00	1000.000	1
0.56282058E+01	0.40853401E-02	-0.15934547E-05	0.28626052E-09	-0.19407832E-13	2				
0.19327215E+05	-0.39302595E+01	0.22517214E+01	0.17655021E-01	-0.23729101E-04	3				
0.17275759E-07	-0.50664811E-11	0.20059449E+05	0.12490417E+02		4				
HCCOH	SRI91C	2O	1H	2	OG	300.000	5000.000	1000.000	1
0.59238291E+01	0.67923600E-02	-0.25658564E-05	0.44987841E-09	-0.29940101E-13	2				
0.72646260E+04	-0.76017742E+01	0.12423733E+01	0.31072201E-01	-0.50866864E-04	3				
0.43137131E-07	-0.14014594E-10	0.80316143E+04	0.13874319E+02		4				
NO3	121286N	1O	3		G	0300.00	5000.00	1000.00	1
0.07120307E+02	0.03246228E-01	-0.14316134E-05	0.02797053E-08	-0.02013007E-12	2				
0.05864479E+05	-0.12137301E+02	0.12210763E+01	0.01878797E+00	-0.13443212E-04	3				
0.12746013E-08	0.13540601E-11	0.07473144E+05	0.01840202E+03		4				
N2H2	J12/65N	2H	2	0	OG	300.000	5000.000	1391.000	01
4.17789510E+00	4.56480666E-03	-1.41875536E-06	2.10366577E-10	-1.19629007E-14	2				
2.33992310E+04	4.99620907E-01	1.86991331E+00	9.88823409E-03	-6.18682259E-06	3				
2.19505186E-09	-3.35933023E-13	2.42170286E+04	1.29348918E+01		4				
N	J 3/61N	1	0	0	OG	300.000	5000.000	1000.000	01
2.50104420E+00	0.00000000E+00	0.00000000E+00	0.00000000E+00	0.00000000E+00	2				
5.61038356E+04	4.17481974E+00	2.50104420E+00	0.00000000E+00	0.00000000E+00	3				
0.00000000E+00	0.00000000E+00	5.61038356E+04	4.17481974E+00		4				
NH	melius/91	N	1H	1	OG	300.000	5000.000	1368.000	01
2.71207542E+00	1.33555860E-03	-3.70230207E-07	4.57845270E-11	-2.13216798E-15	2				
4.24170243E+04	6.21142965E+00	3.49617412E+00	-2.58512197E-04	8.00229766E-07	3				
-3.18729027E-10	3.76580317E-14	4.21181588E+04	1.91107205E+00		4				
NH2	L 9/81N	1H	2	0	OG	300.000	5000.000	1379.000	01
2.81084081E+00	3.24676780E-03	-1.05043681E-06	1.56667098E-10	-8.82503591E-15	2				
2.19519093E+04	6.57719920E+00	4.10811911E+00	-1.25157496E-03	4.38306028E-06	3				
-2.62867774E-09	5.10376771E-13	2.16908327E+04	2.01299833E-01		4				
H2NO	M/JB86	N	1H	20	OG	300.000	5000.000	1398.000	01
4.26222939E+00	4.60071183E-03	-1.52686779E-06	2.32081624E-10	-1.32607907E-14	2				
6.26937941E+03	1.89523882E+00	2.62132814E+00	8.05594293E-03	-4.34199752E-06	3				
1.31067689E-09	-1.79413169E-13	6.89825870E+03	1.08768221E+01		4				
HONO	NBS	N	1H	10	OG	300.000	5000.000	1377.000	11
6.11754445E+00	3.00786121E-03	-1.06923897E-06	1.70344657E-10	-1.00625644E-14	2				
-1.17949476E+04	-6.16262788E+00	2.75201621E+00	1.05958045E-02	-7.62288678E-06	3				
2.77356136E-09	-4.14321183E-13	-1.05902472E+04	1.20246757E+01		4				
NNH	Melius93N	2H	1	0	OG	300.000	5000.000	1571.000	01
4.16742317E+00	2.46673021E-03	-8.65307320E-07	1.36642746E-10	-8.02228303E-15	2				

2.83839159E+04	2.06116000E+00	3.73530535E+00	1.00340348E-03	3.26619841E-06	3						
-2.89569645E-09	6.96522384E-13	2.87981268E+04	5.28804396E+00		4						
HCN	L12/69H	1C	1N	1	OG	300.000	5000.000	1394.000	01		
4.14927783E+00	2.75915264E-03	-9.32137186E-07	1.43421227E-10	-8.26578641E-15	2						
1.47264307E+04	-5.23695997E-01	2.85596121E+00	6.10771304E-03	-4.55238121E-06	3						
2.02415417E-09	-3.88077841E-13	1.51690915E+04	6.34976764E+00		4						
H2CN	MELIUS	88	H	2C	1N	1	OG	300.000	5000.000	1447.000	01
5.10020023E+00	4.02780465E-03	-1.36439689E-06	2.10725393E-10	-1.21898915E-14	2						
2.75503210E+04	-4.27685930E+00	2.45567293E+00	7.78048141E-03	-1.59463967E-06	3						
-1.33785611E-09	5.32582054E-13	2.86868686E+04	1.07457988E+01		4						
AR	120186AR	1			G	300.000	5000.000	1000.000	1		
0.02500000E+02	0.00000000E+00	0.00000000E+00	0.00000000E+00	0.00000000E+00	2						
-0.07453750E+04	0.04366000E+02	0.02500000E+02	0.00000000E+00	0.00000000E+00	3						
0.00000000E+00	0.00000000E+00	-0.07453750E+04	0.04366000E+02		4						
CN	J	6/69C	1N	1	0	OG	300.000	5000.000	1417.000	01	
3.11872424E+00	1.21876263E-03	-3.73455811E-07	5.23704641E-11	-2.79895164E-15	2						
5.13563933E+04	6.24339093E+00	3.15725686E+00	1.05392231E-03	-1.60373461E-07	3						
-5.86681004E-11	1.78191482E-14	5.13535562E+04	6.06796978E+00		4						
C2	RUS	79C	2	0	0	OG	200.000	6000.000	1000.000	1	
0.37913706E+01	0.51650473E-03	-0.25486960E-07	-0.82263554E-11	0.10086168E-14	2						
0.99023059E+05	0.28151802E+01	0.86470550E+00	0.39353120E-01	-0.11981818E-03	3						
0.13908103E-06	-0.55205503E-10	0.98731303E+05	0.11530141E+02	0.99928438E+05	4						
CH3HCO	L	8/88C	2H	4O	1	OG	200.000	6000.000	1000.000	1	
0.54041108E+01	0.11723059E-01	-0.42263137E-05	0.68372451E-09	-0.40984863E-13	2						
-0.22593122E+05	-0.34807917E+01	0.47294595E+01	-0.31932858E-02	0.47534921E-04	3						
-0.57458611E-07	0.21931112E-10	-0.21572878E+05	0.41030159E+01	-0.19987949E+05	4						
CH3CO	T	9/92C	2H	3O	1	OG	200.000	6000.000	1000.000	1	
0.59447731E+01	0.78667205E-02	-0.28865882E-05	0.47270875E-09	-0.28599861E-13	2						
-0.37873075E+04	-0.50136751E+01	0.41634257E+01	-0.23261610E-03	0.34267820E-04	3						
-0.44105227E-07	0.17275612E-10	-0.26574529E+04	0.73468280E+01	-0.12027167E+04	4						
CH2HCO	T04/83O	1H	3C	2	OG	300.	5000.	1000.000	1		
0.59756699E+01	0.81305914E-02	-0.27436245E-05	0.40703041E-09	-0.21760171E-13	2						
0.49032178E+03	-0.50320879E+01	0.34090624E+01	0.10738574E-01	0.18914925E-05	3						
0.71585831E-08	0.28673851E-11	0.15214766E+04	0.95714535E+01	0.30474436E+04	4						
C2O	RUS	79C	2O	1	0	OG	200.000	6000.000	1000.000	1	
0.51512722E+01	0.23726722E-02	-0.76135971E-06	0.11706415E-09	-0.70257804E-14	2						
0.33241888E+05	-0.22183135E+01	0.28648610E+01	0.11990216E-01	-0.18362448E-04	3						
0.15769739E-07	-0.53897452E-11	0.33749932E+05	0.88867772E+01	0.35003406E+05	4						
C2N2	RUS	79C	2N	2	0	OG	200.000	6000.000	1000.000	1	
0.67055078E+01	0.36425829E-02	-0.13094063E-05	0.21643797E-09	-0.13121437E-13	2						
0.34860766E+05	-0.10493904E+02	0.23292532E+01	0.26153785E-01	-0.49000399E-04	3						
0.46191748E-07	-0.16432385E-10	0.35668442E+05	0.98501993E+01	0.37175973E+05	4						
HCNO	120186H	1C	1N	1O	1G	0250.00	4000.00	1000.00	1		
0.06692412E+02	0.02368360E-01	-0.02371510E-05	-0.12755033E-09	0.02407137E-12	2						
0.01694736E+06	-0.12454345E+02	0.03184858E+02	0.09752316E-01	-0.12802028E-05	3						
-0.06163104E-07	0.03226275E-10	0.01797907E+06	0.06123843E+02		4						
NCN	J12/70C	1N	2O	0O	OG	300.000	5000.000	1000.000	1		
0.55626268E+01	0.20860606E-02	-0.88123724E-06	0.16505783E-09	-0.11366697E-13	2						
0.54897907E+05	-0.55989355E+01	0.32524003E+01	0.70010737E-02	-0.22653599E-05	3						
-0.28939808E-08	0.18270077E-11	0.55609085E+05	0.66966778E+01	0.56865046E+05	4						
END											

Appendix D. Reaction Mechanism of Na Species in Chemkin Format

ELEMENTS

O H C N NA AR

END

SPECIES

NH3 O2 NO H2O CO2 N2

NAOH

H2 H O OH HO2 H2O2 CO

NH2 N2O NO2 NA NAO NA2O NAO2 NAH AR

END

REACTIONS

```

!           k = A×Tn exp(-E/RT)
!   Units: A mole-cm-sec-K; E cal/mole
! *****
! *   Na Subset                               *
! *****
! Reactions           A           n           E
NA+N2O=NAO+N2          1.69E+14      0.00      3159.
NAO+H2O=NAOH+OH        1.32E+13      0.00       0.
NAO+O=NA+O2            2.23E+14      0.00       0.
NAO+NO=NA+NO2          9.04E+13      0.00       0.
NAO+H2=NAOH+H          1.25E+13      0.00       0.
NA+O2+M=NAO2+M         1.74E+21     -1.30       0.
  H2O/5/ CO2/3/ CO/2/ H2/2/
NA+OH+M=NAOH+M         1.82E+21     -1.00       0.
!NAOH+M=NA+OH+M        1.51E+21     -1.00    78244.
NAO+OH=NAOH+O          2.00E+13      0.00       0.
NAO+HO2=NAOH+O2        5.00E+13      0.00       0.
NAO+H2=NA+H2O          3.13E+12      0.00       0.
NAO+CO=NA+CO2           1.00E+14      0.00       0.
H+NAO2=HO2+NA          2.00E+14      0.00       0.
NAO+H=NA+OH            2.00E+14      0.00       0.
NAO+OH=NA+HO2          3.00E+13      0.00       0.
NA+HO2=NAOH+O          1.00E+14      0.00       0.
NAO2+H=NAO+OH          5.00E+13      0.00       0.
NAO+HO2=NAO2+OH        5.00E+13      0.00       0.
NAO2+H=NAOH+O          1.00E+14      0.00       0.
NAO2+CO=NAO+CO2        1.00E+14      0.00       0.
NAO2+O=NAO+O2          1.32E+13      0.00       0.
NAO+NH3=NAOH+NH2       5.00E+13      0.00       0.
NAOH+H=NA+H2O          1.07E+13      0.00    1967.
NAO2+OH=NAOH+O2        2.00E+14      0.00       0.

```

END

Appendix E. Thermodynamic Database for Na Species in Chemkin Format

Thermodynamic properties for each species are calculated from polynomial fits to the specific heat at constant pressure:

$$C_p^o/R = a_1 + a_2T + a_3T^2 + a_4T^3 + a_5T^4$$

$$H^o/RT = a_1 + (a_2/2)T + (a_3/3)T^2 + (a_4/4)T^3 + (a_5/5)T^4 + (a_6/T)$$

$$S/R = a_1 \ln(T) + a_2T + (a_3/2)T^2 + (a_4/3)T^3 + (a_5/4)T^4 + a_7$$

These coefficients are stored for two temperature intervals, one between a low temperature and a common temperature, the second between the common temperature and the high temperature. The second line of the database (before any species data) contains the lowest, highest, and default common temperatures. The data for each species occupies four lines (with the line number at the right margin, in column 80) and contains the following information:

Line 1: Species Name

Date (not used in the code)
 up to four atomic symbols and formula
 phase of species (S, L, or G for solid, liquid, or gas, respectively)
 low temperature
 high temperature
 common temperature (or blank for default)
 fifth atomic symbols and formula (if needed)

Line 2: Coefficients a_1 through a_5 , for the upper temperature interval

Line 3: Coefficients a_6 , a_7 for the upper temperature interval and a_1 , a_2 , a_3 for the lower temperature interval

Line 4: Coefficients a_4 , a_5 , a_6 , a_7 for the lower temperature interval

```

THERMO
  300.000  1500.000  5000.000
NA2O      81092NA  20  1          S  0300.00  2000.00  1000.00  1
  0.08804423E+02  0.03253428E-01-0.03530522E-05-0.04324117E-08  0.01394574E-11  2
 -0.05257507E+06-0.04209654E+03  0.04776964E+02  0.01483269E+00-0.01052247E-03  3
  0.01278469E-07  0.01046187E-10-0.05155651E+06-0.02156737E+03  4
NAO2      D=37.2NA  10  2  0          G  300.000  2000.000  1000.00  1
  .24373729D+01  .11708054D-01  -.12465450D-04  .60394798D-08  -.10877028D-11  2
 -.68349080D+04  .15175355D+02  .24373729D+01  .11708054D-01  -.12465450D-04  3
  .60394798D-08  -.10877028D-11  -.68349080D+04  .15175355D+02  4
NAOH      J12/70NA  10  1H  100  OG  300.000  2000.000  1000.00  1
  .45711116D+01  .61346093D-02  -.76237353D-05  .43706135D-08  -.89064713D-12  2
 -.25359026D+05  -.95321963D-01  .45711116D+01  .61346093D-02  -.76237353D-05  3
  .43706135D-08  -.89064713D-12  -.25359026D+05  -.95321963D-01  4
NA        L 4/93NA  100  000  000  OG  300.000  2000.000  1000.00  1
  .25010442D+01  .00000000D+00  .00000000D+00  .00000000D+00  .00000000D+00  2
  .12157060D+05  .42385793D+01  .25010442D+01  .00000000D+00  .00000000D+00  3
  .00000000D+00  .00000000D+00  .12157060D+05  .42385793D+01  4
NAO       J12/67NA  10  100  000  OG  300.000  2000.000  1000.00  1
  .36192660D+01  .29441938D-02  -.35206654D-05  .18827273D-08  -.36198896D-12  2
  .88821327D+04  .62033018D+01  .36192660D+01  .29441938D-02  -.35206654D-05  3
  .18827273D-08  -.36198896D-12  .88821327D+04  .62033018D+01  4
END

```

Attachment F. Spray Evaporation Modeling Studies

Modeling of reacting flow processes based on staged mass injections, even in the simplest time-dependent approaches, requires characterization of the relative timing of each stage of mixing. In one dimensional models, such descriptions can be as simple as the beginning and end time for introduction of each flow and an assumed rate of mass addition during this interval. Instantaneous mixing at a single point along the reactor is a simplification which is commonly employed in one dimensional analysis, but which fails to resolve any influence of mixing rate.

The chemical kinetic modeling presented in *Section 7.0* demonstrates the potential importance of spray evaporation behavior as one of many controllable parameters affecting the performance of emissions control technologies utilizing liquid agent injection, including AR-Lean and SNCR. The previous discussion treats evaporation time as an independent parameter. The following considers how this parameter depends on other spray parameters for a selected set of conditions.

An accurate mixing characterization should consider the dominant physical phenomena. For the common situation of a liquid spray vaporized into a hot gas stream for subsequent reaction in the gas phase, the important phenomena are distribution and evaporation of the liquid spray and subsequent mixing of the vapor with the main gas stream. An additional issue is the overall mixing behavior of a spray co-injected with gases distinct from the main stream (for example, the atomizing air in a twin-fluid atomizer; or a second reactant stream which is co-injected with the spray, as is the case for overfire air co-injected with an N-agent spray). The rate of reactant availability via mixing is the ultimate concern. The focus in the current discussion is on evaporation in a single hot gas stream, with only cursory consideration of gas mixing issues.

An additional issue of particular importance in one dimensional lagrangian modeling of multiple mixing streams is the frame of reference. This consideration is reflected in the flow configuration of the model. Because sprays are typically injected at velocities different from the main stream, the time scale for a model in the main stream's frame of reference would be different from that following the spray. Both time scales were considered here, treating each in context of the mean flow for each stream.

Modeling was conducted using the commercial CFD code *Fluent*, version 5. A generic geometry was used, based loosely on the BSF. Spray droplets were injected into an axisymmetric cylindrical cross-section of length 10 m and radius 1 m, but employing slip wall boundary conditions to allow turbulent plug flow with minimal geometry dependence. Through this duct flowed combustion products of methane combustion at a stoichiometric ratio of 1.21 (corresponding to a flue gas oxygen level of about 4%, dry) at a velocity of 1 m/s. Monosized spray droplets were injected 3 m from the inlet to allow for counter- as well as co-flow injection. The spray material was water injected at a temperature of 300 K.

Injection studies were conducted in which droplet diameter, velocity (both magnitude and direction), and main flow temperature were varied about a baseline condition of 100 micron droplets injected in axial co-flow at 100 m/s into 1400 K gas. The current studies were conducted with a relatively small number of modeling conditions, so plots in which these conditions are varied include discrete modeling points as well as interpolated curves, as an indicator of the resolution of the predicted trends.

Figure F-1(a) shows the baseline evaporation history (fraction of droplet mass remaining as liquid) as a function of the main flow (duct) frame of reference, while Figure F-1(b) shows the same evaporation history from the spray frame of reference. The mass injection profile is nearly linear

over a period of about 880 ms in the duct frame of reference, but in the spray reference is more rapid initially and complete in about 42 ms. The difference is due to the higher velocity and rapid deceleration of the spray. The differences in the magnitude of characteristic time for each frame of reference continue through the parametric studies described below.

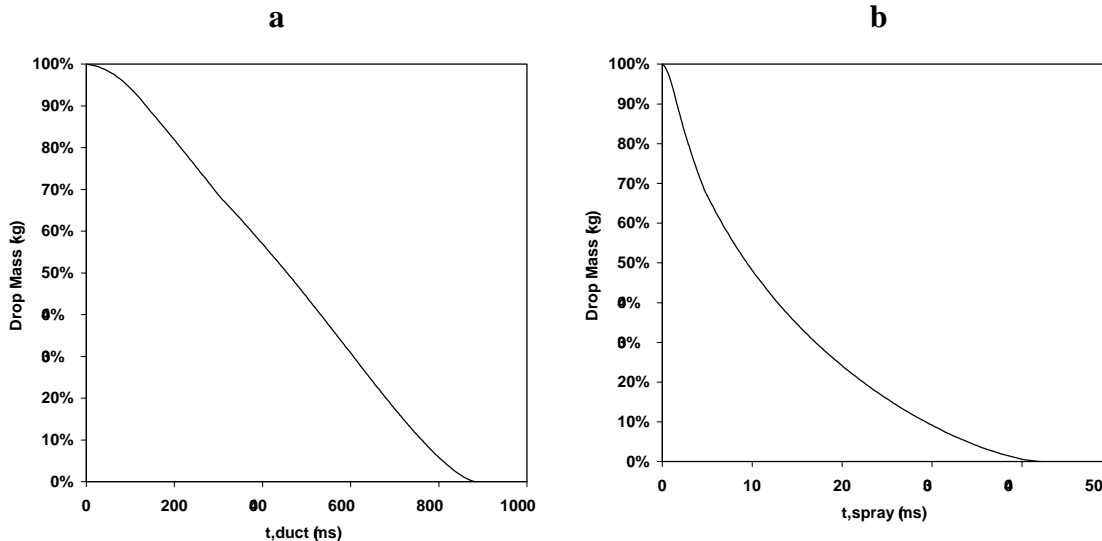


Figure F-1. Droplet evaporation history at baseline conditions. (a) Duct frame of reference, (b) droplet frame of reference.

Figure F-2 shows the effect of varying spray angle relative to the positive x-axis, from co-flow (baseline, 0 degrees) to crossflow (90 degrees) to counterflow injection (180 degrees). All other conditions are as for the baseline. The strong minimum in the duct reference frame, shown in Figure F-2(a), reflects the mapping of two dimensional evaporation onto a one dimensional axis. For crossflow injection under these conditions, evaporation is complete before droplets are carried a significant distance downstream, and so near “instantaneous” evaporation is achieved. The actual evaporation time of the droplets in their own frame of reference has a weaker dependence on spray angle, as shown in Figure F-2(b). At the same time, the view of Figure F-2(a) may be significant in characterizing the thermal environment seen by the droplet, when there is a strong temperature gradient in the direction of the main gas flow due to heat extraction (as in a utility boiler). These differences illustrate how model characteristics are influenced by the mapping of multidimensional physical effects onto one dimension.

Figure F-3 shows the effect of varying droplet diameter from 1 to 300 microns, maintaining all other conditions at baseline conditions. As would be expected, droplet size has a significant impact on evaporation time in either frame of reference, and represents a potential control variable for tailoring the distribution of mass evaporation. It must also be remembered that real injectors release a distribution of droplet sizes which must be considered for accurate characterization.

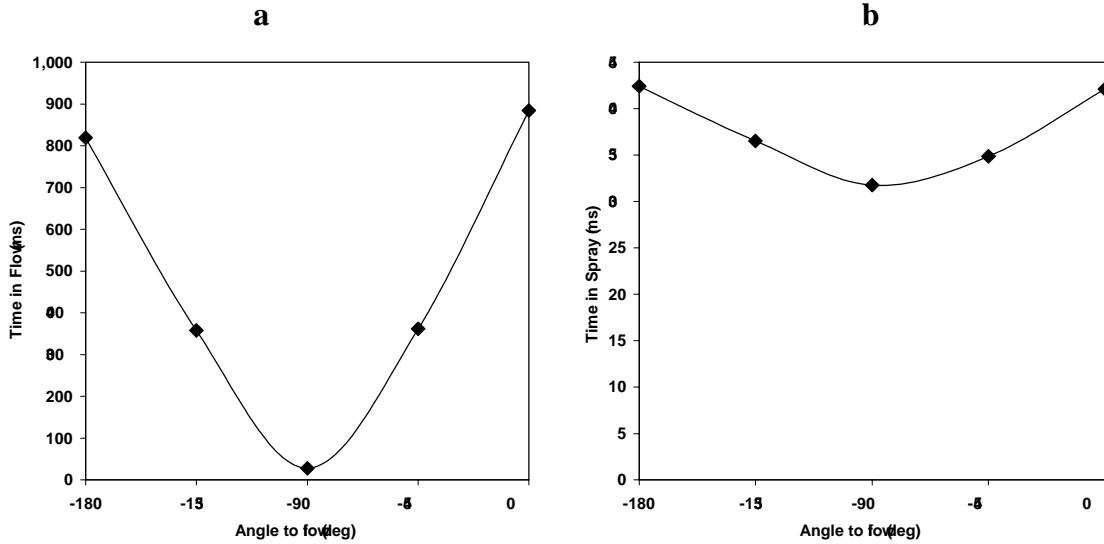


Figure F-2. Evaporation time as a function of angle of injection relative to main gas flow direction. (a) Duct frame of reference, (b) droplet frame of reference.

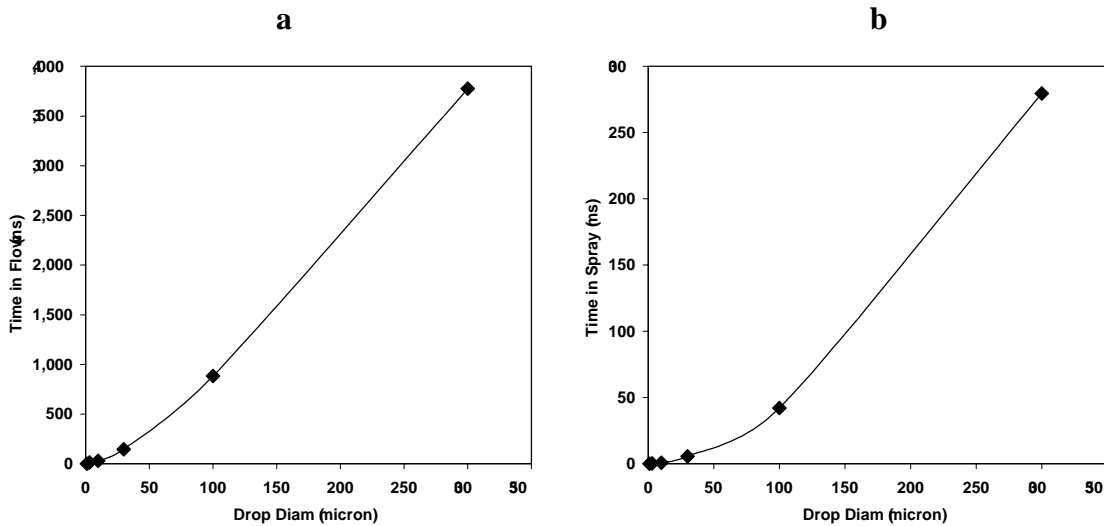


Figure F-3. Evaporation time as a function of droplet diameter. (a) Duct frame of reference, (b) droplet frame of reference.

Figure F-4 shows the effect of varying droplet velocity from 10 to 300 m/s, while maintaining the main flow rate at 1 m/s. All other conditions are the same as for the baseline case. As the droplet velocity increases (assuming coflow with the surrounding gas), the farther it travels in the gas flow direction (hence longer duct reference frame evaporation times), but the more rapidly it evaporates in its own frame of reference. The trend at low velocities in F-4(a) reflects rapid deceleration to main stream velocity when injection velocity is low.

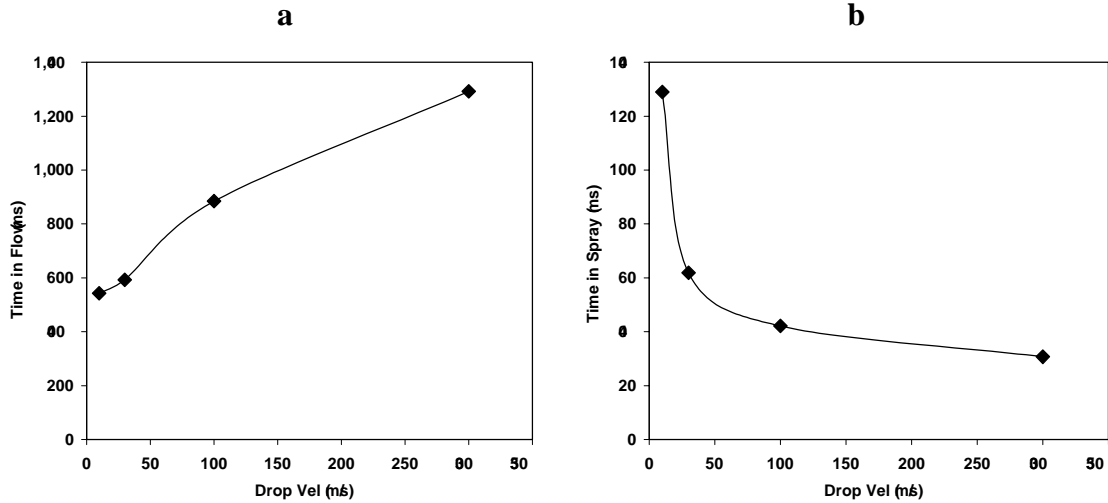


Figure F-4. Evaporation time as a function of droplet velocity. (a) Duct frame of reference, (b) droplet frame of reference.

Figure F-5 shows the effect of varying the main gas temperature from 1200 to 1600 K, while maintaining the initial droplet temperature at 300 K and all other conditions at baseline values. The main effect of this variation is to change the driving force for evaporation, which can be characterized by the initial gas-droplet temperature difference. Because this parameter is changing by percentages, as opposed to parameters discussed above which are changing by orders of magnitude, the results show a relatively weak response. This reflects that the gas is well above the water vaporization temperature over the entire temperature range.

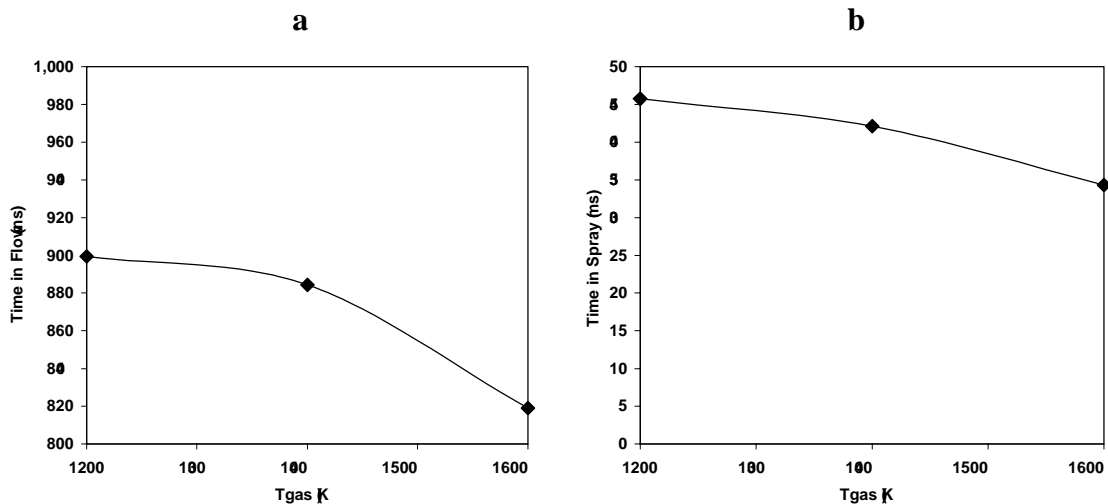


Figure F-5. Evaporation time as a function of gas temperature. (a) Duct frame of reference, (b) droplet frame of reference.

The results of this simple modeling exercise show typical dependencies of spray evaporation time on major spray parameters. The description of evaporation must be done in the context of the lagrangian viewpoint of the overall model, with corresponding mapping of both mass release and thermal history of the spray. Model dependence on some parameters, including spray angle and spray velocity, can be strongly dependent on that viewpoint. Evaporation rate is relatively insensitive to the temperature difference between gas and spray in most practical combustion situations. However, characteristic droplet size is a major parameter for determining the evaporation time scale in either reference frame. For this reason, nozzle selection and characterization is a primary consideration in practical implementation of liquid agent injection technologies.